UNIVERSITÀ
DEGLI STUDI
DI PADOVA

Sede Amministrativa: *Università degli Studi di Padova*

Dipartimento di: *Tecnica e Gestione dei Sistemi Industriali (DTG)*

SCUOLA DI DOTTORATO DI RICERCA IN: INGEGNERIA INDUSTRIALE
INDIRIZZO: INGEGNERIA DELL'ENERGIA
CICLO: XXVIII

APPLICATION OF INNOVATIVE REFRIGERANTS WITH LOW ENVIRONMENTAL IMPACT FOR REFRIGERATION AND THERMAL CONTROL

Direttore della Scuola: Ch.mo Prof. Paolo Colombo
Coordinatore d'indirizzo: Ch.ma Prof.ssa Luisa Rossetto
Supervisore: Ch.mo Prof. Claudio Zilio

Dottoranda: Giulia Righetti

To everyone who has believed in me,
to everyone who has inspired me,
above all: to my Family.

Abstract

After a brief introduction on the global warming effect and on the measures that have been adopted to limit it, this thesis is focused on low GWP refrigerants and, above all, on HFOs, which have been studied during two phase flow in several operating test conditions. To cover a great portion of the existing devices, four heat exchangers have been investigated: a tube in tube heat exchanger, a Brazed Plate Heat Exchanger (BPHE), a roll-bond type heat exchanger, and a Finned Heat Pipe Heat Exchanger (HPFHE).

In Chapter 2 the four experimental test rigs used to collect experimental data are explained and the data reduction processes used to analyze the recorded data are shown.

In Chapter 3 all the experimental data points collected are presented, critically discussed, and compared against some existing correlations. In addition, new analytical procedures are proposed to evaluate the heat transfer coefficient and the pressure drop during vaporization and condensation inside BPHEs respectively. Furthermore a new computational procedure to calculate the heat capacity and the heat transfer coefficients of a HPFHE is presented.

In Chapter 4, the experimental data obtained with different fluids under the same working conditions are grouped and compared to highlight the refrigerant effect on the global performance of the heat exchangers.

Finally some performance evaluation criteria to discriminate the best refrigerants on the basis of thermophysical properties and to select the ones that perform better in terms of heat transfer and pressure drops are presented.

Sommario

Il Capitolo 1 si apre con una breve introduzione riguardante la questione, purtroppo sempre attuale, dell'impatto ambientale dovuto all'attività umana e del surriscaldamento globale, facendo rifermento alle misure adottate negli anni per limitarlo. In seguito viene posta attenzione sul tema dei fluidi refrigeranti a basso impatto ambientale – e dunque a basso indice GWP – e in special modo sulle applicazioni in cui sussiste uno scambio termico bifase. Con l'interesse e lo scopo di coprire il maggior numero di casistiche adottate nella tecnica applicativa, la tesi approfondisce quattro tipi diversi di scambiatore di calore: uno scambiatore tubo in tubo, uno scambiatore a piastre, un evaporatore di tipo roll-bond e un recuperatore a tubi di calore.

Il Capitolo 2 comprende la descrizione degli impianti sperimentali e dei procedimenti di elaborazione dei dati ottenuti.

Il Capitolo 3, invece, presenta tutti i dati sperimentali acquisiti nel corso di questa tesi suddivisi per tipologia di scambiatore di calore, ne riporta un commento critico e li confronta con modelli e correlazioni presenti in letteratura. Inoltre vengono proposti due nuovi modelli basati su dati sperimentali per stimare i coefficienti di scambio termico durante i processi di vaporizzazione e di condensazione di refrigeranti all'interno di scambiatori a piastre. Viene altresì illustrata una procedura di calcolo che permette di ottenere il calore scambiato da un recuperatore a tubi di calore e i coefficienti di scambio termico del fluido operativo all'interno degli stessi tubi di calore.

Il Capitolo 4, infine, riporta un confronto tra dati sperimentali ottenuti nelle medesime condizioni operative con diversi fluidi refrigeranti che mette in luce l'effetto del fluido stesso sulle prestazioni dello scambiatore. Inoltre, per ogni scambiatore, vengono adottati ed implementati dei criteri di valutazione delle prestazioni dei soli refrigeranti sulla base delle proprietà termofisiche e delle prove sperimentali condotte. In tal modo è possibile racchiudere in un unico indice l'effetto combinato del refrigerante su coefficiente di scambio termico e su perdite di carico. Tale discussione può guidare nella scelta di un nuovo fluido, scelta che al giorno d'oggi, inserita all'interno di uno scenario che esige la tutela dell'ambiente e del clima, sta diventando di fondamentale importanza.

Table of Contents

Extended summary

The global warming is universally identified as a concrete and urgent concern (see section 1.1). For this reason also the refrigeration fluids has to be evolved accordingly (section 1.2). Many options have been proposed during years, but the most likely alternatives to the less environmentally friendly fluids can be summed up in few categories (see section 1.3): natural refrigerants, low GWP HydroFluoroCarbons (HFCs) and HydroFluoroOlefins (HFOs), relatively new molecules of which it has been done a detailed and critical review (section 1.3.1).

The aim of this thesis is focused on the use of innovative refrigerants in refrigeration and thermal control applications. To cover a great portion of the existing appliances, four different heat transfer categories were taken into account: tube heat exchangers, plate heat exchangers, roll-bond type heat exchangers and heat pipe finned heat exchangers. For each of the these groups, after a review of the existing scientific works (section 1.5) and an analysis of the flow regimes that occur in it (section 1.4), experimental tests were conducted using several refrigerants aiming to compare their performance.

In Chapter 2 the four experimental set up rigs are described and the procedures adopted to the data regression were illustrated.

In Chapter 3 each set up is analyzed individually and the experimental tests conducted on it are presented. Section 3.1 regards a horizontal smooth tube with an inner diameter of 4 mm. Two couples of refrigerants were tested during vaporization into it: R32 was proposed as low GWP alternative to R410A, and R1234ze(E) as R134a replacement. Heat transfer coefficients and pressure drops were measured at different saturation temperatures and the effects of mass flux, heat flux and temperature were investigated. More in detail the two leading contributions to the boiling process were exploited: nucleate boiling and convective boiling. The first one was affected by high saturation temperatures, low mass fluxes, and high heat fluxes, on the contrary the second one strengthens at low saturation temperatures, high mass fluxes and low heat fluxes, showing a notable dependence on the mean vapor quality (for further details, see section 1.4.1). The 532 experimental data collected were consistent with these theoretical trends, well described by Kim and Mudawar (2014a). In addition, the data were also compared against 13 heat transfer and 8 pressure drop correlations available in literature

(paragraph 3.1.2). The Sun and Mishima (2009) model was the one that matched better (10.4%) the experimental data obtained with R32 and R410A, fluids having high reduced pressure and so relatively high nucleate boiling contribution to vaporization. Besides, the Kim and Mudawar (2014a) model fits the R1234ze(E) and the R134a data within ±6%. The pressure drop of all the fluids tested were well predicted by the Fridel (1979) equation (i.e. absolute percentage deviation around 18.5% for the first couple of refrigerants and 13% for the second couple). In section 4.1 it is carried out a comparison among the fluids of each couple.

R32, the lower GWP component of R410A has higher liquid thermal conductivity (+40%) and higher specific heat (+15%). It also has a 40% higher vaporization latent heat that allows reducing the refrigerant flow rate at the same cooling capacity. The Volumetric Cooling Capacity (VCC) is similar for the two fluids (R32 +3% than R410A) and the saturation pressure is almost the same (R32 around 2% higher than R410A) so they are compatible to a direct drop in operation. On the contrary R32 has a lower reduced pressure (-15%) that disadvantages the pressure drops. Thanks to the more favorable thermophysical properties, the heat transfer coefficients of R32 were up to 17% higher (on average +13%) than those of R410A at the same saturation temperature, mass flux, heat flux and vapor quality. The heat transfer coefficients of both the fluids were strongly affected by the nucleate boiling mechanism under the tested working conditions, but this tendency was more relevant for R410A. As previously anticipated, the R32 pressure drops were on average 18% higher than those of R410A under the same operating conditions and up to 60% higher at 20 °C.

Focusing on the second couple of refrigerants, the saturation pressure is quite different between the two refrigerants: the R134a one is around 35% higher than the R1234ze(E) one and also the R134a reduced pressure is about 20% higher. Furthermore the R134a vapor density is higher than R1234ze(E) (+23%), so theoretically R134a should perform lower pressure drops. On the contrary, the liquid thermal conductivity is similar (around 5% higher for R134a), and also the surface tension (R134a: +9% R1234ze(E)) and the latent heat (R134a: +7% R1234ze(E)) do not vary significantly. There were not great differences in heat transfer coefficients measured: R134a HTCs were on average just 5% higher than R1234ze(E) under the same working conditions but the R1234ze(E) heat transfer coefficients were more influenced by the mean vapor quality and thus by convective boiling, maybe due to the lower pressure and the lower vapor density. This mechanism made the R1234ze(E) HTC increase

and, in some conditions, the R1234ze(E) heat transfer coefficients were higher than the R134a ones (up to 25% at G=600 kg m^{-2} s^{-1} and t_{sat}=10 °C). As for as pressure drop is concerned, the trend as a function of the mean vapor quality was similar for the two refrigerants but, especially due to the higher reduced pressure R134a performed lower pressure drops (around 30% lower at 20 °C but only 5% lower at 10 °C).

Section 3.2 contains the experimental tests carried out in a commercial Brazed Plate Heat Exchanger (BPHE) during both vaporization and condensation.

276 boiling data were collected during R1234ze(E) and R32 vaporization at different saturation temperatures, mass fluxes, heat fluxes and outlet conditions, where four different evaporator outlet conditions were considered (i.e., an outlet vapor quality around 0.8, an outlet vapor quality around 1, a vapor super-heating at the exit of the heat exchanger around 5 °C and a vapor super-heating of around 10 °C). A remarkable effect of the heat flux and of the outlet conditions on the heat transfer coefficients was observed. On the contrary, the impact of the saturation temperature on the heat transfer coefficient appeared relatively less significant. So far as the pressure drop is concerned, fairly linear correlation between them and the kinetic energy per unit volume of the refrigerant flow was detected. Furthermore, a thermography analysis by means of an IR thermo-camera (temperature uncertainty (k=2)=±0.1 °C in the temperature range 5 – 150 °C) was performed to inspect the vaporization process inside the BPHE. This analysis aimed at investigating the heat transfer regimes and to quantify the portion of heat transfer area affected by vapor super-heating and the one in two-phase. This analysis substantially confirmed the experimental measurements and suggested an optimum degree of vapor super-heating at the outlet of the evaporator around 3-5 °C for avoiding a degradation of the evaporator thermal performance and effectiveness but still for guarantee a safe operation of the refrigerating unit.

Moreover, 345 data were collected during R152a, R1234ze(E), R1234ze(Z), and R32 condensation at different saturation temperatures, mass fluxes, heat fluxes and inlet conditions (saturated vapor conditions in which the inlet vapor quality varies around 1 and super-heated vapor conditions of around 10 °C).

A transition point between gravity dominated and forced convection condensation were marked at a refrigerant mass fluxes around 20 kg m^{-2} s^{-1} for all the HFO and HFC refrigerants. For mass fluxes lower than this threshold value the heat transfer coefficients increased for decreasing mass flux as predicted by the Nusselt (1916) analysis for laminar film-

condensation on a vertical surface. While for mass fluxes higher than 20 kg m^{-2} s^{-1} the heat transfer coefficients increased with refrigerant mass flux, highlighting a condensation process governed by the vapor shear mechanism. Furthermore, the heat transfer coefficients were poorly influenced by the saturation temperature and by the outlet conditions. As for vaporization, the frictional pressure drops presented a linear dependence on the kinetic energy per unit volume of the refrigerant flow and therefore a quadratic dependence on the refrigerant mass flux, while they are lightly affected by the saturation temperature.

On the basis of experimental 251 vaporization data and 338 condensation ones collected during several years in the same commercial BPHE, two new correlations have been implemented for both vaporization and condensation heat transfer coefficients. The vaporization procedure (see paragraph 3.2.2.1.1) computed the maximum value between an average convective boiling heat transfer coefficient, obtained by a best fitting procedure on a series of data where convective boiling appeared to be the dominant heat transfer coefficient, and an average nucleate boiling heat transfer coefficient, calculated by a best fitting equation based on the Gorenflo (1992) model. The same procedure, coupled with a single-phase heat transfer coefficient correlation that accounted for the super-heating contribution, was also proposed to predict the average heat transfer coefficient during boiling with outlet vapor super-heating. The mean absolute percentage deviation between calculated and experimental data used to calibrate the new boiling correlation was around 9.0%. Furthermore, this new heat transfer model was compared against a set of 505 experimental data points obtained by several authors available in the open literature, that included different refrigerants (R134a, R410A, R507A, and R22) and different plate geometries. The mean absolute percentage deviation between these latter experimental data and calculated ones by means of the new correlation was around 20%. Similarly, a new model for evaluating the condensation heat transfer coefficient inside BPHEs was presented in section 3.2.2.2.2. It was obtained by a best fit procedure based on 338 experimental data points with R236a, R134a, R410A, R600a, R290, R1270, R1234yf, and R1234ze(E) as two-phase fluids. A transition point between gravity-dominated and forced convection condensation was found for an equivalent Reynolds number around 1600 which corresponded in the tested BPHE to a refrigerant mass flux around 20 kg m^{-2} s^{-1} for HFCs and HFOs and around 16 kg m^{-2} s^{-1} for HCs. The experimental data in the gravity-controlled region were predicted by a simple model based on the Nusselt (1916) equation for vertical surface multiplied by a geometrical enlargement factor, while the

data in forced convection condensation region were predicted by a new non-dimensional equation based on the equivalent Reynolds and Prandtl numbers. To evaluate the super-heated vapor condensation the new model was coupled with the Webb (1998) correlation. The mean absolute percentage deviation between calculated and experimental data was around 4.7%. Then, the new correlation was compared against a set of 516 experimental data points obtained by different laboratories and the mean absolute percentage deviation was lower than 20%.

In section 4.2 the tested fluids were compared against other data collected under the same working conditions in the same BPHE.

R1234ze(E) was correlated with R134a and R1234yf. R1234ze(E) during vaporization exhibited heat transfer coefficients very similar to R134a, while the R1234yf heat transfer coefficients were around 6-8% lower than those of R134a. Then, despite having a similar slope, the R1234ze(E) frictional pressure drops were around 23% higher than R134a, while R1234yf ones were lower (around 10-18%) due to the lower reduced pressure and higher vapor specific volume.

As far as condensation is concerned, R1234ze(E) heat transfer coefficients were slightly lower (4 to 6%) than those of R134a and slightly higher (4 to 6%) than those of R1234yf. While R1234ze(E) frictional pressure drops were higher both than those of R134a (10%) and those of R1234yf (20%) under the same operating conditions.

R32 was once again compared against R410A. The R32 boiling heat transfer coefficients were on average 20-30% lower and the pressure drop were 30-40% higher than the R410A ones, probably mainly due to the lower reduced pressure. While the R32 condensation heat transfer coefficients were around 20% higher than those of R410A, due to difference latent heat of vaporization and liquid thermal conductivity, and the R32 pressure drops during condensation were slightly higher than R410A.

R152a was proposed as low GWP refrigerant to be used in large chiller application working with turbo and screw compressors (see section 4.2.2.2). For this reason it was compared against R134a, R290 and R1234ze(E). It presented condensation heat transfer coefficients higher than those of all the other refrigerants, +19% than R134a, +13% than R290, and +23% than R1234ze(E) at 40 °C due to its high liquid thermal conductivity and latent heat of vaporization. The R152a pressure drops were close to the R290 ones and lightly higher than R134a and R1234ze(E).

Finally R1234ze(Z) was suggested as potential refrigerant for high-temperature heat pumps, mainly due to its high critical temperature, and compared against R134a, R1234ze(E), R600a and R326fa. At a condensation temperature of 40 °C, R1234ze(Z) showed condensation heat transfer coefficients 35% higher than R600a, 65% higher than R134a, 72% higher than R1234ze(E), and 82% higher than R236fa, mainly due to the R1234ze(Z) higher liquid thermal conductivity and latent heat. Furthermore, the R1234ze(Z) frictional pressure drop was similar to R600a but higher than other refrigerants. For example, at 40 °C R1234ze(Z) presented frictional pressure drop 5% lower than R600a but 166% higher than R134a, 125% higher than R1234ze(E), and 73% higher than R236fa, mainly due to the lower reduced pressure.

The third heat exchanger type taken into account was a roll-bond evaporator (section 3.3) where five different refrigerants (R134a, R1234ze(E), R1234yf, R600 and R600a) were tested at two evaporation temperatures and different mass flow rates and their boiling performance was compared.

For each fluid the mass flow rate was incremented from a minimum value, set by the compressor capacity, to a maximum where the two phase flow affects the whole heat transfer surface and the outlet vapor super-heating approaches zero.

For all the fluids tested, the refrigerating capacity was observed to be an almost linear function of the refrigerant mass flow rate. The overall heat transfer coefficient increased with the refrigerating capacity, and it is affected by the saturation temperature. The air-side heat transfer coefficient was fairly constant for all the data points obtained and it weakly depended on the refrigerant used. The mean value was 22.0 W m^{-2} K^{-1} with a standard deviation of 2.0 W m^{-2} K^{-1}. Consequently, the refrigerant heat transfer coefficient increased with the increasing of the refrigerating capacity. In addition, as presented in section 3.3.7, an IR thermo-camera was utilized to monitor the temperature distribution on the front face of the roll-bond evaporator. From that images, it was possible to observe that, increasing the mass flow rate and, thus, the refrigerating capacity, the portion of the heat transfer surface working in vaporization increased with respect to that working in vapor super-heating till the maximum refrigerant flow rate is reached. Thanks to this investigating technique, some deficits in the roll-bond design, for example a non-optimal circuitry and a improvable millwork quality, could be point out.

Finally, 7 nucleate boiling correlations were tested (see paragraph 3.3.8) and the one that fitted better the experimental data taken into account was Cooper (1984) with a mean deviation lower than 20% and an absolute mean deviation around 40%. In section 4.3, after a comparison of all the tested refrigerants inside the roll-bond evaporator under the same working conditions, it was concluded that each fluid tested could be used as working fluid inside a domestic refrigerator. The heat transfer coefficients were comparable between the different refrigerants here analyzed. The mass flow rate could be strongly reduced by using an HC instead of R134a and, consequently, also the pressure drop could be limited. On the other hand, the maximum refrigerating capacity of HFOs was close to the R134a one, while the maximum refrigerating capacity of the HCs was around 20% lower than the R134a one. Finally, since the compressor displacement had to be adjusted to deliver the proper refrigerant mass flow rate, only R1234yf exhibited a volumetric cooling capacity similar to R134a, therefore it only could be considered a direct drop-in alternative for R134a in domestic refrigerator.

The last heat exchanger type analyzed in this thesis is a Heat Pipe Finned Heat Exchanger, commonly used in residential and commercial air conditioning systems as heat recuperator. In paragraph 3.4, 154 experimental data obtained at different heat flow rate, mass flow rates, capacity rate ratios, and working conditions (the supply and the exhaust inlet air temperature were varied to simulate the Mediterranean summer and winter seasons) are presented for three fluids: R134a, one of the most common used in these kind of devices, R152a and R1234ze(E). The principal result shown in this chapter was in terms of heat flow rate, presented as a function of the air flow rate under different working conditions. In fact it linearly increased with the air flow rate, calculated as the average value between the supply and the exhaust lines, and the temperature difference between the two air lines. The maximum air flow rate was fixed at 1000 $m^3\ h^{-1}$ and the maximum heat flow rate achievable was 1616 W with R134a, 1667 W with R1234ze(E), and 1666 W with R152a.

The experimental heat transfer data were later compared against a new computational procedure proposed in section 3.4.2. This new procedure was developed to best fit the data collected with R134a and R1234ze(E) as working fluid. Secondly, it was used to compare the experimental data with R152a as two-phase fluid in the pipes. The heat exchanger was divided into a series of ranks and, after testing several existing correlations: the ones that

fitted better the experimental data were chosen to evaluate the condensation and the vaporization heat transfer coefficient of the refrigerant and of the air heat transfer coefficient. The air temperature, the relative humidity, and the flow rate at the inlet of the condenser and the evaporator sections, and some geometrical parameters were input data.

The simulation proceeded by iterating on the saturation pressure of the fluid inside the heat pipes; given the subdivision of the HPFHE in ranks. The mean absolute percentage deviation between calculated and experimental saturation temperature was around 4.3% for R134a, 4.5% for R1234ze(E), and 6% for R152a. Regarding pressure drops, the data with a Reynolds number from 700 to 1700 were well predicted by the Wang *et al.* (2000) model and probably referred to turbulent flow, whereas the data points with a Reynolds number lower than 700, especially with R1234ze(E) as working fluid exhibited a different trend compatible with a laminar or a transition flow.

In section 4.4 the three fluids performance are compared. It was observed that the heat flow rates of the alternative refrigerants were comparable and even higher than that of the more traditional R134a. In particular, at the extreme summer conditions, $T_{supply.in}$=40 °C, they exchanged similar heat flow rates, (around 5% higher than those of R134a), but at lower inlet supply temperatures ($T_{supply.in}$=35 °C) R152a outperformed, showing heat flow rates up to 11% higher than those of the other fluids, which were similar. Also in winter testing conditions R152a outperformed (15% higher than those of R134a and R1234ze(E) under the same working conditions) the other refrigerants which exhibited almost the same heat transfer performance.

To conclude this thesis some Performance Evaluation Criteria (PEC) were proposed and implemented for the different heat transfer conditions. In fact, they help in a selection between different fluids, gathering together both the heat transfer coefficient and the pressure drop points of views.

On the basis of the Brown *et al.* (2013) PEC, an analysis during flow boiling inside smooth tubes was conducted (see section 4.1.3).

Firstly the saturation temperature drop which occurred due to the refrigerant pressure drop was plotted against the heat transfer coefficients for all the fluids, secondly a PEC called Total Temperature Penalization (TTP), which is the combination of a term related to heat transfer and a term related to pressure drop, was considered.

The analysis based on the TTP suggested that R134a performed better than R1234ze(E), having a TTP value lower at the same heat transfer coefficient value, and similarly R32 gave better performance than R410A at the same HTC. It has also noticed that these temperature differences were strongly affected by the refrigerant saturation pressure. In fact, higher pressure refrigerants had smaller pressure drop penalization values than medium and lower pressure refrigerants.

Section 4.2.3 presents a similar PEC extended to vaporization inside BPHEs. In this particular case the new equations proposed in this thesis were used to evaluate the heat transfer coefficients and the pressure drops. As noticed for the tube case, higher pressure refrigerants have generally smaller saturation temperature drop values than medium and lower pressure refrigerants but the ranking is not strictly linked to saturation pressure. Putting the attention on the refrigerants experimentally tested during vaporization in this thesis R32 was noticed to be a better alternative to R410A on the basis of the saturation temperature drop. While R1234ze(E) had a higher saturation temperature drop than R134a mainly also due to its lower reduced pressure, so its global performance on the basis of this criterion was worse than R134a.

As far as condensation inside BPHEs is concerning, similarly to what has been made for the vaporization process, a saturation temperature drop was defined also for the condensation process inside a Brazed Plate Heat Exchanger (BPHE).

Focusing on the refrigerants experimentally tested during condensation in this it was noticed that, at the same heat transfer coefficient, R152a and R1234ze(E) could be proposed as R134a substitutes. In fact, in terms of saturation temperature drop R152a was slightly better than R134a despite having a lower saturation pressure, while R1234ze(E) had higher Δt_{sr} than R134a. In addition, R1234ze(Z) presented a saturation temperature drop lower than R236fa, so it could be consider as a fair alternative to it. Finally, as presented for the vaporization process, the R32 saturation temperature drop was lower than the R410A one also during condensation. Thus, the R32 energetic and exergetic efficiency should be higher than R410A.

During the shear dominated condensation process, for a specified refrigerant, saturation temperature, vapor quality, and geometry, Cavallini *et al.* (2000, 2002, and 2005) demonstrated that the product of the two penalization components can be expressed only as a function of the heat transfer coefficient. This product was called Penalty Factor (PF) of the

condensation process and it became a useful tool for comparing the exergy losses associated with frictional pressure drop among various fluids.

It was noticed that R32 had PF lower than R410A in fact R410A was affected by the other component R125 having a higher PF value. Furthermore, the HFOs group presented PF values higher than R134a. That means that on the first hand proposing R32 as alternative to R410A is convenient under a refrigerant energetic and exergetic efficiency point of view, on the other hand substituting R134a with some HFOs can be less convenient and so to maintain a high efficiency could be required an optimization of the heat transfer devices.

Finally, it has been chosen to analyze the HPFHE data through a performance criteria proposed by Reay and Kew (2006) for the single heat pipe. They defined a so called Merit number by grouping liquid density, latent heat of vaporization, surface tension, and liquid viscosity.

From a selection of fluids usable in heat pipes operations, with the exception of water that works with pressure very far from the R134a and ammonia that is not compatible to a directly drop-in in the tested copper HPFHE, R152a presented the highest merit number, approximately 78% higher than that of R134a at 40 °C. On the other hand R1234ze(E), the other fluid tested inside this thesis, had a Merit number close to the R134a one (+1% at 40°C). Merit number seemed to be a good criterion to rank the refrigerant performance. In fact R1234ze(E), with a Merit number close to the R134a one, gave heat flow rates similar to the R134a ones. Furthermore R152a, with a Merit number higher to R134a, gave heat flow rates higher than R134a.

To sum up, this thesis aims to investigate the low environmental impact fluids for refrigeration and thermal control. It focuses on the two phase heat transfer in different heat exchangers to cover the great majority of the devices on the market, and it analyzed several refrigerants in order to propose new alternatives. It strengthens the experimental results through the comparison with correlations available in the literature and further it proposes new correlations for BPHEs and HPFHEs. Finally a performance criteria able to condense together the effects of heat transfer coefficient and pressure drop is introduced for each kind of heat exchanger investigated. This analysis reveals to be essential to isolate and to evaluate the refrigerant potentiality and to designate a suitable environmental friendly replacement to the more harmful fluids use at present.

1 Introduction

1.1 Global warming

While this thesis was drafted, the United Nations Conference on Climate Change (COP21) occurred in Paris. There, 186 countries met together to looking for an agreement to limit the effects of global warming and to reduce or to recover the damages connected to it.

The concerns on the climate change have been growing for years, and the 2015 Paris conference is just a step in the long path scientists and politicians have been doing.

The Montreal Protocol, agreed on 16 September 1987 and entered into force on 1 January 1989, was the first international agreement that limited – and later on banned – the production and the consumption of CloroFluoroCarbons (CFCs) and Halons, fluids accountable to damage the ozone layer in order to reduce their abundance in the atmosphere and thereby protect the earth's fragile ozone Layer. (www.ozone.unep.org). The list of harmful substances was made longer during years, for example including also the HydroCloroFluoroCarbons (HCFCs). Specifically for the mostly-developed countries (Non-Article 5), the Montreal Protocol imposed the CFCs stop of production in 1996 and the stop of consumption in 2000. Moreover, the HCFCs phase out was defined gradually until 2030, but most western and central-European countries accelerated it.

In 1992 the United Nations Framework Convention on Climate Change (UNFCCC) was adopted. It acknowledged the existence of an anthropogenic (human-induced) climate change. The industrialized countries were charged with the major part of responsibility and so they were demanded actions for combating it. In 1997 more than 160 countries took part at the Kyoto Protocol where for the first time, binding greenhouse gas emissions reduction targets were set for industrialized countries. This protocol, which entered into force in 2005, after being approved also by Russia, was intended to cover the period 2008-2012. A longer-term vision was introduced by the Bali Action Plan in 2007, which set timelines for the negotiations towards reaching a successor agreement to the Kyoto Protocol, that expired in 2012. Later on, in 2009 at the Copenhagen Conference the common and tangible objective of keeping the increase in global temperature below 2°C was recognized. One year later a list of dedicated instructions and key points was established to reach this target. The following years saw other meetings in Doha (Qatar), Warsaw (Poland) and Lima (Perù). All these Conferences strengthened the unanimous agreement that the earth's atmosphere is growing warmer due to greenhouse gas emissions generated

by human activity and that it is mandatory to keep the rise in temperature below 2 °C. In fact exceeding this threshold limit can have serious consequences, such as an increase in the number of extreme climate events.

Coming back to Paris 2015, the agreement acknowledged that countries have common but differentiated responsibilities when it comes to climate change, depending on their wealth. Furthermore it established an obligation for industrialized countries to fund climate finance for poor countries, while developing countries were invited to contribute on a voluntary basis. $100 billion (in loans and donations) would need to be raised each year from 2020 to finance projects that enable countries to adapt to climate change impacts (rise in sea level, droughts, etc.) or to reduce greenhouse gas emissions. On the basis of these series of conferences and agreements, Nations responsible for more than 90% of global emissions have now to come up with their targets. The EU would cut its emissions by 40%, compared with 1990 levels, by 2030. The US would cut its emissions by 26% to 28%, compared with 2005 levels, by 2025. China would agree that its emissions will peak by 2030.

1.1.1 Environmental metrics

Following the main indexes defined to measure how much a substance is harmful for the environment are listed and briefly explained. A particular attention is given to fluids connected to refrigeration, as the main topic of this thesis.

1.1.1.1 ODP (Ozone Depleting Potential)

One of the greatest environmental effect attributable to chemicals refrigerant is the destruction of the ozone layer. Chlorine and bromine molecules are known to react with ozone, altering the natural chain of reactions that occurs between oxygen and ozone in the stratosphere. The Ozone Depleting Potential (ODP) index was creating to define how much an Ozone Depleting Substance (ODS) is able to destroy the ozone layer. It depends on the number of chlorine and bromine atoms inside the molecule and on the atmospheric life time of the molecule itself. It is defined as ratio between the harmful potential of a compound and the one of R11 molecule, which has been taken as reference value.

1.1.1.2 GWP (Global Warming Potential)

The Global Warming Potential (GWP) is a very commonly used environmental index. It compares the global warming impact of a substance, estimated during a time horizon, in relation to the impact from the emission of similar amount of CO_2. The most adopted time horizon is equal to 100 years. The GWP depends on the infrared radiation absorption of the fluid, its lifetime in the atmosphere, and the time frame selected. Thus, the same gas can have different GWP for different time frames. In any case, the smaller the GWP, the lower is the contribution of a substance to the global warming.

In Table 1 the GWP indexes of some of the commonly used refrigerants are listed. The GWP of the fluids with (*) are evaluated in accordance to EPA (2012) while the ones with (**) according to Hodnebrog *et al.* (2013)

Table 1 Refrigerant GWP indexes.

Fluid	**GWP-100 yr**	**Source**
Ammonia	0	(*)
R1234yf	<1	(**)
R1234ze(E)	<1	(**)
R125	3169	(**)
R1270	1.8	(*)
R134a	1301	(**)
R152a	138	(**)
R236fa	8056	(**)
R245fa	858	(**)
R290	3.3	(*)
R32	677	(**)
R404A	3922	(*)
R410A	2088	(*)
R600a	3	(*)

1.1.1.3 TEWI (Total Equivalent Warming Impact)

The Total Equivalent Warming Impact (TEWI) index takes into account for the global warming impact both the direct and the indirect emissions and it is calculated as a sum of the two contributions.
The direct effect of a refrigerant is linked to the lifetime of the equipment while the indirect impact depends on the CO_2 emissions from fossil fuels used to generate the energy required to operate the equipment throughout its lifetime.
The TEWI index is more difficult to estimate than the GWP and the ODP ones. It can be evaluated according to the definition proposed in Makhnatch and Khodabandeh (2014).

1.1.1.4 LCCP (Life-Cycle Climate Performance)

The TEWI index does not take into account all the relevant indirect emissions involved into refrigerant life cycle, such as the emissions related to the manufacture and transportation of the system and refrigerant. Hence, another indicator is used to account all the contributions to global warming related to the refrigeration system operation, including the environmental impact of substances emitted during the process of refrigerant production and transportation.
This index, called Life-Cycle Climate Performance (LCCP) involves the environmental effect of manufacture and transportation, together with the other effects already accounted in TEWI, but it becomes even harder to be evaluated correctly (Marhnatch and Khodabandeh, 2014).

1.2 History of fluids for refrigeration

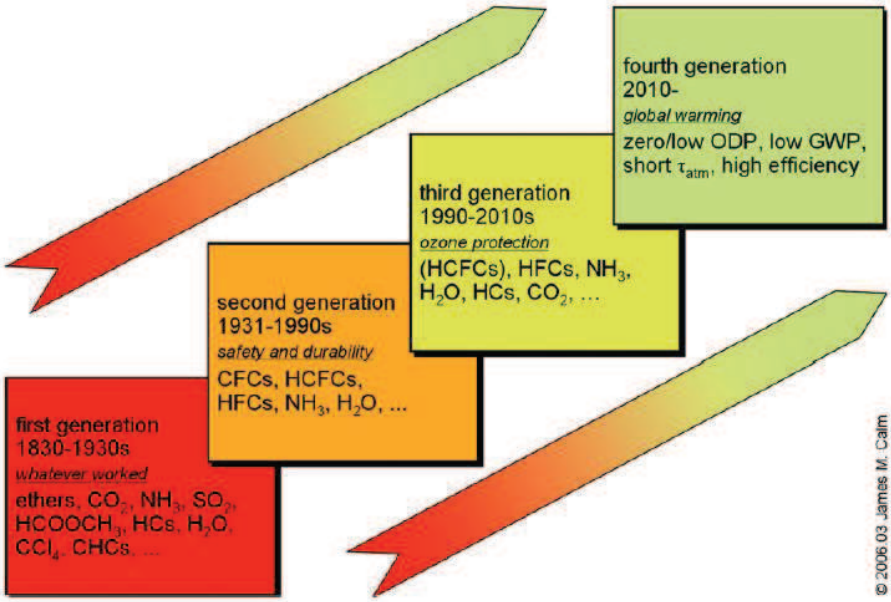

Figure 1. Fluids grouped into four generations by Calm (2008).

The fluids used for refrigeration have changed during years. Calm (2008) proposed four different generations under which subdivide their progression.

The first category is called "whatever worked" and it is made up by whatever fluid could work as refrigerant and was available. At that moment the great majority of these fluids were solvents and other volatile fluids. Nearly all of them were flammable, toxic, or both, and some were also highly reactive.

During years propane prevailed as the "odorless refrigerant" together with ammonia, carbon dioxide in non trans-critical cycles and water.

The second generation is characterized by "safety and durability" and it gathers together a great number of fluoro-chemicals that are stable, but neither toxic nor flammable.

Midgley (1937) completed a methodical research on potential refrigerants starting from the scoured property tables to find chemicals with the desired boiling point.

He firstly eliminated the yielding insufficient volatility molecules, secondly he eliminated those resulting in unstable and toxic compounds, after that he discarded the inert gases due to their low

boiling points. Finally just eight elements remained, namely: carbon, nitrogen, oxygen, sulfur, hydrogen, fluorine, chlorine, and bromine. Midgley (1937) also noted that every known refrigerant at the time combined seven of these elements – all but fluorine.

In the early 1930s the production of R12 and R11 began. ChloroFluoroCarbons (CFCs) and later – especially in residential and small commercial air conditioners and heat pumps by the 1950s – HydroChloroFluoroCarbons (HCFCs) dominated the second generation of refrigerants.

After the 1961 Vienna Convention and the resulting Montreal Protocol (1987) the ozone-depleting substances (ODSs), that included the CFCs and the HCFCs (see section 1.1), are forced to be abandoned. The third generation of refrigerant, called "ozone protection" started here.

The HydroFluoroCarbons (HFCs) were proposed as replacements for the longer term but the interest was focused also in "natural refrigerants", particularly ammonia, carbon dioxide, hydrocarbons, and water. Manufacturers commercialized the first alternative refrigerants in late 1989 and, within 10 years, they introduced replacements for most of the ozone-depleting refrigerants.

Finally the birth of the fourth generation was due to the Kyoto Protocol (1997) which set limits on the greenhouse gas (GHG) emissions based on calculated equivalents of carbon dioxide.

The fourth generation is the so called "global warming".

The Kyoto Protocol (see section 1.1), limited the emissions of carbon dioxide, methane, nitrous oxide, HFCs, perfluorocarbons (PFCs), and sulfur hexafluoride. Thus, HFC refrigerants were pointed as direct greenhouse gases because of their high Global Warming Potential (GWP) (though they have zero Ozone Depletion Potential, ODP), and so they are going to be phasing out.

More recent measures at national, regional, and municipal levels are even more stringent. In Europe the second F-Gas regulation (section 1.2.1) has been approved. It regards the gradual phasing out of high refrigerants, where "high" in some applications means that the maximum acceptable GWP threshold is 150. Similar regulations are under evaluation or introduction also in other developed countries such as, US, Japan, Australia and Canada.

For example in 2014, the United States, Canada and Mexico proposed an amendment to the Montreal Protocol to reduce production and consumption of HFCs by 85% during the period 2016–2035, for non-A5 (developed) countries, while the A5 (developing) countries would reduce HFC production and consumption by 85% during the later period 2025–2045 (Goetzler *et al.*, 2014). Accordingly Australia

have introduced high taxations on the use and on the selling of high GWP refrigerants (i.e. 50 $ each R410A kg).

1.2.1 European Regulation

The European Union has been issued several guidelines to limit the environmental damages connected to refrigerants.

With the EU Regulation No 2037/2000, it has been imposed since the 1st of January, 2000 a ban both in production and in consumption of CFC fluids. Furthermore, it has been gradually limit the use of HCFCs till a complete prohibition in selling in 2010 and in production in 2025.

Table 2 Placing on the market prohibitions by EU Regulation No 517/2014 (Mota-Babiloni *et al.,* 2015).

Products and equipment	**Threshold GWP**	**Date**
Domestic refrigerators and freezers	150	2015
Refrigerators and freezers for commercial use (hermetically sealed equipment)	2500	2020
Refrigerators and freezers for commercial use (hermetically sealed equipment)	150	2022
Stationary refrigeration equipment, that contains, or whose functioning relies upon, HFCs except equipment intended for application designed to cool products to temperatures below -50 °C.	2500	2020
Multipack centralized refrigeration systems for commercial use with a rated capacity>40 kW that contain, or whose functioning relies upon, fluorinated greenhouse gases	150	2022
Movable room air-conditioning equipment (hermetically sealed equipment which is movable between rooms by the end user)	150	2020
Single split air-conditioning systems containing less than 3 kg of fluorinated greenhouse gases, that contain, or whose functioning relies upon, fluorinated greenhouse gases	750	2025

Finally, this Regulation introduced a series of rules concerning the supervision and the maintenance of the machines and the devices containing refrigerants.

After that, the European Directive 2006/40/EC (Directive, 2006/40/EC, 2006) imposed the restriction in the use of refrigerants with GWP values above 150 used in mobile air conditioning systems, banning their use in new systems from 2011 and in the rest onward 2017. In addition it made the inspections and the maintenance programs more strict and rigorous than the previous Regulation.

This directive was following replaced by the EU Regulation No 517/2014 (Regulation (EU) No 517/20, 2014). With this new release the European Commission limited the total amount of a great part of the commonly used refrigerants, depending on their GWP index and their particular application. This regulation has been started since 2015 and is going to proceed until 2030 with even more stringent limits. The main limitations imposed by EU Regulation No 517/2014 are sum up in Table 2 (Mota-Babiloni *et al.,* 2015).

Figure 2 shows a graph of the phasedown schedules given from the European F-gas regulation with respect to the Montreal Protocol ones for the A5 (developing) and non A5 (developed) countries.

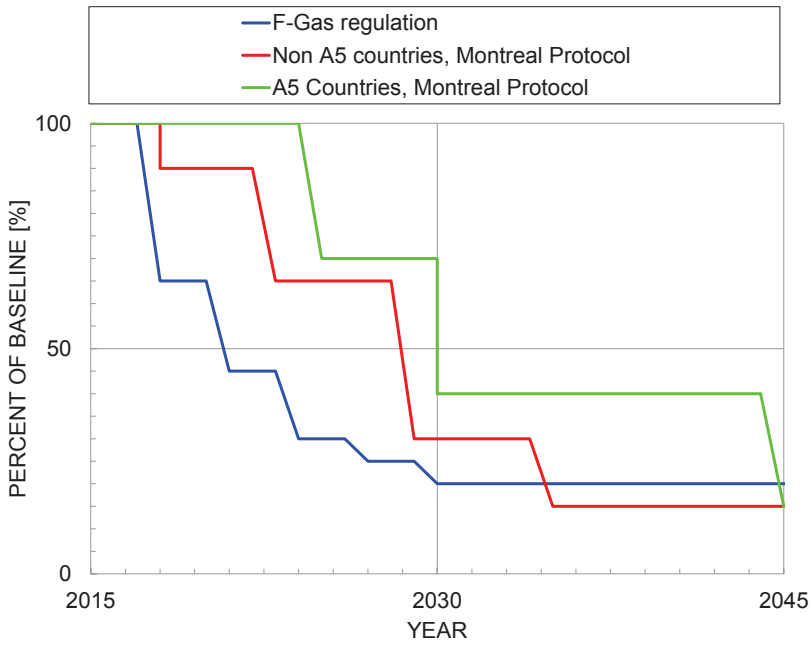

Figure 2 HFC phasedown schedules for European F-gas regulation and the Montreal Protocol (Adapted from Goetzler *et al.*, 2014).

1.3 Low GWP refrigerants

Despite Calm and Didion (1998) said that none of the current or candidate refrigerants are ideal, and future discovery of ideal refrigerants is extremely unlikely, it is mandatory to find some low Global Warming Potential (GWP) alternatives to the fluid that are being phasing out by the Kyoto Protocol and the regional laws.

When looking for new refrigerants, a number of criteria must be considered, for example: the stability within the refrigeration system, a short atmospheric lifetime (which is related to GWP and ozone depletion potential, ODP), thermodynamic properties suitable to the particular application (e.g. normal boiling point, critical temperature, etc.), low flammability and toxicity, and other practical considerations, including cost and compatibility with the materials of construction (McLinden and Didion, 1987).

It has also to be noticed that while short life time is desired to reduce the ODP and the GWP indexes, compounds having too short lifetime may result in high flammability and in degraded air quality, including contribution to urban smog. The impact and the safety of the decomposition products also can be concerns. So, the "optimum" refrigerant depends on many constraints, and the choice of refrigerants must be reconsidered when those constraints change (Velders *et al.*, 2009).

There are many possibilities to replace the refrigerants currently employed (Mohanraj *et al.*, 2009a) but one has to remember that any substitute that lowers the overall efficiency of the system in which it is going to be adopted is likely to have more adverse impact than benefit, on the base of the net global warming impacts (e.g., TEWI or LCCP, see paragraph 1.1.1) (Calm, 2002). Generally the new candidates are less efficient than earlier choices. With a few exceptions, the efficiency gains achieved in machineries that use the alternative refrigerants derive primarily from improvements in equipment design rather than the properties of newer working fluids. Simply put, better optimization with the old refrigerants would have yielded even higher efficiency in most cases, and the alternative refrigerants reduce margins for further product efficiency improvement (Calm and Didion, 1998).

So, besides looking for refrigerants that accomplish the GWP limitations, safe fluids that imply low energy consumption in vapor compression systems should be used (Calm, 2008).

Several alteratives have been proposed in the last years, but a first division can be made from natural refrigerants and new chemicals.

As anticipated in paragraph 1.2.1, carbon dioxide, ammonia, water and hydrocarbons are the most common used natural refrigerants. Even though they were used as first generation refrigerants (see section 1.2), in the last decades their use has been gaining a new growing importance.

They have a lot of advantages, especially connected to their low environmental impact, they are compatible with the common materials found in refrigerating systems (with the exception of ammonia) and they are soluble in conventional oils. On the other hand the concerning linked to safety reasons could limit the use of these fluids. (Bolaji and Huan, 2013)

The three most viable hydrocarbon refrigerants are propane, isobutane, and propylene. They GWP values are equal or lower than 3 (see Table 1) but they are classified as A3 refrigerants due to their high flammability. This feature limits the use of hydrocarbons in applications requiring larger volumes of refrigerant. Hydrocarbons are technically feasible replacements for many R410A systems, despite having slightly lower volumetric capacity and performance. In addition they have significantly lower cost compared to other synthetic alternatives (Goetzler *et al.*, 2014). Hydrocarbons are technically viable for small and medium-sized refrigeration and air conditioning applications, as well as chillers. Furthermore they are promising for secondary expansion systems, for example in supermarkets and in some chiller applications.

Beside natural refrigerants, the chemical industry is continuously proposing new compounds. McLinden *et al.* (2014) selected from a public-domain database of more than 100 million chemical, compounds a set of 56 000 candidate molecules. Following to search for new potential refrigerants they selected only the molecule composed by a limited set of elements (i.e. C, H, F, Cl, Br, O, N, and/or S) and having 15 or fewer atoms in the molecule, because it has been observed that the currently used refrigerants are all small molecules and because McLinden (1990) provided a thermodynamic basis for preferring small molecules. Then the authors estimated the GWP, the flammability, the critical temperature and other thermodynamic parameters and they and filtered out those molecules known to be generally toxic or unstable, those having a high GWP and an high ODP – the authors accepted compounds containing Cl or Br despite their potential to deplete stratospheric ozone if and only if they have a very short atmospheric lifetime – and the molecules having a too high or too low critical temperature (T_{crit} between 300 K and 400 K). A too high-critical temperature would result in a low

volumetric capacity, while a too low-critical-temperature would most likely involve a transcritical cycle and increased expansion losses).

These latter filters limited the number of potential refrigerants to 1200, the vast majority of which were halogenated because of the flammability constraint and over the 60% of the halogenated candidates contain only fluorine, because the addition of heavier chlorine or bromine atoms, despite suppressing flammability, generally increases to much the critical temperature.

Among this great amount of chemicals, just few choices can potentially be adopted in the short term and can respect the constrains of flammability, toxicity, availability, price, etc. It has to be reminded that HFOs are molecules more difficult to manufacture than most HFCs and will inevitably be more costly.

To sum up, McLinden *et al.* (2014) proposed among the few remaining candidates:

- two HFOs already commercially produced and investigated, namely R1234yf and R1234ze(E);
- the two R1132 isomers, despite having unknown risks, they would be interesting for further study;
- R1233zd(E) approved by the U.S. Environmental Protection Agency for the use in chiller applications (U.S. EPA, 2012), despite having a small, but non-zero, ozone depletion potential;
- 3,3,3-trifluoroprop-1-yne, initially screened out because of stability concerns, on the basis of the critical temperature could be a good candidate to replace R410A.

From a more engineering point of view, the performance of R1234yf closely matches that of R134a. For this reason it has been widely adopted mainly in automotive air conditioning, then in chillers and commercial refrigeration applications that currently use R134a. On the other hand R1234ze(E) has a lower volumetric capacity than R1234yf, but it is easier to manufacture and less costly. It could potentially be used for centrifugal, reciprocating, and screw compressors and large chillers, which require high quantities of refrigerant. It is also marketed for blowing agent and propellant applications.

R1233zd(E), despite being few investigated in the literature, could be a valid replacement for R123 in centrifugal chillers. For example, one manufacturer has also announced the launch of a centrifugal chiller in Europe that uses R1233zd(E) (Ejarn, 2015).

HFO blends have started to be developed to be viable alternative in applications that would traditionally use R22, R404A, and R410A. The GWP value of these blends ranges from less than 150 to around 600, which is a value still significantly lower than the ones of the HFCs they would replace.
Cost represents a major concern with HFOs and HFO blends. While actual costs under full scale production conditions are still unknown, current HFO-based refrigerants have a much higher cost than the refrigerants they would replace (Goetzler *et al.,* 2014).

Finally some HFCs can also be considered. In fact, thanks to their relatively low GWP index they can be again used as pure fluid or combined in mixtures Among all, two fluids seem to be particularly attractive, R32 and R152a. R32 is a versatile refrigerant that is particularly suitable for air conditioning and heat pump applications, while R152a has been investigated as an option for replacing R134a in mobile vehicle air conditioning applications, but its A2 flammability classification poses a major limitation to widespread adoption. It might also be a viable alternative refrigerant in commercial refrigeration applications, chillers, and industrial refrigeration.

1.3.1 HydroFluoroOlefins (HFOs)

A particular section is dedicated to the HydroFluoroOlefin (HFO) refrigerants, because actually they are the focus of a considerable interest in industry and scientific community. The halogenated olefins are molecules that contain at least one carbon-carbon double bond. Several dozen fluids are gather in this category but only few are effectively applied in cooling technologies and extensively investigated (McLinden *et al.,* 2014).
Heat transfer and pressure drop studies of HFOs have begun appearing since approximately 2010. The majority of these papers are devoted to R1234yf and R1234ze(E) and their blends with other common refrigerants, while other few molecules have been started to be taken into account by researchers because they seem potentially interesting for future developments, for example R1234ze(Z), R1243zf, R1233xf, R1243zf, and R1233zd(E).
One of the main issues related to the development of these fluids is the uncertainty that already occurs on the estimation of the thermophysical properties. In fact, many properties directly affects the two-

phase heat transfer: among others, vapor pressure, saturated liquid density, saturated vapor density, liquid specific heat, latent heat, liquid dynamic viscosity, liquid thermal conductivity, and surface tension.

Only the R1234yf and R1234ze(E) properties have been considerable measured, while other molecules (i.e. R1234ze(Z), R1233zd(E), R1243zf) properties have just started to be investigated, as reported the detailed literature review reported in Brown *et al.* (2014).

Some estimation techniques have been developed during years, for example Brown *et al.* (2014) demonstrated that it is possible to obtain a quite reasonable engineering estimation of the thermophysical properties of a fluid by knowing only the normal boiling temperature and its molecular structure.

Moving to the heat transfer measurements obtained with HFOs and their blends that were conducted in these years, a detailed list of the existing works is going to be redacted, subdivided by the particular heat transfer mechanism that occurred. A few subsections are created: the pool boiling one collects 4 papers that are available in literature: two regarding R1234yf and two R1234ze(E). One of these latter analyzed also R1234ze(Z) and R1233zd(E). The vaporization-inside-tube section counts 31 experimental works: one on R1234ze(Z), 12 on R1234yf, 8 on R1234ze(E) and 10 on HFO mixtures. Furthermore there are 8 papers on the condensation process inside tubes: three with R1234yf, three with R1234ze(E) and two with mixtures. Just two papers were found on the external condensation process that take into account four fluids: R1234yf, R1234ze(E), R1234ze(Z), and R1233zd(E). Finally a section that collects all the other applications is presented. Here are grouped two works on brazed plate heat exchanger using R1234yf during vaporization and condensation respectively and a paper of R1234ze(Z) condensation inside a plate-fin heat exchanger. Then, a paper on R1234ze(E) boiling inside copper foams, one on R1234ze(E) flow boiling on a micro-particle coated surface and two works that analyze the R1234yf two phase flow inside return bends are reported.

1.3.1.1 Pool boiling

Considering the pool boiling, R1234yf was studied by Park and Jung (2010) and by Moreno *et al.* (2011). Park and Jung (2010) measured the heat transfer coefficients on flat plain and low fin surfaces at 7 °C and at a heat flux going from 10 to 200 kW m^{-2}, while Moreno *et al.* (2011) investigated a

horizontally oriented copper surface with a micro porous coating. They both concluded that the nucleate boiling heat transfer coefficients of R1234yf were similar to those of R134a.

Also Van Rooyen and Thome (2013) studied the pool boiling process, in this case using R1234ze(E) as refrigerant that boiled outside externally enhanced tubes for a saturation temperature ranging from 5 °C to 15 °C and a heat flux ranging from 15 to 70 kW m^{-2}.

Nagata *et al.* (2015) investigated the pool boiling heat transfer of R1234ze(E), R1234ze(Z) and R1233zd(E) on a horizontal plane tube. The HTC of the HFO refrigerants were experimentally quantified and compared to that of conventional refrigerants R134a and R245fa at a saturation temperature from 10 °C to 60 °C and a heat flux from 0.7 to 80 kW·m^{-2}. The HTC of R1234ze(E) was slightly lower than that of R134a, whereas the HTCs of the other three refrigerants were significantly lower than R134a. Finally, the HTC of R1234ze(Z) and R1233zd(E) was slightly higher than R245fa.

1.3.1.2 In-tube flow boiling

With the exception of Kondou *et al.* (2014b) who investigated R1234ze(Z) during flow boiling inside a microfin tube having an outer diameter of 6 mm, at 30 °C of evaporation and at a fixed heat flux equal to 10 kW·m^{-2}, all the other papers published in literature present data of R1234ze(E), R1234yf and some blends obtained by mixing these two latter fluids mainly with R32.

As for as R1234yf is concerned, several authors investigated it as a possible replacement to R134a.

Del Col *et al.* (2013b) measured heat transfer coefficients and pressure drops inside a 0.96 mm diameter circular tube, where the mass velocity ranged from 200 to 600 kg·m^{-2}·s^{-1}. They concluded that there were no significant differences between the flow boiling heat transfer of R1234yf and R134a for the considered test conditions.

Saitoh *et al.* (2011) measured the boiling heat transfer coefficients in a 2 mm smooth tube for a saturation temperature of 15 °C at a mass velocity ranging from 100 to 400 kg·m^{-2}·$s^{-1}$and at a heat flux going from 6 to 24 kW m^{-2}, and an inlet vapor quality from 0 to 0.25. They concluded that the heat transfer coefficients of R1234yf were similar to those of R134a under their testing working conditions.

Anwar *et al.* (2015) presented an experimental campaign on R1234yf during flow boiling inside a tube of 1.6 mm of inner diameter at different saturation temperatures (27 and 32 °C), mass fluxes (ranging from 100 to 500 kg·m^{-2}·s^{-1}) and heat fluxes (ranging from 5 to 130 kW m^{-2}).

Chien *et al.* (2015) investigated a smooth tube of inner diameter equal to 1.5 mm at a saturation temperature of 10 °C, a heat fluxed from 5 to 30 kW m^{-2} and a mass flux ranging from 300 to 500 $kg \cdot m^{-2} \cdot s^{-1}$. They compared R1234yf against R32 and R134a, finding that the nucleate boiling was the dominant phase change mechanism in heat transfer mechanism for all the tested fluids. In addition, since none of the correlations tested were able to predict the data, they developed a new model on the basis of their experimental data.

Choi *et al.* (2013) collected some data during evaporation of R1234yf, R134a, and R22 in horizontal circular small tubes with inner diameters of 1.5 and 3.0 mm, for a heat flux ranging from 10 to 35 kW m^{-2}, a mass flux from 100 to 650 kg m^{-2} s^{-1}, and a saturation temperature of 5, 10, and 15°C, respectively. The R1234yf heat transfer coefficient data were found to be higher than the other fluids ones under the same working conditions.

Diani *et al.* (2015a) compared R1234yf against R134a in a 3.4 mm microfin circular tube at 30 °C of saturation, a mass flux from 190 to 940 $kg \cdot m^{-2} \cdot s^{-1}$ and a heat flux ranging from 10 to 50 $kW \cdot m^{-2}$. The R1234yf heat transfer coefficients were found to be slightly lower than R134a ones. While Diani and Rossetto (2015) proposed R1234yf flow boiling data inside a 2.4 mm microfin circular tube. The authors tested a mass velocities range between 375 and 940 $kg \cdot m^{-2} \cdot s^{-1}$, heat fluxes from 10 to 50 $kW \cdot m^{-2}$, and vapour qualities from 0.10 to 0.99, at a saturation temperature of 30 °C. They finally proposed a comparison against R134a data collected under the same working conditions, finding R134a to outperform R1234yf under the heat transfer point of view, but to present also higher pressure drops.

Padilla *et al.* (2011) visualized the two-phase flow patterns inside horizontal straight tubes with a diameter varying from 7.90 to 10.85 mm at a mass velocity ranging from 187 to 1702 $kg \cdot m^{-2} \cdot s^{-1}$ and a saturation temperature ranging from 4.8 °C to 20.7 °C. They compared the R1234yf results against R134a and R410A.

Mortada *et al.* (2012) for their experiments used a horizontal flattened tube with 6 rectangular minichannels with a hydraulic diameter of 1.1 mm, a mass velocity ranging from 20 to 100 $kg \cdot m^{-2} \cdot s^{-1}$ and a heat flux ranging from 2 to 15 $kW \cdot m^{-2}$. They claimed that the local heat transfer coefficient of R1234yf could be up to 40% higher than R134a for the same mass velocity.

Chien *et al.* (2012) and Oh *et al.* (2012) compared the R1234yf heat transfer coefficient and pressure drop during flow boiling against R134a and R22 (Chien *et al.*, 2012) and against R744, R717 and R290

(Oh *et al.*, 2012) inside stainless steel plain tubes with inner diameters of 1.5 mm and 3.0 mm over a heat flux range of 5 to 70 $kW \cdot m^{-2}$, mass velocity ranging from 50 to 650 $kg \cdot m^{-2} \cdot s^{-1}$, and saturation temperatures going from 0 °C to 15 °C.

R1234yf was also investigated as component inside blends by Li *et al.* (2012) who measured the boiling heat transfer coefficients at 15 °C in a horizontal 2 mm smooth tube for a mass velocity ranging from 100 to 400 $kg \cdot m^{-2} \cdot s^{-1}$and a heat flux ranging from 6 to 24 $kW \cdot m^{-2}$ using R1234yf together with R32 (50:50 and 80:20 by mass%). They concluded that the heat transfer coefficients of the blends were respectively 10% to 30% lower than R1234yf for the same mass velocity and heat flux.

Finally Kedzierski and Park (2013) investigated a R1234yf/R134a (56:44 by mass%) mixture inside a 5.45 mm microfin tube at 30 $kW \cdot m^{-2}$ at a saturation temperature ranging from 5 to 50 °C and a mass flux going from 100 to 418 $kg \cdot m^{-2} \cdot s^{-1}$. They concluded that R134a presented the highest heat transfer coefficients while the ones of the mixture were similar to the pure R1234yf.

In regard to R1234ze(E) the following papers are available in literature.

Tibiriçà *et al.* (2012) tested R1234ze(E) during flow boiling inside two horizontal tubes with inner diameters of 1 mm and 2.2 mm. The mass velocity varied from 50 to 500 $kg \cdot m^{-2} \cdot s^{-1}$, the heat flux varied from 10 to 300 $kW \cdot m^{-2}$ and the saturation temperature from 25 to 35 °C. They concluded that R1234ze(E) exhibited similar heat transfer performance as R134a for similar testing conditions.

Grauso *et al.* (2013a), after analyzing the heat transfer and pressure drop during flow boiling of R1234ze(E) in a 6 mm smooth tube for a mass velocity ranging from 200 to 350 $kg \cdot m^{-2} \cdot s^{-1}$, a saturation temperaturs from 7.0 °C to 12.0 °C and a heat flux from 5.0 to 20.0 $kW \cdot m^{-2}$, concluded that R1234ze(E) had similar performance to R134a for the same operating conditions.

Diani *et al.* (2014) studied R1234ze(E) flow boiling inside a 3.4 mm microfin tube at a constant evaporating temperature of 30 °C and mass velocities between 190 $kg \cdot m^{-2} \cdot s^{-1}$and 940 $kg \cdot m^{-2} \cdot s^{-1}$. They compared the results obtained against R134a, finding that R134a slightly outperformed R1234yf.

In addition, Diani *et al.* (2015c) studied R1234ze(E) flow boiling inside a 2.4 mm microfin tube at 30 °C of saturation temperature, mass flux from 375 to 940, and heat flux from 10 to 50.

Kedzierski and Park (2013) after investigated a R1234yf/R134a (56:44 by mass%) mixture inside a 5.45 mm microfin tube, they studied pure R1234ze(E) and R134a finding that R134a presented the highest heat transfer coefficients.

Costa-Patry *et al.* (2012) measured the R1234ze(E) heat transfer coefficients and pressure drops in a micro-evaporator having 52 microchannels. They compared R1234ze(E) data against R134a and R145fa and they proposed a new flow pattern-based prediction method based on their experimental results.

Szczukiewicz *et al.* (2013) analyzed the two-phase flow boiling of R1234ze(E) together with R245fa, R236fa, and in 100 mm × 100 mm parallel silicon microchannels. They found that, under particular testing conditions, the junction temperature was 14 °C lower with R1234ze(E) than R245fa and 7 °C lower than R236fa.

Vakili-Farahani *et al.* (2013) tested R1234ze(E) inside an aluminum extruded multiport tube with seven parallel rectangular channels and compared their results against R245fa. In addition they developed a new flow pattern-based model that was able to predict their experimental database.

So far as mixtures are concerned, Baba *et al.* (2012) experimentally investigated the flow boiling heat transfer of R1234ze(E)/R32 mixture (50:50% by mass) inside a 6 mm microfin tube with a mass velocity ranging from 150 to 400 $kg \cdot m^{-2} \cdot s^{-1}$ at a constant inlet temperature of 10 °C.

Kondou *et al.* (2014a) studied R1234ze(E) in blend with R744 and R32 inside a microfin tube having an outer diameter of 6 mm at 30 °C of saturation temperature, 10 $kW \cdot m^{-2}$ of heat flux and mass flux ranging from 150 to 300. Accordingly, Kondou *et al.* (2014c) investigated R32/R1234ze(E) flow boiling inside the same microfin tube at a saturation temperature of 10 °C, heat fluxes of 10 and 15 kW m^{-2}, and mass velocities from 150 to 400 $kg \cdot m^{-2} \cdot s^{-1}$. The authors found that the degradation in the HTC of the R32/R1234ze(E) mixture was significant and that the HTC of the mixture was even lower than that of pure R1234ze(E).

Hossain *et al.* (2013) performed a comparative study of the heat transfer of R1234ze(E), R32, R410A, and the zeotropic blend R32/R1234ze(E) (45:55 mass%). They measured that pure R1234ze(E) heat transfer coefficients were lower than R32 and R410A for the same mass velocity, but that they increased when blended with R32. The authors also observed that for the R32/R1234ze(E) blend there was a significant effect of subcooled nucleate boiling that penalized the boiling heat transfer coefficient.

Del Col *et al.* (2014) investigated a R1234ze(E)/R32 mixture flowing inside a 0.96 mm tube at a saturation pressure of 18 bar, a heat flux around 100 $kW \cdot m^{-2}$, and a mass flux ranging from 300 to 600.

Qiu *et al.* (2015), after testing R1234ze(E) and R600a, experimentally assessed also a mixture composed by R1234ze(E) and R32 (L41b) inside a 8 mm smooth tube, at a saturation temperature of 20 °C and a heat flux ranging from 5 to 10 $kW \cdot m^{-2}$. The results showed that the local heat transfer coefficients of R1234ze(E) were averagely 33% and 18% lower than those of R600a and L41b, respectively, while the frictional pressure drops of R1234ze(E) were 21% lower than those of R600a but 6% greater than those of L41b.

Finally Han *et al.* (2013) studied a mixture composed by R1234yf and lubricant oil during flow boiling inside a 7 mm OD microfin tube. The authors evaluated local heat transfer coefficients and pressure drops at 100, 200, 400 $kg \cdot m^{-2} \cdot s^{-1}$ of mass flux, 4, 8, 12 kW m^{-2} of heat flux, 5 and 15 °C of saturation temperature and 0%, 1.5%, 3.0% and 5.0% of oil concentration.

1.3.1.3 External condensation

Park *et al.* (2011) measured the external condensation heat transfer coefficients of R1234yf on a plain surface and two enhanced surfaces at 39 °C of condensation temperature for wall subcooling values ranging from 3 °C to 8 °C. They concluded that the external condensation heat transfer coefficients of R1234yf on these three surfaces were similar to R134a ones.

Nagata *et al.* (2015) tested R1234ze(E), R1234ze(Z) and R1233zd(E) during external condensation on a tube having a diameter of 19.122 mm and a total length of 400 mm at a saturation temperature ranging from 20 to 60 °C. The HTC of R1234ze(E) was found to be slightly lower than that of R134a. While the HTC of R1234ze(Z) was somewhat higher than that of R245fa; and the HTC of R1233zd(E) was comparable to R245fa.

1.3.1.4 In-tube condensation

Park *et al.* (2011) measured the condensation heat transfer coefficients of R234yf in a vertical 7-port minichannel test section with rectangular channels having hydraulic diameters of 1.45 mm for a mass velocity ranging from 50 to 260 $kg \cdot m^{-2} \cdot s^{-1}$, a heat flux from 0.4 to 62 $kW \cdot m^{-2}$, and a saturation

temperature from 30 °C to 70 °C. They measured R1234yf heat transfer coefficients up to 25% lower than R134a and approximately 5% lower than R236fa for the same operating conditions.

Del Col *et al.* (2010) collected the condensation heat transfer coefficients and pressure drop of R1234yf in a single horizontal circular minichannel with a diameter of 0.96 mm for a mass velocity ranging from 200 to 1000 $kg \cdot m^{-2} \cdot s^{-1}$ at a saturation temperature of 40 °C. They concluded that R1234yf had lower heat transfer coefficients than R134a for the same operating conditions, varying from 15% lower for a mass velocity of 200 $kg \cdot m^{-2} \cdot s^{-1}$ to 30% lower for a mass velocity of 800 $kg \cdot m^{-2} \cdot s^{-1}$. They also measured the pressure drop of R1234yf around 10% lower than R134a for the same operating conditions.

In 2015 they investigated the R1234ze(E) condensation heat transfer coefficient and pressure drop in the same test rig (Del Col *et al.*, 2015a) concluding that at the same mass flux and saturation temperature, the condensation heat transfer coefficients of R1234ze(E) resulted lower than those of R32, comparable with those of R134a and higher than those of R1234yf.

Agarwal and Hrnjak (2015) presented a comparison between R1234ze(E), R134a and R32 inside a 6.3 mm tube at 30 and 50 °C of saturation temperature with a heat flux that ranged from 10 to 25 $kW \cdot m^{-2}$ and a mass flux from 100 to 300 kg m^{-2} s^{-1}. They concluded that R1234ze(E) had very similar heat transfer characteristics as R134a due to close thermo-physical properties. However, R1234ze(E) had much higher pressure drop which should be considered while using it as a drop-in replacement. Finally, R32 had higher HTC and lower pressure drop than R1234ze(E) and R134a.

Kondou *et al.* (2014b) investigated the condensation process of R1234ze(E), R134a and R32 inside a microfin 6 mm tube at 65 °C of saturation temperature, 10 $kW \cdot m^{-2}$ of heat flux and a mass flux ranging from 150 to 400 $kg \cdot m^{-2} \cdot s^{-1}$. As for evaporation, also during condensation the pressure gradient of R1234ze(Z) was approximately three times greater than those of R1234ze(E) and the conventional refrigerant R134a. Furthermore, the HTC of R1234ze(Z) was approximately 2.6 times higher than those of R1234ze(E) and R134a, especially at vapor qualities beyond 0.6.

Wang *et al.* (2012) studied the R1234yf condensation in a horizontal 4 mm smooth tube for a mass velocity ranging from 100 to 400 $kg \cdot m^{-2} \cdot s^{-1}$ and for a saturation temperature from 40 °C to 50 °C .

They concluded that the heat transfer coefficients of R1234yf were up to approximately 25% lower than those of R134a for the same mass velocity.

As regarding mixture where HFOs are present as components, by using the same test rig and section, Wang *et al.* (2012) studied the heat transfer coefficients of R1234yf/ R32 mixtures (52:48 and 77:23 wt%) at a saturation pressure of 1848 kPa for a mass velocity ranging from 100 to 300 $kg \cdot m^{-2} \cdot s^{-1}$.

Hossain *et al.* (2012) measured the condensation heat transfer coefficients of R1234ze(E) in a horizontal 4.35 mm tube for a mass velocity ranging from 150 to 400 $kg \cdot m^{-2} \cdot s^{-1}$ and a saturation temperature from 35 °C to 45 °C. They concluded that the heat transfer coefficients of R1234ze(E) were approximately 20% to 45% lower than R32 but 10% to 30% higher than R410A for a saturation temperature of 40 °C. They also concluded that the pressure drop of R1234ze(E) was approximately 26% to 50% higher than R32 and approximately 38% to 70% higher than R410A, for the same vapor quality and mass velocity.

Kondou *et al.* (2014a) investigated the condensation process of a blend made by R1234ze(E), R744, and R32 inside a microfin tube having an outer diameter of 6 mm at 40 °C of saturation temperature, 10 $kW \cdot m^{-2}$ of heat flux and 200 $kg \cdot m^{-2} \cdot s^{-1}$ of mass flux. The authors found that the condensation HTC of pure R32 was somewhat higher than that of R1234ze(E) due to superior thermophysical properties, as predicted by the correlations, while the HTC values of the binary and ternary mixtures were drastically lower than those of the pure components.

1.3.1.5 Other types of heat transfer

Longo (2012b) measured the boiling heat transfer coefficient and pressure drop of R1234yf in a BPHE for a mass velocity ranging from 15 to 36 $kg \cdot m^{-2} \cdot s^{-1}$, a heat flux ranging 4.2 to 17 $kW \cdot m^{-2}$, an inlet vapor quality from 0.16 to 0.33, and a saturation temperature from 5 °C to 20 °C. The author concluded that for a saturation temperature of 20 °C the average heat transfer coefficients and pressure drops of R1234yf were lower by 6% to 10% and 10% to 18%, respectively, when compared with R134a for the same mass velocity and heat flux.

Longo and Zilio (2012) studied also the condensation heat transfer coefficient and pressure drops of R1234yf inside the same BPHE. Under the same operating conditions, R1234yf exhibited lower (10% to 12%) heat transfer coefficients and lower (10% to 20%) frictional pressure drops than does R134a.

Diani *et al.* (2015b) experimentally measured the heat transfer performance of R1234yf and R1234ze(E) during flow boiling heat transfer inside a horizontal high porosity copper foam with 5

Pores Per Inch (PPI) at three different heat fluxes: 50, 75, and 100 $kW \cdot m^{-2}$, at a constant saturation temperature of 30 °C and at refrigerant mass fluxes between 50 and 200 $kg \cdot m^{-2} \cdot s^{-1}$. The authors found that the two alternative HFO refrigerants showed interesting heat transfer capabilities as compared to R134a and the performance of the three fluids were almost similar. But R1234ze(E) exhibited slightly higher two-phase pressure drops than those measured for R134a and R1234yf especially at high mass velocity. While Mancin *et al.* (2015) presented some experimental measurements collected during flow boiling heat transfer R1234yf on a micro-particle coated surface obtained via high pressure cold spray at a constant saturation temperature of 30 °C, a heat flux equal to 50 kW m^{-2} and a mass velocity varying from 30 and 200 kg m^{-2} s^{-1}.

Fukuda *et al.* (2015) investigated experimentally and theoretically the condensation heat transfer of R1234ze(Z) flowing downward in a vertical plate-fin heat exchanger.

Padilla *et al.* (2012) and Padilla *et al.* (2013) studied the two-phase flow regimes of R1234yf in a horizontal and a vertical 6.7 mm return bend respectively and measured the pressure drop of R1234yf in horizontal return bends of inner diameter ranging from 7.90 to 10.85 mm and curvature ratio ($2R/d$) ranging from 3.68 to 4.05. They concluded that the pressure drop of R1234yf was in general lower than R134a for the same operating conditions.

1.3.2 Thermophysical properties

A short section is dedicated to briefly present the major thermophysical properties that contribute to two-phase heat transfer and pressure drop. Table 3 reports the critical pressure and the critical temperature of the most common fluids for refrigeration listed with a crescent critical temperature criteria.

Obviously the critical temperature is a constrain in the application field but it also affects the heat transfer characteristics, as well as the reduced pressure.

Furthermore density, thermal conductivity, viscosity, specific heat, enthalpy, and surface tension are the thermophysical properties that most influence the heat transfer, among others.

Table 4 reports a summary of these properties evaluated at 20 °C of some of the most common fluids used in refrigeration applications.

Table 3 Critical temperature and pressure of the most common refrigerants (Refprop 9.1, 2013).

Refrigerant	$\mathbf{p_{crit}}$	$\mathbf{t_{crit}}$
	[bar]	[°C]
R125	36.18	66.05
R410A	49.00	71.34
R404A	37.35	72.16
R32	57.82	78.17
R1270	45.55	91.09
R1234yf	33.82	94.70
R290	45.51	96.74
R134a	40.59	101.09
R1234ze(E)	36.36	109.39
R152a	45.17	113.30
R236fa	32.00	125.06
R600a	36.29	134.65
R1234ze(Z)	35.33	150.12
R600	37.96	151.97
R245fa	36.51	154.01

Table 4 Thermopysical properties of the most common refrigerants at 20 °C (Refprop 9.1, 2013).

Fluid	p_{in}	p^*	λ_L	λ_G	c_{pL}	c_{pG}	ρ_L	ρ_G	μ_L	μ_G	σ	Δh_{LG}
	[bar]	[-]	[W m^{-1} K^{-1}]	[W m^{-1} K^{-1}]	[J kg^{-1} K^{-1}]	[J kg^{-1} K^{-1}]	[kg m^{-3}]	[kg m^{-3}]	[Pa s]	[Pa s]	[N m^{-1}]	[kJ kg^{-1}]
R125	12.052	0.333	6.15E-02	1.47E-02	1366.6	1023.0	1218.30	77.97	1.52E-04	1.31E-05	4.44E-03	115.57
R410A	14.430	0.294	9.18E-02	1.46E-02	1656.8	1362.7	1083.62	56.81	1.26E-04	1.34E-05	6.04E-03	194.19
R404A	10.844	0.290	6.57E-02	1.52E-02	1498.9	1163.6	1069.23	56.31	1.38E-04	1.18E-05	5.09E-03	145.99
R32	14.746	0.255	1.30E-01	1.42E-02	1885.9	1513.6	981.38	40.86	1.20E-04	1.25E-05	7.59E-03	280.78
R1270	10.170	0.223	1.15E-01	1.79E-02	2614.4	1899.7	514.77	21.40	1.01E-04	8.66E-06	7.58E-03	344.28
R1234yf	5.917	0.175	6.51E-02	1.34E-02	1369.3	1023.7	1109.86	32.80	1.64E-04	1.09E-05	6.80E-03	149.29
R290	8.365	0.184	9.61E-02	1.82E-02	2666.2	1949.2	500.06	18.08	1.02E-04	8.09E-06	7.63E-03	344.31
R134a	5.717	0.141	8.33E-02	1.33E-02	1404.9	1000.7	1225.33	27.78	2.07E-04	1.15E-05	8.69E-03	182.28
R1234ze(E)	4.273	0.118	7.59E-02	1.32E-02	1369.8	954.8	1179.26	22.61	2.11E-04	1.20E-05	9.50E-03	170.63
R152a	5.129	0.114	1.00E-01	1.42E-02	1776.5	1217.3	911.97	15.91	1.73E-04	9.88E-06	1.04E-02	285.32
R236fa	2.294	0.072	7.44E-02	1.23E-02	1227.8	863.4	1376.70	15.59	3.03E-04	1.08E-05	1.02E-02	148.10
R600a	3.022	0.083	9.11E-02	1.63E-02	2398.2	1757.3	556.86	7.91	1.59E-04	7.37E-06	1.06E-02	334.33
R1234ze(Z)	1.487	0.042	9.12E-02	1.24E-02	1249.4	887.0	1233.61	7.45	2.85E-04	1.11E-05	0.00E+00	209.02
R600	2.076	0.055	1.07E-01	1.61E-02	2412.9	1765.3	578.59	5.31	1.66E-04	7.26E-06	1.25E-02	366.50
R245fa	1.227	0.034	8.97E-02	1.26E-02	1311.6	936.1	1352.01	7.15	4.29E-04	1.03E-05	1.43E-02	193.25

1.4 Two phase heat transfer

In the following session it is going to be written about different flow regimes that can occur into two phase heat transfer.

A great multitude of devices and heat exchangers are commonly used for vaporization and condensation, but the majority of them can be grasped in a few categories: two phase flow inside tubes and outside tubes, plate heat exchangers, roll-bond heat exchangers and heat pipes.

In this thesis it will be experimentally analyzed the vaporization inside round tubes and inside Brazed Plate Heat Exchangers (BPHEs), the condensation inside BPHEs, the vaporization in roll-bond type evaporators, and the two phase heat transfer in a Heat Pipe Finned Heat Exchanger (HPFHE).

Thus in this section the flow regimes into these latter devices have been analyzed.

1.4.1 Flow boiling inside circular mini-channel

The boiling process inside a circular tube develops different flow regimes as a function of several parameters: the vapor quality, the refrigerant type and its thermophysical properties, the refrigerant mass flow rate, and the heat flux among others.

While the number and the characteristics of specific flow regimes are somewhat subjective, a few number of these are almost universally accepted.

They are defined as follow and represented by Figure 3, as proposed by Huo *et al.* (2004):

Dispersed bubble: numerous small bubbles float in a continuous liquid phase;

Bubbly: bubble size is growing but bubbles but it is still smaller than the tube diameter;

Slug: bubbles develop into bullet shape due to the tube wall restriction. Sometimes the bullet bubbles are followed by a stream of small bubbles creating a trail;

Churn: bullet bubbles start to distort and small bubbles in liquid slug coalesce into vapor clumps with the increase of the vapor velocity. This is a highly oscillatory flow with chaotic interface;

Annular: vapor phase becomes a continuous flow in the core of the tube;

Mist: liquid film is blown away from tube wall and numerous liquid droplets float in high-speed vapor flow.

To predict the existence of a particular flow regime, or the transition process from one flow regime to another, usually flow regime maps, created on the basis of experimental measures and observations, are used.

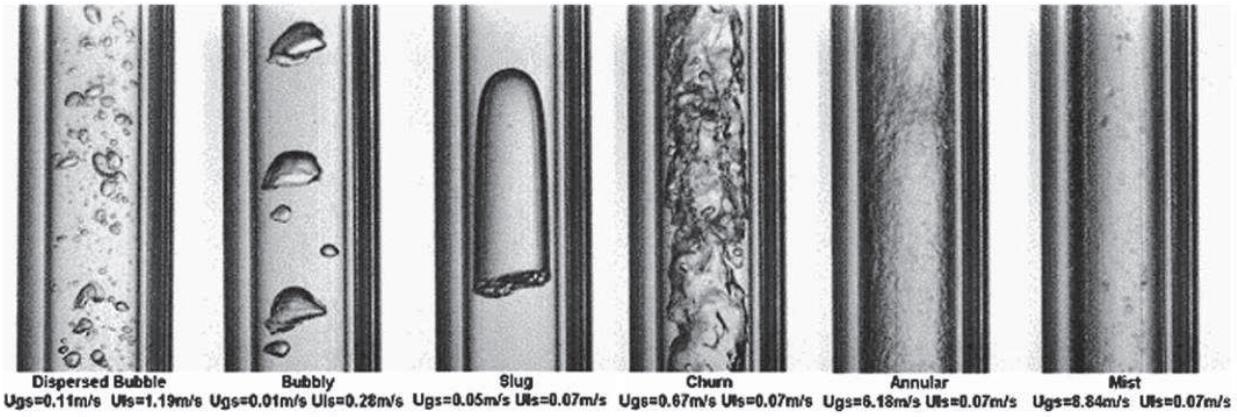

Figure 3 Flow patterns observed in the Huo *et al.* 2004 experiment (4.26 mm internal diameter tube at 10 bar).

On the base of the flow regimes that occur in the tube during boiling, it is possible to define two kind of heat transfer mechanisms: nucleate boiling and convective boiling.

A dominant nucleate boiling heat transfer regime occurs when the bubbly and slug flow regimes occupy a significant fraction of the channel length, while a convective boiling dominant heat transfer regime occurs when a significant fraction of the channel length is occupied by annular flow.

Kim and Mudawar (2014a) described the influence of the flow regime on the heat transfer coefficient, in fact the local heat transfer coefficient depends on the particular flow regime that occurs.

Figure 4 presents the axial local HTC during the boiling process (i.e. passing from a refrigerant vapor quality x=0 to x=1) at uniform heat flux when the nucleate boiling is the dominant heat transfer mechanism.

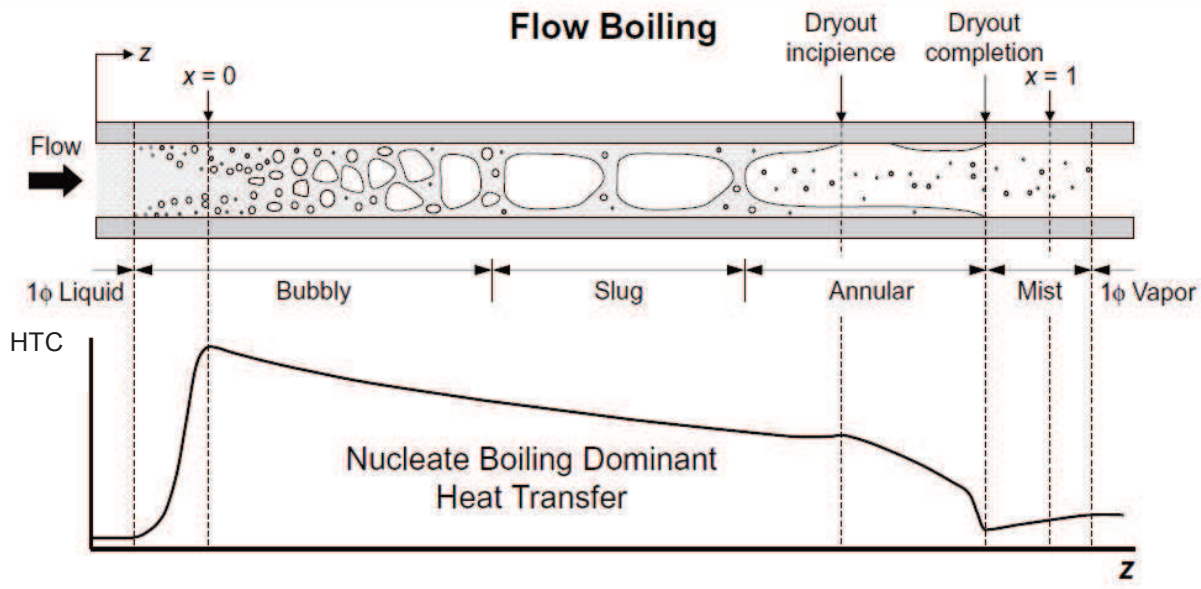

Figure 4 Axial local HTC during the boiling process at uniform heat flux when nucleate boiling is the dominant heat transfer mechanism (Kim and Mudawar, 2014a).

At low vapor qualities the heat transfer coefficient is particularly high, while it decreases when the vapor quality increases due to the gradual suppression of pool boiling.

On the other hand, Figure 5 shows the HTC during the boiling process at uniform heat flux when the convective boiling is the dominant heat transfer mechanism.

In this case the heat transfer coefficient increases when the vapor quality increases due to the gradual thinning of the annual liquid film and so the consequent reduction of the conduction resistance.

Figure 6 summarizes the influences that nucleate boiling and convective boiling have on the vaporization process. It presents the two phase HTC vs. the vapor quality as a function of several parameters: the refrigerant mass flux (G), the heat flux (q), the saturation temperature (t_{sat}), and the hydraulic diameter of the tube (D).

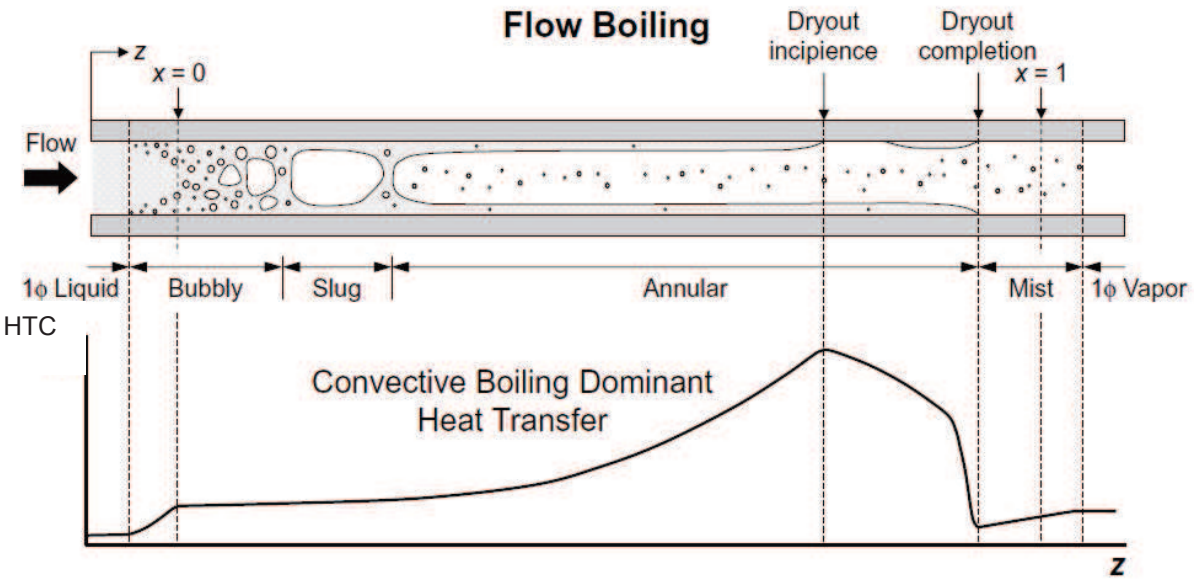

Figure 5 Axial local HTC during the boiling process at uniform heat flux when convective boiling is the dominant heat transfer mechanism (Kim and Mudawar, 2014a).

The HTC variations depend on the particular mechanism that locally controls the heat transfer.

As shown by Figure 4 and Figure 5 when increasing the vapor quality x, the heat transfer coefficient has a negative slope when the nucleate boiling is the dominant heat transfer regime, while it has a positive slope when the convective boiling is the dominant heat transfer regime. When the refrigerant mass flux increases, as can be seen in Figure 6, the convective boiling contribution increases so that the slope of the resulting heat transfer coefficient changing from negative to positive, as the vapor quality increases. In addition if the saturation temperature or the heat flux is decreasing, the region at low vapor qualities where HTC decreases when G increases is extended.

At the contrary the contribution of nucleate boiling is more influent at high saturation temperatures and high heat fluxes. In fact, from Figure 6 it can be noticed that increasing the heat flux q the HTC slope changes from positive to negative, indicating that convective boiling is going to be suppressed.

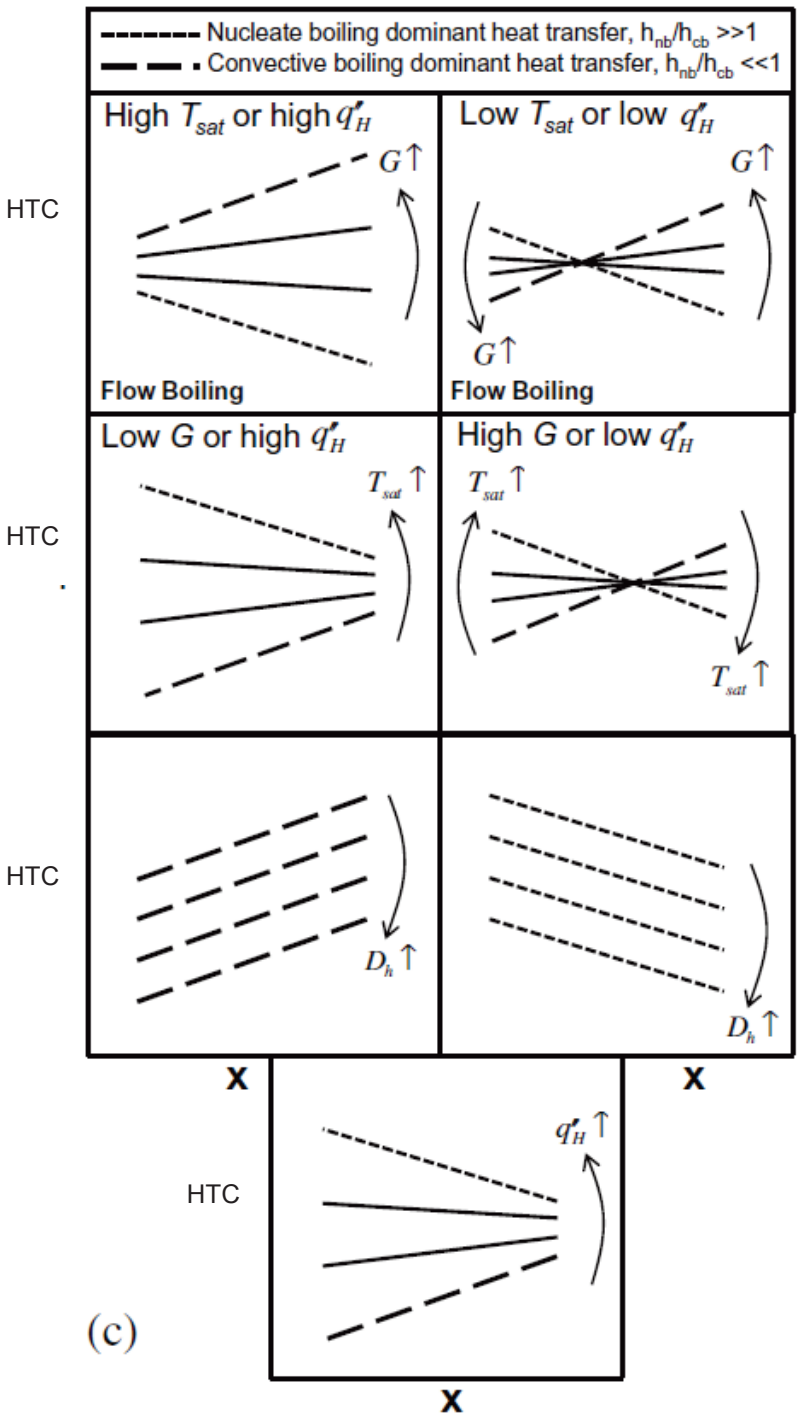

Figure 6 Influence of nucleate boiling and convective boiling mechanisms on the vaporization process (Kim and Mudawar, 2014a).

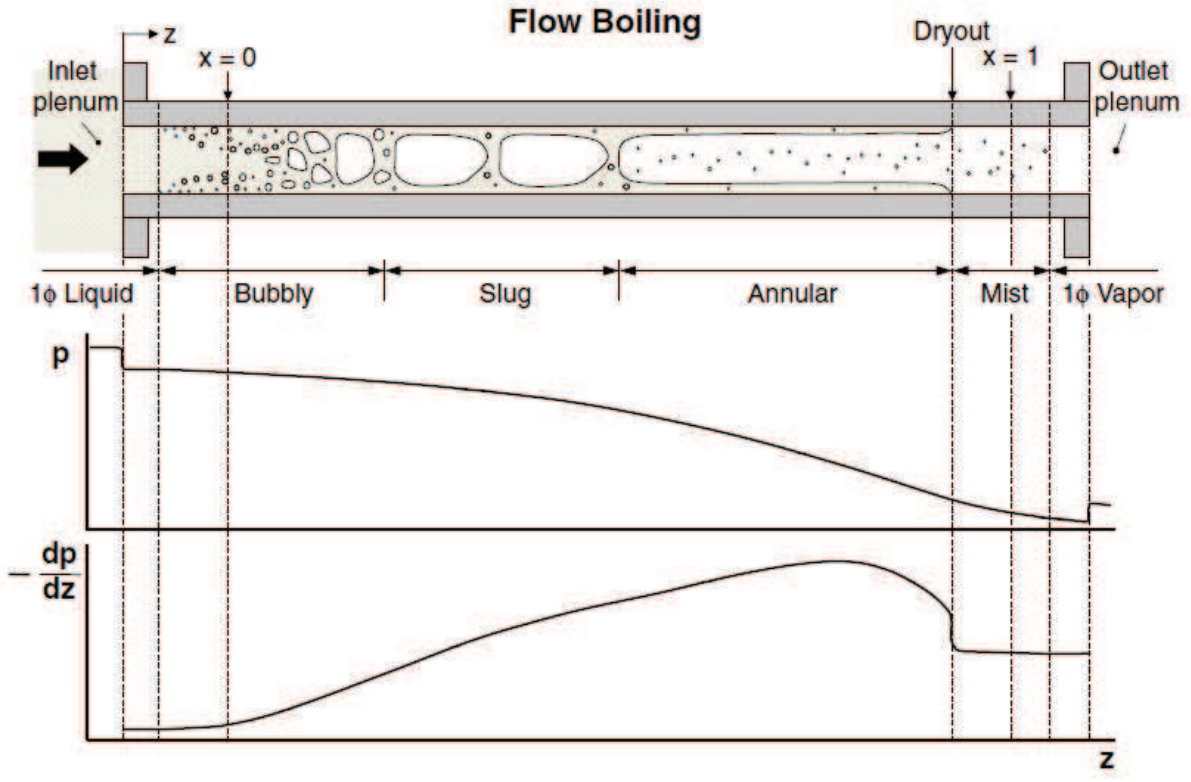

Figure 7 Influence of the flow regimes on the pressure drop during the vaporization process (Kim and Mudawar, 2014b).

Kim and Mudawar (2014b) analyzed also the influence of the flow regimes on pressure drops during the complete boiling process inside a tube.

As represented by Figure 7 a subcooled liquid (x=0) goes inside the tube which walls are heated with a constant heat flux. With the beginning of evaporation, a bubbly flow regime starts. Increasing the vapor quality, the vapor production increases both the size and number of bubbles. This causes an increase in the collision frequency and in the coalescence between bubbles. Further, when slug flow regime occurs large, oblong bubbles are formed and a thin liquid film remains close to the wall. Going at higher vapor qualities, the liquid slugs become vapor and the oblong bubbles merge together and become a continuous vapor core, with just a thin liquid film around the walls. At Critical Heat Flux (CHF) the liquid film is dried and just little liquid droplets entrains in the vapor core.

During the boiling process the pressure is decreasing due to the irreversibility of the process, in addition the evaporation causes an axial acceleration of the refrigerant flow, which increases both the wall shear stress and pressure gradient as the vapor quality increases.

1.4.2 Brazed Plate heat exchanger

The introduction of the traditional gasketed Plate Heat Exchangers (PHEs) on the market can be dated in the 1930s. These devices were used for single-phase (liquid-to-liquid) heat transfer in chemical and food processing industries thanks to their high efficiency and compactness.
Generally, PHEs consist of thin, rectangular, pressed steel (most often stainless steel) plates stacked together. The plates are stamped with corrugated patterns that not only to provide a larger effective heat transfer surface area (on the order of 10-25% compared to the original flat plate) but also to modify the flow field in order to promote enhanced thermal-hydraulic performance. (Amalfi *et al.* 2015)

Tribbe and Müller-Steinhagen (2001) experimentally studied several commercial PHEs and, after conducting on them a two-phase flow visualization analysis, they proposed a simple flow pattern map for PHEs based on the superficial velocities and their flow observations.
In this pattern map five main flow patterns were identified and reported in Figure 8.

Regular bubbly flow: it is made up by individual bubbles of approximately 3–5 mm in diameter that flow along the furrows of both plates. The bubbles are forced toward surface contact points by shear stress. When the bigger bubbles approach the contact point, the shear stress divides them: one part continues along the same furrow while the other parts transfer to an opposite furrow and, therefore, change direction. While when the smaller bubbles approach a contact point, tend to change furrow but remain intact. The tendency toward crossing flow diminishes as chevron angle increases and it is overtaken by longitudinal wavy flow character;

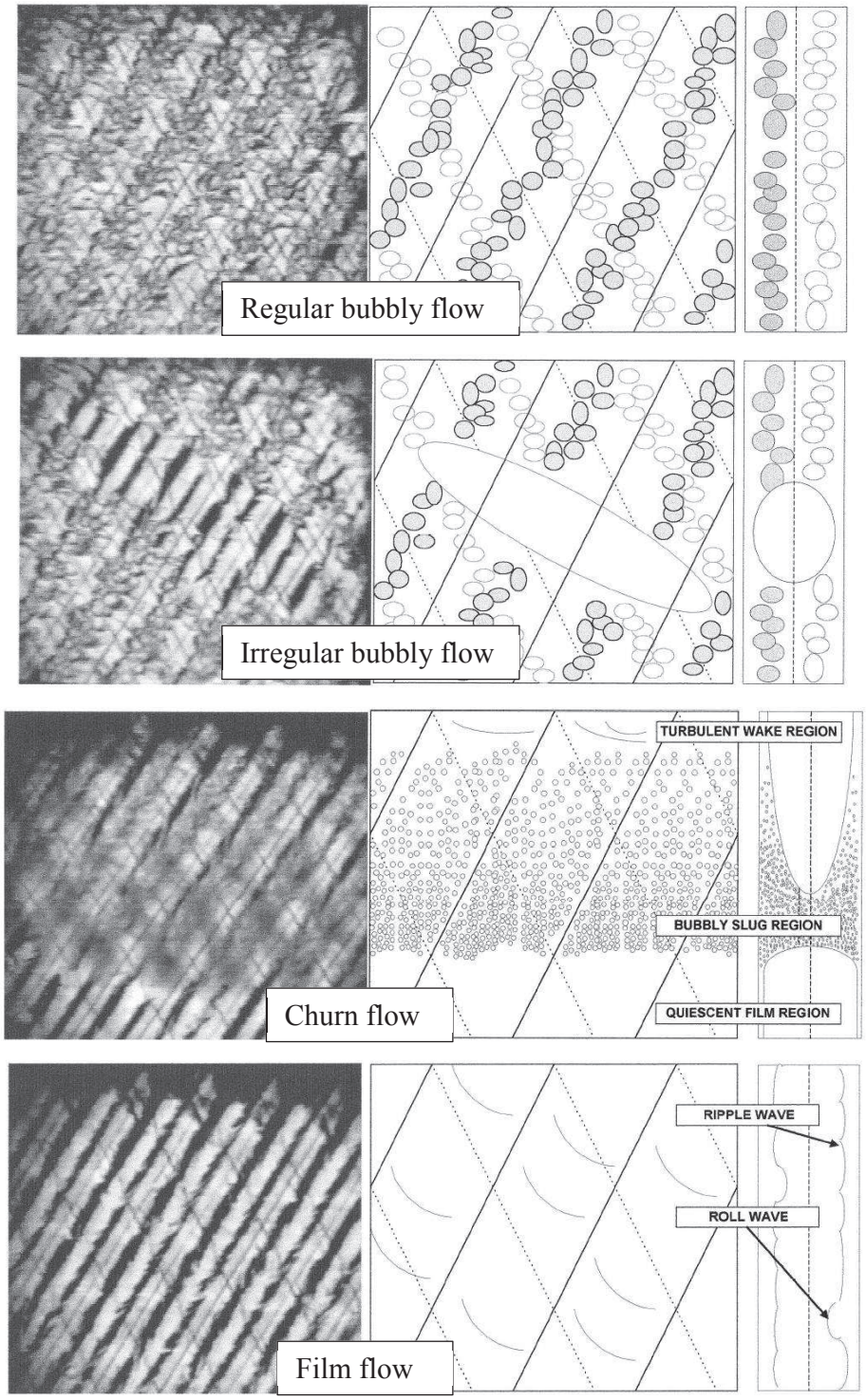

Figure 8 Flow patterns during vaporization inside a PHE (Tribbe and Müller-Steinhagen, 2001).

Irregular bubbly flow: at the increasing of the mass flux, the bubbles are unable to transport the quantity of vapor present. So, large and irregularly shaped regions of vapor appear among the regular bubbly flow;

Churn flow: it is characterized by high-velocity liquid slugs that increase of dimension and frequency at the increase of mass flow. The intermittent appearance of the flow is caused by fast-moving slugs of liquid containing finely dispersed bubbles (diameter around 0.1 mm). The wake region following the slugs consists of a decelerating turbulent film on which surface disruptions occur, such as collapsing of bubbles and liquid bridges;

Film flow: it consists of a thin liquid film flowing along a furrow over which a fast-moving vapor stream flows. It is similar in nature to annular flow, but the liquid film does not form an annulus due to the geometry of the channel;

Partial film flow: when the vapor flow rates increase, the film no longer wets the entire surface and a region of dry surface appears.

The Brazed Plate Heat Exchangers (BPHEs) technology was developed in the 1970s and it allowed to apply this compact and very efficient type of heat exchanger also to condensation and vaporization of high-pressure refrigerant fluids due to the capacity to work also under high pressure conditions. Nowadays BPHEs are widely used in many applications (for instance, refrigerant evaporation and condensation, heat pumps, steam heating, engine or hydraulic oil cooling, district or zone heating systems, various heating and cooling duties, swimming pool heating, etc.). Among their advantages, it can be reminded that they promote an high turbulence level and so they permit an efficient heat transfer with low refrigerant flow rates and they also avoid fouling. Secondly they allow the complete separation between fluids, an extremely important feature for food, chemical and pharmaceutical industry.

Following the vaporization and the condensation processes inside BPHEs are analyzed with the aim to underline the flow regimes that occur during the two phase flow.

1.4.2.1 Vaporization

As for the boiling process inside circular tubes (see paragraph 1.4.1), also for the vaporization inside BPHEs it is possible to find the same two heat transfer mechanisms that govern the process: nucleate boiling and convective boiling. Also in this particular case, the nucleate boiling is dominant when the flow inside the heat exchanger has a significant fraction occupied by the bubbly and the slug flow regimes, while the convective boiling is predominant when the annular flow occupies the major part of the heat transfer flow area.

From an external point of view, the nucleate boiling is mainly governed by the heat flux and the saturation temperature, while it has a weak sensitivity on the mass flux. On the other hand, the convective boiling is strongly affected by vapor quality and mass flux.

In the open literature there is only one quantitative criterion to discriminate the dominant heat transfer mechanism during vaporization inside BPHEs: the one proposed by Thonon *et al.* (1997), which has been applied to analyze the experimental data collected and to find a suitable correlation to predict the heat transfer coefficient (see paragraph 3.2.2.1.1).

1.4.2.2 Condensation

During the condensation process it is possible to point out two different heat transfer mechanisms: gravity-dominated condensation and forced-convection condensation.

During a gravity-dominated condensation the heat transfer coefficient is weakly influenced by the mass flux and therefore by the temperature difference, and it slightly decreases when the mass flux and the vapor quality increase. On the other hand during forced convection condensation the condensate drainage is controlled by the combined actions of gravity and vapor shear, so this mechanism is strongly affected by vapor quality and mass flux.

These two mechanisms can be discriminated on the basis of the mass flux and of the refrigerant properties.

In fact in the condensation experimental data inside BPHEs, it can be found a transition point between gravity-dominated and forced convection condensation for an equivalent Reynolds number around 1600.

In the particular BPHE investigated in this thesis, a Reynolds number of around 1600 corresponds to a refrigerant mass flux of around 20 kg m^{-2} s^{-1} for HFC and HFO refrigerants and around 15 kg m^{-2} s^{-1} for HC refrigerants. This discrepancy in refrigerant mass flux transition point between HFC–HFO and HC refrigerants may be explained considering the large difference in liquid phase density: HFC and HFO refrigerants exhibit liquid phase density twice higher than HC refrigerant (see Table 4).

1.4.2.3 Pressure drop

As presented for the round tube case in section 1.4.1, the pressure drop does not depend on the particular heat transfer mechanism and on the heat flux applied but it exhibits a quadratic dependence on the refrigerant mass flux, that means the friction factor has a constant value as a function of the Reynolds number in the Moody diagram.

1.4.3 Roll-bond evaporator

A roll-bond heat exchanger consists of a plate formed by two powder-coated aluminum sheets, with a channel expanded between them in which the refrigerant evaporation takes place, while a buoyancy-driven air circulation occurs at the outer side.

Among the advantages of roll-bond evaporators the efficient thermal performance, the cost effectiveness, and the ease with they can be shaped and adapted to fit in many applications can be underlined.

In fact, the combination of a low cost and a reasonable performance – compared to plate-and-tube heat exchangers – has led to a steady increase of its application. (Hermes *et al.*, 2008)

The dominating resistance in this heat exchanger is on the air side, which is penalized due to the low air velocity and due to the flat geometry of the external surface. Beside this, on the refrigerant side the flow rates are commonly poor, so that a very low turbulence is generated inside the refrigerant

channels. The mass fluxes and, moreover, the heat fluxes, are too limited to allow the convective boiling mechanism to occur, so the heat transfer is totally governed by pool boiling.

1.4.4 Heat Pipe Finned Heat Exchanger

An heat pipe is a device of very high thermal conductance. (Reay and Kew 2006). It is made by a small quantity of refrigerant sealed inside a tube. The ends of the tube are places at different temperature levels so that evaporation and condensation can take place and the working fluid can circulate into the pipe. The condensate liquid is returned to the hot end by capillary forces.
For a wicked heat pipe (i.e. the capillary forces are created by a wick placed inside the tube) some operating limits exist and they cause the stop of its functioning. They are: entrainment limit, capillary limit, boiling limit, sonic limit, and viscous limit and are represent in Figure 9. They depend on the type of the refrigerant, on the heat flux, and on the saturation temperature.

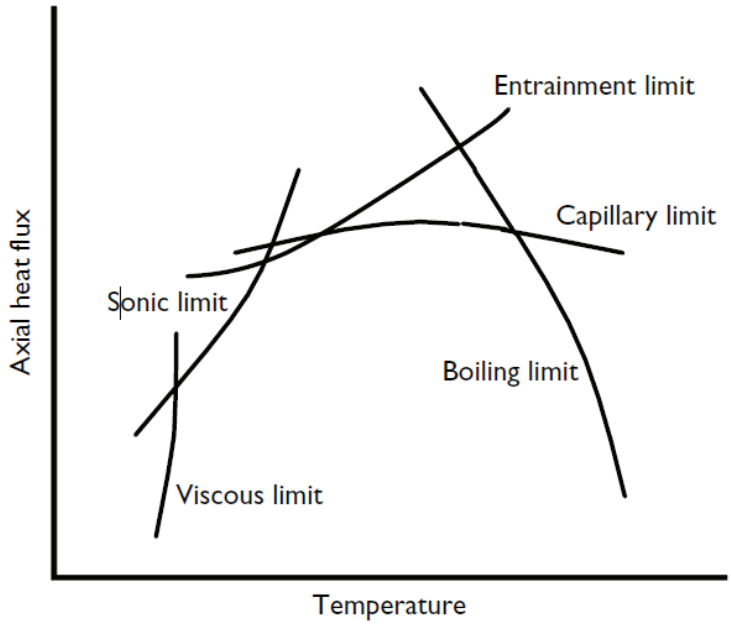

Figure 9 Operating limits for a wicked heat pipe (Reay and Kew, 2006).

The capillary limit determines the maximum heat flux of the operating range over which the wick will dry out in the evaporator region and the heat pipe will not operate.

The sonic limit occurs at during the start-up and with certain high-temperature liquid metal heat pipes, when the vapor velocity may reach sonic values setting a limit on the heat pipe performance.

The viscous – or vapor pressure limit – is also important at start-up. At low temperature, the vapor pressure of the fluid in the evaporator is very low, and, since the condenser pressure cannot be less than zero, the maximum difference in vapor pressure is insufficient to overcome viscous and gravitational forces.

The entrain limit occurs at high heat fluxes, when the vapor velocity necessarily increases and if this velocity is sufficient to entrain liquid returning to the evaporator, then performance will decline.

Finally the boiling limit happens when the temperature difference that accompanies the radial heat flux grows over a critical value where the vapor blankets the evaporator surface.

The flow regime in the liquid phase is almost always laminar so it can be sum up that in the boiling region nucleate boiling occurs while in the condensing region gravity-dominated condensation occurs.

Heat Pipes Heat Exchangers (HPHEs) usually consist of several heat pipes that are mechanically expanded against continuous fins (typically in aluminum), according to the classical construction procedure of finned coils evaporators. HPHE are largely used for energy recovery purposes both in civil (air conditioning) and in industrial (air-to-air or gas-to-gas heat recovery) applications.

Among their advantages, HPHEs can promote relatively high heat transfer effectiveness, they do not need any power input, they do not present moving parts (thus endorsing higher reliability in comparison to “active systems” based on vapor compression heat recovery units) and they allow theoretically complete separation between hot and cold fluids.

1.5 Literature review

As introduced in section 1.4 a great multitude of devices and heat exchangers are used for two phase heat transfer, but the most common ones can be grouped in a few categories: tubes, plate heat exchangers, roll-bond heat exchangers and heat pipes, among others. This thesis aims to analyze a significant part of these multitude of devices and so an example for each category is taken into account. (i.e. a tube-in-tube heat exchanger, a Brazed Plate Heat Exchanger, a roll-bond type evaporator, and a Heat Pipe Finned Heat Exchanger). The experimental studies conducted and following presented are going to analyze the effects the working fluids have on the heat transfer and to rank the refrigerants in order to permit a more conscious choice when substituting old and less environment friendly fluids.
In this section a review of the open literature is presented focusing on the four kind of devices following analyzed and on the impact that the refrigerants have inside them.

1.5.1 Vaporization inside tubes

The vaporization process inside a tube is the primary heat transfer method applied in many heat exchangers, for example, tube-in-tube, fin-and-tube, and shell-and-tube heat exchangers among others.
During years, several refrigerants have been analyzed during flow boiling inside tubes and several correlations were proposed to predict this kind of heat transfer.
In this thesis just two couples of refrigerants are been going to be tested. The first one is composed by R1234ze(E) and R134a. The newer HFO molecule is proposed as a viable R134a alternative, as other researchers have already proposed. A detailed review of the existing works on the HFOs was done in section 1.3.1, where R1234ze(E) and other few fluids (i.e. R1234yf, R1234ze(Z)) were experimentally tested under different heat transfer regimes (i.e. pool boiling, flow boiling, condensation inside and outside tubes, vaporization and condensation in BPHEs, etc.). Table 5 summarizes just the papers regarding the R1234ze(E) vaporization process inside a tube.

Table 5 Literature review on R1234ze(E) flow boiling inside tubes.

Authors	**Tube diameter**	**Vaporization temperature**	**Heat flux**	**Mass flux**
	[mm]	[°C]	[kW m^{-2}]	[kg m^{-2} s^{-1}]
Baba *et al.* (2012)	5.21, microfin	10	6 to 24	150 to 400
Kedzierski and Park (2013)	5.45, microfin	5 to 50	30	100 to 418
Kondou *et al.* (2014)	6, microfin	30	10	150 to 300
Diani *et al.* (2015c)	2.4, microfin	30	10 to 50	375 to 940
Diani *et al.* (2014)	3.4, microfin	30	10 to 50	190 to 940
Grauso *et al.* (2013a)	6	-3 to 12	5 to 20	146 to 520
Qiu *et al.* (2015)	8	20	5 to 10	200 to 400
Tibrica *et al.* (2012)	1 and 2.2	25 to 35	10 to 300	50 to 500

As far as R134a is concerned, it is probably one of the most investigated refrigerants of the last decades. Many researchers tested it, before as zero ODP alternative to HCFCs, after as reference fluid to compare against lower GWP refrigerants. Following only the most recent paper available in literature are reported, while for the oldest ones some reference could be found in Fang (2013) and Xu *et al.* (2016) where new data were also presented. The authors tested three horizontal circular smooth copper tubes with inner diameters of 1.002, 2.168, and 4.065 mm with mass flux from 185 to 935 kg m^{-2} s^{-1}, heat flux from 18.0 to 35.5 kW m^{-2}, and saturation pressure from 0.578 to 0.82 MPa.

In 2016 Abadi *et al.* (2016) analyzed the flow boiling characteristics of R134a and its mixtures with R245fa in a circular tube with a 3 mm inner diameter, mass flux from 300 to 800 kg m^{-2} $s^{-1}$and heat flux from 1 to 69 kW m^{-2} at 32 °C of saturation temperature. The authors compared the results obtained with the pure fluid and the mixture discussing also the mass transfer resistance.

Fang *et al.* (2015) investigated R134a flow boiling heat transfer in a horizontal copper tube with 4.07 mm inner diameter and they observed the effect of gravity on flow boiling heat transfer. The gravity level ranged from 1 to 3.16 g, the mass flux from 185.1 to 412.1 kg m^{-2} s^{-1}, the heat flux from 18.1 to 28.1 kW m^{-2}, the saturation pressure from 0.576 to 0.679 MPa, and the vapor quality from 0.08 to 0.91. The authors concluded that gravity had effects on flow patterns and thus on heat transfer coefficients.

An increase in gravity made the transition from plug/slug flow to intermittent flow appear earlier, while the effects related to vapor quality, mass flux, saturation pressure, and heat flux on under a certain hypergravity level were similar to that under Earth's gravity.

Kundu *et al.* (2014a), Kundu *et al.* (2014b), and Kundu *et al.* (2014c) examined in detail the effects on the heat transfer coefficient and on the two-phase pressure drops of vapor quality, mass velocity, imposed heat flux and fluid thermophysical properties. They tested three refrigerants, R134a, R407C, and R410A in a smooth horizontal tube (7.0 mm ID) uniformly heated by a resistance. The refrigerant mass velocities varied within the range 100 – 400 kg m^{-2} s^{-1}; the heat fluxes within 3.0 – 10.0 kW m^{-2}; and the inlet temperatures within 5 °C – 9 °C. Finally they analyzed the flow patterns obtained during flow boiling and compared them against some flow pattern maps available in the literature.

Mancin *et al.* (2014) investigated the R134a flow boiling inside a 3.4 mm microfin tube at a saturation temperature of 30 °C at three different heat fluxes 10, 25, and 50 kW m^{-2} and refrigerant mass velocity between 190 kg m^{-2} $s^{-1}$and 755 kg m^{-2} s^{-1}.

Finally, *Chiapero et al.* (2014) presented the heat transfer and pressure drop data for R134a at a saturation temperature of approximately 34 °C, heat fluxes of 10.5 and 20 kW m^{-2} and mass fluxes of 300 and 500 kg m^{-2} $s^{-1}$and analyzed the flow patterns thanks to a high speed camera.

The second couple of refrigerants investigated in this thesis is made up by R32 and R410A , where the lower GWP HFC is proposed to replace the commonly used HFC mixture.

In the open literature it is possible to find a limited experimental data on R32 two-phase heat transfer inside tubes.

Shin *et al.* (1996) was probably the first paper reporting about experimental measurements of flow boiling of several fluids, including R32. The authors used a smooth stainless steel tube of 7.7 mm diameter. Cavallini *et al.* (2001b) presented the experimental heat transfer coefficients and pressure drops measured during R32 condensation inside a 8 mm horizontal smooth tube with a refrigerant mass flux varying from 100 to 750 kg m^{-2} s^{-1}. Jung *et al.* (2003, 2004) investigated R32 nucleate boiling inside a 19 mm smooth tube and various 18.6-18.8 mm enhanced tubes.

Del Col *et al.* (2013a) reported the heat transfer coefficients measured during flow boiling of R32 inside a 0.96 mm single circular channel to evaluate the effects of heat flux, mass velocity, vapor quality and fluid properties.

Hossain *et al.* (2012, 2013) measured condensation and boiling heat transfer coefficient of R32 inside a 4.35 mm horizontal smooth tube with a refrigerant mass flux varying from 150 to 445 kg m^{-2} s^{-1}.
Ramírez-Rivera *et al.* (2015) experimentally assessed the two-phase flow pressure drop during both condensation and evaporation of refrigerants R134a and R32 in a multiport extruded aluminum tube with hydraulic diameters of 0.715 and 1.16 mm. The testing conditions ranged from 200 to 1229 kg m^{-2} s^{-1} of mass velocity, from 2.55 to 70 kW m^{-2} of heat flux, and 5, 7.5, 12.5, 30, 35, 40, 45, 50, and 55 °C of saturated temperature.
Wu *et al.* (2015) experimentally investigated the heat transfer and the pressure drops characteristics of R32 when boils in a mini multichannel flat tube with 1.7 mm of diameter and with thirteen 0.16 mm high fins having a 0° helix angle. The working conditions were mass fluxes of 100 – 400 kg m^{-2} s^{-1}, heat fluxes of 10 – 40 kW m^{-2} and saturation temperatures of 10 – 20 °C. The authors found that the flow boiling heat transfer coefficient increased with increasing mass flux, heat flux and saturation temperature.
Recently R32 has been proposed as fluid to be bland with HFOs to create new mixture. Some examples are reported in section 1.3.1, where Li *et al.* (2012) tested several compositions of R1234yf/R32 mixtures during flow boiling in a 2 mm tube, while Del Col *et al.* (2014), Baba *et al.* (2012), Qiu *et al.* (2015), and Hossain *et al.* (2013) proposed a mixture composed by R1234ze(E) and R32. Finally Kondou *et al.* (2014) investigated R32/R744/R1234ze(E) mixture boiling inside a 6 mm microfin tube.

Passing to R410A flow boiling studies available in literature, it is possible to cite, among others, Greco and Vanoli (2005) who tested several refrigerants during flow boiling inside a 6 mm smooth horizontal tube: R22, R134a, R507, R404A and also R410A. The refrigerant mass flux was about 360 kg m^{-2} s^{-1}, while the evaporating pressure was varied within the range 3 – 12 bar, and the heat fluxes within the range 11 – 21 kW m^{-2}. R410A heat transfer coefficients measured by the authors were found to be lower than R134a and R22 but higher than the other two mixtures, when compared as a function of the evaporating pressure.
Padovan *et al.* (2011) presented an experimental study on vaporization of R134a and R410A inside a horizontal microfin tube at 30 °C and 40 °C of saturation temperature. The operating conditions investigated were: mass flux from 80 to 600 kg m^{-2} s^{-1}, heat flux from 14 to 83.5 kW m^{-2} and vapour quality from 0.1 to 0.99.

The group of Ding (i.e. Ding *et al.* 2009; Hu *et al.*, 2008a; and Hu *et al.*2008b) focused on the two-phase characteristics of R410A/POE oil mixture during flow boiling inside a straight microfin tube with the outside diameter of 7.0 mm. They investigated an evaporation temperature of 5 °C, mass flux from 200 to 400 kg m^{-2} s^{-1}, and heat flux from 7.56 to 15.12 kW m^{-2}. They also proposed new correlations to predict the local frictional pressure drop on the base of their experimental measures.

Grauso *et al.* (2013b) experimentally studied flow boiling in a circular, horizontal, smooth tube of 6.00 mm diameter using R410A and CO_2 as refrigerants. They collected flow visualizations and heat transfer coefficient measurements at reduced pressures of 0.57 and 0.64 for CO_2 and 0.19 and 0.52 for R32, heat fluxes of 5.0 kW m^{-2} and 20.0 kW m^{-2} and mass flux from 150 kg m^{-2} s^{-1} to 500 kg m^{-2} s^{-1}.

Also Park and Hrnjak (2007) investigated the flow boiling heat transfer coefficient, pressure drop, and flow pattern inside a horizontal smooth tube of 6.1 mm inner diameter for CO_2, R410A, and R22.

This research was performed at evaporation temperatures of 15 and 30 °C, mass flux from 100 to 400 kg m^{-2} s^{-1}, and heat flux from 5 to 15 kW m^{-2} for vapor qualities ranging from 0.1 to 0.8. This study indicated that CO_2 has better heat transfer and pressure drop characteristics than the conventional refrigerants of R22 and R410A under the testing conditions just told.

Finally, also the work presented by Kundu (2014), already presented before in this section, analyzed the heat transfer coefficients of R134a, R407C, and R410A in a smooth horizontal tube (7.0 mm ID) uniformly heated by a resistance.

1.5.2 Brazed Plate Heat Exchanger

Brazed plate heat exchangers (BPHEs) are a type of compact heat exchanger widely used for industrial applications, such as refrigeration, heating, cooling, chemical processing, etc. They provide a large heat transfer surface area per unit volume, which makes them particularly suited for installation in confined spaces. Consequently, they have a reduced refrigerant charge and require lighter structural supports (Amalfi *et al.,* 2015). Furthermore, a little charge can promote the use of more flammable fluids, that if used in small amounts can be accepted by safety regulations.

In this thesis a few refrigerants are going to be analyzed during phase change inside a commercial BPHE.

During years many works have been conducted to experimentally analyze the plate heat exchanger behavior during refrigerant phase change. Recently R134a is the most investigated fluid together with ammonia and R410A.

For example Hsieh *et al.* (2002) and Hsieh and Lin (2002, 2003) performed experiments on saturated flow boiling with R134a and R410A in a vertical PHE of 60° chevron angle. The effects of vapor quality, mass flux, heat flux and system pressure on the evaporation heat transfer and pressure drop were investigated in detail.

Han *et al.* (2003) performed flow boiling experiments with refrigerants R410A and R22 in PHEs with different chevron angles (45°, 55°, and 70°) and corrugation pitches (7 mm, 5.2 mm, and 4.9 mm).

Jokar *et al.* (2006) analyzed the performance of R134a and ammonia during boiling inside three PHEs, different in size but similar in plate geometry specifications. Their average heat transfer and pressure drop data for complete evaporation were correlated using the dimensional analysis technique applied to both measured and calculated parameters.

Jassim *et al.* (2006) experimentally analyzed the frictional pressure drop in adiabatic two-phase flow of R134a through a PHE with herringbone and bumpy corrugations. They found a linear dependence between their frictional pressure drop data at constant vapor qualities and the associated kinematic energy of refrigerant flow per unit volume.

Djordjevic and Kabelac (2008) evaluated the evaporation of ammonia and R134a in chevron PHEs with angles of 27° and 63°. Their measurement technique enabled the obtaining of quasi-local heat transfer coefficients along the plate, as several thermocouples were welded on the plate wall to measure the surface temperatures. The results indicated that the heat transfer coefficient rose over the entire range of vapor quality for high values of mass flux but decreased for low mass fluxes after a maximum value at vapor qualities at about x=0.5. From these results, they concluded that the parallel flow case yields better overall performance than the counter flow case, and that plates with low chevron angle corrugations increased the evaporation heat transfer.

Ouazia (2001) realized an experimental study to explore heat transfer coefficients and associated frictional pressure drops of R134a in a vertical plate heat exchanger. In this study, three plates with different chevron angles (0°, 30°, and 60°) were tested. The desired test condition at the entrance of the test section was reached with an electrical preheater; two different inlet conditions of 4 K subcooling and 5-10% of vapor were tested. They found that the inlet condition slightly affected the thermal-

hydraulic performance. The heat transfer coefficients and the associated pressure drops were slightly higher for the test condition of 5-10% vapor at the PHE inlet.

Huang *et al.* (2012) experimentally investigated the flow boiling heat transfer coefficient and the associated frictional pressure drop during R134a, R507A, ammonia, and R12 vaporization inside PHEs having 28°, 44°, and 60° chevron angles.

Park and Kim (2004) studied heat transfer and pressure drops of R134a boiling in an oblong shell and plate heat exchanger with a chevron angle of 45°. The effects of the mass flux, the average imposed heat flux, the saturation temperature, and the vapor quality on the measured data were experimentally examined.

Boccardi *et al.* (2000) studied the thermal performance of two compact BHEs using R22, R134a, R407C, and R410A as refrigerants. The thermal performance was found to depend on the refrigerant, the thermal load, and the heat transfer process. Regarding the evaporation process, R410A had the highest and R407C the lowest heat transfer coefficients, respectively. Based on their results the R22 replacement options in PHEs for air conditioning application were discussed.

Kuo *et al.* (2005) reported experimental data on R410A condensation inside a BPHE and proposed empirical correlations for heat transfer and pressure drop. The heat transfer coefficient was found to depend mainly on heat flux, whereas friction factor was strongly influenced by mass flux and vapor quality.

Longo and Gasparella (2007b) and Longo and Gasparella (2007c) experimentally measured heat transfer coefficients and pressure drop measured during R410A and R134a vaporization respectively.

The effects of heat flux, refrigerant mass flux, saturation temperature and outlet conditions were investigated. The experimental results have been reported in terms of refrigerant side heat transfer coefficients and frictional pressure drop.

Yan *et al.* (1999) presented semi-empirical correlations for the heat transfer coefficient and the friction factor based on a single set of R134a condensation data, experimentally collected.

Mancin *et al.* (2011 and 2012) investigated the condensation heat transfer of two refrigerants mixtures, R407C and R410A, in two brazed plate heat exchangers (BPHE) with different plate geometries values of aspect ratio and number of refrigerant channels. They found that for both the BPHEs, the condensation heat transfer coefficient increased with vapor quality and decreased with temperature difference. At low mass velocity, the HTC did not seem to depend on refrigerant mass flux and, by

increasing the specific mass flux at constant outlet vapor quality, the condensation heat transfer coefficient increased.

Also other refrigerants were studying during phase change in BPHEs. Among them the ones having relatively low GWP (i.e. R32, R152a, and R1234yf) are worth to be underlined, in fact they are potentially assumed as substitutes to the commonly used ones.

Palmer *et al.* (2000) measured the average Nusselt number during refrigerant mixture R32/R152a (50/50 wt%) vaporization and condensation inside a BPHE in presence of lubricant oil. The performance of this mixture was compared to HC refrigerant (R290) and HC refrigerant mixture (R290/R600a (70/30 wt.%)).

Mancin *et al.* (2013) presented R32 super-heated vapor condensation data inside a BPHE with refrigerant mass flux from 13 to 37 kg m^{-2} s^{-1} finding heat transfer coefficients higher than those of R410A and R407C.

Del Col *et al.* (2015b) measured the heat transfer coefficient during flow boiling of R32 inside a commercial BPHE. They investigated the effects of refrigerant heat flux, mass velocity, inlet vapor quality and superheating at the outlet at a saturation temperature of 5 °C.

Jung *et al.* (2014) assessed R32 as environment friendly substitute for R22 in condensation and vaporization inside a Plate Heat Exchanger (PHE) for Ocean Thermal Energy Conversion (OTEC), while Lee *et al.* (2014) investigated the application of the refrigerant mixture R32/R152a in a seawater heat pump equipped with PHE.

Bella *et al.* (2014) compared the performance of R32 to that of R410A in a 70 kW packaged air cooled water chiller which presented a BPHE evaporator. R32 was demonstrated to be an effective low GWP substitute for R410A in this specific application.

Longo and Zilio (2013) experimentally measured the heat transfer coefficients and the pressure drop measured during condensation of R1234yf inside a BPHE, investigating the effects of saturation temperature, refrigerant mass flux and vapor super-heating. The condensation heat transfer coefficients of super-heated vapor were founded to be from 8 to 11% higher than those of saturated vapor. R1234yf exhibited heat transfer coefficients lower (10-12%) and frictional pressure drop lower (10-20%) than those of R134a under the same operating conditions.

Finally Longo (2012b) experimentally measured the heat transfer coefficients and the pressure drop measured during vaporization of R1234yf inside the same BPHE investigating the effects of heat flux,

mass flux, saturation temperature and outlet conditions. The saturated boiling heat transfer coefficients were founded to be 15 - 40% higher than those with 10 °C of outlet vapor super-heating.

1.5.3 Roll-bond

Roll-bond type evaporators are used in a great number of domestic refrigerators. The global annual production of domestic refrigerators and freezers is more than 90 million units and in 2009, an estimated 1.5–1.8 billion domestic refrigerators and freezers were in operation worldwide (Björk, 2010). On average a domestic refrigerator contains around 0.05–0.25 kg of refrigerant, but units in Europe and in Asia typically contain about 15–25% less refrigerant charge and 50% less blowing agent than the units produced in the United States (EPA, 2015).

R134a has been the most used refrigerant in this kind of application for years but, due to its high GWP index, it is going to be phased out in most of the countries. For example, in Europe, the EU regulation No 517/2004 (2014) have been banned refrigerants with GWP>150 in new domestic refrigerators since January 2015 (see paragraph 1.2.1).

Hydrocarbons, such as R600a (Isobutane) and R290 (Propane), have already been used in small domestic refrigerators and drink-coolers especially in Europe and in Asia. Due to the flammability of hydrocarbons, safety regulations were stipulated on how the refrigerator should have been designed to avoid fire, including leak protected cooling systems and spark free electronics (Gigiel, 2004).

Through sources such as manufacturers and international safety committees, the estimated number of incidents up to 2014 has been collated. Using the known population of R600a domestic refrigerators (over 500 million), the ignition frequency is estimated to be around 1×10^{-9} per year, although it is recognised that the actual number of incidents may be greater by a factor of 2 to 10 (HSE, 2014). Reasons for ignition were refrigerant leaks migrating into the domestic refrigerators cabinet due to containment faults and then being ignited by the thermostat or lamp switch. In addition the frequency of secondary fire for domestic refrigerators is about 10 to 100 times lower than the ignition frequency (Colbourne and Suen, 2015)

In the literature it is possible to find many works that investigate the performance of domestic refrigerators working with HCs or with HC-HFC mixtures with low GWP instead of high-GWP refrigerants.

In Table 6 are reported some of these works, underlining the refrigerants proposed to replace the old ones.

Table 6 Literature review on HCs used as low GWP refrigerants in domestic refrigerators.

Authors	**Alternative**	**Common**
Akash and Said (2003)	mixture of about 30% of R290, 55% of R600 and 15% of R600a	R12
Almeida *et al*. (2010)	mixtures of R290/R600a with a mass ratio of 60:40, R290/R600a/R134a with a mass ratio of 40:30:30 and R600a/R290 with a mass ratio of 50:50.	R134a
Alsaad and Hammad (1998)	LPG composed by 24.4% R290, 56.4% R600 and 17.2% R600a.	R12
Devotta and Kulkarni (1996)	R290/R600a mixture	R12
El Morsi (2015)	pure propane (R290), pure butane (R600) and commercial LPG (liquefied petroleum gas)	R134a
Fatouh and El Kafafy (2006b)	Liquefied Petroleum Gas (LPG) composed by R290, R600a and R600 (60:20:20 by mass fraction)	R134a
Fatouh and El Kafafy (2006a)	proposed propane, commercial butane and propane/iso-butane/n-butane mixtures	R134a
Hammed and Alsaad (1999)	Mixture of R290:R600:R600a	R12

	(50:38.3:11.7 by weight).	
Joybari *et al.* (2013)	R600a	R134a
Jung *et al.* (2000b)	R290/R600a mixture	R12
Mohanraj *et al.* (2009b) and Mohanraj *et al.* (2007)	composed of R290 and R600a in the ratio of 45.2:54.8 by weight	R134a
Rasti *et al.* (2012) and Rasti *et al.* (2013)	with R436A (a mixture of R290 and R600a with a mass ratio of 56/44).	R134a
Sattar *et al.* (2007)	R600, R600a and a mixture of R290, R600 and R600a	R134a
Wongwises and Chimres (2005)	Mixtures of R290 and R600 at different mass ratio	R134a
Yu and Teng (2015)	Three different R290 and R600 mixtures	R134a

All the experimental works presented in Table 6 found a performance improvement passing from a traditional system working with a CFC to a system that used HCs as refrigerants. The system COP, when measured, was found to be a little bit higher but, above all, thanks to the higher HC latent heat, the energy consumption of the new system was lower and the optimal charge amount required was dramatically reduced. This latter advantage is extremely important for hydrocarbons that are classified as flammable and the possibility to use a little amount of charge allows their use despite the flammability.

Furthermore, some authors proposed to replace high GWP refrigerants with HFC-HC mixtures or with lower GWP refrigerant, such as R152a and R32.

In Table 7 are summarized the most relevant experimental works. Also in all of these works a slight performance enhancement of the system correlated to a reduction of the optimum amount of refrigerant charge was possible to be appreciated..

Finally, also the HydroFluoroOlefin (HFO) refrigerants, especially R1234yf and R1234ze(E), are other suitable candidates for R134a replacement in domestic and small refrigerators.

Table 7 Literature review on HFC and HC mixtures used as low GWP refrigerants in domestic refrigerators.

Authors	Alternative	Common
Bolaji (2010)	R152a and R32	R134a
He *et al.* (2005)	HFC mixture composed of R152a and R125 at different weight percentage (80:20, 85:15 and 90:10)	R12
Mohanraj (2013)	R430A composed of R152a and R600a (in the ratio of 76:24, by mass)	R134a
Sekhar *et al.* (2004)	R134a/R289/R600a mixture	R12
Tashtoush *et al.* (2002)	R600/R290/R134a mixture	R12

Yana Motta *et al.* (2010) found that both R1234yf and R1234ze(E) were suitable for drop-in replacement of R134a in small refrigerators. Karber *et al.* (2012) experimentally investigated the performance of R1234yf and R1234ze(E) as drop-in replacements for R134a in domestic refrigerators. R1234yf exhibits COP and cooling capacity similar to R134a, whereas R1234ze(E), although it performed favorably in term of COP, had a cooling capacity significantly lower than R134a and therefore it was unsuitable for direct drop-in replacement of R134a. Leighton *et al.* (2012) developed a simulation model of a commercially available R134a household refrigerator to evaluate the drop-in performance of several low GWP alternative refrigerants. R1234yf seemed to be the most promising direct drop-in replacement for R134a in domestic refrigeration.

1.5.4 Heat Pipe Finned Heat Exchanger (HPFHE)

Heat pipes heat exchangers are devices widely used for energy recovery purposes inside air conditioning systems.

Several review works are available in the open literature, among them: Riffat and Ma (2007), Srimuang and Amatachaya (2012), Ong (2014), and Jafari *et al.* (2016) where some applications of HPHEs used as heat recovery systems are reported. In fact, these devices have been proposed and used in many fields, they are effective in enhancing dehumidification and in reducing air conditioning costs especially in hot and humid countries.

Following some works in which heat pipes heat exchangers are used for air conditioning purposes are reported. Abd El-Baky and Mohamed (2007) studied an heat pipe recuperator for the heat recovery between two streams of fresh air (at a temperature between 32 and 40 °C) and return air (approximately at 26 °C) inside an air conditioning system. Martinez *et al.* (2003) designed a mixed-energy recovery system consisting of an heat pipes heat exchanger and indirect evaporative recuperators for the air conditioning. They demonstrated that this system improved the energy efficiency and reduced the environmental impact.

Zhang *et al.* (2015) proposed a thermosyphon free cooling system to be used inside data centers, places where cutting down the energy consumption of cooling equipment becomes an urgent need and free cooling is an ideal way.

Noie-Baghban and Majideian (2000) proposed a system based on heat pipes for surgery rooms in hospitals, designed to be used with low-temperature sources (15–55 °C). Lukitobudi *et al.* (1995) applied the HP technology to a medium temperature heat recovery system in bakeries. Yang *et al.* (2003) investigated the possible application of a HPHE in a large bus by recovering the heat from the exhaust gas of the engine. Yuan *et al.* (2014) presented a thermodynamic analysis and a numerical simulation of a heat pipe finned heat exchanger which recovered both sensible and latent heat from the exhaust gases of boiler with a temperature ranged from 450K to 600K.

Wu *et al.* (1997) discussed about the use of a three-row heat pipe heat exchanger filled with R22 as working fluid for the humidity control in air-conditioning systems. Tests were carried out with fresh air/recirculating supply air ratios from 10 to 100%. Rittidech *et al.* (2005) used a heat pipe based system air-preheater for the drying process. The authors connected the condenser section to the fresh-air section, and the evaporator to the heat source from the gas burner. Also Meena *et al.* (2007) presented a similar study to reduce the relative humidity and to save energy in the drying systems.

Yau and Ahmadzadehtalatapeh (2010) investigated the heat pipe heat exchanger applications in tropical, sub-tropical, hot and humid climates, in order to control the temperature and humidity levels in conditioned spaces. In such harsh climate, in fact, the heat recovery based on heat pipe technologies can work with higher efficiencies and, thus, can increase the global benefits.

Among the great number of works cited, it can be highlighted the works by Mathur (1996) and Mathur (1997) who designed and tested systems for the hot and humid climates typical of Southeastern of the United States; Wan *et al.* (2007) who examined the effect of a heat pipe air handling coil on the energy

consumption in a central air conditioning system for an office building; and Yau (2007) and Yau (2008) that conducted a research on the influence of a 8-row HPHEs in a tropical air conditioning system varying the inlet air temperature.

In spite of the large diffusion of this type of heat exchangers, there is relatively poor evidence in the open literature about the optimization and the two-phase working fluid selection inside HPHEs.

It is well known (Reay and Kew, 2006) that the choice of heat pipe working fluid markedly affects the heat pipe effectiveness. R134a is widely adopted as working fluids for HPHE since it is quite widespread as a refrigerant for refrigeration and air conditioning units including finned coil condensers and evaporators. It can be used for working temperatures down to -5 °C or so and up to 90 °C or so (being 101.09 °C its critical temperature, see Table 3).

For example, Yau and Tucker (2003) investigated the overall effectiveness of a 6-row heat pipe heat exchanger filled with R134a in tropical buildings Jouhara and Ezzuddin (2013) experimentally analyzed the performance of a HPHE charged with R134a inside an air handling unit. Furthermore, Grooten and van der Geld (2009) presented a single thermosyphon with a large length-to-diameter ratio (L/D=188) used for air conditioning puroposes using R134a as working fluid concluding that the effect of pressure on the evaporation heat transfer is higher for the long R134a filled thermosyphon than that measured previously for all other, shorter thermosyphons. Also Sukchana and Jaimboonma (2013) investigated the effect of R134a filling ratio and of the adiabatic length on thermal efficiency of the long heat pipe.

In addition Guo and Nutter (2009) experimentally tested a two phase thermosyphon filled with R134a at different heat fluxes and Guo *et al.* (2011) studied a commercially available HPFHE. The effectiveness equations obtained from the experimental results, which represented the variation in effectiveness with several independent operating variables, were used for achieving the minimum life-cycle costs in HVAC design.

R134a, together with other fluids having a GWP index rather high, is going to be phased out (see for instance section 1.2.1). For this reason some authors have been investigating the effects of the working fluid substitution also inside heat pipes.

For example Esen (2003) tested R134a, R407C and R22 as working fluids inside the pipes of a solar cooking system. He found that the thermophysical properties of the refrigerant used influenced the

global performance and that R407C outperforms the other two fluids perhaps be due to its low boiling point and its high latent heat.

Esen and Esen (2005) experimentally investigated R134a, R407C, and R410A as two-phase refrigerants inside a thermosyphon: they measured the best performance by using R410A.

Hassan (2013) investigated the performance of a HPFHE operating with R134a, R22, R410A, and R407C. The Author used heat pipes of 660 mm length, 20 mm outer diameter and 4 mm fin spacing with staggered arrangements. During the test campaign, the air temperature at the evaporator inlet was varied from 35 to 55°C and at the condenser was varied from 20 to 25°C. He concluded that the results obtained using R410A, R134a, and R22 were similar, whereas R407C was the least effective.

Cieslinski and Fiuk (2013) proposed a two-phase thermosyphon heat exchanger using distilled water, methanol and R141b as working fluids. The tested two-phase thermosyphon heat exchanger operated in a vacuum, and therefore the working liquids boiled in a temperature range from 24°C to 62 °C. When low wall superheat is preferable, the best option was to use R141b as working fluid, but for higher wall superheating operations, water gave better heat transfer coefficients than the other fluids maybe because of its different boiling regime.

MacGregor *et al.* (2013) investigated a large number of fluids in terms of merit number, a performance criteria to rank the refrigerants. The analysis suggested that a water-5% ethylene glycol mixture could be a possible solution as R134a replacement fluid in closed-loop heat pipes working as air-to-air heat exchangers with operating temperature ranges of -10 – 50 °C for the cold side and 60 – 80 °C for the hot side. However, the experiments showed that under certain conditions the blend performance was lower than that of R134a.

Some authors presented also theoretical analyses where the thermophysical properties of the working fluids were taken into account for defining performance evaluation criteria.

D. Mishkinis and J. M. Ochterbeck (2003) proposed a correlation of geometrical, structural and physicochemical properties of the Loop Heat Pipes (LHPs) elements and they found that the working fluid played a key role in the heat pipe successful and reliable start-up and operation in required range of temperatures, heat loads and ambient conditions. After listing a huge number of criteria to be adopted in the refrigerant choice to guarantee the correct heat pipe functioning and an high efficiency of the heat exchanger, they proposed a criteria to estimate the values and magnitudes of different forces, to select working fluid (group of fluids) and to develop the heat exchanger design.

Sabharwall *et al.* (2009) performed a dimensional analysis for helping in the heat pipe and thermosyphon design. This analysis yielded two terms: one related to the latent heat of vaporization to the pressure drop across the device, and the other one related to the latent heat of vaporization to the capillary pressure.

Chang and Hung (2014) developed a mathematical model by incorporating the solid wall conduction, together with the continuity, momentum, and energy equations of the liquid and vapor phases. They analyzed the effects of working fluid on the thermal performance by deriving a new non-dimensional group made up by the combination of surface tension, liquid density, latent heat, liquid dynamic viscosity, solid wall temperature difference between evaporator and condenser, thermal conductivity of the pipe material, and total length of the pipe.

Arab and Abbas (2014) proposed a generic model used to analyze and quantify the contribution of each of the thermophysical properties of working fluid on heat pipe thermal resistance. They found that high thermal conductivity, low surface tension, low latent heat of evaporation, high viscosity, and low liquid density are the most favorable thermophysical properties of the working fluid leading to improvement of heat pipe thermal resistance, respectively.

Zhang and Faghri (2008) by analyzing Pulsating Heat Pipes (PHP or OHP) concluded that the main thermophysical properties that are involved in the heat transfer inside an heat pipe are: surface tension, latent heat, specific heat, viscosity, and the rate of change in pressure with respect to temperature at saturated conditions $(dp/dT)_{sat}$. More in details they observed that: a higher surface tensions will increase the maximum allowable diameter and also the pressure drop in the tube; a low latent heat will cause the liquid to evaporate more quickly, so the heat transfer performance will be improved; a high specific heat will increase the amount of sensible heat transferred; a low dynamic viscosity will reduce shear stress along the wall and will consequently reduce pressure drop in the tube; and at a high value of $(dp/dT)_{sat}$ the difference between vapor pressures in the evaporator and condenser will be increased and the performance will be improved.

2 Experimental set up and procedures

2.1 Horizontal smooth tube

2.1.1 Experimental facility

The experimental facility, shown in Figure 10, consists of a refrigerant loop, a water-glycol loop and a refrigerated water loop.

In the first loop the refrigerant is pumped from a sub-cooler heat exchanger into a Brazed Plate Heat Exchanger (BPHE) pre-evaporator, where it is partially evaporated to achieve the set quality at the inlet of the tubular test section. The refrigerant goes through the test section where it is evaporated and then it comes back to ta BPHE condenser and a BPHE sub-cooler. A variable speed volumetric pump varies the refrigerant flow rate, whereas a bladder accumulator connected to a nitrogen bottle and a pressure regulator controls the operating pressure in the refrigerant loop.

The second loop is able to supply a water-glycol flow at a constant temperature in the range of -10 to 30 °C with a stability within ±0.1 K which is used to feed the sub-cooler and the condenser, whereas the third loop supplies a refrigerated water flow at a constant temperature in the range of 3 °C to 30 °C with a stability within ±0.1 K and it is used to feed the test section and the pre-evaporator.

The test-section presented in Figure 11 is a double tube evaporator in which the refrigerant evaporates in the inner tube while the refrigerated water flows in the annulus.

The test-section is subdivided in two different parts: a 200 mm long pre-section, in which the refrigerant achieves a fully developed flow regime and a 800 mm long measurement section, in which the heat transfer coefficient is measured. This arrangement is obtained using a single inner smooth tube, 4 mm in diameter, 1300 mm long and two separated cooling water jackets fed in series. The inner tube is instrumented with four copper-constantan thermocouples (uncertainty (k=2) within ±0.1 K) embedded in its wall to measure the surface temperature. The thermocouples are inserted into two equidistant axial grooves, at the top and at the bottom of the cross section, 100 mm from the inlet and outlet of the cooling water. Each groove is sealed with a copper wire fixed by epoxy. Table 8 shows the main geometrical characteristics of the test section including also the measured surface roughness of the tube.

Table 8 Horizontal smooth tube test facility main features.

Parameter	Measure
Tube inside diameter d (mm)	4.0
Measure section length L(mm)	800.0
Pre-section length (mm)	200.0
Total section length (mm)	1300.0
Inside tube surface roughness R_a(μm) (ISO 4287/1)	0.7
Inside tube surface roughness R_p (μm) (DIN 4762/1)	1.8

T-type thermocouples (uncertainty (k=2) within ±0.1 K) measure the temperatures of refrigerant and water at the inlet and outlet of the test section and of the pre-evaporator. T-type thermopiles (uncertainty (k=2) within ±0.05 K) measure the water temperature drops through the test section and the pre-evaporator. The refrigerant pressures at the inlet of the test-section and the pre-evaporator are measured by two absolute strain-gage pressure transducers (uncertainty (k=2) within 0.075% f.s.), whereas the refrigerant pressure drop through the test section is measured by a strain-gage differential pressure transducer (uncertainty (k=2) within 0.075% f.s.). The refrigerant mass flow rate is measured by means of a Coriolis effect mass flow meter (uncertainty (k=2) of 0.1% of the reading), whereas the water flow rates through the test section and the pre-evaporator are measured by means of magnetic flow meters (uncertainty (k=2) of 0.15% of the f.s.). All the measurements are scanned and recorded by a data logger linked to a PC. Table 9 outlines the main features of the different measuring devices in the experimental rig.

Before each test the refrigerant is re-circulated through the circuit, the condenser and the sub-cooler are fed with water-glycol at a constant temperature and the test section and pre-evaporator are fed with water at a constant temperature. The refrigerant pressure and vapor quality at the inlet of the evaporator and the vapor quality at the outlet of the evaporator are controlled by adjusting the bladder accumulator, the volumetric pump, the flow rate and the temperature of the water-glycol and the refrigerated water. Once temperature, pressure, flow rate and vapor quality steady have reached state conditions at the test section inlet and outlet, both on refrigerant and water sides, all the readings are recorded for a set time and the average value during this time is computed for each parameter collected.

The experimental results are reported in terms of refrigerant side heat transfer coefficients α_r and frictional pressure drop Δp_f.

Table 9 Specification of the different measuring devices used in the horizontal smooth tube test facility.

Devices	**Uncertainty** (k=2)	**Range**
T-type thermocouples	0.1 K	-20/80 °C
T-type thermopiles	0.05 K	-20/80 °C
Abs. pressure transducers	0.075% f.s.	0/3.0 MPa
Diff. pressure transducers	0.075% f.s.	0/0.3 MPa
Coriolis effect flow meters	0.1%	0/300 kg h^{-1}
Magnetic flow meters	0.15% f.s.	100/1200 l h^{-1}
Data logger	± 2.7 μV	0 / 100 mV

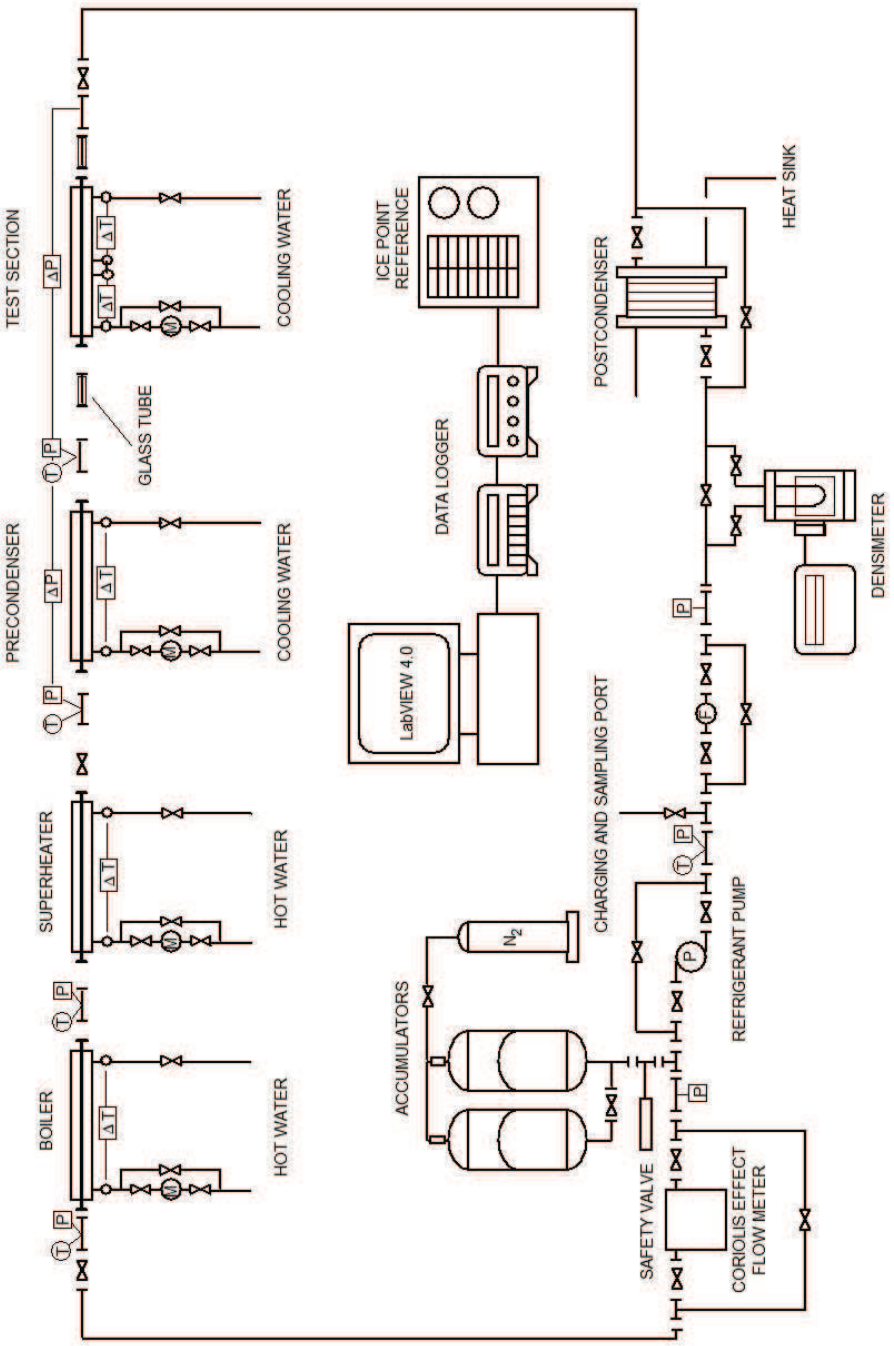

Figure 10 Horizontal smooth tube experimental facility scheme.

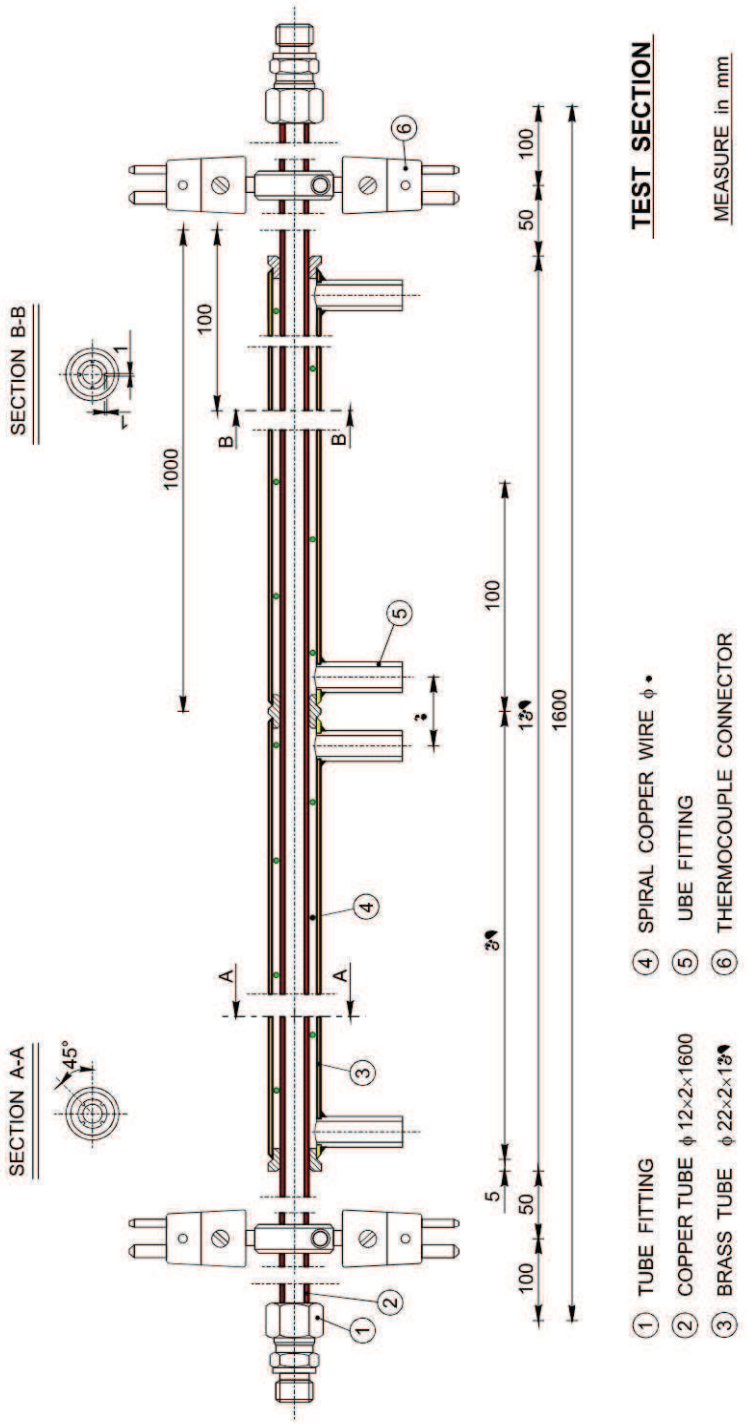

Figure 11 Horizontal smooth tube test section scheme.

2.1.2 Data reduction

The average refrigerant heat transfer coefficient α_r (Eq. 1) is equal to the ratio between the heat flow rate Q, the heat transfer area A and the mean temperature difference ΔT:

$$\alpha_r = \frac{Q}{A\,\Delta T} \qquad \text{Eq. 1}$$

The heat flow rate (Eq. 2) is derived from a thermal balance on the water-side of the measurement section:

$$Q = m_w\, c_{pw}\, |\Delta T_w| \qquad \text{Eq. 2}$$

where m_w is the water flow rate, c_{pw} the water specific heat capacity and $|\Delta T_w|$ the absolute value of the temperature variation on the water-side of the measurement section. The heat transfer area of the measurement section (Eq. 3) is equal to

$$A = \pi\, d\, L \qquad \text{Eq. 3}$$

The mean temperature difference (Eq. 4) is equal to:

$$\Delta T = (T_{wall} - T_{sat}) \qquad \text{Eq. 4}$$

where T_{sat} is the average saturation temperature derived from the average pressure measured on refrigerant side and T_{wall} is the average surface temperature equal to the arithmetical mean value of the reading of the four thermocouples embedded in the tube wall.
The refrigerant vapor quality at the measurement section inlet and outlet x_{in} (Eq. 5) and x_{out} (Eq. 6) are computed starting from the refrigerant temperature $T_{pb.in}$ and pressure $p_{pb.in}$ at the inlet of the pre-evaporator (sub-cooled liquid condition) considering the heat flow rate exchanged in the pre-

evaporator, in the pre-section and in the measurement section Q_{pb} (Eq. 9), Q_{ps} (Eq. 10) and Q (Eq. 2) and the pressure at the inlet and outlet p_{in} and p_{out} of the test section as follows:

$$x_{in}=f(h_{in}, p_{in}) \quad \text{Eq. 5}$$

$$x_{out}=f(h_{out}, p_{out}) \quad \text{Eq. 6}$$

$$h_n=h_{pb.in}(T_{pb.in}, p_{pb.in}) + \frac{Q_{pb}}{\dot{m}_r} + \frac{Q_{ps}}{\dot{m}_r} \quad \text{Eq. 7}$$

$$h_{out}=h_{in} + \frac{Q}{\dot{m}_r} \quad \text{Eq. 8}$$

$$Q_{pb}=m_{pb.w}\, c_{pw}\, |\Delta T_{pb.w}| \quad \text{Eq. 9}$$

$$Q_{ps}=m_{w}\, c_{pw}\, |\Delta T_{ps.w}| \quad \text{Eq. 10}$$

where h is the specific enthalpy of the refrigerant, $\dot{m}_r$ the refrigerant mass flow rate, $\dot{m}_{pb.w}$ the water flow rate and $|\Delta T|_{pb.w}$ the absolute value of the temperature variation on the water side of the pre-evaporator, $|\Delta T|_{ps.w}$ the absolute value of the temperature variation on the water side of the pre-section. Therefore the mean vapor quality (Eq. 11) in the measurement section results:

$$x_m = \frac{x_{out} + x_{in}}{2} \quad \text{Eq. 11}$$

The frictional refrigerant pressure drop Δp_f (Eq. 12) is computed by subtracting the inlet / outlet local pressure drops Δp_c, and the momentum pressure drops Δp_a from the total pressure drop measured Δp_t:

$$\Delta p_f=\Delta p_t - \Delta p_c - \Delta p_a \quad \text{Eq. 12}$$

It should be noted that the pressure drops refers to the whole length of the test section, 1300 mm, including the pre-section, the measurement section and the adiabatic parts of the tube.
The momentum pressure drops (Eq. 13) are estimated by the homogeneous model for two-phase flow as follows:

$$\Delta p_a=G^2\,(v_G - v_L)\,|\Delta x| \quad \text{Eq. 13}$$

where G is the refrigerant mass flux, v_L and v_G are the specific volume of liquid and vapor phase, $|\Delta x|$ is the absolute value of the vapor quality change through the whole test section.
The inlet and the outlet local pressure drops Δp_c (Eq. 14) are empirically estimated, in accordance with (ASHRAE Handbook Fundamentals, 1989), as follows:

$$\Delta p_c = 1.5 \frac{G^2}{2\,\rho_{m.w}} \qquad \text{Eq. 14}$$

where

$$\rho_{m.w} = \left(\frac{x_{m.w}}{\rho_G} + \frac{1 - x_{m.w}}{\rho_L}\right)^{-1} \qquad \text{Eq. 15}$$

is the average two-phase density between inlet and outlet calculated by the homogeneous model at the mean vapor quality $x_{m.w}$ in the whole test section.
Being the test section horizontal, no gravity pressure drops component Δp_g occur.
The refrigerant properties are evaluated according with Refprop9.1(2013).

2.2 Brazed Plate Heat Exchanger (BPHE)

2.2.1 Experimental facility

The experimental facility consists of a refrigerant loop, two water-glycol loops and two water loops. It provides the required inlet conditions at the testing BPHE and it allows obtaining in it both the condensation and the vaporization process.

2.2.1.1 Condensation mode

When the facility works in condensation mode (Figure 12), that is condensation occurs into the BPHE under testing, in the first loop the refrigerant is pumped from the sub-cooler into a first plate heat exchanger fed by a water loop that works as an evaporator where it is evaporated and eventually super-heated to achieve the set condition for the test. The refrigerant goes through the measurement section where it is condensed and eventually sub-cooled and then it comes back to another plate heat exchanger that works as post-condenser and it is fed by the first water-glycol loop. Finally the liquid refrigerant is sub-cooled by the last plate heat exchanger fed by the second water-glycol loop. A variable speed volumetric pump varies the refrigerant flow rate and a bladder accumulator connected to a nitrogen bottle and a pressure regulator controls the operating pressure in the refrigerant loop. The first water-glycol loop of the condenser is able to supply a water–glycol (70–30%) flow at a constant temperature in the range of -10 to 30 °C with stability within ±0.1 K, while the one of the sub-cooler supplies a water–glycol (50–50%) flow at a constant temperature in the range of -10 to 30 °C with stability within ±0.1 K. Finally, to feed the evaporator and the BPHE under testing, the two water loops supply refrigerated water at a constant temperature in the range of 3–40 °C with a stability within ±0.1 K. The use of water minimizes fouling inside the evaporator and eliminates the errors in the estimation of water–glycol mixture properties due to the uncertainty in the brine composition.

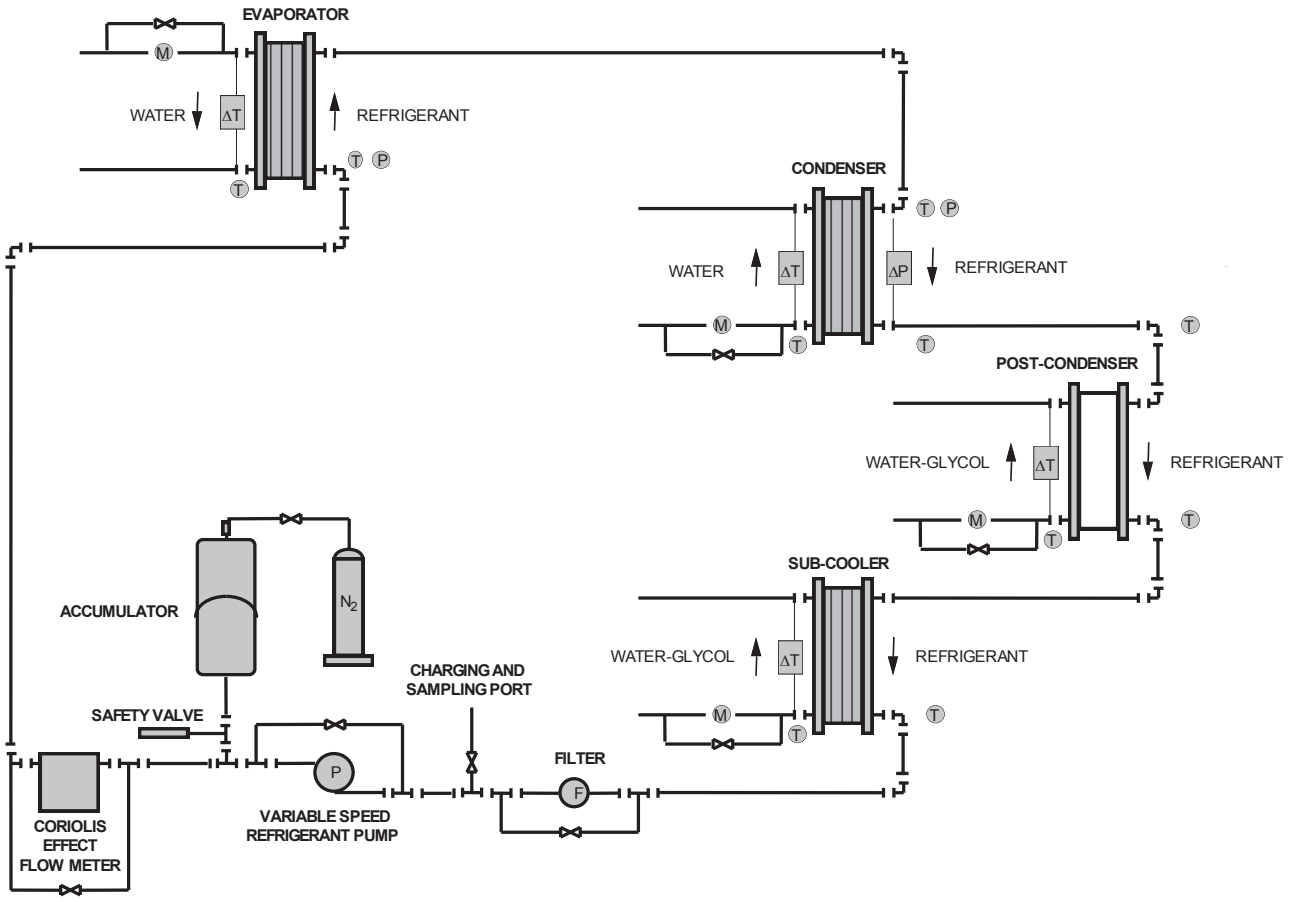

Figure 12 BPHE experimental facility scheme during condensation tests.

2.2.1.2 Vaporization mode

When the facility works in vaporization mode (Figure 13), that is vaporization occurs into the BPHE, in the first loop the refrigerant is pumped from the sub-cooler into a first plate heat exchanger fed by a water loop that works as pre-evaporator. Here the refrigerant is partially evaporated to achieve the set quality at the inlet of the BPHE evaporator. The refrigerant goes through the measurement section where it is evaporated and eventually super-heated and then it comes back to another plate heat exchanger that works as condenser and it is fed by the first water-glycol loop. After the liquid refrigerant is sub-cooled by the last plate heat exchanger fed by the second water-glycol loop. The same variable speed volumetric pump is used to regulate the refrigerant flow rate and the bladder accumulator and the pressure regulator to control the operating pressure in the refrigerant loop.

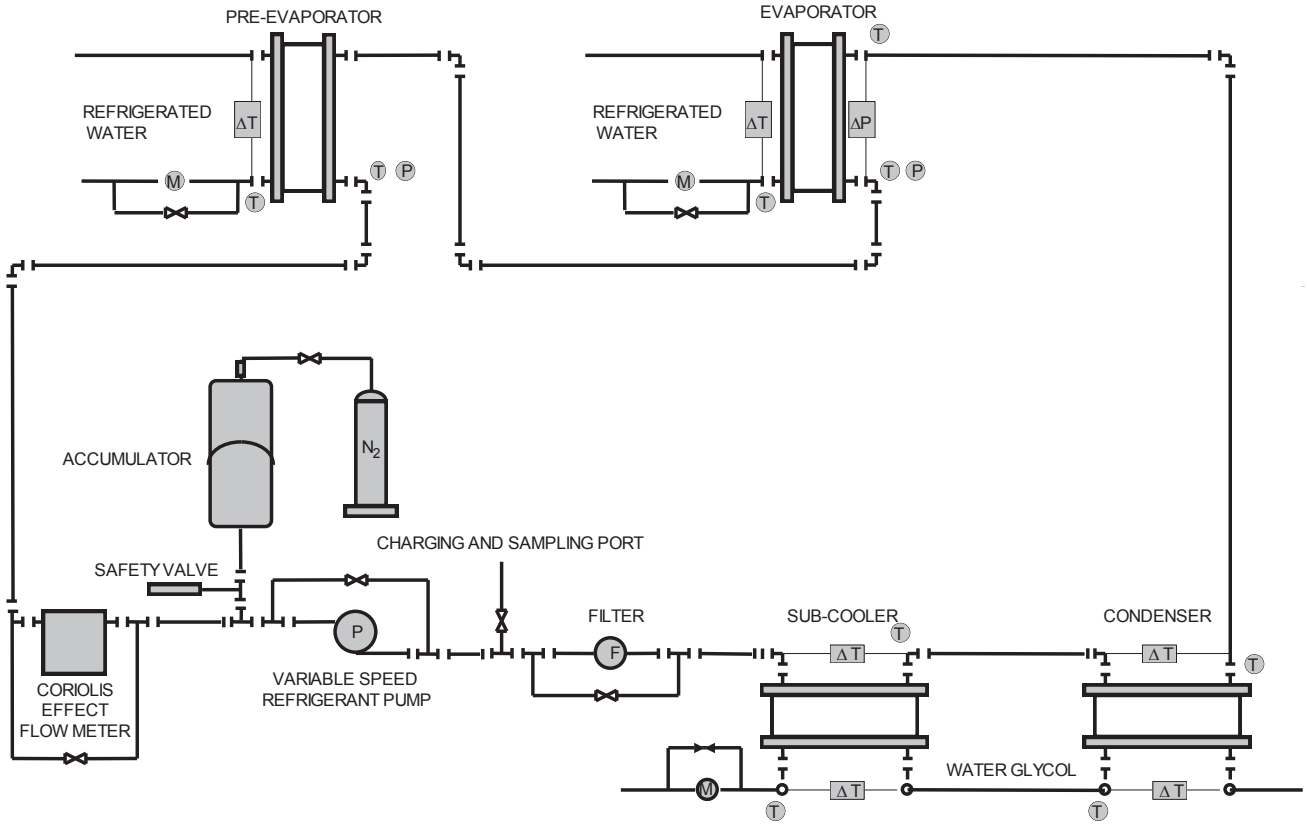

Figure 13 BPHE experimental facility scheme during vaporization tests.

2.2.1.3 Heat exchanger

The tested BPHE consists of 10 plates, 72 mm in width and 310 mm in length, with a macro-scale herringbone corrugation, an inclination angle of 65° and a corrugation amplitude of 2 mm. Figure 14 and Table 10 give the main geometrical characteristics of the BPHE tested.

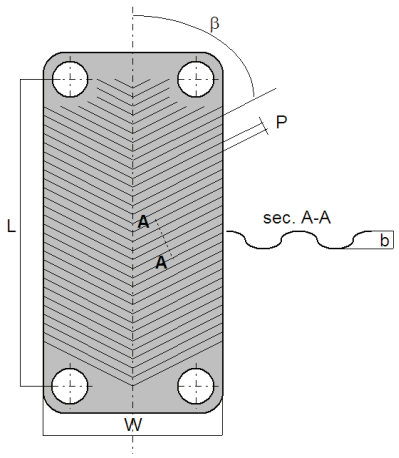

Figure 14 Schematic view of the plate of the BPHE taken into account.

Table 10 Geometrical characteristic of the plate of the BPHE taken into account.

Parameter	**Measure / Type**
Fluid flow plate length *L* [mm]	278.0
Plate width *W* [mm]	72.0
Area of the plate *A* [m^2]	0.020
Corrugation type	Chevron
Angle of the corrugation β [°]	65
Corrugation deep *b* [mm]	2.0
Corrugation pitch *P* [mm]	8.0
Plate roughness R_a [μm]	0.4
Plate roughness R_p [μm]	1.0
Total number of plates	10
Number of effective plates	8
Channels on refrigerant side	4
Channels on water side	5

2.2.1.4 Measurement set up

The temperatures of refrigerant and water at the inlet and outlet of the BHPE under test and of the first BPHE, used as evaporator in condensation mode and as pre-evaporator in vaporization mode, are measured by T-type thermocouples (uncertainty (k=2) within ±0.1 K) and the water temperature drops through the same heat exchangers are measured by T-type thermopiles (uncertainty (k=2) within±0.05 K). The refrigerant pressures at the inlet of these heat exchangers are measured by two absolute strain-gage pressure transducers (uncertainty (k=2) within 0.075% f.s.) and the refrigerant pressure drop through the tested BPHE is measured by a strain-gage differential pressure transducer (uncertainty (k=2) within 0.075% f.s.). The refrigerant mass flow rate is measured by means of a Coriolis effect mass flow meter (uncertainty (k=2) of 0.1% of the measured value); the water flow rates through the BHPE under test and the first BPHE are measured by means of magnetic flow meters (uncertainty (k=2) of 0.15% of the f.s.). All the measurements are scanned and recorded by a data logger linked to a PC. Table 11 gives the main features of the different measuring devices in the experimental rig. Before each test the refrigerant is re-circulated through the circuit and all the heat exchanger are fed by water or water-glycol at a constant temperature. The refrigerant pressure and the vapor quality at the inlet and at the outlet of the measurement section are controlled by adjusting the volumetric pump, the throttling valve, the flow rate and the temperature of the water–glycol and the refrigerated water. Once temperature, pressure, flow rate and vapor quality steady-state conditions are achieved at the testing BPHE inlet and outlet both on refrigerant and on the water side, all the readings are recorded for a set time (10 min) and the average value during this time is computed for each parameter recorded.

Table 11 Specification of the different measuring devices used in the brazed plate heat exchanger test facility.

Devices	**Uncertainty** (k=2)	**Range**
T-type thermocouples	0.1 K	-20/80°C
T-type thermopiles	0.05 K	-20/80°C
Abs. pressure transducers	0.075% f.s.	0/3.0 MPa
Diff. pressure transducers	0.075% f.s.	0/0.3 MPa
Coriolis effect flow meters	0.1%	0/300 kg h^{-1}
Magnetic flow meters	0.15% f.s.	100/1200 l h^{-1}

2.2.2 Data reduction

The experimental results are reported in terms of refrigerant side heat transfer coefficients and frictional pressure drop.

2.2.2.1 Condensation mode

The overall heat transfer coefficient in the BPHE condenser K is equal to the ratio between the heat flow rate Q, the nominal heat transfer area S and the logarithmic mean temperature difference ΔT_{ln} (Eq. 16)

$$K = \frac{Q}{A\,\Delta T_{ln}} \qquad \text{Eq. 16}$$

The heat flow rate is derived from a thermal balance on the water-side of the condenser (Eq. 17):

$$Q = m_w\, c_{pw}\, |\Delta T_w| \qquad \text{Eq. 17}$$

where m_w is the water mass flow rate, c_{pw} the water specific heat capacity and $|\Delta T_w|$is the absolute value of the water temperature lift across the condenser. The reference heat transfer area of the condenser A is defined as

$$A = N\,A' \qquad \text{Eq. 18}$$

and it is equal to the nominal projected area A'=L x W of the single plate multiplied by the number N of the effective elements in heat transfer. The logarithmic mean temperature difference ΔT_{ln} (Eq. 19) is equal to:

$$\Delta T_{ln} = \frac{T_{w.out} - T_{w.in}}{\ln \frac{T_{sat} - T_{w.in}}{T_{sat} - T_{w.out}}} \quad \text{Eq. 19}$$

where T_{sat} is the average saturation temperature of the refrigerant computed from the measurement of refrigerant temperature at the inlet and at the outlet of the condenser, and $T_{w.in}$ and $T_{w.out}$ are the water temperatures measured at the inlet and the outlet of the condenser.

The average refrigerant heat transfer coefficient $\alpha_{r.ave}$ (Eq. 20 defined by)is derived from the global heat transfer coefficient K assuming no fouling resistances:

$$\alpha_{r.ave} = \left(\frac{1}{K} - \frac{s}{\lambda_p} - \frac{1}{\alpha_w}\right)^{-1} \quad \text{Eq. 20}$$

by computing the water-side heat transfer coefficient α_w using a modified Wilson plot technique. A specific set of experimental water-to-water tests is carried out on the condenser to determine the calibration correlation for heat transfer on the water-side, in accordance with Muley and Manglik (1999).

This modification of the classical Wilson plot technique incorporates an account of variable fluid property effects. Figure 15 shows the water-to-water data plotted on the co-ordinates defined by Eq. 21 and Eq. 22:

$$X = \frac{\lambda_I}{\lambda_E}\left(\frac{Re_I}{Re_E}\right)^{0.766}\left(\frac{Pr_I}{Pr_E}\right)^{0.333} \quad \text{Eq. 21}$$

$$Y = \left(\frac{1}{K} - \frac{s}{\lambda_P}\right)\left[\left(\frac{\lambda_I}{d_h}\right) Re_I^{0.766}\, Pr_I^{0.333}\right] \quad \text{Eq. 22}$$

where subscripts I and E refer to the internal channels (normally refrigerant side) and the external channels (normally water side) of the tested BPHE, respectively.

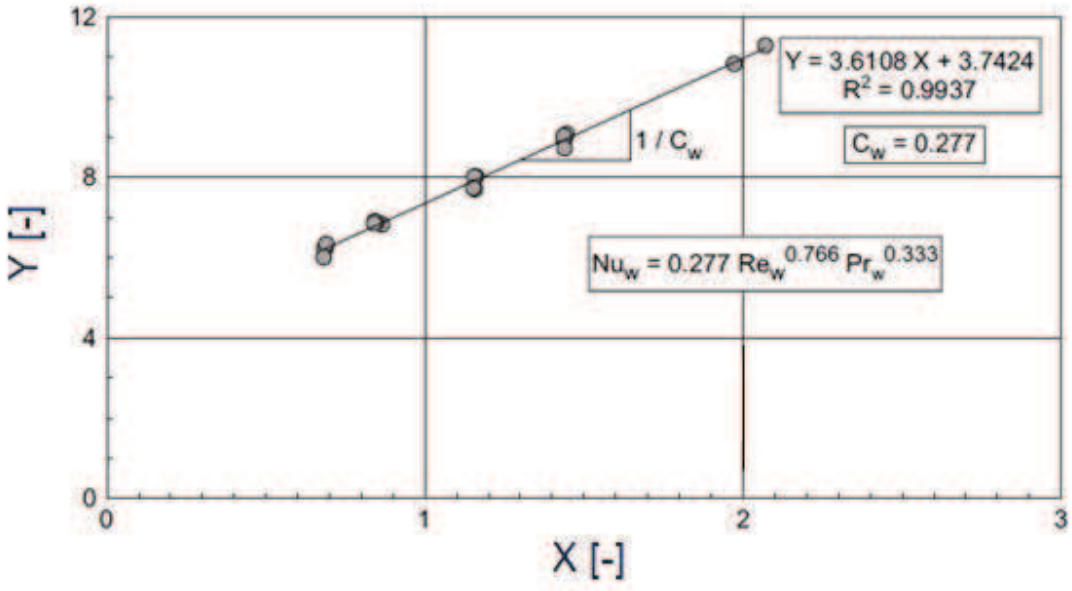

Figure 15 Modified Wilson plot results for calibration of water side heat transfer coefficient. (Longo and Gasparella 2007a).

The slope of the plot gives the constant in the calibration correlation, a power-law type, for heat transfer coefficients on the water side. The exponent on Reynolds number Re_l 0.766 results from a best fitting procedure on the experimental data. The calibration correlation for water-side heat transfer coefficient is (Eq. 23):

Eq. 23

$$\alpha_w = 0.277 \frac{\lambda_w}{d_h} Re_w^{0.766} Pr_w^{0.333}$$

and it is valid for:

$5<Pr_w<10$ $200<Re_w<1200$

The refrigerant vapor quality at the condenser inlet and outlet x_{in} and x_{out} are computed starting from the refrigerant temperature $T_{e.in}$ and pressure $p_{e.in}$ measured at the inlet of the evaporator (sub-cooled liquid condition) considering the heat flow rate exchanged in the evaporator and in the condenser (Q_e

and Q, respectively) and the pressures p_{in} and p_{out} measured at the inlet and outlet of the condenser as follows (equations from Eq. 24 to Eq. 28):

$$x_{in}=f(h_{in}, p_{in})$$ Eq. 24

$$x_{out}=f(h_{out}, p_{out})$$ Eq. 25

$$h_{in}=h_{e.in}(T_{e.in}, p_{e.in}) + \frac{Q_e}{m_r}$$ Eq. 26

$$h_{out}=h_{in} - \frac{Q}{m_r}$$ Eq. 27

$$Q_e=m_{e.w}\, c_{pw}\, |\Delta T_{e.w}|$$ Eq. 28

where h is the specific enthalpy of the refrigerant, $\dot{m}_r$ the refrigerant mass flow rate, $\dot{m}_{e.w}$ the water flow rate and $|\Delta T_{e.w}|$ the absolute value of the temperature variation on the waterside of the evaporator. The refrigerant properties are evaluated by Refprop 9.1 (2013).

2.2.2.2 Vaporization mode

The overall heat transfer coefficient of the BPHE evaporator is defined as in Eq. 16. The heat power exchanged is derived from a thermal balance on the water side of the evaporator, as in Eq. 17. The nominal heat transfer area of the evaporator A is defined in Eq. 18 and it is equal to the nominal projected area A' of the single plate multiplied by the number N of the effective elements in heat transfer, as suggested by Shah and Focke (1988).
When the evaporator works only in two-phase heat transfer the logarithmic mean temperature difference is equal to:

$$\Delta T_{ln} = \frac{T_{w.in} - T_{w-out}}{\ln \frac{T_{w.in} - T_{sat}}{T_{w.out} - T_{sat}}}$$ Eq. 29

where T_{sat} is the average saturation temperature of the refrigerant derived from the average pressure measured on refrigerant side and $T_{w.in}$ and $T_{w.out}$ the water temperatures at the inlet and the outlet of the evaporator, respectively.

Claesson (2005) shows that, although the boiling heat transfer coefficient and the overall heat transfer coefficient are not constant along a BPHE evaporator, the logarithmic mean temperature difference approach may be used if the boiling heat transfer is governed by heat flux and the logarithmic mean temperature difference is not too small (>4-5 °C).

When the evaporator works both in vaporization and super-heating, Dutto *et al.* (1991) and Fernando *et al.* (2004) suggested the Eq. 30 for the logarithmic mean temperature difference:

$$\Delta T_{ln} = \frac{Q}{\frac{Q_{boil}}{\Delta T_{ln.boil}} + \frac{Q_{sup}}{\Delta T_{ln.supl}}} \quad \text{Eq. 30}$$

Where:

$$Q_{boil} = m_w \, c_{pw} \, (T_{wm} - T_{w.out}) \quad \text{Eq. 31}$$

$$Q_{sup} = m_w \, c_{pw} \, (T_{w.in} - T_{wm}) \quad \text{Eq. 32}$$

are the heat power exchanged in the boiling and superheating zones, respectively, and

$$\Delta T_{ln,boil} = \frac{T_{wm} - T_{w.out}}{\ln \frac{T_{wm} - T_{sat}}{T_{w.out} - T_{sat}}} \quad \text{Eq. 33}$$

$$\Delta T_{ln,sup} = \frac{(T_{w.in} - T_{r.out})(T_{wm} - T_{sat})}{\ln \frac{T_{w.in} - T_{r.out}}{T_{wm} - T_{sat}}} \quad \text{Eq. 34}$$

are the logarithmic mean temperature difference in the boiling and super-heating zones, respectively, whereas $T_{w.m}$ is the water temperature between the super-heating and the boiling zone and $T_{r.out}$ is the refrigerant temperature at the outlet of the evaporator. This approach computes the overall heat transfer

coefficient of the whole evaporator K as the average value between the overall heat transfer coefficient of the boiling zone K_b and that of the super-heating zone K_{sup} weighted on the basis of the respective heat transfer areas. In this way it is possible to directly compare the heat transfer performance of an evaporator working only in two-phase heat transfer with that of an evaporator working also in vapor super-heating.

The average refrigerant heat transfer coefficient α_r is derived from the overall heat transfer coefficient K assuming no fouling resistances (Eq. 20) by computing the water side heat transfer coefficient α_w using a modified Wilson plot technique. Eq. 23 is used as calibration correlation for water side heat transfer coefficient.

The refrigerant vapor quality at the evaporator inlet and outlet x_{in} and x_{out} are computed starting from the refrigerant temperature $T_{pb.in}$ and pressure $p_{pb.in}$ at the inlet of the pre-evaporator (sub-cooled liquid condition) considering the heat power exchanged in the pre-evaporator and in the evaporator Q_{pb} and Q and the pressure at the inlet and outlet p_{in} and p_{out} of the evaporator as follows (equations from Eq. 35 to Eq. 39):

$$x_{in}=f(h_{in}, p_{in}) \quad \text{Eq. 35}$$

$$x_{out}=f(h_{out}, p_{out}) \quad \text{Eq. 36}$$

$$h_{in}=h_{pb.in}(T_{pb.in}, p_{pb.in}) + \frac{Q_{pb}}{\dot{m}_r} \quad \text{Eq. 37}$$

$$h_{out}=h_{in} - \frac{Q}{\dot{m}_r} \quad \text{Eq. 38}$$

$$Q_{pb}=m_{pb.w}\, c_{pw}\, |\Delta T_{pb.w}| \quad \text{Eq. 39}$$

where $m_{pb.w}$ is the water flow rate and $|\Delta T_{pb.w}|$ the absolute value of the temperature variation on the water side of the pre-evaporator.

2.2.2.3 Pressure drop

The frictional pressure drop Δp_f (Eq. 40) is computed by subtracting the manifolds and ports pressure drops Δp_c and adding the momentum pressure rise (deceleration) Δp_a and the gravity pressure rise (elevation) Δp_g to the total pressure drop measured Δp_t:

$$\Delta p_f = \Delta p_t - \Delta p_c + \Delta p_a + \Delta p_g \quad \text{Eq. 40}$$

The momentum and gravity pressure drops are estimated by the homogeneous model for two-phase flow (Eq. 41)

$$\Delta p_g = g\, \rho_m\, L \quad \text{Eq. 41}$$

While, the manifold and port pressure drops are empirically estimated, in accordance with Shah and Focke (1998) as in Eq. 14 and the momentum pressure rise (deceleration) Δp_a are evaluated through Eq. 13.

2.3 Roll-bond evaporator

2.3.1 Experimental facility

The experimental facility consists of four main components: a roll-bond evaporator, a compressor, a condenser and a throttling device. Figure 16 shows a schematic of the test rig, including the locations of the measurement devices and some of the additional components essential to run the facility.

The compressor is a 1.9 cm^3 rotary model made by Aspen and it is driven by a DC brushless motor with variable speed control. The condenser is split in two water cooled tube-in-tube heat exchangers. Each of them is fed by a thermostatic bath so it is possible to independently control the condensing and the sub cooling temperatures. Therefore the desired specific enthalpy and vapor quality can be set at the inlet of the roll-bond evaporator. A liquid accumulator is placed among the two heat exchangers to ensure the necessary amount of refrigerant during high load tests.

Once out of the condenser, the fluid finds a filter then it passes through the throttling device (a Swagelok metering valve). By suitably tuning the compressor rotation speed and the throttling valve stem position it is possible to set the refrigerant mass flow rate and the evaporation pressure.

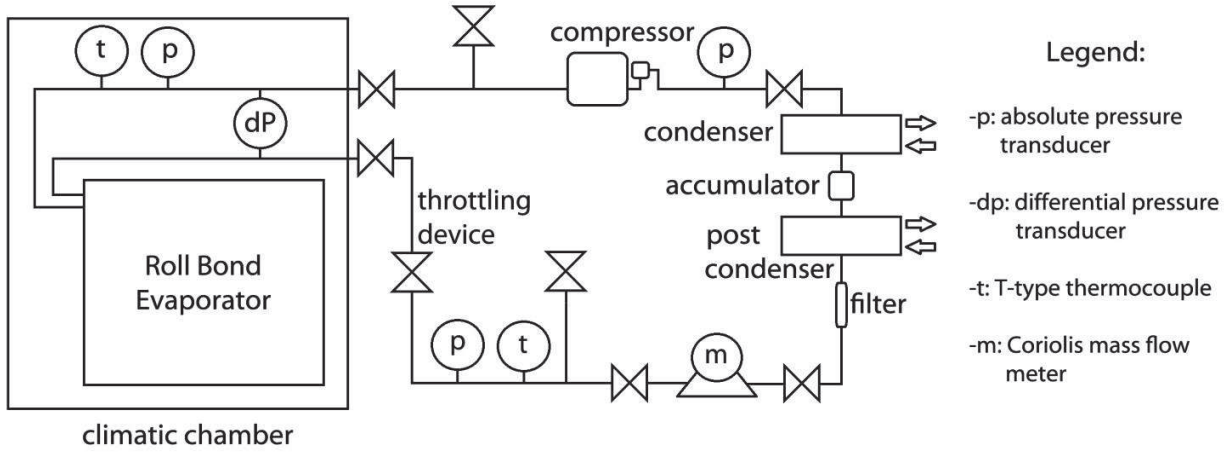

Figure 16 Roll-bond evaporator experimental facility scheme.

The evaporator is put inside a climate test chamber at 3°C to reproduce the refrigerate cavity of a domestic refrigerator, the major application of this kind of devices. The chamber is a Weiss WK111-180 model with an internal volume of 750x580x450 mm, able to maintain the air temperature deviation within ±1 K (spatial distribution) and ±0.3 K (time).

To monitor the air temperature during experimental tests, two T-type thermocouples were positioned inside the chamber: one about 3 cm above the floor and the other one about 3 cm below the ceiling.

The air velocity inside the chamber is the minimum value to avoid excessive air stratification (within 1 K) and it is comparable to air velocity of real domestic refrigerators. It has also been mounted a desiccant rotor (Munters MG 50) with a rated airflow of 50 m^3 h^{-1} to limit the humidity inside the chamber. Thanks to this device the chamber air dew temperature was kept below -5 °C in all the tests.

The roll-bond evaporator investigated is an off the shelf component, normally used for small domestic refrigerators. A scheme of the geometry and the main dimensions are reported in Figure 17 and Table 12 respectively. The evaporator back face has been covered with a thick layer of flexible insulation so that just the front face is able to exchange heat, than the whole system has been hung up on the internal climate chamber wall.

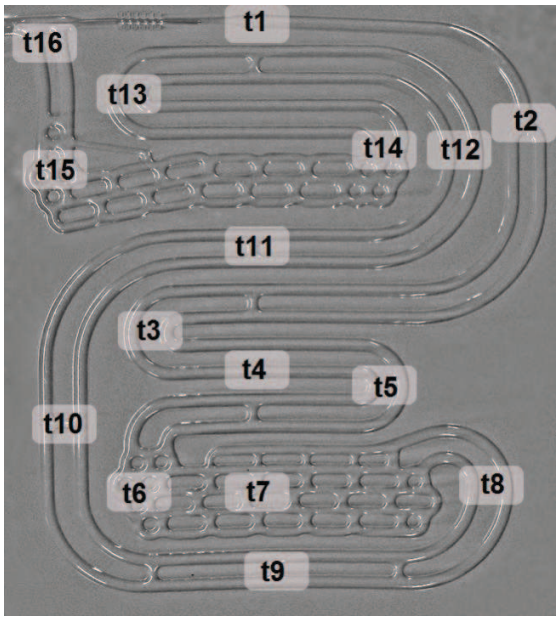

Figure 17 Schematic view of the roll-bond evaporator with the thermocouple positioning.

Table 12 Roll-bond evaporator main features.

Parameter	**Measure**
Plate length L [m]	0.42
Plate width W [m]	0.52
Plate thickness [mm]	0.8
A / A_r	1.69

To evaluate the temperature field during experimental tests 16 T-type (Copper-Constantan) thermocouples (uncertainty (k=2) within ±0.1 K) have been attached on the aluminum plate, among the roll-bond rear face and the insulation panel. Their spatial distribution is represented in Figure 17.

In addition, an infrared camera (Agema, Thermovision 550, temperature uncertainty (k=2) within ±0.1 K) has been positioned in front of the evaporator and used to monitor its temperature field. The collected data points showed good agreement in temperatures between the wall thermocouples and the thermo camera images.

The measurement set-up was competed as follow:

- a Coriolis mass flow meter (uncertainty (k=2) within ±0.1% of the reading) has been used to measure the refrigerant mass flow rate;
- three strain gauge absolute pressure transducers were positioned at the outlet of the evaporator (uncertainty (k=2) within ± 0.075% f.s.; f.s=10 bar), at the inlet of the throttling device (uncertainty (k=2) within ± 0.075% f.s.; f.s=20 bar) and at the compressor discharge (uncertainty (k=2) within ± 0.5% of the upper range limit; f.s=40 bar) respectively. In addiction two T-type thermocouples (uncertainty (k=2) within ±0.1 K) were placed inside adiabatic mixing chambers, one just before the throttling valve and one at the evaporator outlet. Thanks to the measured temperatures and pressures it is possible to evaluate specific enthalpy and refrigerant quality at the evaporator inlet and the specific enthalpy at the evaporator outlet. Table 13 summarizes the uncertainty of the major measuring devices used in the test rig.

Table 13 Specification of the different measuring devices used in the roll-bond evaporator test facility.

Devices	**Type**	**Uncertainty** (k=2)	**Range**
Thermometer	T-type thermocouple	± 0.1°C	-30 / 60°C
Mass flow meter	Coriolis effect	± 0.1%	0 / 20 kg/h
Absolute pressure transducer	Strain gage	± 0.15% f.s.	0 / 30 bar
Data logger	20 channels Multiplexer 6½ digit Multimeter	± 2.7 μV	0 / 100 mV
Thermo camera	IR analysis	± 0.1°C	-20 / 250°C

2.3.2 Data reduction

Once steady state conditions in temperature, pressure and refrigerant mass flow are reached, all the data collected are scanned and recorded by a data logger for a set time after which an average value is computed for each parameter.
From the average values of the measurements recorded during the steady state conditions, it is possible to compute the following characteristic parameters:

2.3.2.1 Refrigerant mass flow ratio

$$MFR = \frac{\dot{m}}{\dot{m}_{max}} \qquad \text{Eq. 42}$$

Is the ratio between the refrigerant mass flow rate and the maximum refrigerant mass flow rate achieved in the corresponding set of tests.

2.3.2.2 Refrigerating capacity Q

$$Q = \dot{m}\,(h_{out} - h_{in}) \qquad \text{Eq. 43}$$

where ṁ is the refrigerant mass flow measured by the Coriolis mass flow meter and h_{in} and h_{out} are the specific enthalpies at the inlet and outlet of the roll-bond evaporator respectively.

2.3.2.3 Mean overall heat transfer coefficient K

$$K = \frac{Q}{A\,(t_a - t_r)} \qquad \text{Eq. 44}$$

where A=L x W (Values in
Table 12 12) is the surface area of the whole front face of the evaporator; t_a is the mean value between two T-type thermocouples respectively installed close to the floor and to the ceiling of the climate chamber and t_r is the refrigerant saturation temperature evaluated thanks to Refprop 9.1 (2013)

2.3.2.4 Mean air side heat transfer coefficient α_a

$$\alpha_a = \frac{Q}{A\,(t_a - t_w)} \qquad \text{Eq. 45}$$

where t_w is the mean value of 16 thermocouples positioned on the rear face of the roll-bond evaporator. Also in this case the area A=L x W (Values in Table 12) is the frontal surface of the evaporator.

2.3.2.5 Mean refrigerant side heat transfer coefficient α_r

It derives from the overall heat transfer coefficient, assuming no fouling resistances and neglecting the wall resistance:

$$\alpha_r = \frac{1}{\left(\frac{1}{K} - \frac{1}{\alpha_a}\right)\left(\frac{A}{A_t}\right)} \qquad \text{Eq. 46}$$

where A_t is the plate surface occupied by the tube in which the refrigerant flows.

2.4 Heat pipe finned heat exchanger

2.4.1 Experimental facility

The experimental rig, shown in Figure 18, consists of two air lines, one for the exhaust air and one for the supply air, linked by a HPFHE. Each line prepare the air for the requiring inlet testing conditions at the inlet of the heat exchanger. So, the ambient air flow rate is modulate by a variable speed fan, then it can be cooled and dehumidified in a fin and coil heat exchanger, heated by electric heating elements and humidified by a steam injection system. The exhaust and the supply air streams pass through the tested heat exchanger where the heat transfer takes place and then they are discharged. Both the air lines contain two measurement sections located at the inlet and at the outlet of the regenerative HPFHE where temperature and humidity ratio are measured.

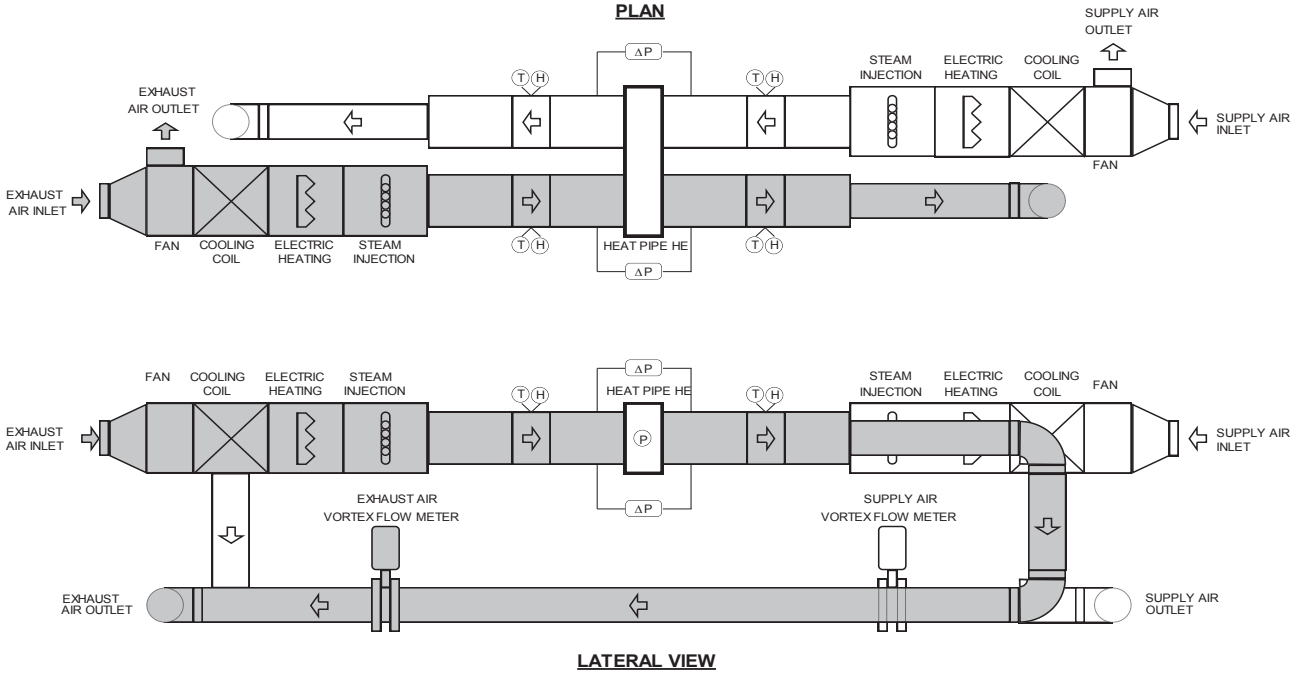

Figure 18 HPFHE experimental facility scheme.

Each measuring section consists of four T-type thermocouples (uncertainty (*k*=2) within ±0.1 K) and a humidity tap connected to a dew point temperature probe (uncertainty (*k*=2) within ±0.2 K). The pressure drops on both sides of the heat exchanger are measured by means of differential strain-gauge pressure transducers (uncertainty (*k*=2) within 0.1% f.s., f.s.=0.04 bar), whereas the air flow rates are measured by vortex-shedding flow meters (uncertainty (*k*=2) within ±1.0% of the reading.). A barometer (uncertainty (*k*=2) within ±0.08% f.s.) measures the absolute atmospheric pressure. The refrigerant pressure inside the third row of heat pipes is measured by means of an absolute strain-gage pressure transducer (uncertainty (*k*=2) within 0.075% f.s., f.s.=10 bar). All the readings are scanned by a data acquisition system consisting of a 20 channel switch unit and a 6½ digit multimeter (uncertainty (*k*=2) within ±2.7 μV) and then recorded.

Table 14 gives the uncertainties (k=2) of the different measuring devices in the experimental rig.

The HPFHE tested (Figure 19 is a heat pipe fin and coil consisting of 12.7 mm copper microfin tubes and aluminum fins divided into two sections on the air side by a 160 mm separation panel which separates completely the exhaust air flow from the supply air flow. All the tubes are filled up with a two-phase fluid: in present experimentation R-152a was tested. The refrigerant charge was set in accordance with the recommendation by Reay and Kew (2006) for a proper charge of the heat pipes.

Table 14. Specification of the different measuring devices used in the heat pipe finned heat exchanger test facility.

Measurement device	**Uncertainty (**k=2**)**
t-type thermocouple	±0.1 K
dew point temperature probe	±0.2 K
differential strain-gauge pressure transducers	0.1% f.s., f.s.=0.04 bar
vortex-shedding flow meter	±1.0% of the reading
barometer	±0.08% f.s.
absolute strain-gage pressure transducer	0.075% f.s., f.s.=10 bar
Multi-meter	±2.7 μV

Table 15 provide the main geometrical characteristics of the tested HPFHE. The heat pipes are perfectly horizontal and the back flow of the condensate is governed only by the capillary forces acting along the spiral grooves of the microfin in-tube surface.

Table 15 HPFHE main features.

Specification	**Unit**	**Measure/type**
Enhanced tube type		microfin
Tube material		copper
Tube outside diameter d_{ext}	mm	12.70
Number of grooves n_g		65
Groove depth h_g	mm	0.20
Helix angle β_g	°	18
Total tube length L_t	mm	700
Effective tube length L_t'	mm	540
Number of rows n_r		6
Number of tubes per row n_t		9
Tube pitch l_t	mm	30
Row pitch l_r	mm	26
Fin type		corrugated
Fin material		aluminum
Fin thickness s_f	mm	0.115
Fin pitch l_f	mm	3
Supply air side dimension	mm	270 × 270
Exhaust air side dimension	mm	270 × 270

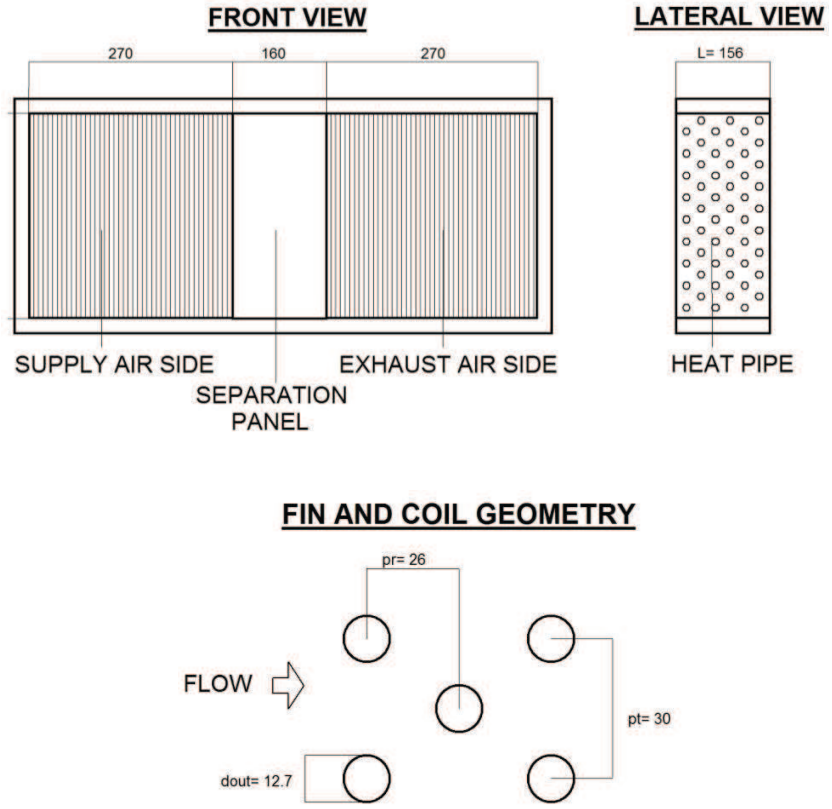

Figure 19 Scheme of the HPFHE geometry and of the heat pipes positioning.

Temperature, humidity ratio, and flow rate of the exhaust and supply air streams at the inlet of the regenerative heat pipe heat exchanger are adjusted to obtain the desired inlet conditions. Once steady state conditions in temperature, humidity ratio, and flow rate at the heat pipe heat exchanger inlet and outlet on both the supply and exhaust air sides are reached, all values are recorded for a set time after which an average value is computed for each recorded parameter.

2.4.2 Data reduction

From the average values of the measurements recorded during the steady state conditions, it is possible to compute the following characteristic parameters.

2.4.2.1 Sensible Heat Recovery Q

$$Q_{\text{supply}} = m_{\text{supply}} c_{p_{\text{supply}}} |T_{supply_{out}} - T_{supply_{in}}| \quad \text{Eq. 47}$$

$$Q_{exh} = m_{exh} c_{p_{exh}} |T_{exh_{out}} - T_{exh_{in}}| \quad \text{Eq. 48}$$

$$Q = \frac{(Q_{\text{supply}} + Q_{exh})}{2} \quad \text{Eq. 49}$$

where s_{upply} and m_{exh} are the supply and the exhaust air mass flow rates measured by the vortex-shedding flow meter, $c_{\text{p.supply}}$ and $c_{\text{p.exh}}$ are the supply and the exhaust air specific heat capacities and $T_{\text{supply.in}}$ and $T_{\text{supply.out}}$ and $T_{\text{exh.in}}$ and $T_{\text{exh.out}}$ are the supply and the exhaust air temperatures at the inlet and outlet of the regenerative heat exchanger measured by the installed thermocouples. During the experimental tests the average absolute misbalance between the supply and the exhaust air side is always lower than 7.0% with an average absolute value of 2.2%.

2.4.2.2 Sensible Thermal Effectiveness ε

$$\varepsilon = \frac{MAX\,[\,|T_{supply_{out}} - T_{supply_{in}}|\,,|T_{exh_{out}} - T_{exh_{in}}|\,]}{|T_{supply_{in}} - T_{exh_{in}}|} \quad \text{Eq. 50}$$

which depends on the ratio between the heat capacity rates

$$C_{min} = MIN\,[m_{\text{supply}} c_{p_{\text{supply}}}, m_{exh} c_{p_{exh}}\,] \quad \text{Eq. 51}$$

$$C_{max} = MAX\,[m_{\text{supply}} c_{p_{\text{supply}}}, m_{exh} c_{p_{exh}}\,] \quad \text{Eq. 52}$$

and the number of transfer units

$$NTU = \frac{K\,A}{C_{min}} \quad \text{Eq. 53}$$

$$K\,A = \frac{Q}{\Delta T_{ln}} \quad \text{Eq. 54}$$

$$\Delta T_{ln} = \frac{(T_{supply_{in}} - T_{exh_{out}}) - (T_{supply_{out}} - T_{exh_{in}})}{ln \frac{(T_{supply_{in}} - T_{exh_{out}})}{(T_{supply_{out}} - T_{exh_{in}})}} \quad \text{Eq. 55}$$

(10)

2.4.2.3 Fanning friction factor *f*

$$f = \frac{\Delta p}{4 \frac{L}{d_h} \frac{\rho w^2}{2}} \quad \text{Eq. 56}$$

where Δp_{supply} and Δp_{exh} are the pressure drop measured by the differential pressure transducers, L=156 mm is the depth and d_h=3.561 mm the hydraulic diameter of the fin and coil, ρ_{supply} and ρ_{exh} the average density and w_{supply} and w_{exh} the incoming face velocity of the supply and exhaust air. The Fanning friction factor f depends on the Reynolds number:

$$Re = \frac{\rho w d_h}{\mu} \quad \text{Eq. 57}$$

where μ stays for μ_{supply} or μ_{exh} (i.e. the average dynamic viscosity of the supply or the exhaust air).

2.4.2.4 Average saturation temperature of the refrigerant within the pipes

$T_{ref}=T_{sat}(p_{ref})$ Eq. 58

where p_{ref} is the refrigerant pressure measured by the absolute pressure transducer installed on the third row of pipes. The refrigerant properties are evaluated by Refprop 9.1 (2013).

All the experimental tests conducted refer directly to the sensible heat recovery and the sensible thermal effectiveness, as the operating conditions on both the supply and the exhaust air sides are always far from saturation conditions.

The instrumentation, the procedures and the data reduction techniques used in present work are consistent with the AHRI Standard 410 (2001) and the ANSI/ASHRAE Standard 33 (2000) for testing air-to-air heat exchangers.

3 Analysis of the results

3.1 Horizontal smooth tube

3.1.1 Experimental results

The vaporization process inside a smooth tube having an inner diameter D equal to 4 mm has been experimentally investigated. Two couples of refrigerants: R410A and R32, and R134a and R1234ze(E) have been tested during vaporization in counter-flow against water at four different saturation temperatures, 5, 10, 15, and 20 °C.

During this experimental campaign 108 data points were collected with R410A as refrigerant, 185 points with R32,108 with R134a, and 131 with R1234ze(E) under similar operating conditions.

The vaporization process inside the tube was studied at three different saturation levels. R401A and R32 were investigated at 20 °C, 10 °C and 5 °C of saturation temperature, while R134a and R1234ze(E) at 20 °C, 15 °C and 5 °C. The mass flux was varied from 200 kg m^{-2} s^{-1} to 800 kg m^{-2} s^{-1} for the first couple (R410A and R32) while from 200 kg m^{-2} s^{-1} to 600 kg m^{-2} s^{-1} for the second couple (R134a and R1234ze(E)). Finally, the heat flux was varied from 12 W m^{-2} to 51 W m^{-2} for the first couple while from 15 W m^{-2} to 30 W m^{-2} for the second couple.

The experimental tests were managed in order to separate the contribution of heat flux, refrigerant mass flux, and mean vapor quality. Therefore firstly, at each saturation temperature and constant refrigerant mass flux, four different heat fluxes were set at increasing mean vapor quality up to incipient dryout. Secondly, at each saturation temperature and constant heat flux, four different refrigerant mass fluxes were applied at increasing mean vapor quality up to incipient dryout.

Table 16 sums up the limit operating conditions obtained during the four refrigerants vaporization in terms of: refrigerant saturation temperature t_{sat} and pressure p_{sat}, mean vapor quality x_m, refrigerant mass flux G, and heat flux q.

The final results of a detailed error analysis performed in accordance with Kline and McClintock (1953) were reported in Table 17 in terms of refrigerant heat transfer coefficient and of total pressure drop measurement (k=2).

Table 16 Operating conditions during refrigerant vaporization in a horizontal smooth tube.

Fluid	**R32**	**R410A**	**R1234ze(E)**	**R134a**
Runs	185	108	131	108
$\mathbf{t_{sat}}$ [°C]	4.8–20.2	4.8–20.2	9.8-20.2	9.8-20.2
$\mathbf{p_{sat}}$ [MPa]	0.95-1.48	0.93-1.45	0.31-0.46	0.42-0.59
$\mathbf{x_m}$ [-]	0.06–0.90	0.09-0.87	0.11-0.97	0.10-0.95
G [kg $m^{-2}s^{-1}$]	196.1-821.3	199.1-810.2	196.2-597.7	200-609
q [kW m^{-2}]	12.0–51.6	11.7-51.4	14.7-30.8	10.6-30.6

Table 17 Refrigerant Heat Transfer Coefficient (HTC) and total pressure drop overall uncertainty obtained with the Kline and McClintock (1953) procedure for the four refrigerants tested.

Fluid	**Refrigerant HTC**	**Total pressure drop**
R410A	±6.3%	±14.4%
R32	±7.5%	±13.7%
R134a	±5.8%	±19.4%
R1234ze(E)	±6.1%	±20.7%

3.1.1.1 Heat transfer coefficient

3.1.1.1.1 R410A

Figure 20, Figure 21, and Figure 22 show the average refrigerant Heat Transfer Coefficient (HTC) plotted against mean vapor quality at constant refrigerant mass flux (G=400 kg m^{-2} s^{-1}) and four different heat fluxes (q=12, 25, 38, and 51 kW m^{-2}) at 5, 10, and 20 °C of saturation temperature, respectively.

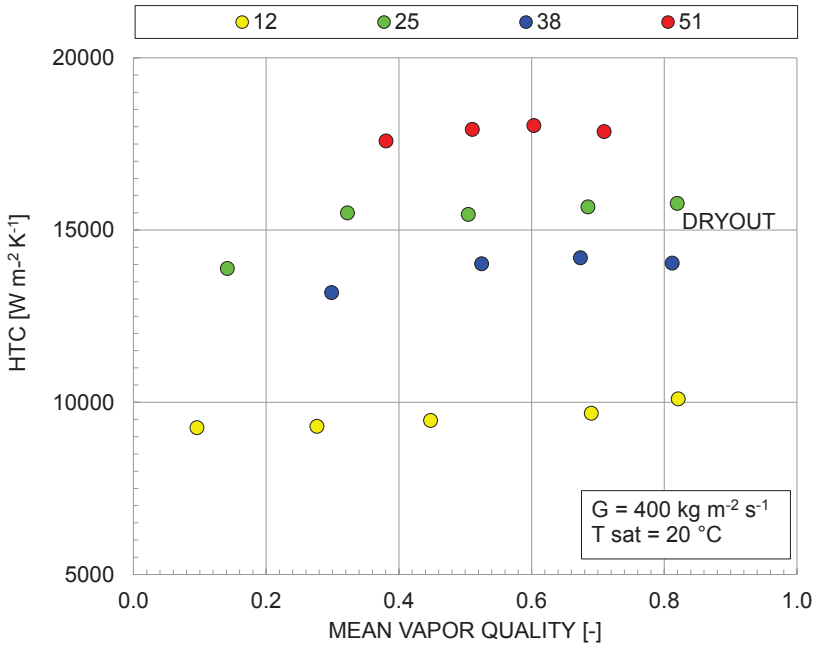

Figure 20 R410A Heat Transfer Coefficient (HTC) vs. mean vapor quality as a function of the heat flux (kW m^{-2}) at fixed mass flux G=400 kg m^{-2} s^{-1}and saturation temperature t_{sat}=20 °C.

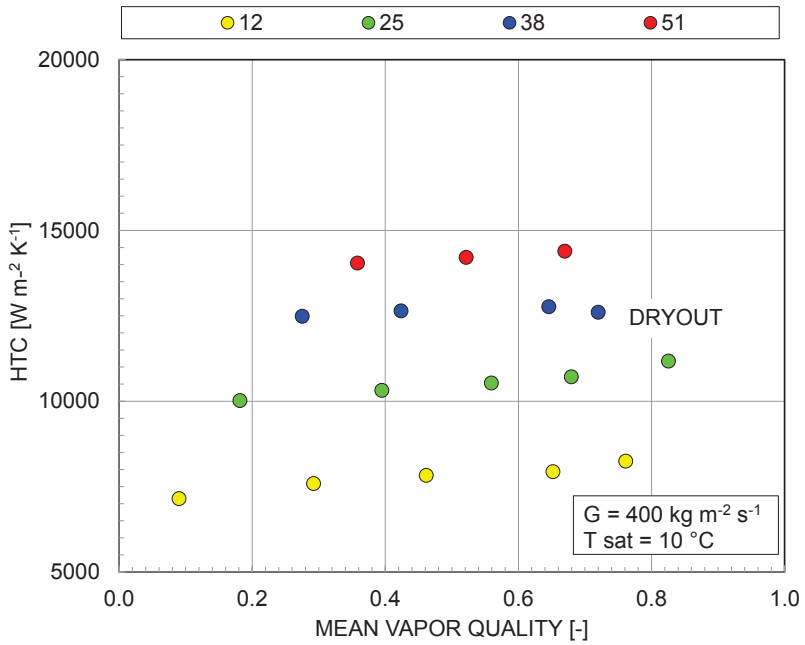

Figure 21 R410A Heat Transfer Coefficient (HTC) vs. mean vapor quality as a function of the heat flux (kW m^{-2}) at fixed mass flux G=400 kg m^{-2} $s^{-1}$and saturation temperature t_{sat}=10 °C.

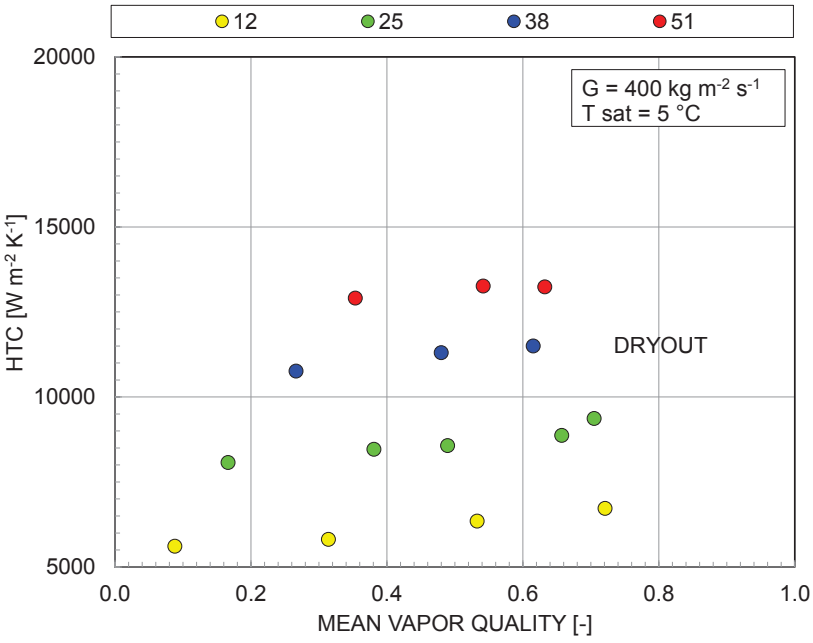

Figure 22 R410A Heat Transfer Coefficient (HTC) vs. mean vapor quality as a function of the heat flux (kW m^{-2}) at fixed mass flux G=400 kg m^{-2} s^{-1} and saturation temperature t_{sat}=5 °C.

The heat transfer coefficient is strongly influenced by the heat flux. Doubling the heat flux (from 25 to 50 kW m^{-2}), the refrigerant HTC increases around 30% at 20 °C of saturation temperature, 35% at 10 °C, and 50% at 5 °C. The HTC is poorly affected by the mean vapor quality: it slightly increases at the increasing of the vapor quality especially at low heat fluxes and low saturation temperatures (for instance, +20% going from x_m=0.1 to x_m=0.7 at q=12 kW m^{-2} and t_{sat}=5 °C).
The onset of dryout appears at lower vapor qualities with higher heat fluxes and it can be depicted from x_m=0.60 to x_m=0.82.

Figure 23, Figure 24, and Figure 25 show the average Heat Transfer Coefficient (HTC) plotted against mean vapor quality at constant heat flux (q=25 kW m^{-2}) and four different refrigerant mass fluxes (G=200, 400, 600, and 800 kg m^{-2} s^{-1}) at 5, 10, and 20 °C of saturation temperature, respectively.

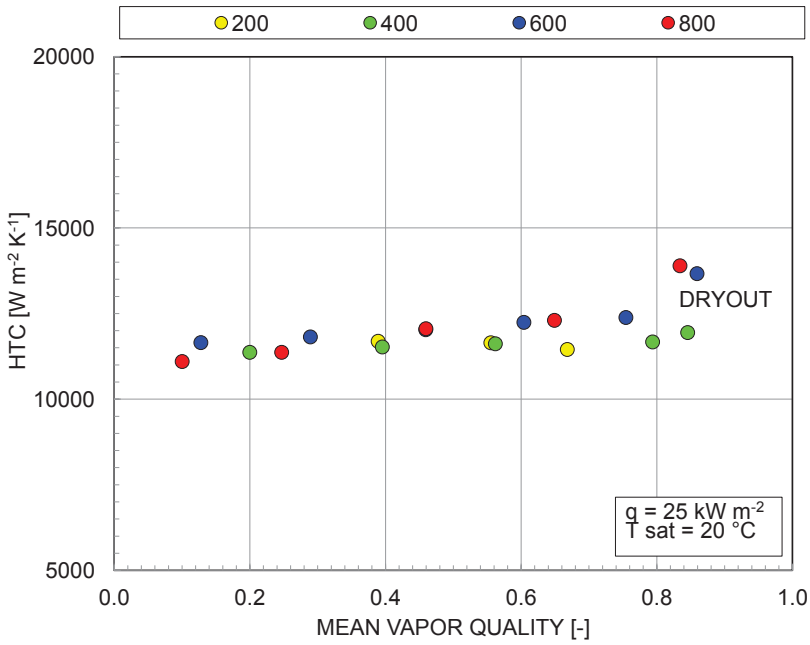

Figure 23 R410A Heat Transfer Coefficient (HTC) vs. mean vapor quality as a function of the mass flux (kg m^{-2} s^{-1}) at fixed heat flux q=25 kW m^{-2} and saturation temperature t_{sat}=20 °C.

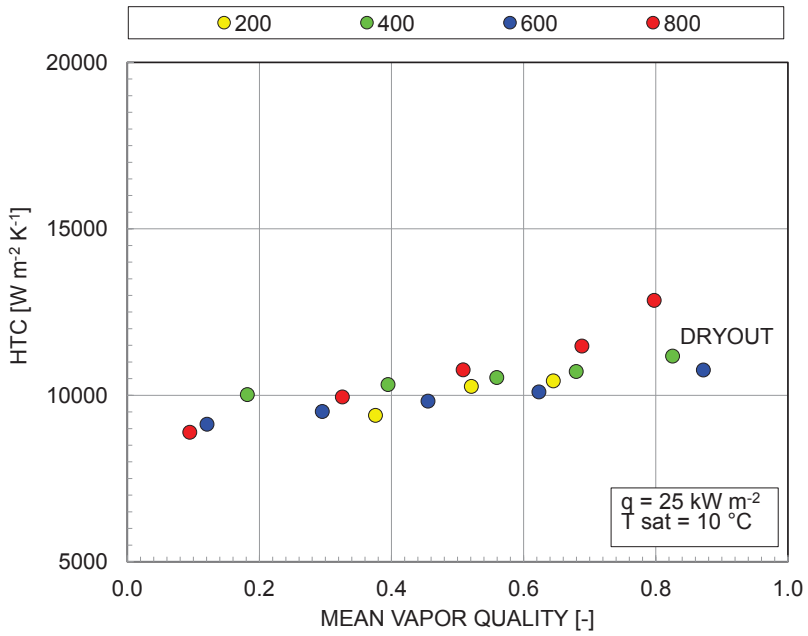

Figure 24 R410A Heat Transfer Coefficient (HTC) vs. mean vapor quality as a function of the mass flux (kg m^{-2} s^{-1}) at fixed heat flux q=25 kW m^{-2} and saturation temperature t_{sat}=10 °C.

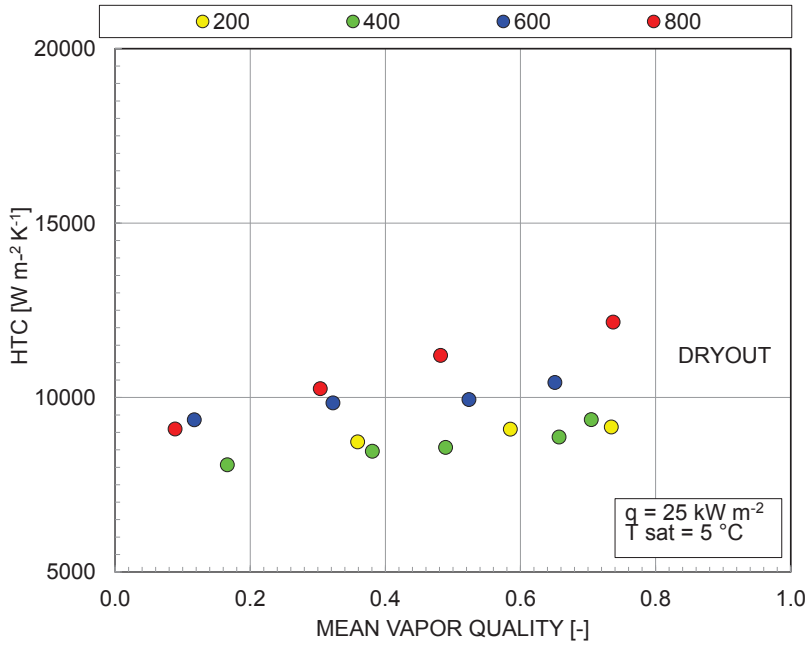

Figure 25 R410A Heat Transfer Coefficient (HTC) vs. mean vapor quality as a function of the mass flux (kg m^{-2} s^{-1}) at fixed heat flux q=25 kW m^{-2} and saturation temperature t_{sat}=5 °C.

The heat transfer coefficient is weakly influenced by the mass flux, especially at high saturation temperatures where the nucleate boiling is the dominating heat transfer mechanism. At 5 °C of saturation temperature (Figure 25) the HTC increases of around 30% when doubling the mass flux (from G=400 kg m^{-2} s^{-1} to G=800 kg m^{-2} s^{-1}). In addition, the refrigerant HTC slightly increases at the increasing of the vapor quality especially at high mass fluxes and low saturation temperatures where it is possible to appreciate the convective boiling contribution that takes place thanks to the higher flow velocity and the lower vapor density (for instance, +35% going from x_m=0.1 to x_m=0.73 at G=800 kg m^{-2} s^{-1} and t_{sat}=5 °C).

The onset of dryout is not hardly influenced by the refrigerant mass flux and it appears from x_m=0.68 to x_m=0.87.

Finally a comparison as a function of the saturation temperature is going to be made.

Figure 26 and Figure 27 present the heat transfer coefficient at a fixed heat flux (q=25 kW m^{-2}) and fixed mass flux (G=200 kg $m^{-2}s^{-1}$ and G=800 kg $m^{-2}s^{-1}$, respectively) as a function of the saturation temperature that ranges from 20 °C to 5 °C.

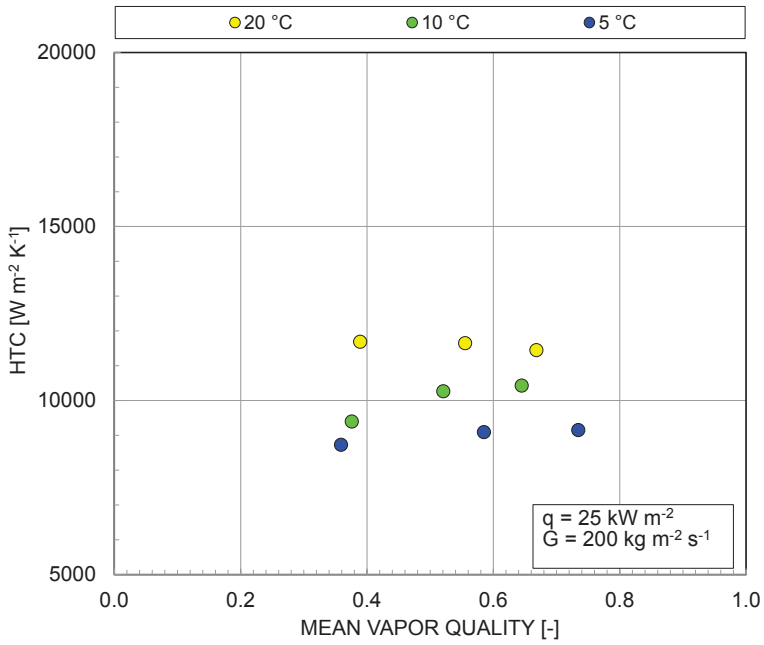

Figure 26 R410A Heat Transfer Coefficient (HTC) vs. mean vapor quality as a function of the saturation temperature at fixed mass flux G=200 kg m^{-2} $s^{-1}$and heat flux q=25 kW m^{-2}.

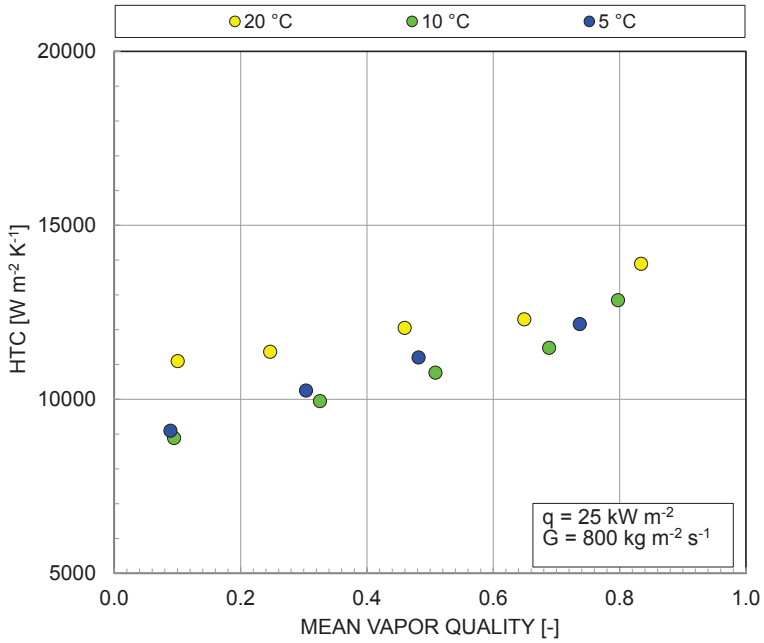

Figure 27 R410A Heat Transfer Coefficient (HTC) vs. mean vapor quality as a function of the saturation temperature at fixed mass flux G=800 kg m^{-2} s^{-1} and heat flux q=25 kW m^{-2}.

At low refrigerant mass fluxes (Figure 26) the heat transfer is governed by nucleate boiling. In fact, as presented in the introduction (see paragraph 1.4.1) the heat transfer coefficient is lightly affected by the vapor quality. This can be appreciated especially at high saturation temperatures where the density is higher and the HTC slightly decreases with the increasing of the mean vapor quality. Due to nucleate boiling plays an important role into the heat transfer, the HTC is also influenced by the saturation temperature and it increases when the saturation temperature increases (+35% passing from t_{sat}=5 °C to t_{sat}=20 °C).

On the other hand, when the refrigerant mass flux is high (Figure 27) the convective mechanism starts to become more influent and its effects characterize especially the low saturation temperatures where the HTC is growing with the vapor quality. In addition the HTC is less affected by the saturation temperature, especially at high vapor qualities (from +8% to +22% when passing from t_{sat}=5 °C to t_{sat}=20 °C).

Figure 28 and Figure 29 present the heat transfer coefficient at a fixed heat flux (q=12 kW m^{-2} and q=50 kW m^{-2}, respectively) and fixed mass flux (G=400 kg $m^{-2}s^{-1}$) as a function of the saturation temperature that ranges from 20 °C to 5 °C.

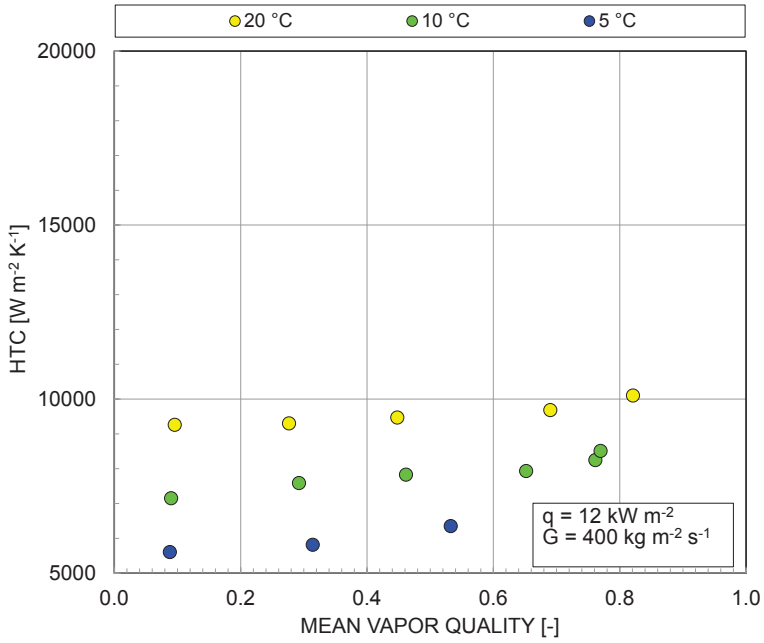

Figure 28 R410A Heat Transfer Coefficient (HTC) vs. mean vapor quality as a function of the saturation temperature at fixed mass flux G=400 kg m^{-2} s^{-1} and heat flux q=12 kW m^{-2}.

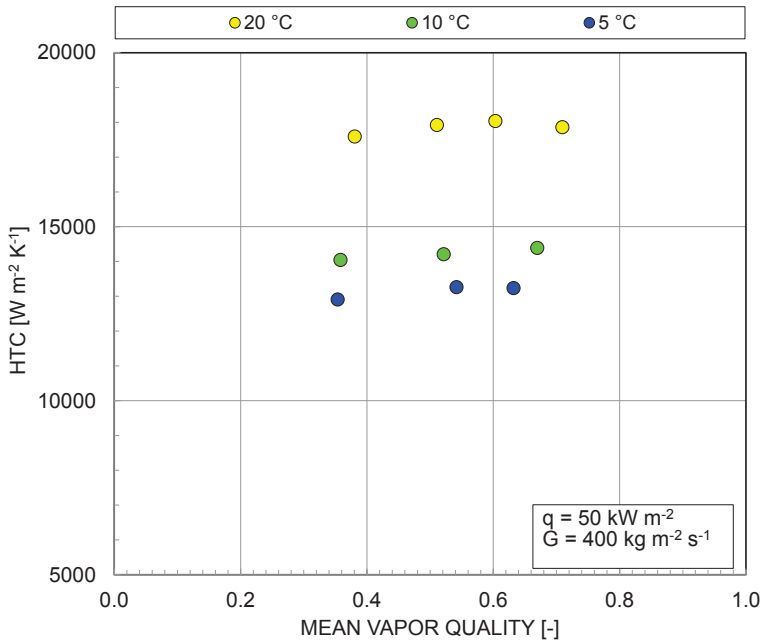

Figure 29 R410A Heat Transfer Coefficient (HTC) vs. mean vapor quality as a function of the saturation temperature at fixed mass flux G=400 kg m^{-2} $s^{-1}$and heat flux q=50 kW m^{-2}.

At a mass flux equal to 400 kg m^{-2} s^{-1}, the nucleate boiling dominates the heat transfer. In fact, as presented in section 1.4.1, the HTC increases with the increasing of the saturation temperature but it is marginally influenced by the mean vapor quality. Only at low heat fluxes (Figure 28) some convective boiling effects are evident, and the HTC lightly increases with the vapor quality (+15% at t_{sat}=5 °C going from x=0.09 to x=0.54).

3.1.1.1.2 R32

Figure 30, Figure 31, and Figure 32 show the average Heat Transfer Coefficient (HTC) plotted against mean vapor quality at constant refrigerant mass flux (G=400 kg m^{-2} s^{-1}) and four different heat fluxes (q=12, 25, 38, and 51 kW m^{-2}) at 5, 10, and 20 °C of saturation temperature, respectively.

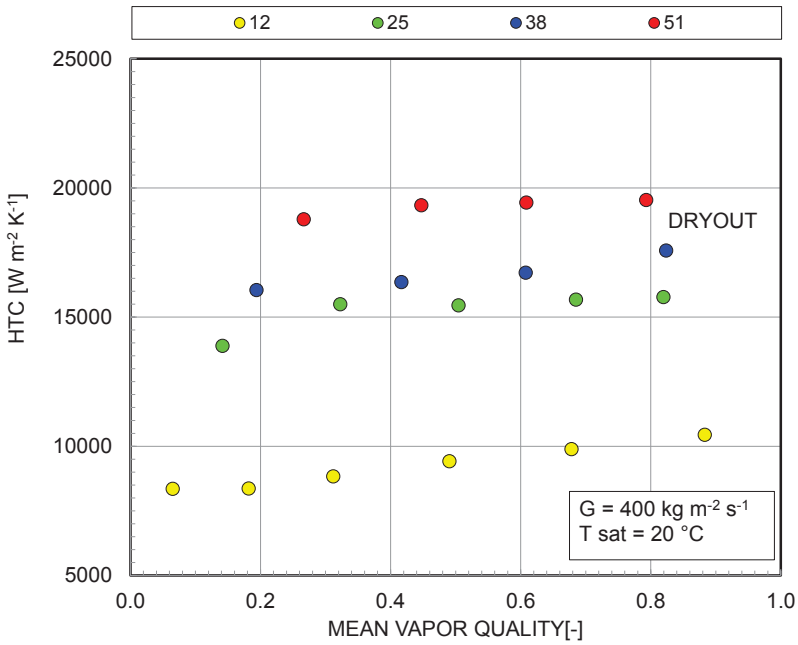

Figure 30 R32 Heat Transfer Coefficient (HTC) vs. mean vapor quality as a function of the heat flux (kW m^{-2}) at fixed mass flux G=400 kg m^{-2} s^{-1} and saturation temperature t_{sat}=20 °C.

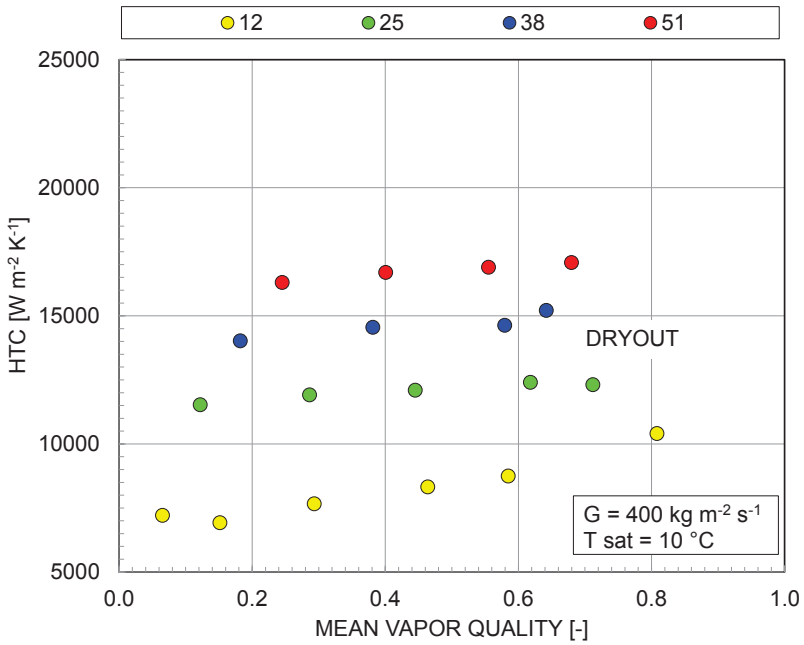

Figure 31 R32 Heat Transfer Coefficient (HTC) vs. mean vapor quality as a function of the heat flux (kW m^{-2}) at fixed mass flux G=400 kg m^{-2} s^{-1} and saturation temperature t_{sat}=10 °C.

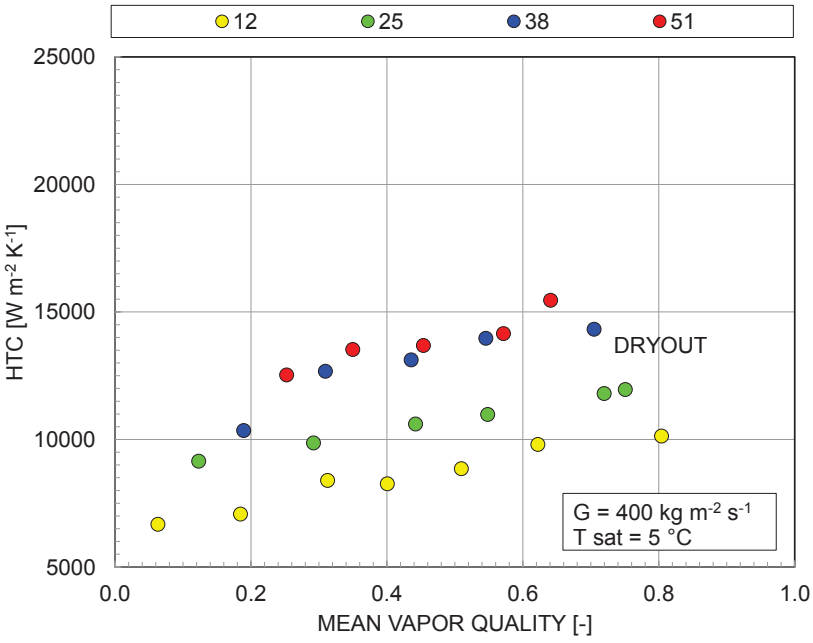

Figure 32 R32 Heat Transfer Coefficient (HTC) vs. mean vapor quality as a function of the heat flux (kW m^{-2}) at fixed mass flux G=400 kg m^{-2} s^{-1} and saturation temperature t_{sat}=5 °C.

As presented for R410A in section 3.1.1.1.1, the heat transfer coefficient is deeply affected by the heat flux. When doubling the heat flux (from 25 to 50 kW m^{-2}), the refrigerant HTC increases around +25% – 35% and +90% – 120% when the heat flux becomes 4 times higher (from 12 to 50 kW m^{-2}).

The HTC is influenced by the mean vapor quality at low heat fluxes and low saturation temperatures due to a convective boiling contribution to heat transfer (for instance, +45% going from x_m=0.07 to x_m=0.8 at q=12 kW m^{-2} and t_{sat}=5 °C) but at higher heat fluxes and higher saturation temperatures the HTC sensitivity to vapor quality becomes negligible and the nucleate boiling remains the predominant heat transfer mechanism.

The onset of dryout appears at lower vapor qualities with higher heat fluxes and it is included from x_m=0.60 to x_m=0.82.

Figure 33, Figure 34, and Figure 35 show the average Heat Transfer Coefficient (HTC) plotted against mean vapor quality at constant heat flux (q=38 kW m^{-2}) and four different refrigerant mass fluxes (G=300, 400, 600, and 800 kg m^{-2} s^{-1}) of at 5, 10 and 20 °C saturation temperature, respectively.

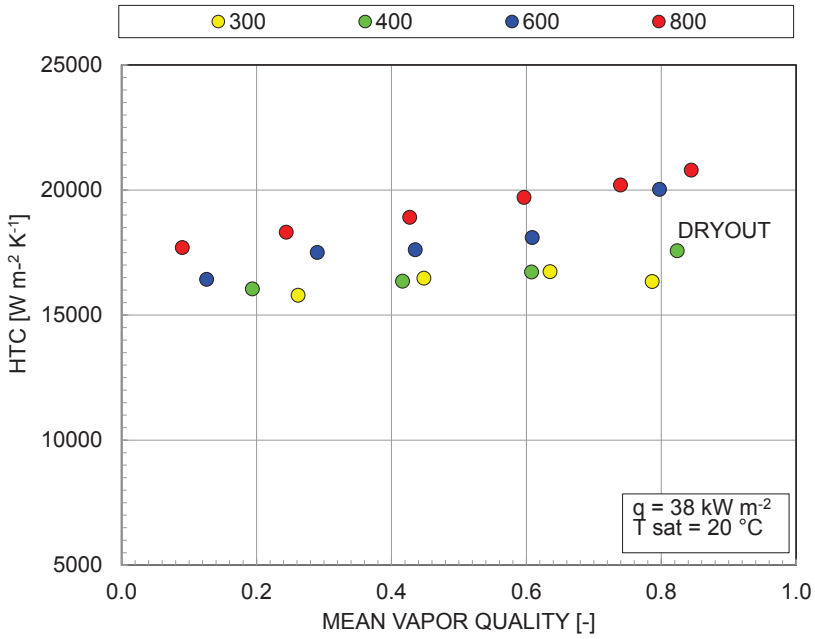

Figure 33 R32 Heat Transfer Coefficient (HTC) vs. mean vapor quality as a function of the mass flux (kg m^{-2} s^{-1}) at fixed heat flux q=38 kW m^{-2} and saturation temperature t_{sat}=20 °C.

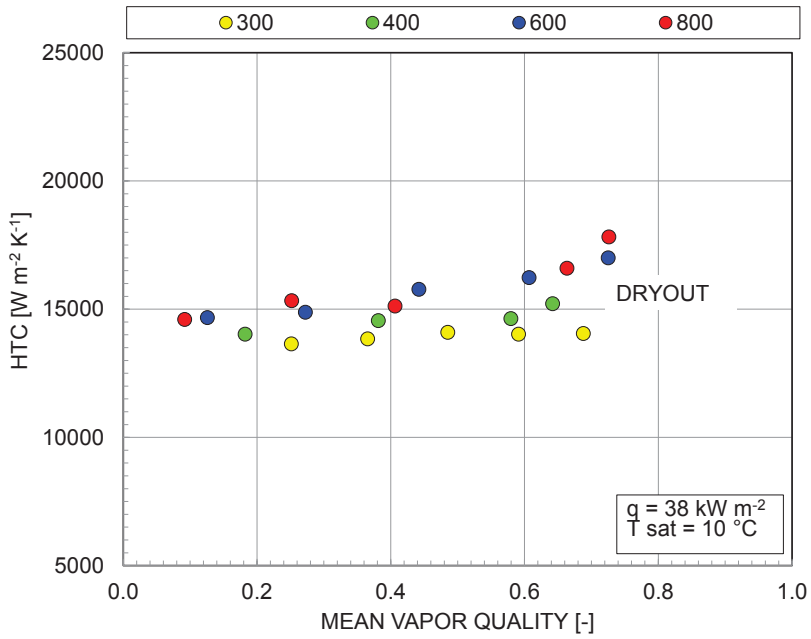

Figure 34 R32 Heat Transfer Coefficient (HTC) vs. mean vapor quality as a function of the mass flux (kg m^{-2} s^{-1}) at fixed heat flux q=38 kW m^{-2} and saturation temperature t_{sat}=10 °C.

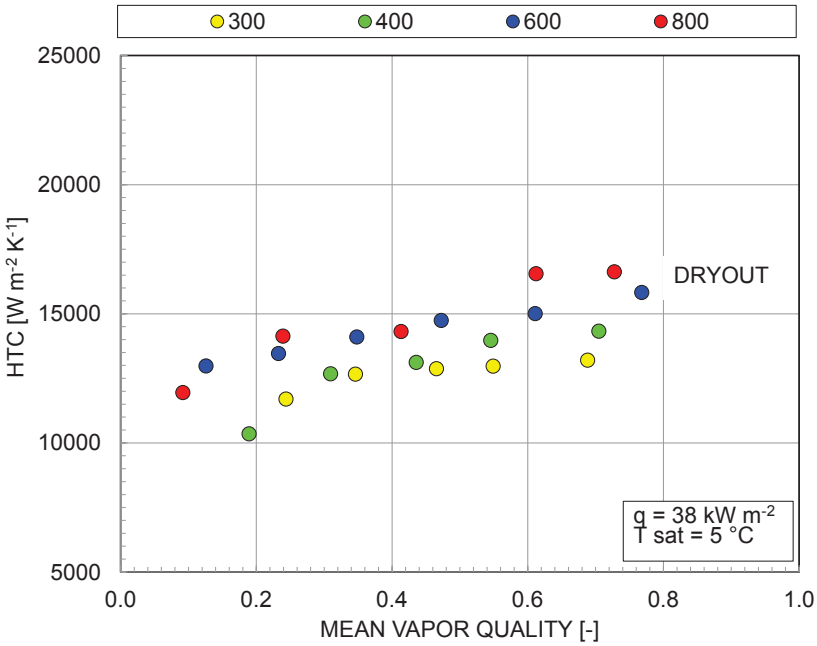

Figure 35 R32 Heat Transfer Coefficient (HTC) vs. mean vapor quality as a function of the mass flux (kg m^{-2} s^{-1}) at fixed heat flux q=38 kW m^{-2} and saturation temperature t_{sat}=5 °C.

It can be noticed a slight influence of the refrigerant mass flux on the HTC, that is up to +25% when the refrigerant mass flux varies from G=400 kg m^{-2} s^{-1} to G=800 kg m^{-2} s^{-1} at t_{sat}=5 °C (Figure 35). HTC is marginally dependent on the vapor quality at low saturation temperature (+10% going from x_m=0.24 to x_m=0.69 at t_{sat}=5 °C and G=800 kg m^{-2} s^{-1}) while at high saturation temperatures the dependency is negligible, so a convective boiling occurs when the pressure is low.

Figure 36, Figure 37, Figure 38 present the average Heat Transfer Coefficient (HTC) plotted against mean vapor quality at constant heat flux (q=25 kW m^{-2}) and four different refrigerant mass fluxes (G=200, 400, 600, and 800 kg m^{-2} s^{-1}) at 5, 10 and 20 °C of saturation temperature, respectively.

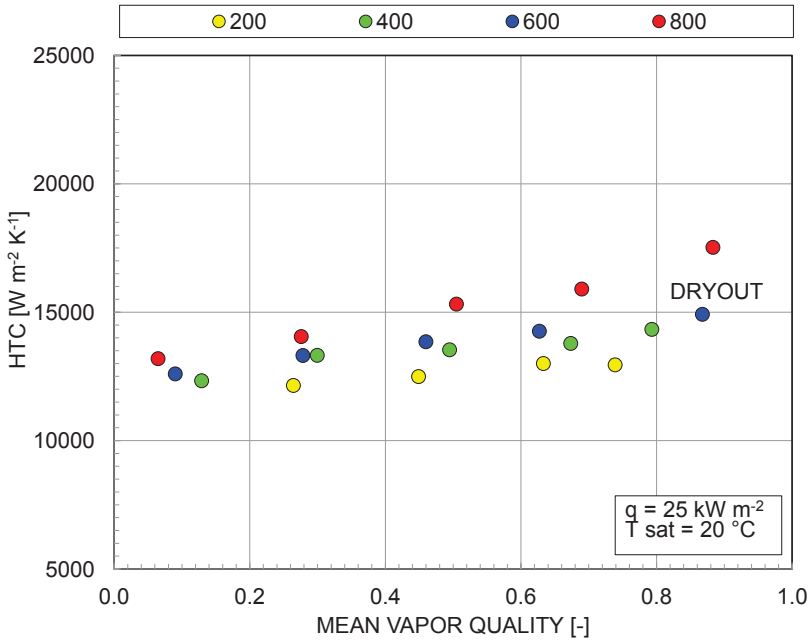

Figure 36 R32 Heat Transfer Coefficient (HTC) vs. mean vapor quality as a function of the mass flux (kg m^{-2} s^{-1}) at fixed heat flux q=25 kW m^{-2} and saturation temperature t_{sat}=20 °C.

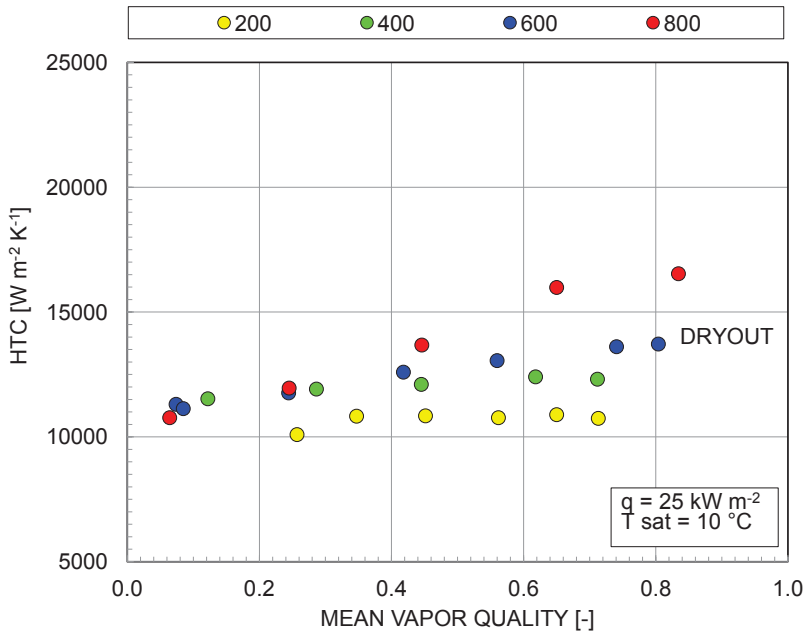

Figure 37 R32 Heat Transfer Coefficient (HTC) vs. mean vapor quality as a function of the mass flux (kg m^{-2} s^{-1}) at fixed heat flux q=25 kW m^{-2} and saturation temperature t_{sat}=10 °C.

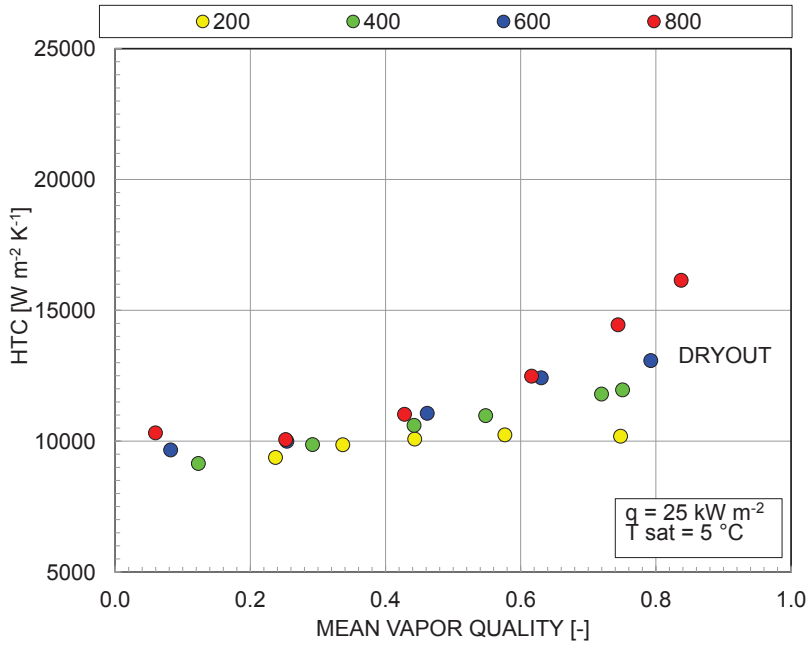

Figure 38 R32 Heat Transfer Coefficient (HTC) vs. mean vapor quality as a function of the mass flux (kg m^{-2} s^{-1}) at fixed heat flux q=25 kW m^{-2} and saturation temperature t_{sat}=5 °C.

The heat transfer coefficient exhibits a low but not negligible sensitivity to mass flux. At 5 °C saturation temperature, the HTC increases of 20% doubling the mass flux (from 400 to 800 kg m^{-2} s^{-1}) and of +40% the mass flux becomes 4 times higher (from 200 to 800 kg m^{-2} s^{-1}). In addition, the refrigerant HTC increases at the increasing of the vapor quality especially at high mass fluxes and low saturation temperatures. (for instance, +60% going from x_m=0.06 to x_m=0.84 at G=800 kg m^{-2} s^{-1} and t_{sat}=5 °C).

By comparing Figure 35, where q=35 kW m^{-2}, to Figure 38, where q=25 kW m^{-2}, it can be highlighted the heat flux effect on the heat transfer mechanism. In fact in Figure 38 the convective boiling effect is higher, especially at high mass fluxes, than in Figure 35 where the nucleate boiling governs the heat transfer. The onset of dryout appears at higher vapor qualities when the mass flux is higher. It ranges from x_m=0.70 to x_m=0.88.

Finally a comparison as a function of the saturation temperature is showed in Figure 39 and Figure 40, which present the heat transfer coefficient at a fixed heat flux (q=25 kW m^{-2}) and fixed mass flux (G=200 kg $m^{-2}s^{-1}$ and G=800 kg $m^{-2}s^{-1}$, respectively) as a function of the saturation temperature that ranges from 20 °C to 5 °C.

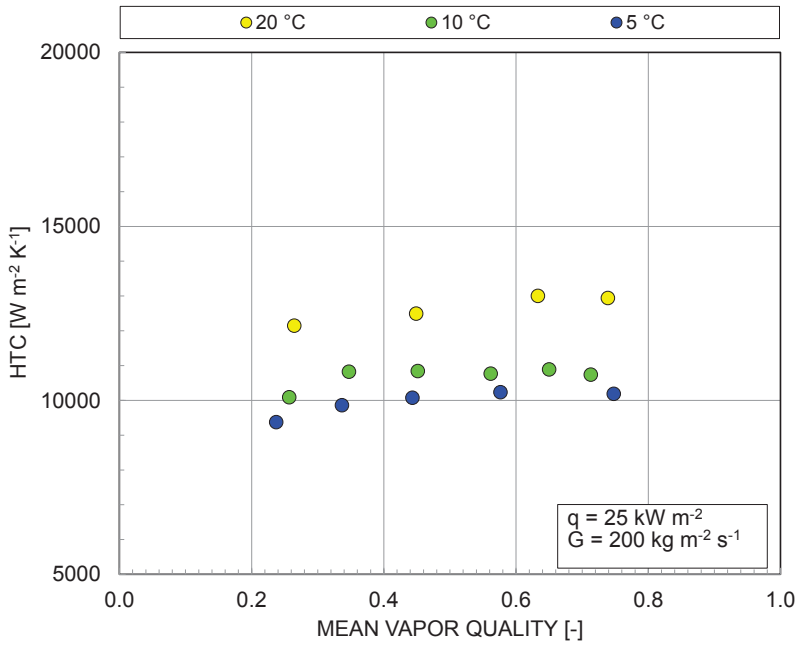

Figure 39 R32 Heat Transfer Coefficient (HTC) vs. mean vapor quality as a function of the saturation temperature at fixed mass flux G=200 kg m^{-2} s^{-1} and heat flux q=25 kW m^{-2}.

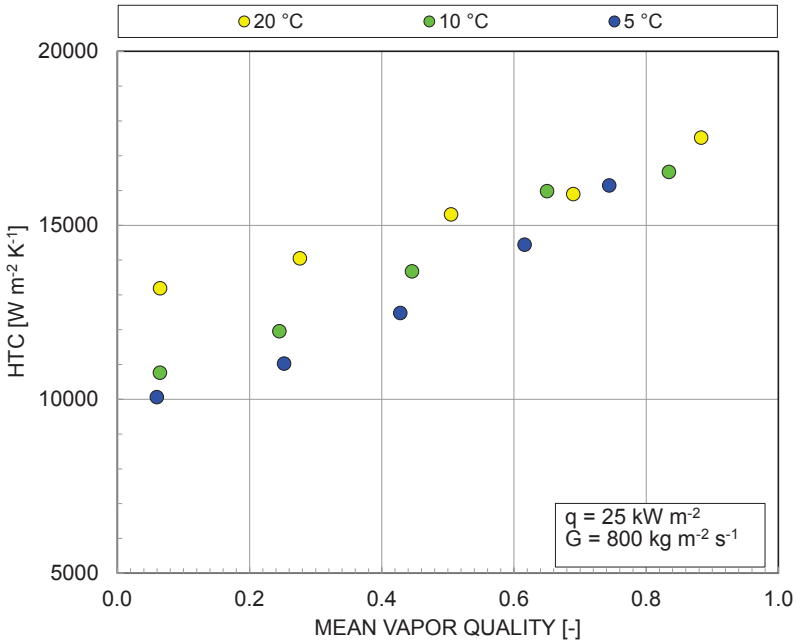

Figure 40 R32 Heat Transfer Coefficient (HTC) vs. mean vapor quality as a function of the saturation temperature at fixed mass flux G=800 kg m^{-2} s^{-1} and heat flux q=25 kW m^{-2}.

The saturation temperature affects the heat transfer inside the 4 mm inner tube. In fact the HTC increases when the saturation temperature increases. In addition, the saturation temperature influences also the heat transfer regime. When it is low, the density is low and thus the velocity inside the tube increases promoting the convective heat transfer (see paragraph 1.4.1). This can be seen in Figure 40 where at low evaporation temperatures the HTC is strongly dependent on the vapor quality (+60% from x=0.05 to x=0.74), while at higher evaporation temperatures this dependence is clearly lower (+22% from x=0.05 to x=0.71).

Figure 41 and Figure 42 present the heat transfer coefficient at a fixed heat flux (q=15 kW m^{-2} and q=30 kW m^{-2}, respectively) and fixed mass flux (G=400 kg $m^{-2}s^{-1}$) as a function of the saturation temperature that ranges from 20 °C to 5 °C.

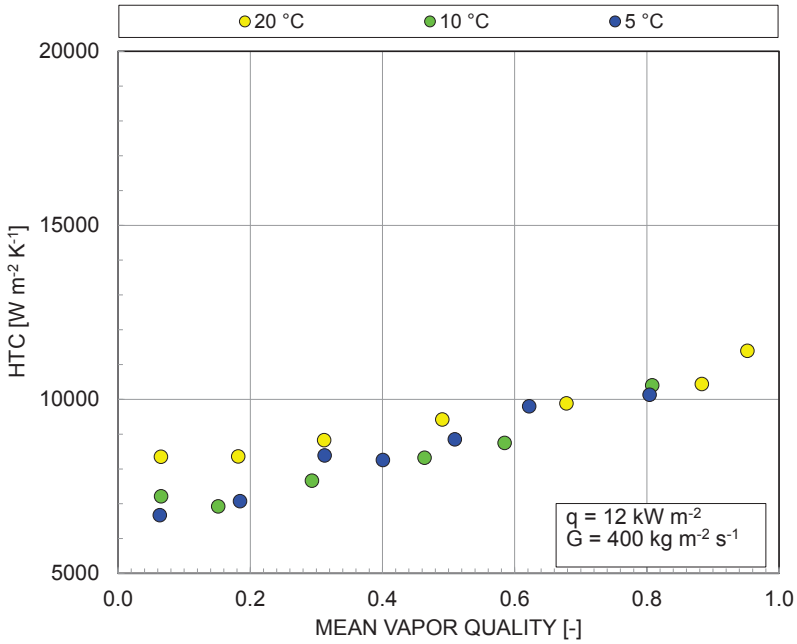

Figure 41 R32 Heat Transfer Coefficient (HTC) vs. mean vapor quality as a function of the saturation temperature at fixed mass flux G=400 kg m^{-2} s^{-1} and heat flux q=12 kW m^{-2}.

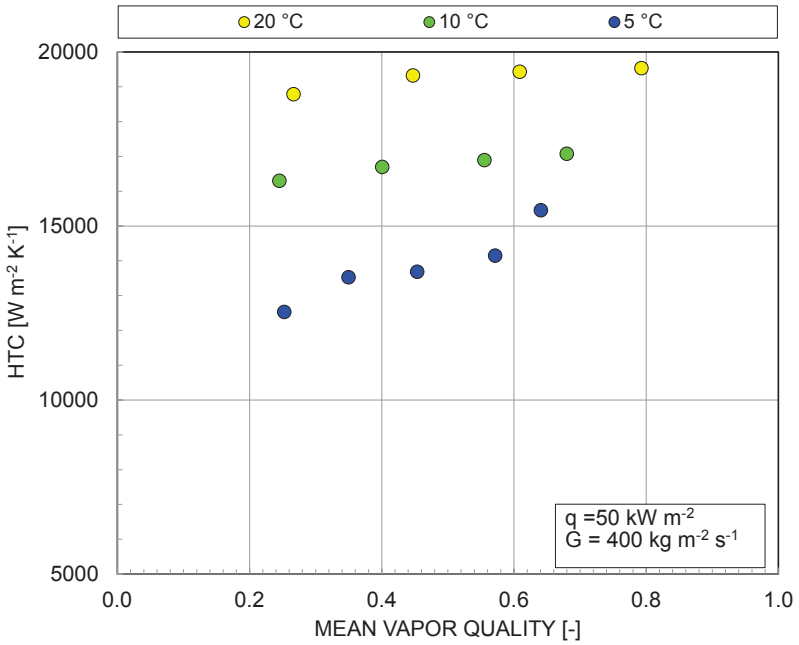

Figure 42 R32 Heat Transfer Coefficient (HTC) vs. mean vapor quality as a function of the saturation temperature at fixed mass flux G=400 kg m^{-2} s^{-1} and heat flux q=50 kW m^{-2}.

Oppositely to R410A (Figure 28, section 3.1.1.1.1), the refrigerant HTC depends on the vapor quality at low heat fluxes and it increases up to 63% going from x=0.06 to x=0.8, so convective boiling occurs. At higher heat fluxes (Figure 42) the nucleate boiling prevails on the convective boiling mechanism; in fact the influence of mass flux on HTC is reduced while the influence of saturation temperature strengthens.

3.1.1.1.3 R134a

Figure 43, Figure 44, and Figure 45 show the average Heat Transfer Coefficient (HTC) plotted against then mean vapor quality at a constant refrigerant mass flux (G=400 kg m^{-2} s^{-1}) at four different heat fluxes (q=15, 20, 25, and 30 kW m^{-2}) at 20 °C, 15 °C, and 10 °C of saturation temperature, respectively.

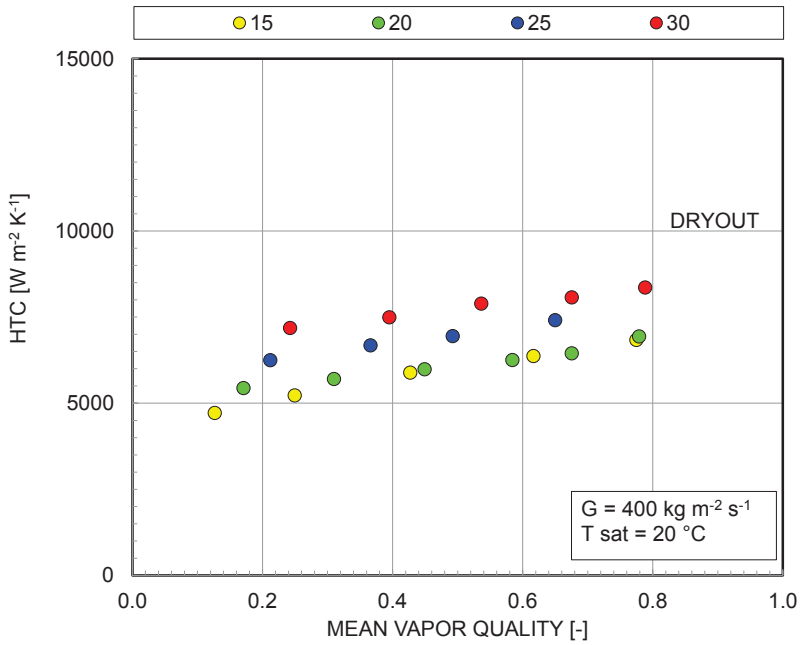

Figure 43 R134a Heat Transfer Coefficient (HTC) vs. mean vapor quality as a function of the heat flux (kW m^{-2}) at fixed mass flux G=400 kg m^{-2} s^{-1} and saturation temperature t_{sat}=20 °C.

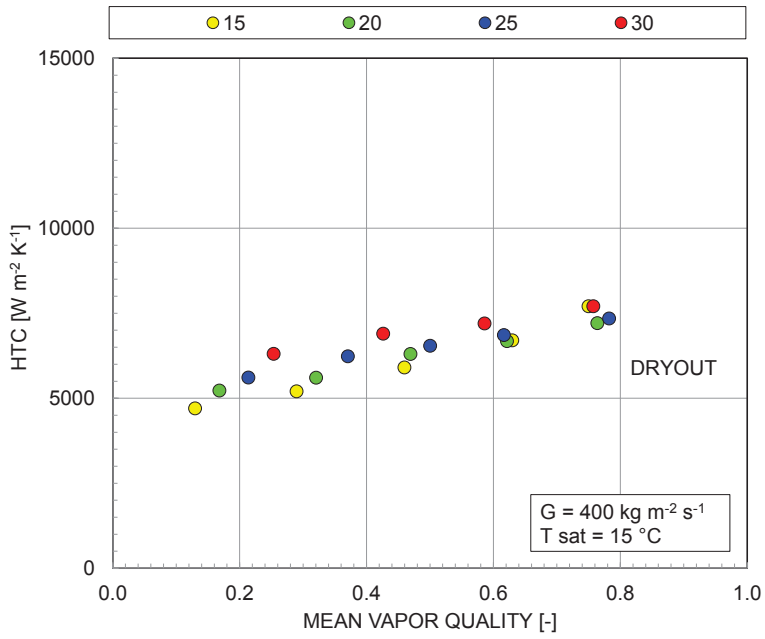

Figure 44 R134a Heat Transfer Coefficient (HTC) vs. mean vapor quality as a function of the heat flux (kW m^{-2}) at fixed mass flux G=400 kg m^{-2} s^{-1} and saturation temperature t_{sat}=15 °C.

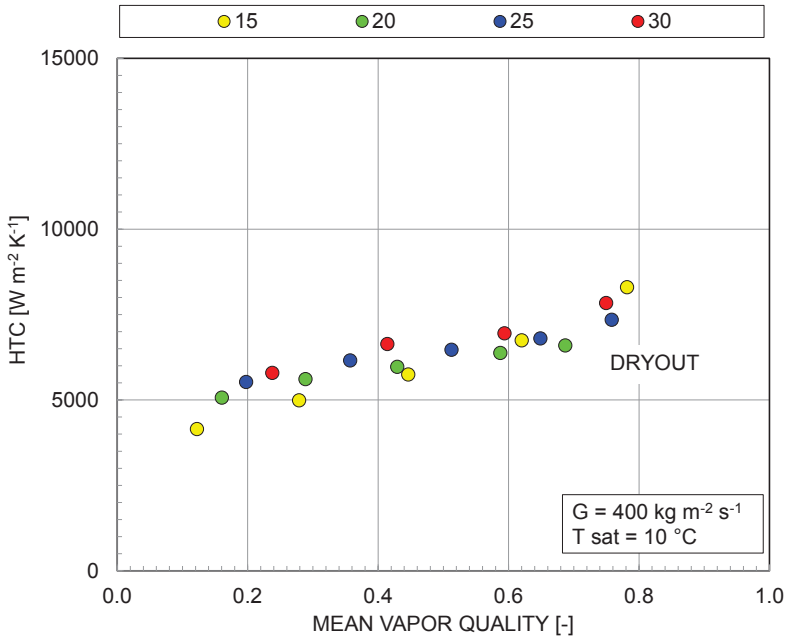

Figure 45 R134a Heat Transfer Coefficient (HTC) vs. mean vapor quality as a function of the heat flux (kW m^{-2}) at fixed mass flux G=400 kg m^{-2} s^{-1} and saturation temperature t_{sat}=10 °C.

The heat transfer coefficient is influenced by the mean vapor quality and this dependence is higher at low saturation temperatures (+46% passing from x=0.13 to x=0.78 at t_{sat}=20°C, Figure 43, and +93% passing from x=0.13 to x=0.78 at t_{sat}=10°C, Figure 45). Beside this the HTC is sensible to the heat flux especially at high saturation temperatures (Figure 43), where it increases up to 40% when doubling the heat flux (from 15 to 30 kW m^{-2}).

These behaviors can be explain thanks to the theory of the heat transfer mechanisms that take place inside a tube during flow boiling (see section 1.4.1). Nucleate boiling is dominant at high saturation temperatures (Figure 43), while at lower saturation temperatures (Figure 45) also convective boiling affects the phase change mechanism.

Figure 46, Figure 47, and Figure 48 show the average Heat Transfer Coefficient (HTC) plotted against the mean vapor quality at a constant heat flux (q=20 kW m^{-2}) and at four different refrigerant mass fluxes (G=200, 300, 400, and 600 kg m^{-2} s^{-1}) at 20 °C, 15 °C, and 10 °C of saturation temperature, respectively.

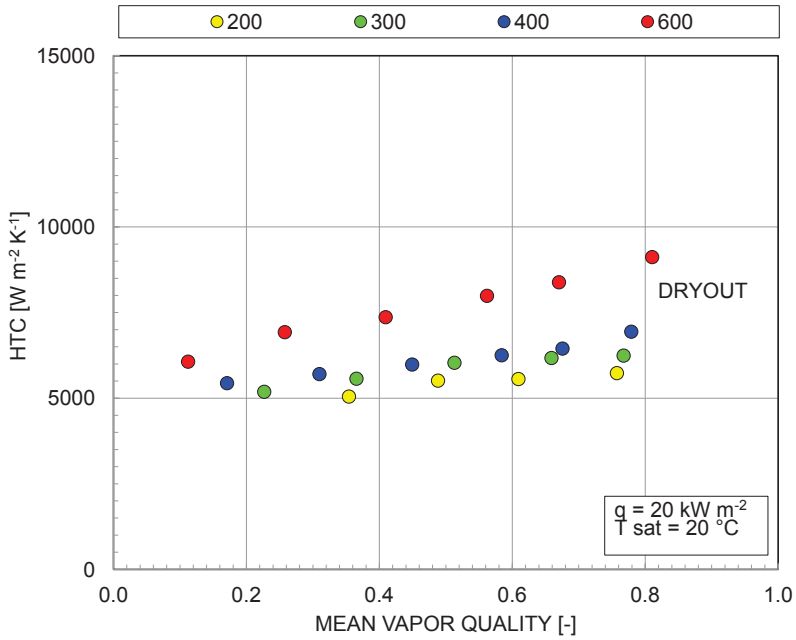

Figure 46 R134a Heat Transfer Coefficient (HTC) vs. mean vapor quality as a function of the mass flux (kg m^{-2} s^{-1}) at fixed heat flux q=20 kW m^{-2} and saturation temperature t_{sat}=20 °C.

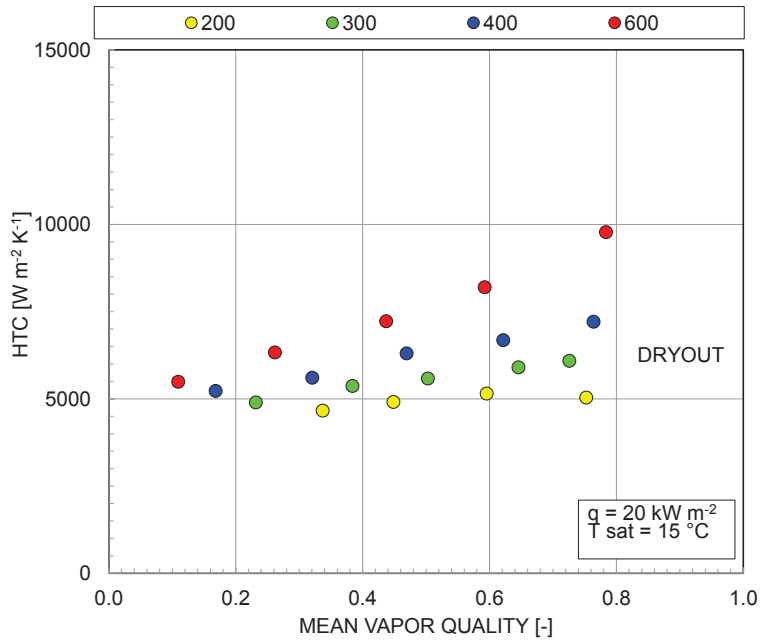

Figure 47 R134a Heat Transfer Coefficient (HTC) vs. mean vapor quality as a function of the mass flux (kg m^{-2} s^{-1}) at fixed heat flux q=20 kW m^{-2} and saturation temperature t_{sat}=15 °C.

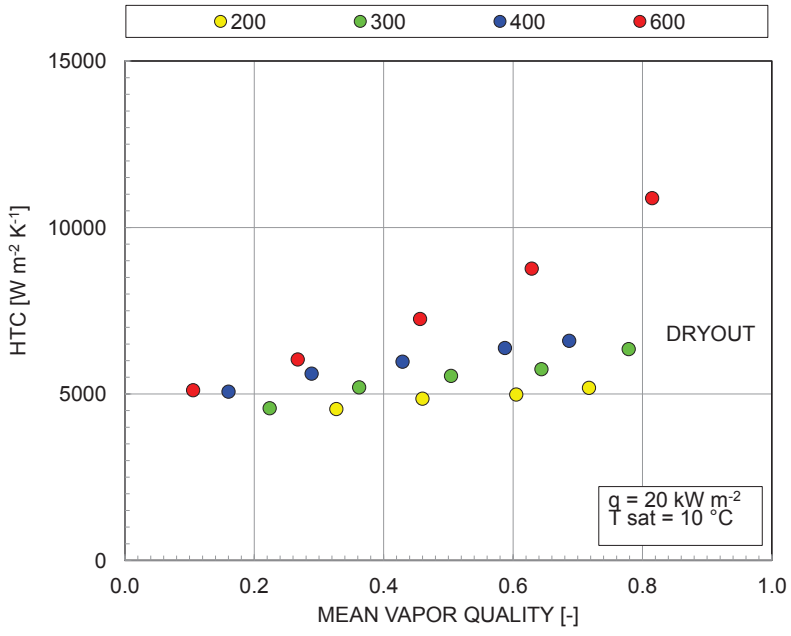

Figure 48 R134a Heat Transfer Coefficient (HTC) vs. mean vapor quality as a function of the mass flux (kg m^{-2} s^{-1}) at fixed heat flux q=20 kW m^{-2} and saturation temperature t_{sat}=10 °C.

A remarkable effect of the refrigerant mass flux and of the mean vapor quality is displayed on the heat transfer coefficient, which increases when they increase. The most notable effects are exhibit at lower saturation temperature where the convective boiling mechanism affects more the heat transfer. For example (Figure 48), HTC becomes more than 2 times greater when the mean vapor quality goes from 0.11 to 0.82 and it goes up to +95% when the refrigerant mass flux passes from 200 kg m^{-2} s^{-1} to 600 kg m^{-2} s^{-1}.

Figure 49 and Figure 50 present the refrigerant HTC at a fixed heat flux (q=20 kW m^{-2}) and at a fixed mass flux (G=200 kg m^{-2} s^{-1} and 600 kg m^{-2} s^{-1}, respectively) as a function of the saturation temperature that ranges from 20 °C to 10 °C.

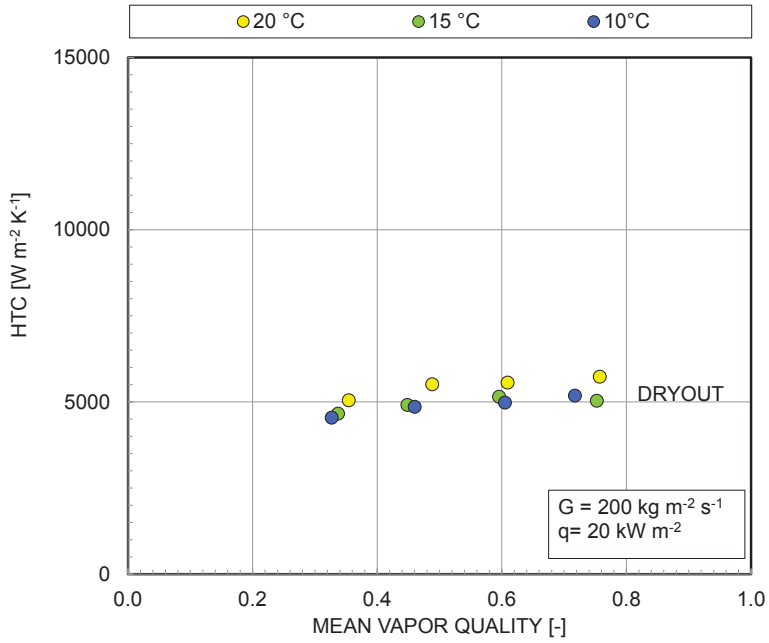

Figure 49 R134a Heat Transfer Coefficient (HTC) vs. mean vapor quality as a function of the saturation temperature at fixed mass flux G=200 kg m^{-2} s^{-1} and heat flux q=20 kW m^{-2}.

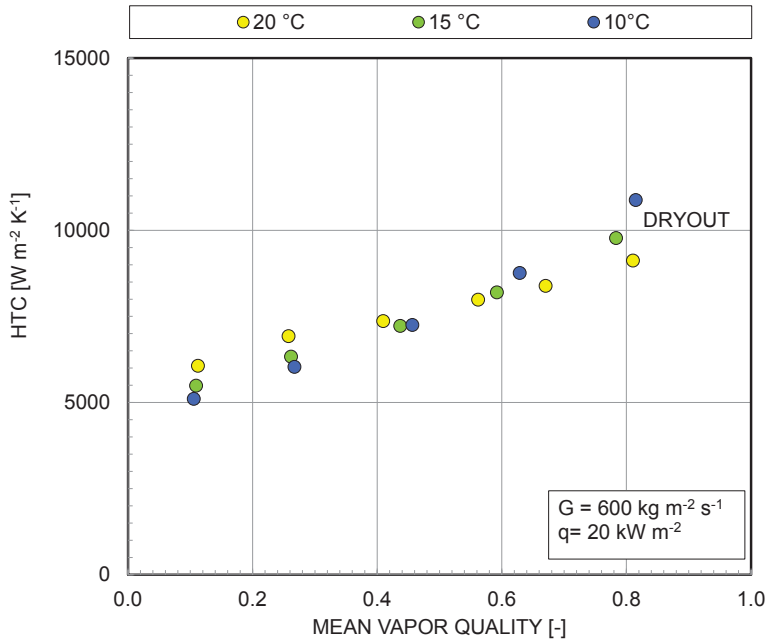

Figure 50 R134a Heat Transfer Coefficient (HTC) vs. mean vapor quality as a function of the saturation temperature at fixed mass flux G=600 kg m^{-2} s^{-1} and heat flux q=20 kW m^{-2}.

Figure 51 and Figure 52 present the refrigerant HTC at a fixed heat flux (q=15 kW m^{-2} and 30 kW m^{-2}, respectively) and at a fixed mass flux (G=400 kg m^{-2} s^{-1}) as a function of the saturation temperature that ranges from 20 °C to 10 °C.

As presented in section 1.4.1, the nucleate boiling controls the heat transfer at high saturation temperatures, low mass fluxes and high heat fluxes. On the contrary, the convective boiling affects the phase change mechanism mainly at low saturation temperatures, high mass fluxes and low heat fluxes and shows a great dependence of the heat transfer coefficient with the mean vapor quality.

The experimental data collected with R134a during flow boiling inside a circular tube and presented in Figure 49, Figure 50, Figure 51, and Figure 52 are consistent with the theoretical trends. In fact in Figure 49, where the mass flux is low, the heat transfer is dominated by the nucleate boiling and, consequently, the HTCs are weakly influenced by the vapor quality, while in Figure 50, where the mass flux is high, the HTCs increase with the vapor quality and the strongest slope is reached at 10 °C of saturation temperature, conditions in which the convective boiling takes place.

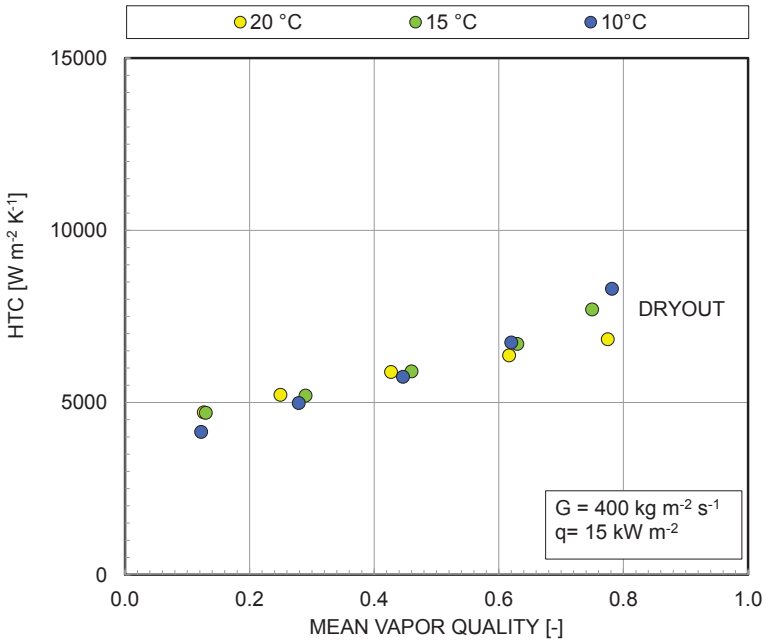

Figure 51 R134a Heat Transfer Coefficient (HTC) vs. mean vapor quality as a function of the saturation temperature at fixed mass flux G=400 kg m^{-2} s^{-1} and heat flux q=15 kW m^{-2}.

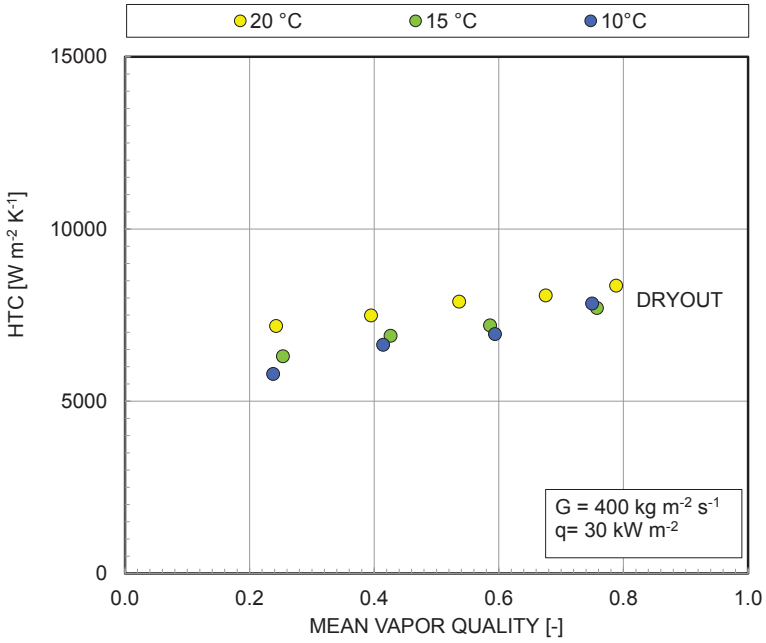

Figure 52 R134a Heat Transfer Coefficient (HTC) vs. mean vapor quality as a function of the saturation temperature at fixed mass flux G=400 kg m^{-2} s^{-1} and heat flux q=30 kW m^{-2}.

3.1.1.1.4 R1234ze(E)

Figure 53, Figure 54, and Figure 55 show the average Heat Transfer Coefficient (HTC) plotted against then mean vapor quality at a constant refrigerant mass flux (G=400 kg m^{-2} s^{-1}) at four different heat fluxes (q=15, 20, 25, and 30 kW m^{-2}) at 20 °C, 15 °C, and 10 °C of saturation temperature, respectively.

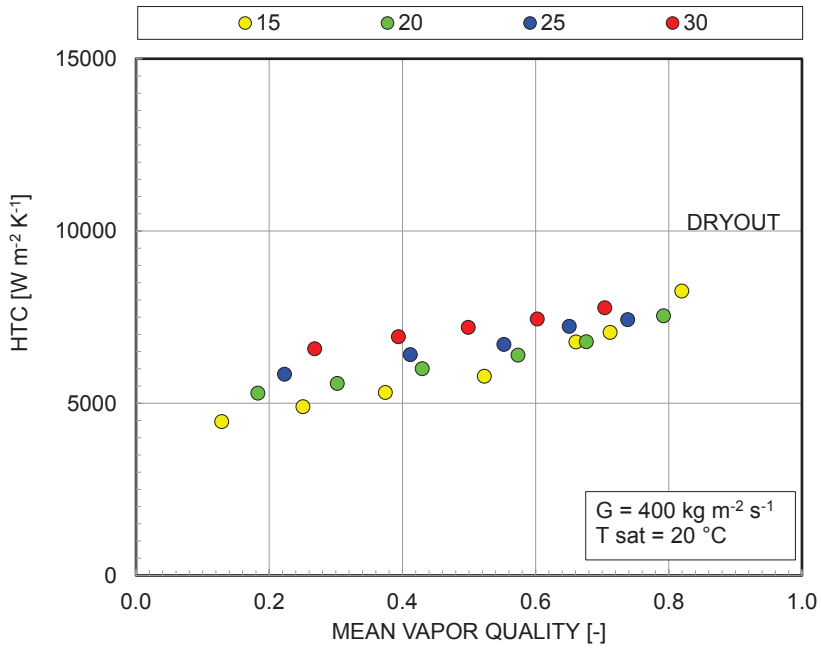

Figure 53 R1234ze(E) Heat Transfer Coefficient (HTC) vs. mean vapor quality as a function of the heat flux (kW m^{-2}) at fixed mass flux G=400 kg m^{-2} s^{-1} and saturation temperature t_{sat}=20 °C.

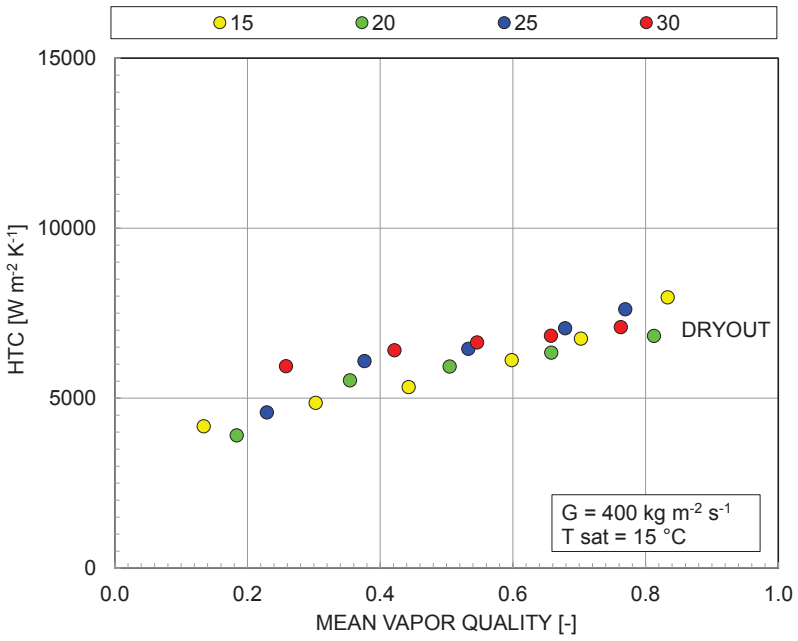

Figure 54 R1234ze(E) Heat Transfer Coefficient (HTC) vs. mean vapor quality as a function of the heat flux (kW m^{-2}) at fixed mass flux G=400 kg m^{-2} s^{-1} and saturation temperature t_{sat}=15 °C.

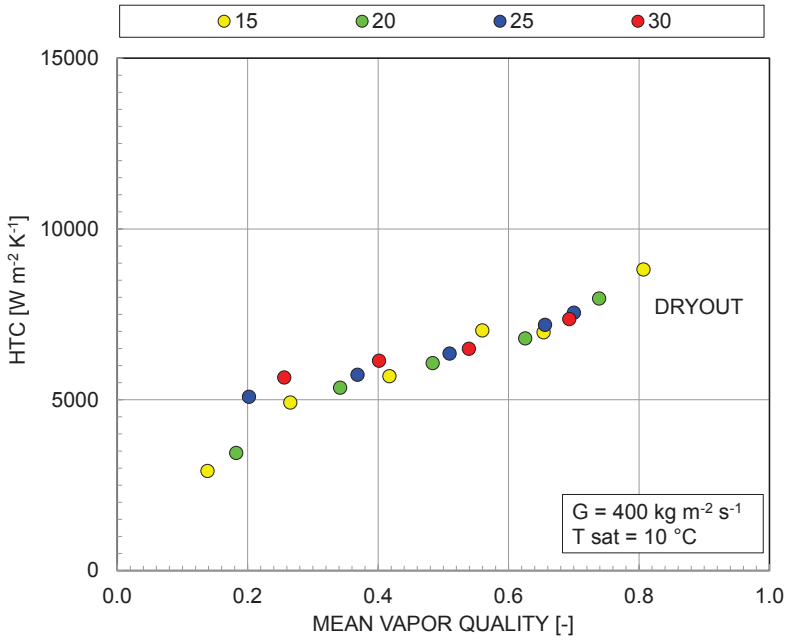

Figure 55 R1234ze(E) Heat Transfer Coefficient (HTC) vs. mean vapor quality as a function of the heat flux (kW m^{-2}) at fixed mass flux G=400 kg m^{-2} s^{-1} and saturation temperature t_{sat}=10 °C.

At high saturation temperature (for instance, 20 °C) and at low vapor qualities the refrigerant heat transfer coefficient exhibits a notable sensitivity to heat flux. In fact, doubling the heat flux (from 15 to 30 kW m^{-2}) at a saturation temperature equal to 20 °C, the refrigerant HTC increases around 45%. At the contrary, at low saturation temperatures and high vapor qualities the refrigerant HTC presents a negligible sensitivity to heat flux.

Furthermore, the refrigerant heat transfer coefficient increases at the increasing of the mean vapor quality especially at low heat fluxes and low saturation temperatures where the convective mechanism is more relevant (around 3 times greater going from x_m=0.15 to x_m=0.8 at q=15 kW m^{-2} and t_{sat}=10 °C, +20% going from x_m=0.25 to x_m=0.7 at q=15 kW m^{-2} and t_{sat}=20 °C).

The onset of dryout appears at lower vapor qualities with higher heat fluxes and lower saturation temperature. It is included from x_m=0.69 to x_m=0.83.

Figure 56, Figure 57, and Figure 58 show the average Heat Transfer Coefficient (HTC) plotted against the mean vapor quality at a constant heat flux (q=20 kW m^{-2}) and at four different refrigerant mass fluxes (G=200, 300, 400, and 600 kg m^{-2} s^{-1}) at 20 °C, 15 °C, and 10 °C of saturation temperature, respectively.

The refrigerant side heat transfer coefficient is strongly affected by the mass flux, especially at low saturation temperatures and high mean vapor qualities, where the convective mechanism plays an important role into the phase change process. At 10 °C of saturation temperature (Figure 58) the HTC increases of around 2.5 times when the mass flux going from 200 to 600 kg m^{-2} s^{-1}, while at 20 °C of saturation temperature the HTC becomes 70% greater.

In addition, the refrigerant HTC increases at the increasing of the vapor quality especially at high flow rates and low saturation temperatures. (around 3.5 times greater going from x_m=0.11 to x_m=0.71 at G=600 kg m^{-2} $s^{-1}$and t_{sat}=10 °C against +2% going from x_m=0.35 to x_m=0.71 at G=200 kg m^{-2} $s^{-1}$and t_{sat}=20 °C). At low mass fluxes the nucleate boiling mechanism becomes more consistent and the heat transfer coefficient is fairly constant as a function of the mean vapor quality.

The onset of dryout occurs at higher vapor qualities when the refrigerant mass flux is higher. It appears from x_m=0.66 to x_m=0.85.

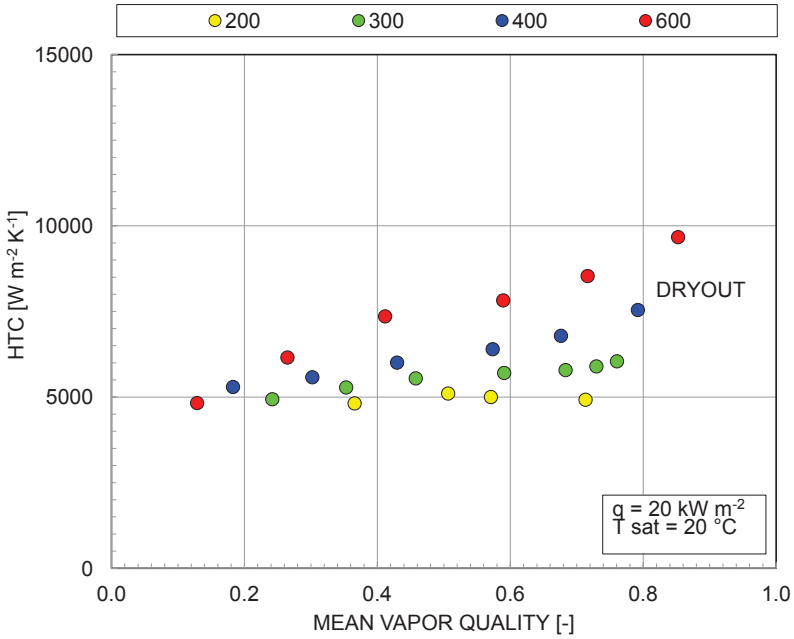

Figure 56 R1234ze(E) Heat Transfer Coefficient (HTC) vs. mean vapor quality as a function of the mass flux (kg m^{-2} s^{-1}) at fixed heat flux q=20 kW m^{-2} and saturation temperature t_{sat}=20 °C.

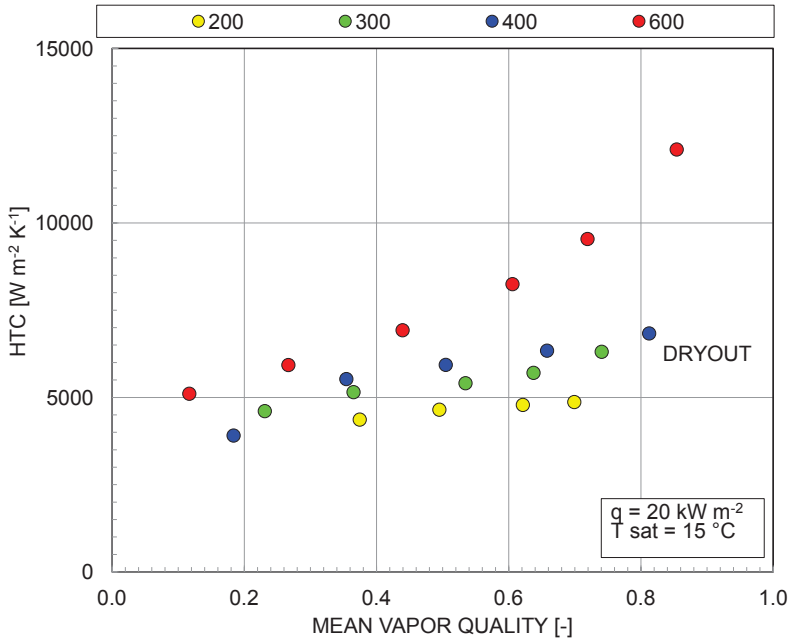

Figure 57 R1234ze(E) Heat Transfer Coefficient (HTC) vs. mean vapor quality as a function of the mass flux (kg m^{-2} s^{-1}) at fixed heat flux q=20 kW m^{-2} and saturation temperature t_{sat}=15 °C.

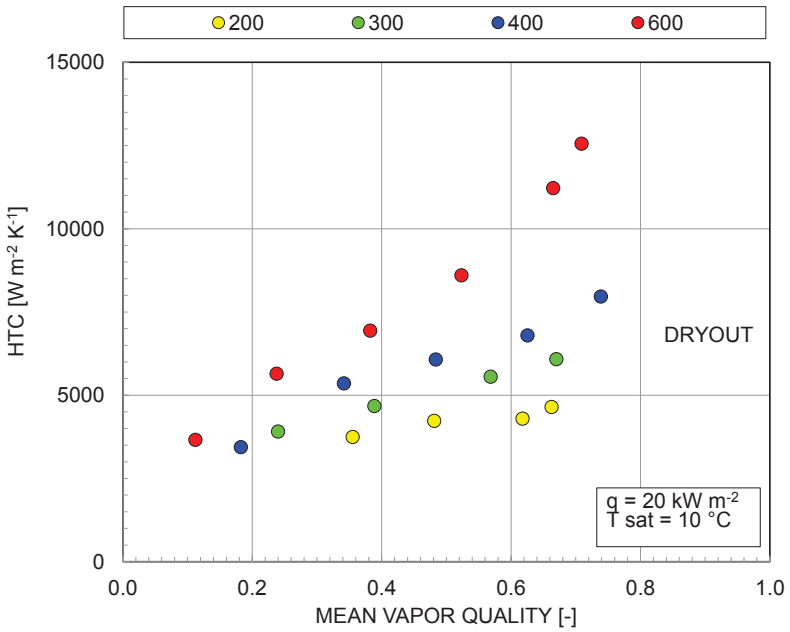

Figure 58 R1234ze(E) Heat Transfer Coefficient (HTC) vs. mean vapor quality as a function of the mass flux (kg m^{-2} s^{-1}) at fixed heat flux q=20 kW m^{-2} and saturation temperature t_{sat}=10 °C.

Figure 59 and Figure 60 present the refrigerant HTC at a fixed heat flux (q=20 kW m^{-2}) and at a fixed mass flux (G=200 kg m^{-2} $s^{-1}$and 600 kg m^{-2} s^{-1}, respectively) as a function of the saturation temperature that ranges from 20 °C to 10 °C.

When the refrigerant mass flux is low (Figure 59) the saturation temperature has a weak influence on the HTC, furthermore the HTC is poorly affected also by the mean vapor quality. The convective boiling mechanism is negligible at these operating conditions.

At the contrary, when the refrigerant mass flux is higher (Figure 60) the slope of the HTC has a great sensitivity of the saturation temperature. In fact, at low saturation temperatures, the refrigerant heat transfer coefficient strongly increases at the increasing of the average vapor quality and it reaches absolute values higher than the ones at high saturation temperature, due to the increasing of the flow velocity that increments the convective boiling effect (see paragraph 1.4.1).

Figure 61 and Figure 62 present the refrigerant HTC at a fixed heat flux (q=15 kW m^{-2} and 30 kW m^{-2}, respectively) and at a fixed mass flux (G=400 kg m^{-2} s^{-1}) as a function of the saturation temperature that ranges from 20 °C to 10 °C.

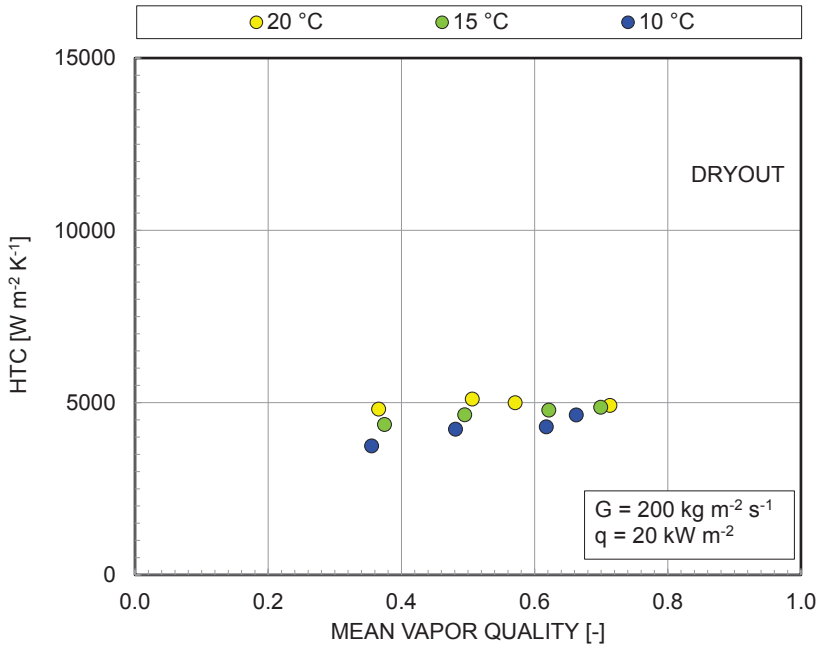

Figure 59 R1234ze(E) Heat Transfer Coefficient (HTC) vs. mean vapor quality as a function of the saturation temperature at fixed mass flux G=200 kg m^{-2} s^{-1} and heat flux q=20 kW m^{-2}.

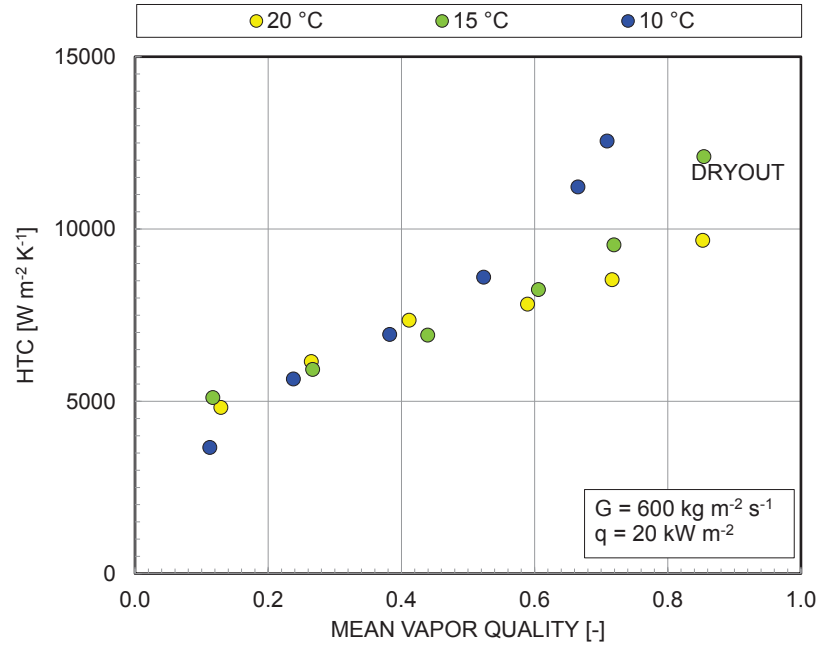

Figure 60 R1234ze(E) Heat Transfer Coefficient (HTC) vs. mean vapor quality as a function of the saturation temperature at fixed mass flux G=600 kg m^{-2} s^{-1} and heat flux q=20 kW m^{-2}.

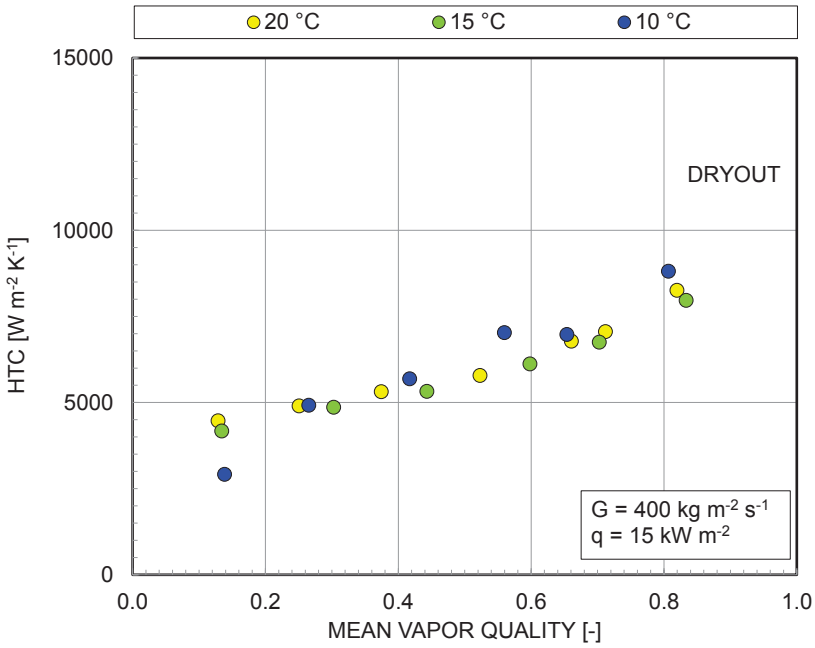

Figure 61 R1234ze(E) Heat Transfer Coefficient (HTC) vs. mean vapor quality as a function of the saturation temperature at fixed mass flux G=400 kg m^{-2} s^{-1} and heat flux q=15 kW m^{-2}.

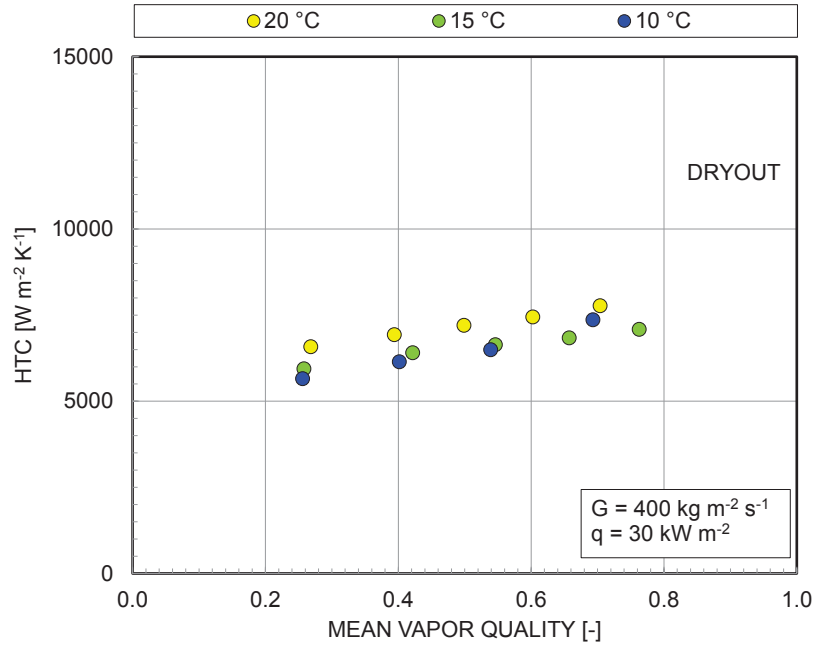

Figure 62 R1234ze(E) Heat Transfer Coefficient (HTC) vs. mean vapor quality as a function of the saturation temperature at fixed mass flux G=400 kg m^{-2} s^{-1} and heat flux q=30 kW m^{-2}.

An increase in heat flux leads to an increment of the nucleate boiling effect, as presented in paragraph 1.4.1. This can be seen in Figure 62 (q=30 kW m^{-2}) where the HTC is lightly influenced by the vapor quality, while in Figure 61 (q=15 kW m^{-2}) the influence of vapor quality to HTC is higher, underlining a great effect of convective boiling.

3.1.1.2 Pressure drop

3.1.1.2.1 R410A

Figure 63, Figure 64, and Figure 65 show the frictional pressure drop plotted against refrigerant mass flux for R410A at three different ambient temperatures 20 °C, 10 °C, and 5 °C, respectively.

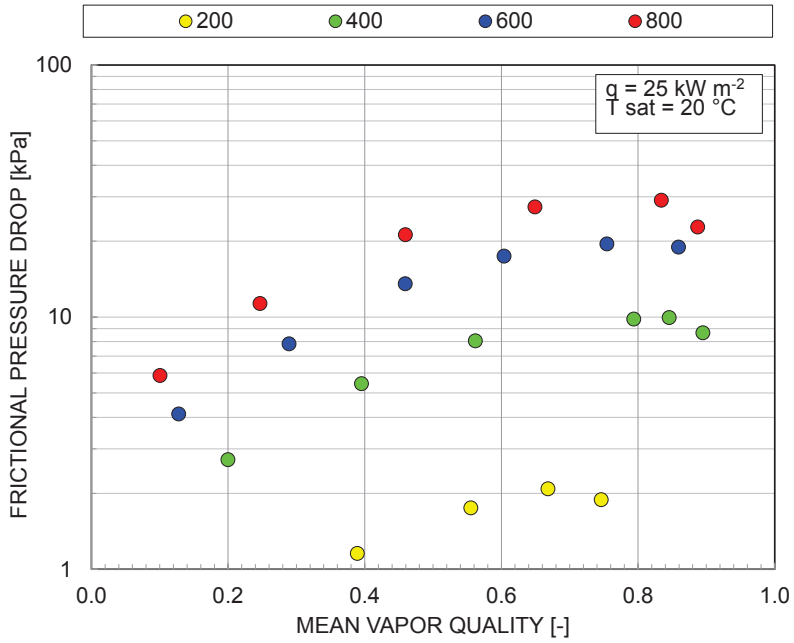

Figure 63 R410A frictional pressure drop vs. mean vapor quality as a function of the mass flux (kg m^{-2} s^{-1}) at fixed heat flux q=25 kW m^{-2} and saturation temperature t_{sat}=20 °C.

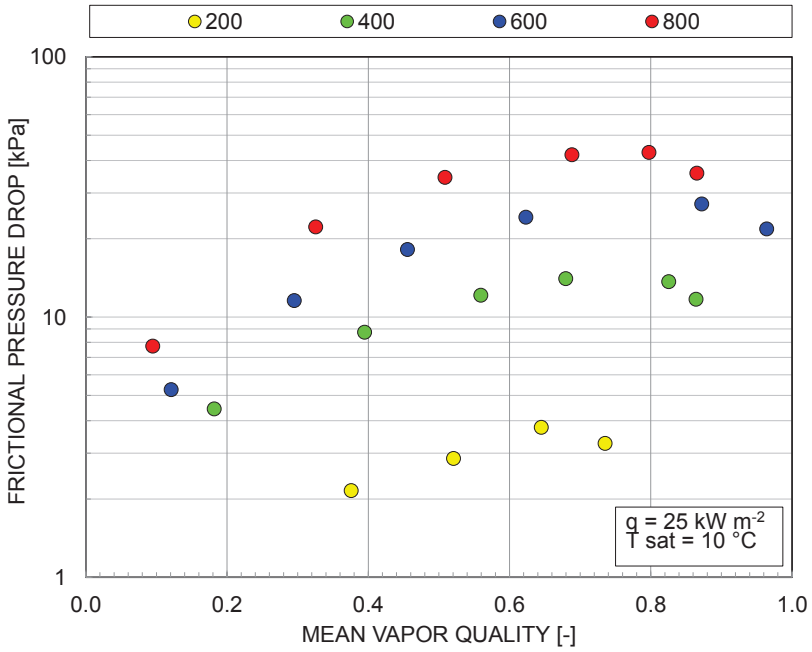

Figure 64 R410A frictional pressure drop vs. mean vapor quality as a function of the mass flux (kg m^{-2} s^{-1}) at fixed heat flux q=25 kW m^{-2} and saturation temperature t_{sat} =10 °C.

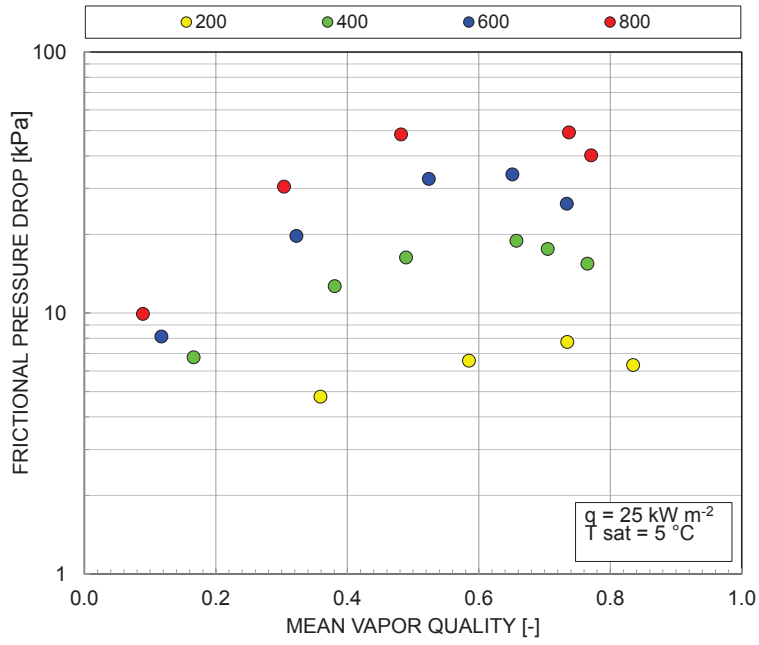

Figure 65 R410A frictional pressure drop vs. mean vapor quality as a function of the mass flux (kg m^{-2} s^{-1}) at fixed heat flux q=25 kW m^{-2} and saturation temperature t_{sat} =5 °C.

Frictional pressure drops are deeply influenced by the refrigerant mass flux and obviously they increase when the flow rate increases. For example, they become up to 15 times higher when the refrigerant mass flux varies from 200 kg m^{-2} s^{-1} to 800 kg m^{-2} s^{-1} at constant heat flux.

The mean vapor quality also affects the pressure drops that increase with the increasing of the vapor quality up to a certain value in which they start to decrease toward the single phase gas value.

On the other hand pressure drops are lightly influenced by the heat flux as demonstrated by Figure 66 which presents the frictional pressure drops as a function of the average vapor quality and the heat flux (q is equal to 12, 25, 38, and 50 kW m^{-2} respectively) at fixed saturation temperature and refrigerant mass flux (G=400 kg m^{-2} s^{-1}).

Finally, Figure 67 presents the frictional pressure drops as a function of the average vapor quality and the saturation temperature (that varies from 5 °C to 20 °C) at a fixed refrigerant mass flux (G=400 kg m^{-2} s^{-1}) and heat flux (q=25 kW m^{-2}).

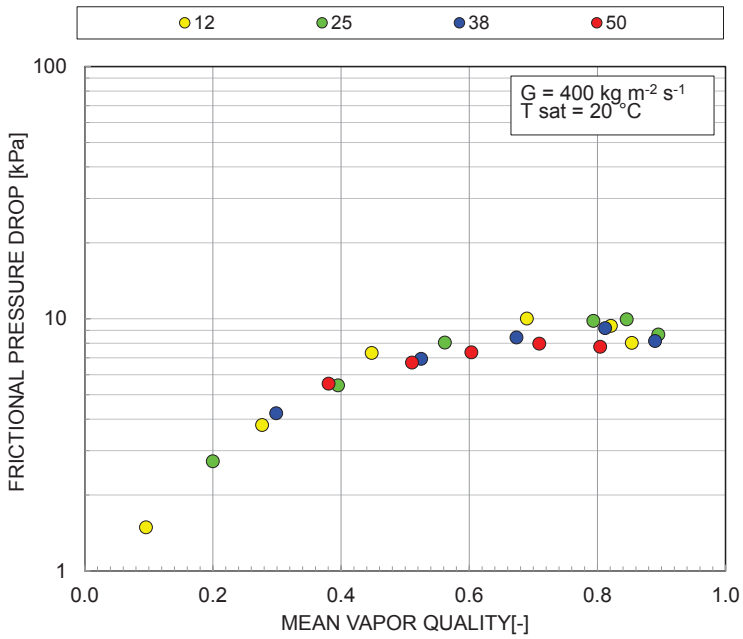

Figure 66 R410A frictional pressure drop vs. mean vapor quality as a function of the heat flux at fixed mass flux (kg m^{-2} s^{-1}) G=400 kg m^{-2} s^{-1} and t_{sat}=20 °C.

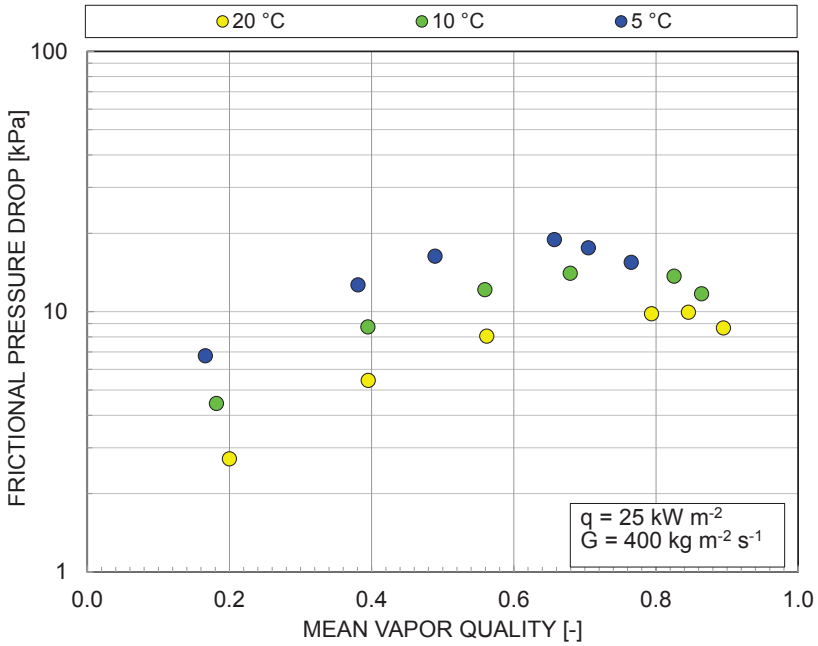

Figure 67 R410A frictional pressure drop vs. mean vapor quality as a function of saturation temperature at fixed mass flux G=400 kg m^{-2} s^{-1} and heat flux q=25 kW m^{-2}.

The frictional pressure drop increases with the decreasing of the saturation temperature. At lower mean vapor quality the saturation temperature effect is higher. The pressure drop decreases up to 2 times going from 5 °C to 20 °C saturation temperature at x_m=0.2, while they decreases up to 80% going at x_m=0.8.

3.1.1.2.2 R32

Figure 68, Figure 69, and Figure 70 show the frictional pressure drop plotted against refrigerant mass flux for R32 at three different ambient temperatures 20°C, 10°C, and 5°C, respectively.

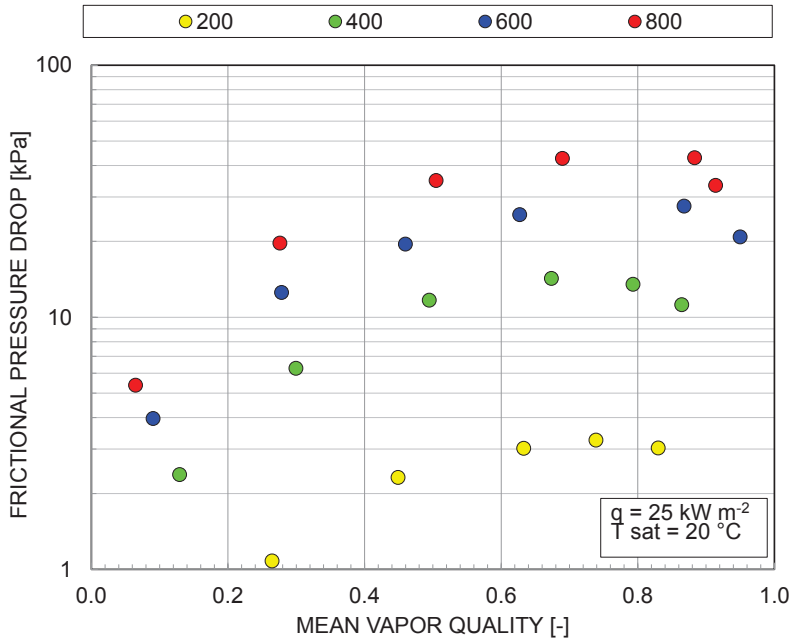

Figure 68 R32 frictional pressure drop vs. mean vapor quality as a function of the mass flux (kg m^{-2} s^{-1}) at fixed heat flux q=25 kW m^{-2} and saturation temperature t_{sat}=20 °C.

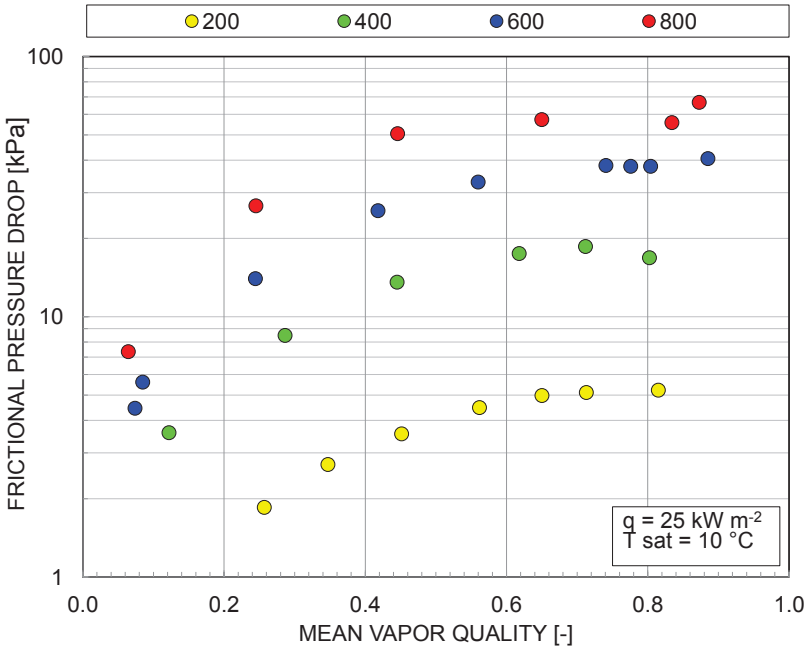

Figure 69 R32 frictional pressure drop vs. mean vapor quality as a function of the mass flux (kg m^{-2} s^{-1}) at fixed heat flux q=25 kW m^{-2} and saturation temperature t_{sat}=10 °C.

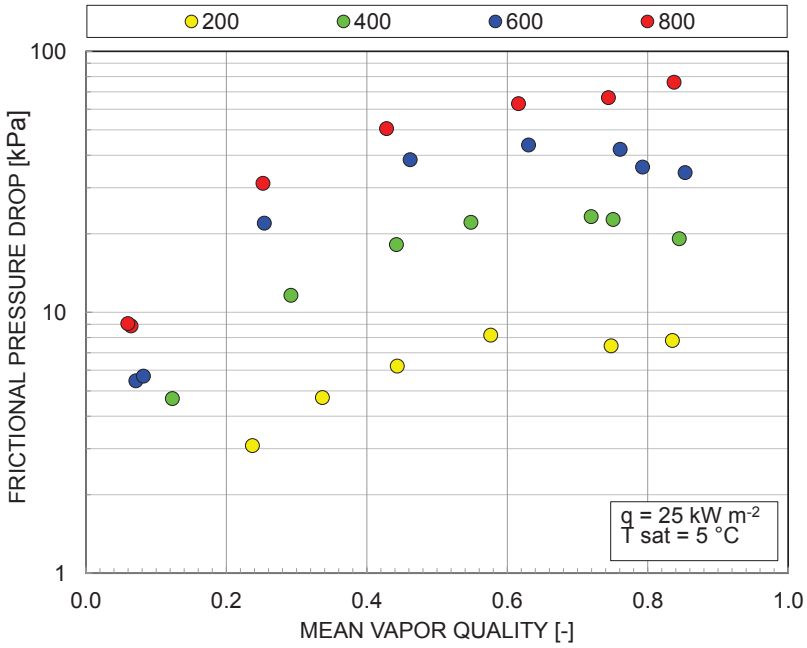

Figure 70 R32 frictional pressure drop vs. mean vapor quality as a function of the mass flux (kg m^{-2} s^{-1}) at fixed heat flux q=25 kW m^{-2} and saturation temperature t_{sat}=5 °C.

As presented in section 3.1.1.2.1 during R410A vaporization tests, the R32 frictional pressure drops are significantly affected by the mass flux and the mean vapor quality while they weakly influenced by the heat flux.

The frictional pressure drop becomes up to 13 times higher when the refrigerant mass flux increases from 200 kg m^{-2} s^{-1} to 800 kg m^{-2} s^{-1} at constant heat flux, while the variation is negligible varying the heat fluxes at a constant mass flux, as presented in Figure 71. In this figure, in fact, the frictional pressure drops are presented as a function of the heat flux (from 12 to 50 kW m^{-2}) at a constant refrigerant mass flux (G=800 kg m^{-2} s^{-1}) and saturation temperature (t=20°C).

Finally, Figure 72 presents the frictional pressure drop as a function of the average vapor quality and the saturation temperature at a fixed refrigerant mass flux G=400 kg m^{-2} s^{-1} and fixed heat flux q=25 kW m^{-2}.

Here the frictional pressure drop increases with the decreasing of the saturation temperature. The pressure drop decreases up to 95% going from 5 °C to 20 °C saturation temperature.

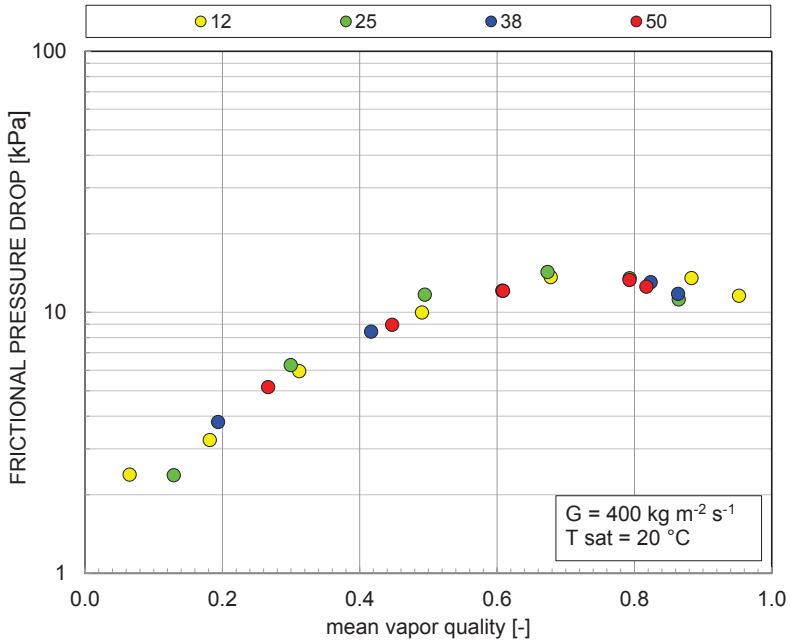

Figure 71 R32 frictional pressure drop vs. mean vapor quality as a function of the heat flux (kW m^{-2}) at fixed mass flux G=400 kg m^{-2} s^{-1} and t_{sat}=20 °C.

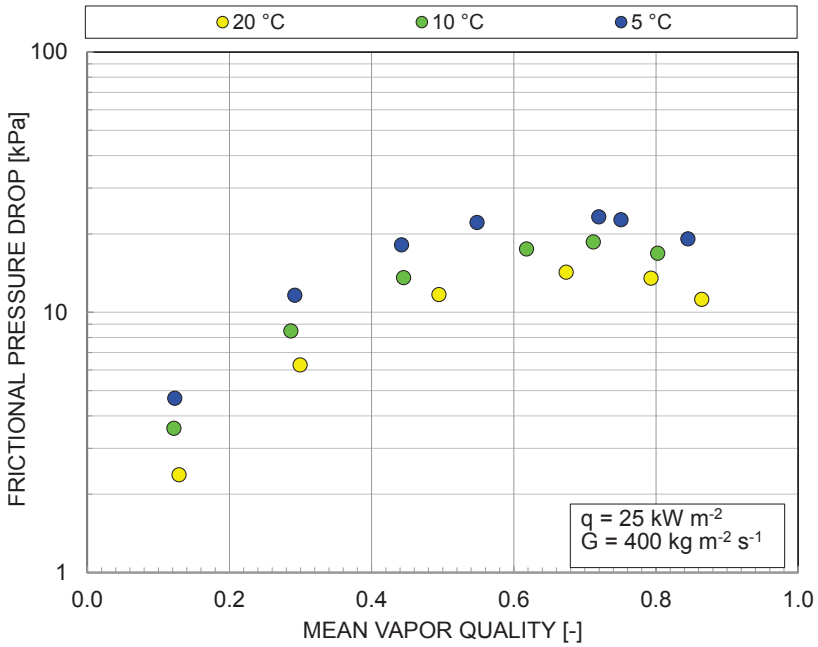

Figure 72 R32 frictional pressure drop vs. mean vapor quality as a function of the saturation temperature at fixed mass flux G=400 kg m^{-2} s^{-1} and heat flux q=25 kW m^{-2}.

3.1.1.2.3 R134a

Figure 73, Figure 74, and Figure 75 show the frictional pressure drop plotted against the refrigerant mass flux at three different ambient temperatures 20 °C, 15 °C, and 10 °C, respectively.

Frictional pressure drops are strongly dependent on the mean vapor quality. The slope is not linear but it is higher at low vapor qualities than it becomes more flat when almost the totally of the flow is vaporized. In addition the pressure drops are influenced by the refrigerant mass flux and they increase at the increasing of the mass flux. For example, the frictional pressure drops become up to 8 times higher when the refrigerant mass flux varies from 200 kg m^{-2} s^{-1} to 600 kg m^{-2} s^{-1} at constant heat flux.

Figure 76 presents the frictional pressure drop as a function of the heat flux at 20 °C of saturation temperature at a refrigerant mass flux G=400 kg m^{-2} s^{-1}. The heat flux does not affect the frictional pressure drop, in fact the variation in pressure drop is smaller than the experimental uncertainty.

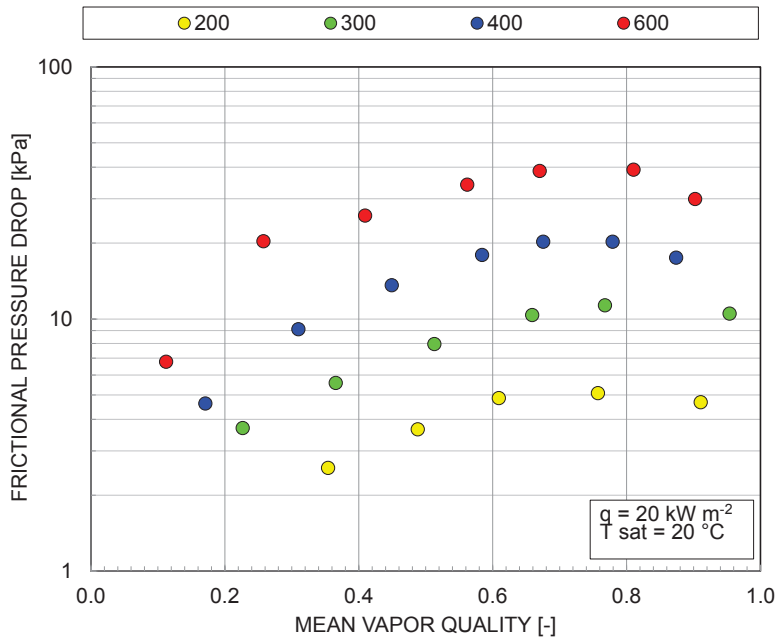

Figure 73 R134a frictional pressure drop vs. mean vapor quality as a function of the mass flux (kg m^{-2} s^{-1}) at fixed heat flux q=20 kW m^{-2} and saturation temperature t_{sat}=20 °C.

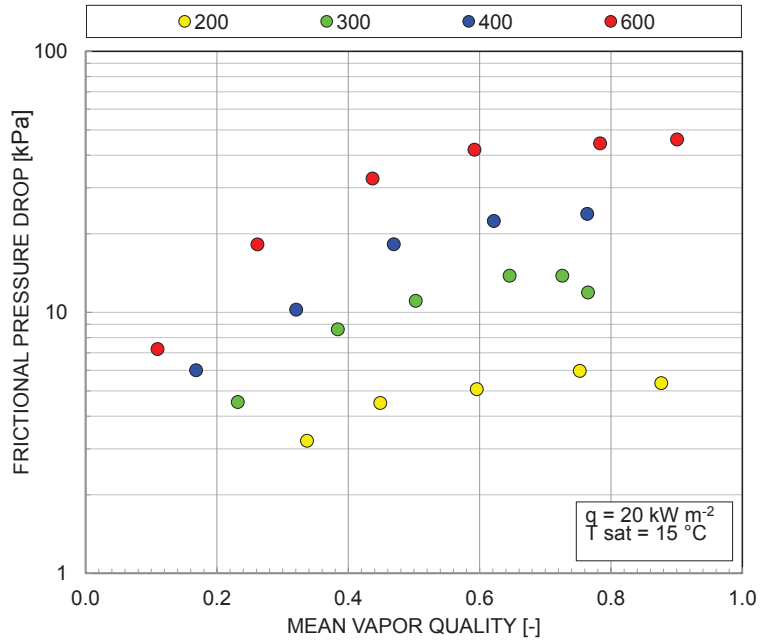

Figure 74 R134a frictional pressure drop vs. mean vapor quality as a function of the mass flux (kg m^{-2} s^{-1}) at fixed heat flux q=20 kW m^{-2} and saturation temperature t_{sat}=15 °C.

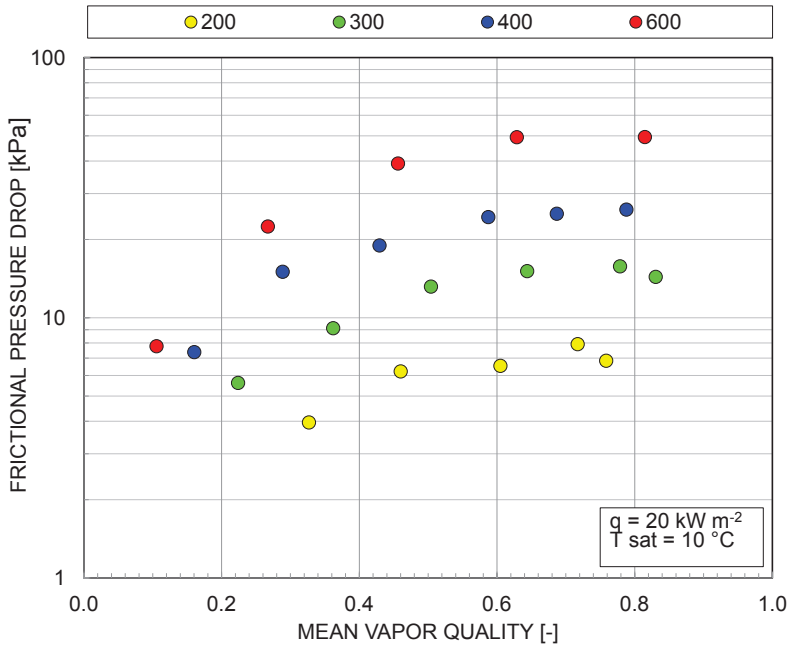

Figure 75 R134a frictional pressure drop vs. mean vapor quality as a function of the mass flux (kg m^{-2} s^{-1}) at fixed heat flux q=20 kW m^{-2} and saturation temperature t_{sat}=10 °C.

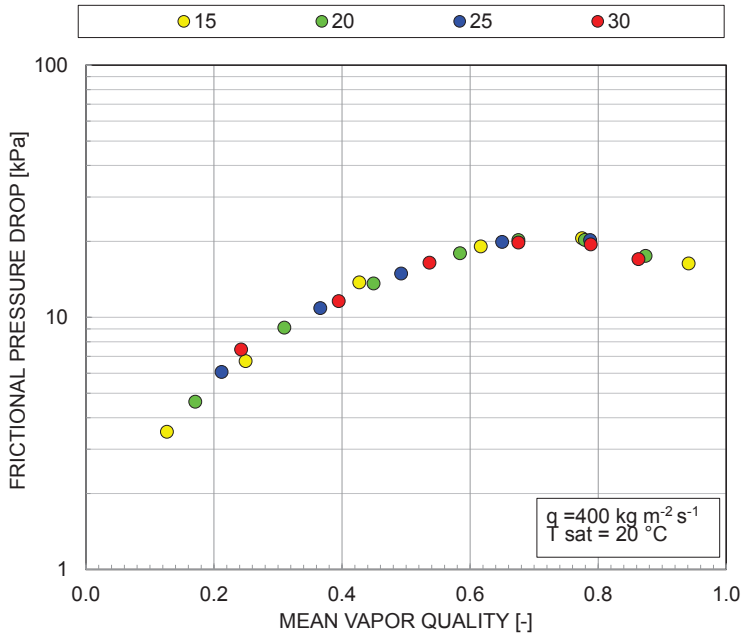

Figure 76 R134a frictional pressure drop vs. mean vapor quality as a function of the heat flux (kW m^{-2}) at fixed mass flux G=400 kg m-2 s-1 and t_{sat}=20 °C.

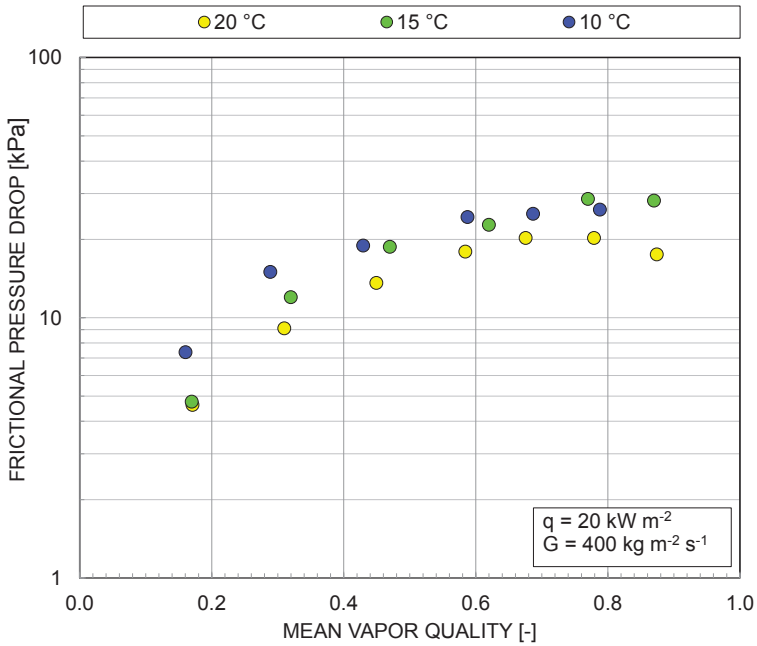

Figure 77 R134a frictional pressure drop vs. mean vapor quality as a function of the saturation temperature at fixed mass flux G=400 kg m^{-2} s^{-1} and heat flux q=20 kW m^{-2}.

Figure 77 presents the frictional pressure drop as a function of the average vapor quality and of the saturation temperature at fixed refrigerant mass flux G=400 kg m^{-2} s^{-1} and heat flux q=20 kW m^{-2}.
The frictional pressure drops are lightly affected by the saturation temperature. From Figure 77 it can be noticed that a lower saturation temperature contributes to higher frictional pressure drop, around 40% higher passing from 20 to 10 °C.

3.1.1.2.4 R1234ze(E)

Figure 78, Figure 79, and Figure 80 show the frictional pressure drop plotted against the refrigerant mass flux at three different ambient temperatures 20 °C, 15 °C, and 10 °C, respectively.

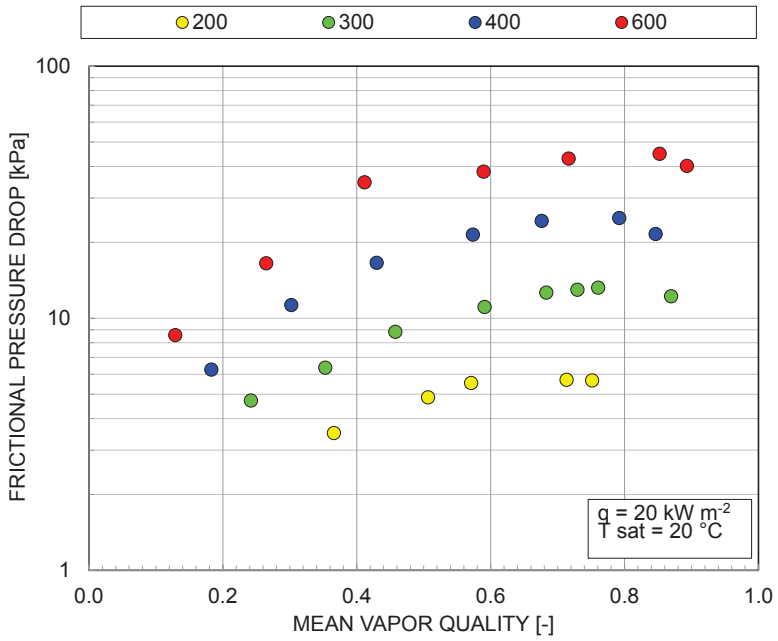

Figure 78 R1234ze(E) frictional pressure drop vs. mean vapor quality as a function of the mass flux (kg m^{-2} s^{-1}) at fixed heat flux q=20 kW m^{-2} and saturation temperature t_{sat}=20 °C.

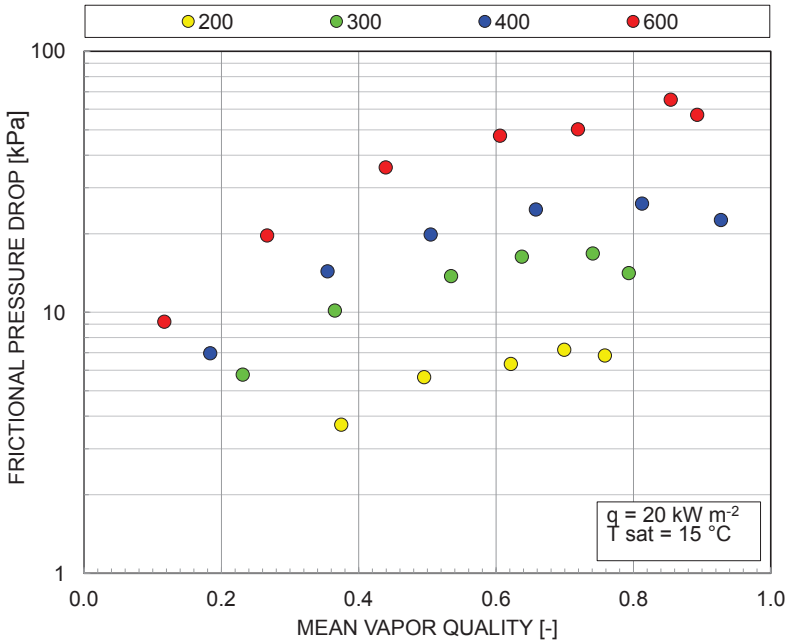

Figure 79 R1234ze(E) frictional pressure drop vs. mean vapor quality as a function of the mass flux (kg m^{-2} s^{-1}) at fixed heat flux q=20 kW m^{-2} and saturation temperature t_{sat}=15 °C.

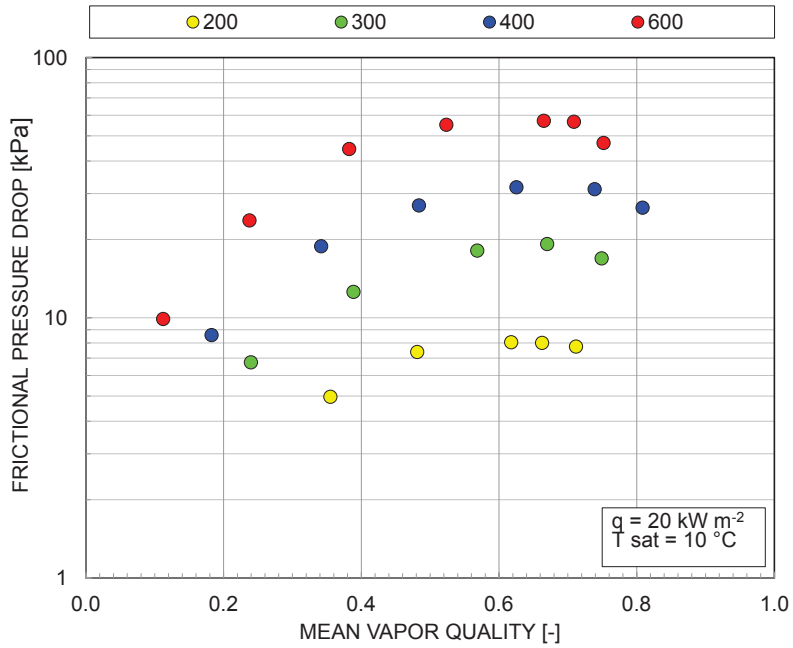

Figure 80 R1234ze(E) frictional pressure drop vs. mean vapor quality as a function of the mass flux (kg m^{-2} s^{-1}) at fixed heat flux q=20 kW m^{-2} and saturation temperature t_{sat}=10 °C.

Frictional pressure drops exhibit great sensitivity to refrigerant mass flux and mean vapor quality. In fact becomes up to 7 times higher when the refrigerant mass flux passes from 200 kg m^{-2} s^{-1} to 600 kg m^{-2} s^{-1} at constant heat flux and 5 times higher when the vapor quality passes from 0.1 to 0.6.

Figure 82 presents the frictional pressure drop as a function of the average vapor quality and heat flux q that varies from 15 kW m^{-2} to 30 kW m^{-2} at a fixed refrigerant mass flux G=400 kg m^{-2} s^{-1} and fixed saturation temperature of 20 °C.

The frictional pressure drops are not affected by the heat flux. In fact a great increment in the heat flux – that passes from q=15 kW m^{-2} to q=50 kW m^{-2} – implies a light increase of the frictional pressure drop (around 5%) which is comparable with the uncertainty of the measure.

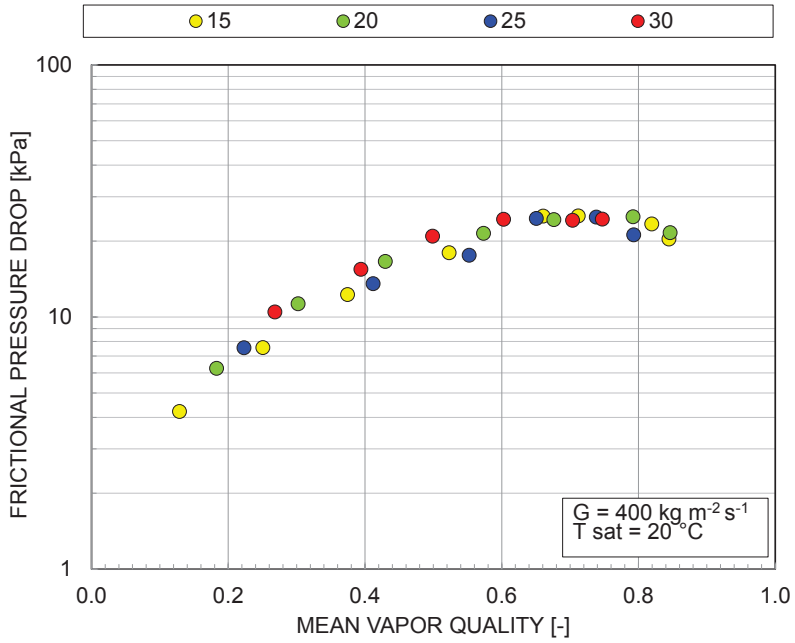

Figure 81 R1234ze(E) frictional pressure drop vs. mean vapor quality as a function of the heat flux (kW m^{-2}) at fixed mass flux G=400 kg m^{-2} s^{-1} and t_{sat}=20 °C.

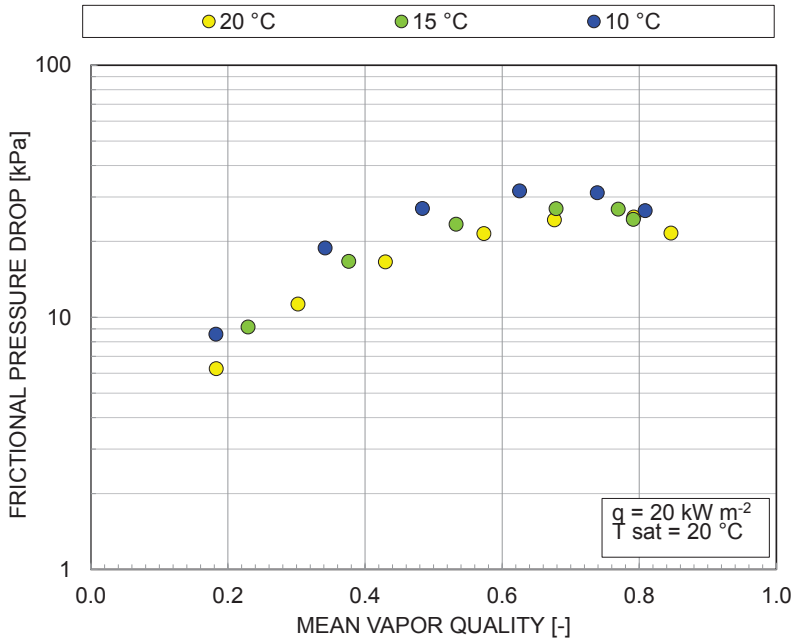

Figure 82 R1234ze(E) frictional pressure drop vs. mean vapor quality as a function of the saturation temperature at fixed mass flux G=400 kg m^{-2} s^{-1} and heat flux q=25 kW m^{-2}.

Figure 82 presents the frictional pressure drop as a function of the average vapor quality and the saturation temperature at a fixed refrigerant mass flux G=400 kg m^{-2} s^{-1} and fixed heat flux q=20 kW m^{-2}.

Frictional pressure drops are weakly influenced by saturation temperature, in fact they increase up to 20% when the saturation temperature goes from 20 °C to 10 °C.

3.1.2 Comparison against literature correlations

3.1.2.1 Heat transfer coefficient

The experimental heat transfer coefficients were compared against different heat transfer correlations for boiling inside tube. The following correlations available in the open literature were implemented: Chen (1966), Cooper (1984), Gorenflo (1993), Gungor and Wintertorn (1986), Kim and Mudawar (2014a), Lazarek and Black (1982), Liu and Winterton (1991), Oh and Son (2011), Sun and Mishima (2009), Tran *et al.* (1996), Wojtan *et al.* (2005), Yu *et al.* (1999), and Zhang *et al.* (2004).

It has to be noticed that the Cooper (1984) correlation is for nucleate pool boiling, the ones of Gorenflo (1993), Lazarek and Black (1982), Tran *et al.* (1996), and of Yu *et al.* (1999) are for a dominant nucleate boiling regime, the ones of Chen (1966), Gungor and Wintertorn (1986), Kim and Mudawar (2014a), and Liu and Winterton (1991) combine the contribution of both nucleate boiling and convective boiling, the ones of Oh and Son (2011), Sun and Mishima (2009), and Zhang *et al.* (2004) propose a best fitting equation based on the adimensional groups that govern the boiling heat transfer and finally the Wojtan *et al.* (2005) correlation defines a HTC on the basis of the particular flow regime that locally occurs inside the tube.

Table 18 lists the mean absolute percentage deviation between experimental and calculated values for both R410A, R32, R134a and R1234ze(E), respectively.

For the first couple of refrigerants, namely R410A and R32, the correlation of Sun and Mishima (2009) reports the best performance with a mean absolute percentage deviation of 9.8% and 10.8% for R32 and R410A data, respectively.

Figure 83 and Figure 84 show the deviation between the experimental data and the calculated data for Sun and Mishima (2009) correlation for R410A and R32 data, respectively. It should be noted that this correlation is able to reproduce very well R410A and R32 data both in magnitude and tendency.

Table 18 Mean absolute percentage deviation between experimental and calculated values for R410A, R32, R134a, and R1234ze(E), respectively.

Correlation	R410A	R32	R134a	R1234ze(E)
Chen (1966)	32.3%	28.5%	12.1%	20.8%
Cooper (1984)	36.2%	37.6%	37.0%	36.4%
Gorenflo (1993)	11.9%	11.5%	17.6%	18.1%
Gungor and Wintertorn (1986)	16.9%	15.2%	12.2%	8.5%
Kim and Mudawar (2014a)	28.1%	29.0%	**6.1%**	**6.5%**
Lazarek and Black (1982)	34.5%	33.4%	38.4%	42.4%
Liu and Winterton (1991)	38.6%	37.2%	11.1%	8.2%
Oh and Son (2011)	41.5%	34.6%	26.5%	14.4%
Sun and Mishima (2009)	**10.8%**	**9.8%**	25.7%	29.9%
Tran *et al.* (1996)	29.4%	28.1%	36.2%	40.3%
Wojtan *et al.* (2005)	30.9%	29.4%	16.3%	15.8%
Yu *et al.* (1999)	20.4%	28.1%	10.4%	11.3%
Zhang *et al.* (2004)	45.0%	43.7%	32.6%	34.1%

As for as the second couple of refrigerants – namely R134a and R1234ze(E) – is concerned, the Kim and Mudawar (2014a) correlation is the one that better fits the experimental data. It can be noticed that also other correlations can reproduce this vaporization data, as presented in Table 18, for example Gungor and Wintertorn (1986), Liu and Winterton (1991), and Yu *et al.* (1999) can reproduce the experimental data with an mean average deviation around 10%.

Figure 85 and Figure 86 show the calculated data with the Kim and Mudawar (2014a) correlation vs. the experimental ones obtained with R134a and R1234ze(E) respectively.

The mean average deviation is around 6% for both the refrigerants, so this model can fairly predict this experimental data.

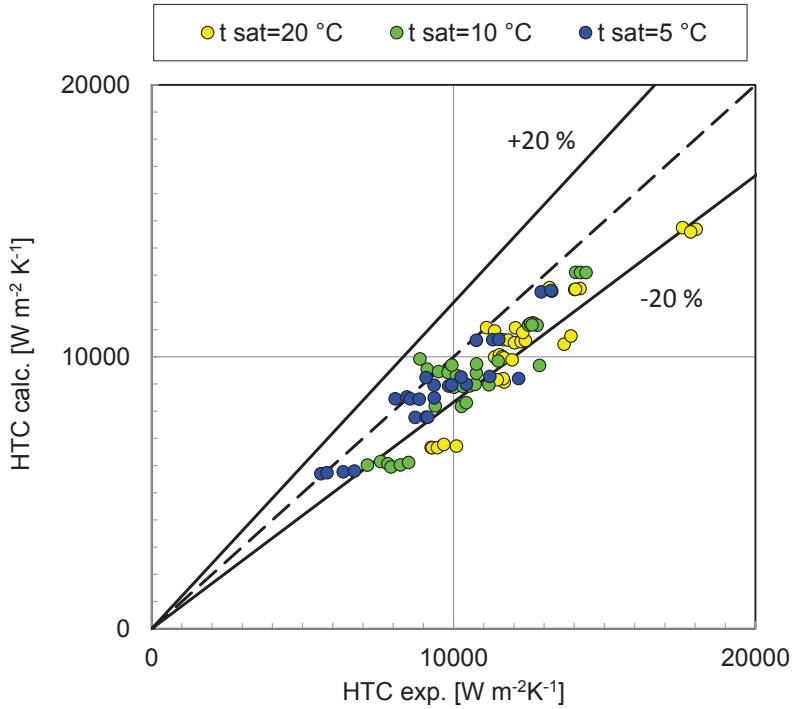

Figure 83 Heat Transfer Coefficient (HTC) calculated by Sun and Mishima (2009) correlation vs. esperimental value for R410A at 20 °C, 10 °C and 5 °C of saturation temperature.

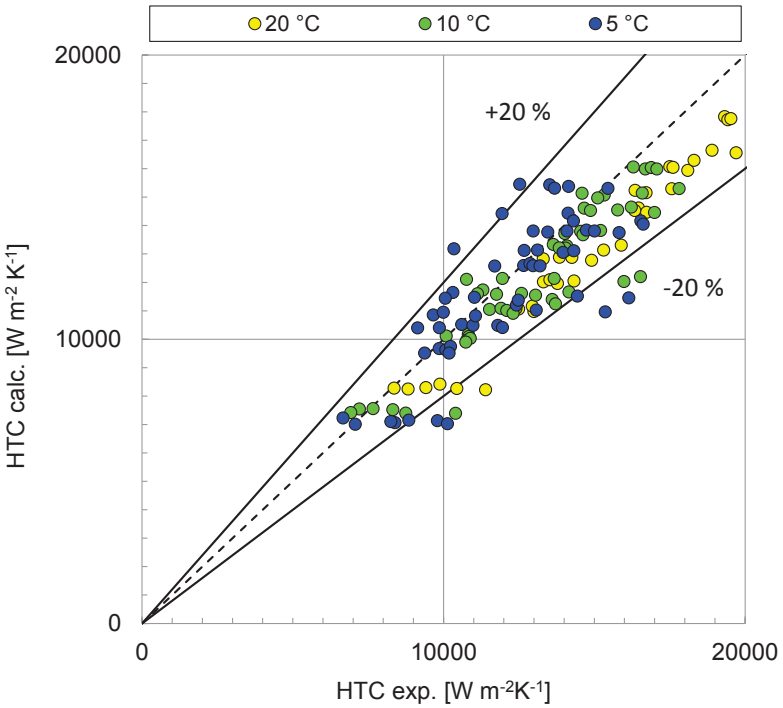

Figure 84 Heat Transfer Coefficient (HTC) calculated by Sun and Mishima (2009) correlation vs. esperimental value for R32 at 20 °C, 10 °C and 5 °C of saturation temperature.

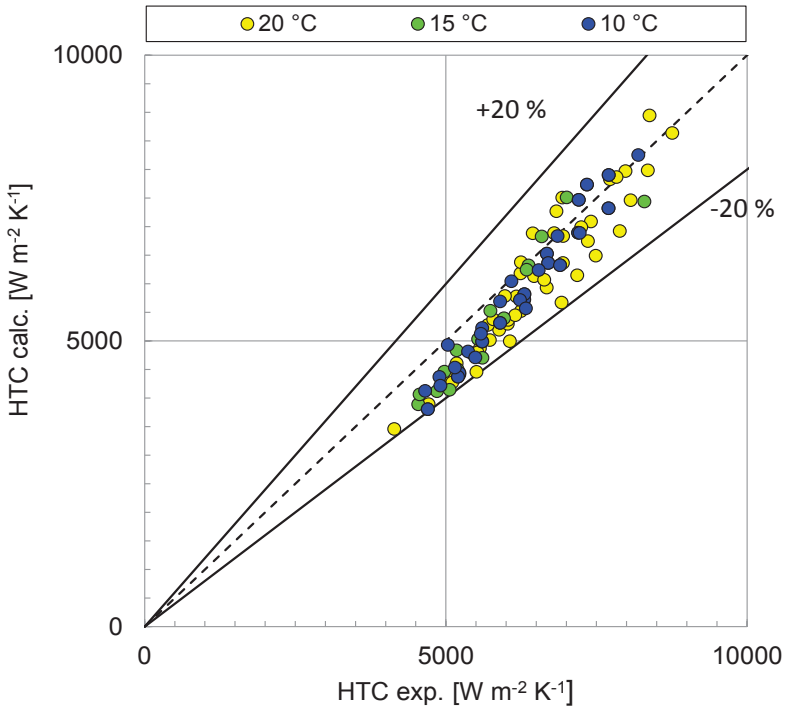

Figure 85 Heat Transfer Coefficient (HTC) calculated by Kim and Mudawar (2014a) correlation vs. esperimental value for R134a at 20 °C, 15 °C and 10 °C of saturation temperature.

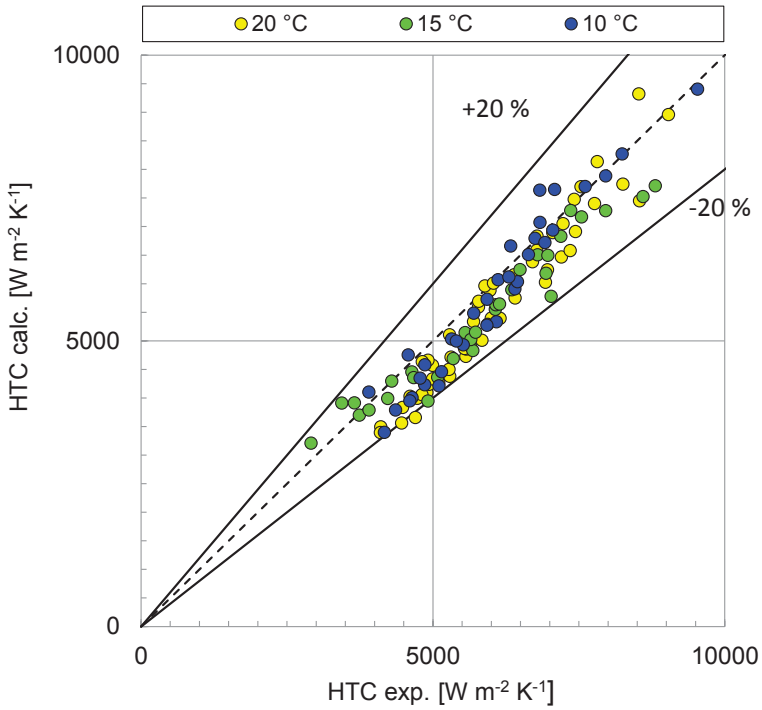

Figure 86 Heat Transfer Coefficient (HTC) calculated by Kim and Mudawar (2014a) correlation vs. esperimental value for R1234ze(E) at 20 °C, 15 °C and 10 °C of saturation temperature.

3.1.2.2 Pressure drop

As presented by Kim and Mudawar (2013), several studies on two-phase flow inside channels were realized and different approaches to predict pressure drops were proposed. The vast majority of these studies are based on the homogeneous equilibrium model or semi-empirical correlations, but the number of studies is continuously increasing.

Present experimental data points were compared against a few different correlations for two-phase pressure drop inside tube among the most common ones: Friedel (1997), Jung (2003), Mishima and Hibiki (1996), Moreno Quiben and Thome (2007), Muller- Steinhagen and Heck (1986), Sun and Mishima (2009), and Wang *et al.* (1997) are used. Table 19 shows the mean absolute percentage deviation between experimental and calculated pressure drop values for R410A, R32, R134a and R1234ze(E), respectively.

Regarding R410A and R32, the Friedel (1979) correlation shows the best performance with a mean absolute percentage deviation of 18.5 % for R410A and R32 data; furthermore, more than 60% of these data are predicted within ± 20%. Figure 87 and Figure 88 show the deviation between the experimental data and the calculated data for Friedel (1979) correlation for R410A and R32 data, respectively.

Table 19 Mean absolute percentage deviation between experimental and calculated pressure drop for R410A and R32.

Correlation	**R410A**	**R32**	**R134a**	**R1234ze(E)**
Friedel (1979)	**18.50%**	**18.5%**	**11.2%**	**15.4%**
Jung (2003)	59.6%	34.4%	35.3%	37.6%
Mishima and Hibiki (1996)	33.4%	30.1%	21.2%	20.8%
Moreno Quiben and Thome (2007)	53.5%	50.3%	11.4%	15.1%
Muller- Steinhagen and Heck (1986)	63.2%	52.8%	17.7%	14.2%
Sun and Mishima (2009)	31.4%	35.4%	24.1%	23.2%
Wang *et al.* (1997)	22.8%	20.4%	14.7%	13.4%
Kim and Mudawar (2013)	24.1%	23.5%	14.2%	18.5%

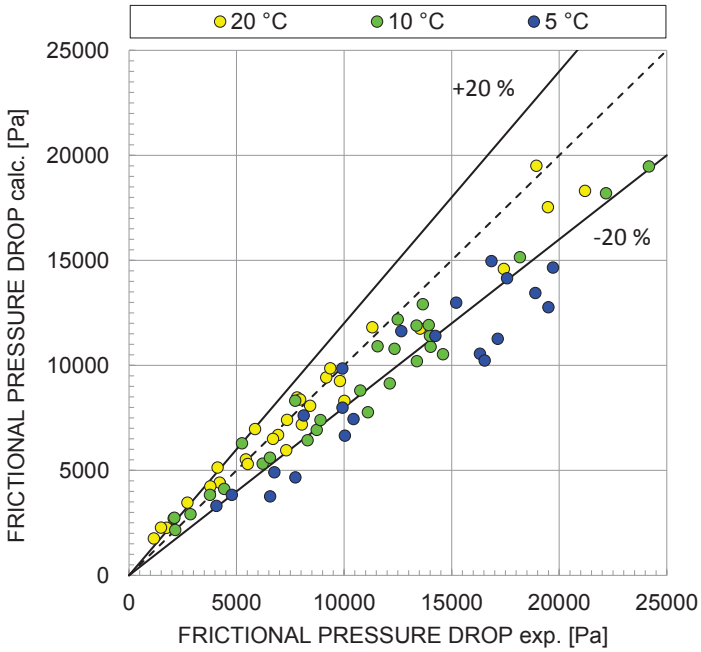

Figure 87 Pressure drop calculated by Friedel (1979) correlation vs. esperimental value for R410A at 20 °C, 10 °C and 5 °C of saturation temperature.

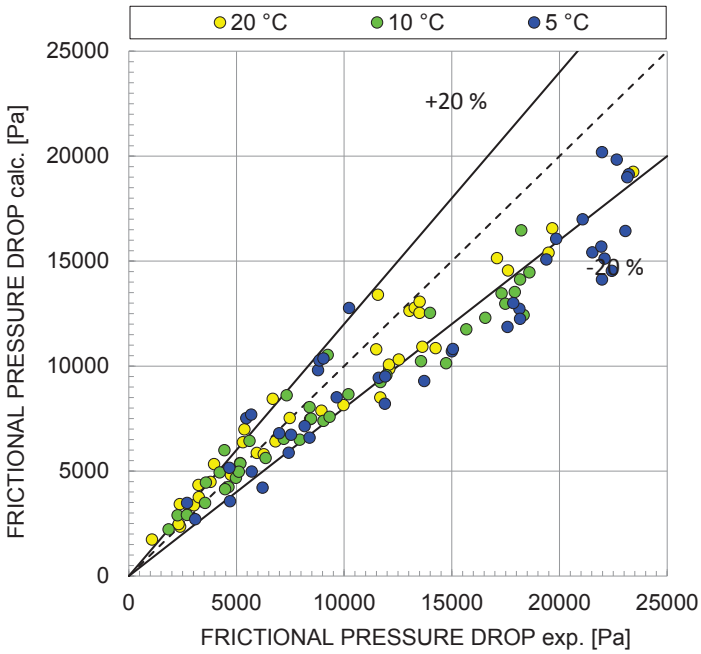

Figure 88 Pressure drop calculated by Friedel (1979) correlation vs. esperimental value for R32 at 20 °C, 10 °C and 5 °C of saturation temperature.

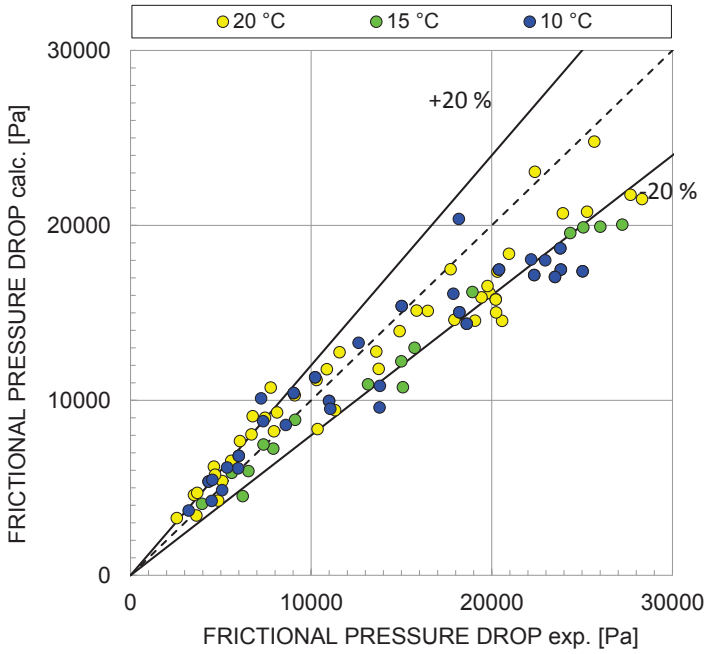

Figure 89 Pressure drop calculated by Friedel (1979) correlation vs. esperimental value for R134a at 20 °C, 15 °C and 10 °C of saturation temperature.

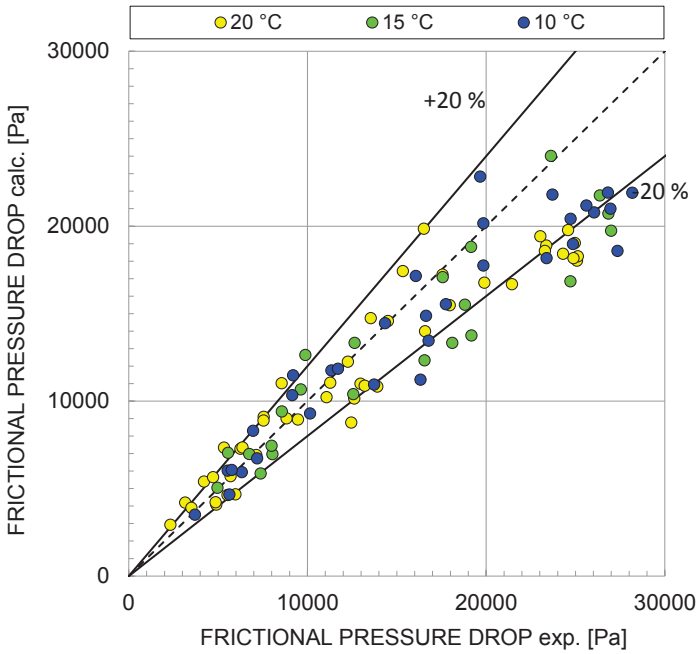

Figure 90 Pressure drop calculated by Friedel (1979) correlation vs. esperimental value for R1234ze(E) at 20 °C, 15 °C and 10 °C of saturation temperature.

As far as the couple R134a and R1234ze(E) is concerned, many correlations fit the experimental data with a fair agreement, as presented in Table 19.

For the sake of homogeneity, it has been chosen to represent the comparison between the experimental data and Fridel model (1979). Moreover it has to be underlined that this correlation is the one that presents the best results for all the data together. So, Figure 89 and Figure 90 show the calculated pressure drop using the Fridel model (1979) vs. the calculated ones when R134a and R1234ze(E) are using as refrigerant, respectively.

The data are well represented by this correlation both in magnitude and in tendency and the mean absolute deviation is 11.2% and 15.4% for R134a and R1234ze(E) respectively.

3.2 Brazed Plate Heat Exchanger

3.2.1 Experimental results

Heat Transfer Coefficients (HTCs) and pressure drop of several low GWP refrigerants were analyzed inside a commercial Brazed Plate Heat Exchanger (BPHE). R1234ze(E) and R32 were studied during both condensation and vaporization processes, and R152a and R1234ze(Z) during the condensation process.

For each fluid the heat transfer coefficients and pressure drops were experimentally measured and the effects of heat flux, saturation temperature, and outlet conditions were investigated.

3.2.1.1 Vaporization

Two sets made up of 138 vaporization tests with refrigerant up-flow and water down-flow were carried with two different fluids R1234ze(E) and R32.

For each set four different evaporator outlet conditions were investigated: an outlet vapor quality around 0.8, an outlet vapor quality around 1, a vapor super-heating at the exit of the heat exchanger around 5 °C and a vapor super-heating of around 10 °C). The inlet vapor quality ranges between 0.19 and 0.33, which is a common working condition for brazed plate evaporators.

Different saturation temperatures were tested: 10 °C, 15 °C and 20 °C with R1234ze(E) as refrigerant, and 5 °C , 10 °C, and 20 °C with R32.

Table 20 gives the main operating conditions in the evaporator under experimental tests: refrigerant saturation temperature t_{sat} and pressure p_{sat}, inlet and outlet refrigerant vapor quality x_{in} and x_{out}, outlet refrigerant super-heating Δt_{sup}, mass flux on refrigerant side G_r and water side G_w, and heat flux q.

A detailed error analysis performed in accordance with Kline and McClintock (1953) indicates an overall uncertainty within ±12.0% for the refrigerant heat transfer coefficient measurement and within ±6.6% and ±17.3% for the total pressure drop measurement for R1234ze(E) and R32, respectively.

Table 20 Operating conditions during vaporization tests inside the BPHE.

Refrigerant	R1234ze(E)	R32
t_{sat} [°C]	9.9–20.2	5.0–20.1
p_{sat} [MPa]	0.30–0.43	0.95–2.30
x_{in} [-]	0.19–0.30	0.19–0.33
x_{out} [-]	0.79–1.00	0.79–0.98
Δt_{sup} [°C]	4.6–10.3	4.7–10.9
G_r [kg $m^{-2}s^{-1}$]	11.1–31.4	9.5–29.1
G_w [kg$m^{-2}s^{-1}$]	49.0–141.9	55.6–190.0
q [kWm^{-2}]	3.7–16.7	5.2–24

3.2.1.1.1 Heat transfer coefficient

3.2.1.1.1.1 R1234ze(E)

Figure 91, Figure 92, and Figure 93 represent the boiling heat transfer coefficients vs. the heat flux as a function of the different evaporator outlet conditions (i.e. outlet vapor quality around 0.8 and 1., vapor super-heating at the exit of the heat exchanger around 5 °C and 10 °C) for 10 °C, 15 °C and 20 °C of saturation temperature, respectively.

A remarkable effect of the heat flux and of the outlet conditions on the heat transfer coefficients is displayed. On the contrary, the impact of the saturation temperature on the heat transfer coefficient appears relatively less significant. In fact, the HTCs when the outlet vapor quality is around 0.8 are 6-11% higher than those when the outlet vapor quality is around 1, 13-16% higher than those when the vapor at the outlet is super-heated of around 5 °C, and 39-46% higher than those when the vapor exits with 10 °C of super-heating.

The inception of the dry-out might justify the slight decrease of the boiling heat transfer coefficient when outlet vapor quality increases from 0.8 to 1, whereas the increase of the outlet vapor super-heating involves a considerable degradation of the boiling heat transfer coefficients.

Examining the heat flux influence, a lower heat flux affects the decreasing of the HTCs. For example, doubling the heat flux the HTC becomes up to 2.5 times greater at 20 °C of saturation temperature.

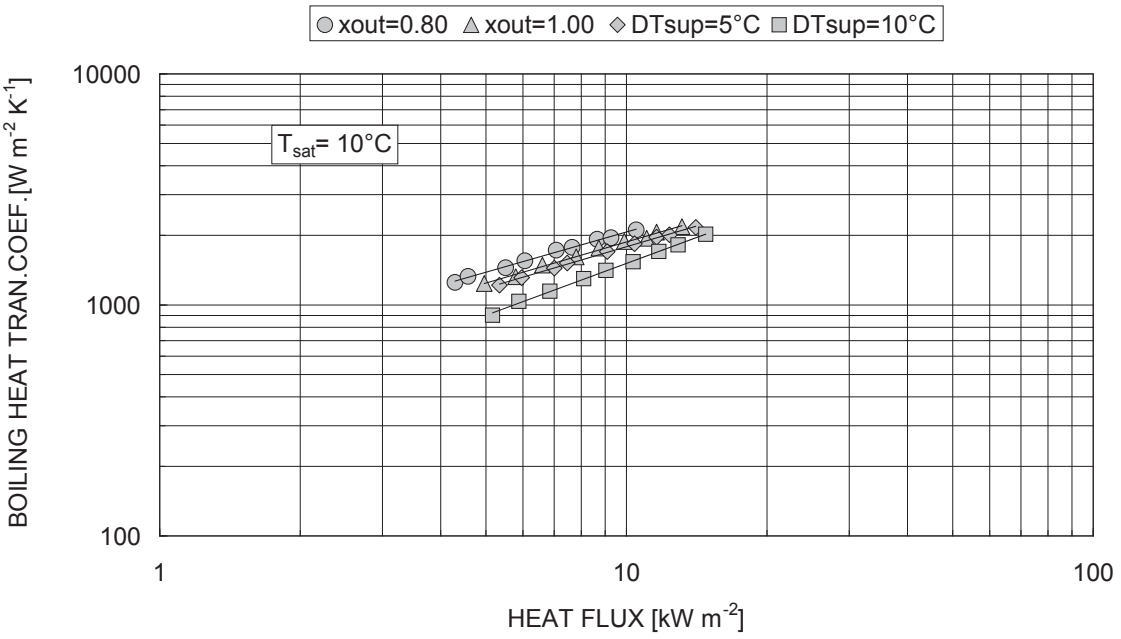

Figure 91 Average boiling heat transfer coefficient vs. heat flux at t_{sat}=10 °C as a function of the refrigerant outlet conditions.

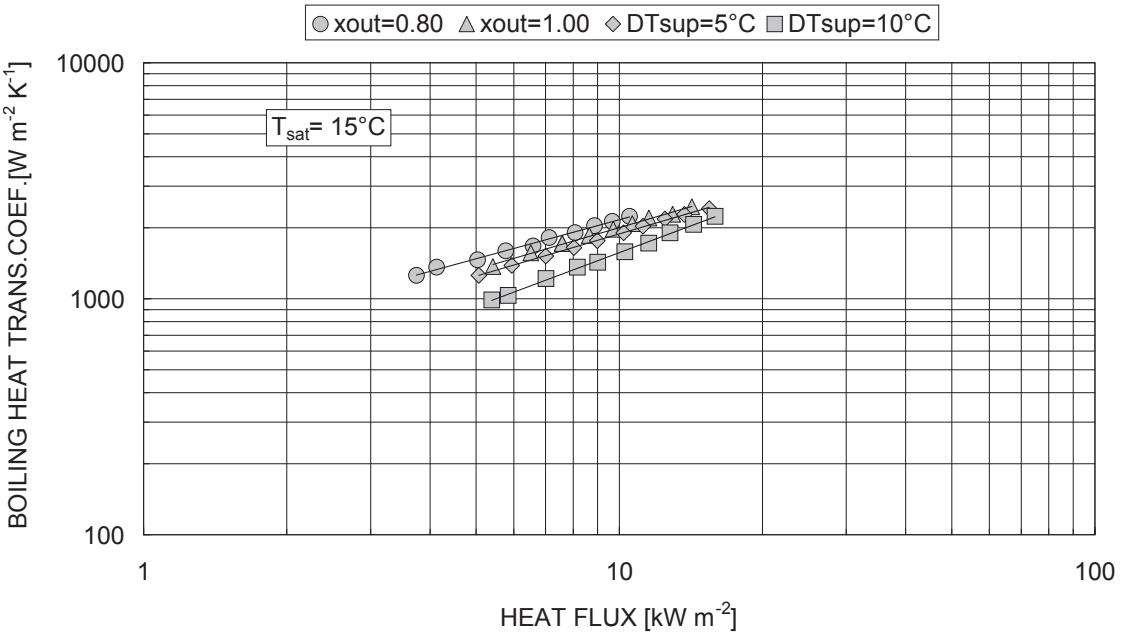

Figure 92 Average boiling heat transfer coefficient vs. heat flux at t_{sat}=15 °C as a function of the refrigerant outlet conditions.

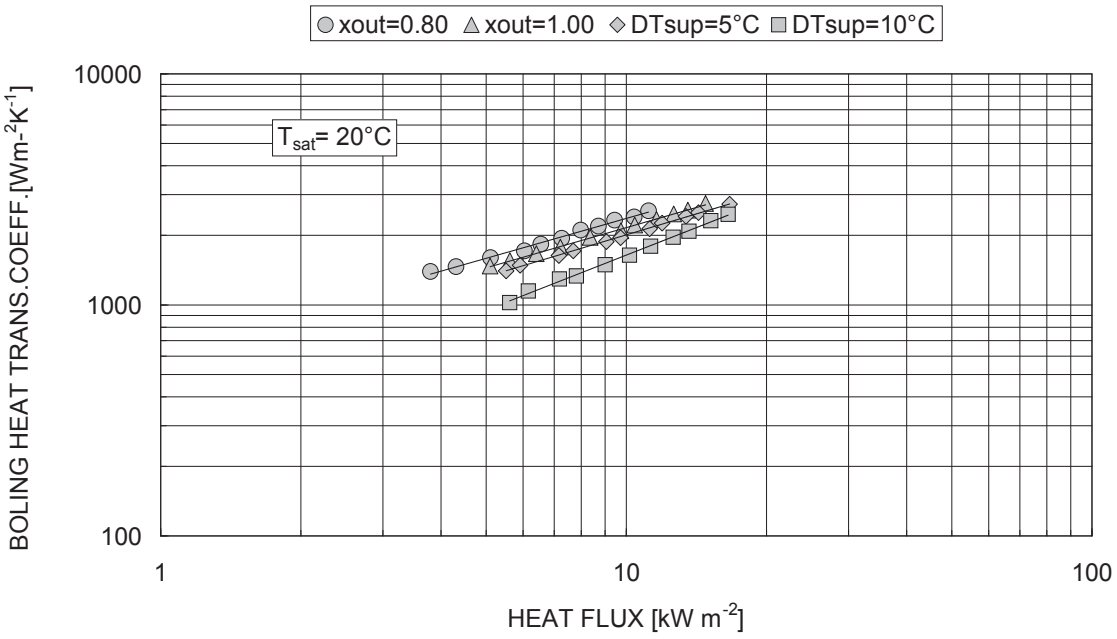

Figure 93 Average boiling heat transfer coefficient vs. heat flux at t_{sat}=20 °C as a function of the refrigerant outlet conditions.

3.2.1.1.1.2 R32

Figure 94, Figure 95, and Figure 96 show the average HTC as a function of the heat flux at four different evaporator outlet conditions (vapor quality around 0.8 and 1, and vapor super-heating around 5 °C and 10 °C) and at three saturation temperatures: 5 °C , 10 °C and 20 °C, respectively.

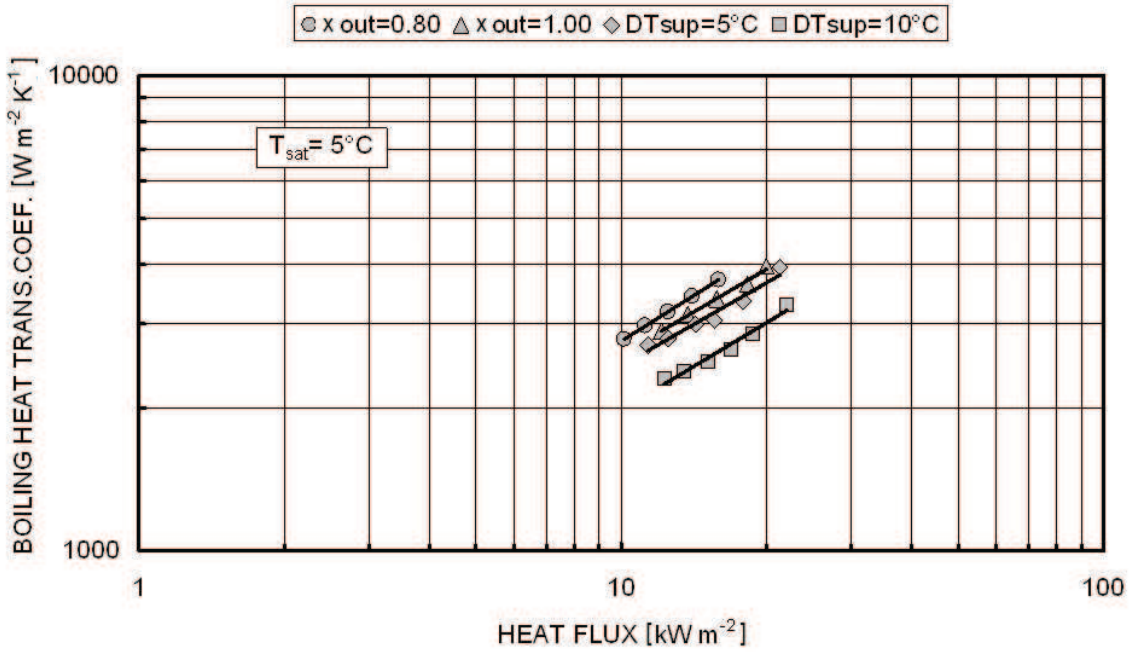

Figure 94 Average boiling heat transfer coefficient vs. heat flux at t_{sat}=5 °C as a function of the refrigerant outlet conditions.

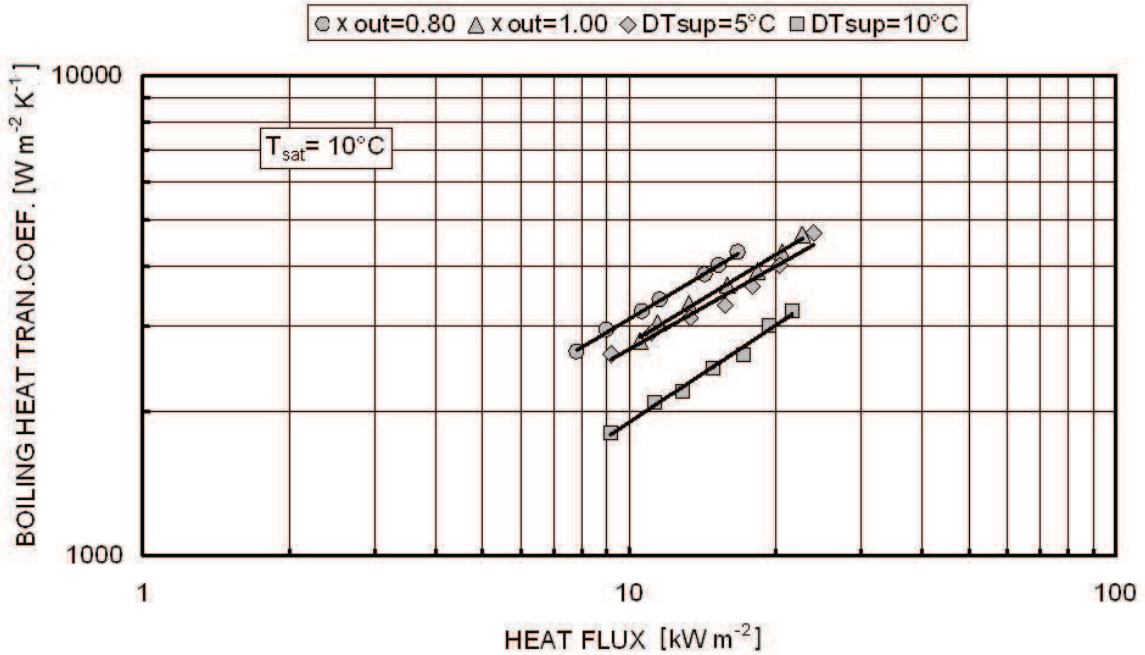

Figure 95 Average boiling heat transfer coefficient vs. heat flux at t_{sat}=10 °C as a function of the refrigerant outlet conditions.

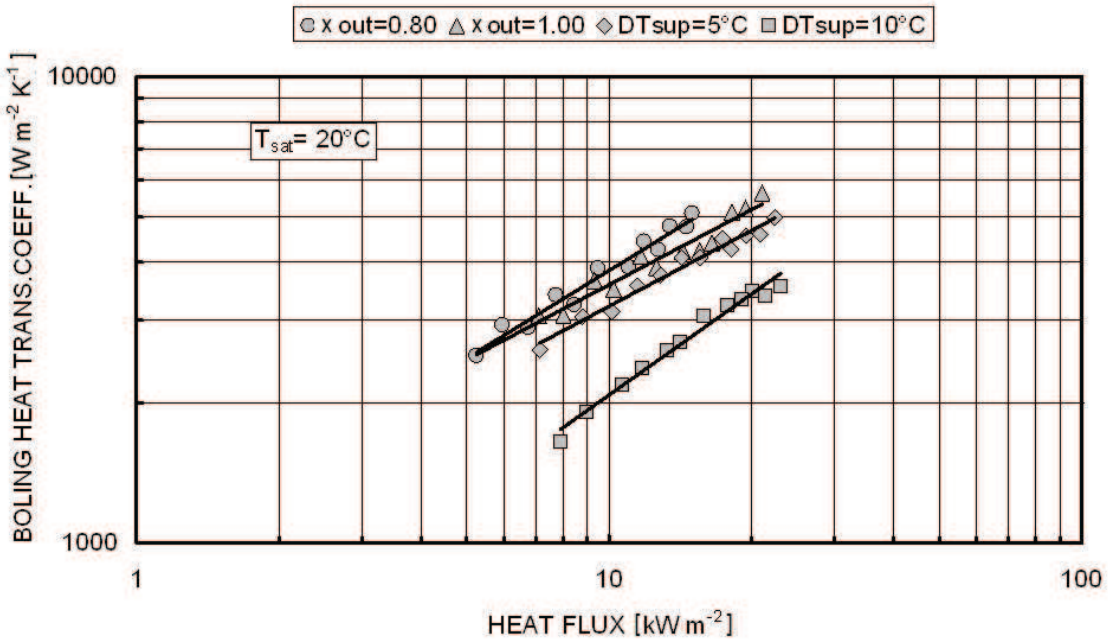

.

Figure 96 Average boiling heat transfer coefficient vs. heat flux at t_{sat}=20 °C as a function of the refrigerant outlet conditions.

The saturated boiling Heat Transfer Coefficients (HTCs) depend on the outlet conditions: in fact the HTCs when the outlet vapor quality is around 0.8 are 6-11% higher than the heat transfer coefficients when the outlet vapor quality is around 1, 13-15% higher than the heat transfer coefficients when the evaporator works with 5 °C of outlet vapor super-heating, and 39-46% higher than the heat transfer coefficients when the evaporator works with 10°C of outlet vapor super-heating.

The slight decrease of the heat transfer coefficients with increasing vapor quality is probably due to a dry-out inception in the upper part of the evaporator. The marked decrease of the heat transfer coefficients with vapor super-heating is due to the increase in the super-heating portion of the heat transfer surface which is affected by gas single phase heat transfer coefficients that are one or two orders of magnitude lower than the two phase heat transfer coefficients ones.

In addition the HTCs are strongly affected by heat flux. For example at t_{sat}=20 °C (Figure 96) increasing the heat flux 2.5 times, the boiling HTC becomes 2.2 times greater when ΔT_{sup}=10 °C and 2 times greater when x_{out}=0.8. On the contrary they are weakly affected by the saturation temperature.

3.2.1.1.2 Pressure drop

3.2.1.1.2.1 R1234ze(E)

Figure 97 shows the frictional pressure drop plotted against the kinetic energy per unit volume of the refrigerant flow computed by the homogeneous model (defined as in Eq. 59) at different saturation temperatures: 10 °C, 15 °C and 20 °C.

$$KE/V=G^2/(2\,\rho_m) \qquad \text{Eq. 59}$$

There is a fairly linear correlation between frictional pressure drop and the kinetic energy per unit volume of the refrigerant flow.

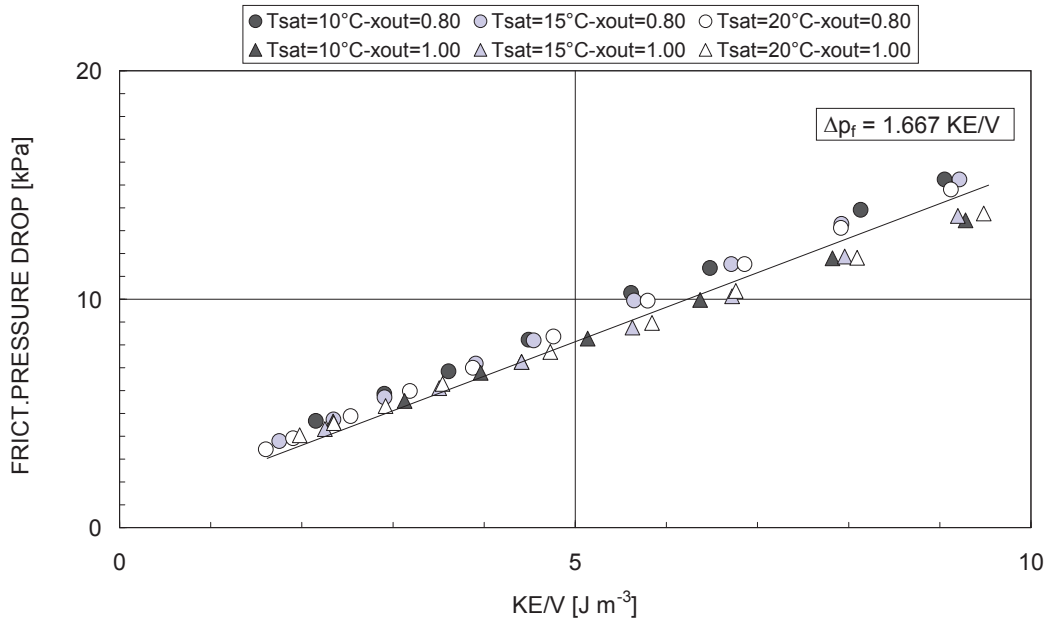

Figure 97 Frictional pressure drop vs. kinetic energy per unit volume of R1234ze(E) refrigerant flow at different saturation temperatures and refrigerant outlet conditions.

Eq. 60 derives from a best fit operation on the experimental data collected, where the frictional pressure drop are reported in kPa.

$\Delta p_f = 1.667\ KE/V$ Eq. 60

This linear correlation reproduces present set of experimental data points with a mean absolute percentage deviation around 7.2%.

3.2.1.1.2.2 R32

Figure 98 shows the frictional pressure drop plotted against the kinetic energy per unit volume of the refrigerant flow computed by the homogeneous model (Eq. 59) at different saturation temperatures:

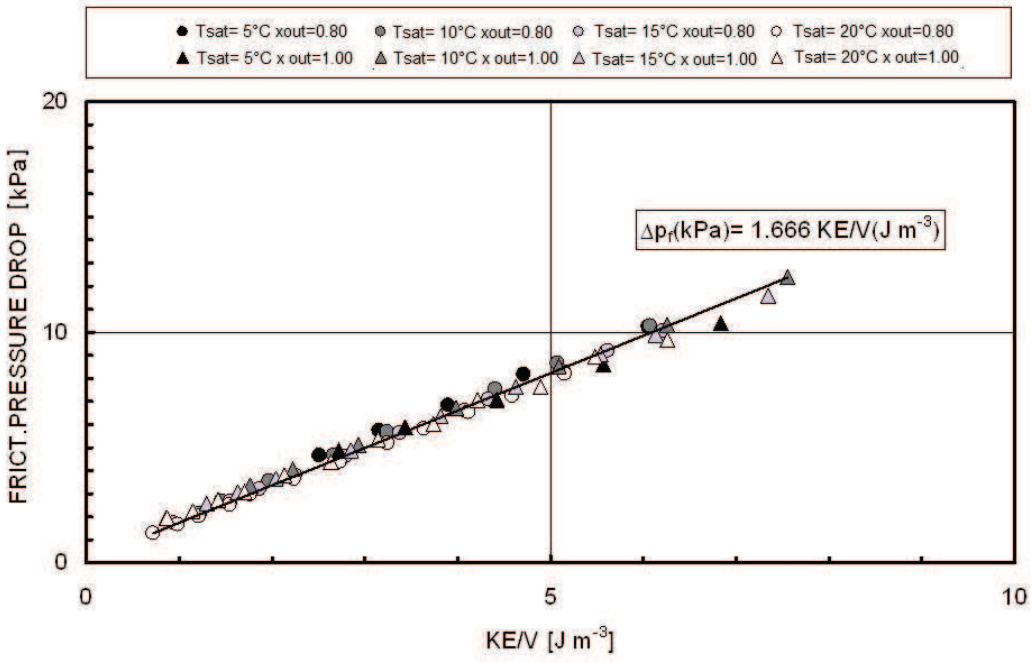

Figure 98 Frictional pressure drop vs. kinetic energy per unit volume of R32 refrigerant flow at different saturation temperatures and refrigerant outlet conditions.

The frictional pressure drop presents a linear dependence on the kinetic energy per unit volume of the refrigerant flow and therefore a quadratic dependence on the refrigerant mass flux. It does not depend on the outlet conditions and on the saturation temperature.

Eq. 61 derives from a best fitting operation among the R32 vaporization experimental data, where the frictional pressure drop are reported in kPa. It reproduces the present experimental data with a mean absolute percentage deviation around 5.3%.

$$\Delta p_f = 1.666\ KE/V \qquad \text{Eq. 61}$$

3.2.1.1.3 Infrared analysis

A thermography analysis was accomplished to study the vaporization process inside the BPHE. This analysis is aimed at investigating the heat transfer regimes and to quantify the portion of heat transfer area affected by vapor super-heating and the one that works in two-phase. In fact, in the real operating conditions of a BPHE evaporator inside a refrigerating machine, some degrees of vapor super-heating are requested at the outlet of the evaporator to prevent wet compression depending on the nature of the refrigerant (low, medium or high molecular weight), the type of compressor (alternative, scroll, screw, centrifugal), and the type of expansion device (thermostatic or electronic valve).
In order to quantify the portion of the heat transfer surface affected by vapor super-heating, the side of the BPHE was filmed during the experimental tests by an IR thermo-camera (temperature uncertainty (k=2)=±0.1 °C in the temperature range 5 – 150 °C). The dotted line indicates the BPHE profile, the red color represents the hottest areas while the blue color the coldest ones, at a temperature close to the saturation one.

3.2.1.1.3.1 R1234ze(E)

Figure 99 and Figure 100 show the IR thermography realized during the vaporization tests with R1234ze(E) as refrigerant at 20 °C with a heat flux of 6 and 10 kWm^{-2}, respectively. The four different evaporator outlet conditions, presented in section 3.2.1.1, were analyzed (i.e. outlet vapor quality 0.8 and 1, vapor super-heating at the outlet 5 °C and 10 °C).
In the saturated boiling tests the heat transfer surface has a temperature close to the saturation one and therefore it is probably affected only by two-phase heat transfer. No evidences of dry-out inception can be observed in these tests. In the tests with 5 °C of outlet vapor super-heating around 15-30% of the heat transfer surface is affected by gas single-phase heat transfer (yellow-green area in the upper part of the BPHE), and this portion of the heat transfer surface increases up to 40-50% (red area in the upper part of the BPHE) at 10°C of outlet vapor super-heating.
The gas single-phase heat transfer coefficients that occur in the vapor super-heated region are one or two orders of magnitude lower than the two-phase heat transfer coefficients that occur in the two-phase

region, therefore the degrees of vapor super-heating at the outlet of the evaporator must be limited at the minimum value for a safe operation of the refrigerating unit, 3-5 °C, for avoiding a degradation of the evaporator thermal performance and effectiveness.

The IR thermography analysis substantially confirms the experimental measurement of the boiling heat transfer coefficients.

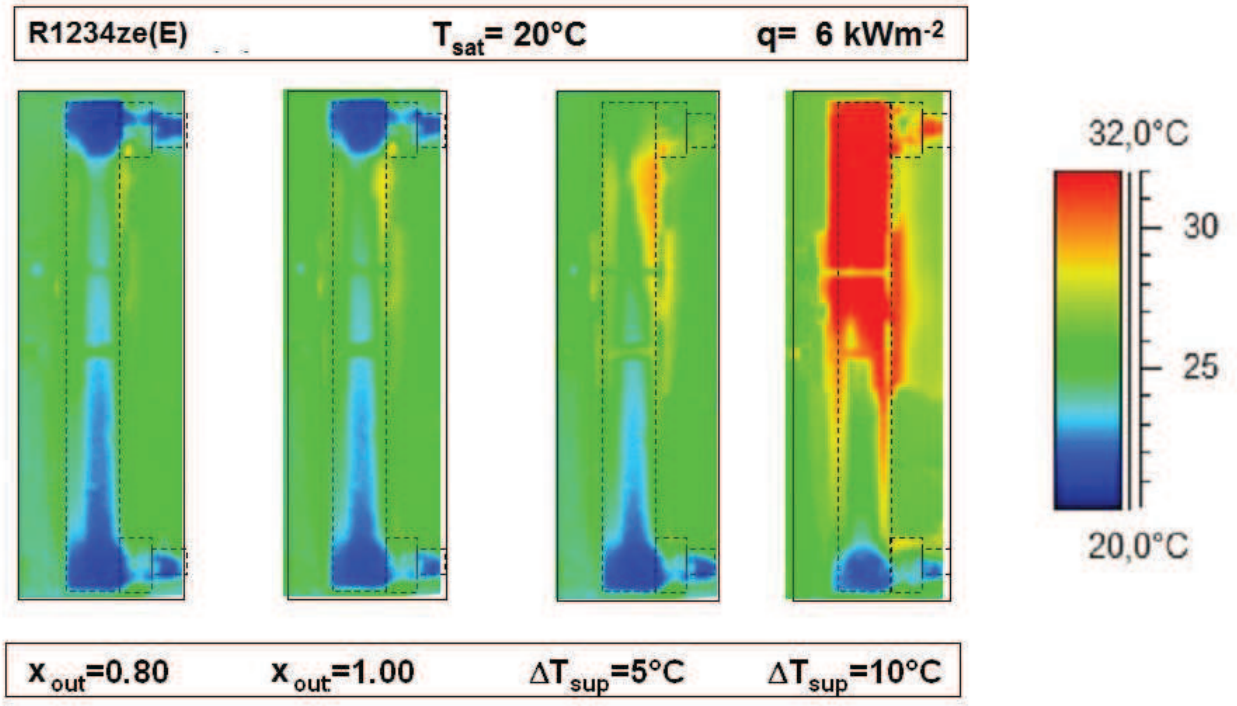

Figure 99 IR thermography during R1234ze(E) vaporization in a BPHE with different refrigerant outlet conditions. t_{sat}=20 °C, q=6 kW m^{-2}.

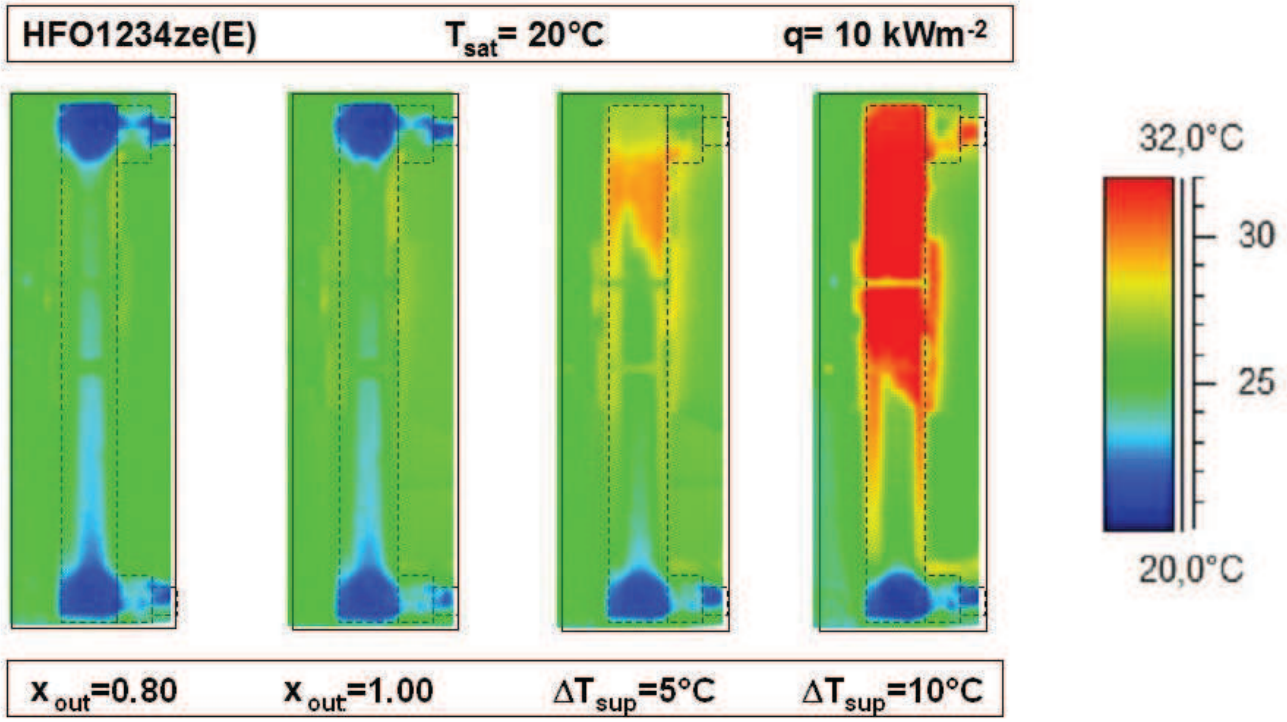

Figure 100 IR thermography during R1234ze(E) vaporization in a BPHE with different refrigerant outlet conditions. t_{sat}=20 °C, q=20 kW m^{-2}.

3.2.1.1.3.2 R32

Figure 101, Figure 102, Figure 103, and Figure 104 show the results of the IR thermography effectuated during R32 vaporization tests as a function of various outlet conditions at fixed heat flux (around 10 and 20 kWm^{-2}) at 10 and 20 °C of saturation temperature, respectively.

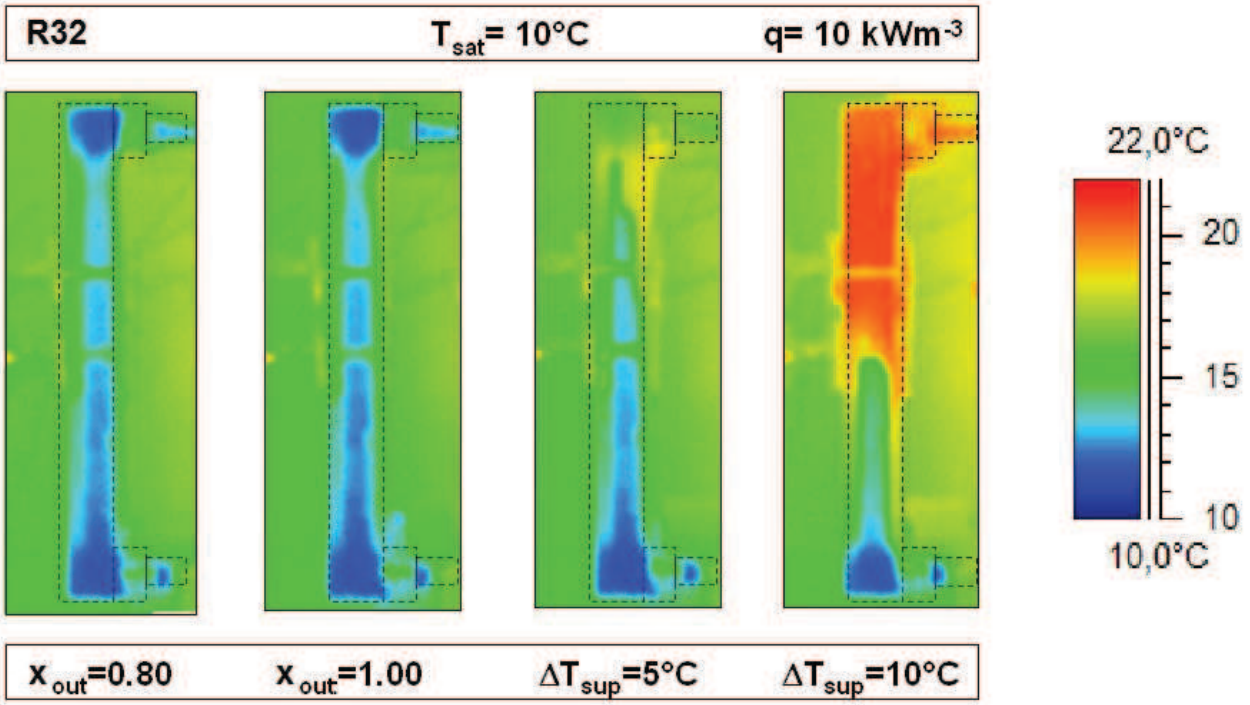

Figure 101 IR thermography during R32 vaporization with different outlet conditions. t_{sat}=10 °C, q=10 kW m^{-2}

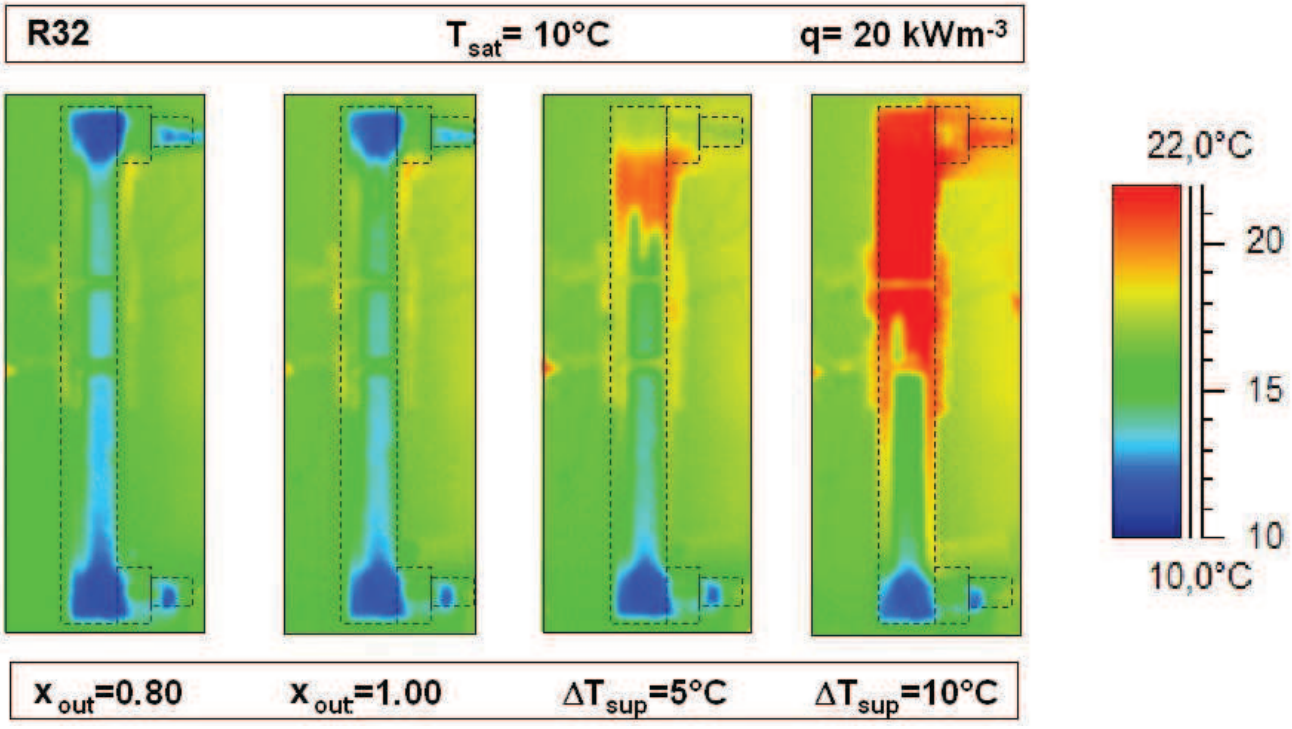

Figure 102 IR thermography during R32 vaporization with different outlet conditions. t_{sat}=10 °C, q=20 kW m^{-2}.

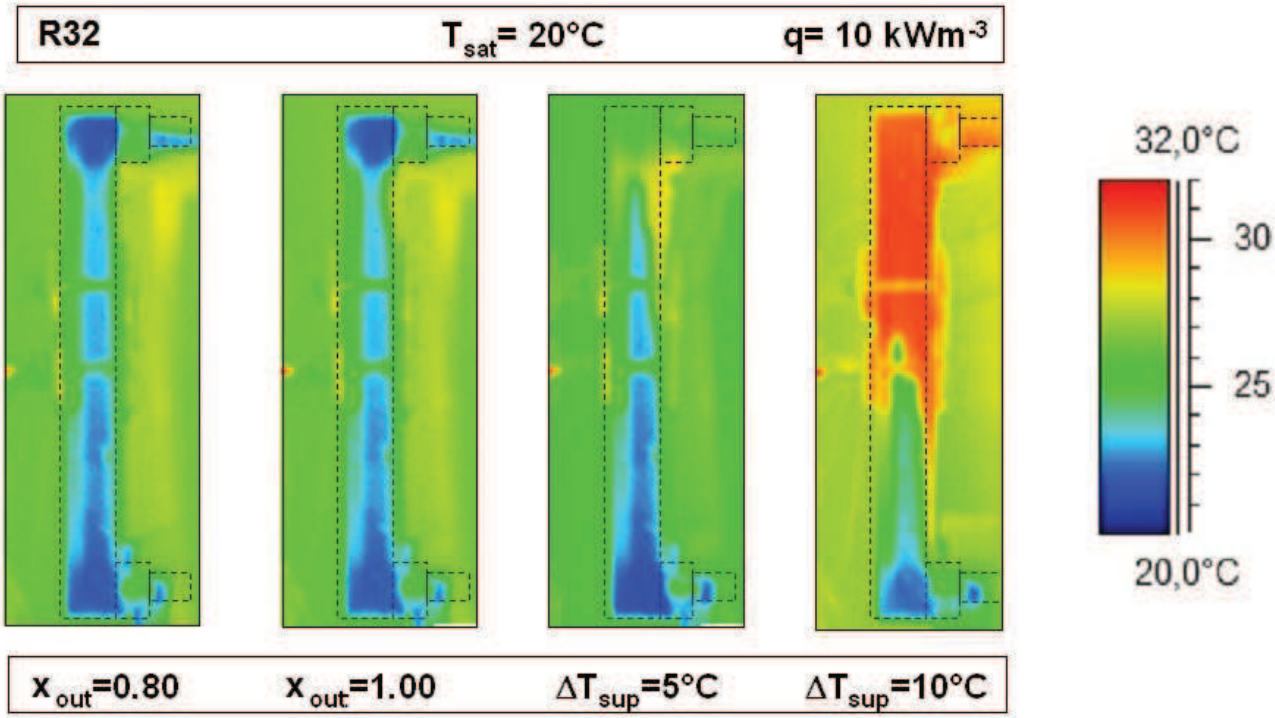

Figure 103 IR thermography during R32 vaporization with different outlet conditions. t_{sat}=20 °C, q=10 kW m^{-2}.

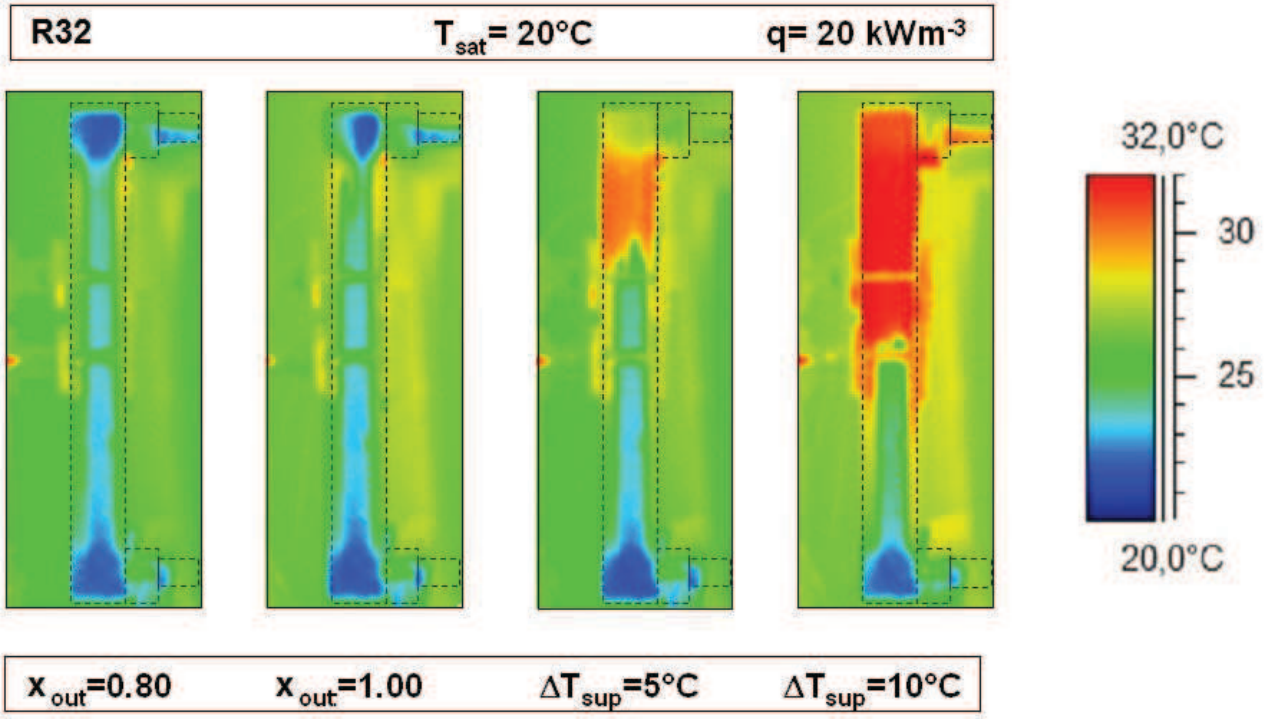

Figure 104 IR thermography during R32 vaporization with different outlet conditions. t_{sat}=20 °C, q=20 kW m^{-2}.

During the saturated boiling tests (x_{out}=0.8 and 1) the whole heat transfer surface works in two-phase heat transfer and it is near to saturation temperature (blue color). At 5 °C of outlet vapor super-heating, around 15-30% of the heat transfer surface (yellow-green area in the upper part of the BPHE) is affected by super-heating, whereas at 10 °C of outlet vapor super-heating this portion increases up to 40-50% (red area in the upper part of the BPHE).
The results of the IR thermography analysis contribute to explain the great sensitivity of the heat transfer coefficients to the evaporator outlet conditions confirming that the dry-out phenomena leads to a great degradation of the heat transfer performance of the BPHE evaporators.

3.2.1.2 Condensation

Four different refrigerants, namely R152a, R1234ze(E), R1234ze(Z), and R32, were tested during condensation inside a BPHE. Different saturation temperatures were investigated: 25 °C, 30 °C, 35 °C, and 40 °C.
Two types of condensation tests were conducted: in the first one the inlet vapor quality varies around 1 and the outlet vapor quality around 0 (saturated vapor conditions). While in the second one super-heated (around 10 °C) vapor conditions are reached at the inlet of the heat exchanger and sub-cooled (from 0 °C to 5 °C) conditions at the outlet, these working conditions are similar to chiller and heat pump applications real ones. (Palm and Claesson, 2006).

Table 21 summarizes the operating conditions during all the tests conducted during refrigerant condensation inside the commercial BPHE under analysis: the refrigerant saturation temperature t_{sat}, the inlet and outlet refrigerant vapor quality x_{in} and x_{out}, the inlet vapor super-heating Δt_{sup} and outlet condensate sub-cooling Δt_{sub}, the refrigerant mass flux G_r and the heat flux q are reported.
A detailed error analysis following the method of Kline and McClintock (1954) is reported in Table 22 for each refrigerant with an overall uncertainty (k=2).

Table 21 Operating conditions during condensation tests in a BPHE.

Refrigerant	Runs	t_{sat} [°C]	x_{in} [-]	x_{out} [-]	Δt_{sup} [°C]	Δt_{sub} [°C]	G_r [kg m^{-2} s^{-1}]	q [kW m^{-2}]
R152a	45	25-40	0.94-0.99	0.0-0.06	-	-	7.3-32.6	7.1-30.8
R152a	46	25-40	-	-	9.2-11.2	0.1-1.6	9.1-32.2	9.3-33.4
R1234ze(E)	53	25-40	0.92-1.00	0.0-0.09	-	-	10.7-39.6	5.3-23.5
R1234ze(E)	55	25-40	-	-	9.8-11.0	0.3-3.64.9	11.9-39.9	7.2-26.0
R1234ze(Z)	42	30-40	0.91-0.97	0.0-0.06	-	-	7.7-33.0	5.1-23.3
R32	53	25-40	0.92-0.99	0.0-0.05	-	-	10.3-37.6	7.9-34.4
R32	55	25-40	-	-	9.6-10.9	0.4-3.6	10.2-39.1	10.1-40.1

Table 22 Heat transfer and pressure drop uncertainty (k=2) in a BPHE during condensation

Refrigerant	Heat transfer uncertainty (k=2)	Pressure drop uncertainty (k=2)
R152a	±12.0%	±13.8%
R1234ze(E)	±12.0%	±11.8%
R1234ze(Z)	±12.0%	±10%
R32	±12.0%	±20%

3.2.1.2.1 Heat transfer coefficient

3.2.1.2.1.1 R1234ze(E)

Figure 105 shows condensation Heat Transfer Coefficient (HTC) vs. refrigerant mass flux for saturated vapor and super-heated vapor condensation at 25 °C, 30 °C, 35 °C and 40 °C of saturation temperature. The heat transfer coefficients are weakly influenced by the saturation temperature and, furthermore, they are lightly dependent on the outlet conditions. The super-heated vapor heat transfer coefficients are from 8% to 11% higher than those of saturated vapor for the same refrigerant mass flux. In fact, vapor super-heating affects condensation kinetics reducing the condensate film thickness and increasing the heat transfer coefficient with respect to saturated vapor as demonstrated by Fujii (1991) and by Mitrovic (2000) for laminar film condensation and by Webb (1998) for forced convection condensation.

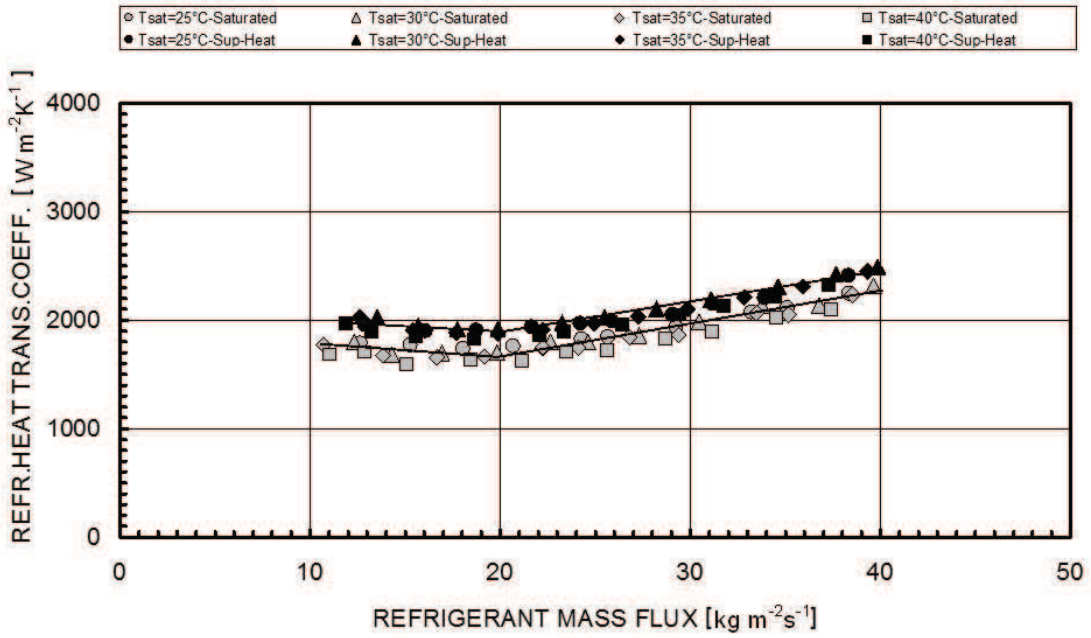

Figure 105 R1234ze(E) HTC vs. refrigerant mass flux at 25, 30, 35 and 40 °C of saturation temperature at different refrigerant inlet conditions.

The saturated vapor data and the super-heated vapor data show the same trend vs. refrigerant mass flux. At low refrigerant mass fluxes (G<20 kg $m^{-2}s^{-1}$) the heat transfer coefficients are independent of mass flux and, as presented in section 1.4.2.2, the condensation is likely gravity-dominated. For higher refrigerant mass fluxes (G>20 kg $m^{-2}s^{-1}$) the heat transfer coefficients depend on mass flux and forced convection condensation occurs. In the forced convection condensation region a doubling of the refrigerant mass flux (from G=20 kg $m^{-2}s^{-1}$ to G=40 kg $m^{-2}s^{-1}$) involves a 32% to 35% enhancement in the heat transfer coefficient (from 1700 W $m^{-2}K^{-1}$ to 2300 W $m^{-2}K^{-1}$ for saturated vapor and from 1900 W $m^{-2}K^{-1}$ to 2500 W $m^{-2}K^{-1}$ for super-heated vapor condensation).

3.2.1.2.1.2 R1234ze(Z)

Figure 106 shows the average HTC vs. the refrigerant mass flux for R1234ze(Z) during a saturated vapor condensation at different saturation temperatures (30 °C, 35 °C, and 40 °C).
The heat transfer coefficient presents a relationship with the saturation temperature. In fact, decreasing the saturation temperature from 40 °C to 30 °C, the HTC increases of around +15-20%. In addition the HTC is strongly affected by the refrigerant mass flux. At low refrigerant mass flux (G<15 kg m^{-2} s^{-1}) the heat transfer coefficients does not dependent on mass flux and probably condensation is controlled by gravity. For higher refrigerant mass flux (G>15 kg m^{-2} s^{-1}) the heat transfer coefficients depend on mass flux and forced convection condensation seems to be dominant. In the forced convection condensation region a doubling of the refrigerant mass flux (from 15–16 kg m^{-2} s^{-1} to 30–33 kg m^{-2} s^{-1}) involves a 30% enhancement in the heat transfer coefficient (from 2500 to 3300W m^{-2} K^{-1}).

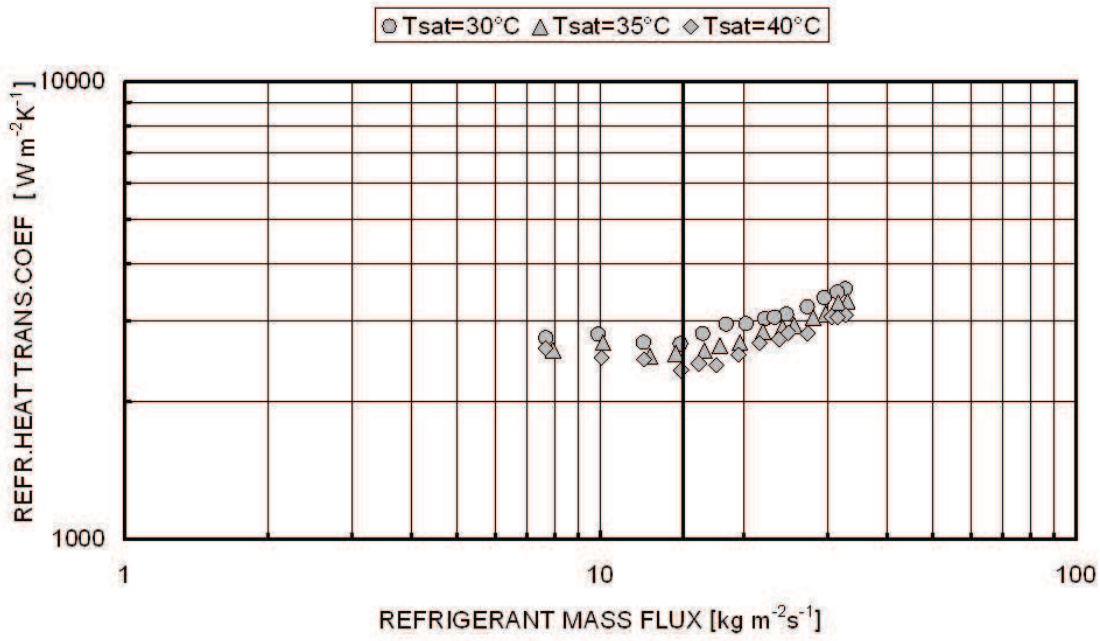

Figure 106 Saturated R1234ze(Z) HTC vs. refrigerant mass flux at 30, 35 and 40 °C of saturation temperature.

3.2.1.2.1.3 R152a

Figure 107 shows the refrigerant-side Heat Transfer Coefficient (HTC) vs. the refrigerant mass flux for saturated vapor and super-heated vapor condensation at 25 °C, 30 °C, 35 °C, and 40 °C of saturation temperature.

At low refrigerant mass fluxes (G<15 kg m^{-2} s^{-1}) heat transfer coefficients are negligibly influenced by the saturation temperature, while they present a weak dependency to the outlet conditions. In fact the super-heated vapor HTCs are 6–8% higher than those of saturated vapor at the same refrigerant mass flux.

The collected experimental data having low mass fluxes exhibit a trend similar to that predicted by the Nusselt analysis. In fact the heat transfer coefficient slightly increases for decreasing mass flux and heat flux (temperature difference).

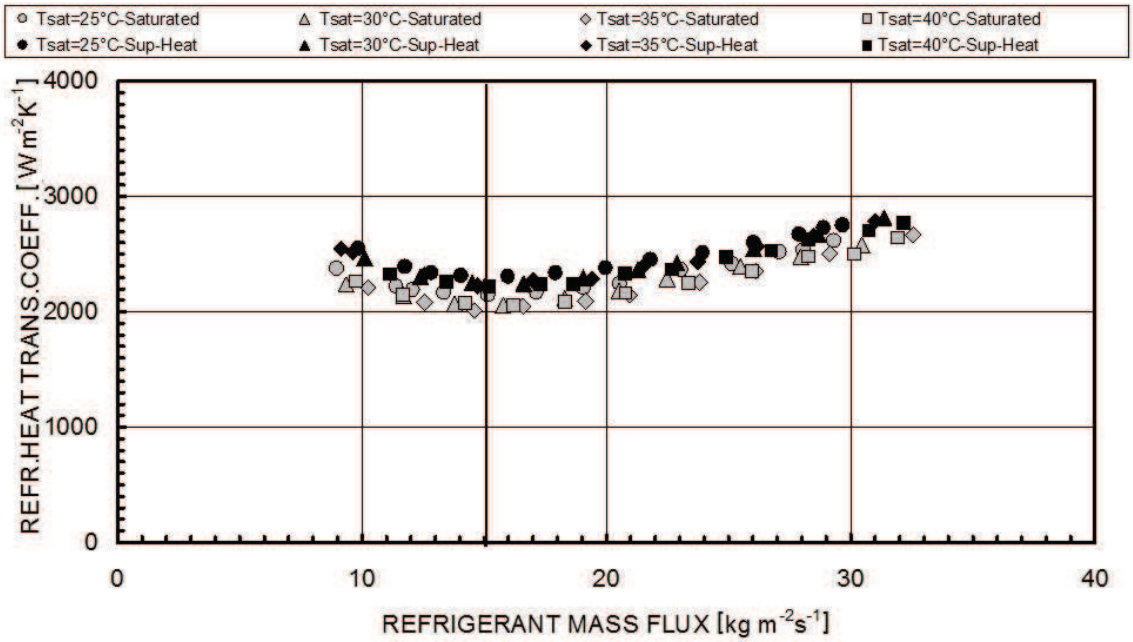

Figure 107 R32 HTC vs. refrigerant mass flux at 25, 30, 35 and 40 °C of saturation temperature at different refrigerant inlet conditions.

It should be noted that, as the experimental tests were performed with an almost constant vapor quality change through the condenser, there is a direct relationship between mass flux and heat flux. In this zone the condensation is likely gravity-dominated, as presented in section 1.4.2.2.

On the other hand, for higher refrigerant mass fluxes (G>15 kg m^{-2} s^{-1}) the heat transfer coefficients increase with increasing mass flux and forced convection condensation occurs. In the forced convection condensation region a doubling of the refrigerant mass flux (from 15–16 kg m^{-2} s^{-1} to 30–32 kg m^{-2} s^{-1}) involves a 27% to 29% enhancement in the heat transfer coefficient (from 2050 W m^{-2} K^{-1} to 2650 W $m^{-2}K^{-1}$ for saturated vapor and from 2200 W m^{-2} K^{-1} to 2800 W m^{-2} K^{-1} for super-heated vapor condensation).

3.2.1.2.1.4 R32

Figure 108 shows the refrigerant-side Heat Transfer Coefficient (HTC) vs. the refrigerant mass flux for saturated vapor and super-heated vapor condensation at 25 °C, 30 °C, 35 °C, and 40 °C of saturation temperature.

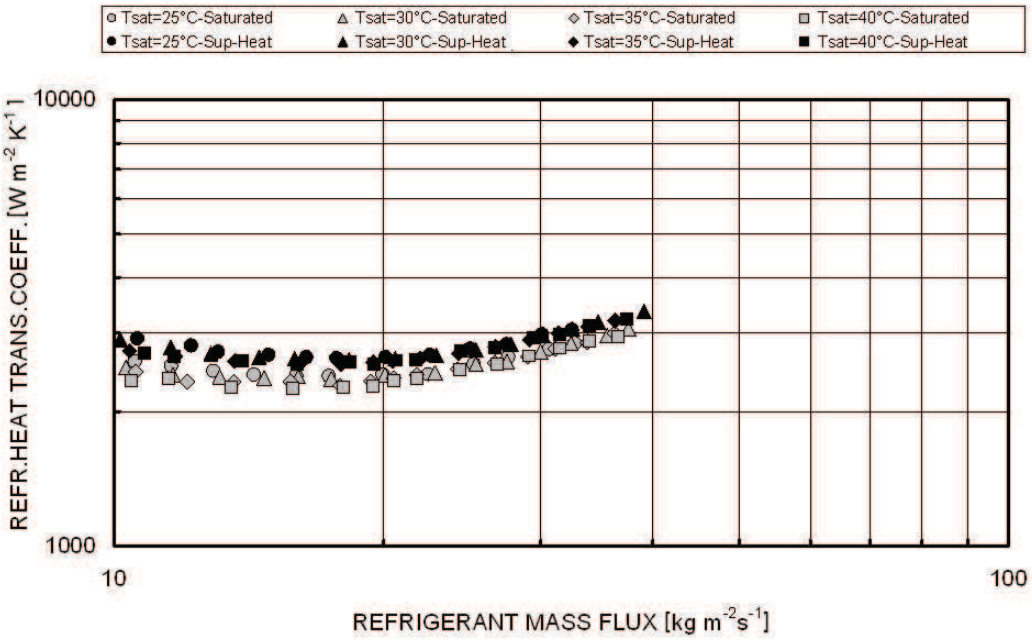

Figure 108 R32 HTC vs. refrigerant mass flux at 25, 30, 35, and 40 °C of saturation temperature at different refrigerant inlet conditions.

The heat transfer coefficients show a low to negligible sensitivity to saturation temperature (maximum difference around 10% at the lowest mass fluxes), while they are weakly influenced by the outlet conditions. In fact the super-heated vapor HTCs are 8-10% higher than those of saturated vapor at the same refrigerant mass flux.

A transition point between gravity dominated and forced convection condensation can be observed at a refrigerant mass flux around 20 kg $m^{-2}s^{-1}$. For refrigerant mass flux lower than 20 kg $m^{-2}s^{-1}$ the heat transfer coefficients increase for decreasing mass flux and therefore for decreasing temperature difference as predicted by the Nusselt (1916) analysis for laminar film-condensation on a vertical surface. For refrigerant mass flux higher than 20 kg $m^{-2}s^{-1}$ the heat transfer coefficients increase with refrigerant mass flux up to a 27-30% enhancement for a doubling of the refrigerant mass flux.

3.2.1.2.2 *Pressure drop*

3.2.1.2.2.1 *R1234ze(E)*

Figure 109 presents the saturated vapor condensation frictional pressure drop against the kinetic energy per unit volume of refrigerant flow computed by the homogeneous model (Eq. 59).

The frictional pressure drops show a linear dependence on the kinetic energy per unit volume of the refrigerant flow and therefore a quadratic dependence on the refrigerant mass flux.

They are lightly affected by the saturation temperature, on the contrary they have a strong relationship with the kinetic energy and, thus, with the refrigerant mass flux. The Eq. 62 is obtained as experimental data best fitting and presents the relation between the saturated vapor condensation frictional pressure drop (in kPa) and the kinetic energy per unit volume of the refrigerant flow (defined as in Eq. 59). This correlation reproduces the present experimental data with a mean absolute percentage deviation of 11.6%.

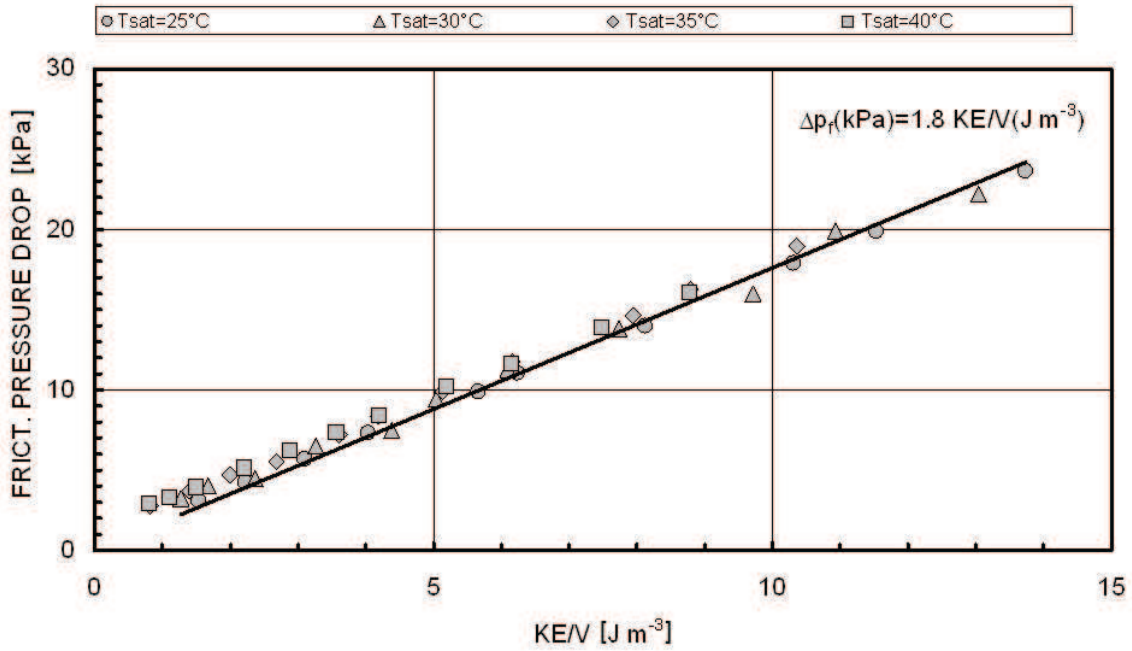

Figure 109 Saturated condensation frictional pressure drop vs. kinetic energy per unit volume of R1234ze(E) refrigerant flow at different saturation temperatures.

$\Delta p_f = 1.8\ KE/V$ Eq. 62

It should be also noted that for the present set of experimental data the momentum and gravity pressure drop components (Eq. 40) ranges from 1% to 8% of the total pressure drop measured.

3.2.1.2.2.2 R1234ze(Z)

Figure 110 presents the saturated vapor condensation frictional pressure drop against the kinetic energy per unit volume of the refrigerant flow computed by the homogeneous model (Eq. 59).

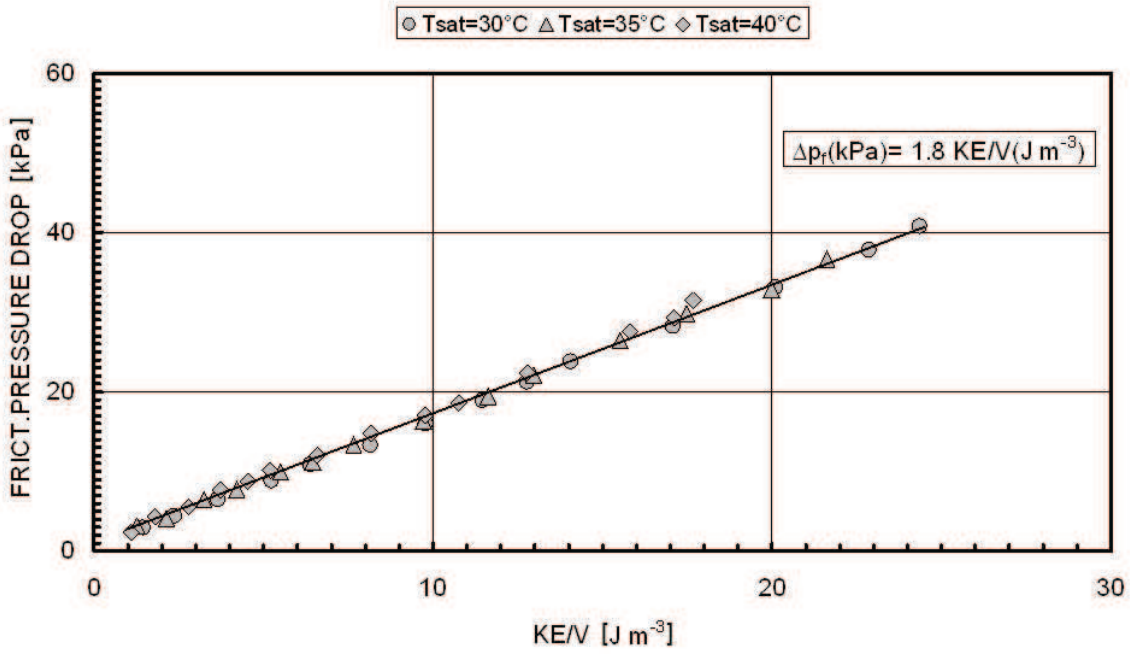

Figure 110 Saturated condensation frictional pressure drop vs. kinetic energy per unit volume of R1234ze(Z) refrigerant flow at different saturation temperatures.

Again, the frictional pressure drops showed a linear dependence with the kinetic energy per unit volume of the refrigerant flow and therefore a quadratic dependence on the refrigerant mass flux.
The sensitivity on the saturation temperature is almost negligible. By a best fitting operation on the experimental one can obtain Eq. 62 that presents the relation between the saturated vapor condensation frictional pressure drop (in kPa) and the kinetic energy per unit volume of the refrigerant flow (Eq. 59). This correlation reproduces present experimental data with a mean absolute percentage deviation around 7.7%.

$\Delta p_f = 1.8\ KE/V$ Eq. 63

3.2.1.2.2.3 R152a

Figure 111 shows the saturated vapor condensation frictional pressure drop against the refrigerant mass flux.

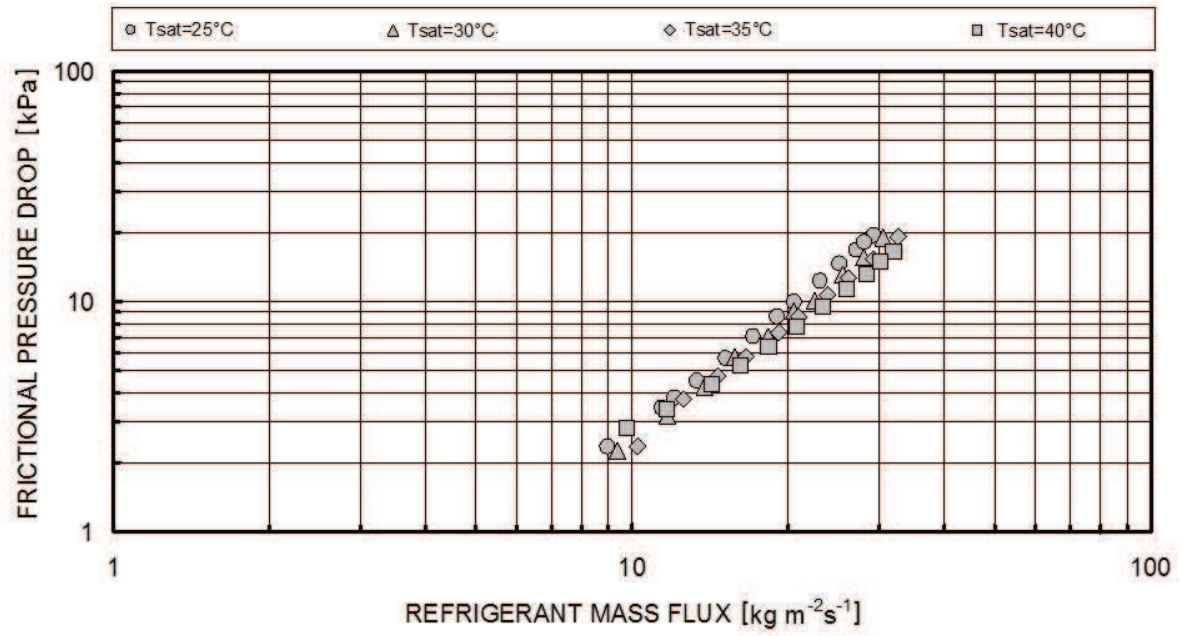

Figure 111 Saturated R152a vapor condensation frictional pressure drop vs. R152a refrigerant mass flux at different saturation temperatures.

The saturated vapor condensation frictional pressure drop presents a quadratic dependence on the mass flux. When doubling the mass flux the frictional pressure drop becomes 4 times higher. Besides, there is a weak dependence on the saturation temperature (up to +30% going from 40 °C to 25 °C of saturation temperature).

3.2.1.2.2.4 R32

Figure 112 shows the saturated vapor condensation frictional pressure drop against the refrigerant mass flux. Also with R32, the saturated vapor condensation frictional pressure drops evidence a quadratic dependence on the refrigerant mass flux that means a constant value for the friction factor vs. Reynolds number as it occurs in the Moody diagram. When doubling the mass flux, the frictional pressure drops become around 2 times higher. There is a weak sensitivity on the saturation temperature: in fact, passing from 40 °C to 25 °C of saturation temperature, the frictional pressure drops increase of around 40%.

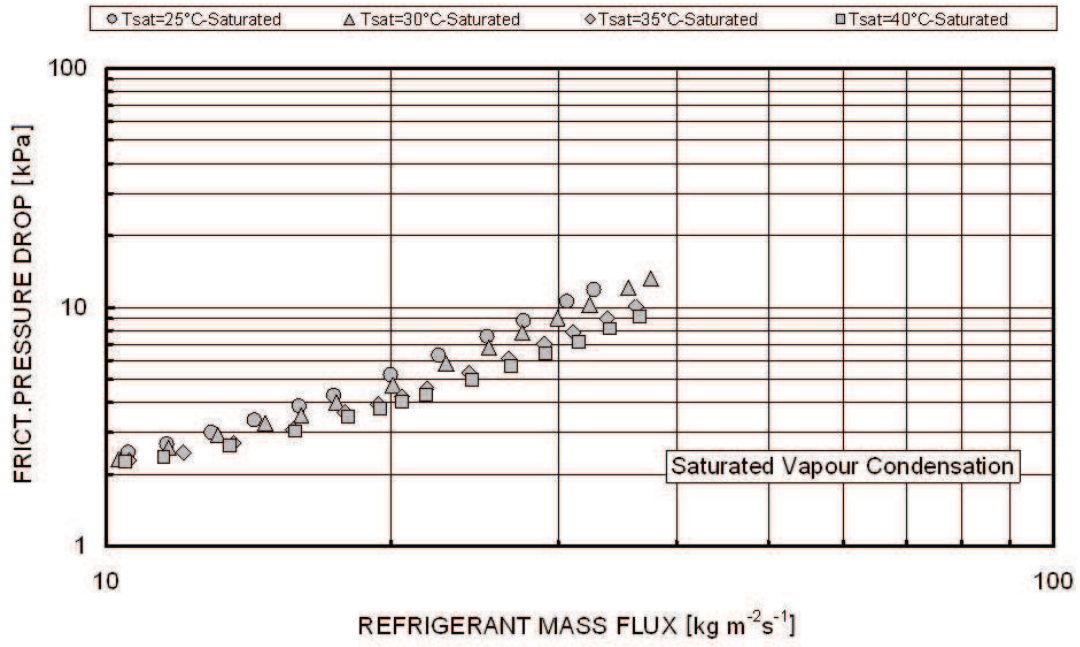

Figure 112 R32 saturated vapor condensation frictional pressure drop vs. R32 refrigerant mass flux at different saturation temperatures.

3.2.2 Development of new correlations

3.2.2.1 Vaporization

Despite the wide spread of BPHEs inside the technical applications, just few models have been presented during years to estimate the heat transfer coefficients during vaporization in plate heat exchangers.

Kumar (1984) proposed a correlation for vaporization in PHEs where the boiling coefficient is the result of two contributions: nucleate boiling and convective boiling.

Pelletier and Palm (1997) tested several refrigerants (among them R22 and propane) as working fluids in a heat pump with a plate heat exchanger as evaporator. The authors compared their experimental data against several correlations available in the open literature and concluded that the pool boiling ones (Cooper, 1984; Gorenflo, 1997; Stephan and Abdelsalam, 1980) were the bests . Also Engelhorn and Reinhart (1990) after conducted a new series of experimental data, found that Gorenflo (1997) and Slipcevic (1988) correlations were the most accurate ones.

Margat *et al.* (1997) investigated the R134a vaporization process in a single channel PHE. The authors observed that in the testing conditions they operated the heat transfer was independent of the heat flux and strongly dependent on the vapour quality, which indicated that the effect of nucleate boiling was not significant. They proposed a correlation based on the liquid-phase heat transfer coefficient, calculated through the specific correlation for corrugated channels, and enhanced by a correction factor.

Yan and Lin (1999) developed empirical correlations for heat transfer coefficient and friction factor based on their experimental data experimentally collected during R134a vaporization inside a BPHE.

Donowski and Kandlikar (2000) developed correlations for both single-phase and two-phase heat transfer inside a PHE. They also noticed that the evaporation process was dominated by the convective mechanism and so that the predicted Nusselt number was strongly dependent on the vapor quality.

Hsieh and Lin (2002) reported experimental data on vaporization heat transfer and pressure drop of R410A in a BPHE. The effects of mean vapor quality, mass flux, heat flux, and saturation pressure were evaluated and non-dimensional equations were proposed for heat transfer coefficient and friction

factor. The authors proposed to correlate the heat transfer coefficients with the Gungor and Winterton (1986) model.

Han *et al.* (2003) performed heat transfer and pressure drop measurements on R410A vaporization inside a BPHE to evaluate the effects of mass flux, heat flux, saturation temperature, and plate geometry (inclination angle of the corrugation). Non-dimensional equations for heat transfer coefficient and pressure drop based on the equivalent Reynolds number and the equivalent Boiling number were also presented.

Ayub (2003) developed a literature survey on heat transfer and pressure drop correlations for PHE evaporators, whereas Palm and Claesson (2006), after collecting R22 and R134a vaporization data in PHEs with different geometries, concluded that all data could be fitted by the Cooper pool boiling correlation (1984) by introducing a constant factor of 1.5.

Jokar *et al.* (2006) reported experimental data on R134a condensation and vaporization inside BPHE and proposed empirical correlations for heat transfer and pressure drop.

Djordjevic and Kabelac (2008) compared their experimental data against the Steiner and Taborek (1992) correlation multiplied by a decrement factor derived from a best fit operation.

Finally, Táboas *et al.* (2012) after conducted an exhaustive literature review on PHEs, proposed a new flow boiling correlation based on previous results from other authors. It was made up of two contributions: a convective boiling one inspired by the Margat *et al.* (1997) method and a nucleate boiling term calculated based on the Hsieh and Lin (2002) correlation. This model was able to predict the transition between nucleate and convective boiling and 98% of the heat transfer coefficient data they considered were calculated within 20% .

3.2.2.1.1 A new model for vaporization inside BPHEs

The development of a new heat transfer model was based on the analysis of a wide set of experimental data on saturated refrigerant vaporization inside a commercial BPHE experimentally collected, which includes 251 data points on HFC refrigerants (R236a, R134a, and R410A) published in Longo and Gasparella (2007a,b and c), HC refrigerants (R600a, R290, and R1270) presented in Longo (2012a)

and also the new low Global Warming Potential (GWP) HFO refrigerant R1234yf, published in Longo (2012b).

The first step to analyze some experimental data is to define which dominant heat transfer mechanism is actually occurring. In fact the boiling process can be governed by two different mechanisms (convective boiling and nucleate boiling), described in section 1.4.2.1.
In the open literature there is only one quantitative criterion to discriminate the dominant heat transfer mechanism in refrigerant vaporization inside BPHEs: the one proposed by Thonon *et al.* (1997).
This criterion is based on the Boiling number Bo (Eq. 64) and the Martinelli parameter X_{tt} (Eq. 65) evaluated at the mean vapor quality x_m between inlet and outlet.

$$\mathrm{Bo} = \frac{\mathrm{q}}{\mathrm{G}\,\mathrm{h_{LG}}} \qquad \text{Eq. 64}$$

$$X_{tt} = \left(\frac{1 - x_m}{x_m}\right)^{0.9} \left(\frac{\rho_G}{\rho_L}\right)^{0.5} \left(\frac{\mu_L}{\mu_G}\right)^{0.1} \qquad \text{Eq. 65}$$

When Bo X_{tt}>0.15 × 10^{-3} nucleate boiling occurs; while when Bo X_{tt}<0.15 × 10^{-3} convective boiling occurs.
Figure 113 places the 251 experimental data points used to base the new correlation on the Thonon *et al.* (1997) map. According to this method, all the experimental data belong to the nucleate boiling zone, however R236fa, R600a and R134a data points approach the boundary between nucleate boiling area and convective boiling area.
It is worth underlining that the Thonon *et al.* (1997) procedure is based on a set of experimental data relative to saturated R22 boiling inside plain rectangular and corrugated channels. The authors suggested to normalize the experimental HTCs by the pool boiling HTC calculated by the Gorenflo (1993) correlation. So, if the ratio between experimental and calculated heat transfer coefficient is higher than unity, convective boiling occurs; if it is around unity, nucleate boiling occurs.

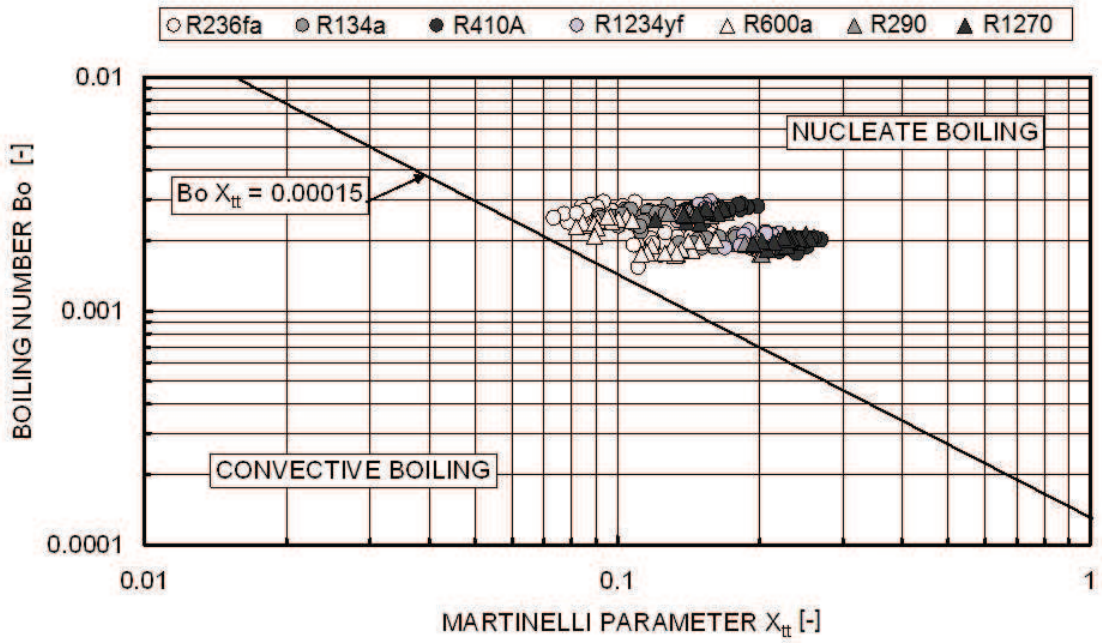

Figure 113 Experimental data plotted on the Thonon *et al.* (1997) map.

To reproduce this procedure, first of all in Figure 114 the heat transfer coefficient experimentally obtained on the BPHE are plotted against the calculated ones by means of the Gorenflo (1993) correlation. One can point out that the R236fa, R600a and R134a data points are not well fitted by the Gorenflo (1993) correlation, while the R410A, R1234yf, and R1270 data are fairly reproduced both in tendency and magnitude.

Secondly, as suggested by the Thonon *et al.* (1997) criterion, the same experimental HTCs have been normalized by using the Gorenflo (1993) correlation. Figure 115 presents them as a function of the heat flux.

It is notable that R236fa, R600a, and R134a normalized heat transfer coefficients are significantly higher than unity indicating a dominant effect of convective boiling, whereas the other normalized heat transfer coefficients are around – or slightly lower – than unity indicating a dominant effect of nucleate boiling.

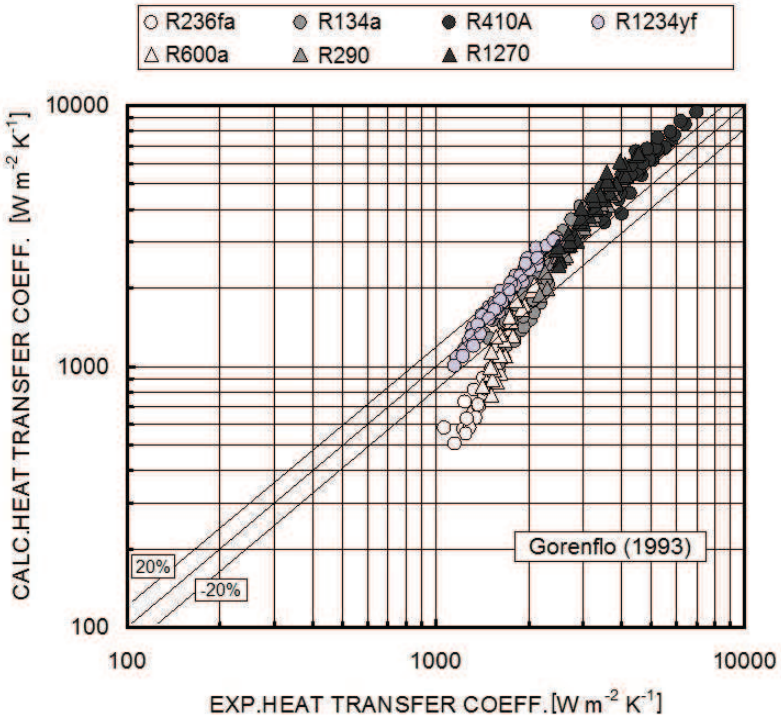

Figure 114 Experimental heat transfer coefficient vs. Gorenflo (1993) correlation.

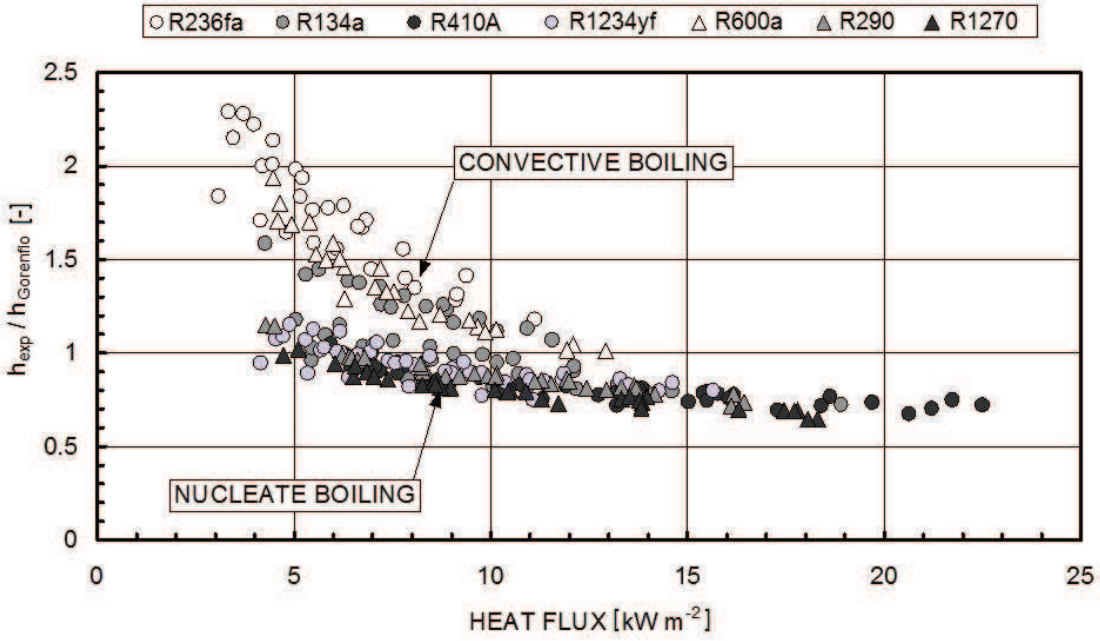

Figure 115 Gorenflo (1993) normalized heat transfer coefficient vs. heat flux (kW m^{-2}).

The first set of data (where the convective boiling is the dominant effect) was used to developed a new non-dimensional equation for convective boiling inside a BPHE based on the equivalent Reynolds number Re_{eq} and the liquid Prandtl number Pr_L (Eq. 66):

$$\alpha_{\mathrm{cb}} = 0.122\Phi\frac{\lambda_L}{d_{\mathrm{h}}}R_{eq}^{\ 0.8}\ Pr_L^{\frac{1}{3}} \qquad \text{Eq. 66}$$

$$\Phi = \frac{A_{actual}}{A_{proiected}} \qquad \text{Eq. 67}$$

where Φ is the enlargement factor of the corrugated plates (Eq. 67), the constant 0.122 and the exponent 0.8 are obtained by a best fitting procedure. The equivalent Reynolds number is computed at the mean vapor quality x_m between inlet and outlet, therefore α_{cb} (Eq. 66) represents the average heat transfer coefficient due to the convective boiling contribution on the whole heat transfer surface.

Figure 116 plots the first set of data (convective boiling) on non-dimensional co-ordinates: J_H (Eq. 68) vs. the equivalent Reynolds number (Eq. 69) calculated at the average vapor quality x_m between inlet and outlet and the new correlation (Eq. 66) trend is highlighted.

$$\mathrm{J_H} = \frac{\mathrm{Nu}}{\mathrm{Pr_L}^{\frac{1}{3}}} \qquad \text{Eq. 68}$$

$$\mathrm{Re_{eq}} = G\left[(1-x)+x\left(\frac{\rho_L}{\rho_G}\right)^{\frac{1}{2}}\right]\frac{d_h}{\mu_L} \qquad \text{Eq. 69}$$

where

$$Nu\ = \alpha\ \frac{d_{\mathrm{h}}}{\lambda_L} \qquad \text{Eq. 70}$$

Eq. 71

$$Pr_L = \frac{\mu_L c_{pL}}{\lambda_L}$$

The second set of data (where the nucleate boiling is the dominant effect) was used to develop a new equation for nucleate boiling inside a BPHE based on the Gorenflo (1993) correlation.α_{nb} (Eq. 72) represents the average heat transfer coefficient due to the nucleate boiling mechanism on the whole heat transfer surface.

The original Gorenflo (1993) correlation was multiplied by a correction term C_{nb} and by the enlargement factor Φ; than the exponent n was changed, whereas the other terms remained unchanged. The correction term C_{nb} and the exponent n were determined by a best fitting procedure.

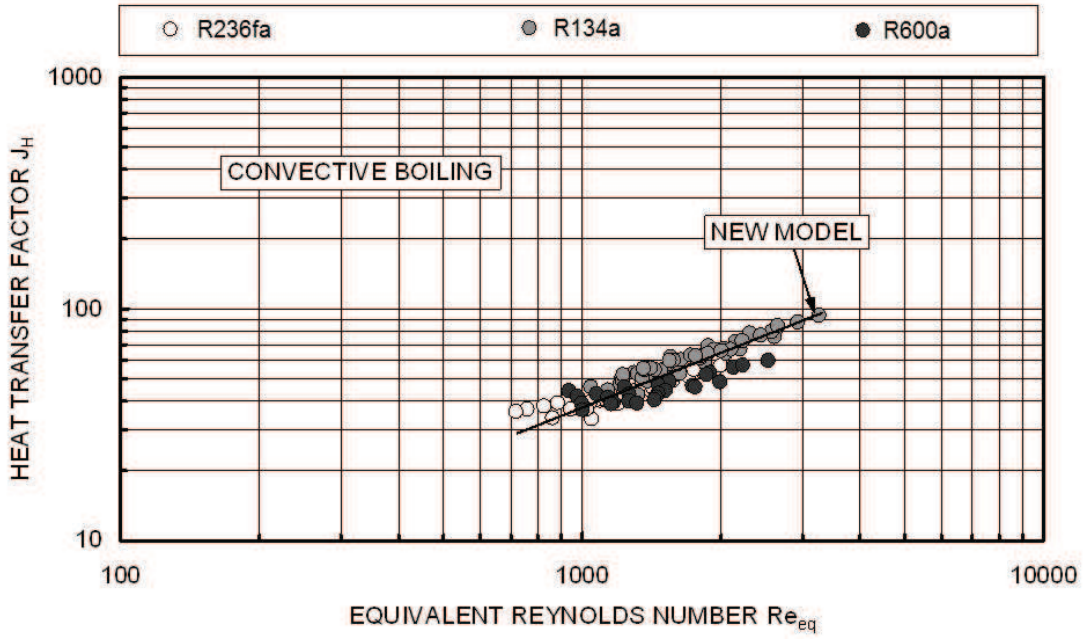

Figure 116 Convective boiling data plotted on non-dimensional co-ordinates: J_H vs. Re_{eq}.

Eq. 72

$$\alpha_{nb} = C_{nb} \Phi \alpha_0 C_{Ra} F(p^*) \left(\frac{q}{q_0}\right)^n$$

Where:

- C_{nb}=0.58 is the correction term;
- Φ is the enlargement factor of the corrugated plates, defined in Eq. 67;
- α_0 is the reference value (p^*_0=0.1, q_0=20000 W m^{-2}, Ra_0=0.4 μm) of the heat transfer coefficient specific for each refrigerant;

Eq. 73

- $C_{Ra} = \left(\frac{R_a}{0.4\ \mu m}\right)^{0.1333}$

  accounts for the effect of the arithmetic mean roughness R_a (μm) of the plates as defined in ISO4287/1;

Eq. 74

- $F(p^*) = 1.2p^{*0.27} + \left(2.5 + \frac{1}{1-p^*}\right)p^*$

  accounts for reduced pressure p^* effect;

n=0.467 Eq. 75

- $\left(\frac{q}{q_0}\right)^n = \left(\frac{q}{20000} W m^{-2}\right)^n$

  accounts for the heat flux q (W m^{-2}) effect.

The final average boiling heat transfer coefficient α_b (Eq. 76) is computed as the maximum between the average convective boiling heat transfer coefficient α_{cb}, calculated by Eq. 66, and the average nucleate boiling heat transfer coefficient α_{nb}, calculated by Eq. 72 as shown by Eq. 76.

α_b=MAX (α_{cb}, α_{nb}) Eq. 76

The heat transfer coefficients α_b, α_{cb}, α_{nb} and the heat flux q are referred to the projected area of the plates.

Figure 117 presents the 251 saturated boiling heat transfer coefficients used to calibrate the new boiling correlation vs. the calculated values obtained with the procedure here presented (Eq. 76): the mean absolute percentage deviation between calculated and experimental data is around 9.0%, with more than 90% of the data points within ± 20%. Around 55% of the data points belong to nucleate boiling regime, so Eq. 72 was used, and the other 45% belong to convective boiling heat transfer regime so Eq. 66 was used.

In addition, this new model for saturated refrigerant boiling has been modified to be adapted to predict the average heat transfer coefficient during boiling with outlet vapor super-heating.

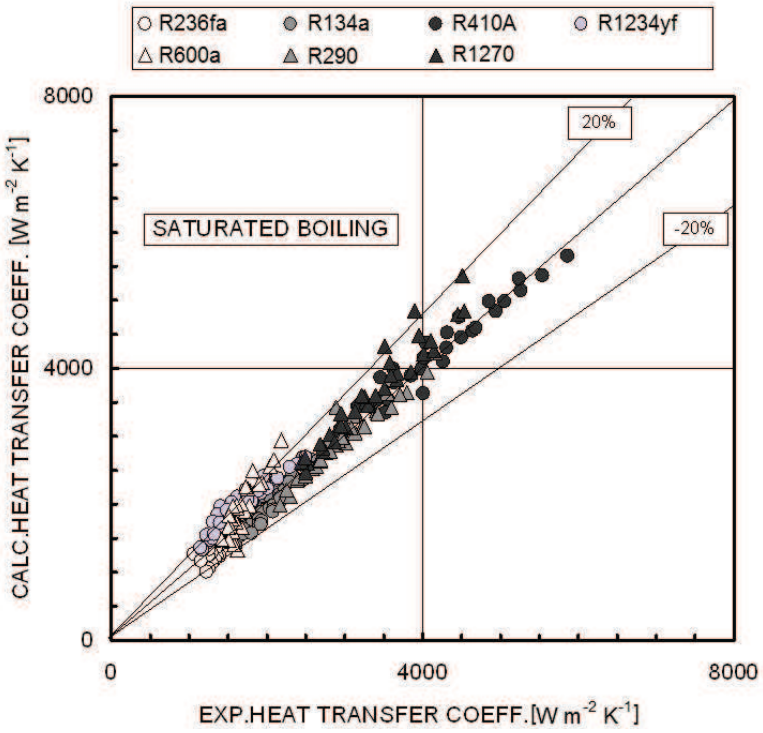

Figure 117 Experimental vs. calculated saturated boiling heat transfer coefficients data.

The original model, presented in Eq. 76, was coupled with a single-phase heat transfer coefficient correlation that accounts for the super-heating contribution (α_s). For this reason, when the evaporator works both in boiling and super-heating, the average heat transfer coefficient on the refrigerant-side of the whole evaporator $\alpha_{\text{ave.clc}}$ (Eq. 77) is computed as the average value between the heat transfer coefficient of the boiling zone α_b (Eq. 76) and that of the super-heating zone α_s weighted on the base of the respective heat transfer area.

Eq. 77

$$\alpha_{\text{ave.clc}} = \alpha_{\text{b}} \frac{A_b}{A} + \alpha_{\text{a}} \frac{A_a}{A}$$

The heat transfer coefficient of the boiling zone α_b is computed by the new model (Eq. 76), whereas the heat transfer coefficient of the super-heating zone α_s is compute by a single-phase heat transfer equation valid for the specific BPHE.
In this case Eq. 78 is applied for the computation of the single-phase heat transfer coefficient in the vapor-superheating zone:

Eq. 78

$$\alpha_{sup} = 0.277 \frac{\text{s}}{d_{\text{h}}} \text{Re}_{\text{s}}^{0.766} \text{Pr}_{\text{s}}^{0.333}$$

The heat transfer area of the boiling and the super-heating zones A_b (Eq. 79) and A_{sup} (Eq. 80) are calculated by the following equations:

Eq. 79

$$A_{\text{b}} = \frac{Q_{\text{b}}}{\alpha_b \Delta T_{\text{ln.b}}}$$

Eq. 80

$$A_{\text{sup}} = \frac{Q_{\text{sup}}}{\alpha_s \Delta T_{\text{ln.sup}}}$$

where Q_b and Q_{sup}, $\Delta T_{ln.b}$ and $\Delta T_{ln.sup}$ are the heat flow rate and the logarithmic mean temperature difference in the boiling and the super-heating zones, respectively.

Finally, Figure 118 shows the comparison between the experimental heat transfer coefficients relative to boiling with outlet vapor-superheating previously obtained by Longo *et al.* (2007, 2012a, 2012b) and the average heat transfer coefficients calculated by Eq. 78.

The set of vapor-superheating data includes 281 data points and the mean absolute percentage deviation between calculated and experimental data is around 11.2%.

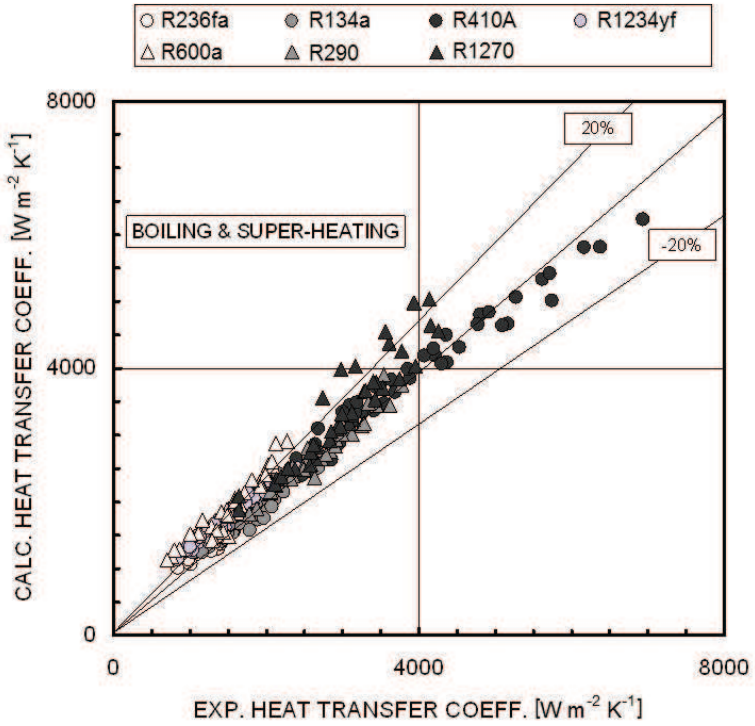

Figure 118 Experimental boiling with outlet vapor-superheating heat transfer coefficients previously obtained by Longo *et al.* (2007, 2012a, 2012b) vs. calculated heat transfer coefficients (new model).

3.2.2.1.2 Comparison against experimental data available in literature

The new heat transfer model, presented in section 3.2.2.1.1, was compared against a set of 505 experimental data points obtained by different authors available in the open literature.

The database includes different refrigerants (R134a, R410A, R507A, and R22) and different plate geometries.

Following the data used for this comparison are listed:

- R134a saturated boiling data by Yan and Lin (1999): 51 data points relative to two different refrigerant mass fluxes (55 and 70 kg m^{-2} s^{-1}) and heat fluxes (11 and 15 kW m^{-2}).
- R410A saturated boiling data by Hsieh and Lin (2002): 154 data points relative to four different refrigerant mass fluxes (50, 75, 100, and 125 kg m^{-2} s^{-1}).
- R410A and R22 saturated boiling data by Han *et al.* (2003): 52 data points relative to three different plate corrugation angles (45, 55, and 70°) and three different heat fluxes (3, 6.4, and 10 kW m^2).
- R134a saturated boiling data by Djordjević *et al.* (2007): 27 data points relative to three different refrigerant mass fluxes (45, 55, and 65 kg m^{-2} s^{-1}).
- R134a and R507A saturated boiling data by Huang *et al.* (2012): 220 data points relative to three different plate corrugations angles (28 and 60°) and five different heat fluxes (between 1.9 kW m^{-2} and 6.3 kW m^{-2}).

Table 23 and Table 24 report the corrugated plate geometries and the operating conditions respectively of all the experimental data considered and listed before. All the experimental heat transfer coefficients and the relative heat fluxes were re-calculated with reference to the projected area of the plates.

Table 23 Corrugated plate geometry of the BPHE experimental data base found in literature.

Authors	**L** [mm]	**W** [mm]	**Φ**	**β** [°]	***b*** [mm]	***p*** [mm]	**R_a** [μm]
Longo *et al.* (2007, 2012a, 2012b)	278	72	1.24	65	2.0	8.0	0.4
Yan and Lin (1999)	450	120	1.28	60	2.9	10.0	0.4
Hsieh and Lin (2002)	450	120	1.28	60	2.9	10.0	0.4
Han *et al.* (2003)	476	115	1.17	45-70	2.15	4.9-7.0	0.4
Djordjevic *et al.* (2007)	872	486	1.26	63.26	3.26	12.0	0.4
Huang *et al.* (2012)	519	180	1.24	28-60	2.0	8.1	0.4

Table 24 Operating conditions of the BPHE experimental data base found in literature.

Authors	**Data**	**Refrigerants**	t_{sat} [°C]	G_r [kg $m^{-2}s^{-1}$]	***q*** [kW m^{-2}]
Longo and Gasparella (2007)	247	R236fa, R134a, R410A	4.8 - 20.3	11.4 - 39-8	3.1 - 21.2
Longo (2012a)	197	R600a, R290, R1270	9.8 - 20.2	6.8 - 23.9	4.3 - 22.2
Longo (2012b)	88	R1234yf	4.8 - 20.2	15.4 - 35.1	4.2 - 15.7
Yan and Lin (1999)	51	R134a	25.5 - 31.3	55 - 70	11 - 15
Hsieh and Lin (2002)	154	R410A	10 - 20	50 - 125	2.7 - 36.5
Han *et al.* (2003)	52	R410A, R22	5 - 15	13 - 34	3.0 - 10.0
Djordjevic *et al.* (2007)	27	R134a	-1.3	45 - 65	15.8
Huang *et al.* (2012)	220	R134a, R507A	9.4 - 9.5	5.7 - 31.4	1.9 - 6.9

Figure 119 shows the comparison between the new model and the saturated boiling heat transfer coefficients available in the open literature.

The new model reproduces the R134a data by Yan and Lin (1999), the R410A data by Hsieh and Lin (2002), the R134a data by Djordjevic *et al.* (2007), and the R507A data by Huang *et al.* (2012) with a reasonable agreement, whereas the comparison with the other sets of data is less satisfactory. The mean absolute percentage deviation between experimental and calculated heat transfer coefficients on the whole set of 505 data points obtained by researchers different from present authors was around 20% with around 50% of the data points within ± 20%. Around 65% of the data points belong to nucleate boiling regime, while the remaining 35% belongs to convective boiling heat transfer regime.

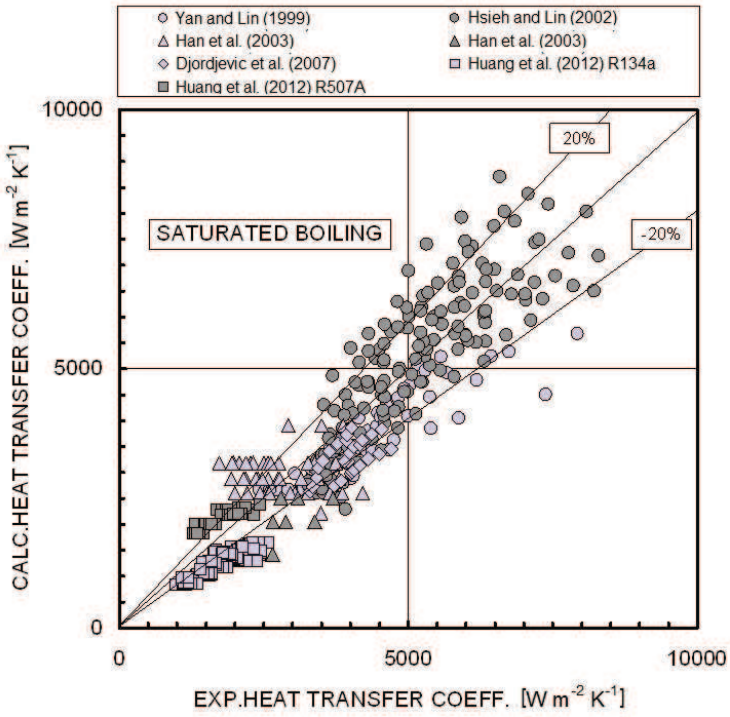

Figure 119 Comparison between experimental and calculated heat transfer coefficient by the new model.

3.2.2.1.2.1 R1234ze(E)

The heat transfer coefficients obtained during the experimental vaporization data inside a commercial BPHE, described in section 3.2.1.1.1.1, were compared against traditional equations for nucleate boiling, such as Cooper (1984) and Gorenflo (1993), and also against the new model presented in section 3.2.2.1.1.

The absolute mean percentage deviation between calculated and experimental data is 13.4% for Cooper equation (1984), 13.1% for the Gorenflo equation (1993), and 7.1% for the new vaporization model, which has not been developed as best fit of these experimental data.

Figure 120 shows the comparison between the experimental saturated boiling heat transfer coefficients and the calculated values by the new model presented in section 3.2.2.1.1.

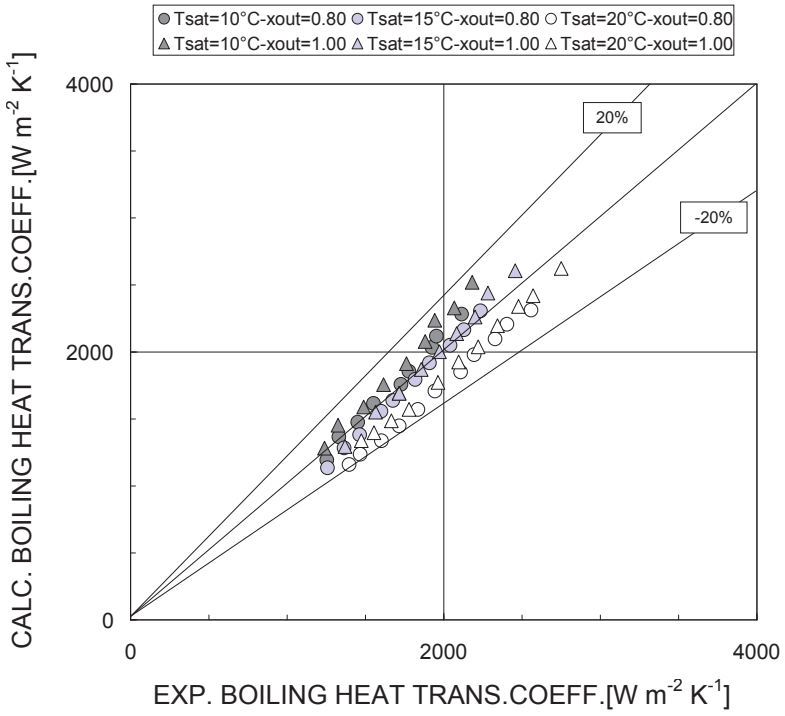

Figure 120 Experimental R1234ze(E) boiling heat transfer coefficients vs. calculated values by the new condensation model in BPHE.

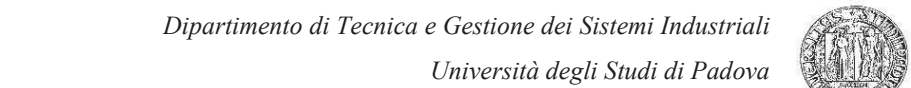

3.2.2.1.2.2 R32

The experimental saturated boiling heat transfer coefficients were also compared against the new model for refrigerant vaporization inside BPHE presented in section 3.2.2.1.1.

Figure 121 shows the comparison between the experimental saturated boiling heat transfer coefficients and the calculated values by the new model described in section 3.2.2.1.1: the absolute mean percentage deviation is 4.7% and one can notice that there is good agreement between calculated and experimental data both in magnitude and tendency.

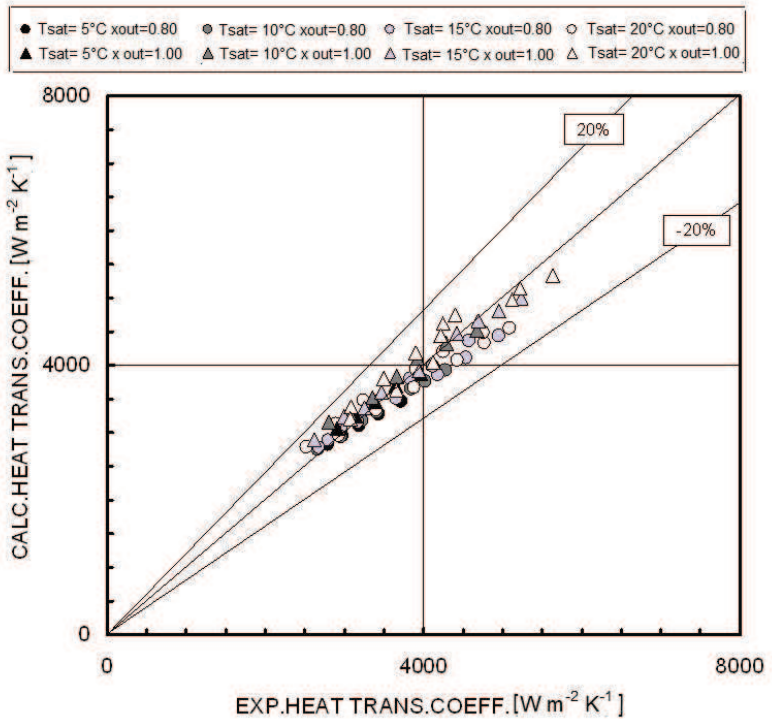

Figure 121 Experimental R32 boiling heat transfer coefficients vs. calculated values by the new condensation model in BPHE.

3.2.2.2 Condensation

In open literature, it is possible to find several experimental works on refrigerant condensation inside BPHE, whereas only a few models were specifically developed. Among them, Yan *et al.* (1999)

presented semi-empirical correlations for the heat transfer coefficient and the friction factor based on a set of data obtained during condensation. Würfel and Ostrowski (2004) developed a non-dimensional equation for the heat transfer coefficient during condensation that takes into account among others also the geometry of the corrugated plates. This correlation is based on a set of data obtained with two fluids, water and n-heptane, and three different corrugated plates. Kuo *et al.* (2005) proposed empirical correlations for the heat transfer coefficient and the friction factor obtained by a best fitting procedure based on their experimental R410A data. Jokar *et al.* (2006), after collecting some R134a condensation data inside a BPHE, developed a non-dimensional equation for the heat transfer coefficient and the friction factor. Shi *et al.* (2010) proposed a heat transfer model by applying the Shah (1979) approach for forced convection condensation in plain tube to condensation inside the corrugated channels of a BPHE. Finally, Mancin *et al.* (2011) presented a new heat transfer model based on an asymptotic approach which takes into account both the gravity and the vapor shear contributions.

3.2.2.2.1 Condensation models from the literature

Depending on the heat transfer mechanism that is predominant in each single data collected during condensation inside a commercial BPHE, the heat transfer coefficients have been compared against the Nusselt (1916) correlation for laminar film condensation on a vertical surface or the Akers *et al.* (1959) equation for forced in-tube convection condensation.
While the data collected with a super-heated vapor at the inlet oh the BPHE have been compared against the model developed by Webb (1998).
The Nusselt (1916) one is valid for gravity controlled laminar film condensation: the average heat transfer coefficient on the vertical surface results (Eq. 81)

Eq. 81

$$\alpha_{\mathrm{NUSSELT}} = 0.943 \left(\frac{\lambda_l^3 \rho_l^2 g \Delta h_{LG}}{\mu_L \, \Delta T \, L} \right)^{\frac{1}{4}}$$

where ρ_L, λ_L and μ_L are the condensate density, thermal conductivity and dynamic viscosity respectively, Δh_{LG} is the specific enthalpy of vaporization, g is the gravity acceleration, ΔT the difference between saturation and wall temperature and L the length of the vertical surface.
This equation has been multiplied by the enlargement factor Φ (Eq. 67) to take account of the enhanced are of the plates and so to compute the heat transfer coefficient referred to the projected area of the plates (Eq. 82).

$$\alpha_{r.ave}=\Phi\,\alpha_{NUSSELT} \qquad \text{Eq. 82}$$

The enlargement factor Φ for the BPHE tested is equal to 1.24.
On the other hand, the Akers *et al.* (1959) equation (Eq. 83) that was developed for forced convection condensation inside tube, is presented in Eq. 83.

$$\alpha_{AKERS} = 5.03\,\frac{L}{d_h}\,\mathrm{Re}_{eq}^{\frac{1}{3}}\,\mathrm{Pr}_L^{\frac{1}{3}} \qquad \text{Eq. 83}$$

Where Re_{eq} and Pr_L are the equivalent Reynolds number and the Prandtl number and are reported by Eq. 69 and Eq. 66, respectively.
The Eq. 83, valid for $Re_{eq}<50000$, gives the local heat transfer coefficient which has to be multiplied by the enlargement factor Φ (Eq. 67) and integrated by a finite difference approach along the heat transfer area to compute the average condensation heat transfer coefficient inside BPHE referred to the projected area of the plates (Eq. 84):

$$\alpha_{r\,ave} = \alpha_{sat}\,\frac{1}{A}\int_0^A \Phi\;\alpha_{AKERS}\,dA \qquad \text{Eq. 84}$$

In addition, the super-heated vapor condensation heat transfer coefficients have been compared against the model developed by Webb (1998) for forced convection condensation of super-heated vapor and described in Eq. 85:

Eq. 85

$$\alpha_{\mathrm{sup}} = \alpha_{\mathrm{sat}} + F\left(\alpha_{\mathrm{fc}} + \frac{c_p \mathrm{G}\, q_{\mathrm{lat}}}{\Delta h_{\mathrm{LG}}}\right)$$

Where:

- α_{sat} is the local heat transfer coefficient for forced convection condensation of saturated vapor;
- α_{fc} is the local single-phase heat transfer coefficient between super-heated vapor and the condensate interface;
- the group $c_{pv}\, q_{lat} / \Delta h_{LG}$ is a correction term which accounts for the effect of mass transfer on sensible heat transfer between super-heated vapor and condensate interface.
- F a factor equal to the ratio between the local degrees of super-heat and the driving temperature difference (Eq. 85.). It approaches zero as the super-heat is depleted.

Eq. 86

$$F = \frac{T_{\mathrm{sup}} - T_{\mathrm{sat}}}{T_{\mathrm{sat}} - T_{\mathrm{wall}}}$$

The super-heated vapor condensation heat transfer coefficient α_{sup} is referred to the temperature difference between average saturation temperature T_{sat} and average wall temperature T_{wall}.

This model may be applied to different type of condenser by using the appropriate correlations to compute the saturated vapor condensation heat transfer coefficient α_{sat} and the single-phase heat transfer coefficient α_{fc}. In this case, the Webb (1998) model has been applied to forced convection condensation of super-heated vapor inside BPHE by using the Akers *et al.* (1959) equation multiplied by the enlargement factor Φ for the computation of the local saturated vapor condensation heat transfer coefficient (Eq. 87):

$\alpha_{sat}=\Phi\ \alpha_{AKERS}$ Eq. 87

and the Thonon (1995) equation (Eq. 88) for the computation of the local single-phase heat transfer coefficient:

Eq. 88

$$\alpha_{fc} = 0.2267 \frac{\lambda_c}{d_h} {Re_G}^{0.631} {Pr_G}^{\frac{1}{3}}$$

$50<Re_G<15000$

The Webb (1998) model gives the local heat transfer coefficient which has been integrated by a finite difference approach along the heat transfer area to compute the average condensation heat transfer coefficient inside the BPHE (Eq. 89):

Eq. 89

$$\alpha_{\text{sup.ave}} = \frac{1}{A}\int_0^A \alpha_{\text{sup}}\,\text{dA}$$

3.2.2.2.1.1 R1234ze(E)

The Nusselt correlation (1916) has been used to compare the experimental data having a refrigerant mass flux lower than 20 kg $m^{-2}s^{-1}$. In fact, for these points the condensation is dominated by the gravity forces.

Figure 122 presents the comparison between the saturated vapor condensation heat transfer coefficients of the low refrigerant mass fluxes data points (G_r<20 kg $m^{-2}s^{-1}$) and the average heat transfer

coefficients calculated by Nusselt correlation (1916) (Eq. 82) as a function of the saturation temperature.

On the contrary, the saturated vapor condensation heat transfer coefficients of the high refrigerant mass fluxes data points (G_r>20 kg $m^{-2}s^{-1}$) have been compared against the Akers *et al.* (1959) model (Eq. 84). Figure 123 present a comparison between experimental and calculated average heat transfer coefficients as a function of the saturation temperature.

Finally, the heat transfer coefficients of the super-heated vapor condensation data obtained at high refrigerant mass fluxes (G_r>20 kg $m^{-2}s^{-1}$) have been compared against the Webb (1998) model (Eq. 89). In Figure 124 are presented the average heat transfer coefficients experimentally obtained vs. the calculated ones as a function of the saturation temperature.

The Nusselt (1916) equation (Eq. 82) reproduces the saturated vapor condensation data at low refrigerant mass fluxes (G_r<20 kg $m^{-2}s^{-1}$) with an absolute mean percentage deviation of 5.6%. The Akers *et al.* (1959) model (Eq. 83) predicts the saturated vapor condensation data at high refrigerant mass fluxes (G_r>20 kg $m^{-2}s^{-1}$) with an absolute mean percentage deviation of 14.2%. The Webb (1998) model (Eq. 89) reproduces the super-heated vapor condensation data at high refrigerant mass fluxes (G_r>20 kg $m^{-2}s^{-1}$) with an absolute mean percentage deviation of 10.0%.

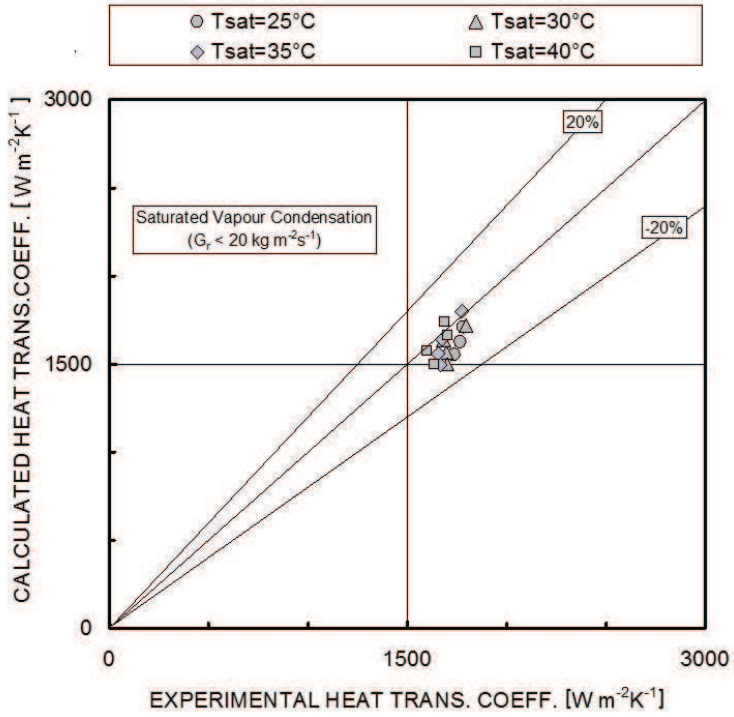

Figure 122 Condensation HTC (G_r<20 kg m^{-2}s^{-1}) vs. average HTC calculated by Nusselt (1916).

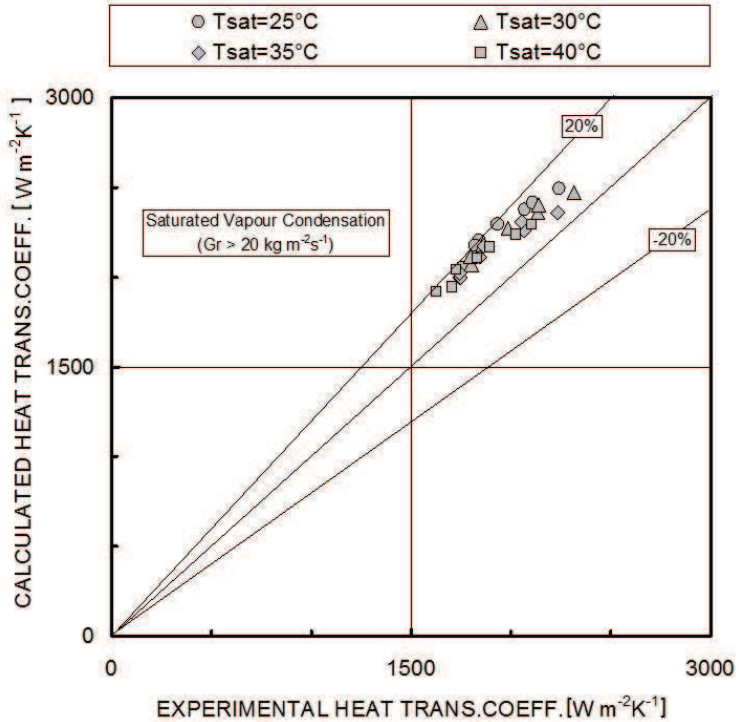

Figure 123 Condensation HTC (G_r>20 kg m^{-2}s^{-1}) vs. average HTC calculated by Akers *et al.* (1959).

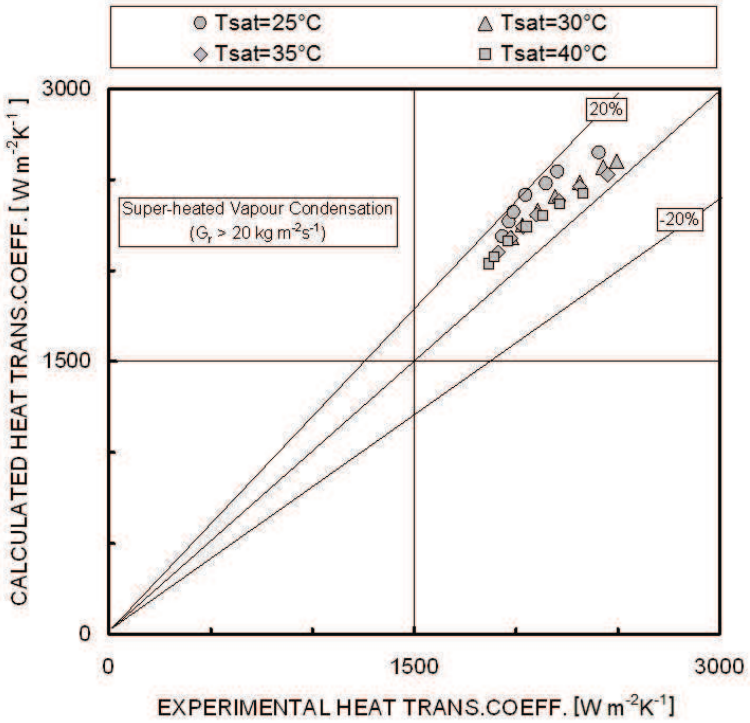

Figure 124 Super-heated vapor condensation heat transfer coefficients (G_r>20 $m^{-2}s^{-1}$) vs. average heat transfer coefficients calculated by Webb (1998) model.

3.2.2.2.1.2 R1235ze(Z)

Figure 125 shows the comparison between the R1234ze(Z) heat transfer coefficients of the low refrigerant mass flux data points (G_r<15 kg $m^{-2}s^{-1}$) and the average heat transfer coefficients calculated by Nusselt (1916) correlation (Eq. 82).

In Figure 126 are presented the saturated vapor condensation heat transfer coefficients at high refrigerant mass fluxes (G_r>15 kg $m^{-2}s^{-1}$) plotted against the average heat transfer coefficients calculated by Akers *et al.* (1959) correlation (Eq. 84).

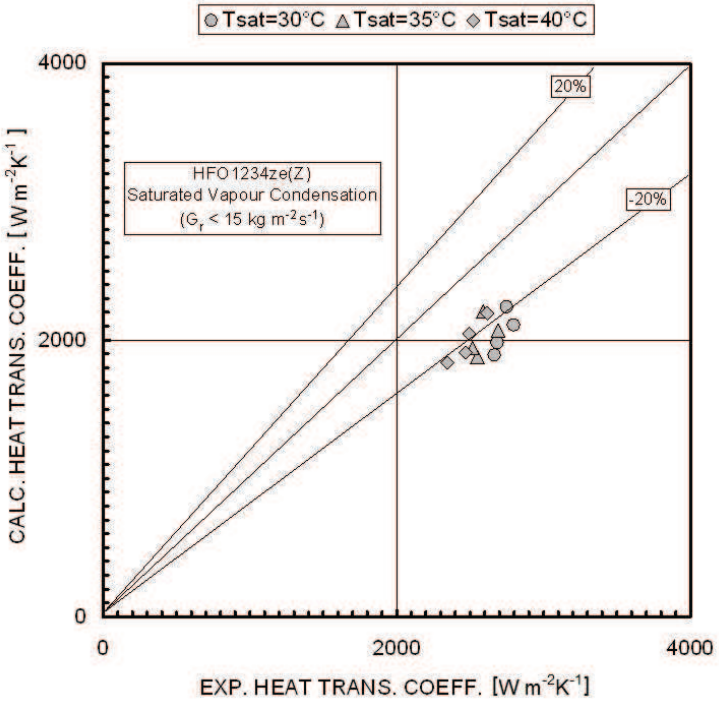

Figure 125 Saturated vapor condensation heat transfer coefficients (G_r<20 kg m^{-2}s^{-1}) vs. average heat transfer coefficients calculated by Nusselt (1916).

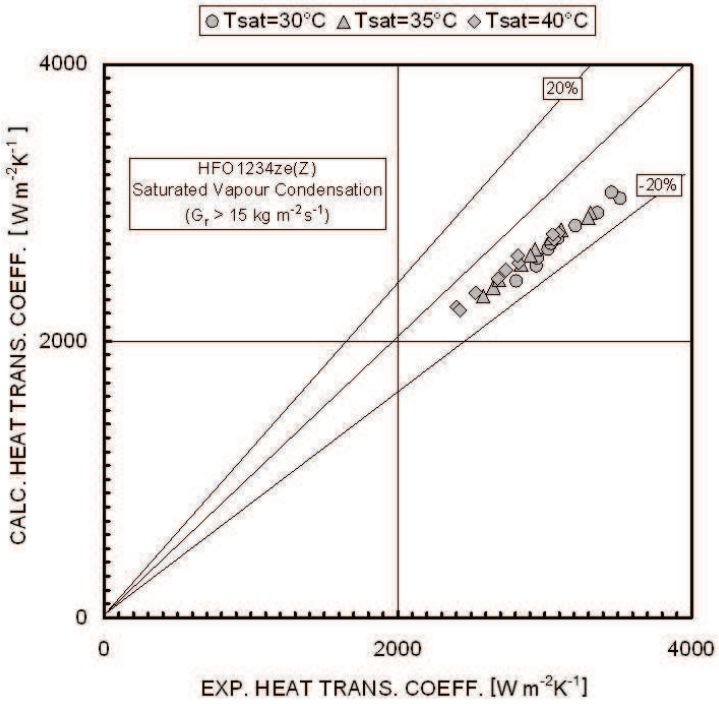

Figure 126 Saturated vapor condensation heat transfer coefficients (G_r>20 kg m^{-2}s^{-1}) vs. average heat transfer coefficients calculated by Akers *et al.* (1959).

The Nusselt (1916) equation reproduces the experimental data at low refrigerant mass flux with an absolute mean percentage deviation of 22.0%, whereas Akers *et al.* (1959) model predicts the experimental data at high refrigerant mass flux with an absolute mean percentage deviation of 10.4%.

3.2.2.2.2 A new model for condensation inside BPHEs

In what follows the development procedure of a new computational model for condensation inside BPHEs based on the analysis of a wide set of experimental data collected with pure or near azeotropic refrigerants during condensation inside a commercial herringbone-type BPHE previously obtained is presented.

This data set includes 338 data points on HFC refrigerants (R236a, R134a, R410A) collected by Longo (2010a), HC refrigerants (R600a, R290, R1270) presented in Longo (2010b), and the new low Global Warming Potential HFO refrigerants R1234yf published by Longo and Zilio (2013), and R1234ze(E), described in section 3.2.1.2.1.1.

Figure 127 plots all these data points on non-dimensional co-ordinates showing the heat transfer factor J_H (Eq. 68) vs. the equivalent Reynolds number Re_{eq} (Eq. 69) calculated at the average vapor quality x_m between inlet and outlet.

As presented in section 1.4.2.2 the condensation process can be governed either by the gravity or by the vapor shear. Observing Figure 127, a transition point between gravity-dominated and forced convection condensation can be found for an equivalent Reynolds number around 1600 which corresponds to a refrigerant mass flux around 20 kg $m^{-2}s^{-1}$ for HFC and HFO refrigerants and around 15 kg $m^{-2}s^{-1}$ for HC refrigerants for the specific case of the tested BPHE.

At low equivalent Reynolds number (Re_{eq}<1600) the heat transfer coefficients are independent of mass flux so the condensation process can be defined as “gravity-dominated”. While, for higher equivalent Reynolds number (Re_{eq}>1600) the heat transfer coefficients depend on mass flux and the condensate drainage is controlled by the combined actions of gravity and vapor shear. Here forced convection condensation also affects the heat transfer.

The experimental data in the gravity-controlled region was well predicted by a simple model based on the Nusselt (1916) equation for vertical surface (Eq. 81).

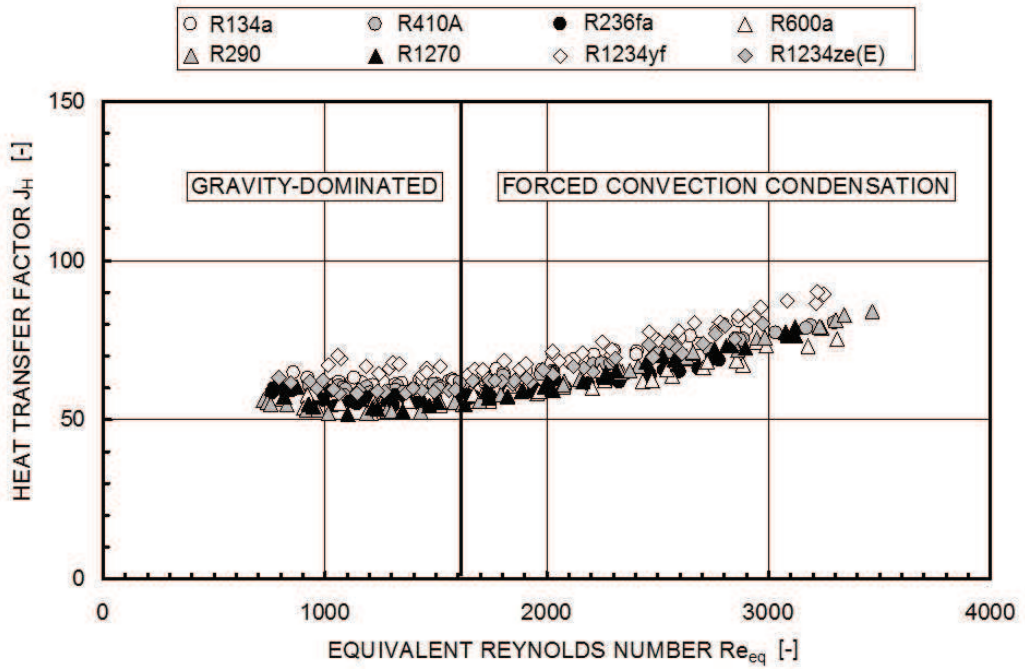

Figure 127 Saturated vapor condensation data plotted on the non-dimensional co-ordinates J_H vs. Re_{eq}.

This equation, as presented in the previous section (see paragraph 3.2.2.2.1) was multiplied by the enlargement factor Φ (Eq. 67) to compute the average condensation heat transfer coefficient referred to the projected area of the plates (Eq. 82).

Figure 128 shows the comparison between the model based on the Nusselt (1916) analysis (Eq. 82) and the experimental saturated vapor condensation heat transfer coefficients in the gravity-dominated region (Re_{eq}<1600): the mean absolute percentage deviation between calculated and experimental data is around 11.2%.

The experimental data in the forced convection condensation region were well predicted by a new non dimensional equation based on the equivalent Reynolds number Re_{eq} and the liquid Prandtl number Pr_L (Eq. 90):

Eq. 90

$$\alpha_{fc} = 1.875\Phi \frac{\lambda_L}{d_h} {Re_{eq}}^{0.445} {Pr_L}^{\frac{1}{3}}$$

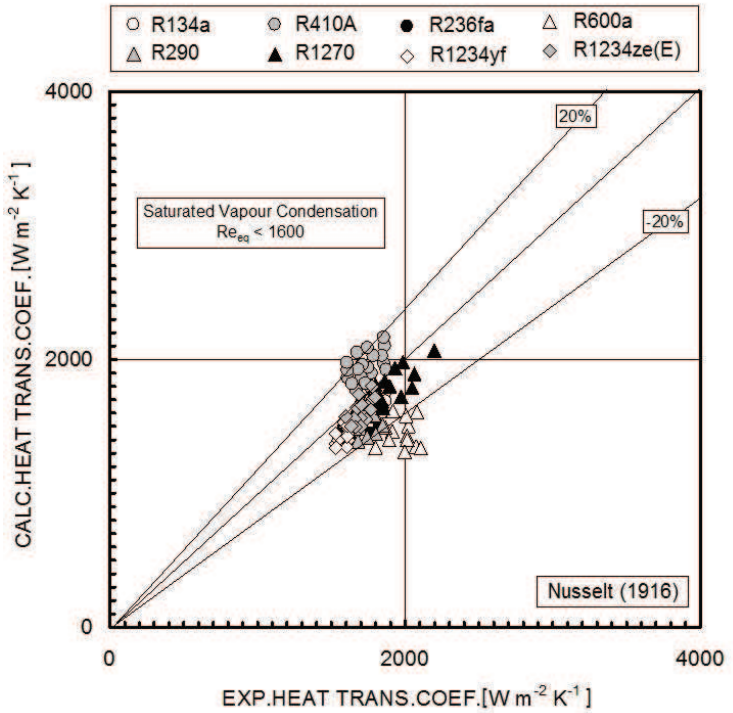

Figure 128 Comparison between gravity-dominated region (Re_{eq}<1600) experimental data and calculated saturated vapor condensation heat transfer coefficient by Nusselt (1916).

where the characteristic constant 1.875 and the exponent 0.445 on the equivalent Reynolds number were obtained by a best fitting procedure on all the experimental data collected.

Eq. 90 gives a local heat transfer coefficient, so it has to be integrated by a finite difference approach along the heat transfer area to compute the average condensation heat transfer coefficient referred to the projected area of the plates (Eq. 91).

Eq. 91

$$\alpha_{fc,ave} = \frac{1}{A}\int_{0}^{A} \alpha_{fc}\, dA$$

Figure 129 presents the heat transfer coefficients calculated with the new model for forced convection condensation (Eq. 91) plotted against the experimental ones obtained in the forced-convection condensation region (Re_{eq}>1600). The mean absolute percentage deviation between calculated and experimental data is around 4.1%.

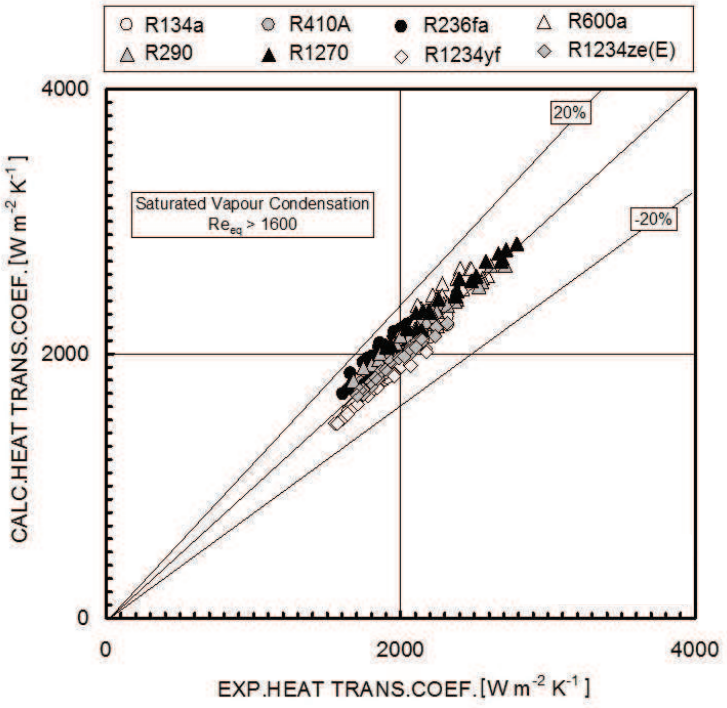

Figure 129 Comparison between experimental and calculated saturated vapor condensation heat transfer coefficient evaluated by the new model. Data in forced-convection condensation region (Re_{eq}>1600).

Finally, as proposed in section 3.2.2.2.1, the Webb (1998) model coupled with the new model for forced-convection condensation was applied to evaluate the super-heated vapor condensation heat transfer coefficients as presented by Eq. 85.

In this particular case the Webb (1998) model (Eq. 85) was applied by using the new model for forced convection condensation (Eq. 91) for the computation of the local saturated vapor condensation heat transfer coefficient $\alpha_{sat}=\alpha_{fc}$ and the Thonon (1995) equation for the local single-phase heat transfer coefficient (Eq. 88)

To compute the average condensation heat transfer coefficients referred to the projected area of the plates, the local heat transfer coefficients estimated by means the Webb (1998) model were integrated by a finite difference approach along the heat transfer area as in Eq. 89.

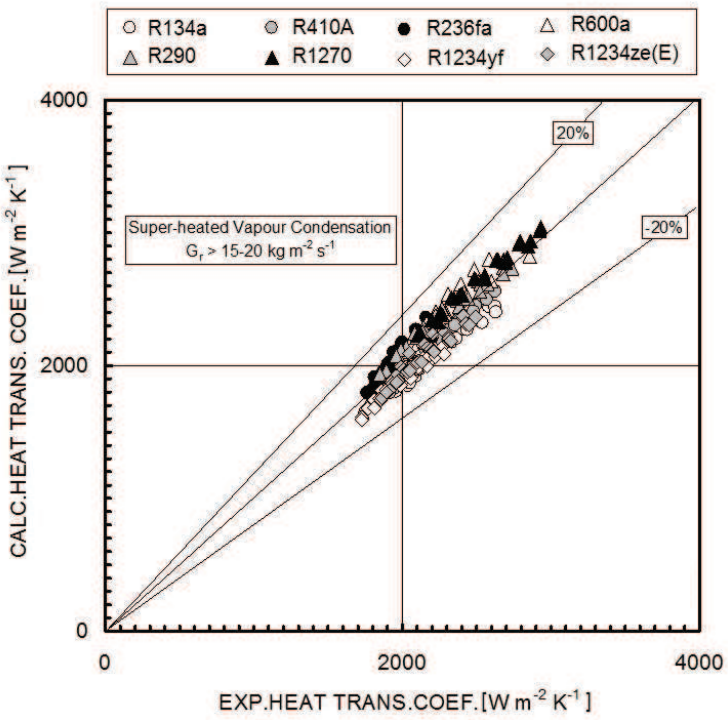

Figure 130 Comparison between experimental and calculated super-heated vapor condensation heat transfer coefficient by the Webb (1998) model together with the new model: data in forced-convection condensation region (G_r>15-20 $m^{-2}s^{-1}$).

Figure 130 shows the comparison between the experimental super-heated vapor condensation heat transfer coefficients in the forced-convection condensation region (G_r>15-20 kg $m^{-2}s^{-1}$) vs. the average heat transfer coefficients calculated by the Webb (1998) model (Eq. 85) implemented using the new model (Eq. 91).

The mean absolute percentage deviation between calculated and experimental data is around 4.7%.

3.2.2.2.2.1 Comparison against experimental data available in literature

The new computational procedure was compared against a set of 516 experimental data points obtained by different laboratories. The database includes saturated and super-heated HCFC, HFC, HC refrigerants, and Carbon Dioxide with different plate geometries.

The experimental heat transfer coefficients and the relative heat fluxes were re-calculated with reference to the projected area of the plates.

The following experimental data have been used:

- R134a saturated vapor condensation data by Yan *et al.* (1999): 88 data points relative to a single plate geometry and five different refrigerant mass fluxes: 60, 70, 80, 100, and 120 kg m^{-2} s^{-1}.
- R410A saturated vapor condensation data by Kuo *et al.* (2004): 121 data points relative to a single plate geometry and three different refrigerant mass fluxes: 50, 100, and 150 kg m^{-2} s^{-1}.
- R134a saturated vapor condensation data by Djordjević *et al.* (2008): 74 local heat transfer coefficient data points relative to a single plate geometry and three different refrigerant mass fluxes, 35, 50, and 65 kg m^{-2} s^{-1}.
- R22 and R290 super-heated vapor condensation data by Palmer *et al.* (2000): 36 data points relative to a single plate geometry and refrigerant mass flux from 2.6 to 19.2 kg m^{-2} s^{-1}.
- R744 super-heated vapor condensation by Hayes *et al.* (2009): present analysis considered only the 33 data points with a mis-balance between refrigerant side and coolant side lower than 10%. Data relative to three different plate geometries: low (30°/30°), medium (30°/63°), and high (63°/63°) were tested.
- R410A and R32 super-heated vapor condensation data by Mancin *et al.* (2011, 2012, and 2013): 61 data points for R410A and 103 data points for R32. Two different plate geometries were tested: type B and C with refrigerant mass flux from 13 to 37 kg m^{-2} s^{-1}.

Table 25 and Table 26 report the corrugated plate geometry and the operating conditions respectively of all the experimental data considered in present paper.

Table 25 Corrugated plate geometry of the BPHE experimental data found in literature.

Authors	**L** [mm]	**W** [mm]	**Φ** [–]	**β** [°]	**b** [mm]	**p** [mm]
Longo *et al.* (2010a, 2010b, 2013)	278	72	1.24	65	2.0	8.0
Yan *et al.* (1999)	450	120	1.28	60	2.9	10.0
Kuo *et al.* (2005)	450	120	1.28	60	2.9	10.0
Djordjevic *et al.* (2008)	872	486	1.26	63.26	3.2	12.0
Palmer *et al.* (2000)	479	116	1.24	65	2.0	8.0
Hayes *et al.* (2009)	444.5	127	1.20	30 - 63	2.0	6.03 - 6.27
Mancin *et al.* (2011, 2012, 2013)	269 - 466	94 - 111	1.2 - 1.22	65	1.2 - 2.05	6.0 - 8.8

Table 26 Operating conditions of the BPHE experimental data found in literature.

Authors	**Data**	**Refrigerant**	**Type**	t_{sat} [C]	G_r [kg m^{-2}s^{-1}]	q [kW m^{-2}]
Longo (2010a)	140	R236fa, R134a, R410A	Saturated	24.6 / 40.2	11.2 - 41.4	5.2 - 25.0
Longo (2010b)	113	R600a, R290, R1270	Saturated	24.8 / 40.3	5.3 - 27.9	6.2 - 34.4
Longo and Zilio (2013)	84	R1234yf	Saturated & Super-heated	24.9 / 40.2	11.0 - 40.8	5.3 - 23.2
Present thesis section	85	R1234ze(E)	Saturated &	24.8 / 40.2	10.7 - 39.9	5.3 - 26.0

3.2.1.2.1.1			Super-heated			
Longo (2010a)	44	R134a	Super-heated	24.9 / 40.1	11.6 - 41.3	7.6 - 28.1
Longo (2010a)	47	R410A	Super-heated	24.8 / 40.0	11.2 - 41.4	7.8 - 30.0
Longo (2010b)	112	R600a, R290, R1270	Super-heated	24.8 / 40.2	6.2 - 28.3	7.8 - 35.2
Yan *et al.* (1999)	88	R134a	Saturated	26.7 / 35.5	60 - 120	10 – 16
Kuo *et al.* (2005)	121	R410A	Saturated	20.0 / 31.5	50 - 150	10 – 15
Djordjević *et al.* (2008)	74	R134a	Saturated Local	26.0 / 29.0	30 - 65	11 – 17
Palmer *et al.* (2000)	36	R22, R290	Super-heated	30.4 / 42.9	2.6 - 19.2	2.0 - 8.3
Hayes *et al.* (2009)	33	R744	Super-heated	-36.4 / -17.0	12.4 - 41.8	4.7-28.7
Mancin *et al.* (2011, 2012)	61	R410A	Super-heated	36.6	13.1 - 36.9	3 - 14.4
Mancin *et al.* (2013)	103	R32	Super-heated	36.6	13.0 - 36.7	4.6 - 20.5

Figure 131 plots the saturated vapor condensation data points on the non-dimensional co-ordinates heat transfer factor J_H (Eq. 68) vs. equivalent Reynolds number Re_{eq} (Eq. 69), both calculated at the average vapor quality between inlet and outlet. For comparison, also the trends of the Nusselt (1916) equation (Eq. 81) and of the new model for forced convection condensation (Eq. 91) computed with an enlargement factor (Eq. 67) Φ=1.26 are reported.

Although the experimental data points cover a very wide range of equivalent Reynolds number, from 724 to 24317, the different sets exhibit trends in a fair agreement with the new computational procedure.

Figure 132 shows the comparison between the new model for forced convection condensation (Eq. 91) and the experimental heat transfer coefficients derived from the open literature.

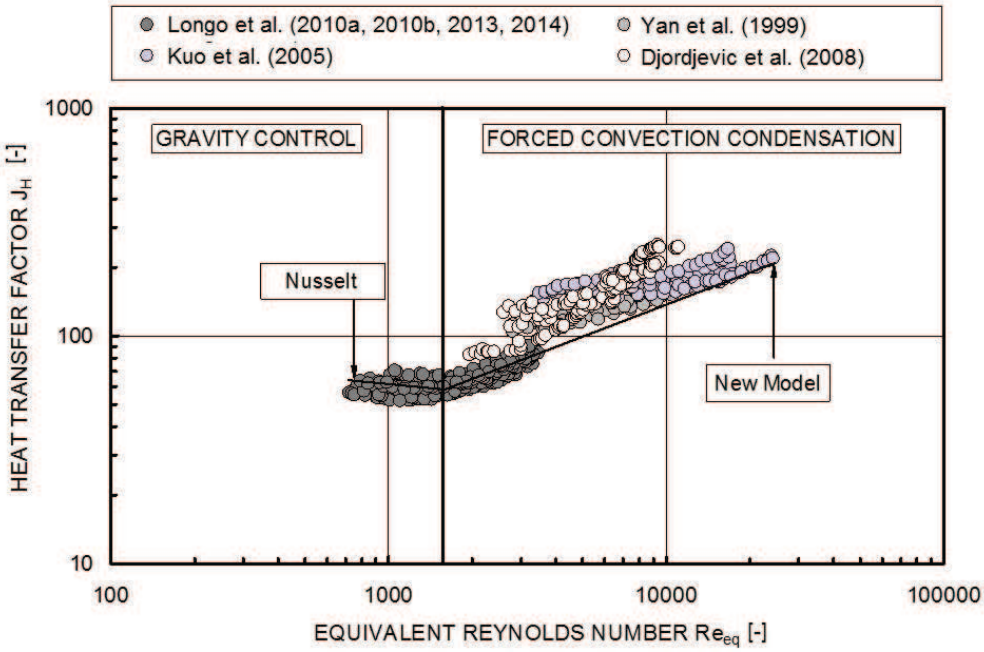

Figure 131 Saturated vapor condensation data available in literature plotted on the non-dimensional co-ordinates J_H vs. Re_{eq}.

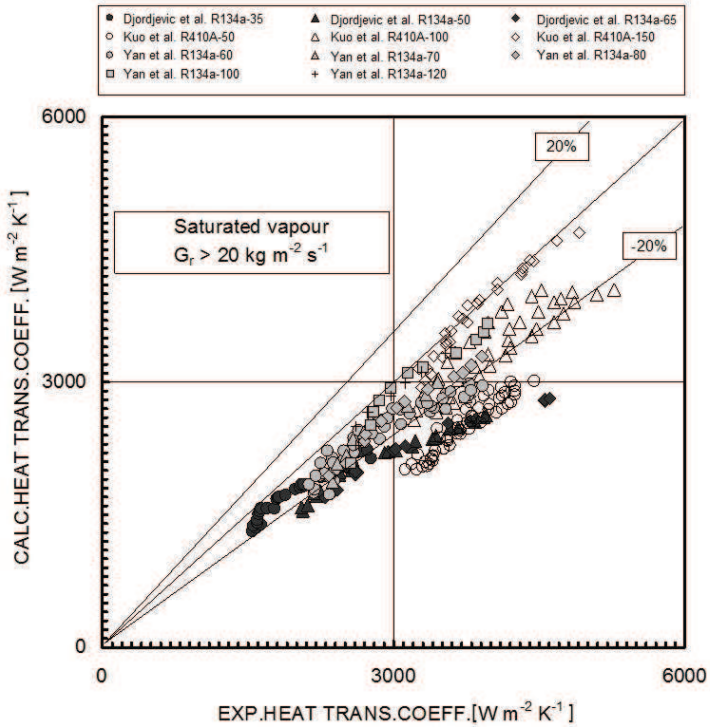

Figure 132 Comparison between experimental and calculated saturated vapor condensation heat transfer coefficient by the new model: data in forced-convection condensation region (Re_{eq}>1600) available in literature.

The available sets of saturated vapor condensation data are limited to R134a and R410A with two different plate geometries. The new model reproduces the experimental data within 20%, except for the R134a data at 50 and 65 kg $m^{-2}s^{-1}$ by Djordjević *et al.* (2008) and for the R410A data at 50 kg $m^{-2}s^{-1}$ by Kuo *et al.* (2005).

Finally, Figure 133 shows the comparison between the Webb (1998) model (Eq. 89) evaluated with the new model (Eq. 91) and the super-heated vapor condensation heat transfer coefficients available in the open literature. The mean absolute percentage deviation between experimental and calculated heat transfer coefficients on the whole set of 516 data points listed in this paragraph was lower than 16%.

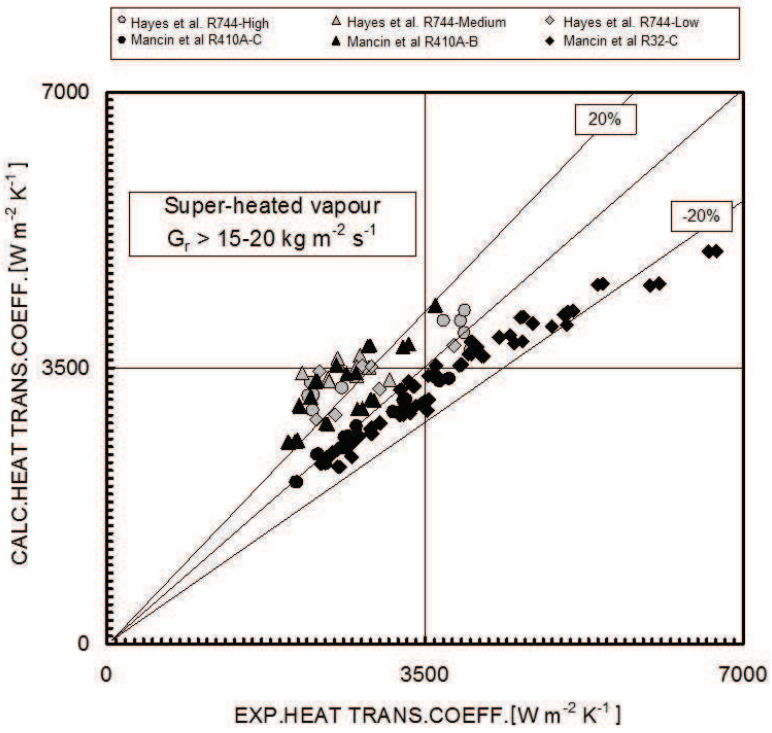

Figure 133 Comparison between experimental and calculated super-heated vapor condensation heat transfer coefficient by the Webb (1998) model together with the new model: data in forced-convection condensation region (G_r>15-20 kg $m^{-2}s^{-1}$) available in literature.

3.2.2.2.2.1.1 R152a

The R152a experimental data were analyzed with both the correlations presented in section 3.2.2.2.1 and 3.2.2.2.2 respectively. It has to be notice that the new correlation (see paragraph 3.2.2.2.2) was not developed using this set of data. The absolute mean percentage deviation between calculated and experimental data is 12.8% for Akers *et al.* (1959) equation, 23.2% for Yan *et al.* (1999) equation, and 6.0% for the here presented computational procedure (paragraph 3.2.2.2.2).

3.2.2.2.2.1.2 R32

Figure 134 presents the experimental heat transfer coefficients plotted against the calculated values obtained by the new computational procedure presented in section 3.2.2.2.2: the absolute mean percentage deviation is 4%. Again, it is worth underlining that the new correlation was not developed using this set of data.

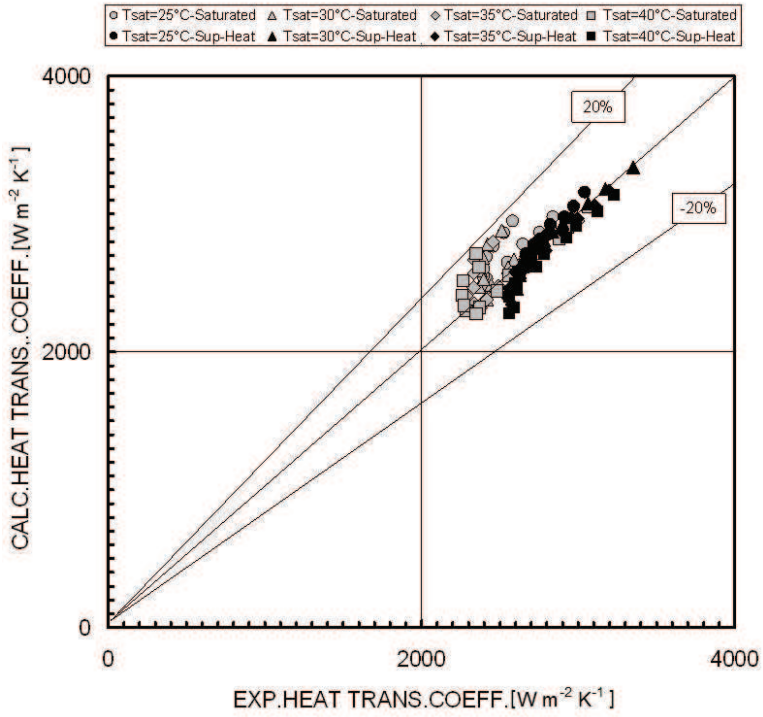

Figure 134 Experimental R32 heat transfer coefficients vs. calculated values obtained by the new computational procedure.

3.3 Roll-bond evaporator

Five different refrigerants were tested in an off-the-shelf roll-bond evaporator and their boiling performance were compared.
R134a was used as reference for the comparison and two HFOs, namely R1234yf and R1234ze(E), and two HCs, R600a and R600, were proposed and tested as low GWP alternatives.

3.3.1 Experimental results

Two different evaporation temperatures were investigated, -15 °C and -20 °C, while the condensing temperature was fixed around 40 °C, the sub-cooling temperature was between 20 and 30 °C, and the vapor quality at the inlet of the evaporator was in the range 0.25 – 0.35. The refrigerating chamber air temperature was maintained constant at 3 °C and dew temperature below -5 °C, to reproduce the refrigerated cavity of a domestic refrigerator.
Beside the optimization of the system for the new low GWP refrigerants, the variable refrigerant flow rate modulation is a solution adopted in many cooling applications to enhance the efficiency. This technology is going to be applied also in the domestic refrigerator field. In the open literature is possible to find some works that analyze the transient period during ON-OFF control, for example Hermes *et al.* (2008), Berger *et al.* (2012) and Porkhial *et al.* (2004). But there are no studies that analyze the problem under the variable flow rate approach point of view. For this reason it was chosen to examine the evaporator behavior focusing on several steady state conditions at different mass flow rates, to simulate a variable speed system behavior.
So each series of data points was run varying the refrigerant mass flow rate that ranged from the minimum value achievable by the compressor at the minimum speed up to the maximum value where the vapor super-heating at the outlet of the roll-bond evaporator approaches zero. Table 27 summarizes the operating conditions during all the experimental tests showing evaporation temperature T_e, condensation temperature T_c, sub-cooling temperature T_{sub}, inlet refrigerant vapor quality x_{in}, refrigerant mass flux G_r, and maximum refrigerant mass flow rate $\dot{m}_{r.max}$.
A detailed error analysis in accordance with Kline and McClintock (1954) is summarized in Table 28.

Table 27 Operating conditions during experimental tests of vaporization inside a roll-bond type evaporator.

Experimental data set	t_{cond}	t_{sub}	x_{in}	**G**	$\dot{m}_{max}$
	[°C]	[°C]	[-]	[kg $m^{-2}s^{-1}$]	[kg h^{-1}]
R134a (t_{evap}=-15°C)	40—42	21—33	0.26—0.32	11—49	2.24
R134a (t_{evap}=-20°C)	40—43	21—34	0.27—0.35	11—60	2.74
R1234ze(E) (t_{evap}=-15°C)	41—42	22—25	0.27—0.28	10—50	2.24
R1234ze(E) (t_{evap}=-20°C)	40—41	21—24	0.28—0.30	10—56	2.53
R1234yf (t_{evap}=-15°C)	39—42	23—28	0.30—0.33	16—60	2.71
R1234yf (t_{evap}=-20°C)	39—42	23—30	0.33—0.38	16—65	2.98
R600a (t_{evap}=-15°C)	41—42	22—32	0.23—0.29	6—23	1.06
R600a (t_{evap}=-20°C)	40—41	23—29	0.28—0.29	6—23	1.06
R600 (t_{evap}=-15°C)	41—42	26—31	0.24—0.25	6—22	1.01

Table 28 Mean uncertainty values of the roll-bond evaporator test facility evaluated by Kline and McClintock (1954) method.

Uncertainty	
Specific enthalpy	±1% (*)
Evaporator cooling capacity	±2.9%
Overall heat transfer coefficient	±7.6%
Air heat transfer coefficient	±2.0%
Refrigerant heat transfer coefficient	±20.0%
(*) Estimated from the measured values of temperature and/or pressure using Refprop 9.1 (2013)	

3.3.2 Refrigerating capacity

Figure 135, Figure 136, Figure 137, Figure 138, and Figure 139 show the cooling refrigerating capacity vs. the refrigerant mass flow rate as a function of the evaporation temperature for R134a, R1234ze(E), R1234yf, R600a and R600, respectively.

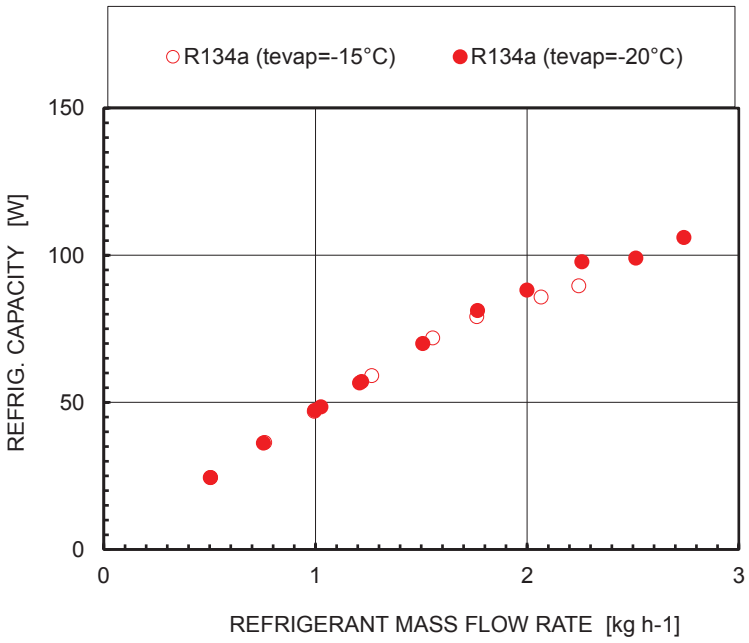

Figure 135 Refrigerating capacity vs. refrigerant mass flow rate at -15 °C and -20 °C of evaporation temperature with R134a.

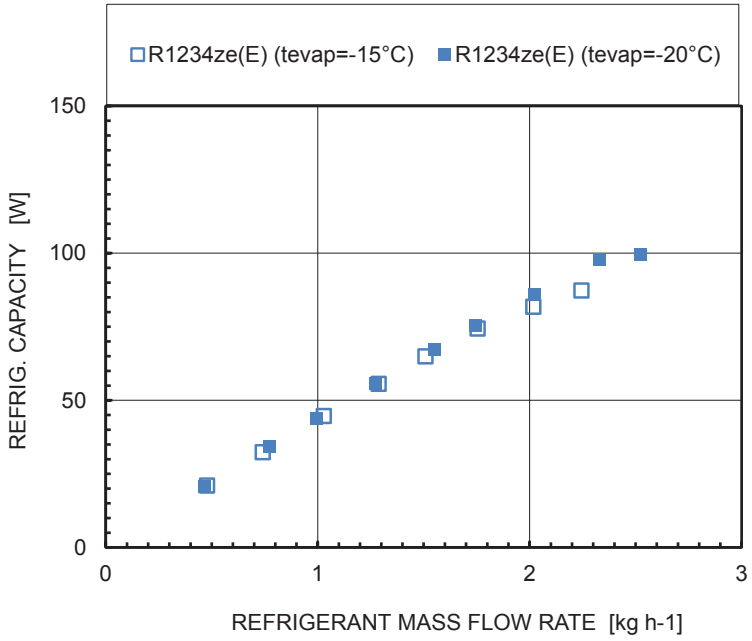

Figure 136 Refrigerating capacity vs. refrigerant mass flow rate at -15 °C and -20 °C of evaporation temperature with R1234ze(E).

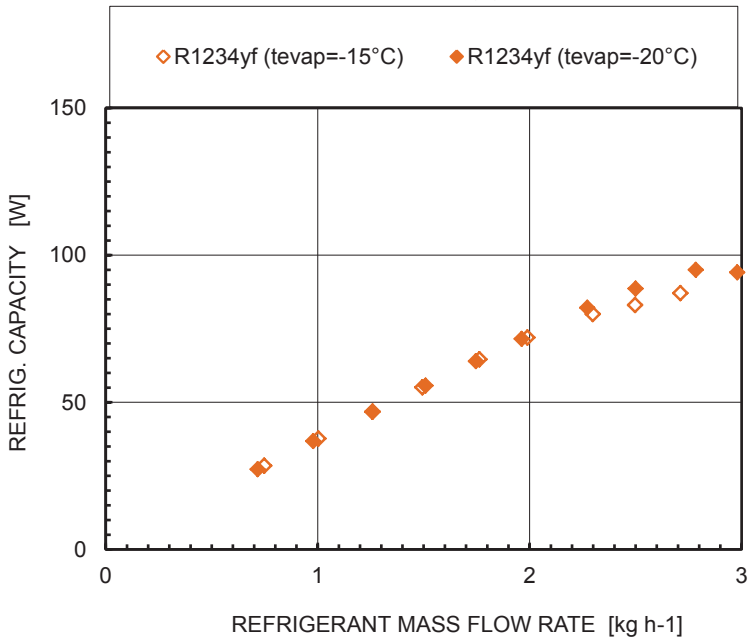

Figure 137 Refrigerating capacity vs. refrigerant mass flow rate at -15 °C and -20 °C of evaporation temperature with R1234yf.

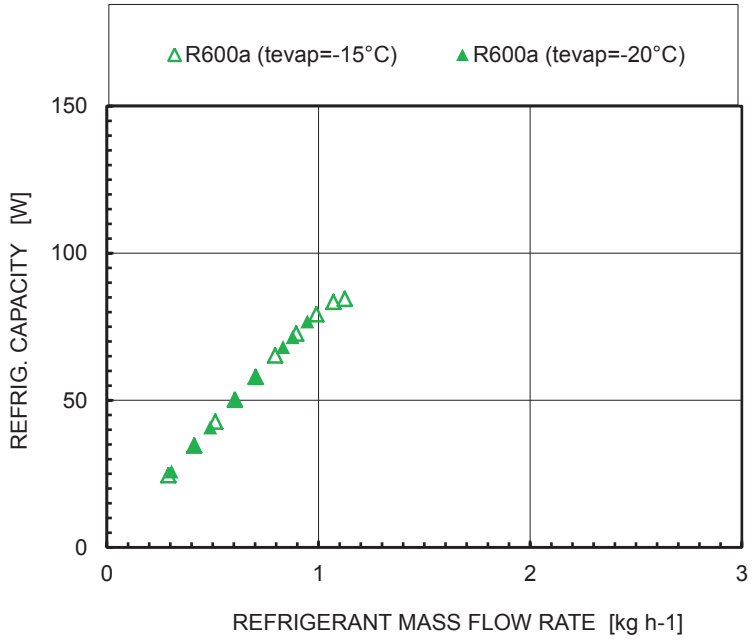

Figure 138 Refrigerating capacity vs. refrigerant mass flow rate at -15 °C and -20 °C of evaporation temperature with R600a.

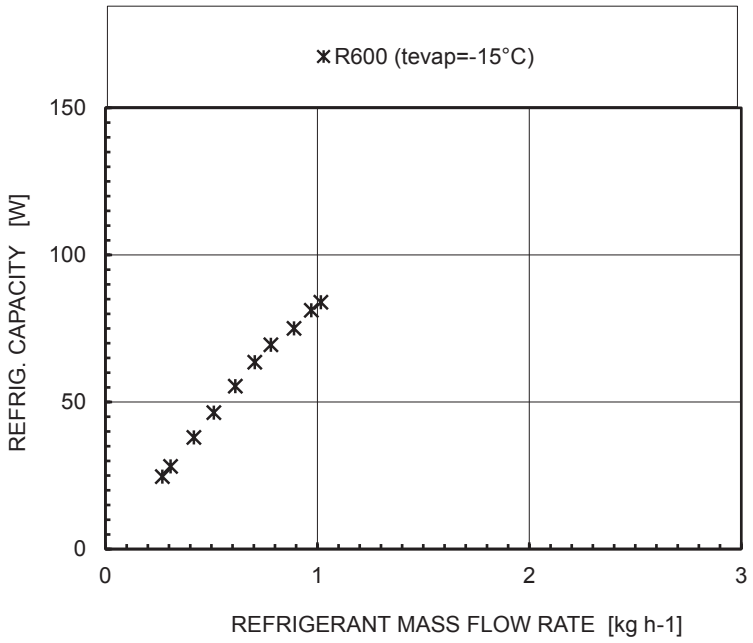

Figure 139 Refrigerating capacity vs. refrigerant mass flow rate at -15 °C of evaporation temperature with R600.

The cooling capacity can be fairly considered as a linear function of the refrigerant mass flow rate. For each evaporation temperature and each refrigerant the mass flow rate, the upper limit in refrigerating capacity is fixed by the roll-bond geometry. In fact, at the maximum refrigerant mass flow rate, the vapor super-heating at the evaporator outlet approaches zero, almost all the heat transfer area is interested by two-phase heat transfer and the compressor is closely near to a wet compression condition.

The maximum refrigerating capacity is 106 W for R134a, 99 W for R1234ze(E), 95 W for R1234yf, 83 W for R600a, and 81 W for R600.

The minimum refrigerant capacity is connected to the minimum flow rate driven by the being this value around 25 W for each refrigerant.

The evaporation temperature does not affect the refrigerating capacity at a fixed refrigerant mass flow rate. At lower saturation temperatures the evaporator can elaborate a greater mass flow rate before reaching the condition of "zero vapor superheating" at the evaporator outlet.

3.3.3 Overall heat transfer coefficient

Figure 140, Figure 141, Figure 142, Figure 143, and Figure 144 show the overall heat transfer coefficient vs. the refrigerating capacity at -15 °C and -20 °C of evaporation temperature for R134a, R1234ze(E), R1234yf, R600a and R600, respectively.

The overall heat transfer coefficient (Eq. 44) can be fairly considered as a linear function of the refrigerating capacity. The maximum value of K is 22.14 W $m^{-2}K^{-1}$, 21.55 W $m^{-2}K^{-1}$, 19.34 W $m^{-2}K^{-1}$, 23.50 W $m^{-2}K^{-1}$, and 22.78 W $m^{-2}K^{-1}$ for R134a, R1234ze(E), R1234yf, R600a, and R600, respectively.

The saturation temperature affects the overall heat transfer coefficient: at higher evaporation temperatures the overall heat transfer coefficient is higher, especially at higher refrigerating capacities.

For example, K is up to 30% higher when the system is evaporating at -15 °C instead of -20 °C with R134a as refrigerant (Figure 140). This enhancement is lower (up to +13%) when the system is working with R600a (Figure 143).

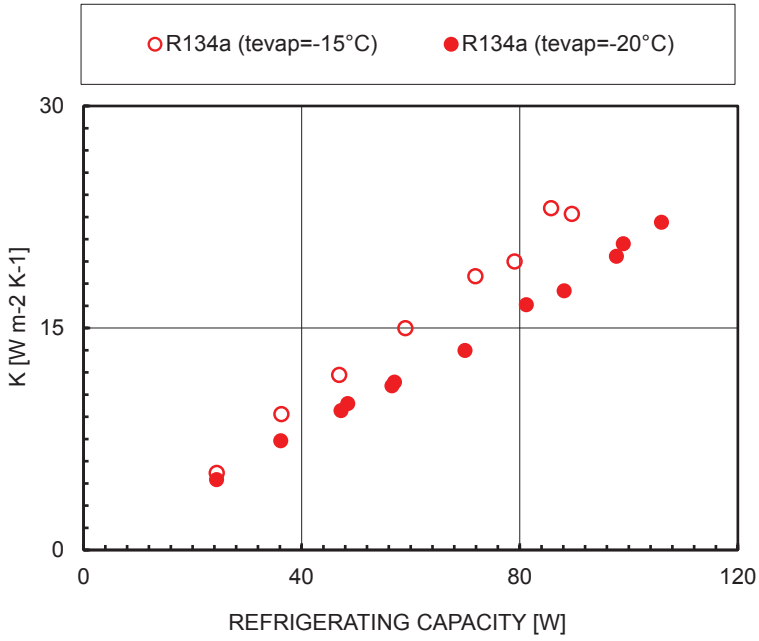

Figure 140 Overall heat transfer coefficient (K) vs. refrigerating capacity at -15 °C and -20 °C of evaporation temperature with R134a.

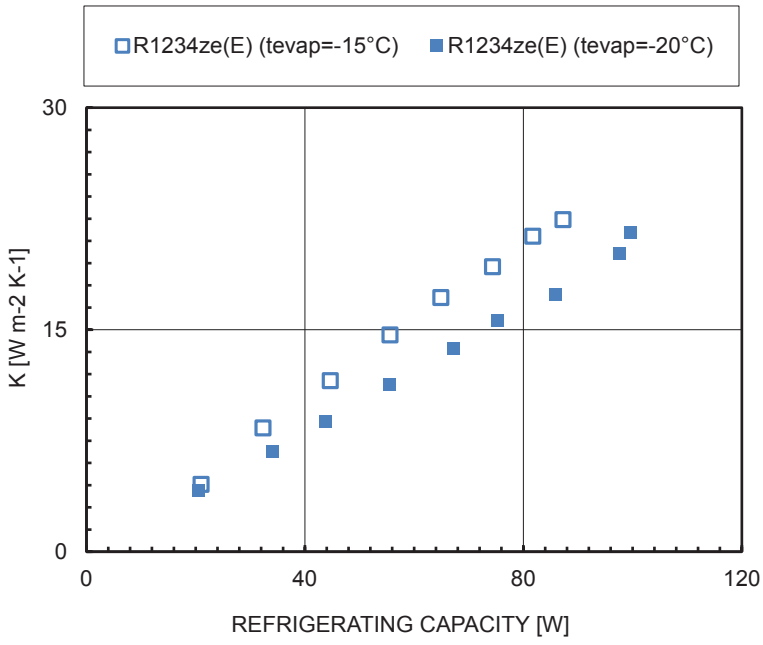

Figure 141 Overall heat transfer coefficient (K) vs. refrigerating capacity at -15 °C and -20 °C of evaporation temperature with R1234ze(E).

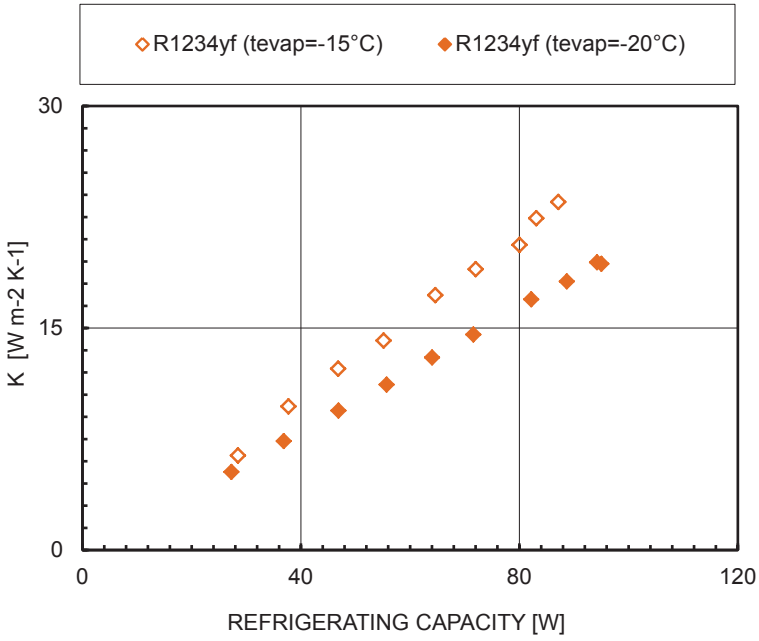

Figure 142 Overall heat transfer coefficient (K) vs. refrigerating capacity at -15 °C and -20 °C of evaporation temperature with R1234yf.

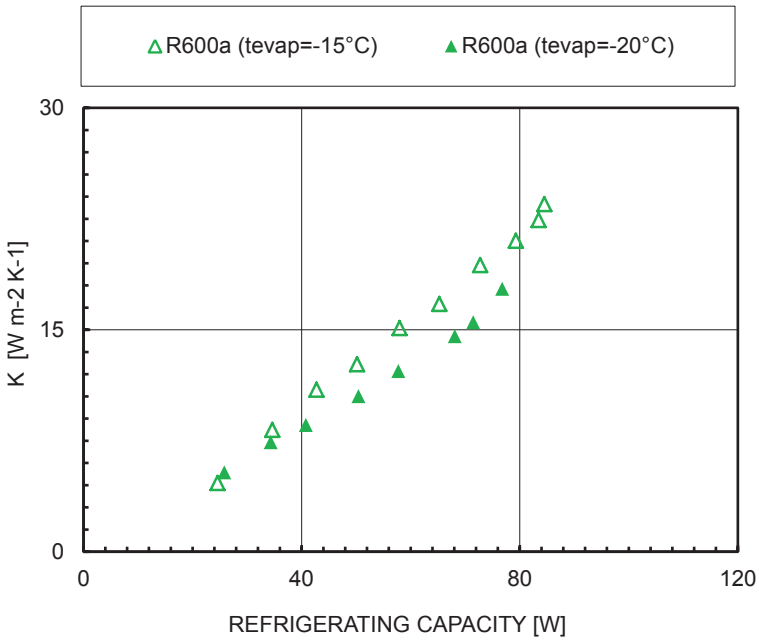

Figure 143 Overall heat transfer coefficient (K) vs. refrigerating capacity at -15 °C and -20 °C of evaporation temperature with R600a.

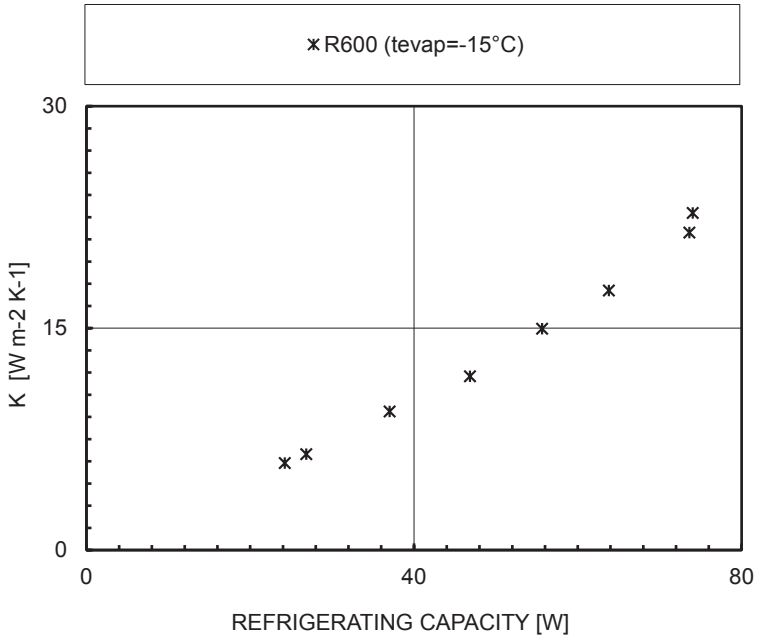

Figure 144 Overall heat transfer coefficient (K) vs. refrigerating capacity at -15 °C of evaporation temperature with R600.

3.3.4 Air side heat transfer coefficient

Figure 145, Figure 146, Figure 147, Figure 148, and Figure 149 show the air-side heat transfer coefficient vs. the refrigerant mass flow rate at -15 °C and -20 °C for R134a, R1234ze(E), R1234yf, R600a, and R600, respectively.

The air-side heat transfer coefficient (Eq. 45) is almost constant for all the data points obtained and it depends weakly on the refrigerant used. The mean air-side heat transfer coefficient value is 22.0 W m^{-2} K^{-1} with a standard deviation of 2.0 W m^{-2} K^{-1}.

At lower refrigerating capacity the air-side heat transfer coefficient is higher because the average wall temperature is hardly affected by the evaporation process; in fact the evaporator works mainly with super-heated vapor (See for instance the infrared images in section 3.3.7).

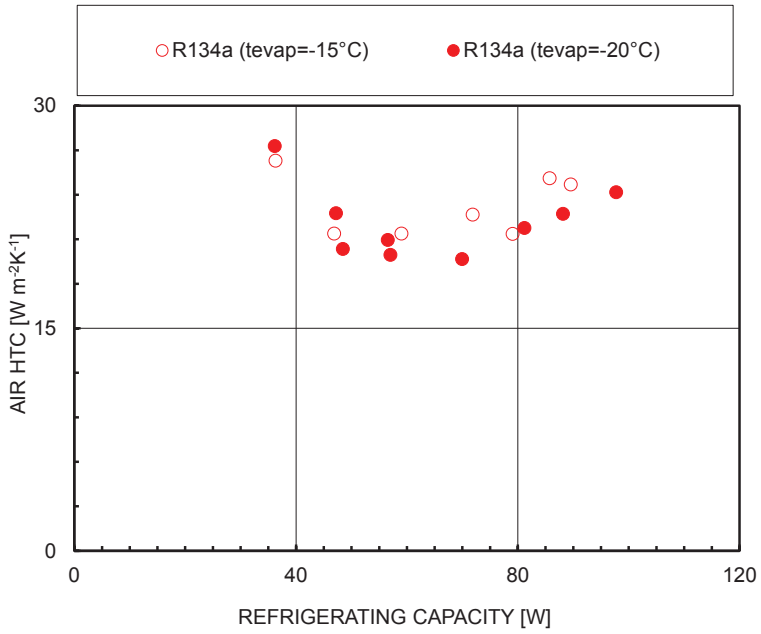

Figure 145 Air side HTC vs. refrigerating capacity at -15 °C and -20 °C of evaporation temperature with R134a.

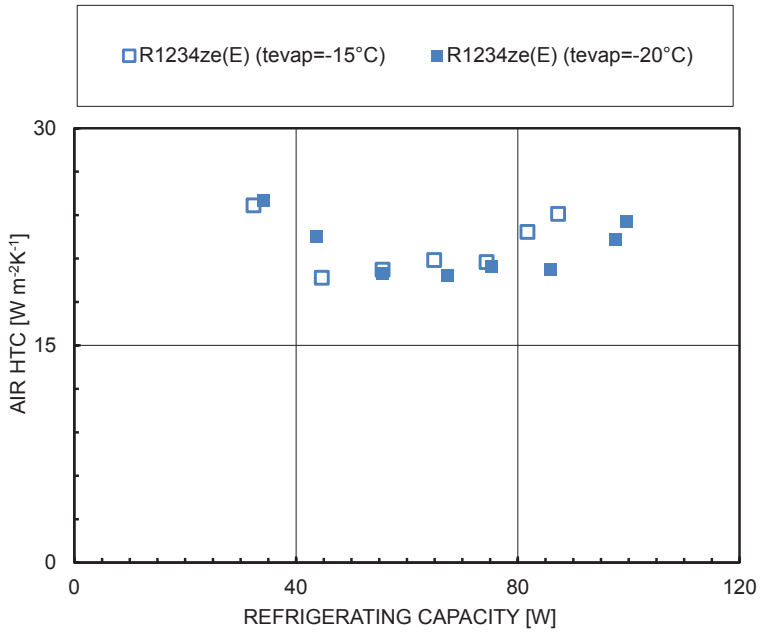

Figure 146 Air side HTC vs. refrigerating capacity at -15 °C and -20 °C of evaporation temperature with R1234ze(E).

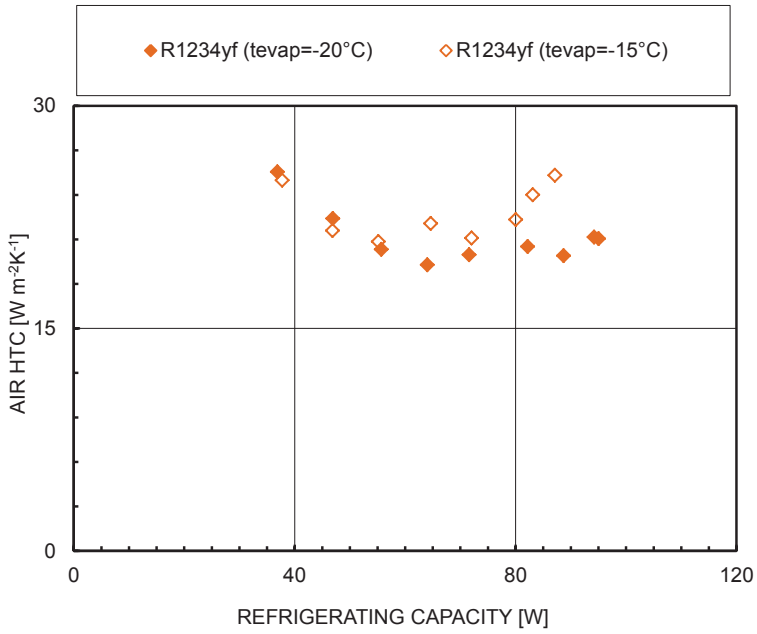

Figure 147 Air side HTC vs. refrigerating capacity at -15 °C and -20 °C of evaporation temperature with R1234yf.

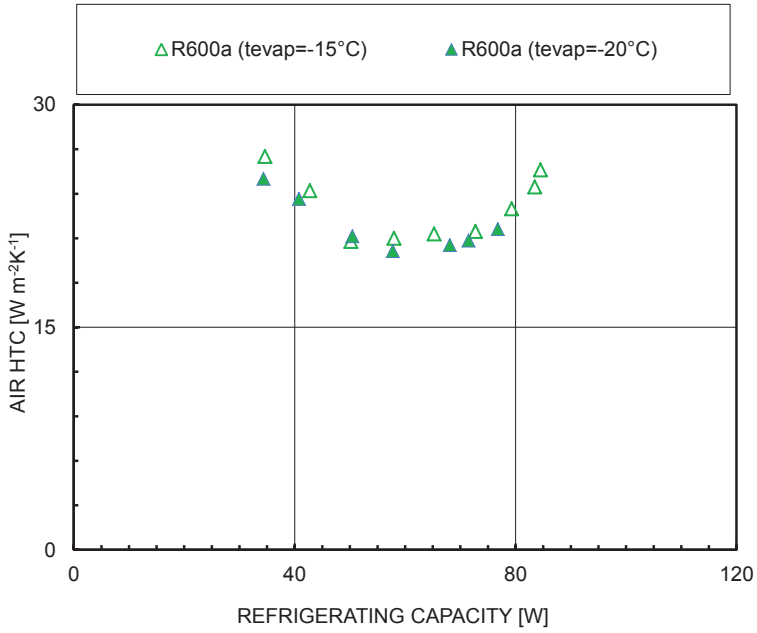

Figure 148 Air side HTC vs. refrigerating capacity at -15 °C and -20 °C of evaporation temperature with R600a.

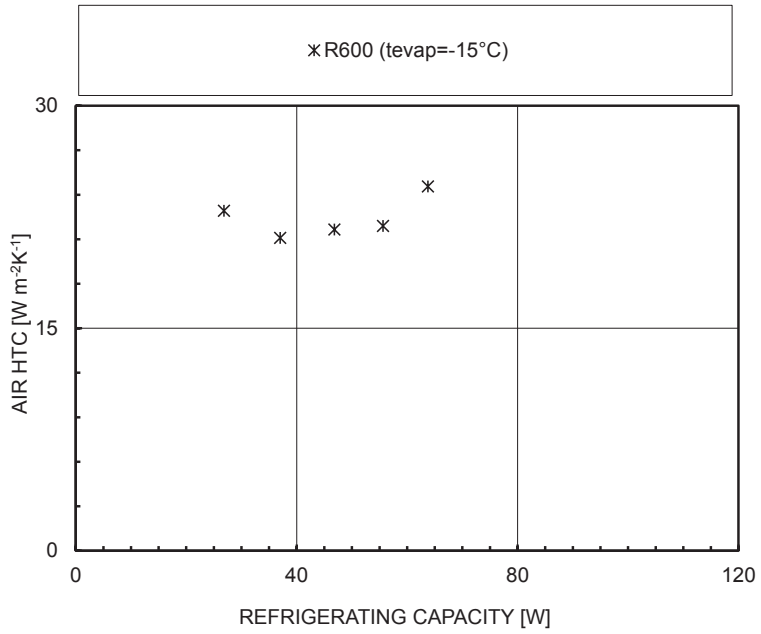

Figure 149 Air side HTC v.s refrigerating capacity at -15 °C of evaporation temperature with R600.

3.3.5 Refrigerant-side heat transfer coefficient

Figure 150, Figure 151, Figure 152, Figure 153, and Figure 154 show the refrigerant-side heat transfer coefficient vs. the refrigerating capacity at -15 °C and -20 °C of evaporation temperature for R134a, R1234ze(E), R1234yf, R600a, and R600, respectively.

At lower refrigerating capacity the refrigerant heat transfer coefficient can be fairly considered as a linear function of the refrigerating capacity. At higher refrigerating capacity, when almost all the heat transfer area is interested by two-phase heat transfer, the slope of the linear relation between refrigerant heat transfer coefficient and refrigerating capacity changes and one can affirm that the refrigerant heat transfer coefficient is almost constant with respect to the refrigerating capacity.

The maximum value of the refrigerant heat transfer coefficient, obtained at -15°C saturation temperature, is 486 W $m^{-2}K^{-1}$, 540 W $m^{-2}K^{-1}$, 571 W $m^{-2}K^{-1}$, 457 W $m^{-2}K^{-1}$, and 453 W $m^{-2}K^{-1}$ for R134a, R1234ze(E), R1234yf, R600a, and R600, respectively.

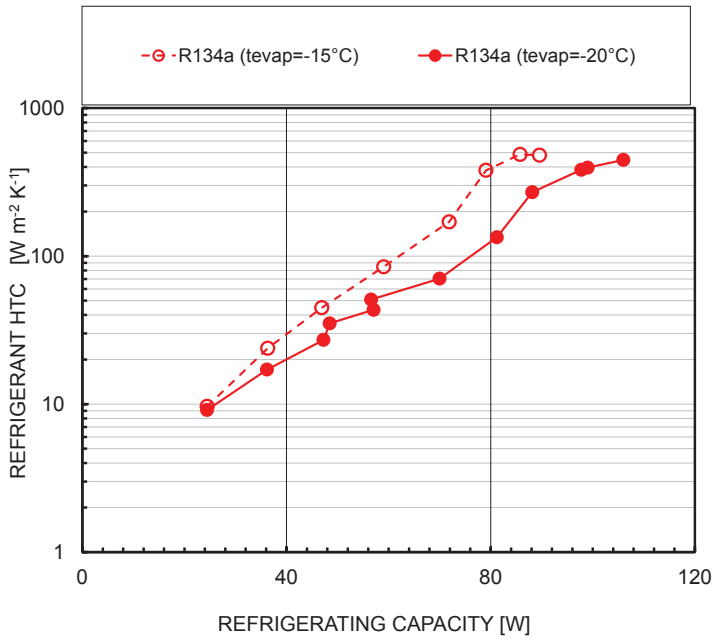

Figure 150 Refrigerant HTC vs. refrigerating capacity at -15 °C and -20 °C of evaporation temperature with R134a.

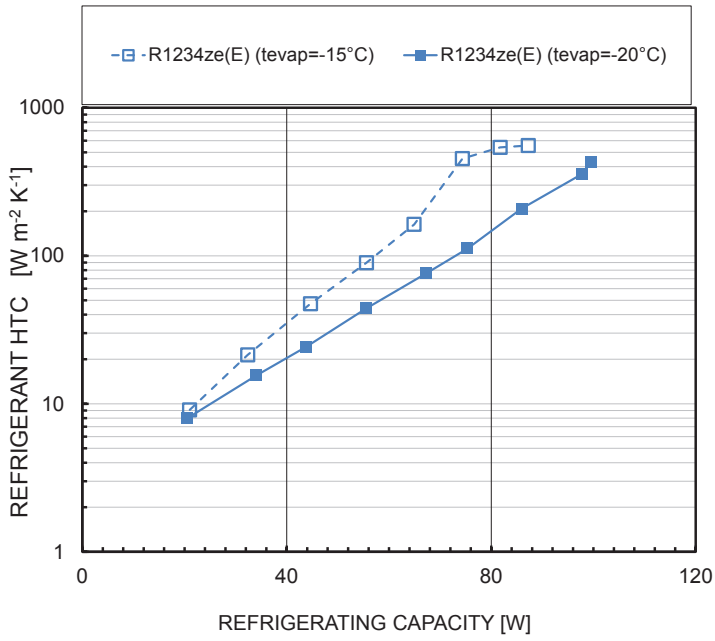

Figure 151 Refrigerant HTC vs. refrigerating capacity at -15 °C and -20 °C of evaporation temperature with R1234ze(E).

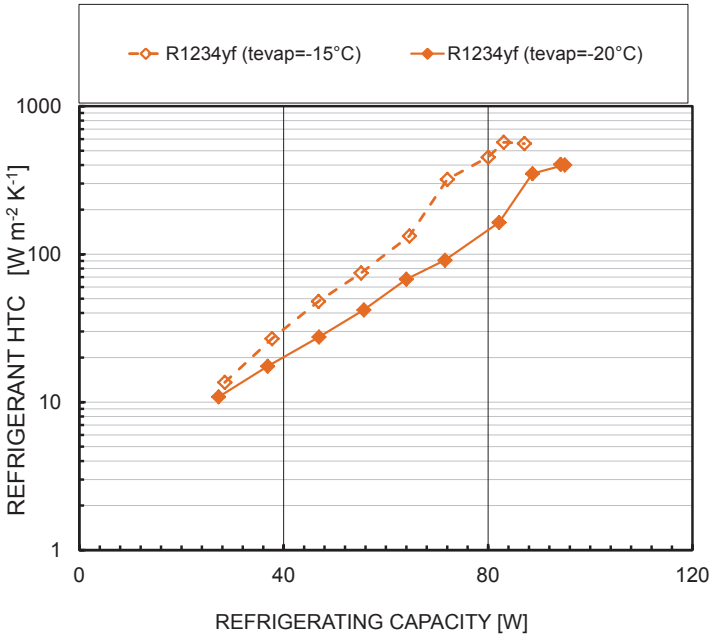

Figure 152 Refrigerant HTC vs. refrigerating capacity at -15 °C and -20 °C of evaporation temperature with R1234yf.

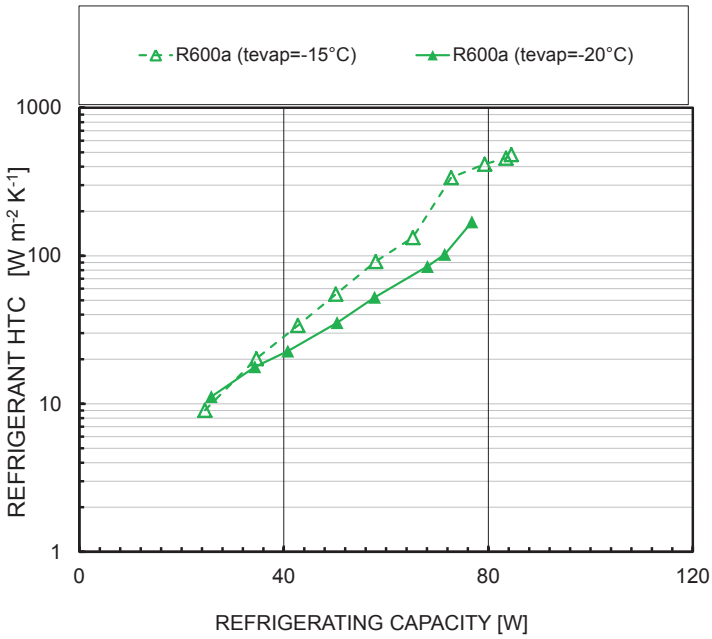

Figure 153 Refrigerant HTC vs. refrigerating capacity at -15 °C and -20 °C of evaporation temperature with R600a.

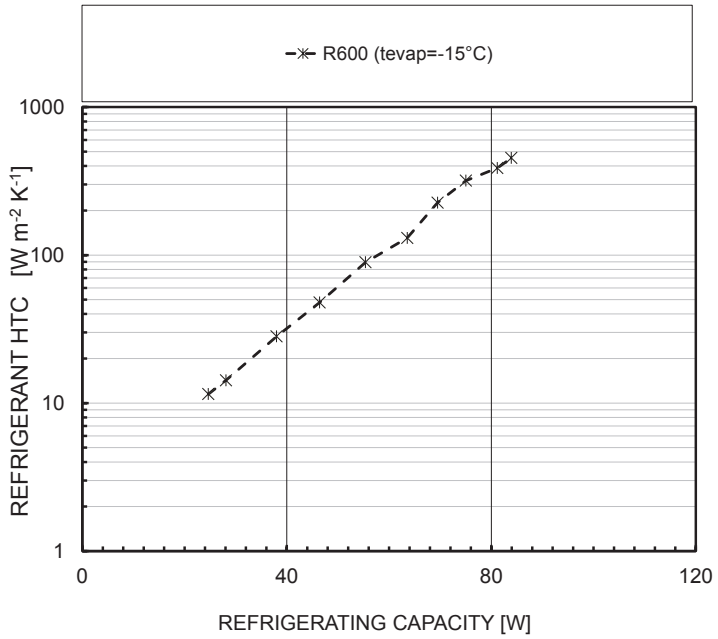

Figure 154 Refrigerant HTC vs. refrigerating capacity at -15 °C of evaporation temperature with R600a.

As for K, presented in section 3.3.3, the saturation temperature affects the refrigerant heat transfer coefficient: the higher evaporation temperatures, the higher refrigerant heat transfer coefficient is, especially at higher refrigerating capacities.

When the system is evaporating at -15 °C instead of -20 °C, the refrigerating HTC is up to 2.8 times higher with R134a as refrigerant, up to 4 times higher with R1234ze(E), up to 2.7 times higher with R1234yf, and up to 2 times higher with R600a.

3.3.6 Pressure drop

Figure 155, Figure 156, Figure 157, Figure 158, and Figure 159 show pressure drop vs. refrigerant mass flow rate at -15 °C and -20 °C of saturation temperature for R134a, R1234ze(E), R1234yf, R600a and R600, respectively.

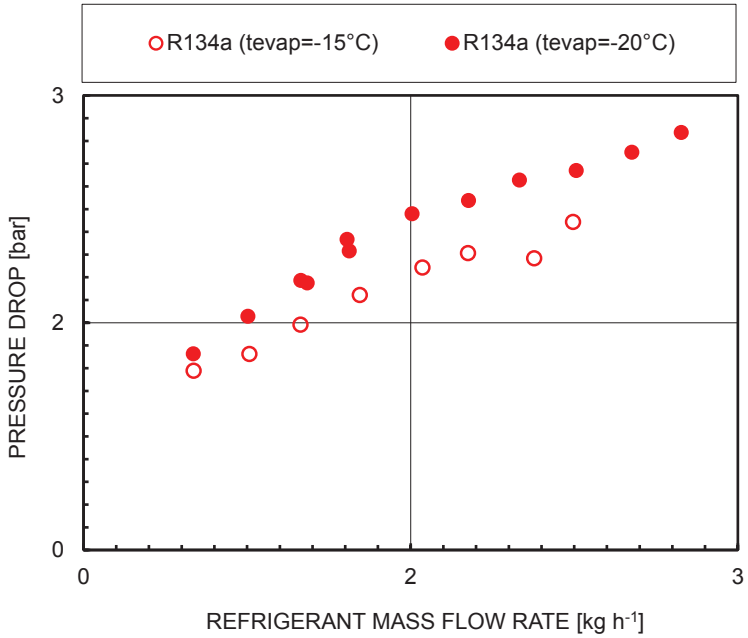

Figure 155 Pressure drop vs. refrigerant mass flow rate at -15 °C and -20 °C of evaporation temperature with R134a.

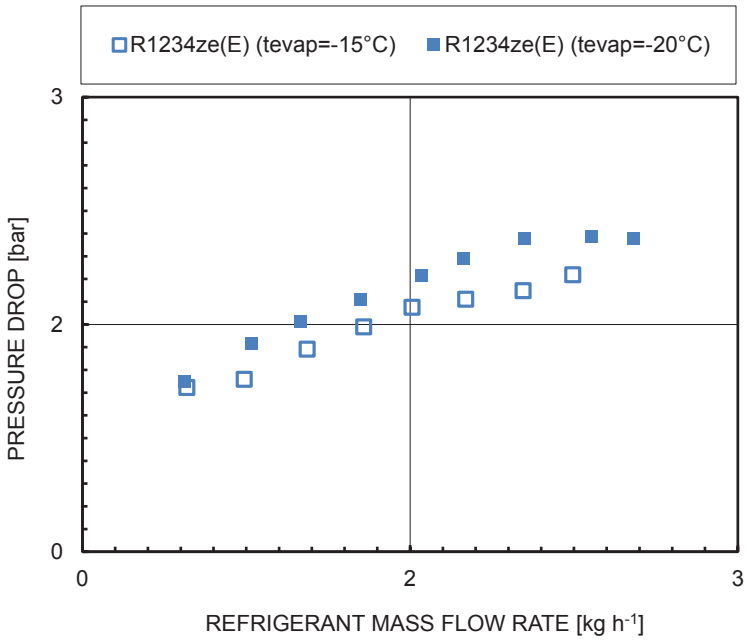

Figure 156 Pressure drop vs. refrigerant mass flow rate at -15 °C and -20 °C of evaporation temperature with R1234ze(E).

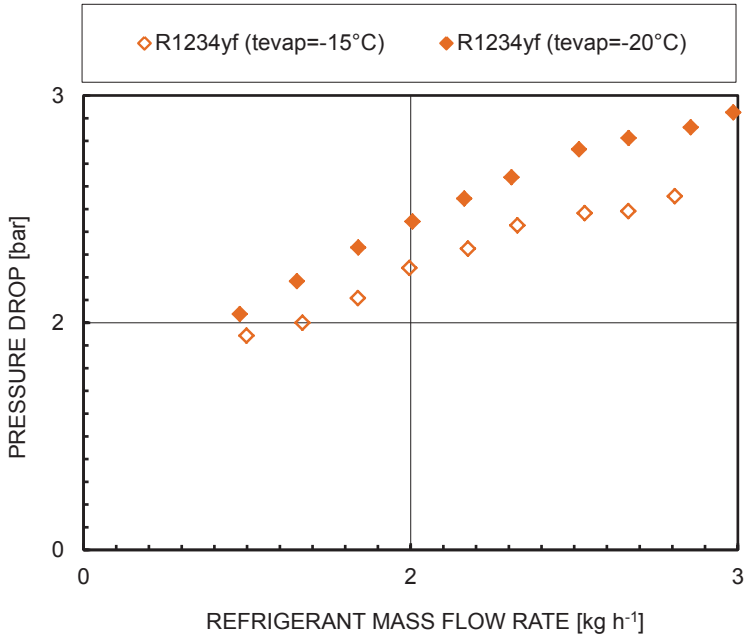

Figure 157 Pressure drop vs. refrigerant mass flow rate at -15 °C and -20 °C of evaporation temperature with R1234yf.

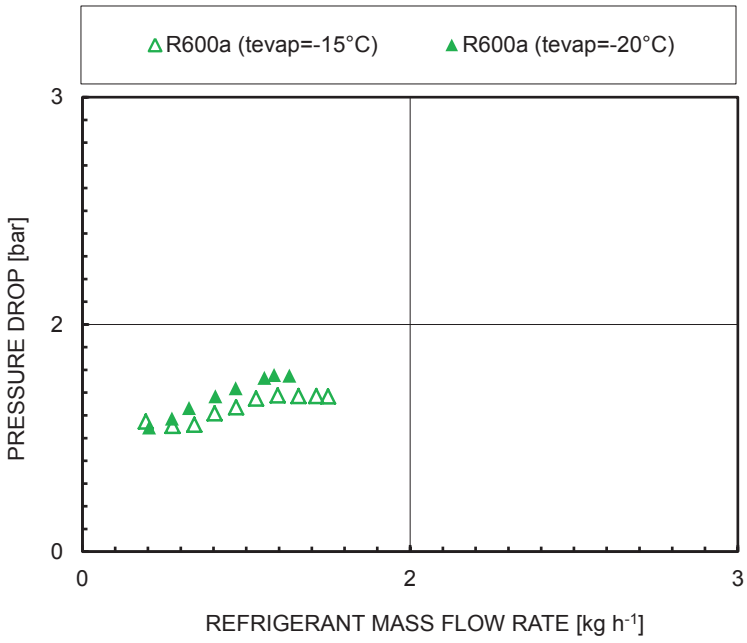

Figure 158 Pressure drop vs. refrigerant mass flow rate at -15 °C and -20 °C of evaporation temperature with R600a.

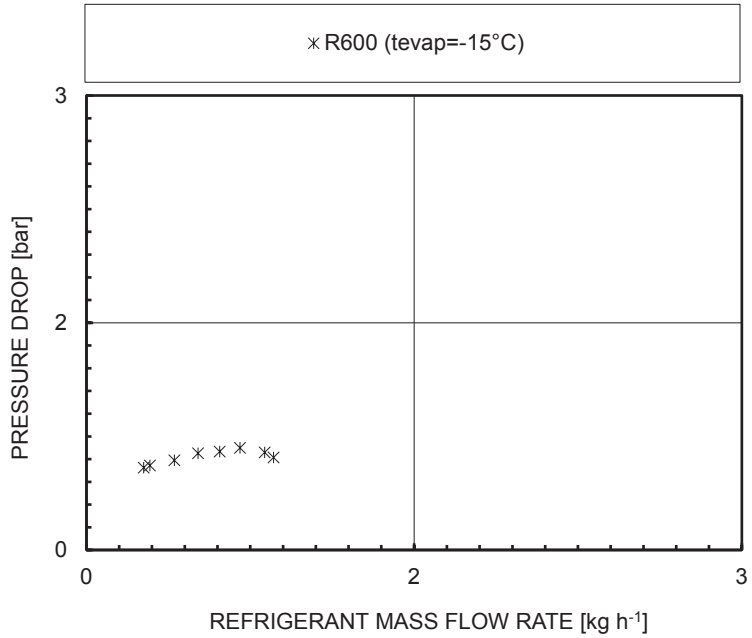

Figure 159 Pressure drop vs. refrigerant mass flow rate at -15 °C of evaporation temperature with R600.

The pressure drop increases with the increasing of the refrigerant mass flow rate, but the trend is not linear. Generally the slope is lower when the refrigerant mass flux is high, maybe because all the plate is working under two phase heat transfer and the heat transfer area is almost constant.

The maximum value of the pressure drop is reached at a saturation temperature of -20 °C and it is equal to 2.76, 2.06, 2.88, 1.16, 0.61 bar for R134a, R1234ze(E), R1234yf, R600a, and R600, respectively.

The saturation temperature affects the pressure drop: on average it becomes 25% higher when the saturation temperature passes from -15 °C to -20 °C with R134a and the HFOs, while when R600a is used as refrigerant this increment is reduced up to around 10%.

3.3.7 Infrared analysis

An IR thermo-camera was utilized to monitor the temperature distribution on the front face of the roll-bond evaporator. The temperature field recorded by the IR camera was validated against the local temperature readings made by the 16 thermocouples located on the rear face of the plate.

Figure 160 shows the comparison between the thermocouple measurements and the IR thermo-camera analysis during a typical test with R134a under steady state condition. A fair agreement can be observed between IR analysis and thermocouple measurements.

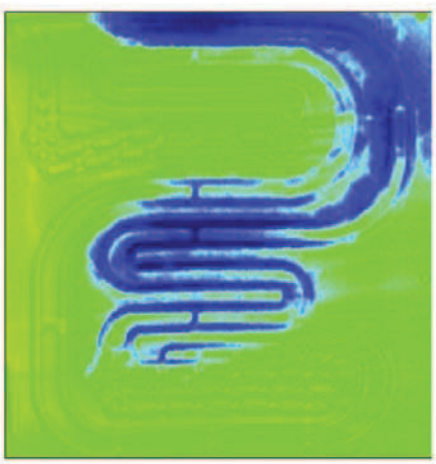

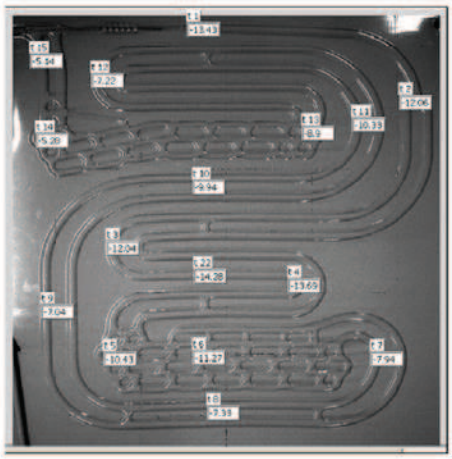

t_1(°C)	-13.43
t_2(°C)	-12.06
t_3(°C)	-12.04
t_4(°C)	-13.69
t_5(°C)	-10.43
t_6(°C)	-11.27
t_7(°C)	-7.94
t_8(°C)	-7.33
t_9(°C)	-7.04
t_{10}(°C)	-9.94
t_{11}(°C)	-10.33
t_{12}(°C)	-7.22
t_{13}(°C)	-8.90
t_{14}(°C)	-5.28
t_{15}(°C)	-5.14
t_{22}(°C)	-14.28

Figure 160 Comparison between an IR image and the corresponding thermocouples temperature profile.

Each figure from Figure 161 to Figure 168 reports eight IR images taken at steady state conditions at a fixed evaporation temperature and refrigerant mass flow rate. Figure 161 and Figure 162 refer to R134a, Figure 163 and Figure 164 refer to R1234ze(E), Figure 165 and Figure 166 refer to R1234yf, and Figure 167 and Figure 168 refer to R600a at -15 °C and -20 °C of evaporation temperature, respectively.

Red color represents the hottest surfaces while blue color the coldest ones. In this way, one can associate at a first sight the blue colored parts with the areas interested by two-phase heat transfer and the red-yellow parts with the super-heated areas.

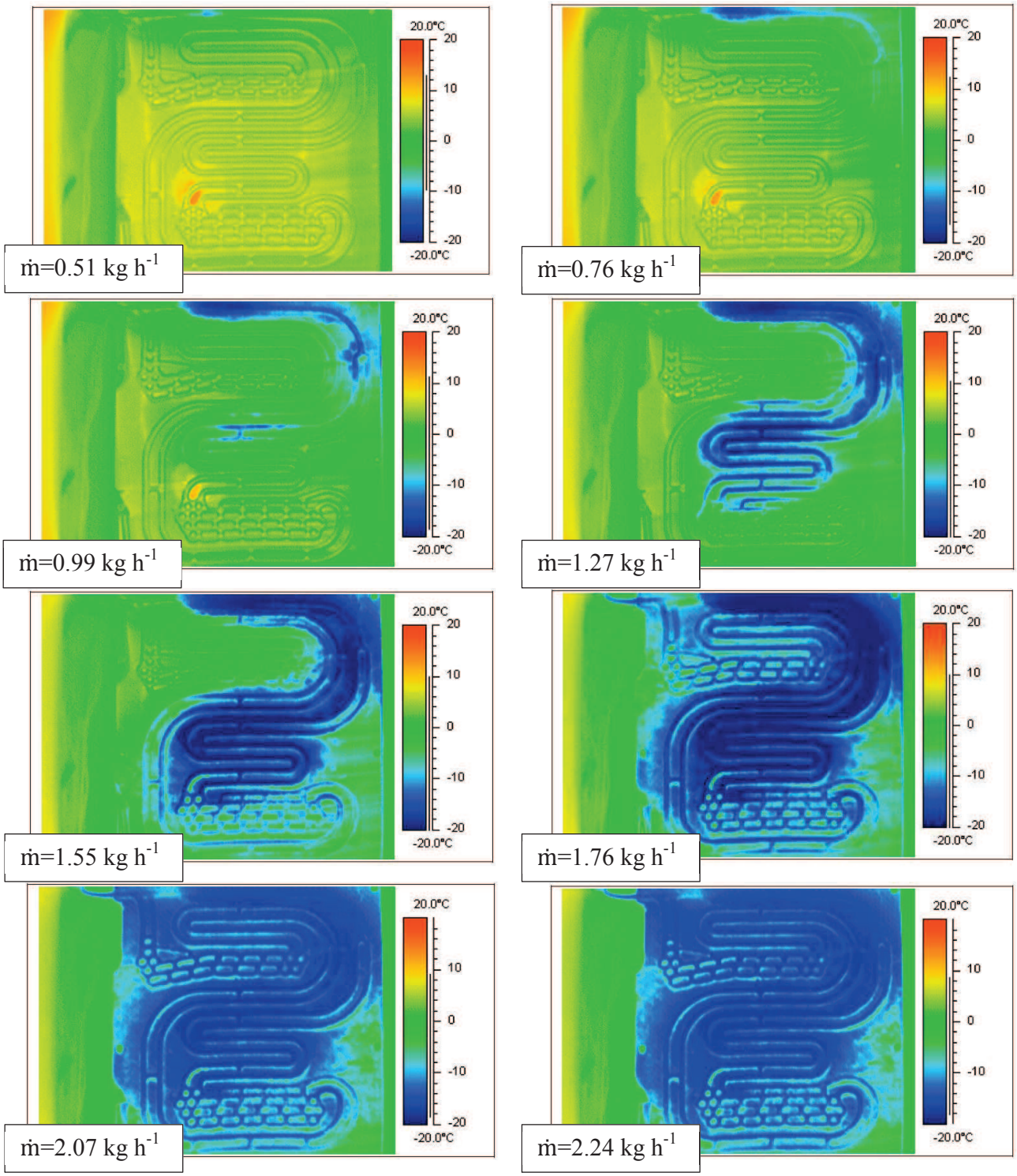

Figure 161 Roll-bond images collected by the thermal camera. Data with R134a at t_{evap}=-15 °C.

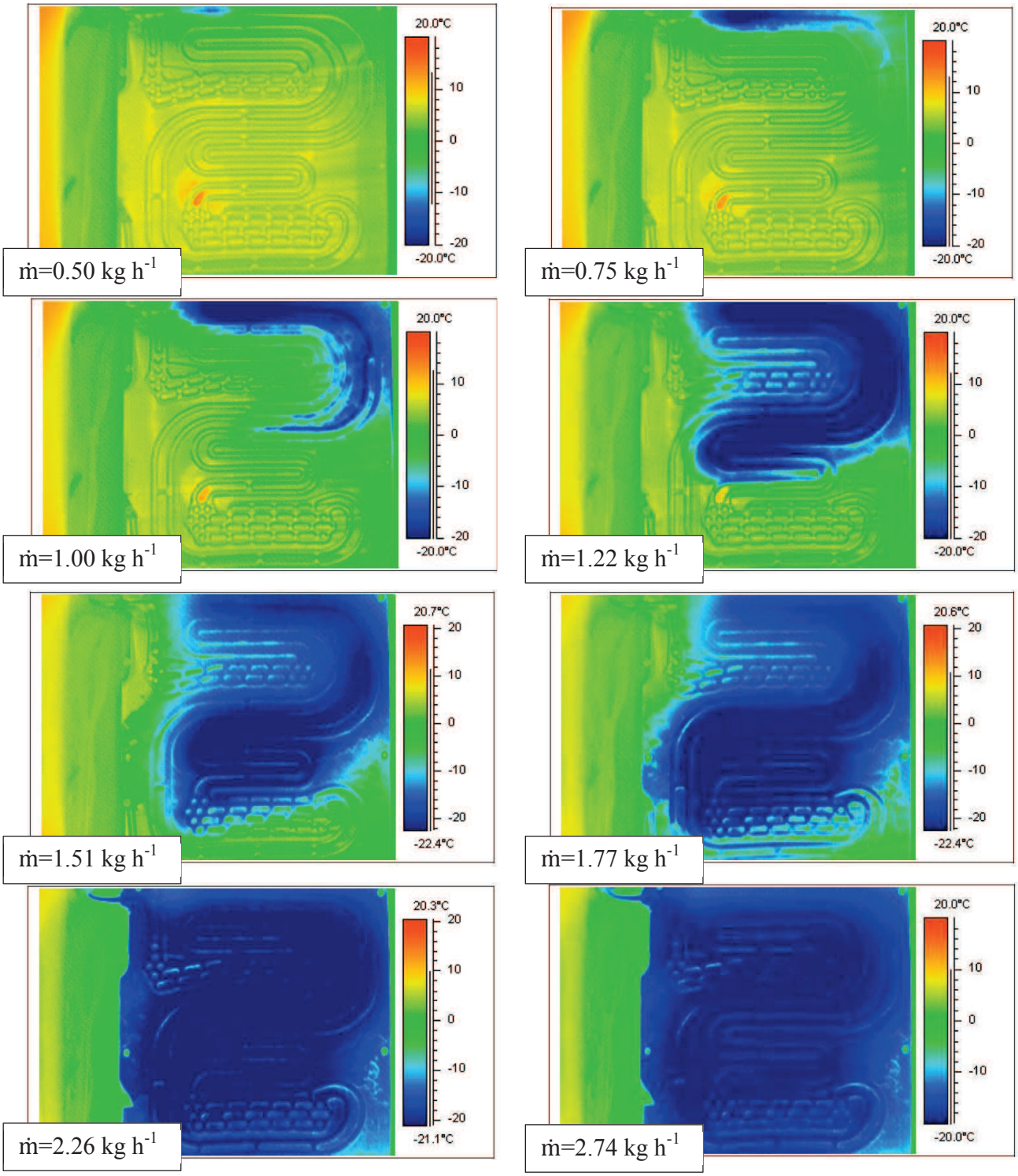

Figure 162 Roll-bond images collected by the thermal camera. Data with R134a at t_{evap}=-20 °C.

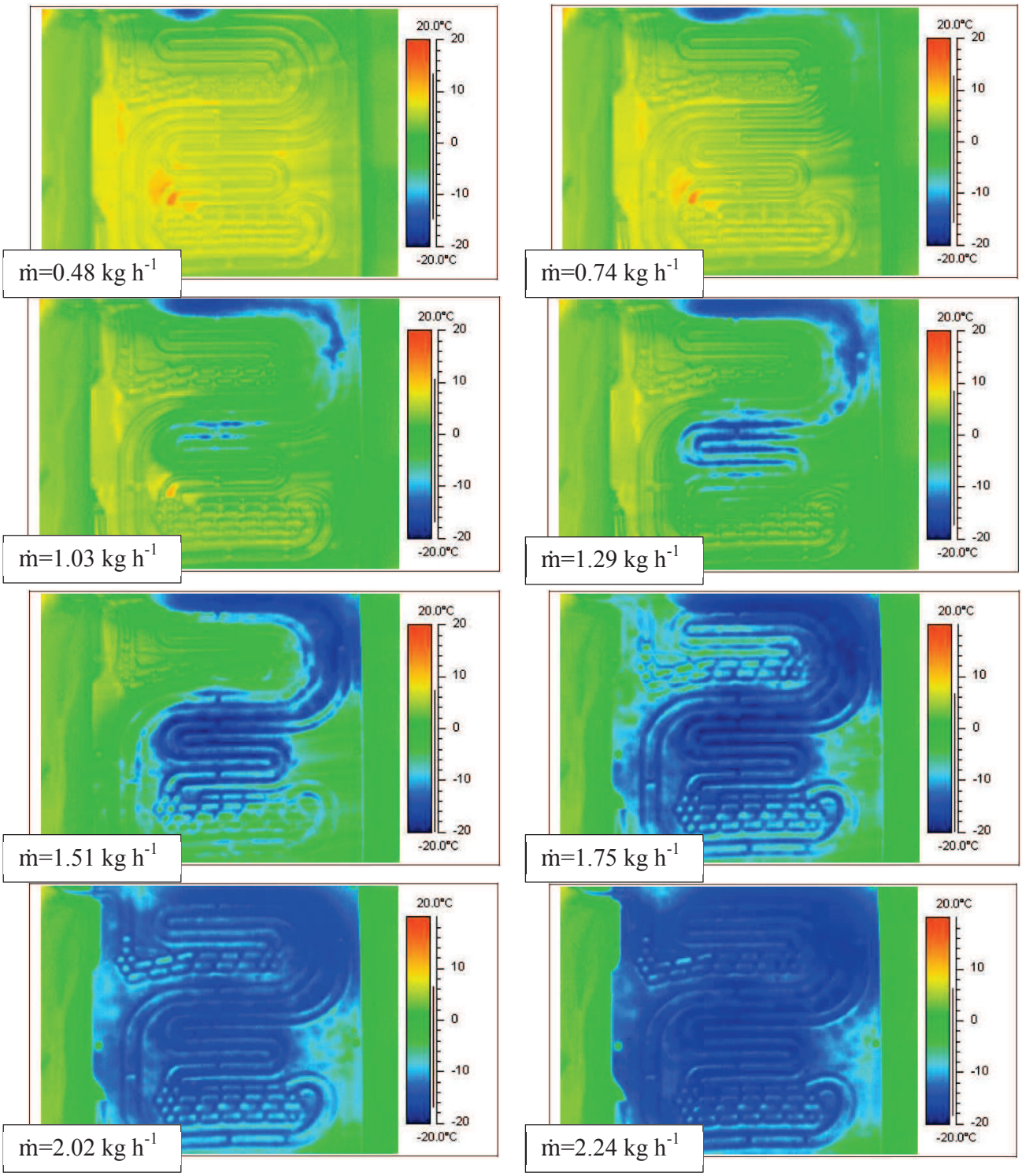

Figure 163 Roll-bond images collected by the thermal camera. Data with R1234ze(E) at t_{evap}=-15 °C.

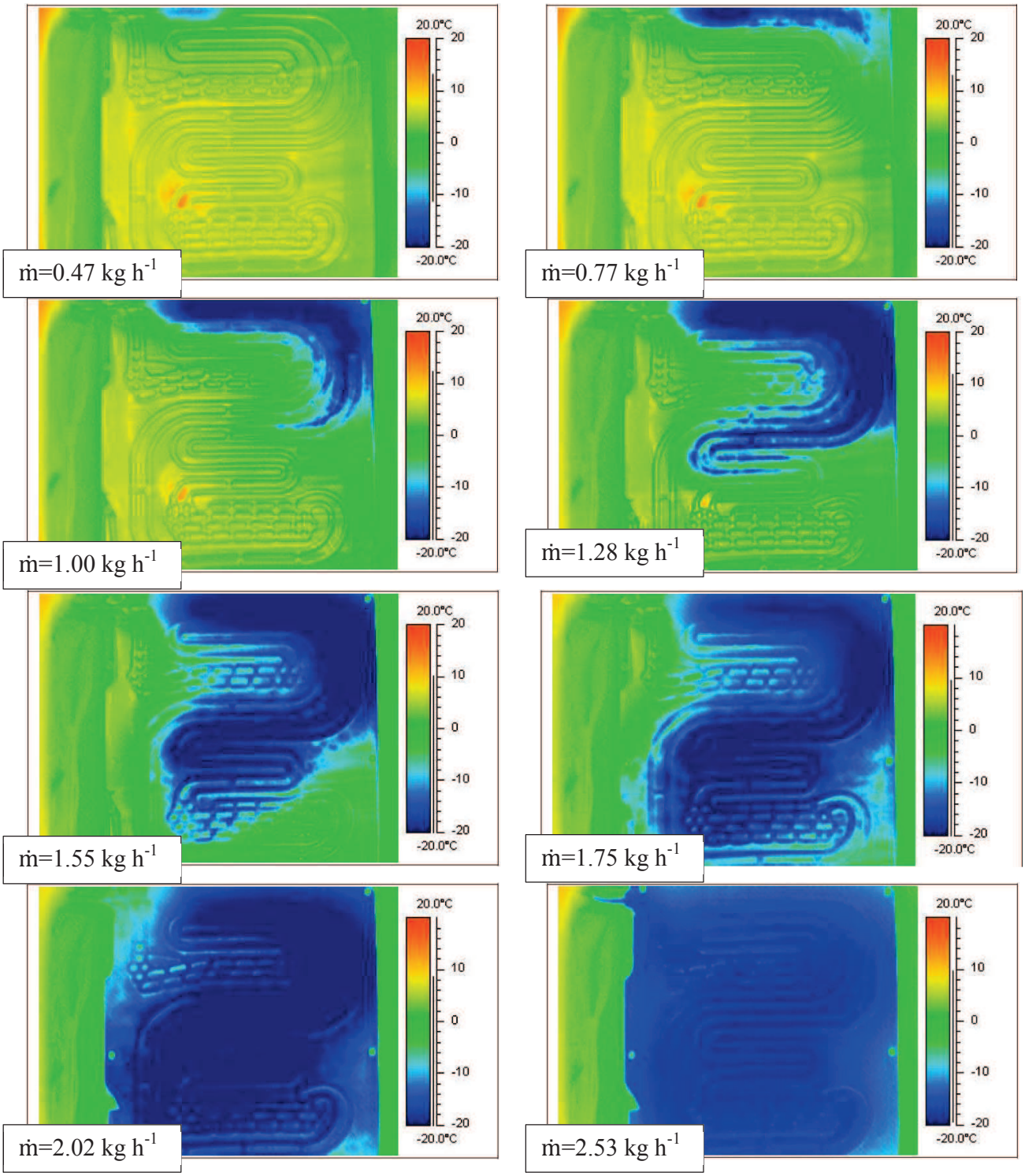

Figure 164 Roll-bond images collected by the thermal camera. Data with R1234ze(E) at t_{evap}=-20 °C.

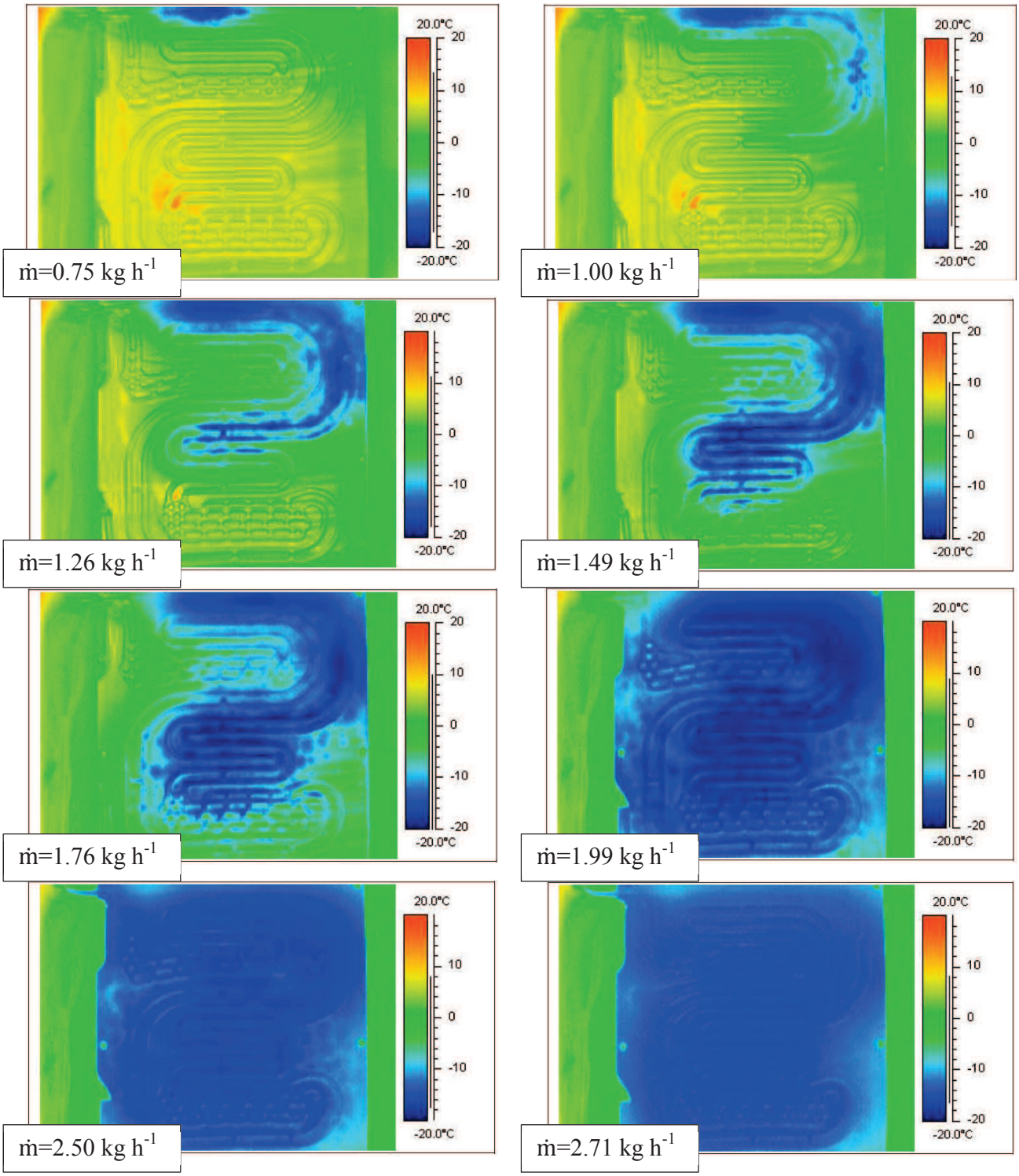

Figure 165 Roll-bond images collected by the thermal camera. Data with R1234yf at t_{evap}=-15 °C.

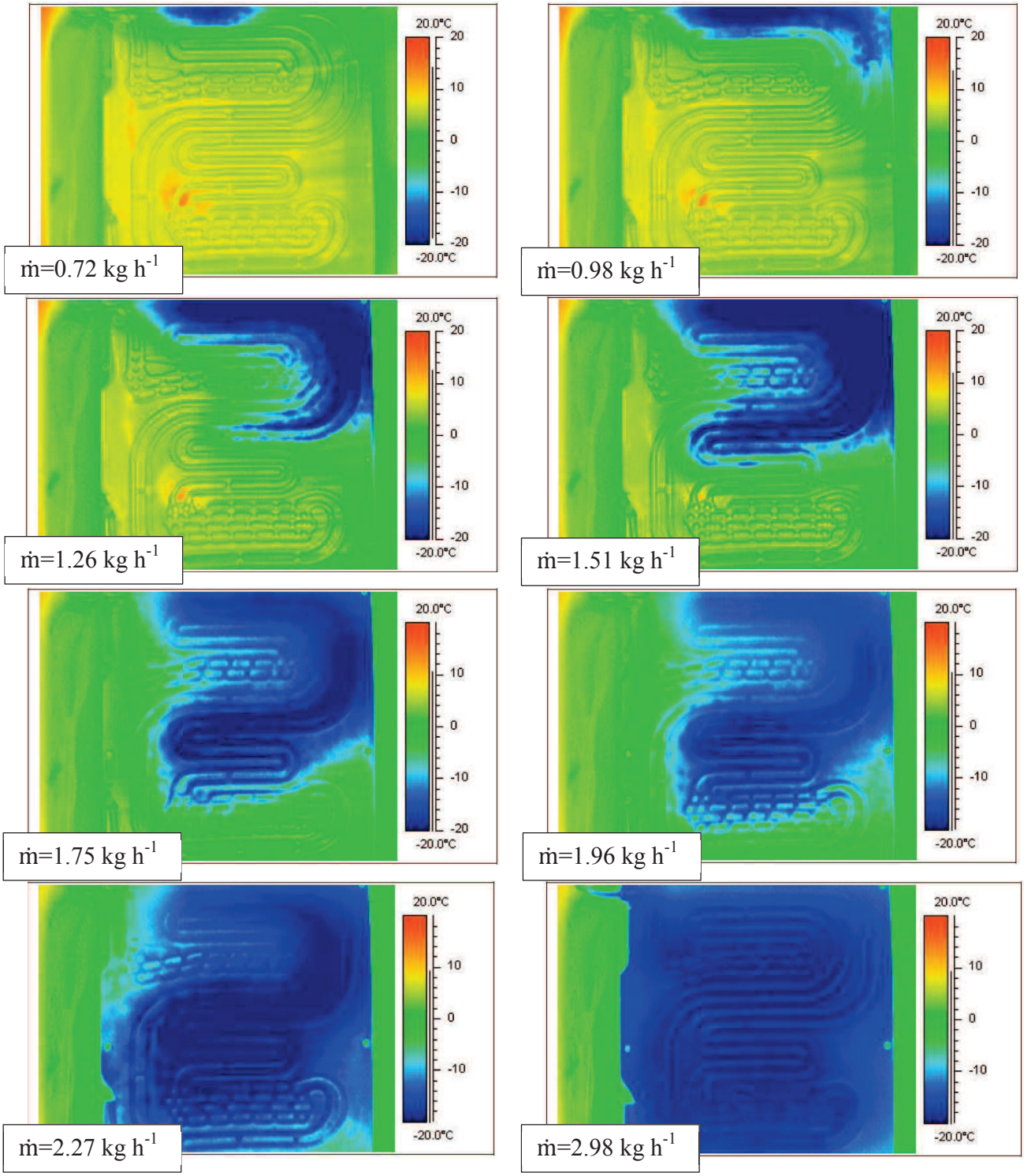

Figure 166 Roll-bond images collected by the thermal camera. Data with R1234yf at t_{evap}=-20 °C.

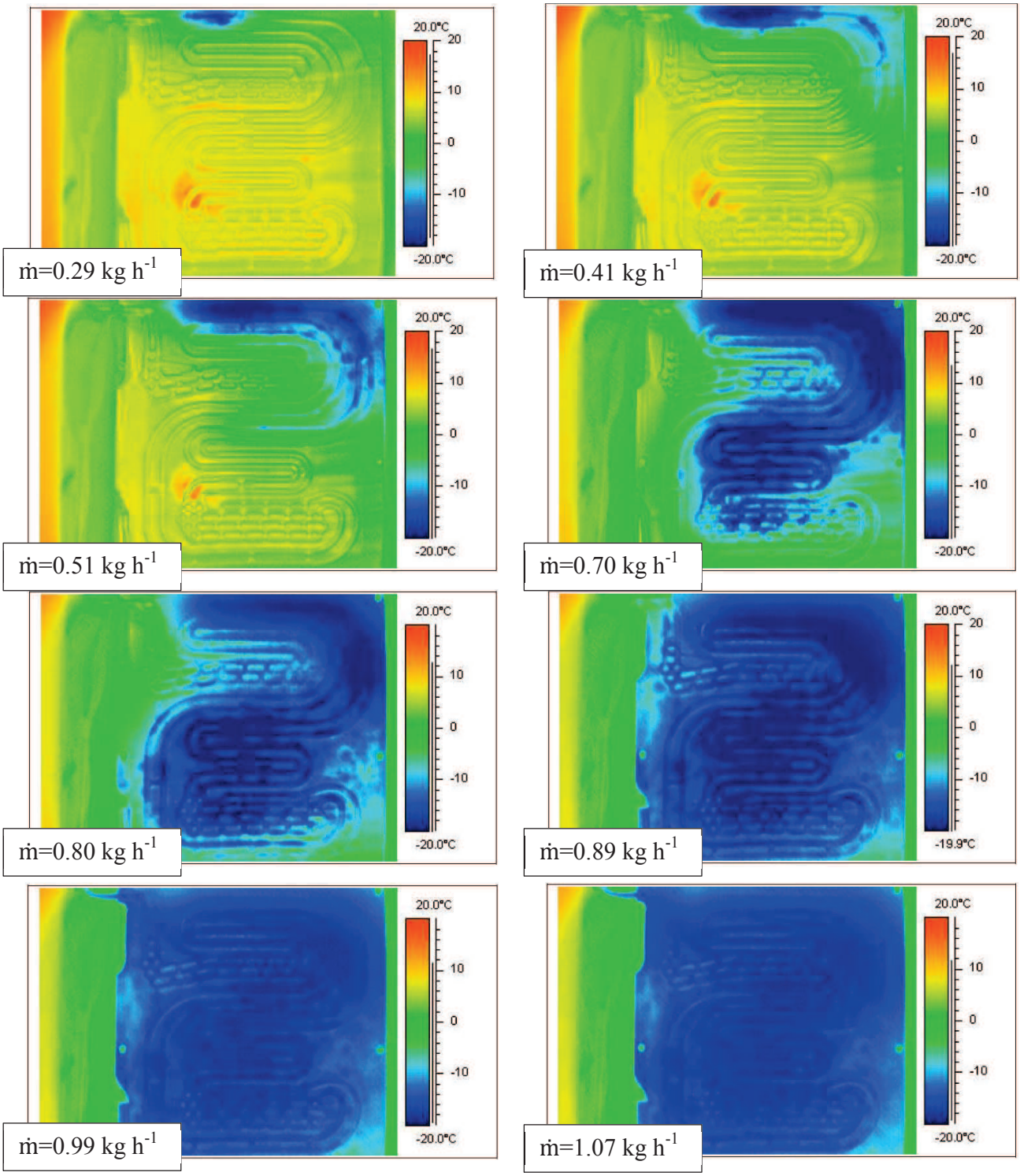

Figure 167 Roll-bond images collected by the thermal camera. Data with R600a at t_{evap}=-15 °C.

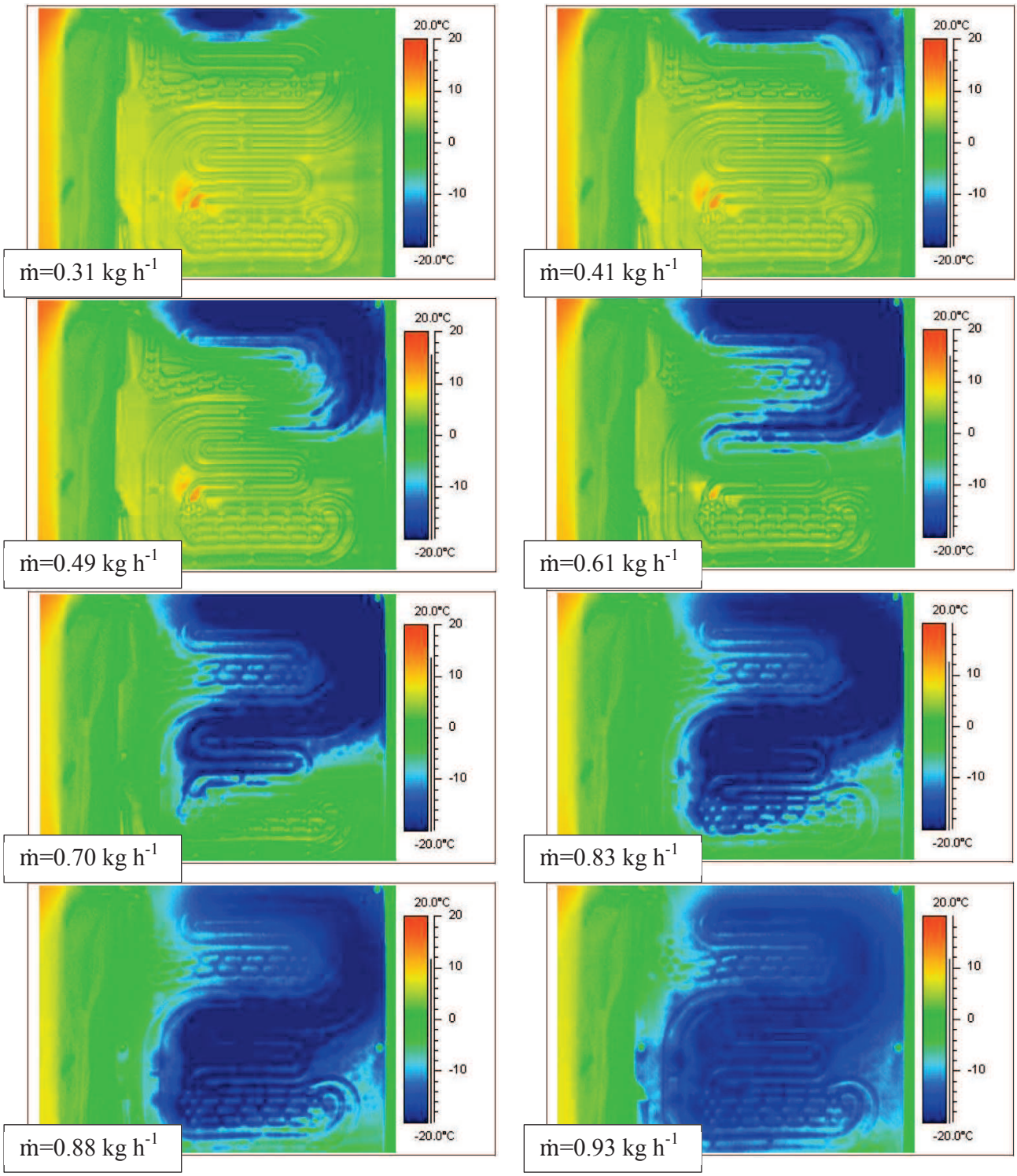

Figure 168 Roll-bond images collected by the thermal camera. Data with R600a at t_{evap}=-20 °C.

It is possible to observe that, when increasing the mass flow (i.e. the refrigerating capacity) the portion of the heat transfer surface working in vaporization (blue-light blue colors) increases with respect to that interested by vapor super-heating (yellow-green colors). When the maximum refrigerant flow rate is reached, the two phase vaporization process affects the whole heat transfer surface and the outlet vapor super-heating approaches zero (evaporator outlet tube in dark blue color). However, also at the maximum refrigerant mass flow rate, when the outlet vapor super-heating is less than 1 K, one can point out some areas having higher temperature than that of the rest of the roll-bond evaporator. So also at full load operation is possible to improve roll-bond efficiency, for example changing the circuitry layout or enhancing the aluminum millwork quality.

Furthermore, the infrared analysis is useful for the identification of the super-heated portions of the roll-bond evaporator. Figures from Figure 169 to Figure 173 report the vapor super-heating area as a function of the refrigerant mass flow ratio at -15 °C and -20 °C of saturation temperature for R134a, R1234ze(E), R1234yf, R600a, and R600, respectively. The super heating area is defined as the portion of the roll-bond evaporator having a temperature more than 10 °C higher than the saturation one.

At high mass flow ratio (i.e. greater than 0.8) the super-heating area is almost zero, and so all the roll-bond works under two phase conditions.

There is no a unique relation valid for all the refrigerants between super-heating area and refrigerant mass flow rate as a function of the saturation temperature. In fact, with R134a and R1234ze(E) the super heating region is greater at higher mass flow rates, while with R1234yf and R600a the super heating region is lower at higher mass flow rates.

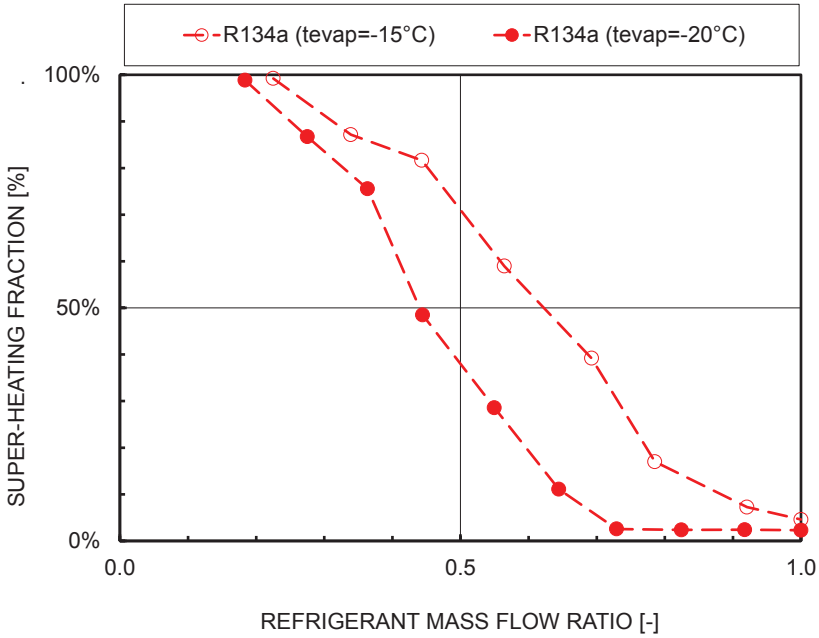

Figure 169 Percentual of super heating area of the plate vs. refrigerant mass flow ratio at -15 °C and -20 °C evaporating temperature with R134a.

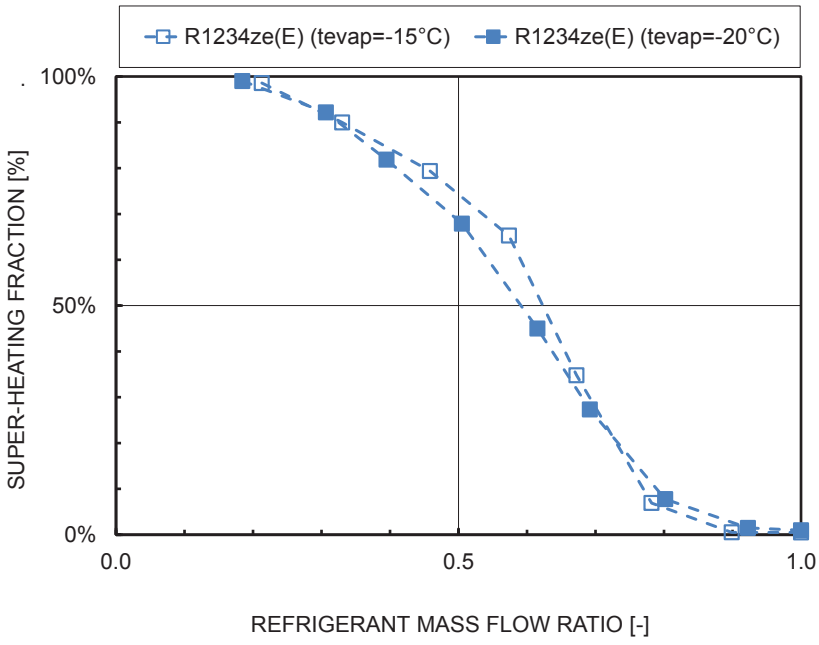

Figure 170 Percentual of super heating area of the plate vs. refrigerant mass flow ratio at -15 °C and -20 °C evaporating temperature with R234ze(E).

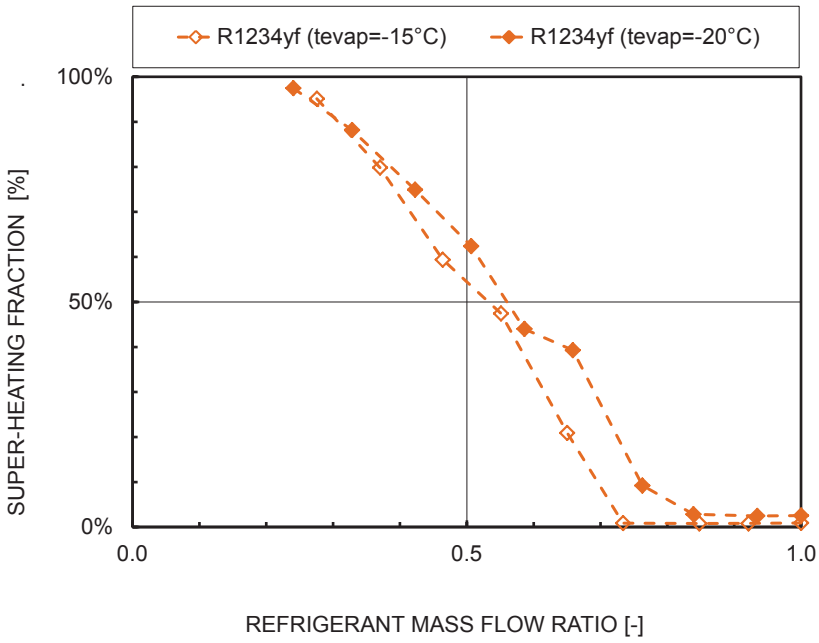

Figure 171 Percentual of super heating area of the plate vs. refrigerant mass flow ratio at -15 °C and -20 °C evaporating temperature with R1234yf.

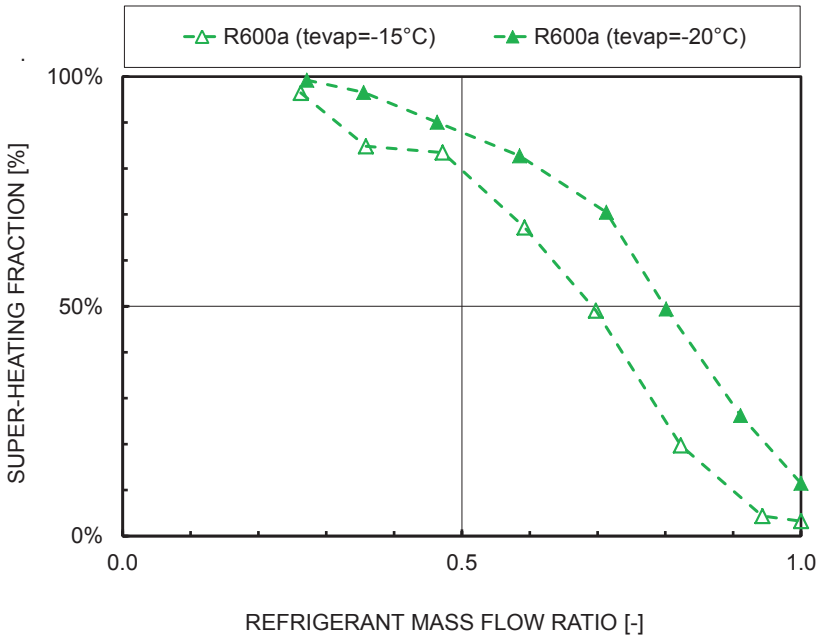

Figure 172 Percentual of super heating area of the plate vs. refrigerant mass flow ratio at -15 °C and -20 °C evaporating temperature with R600a.

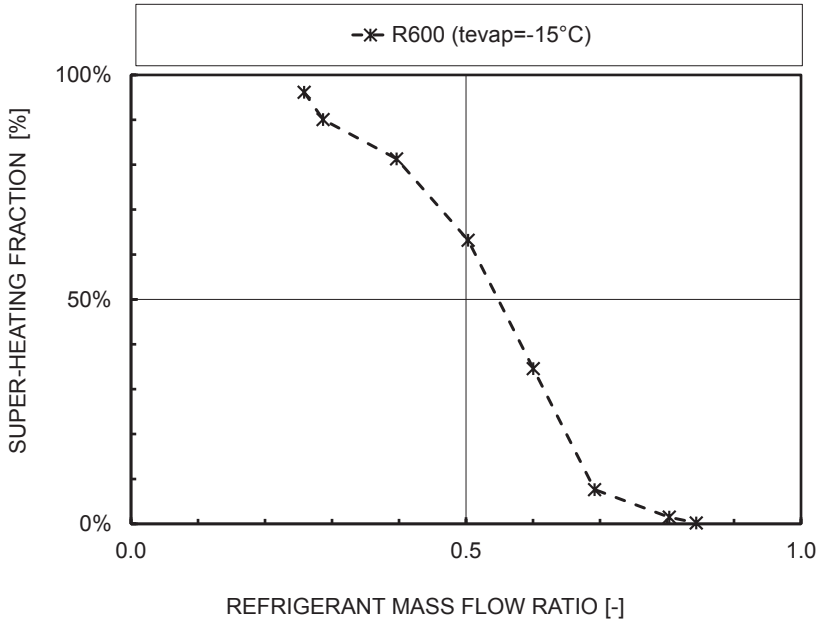

Figure 173 Percentual of super heating area of the plate vs. refrigerant mass flow ratio at -15 °C evaporating temperature with R600.

3.3.8 Comparison against literature correlations

It is not easy to find a unique correlation to model the whole roll-bond evaporator. In fact the real heat transfer area during the partial load functioning is not well defined and the liquid line moves along the plate under different test conditions. In addition the refrigerant flow rate is rather low and few two-phase correlations take into account this kind of operating conditions.

To remedy at the undefined heat transfer area issue, just the data with no superheating (refrigerant mass flow ratio greater than 0.8) were taken into account to be compared against literature correlations. For all these points the heat transfer area could be assumed equal to the whole plate area, as can be seen by Figure 169, Figure 170, Figure 171, Figure 172, and Figure 173 that present the superheating area fraction vs. the refrigerant mass flow ratio for R134a, R1234ze(E), R1234yf, R600a and R600, respectively, without introducing a high uncertainty.

thus, a few literature correlations were implemented and compared only for the two higher mass flow rate data points for each set of experimental tests. Among them: Chen (1966), Cooper (1984), Forster

and Zuber (1955), Zhang *et al.* (2004), Shah (1982), Steiner and Taborek (1992), and Wattelet *et al.* (1994).

Table 29 summarizes the mean deviation and the absolute mean deviation between experimental data and each correlation tested.

Table 29 Mean deviation between boiling literature correlations and vaporization inside a roll-bond evaporator experimental data.

Correlation	**Mean deviation** [%]
Chen (1966)	41.58
Cooper (1984)	19.24
Foster and Zuber (1955)	-73.69
Mishima and Hibiki (1996)	63.04
Shah (1982)	50.18
Steiner and Taborek (1992)	45.85
Wattelet *et al.* (1994)	-3.64
	Absolute mean deviation [%]
Chen (1966)	66.63
Cooper (1984)	40.21
Foster and Zuber (1955)	124.99
Mishima and Hibiki (1996)	65.48
Shah (1982)	59.85
Steiner and Taborek (1992)	54.08
Wattelet *et al.* (1994)	48.40

The Cooper (1984) correlation seems to be the one that works better in terms of absolute mean deviation. For this reason Figure 174 and Figure 175 show the refrigerant-side heat transfer coefficient vs. the refrigerant heat flux at -15 °C and -20 °C of evaporation temperature respectively for all the refrigerant tested, reporting also the behavior of the Cooper (1984) correlation (Eq. 92) calculated at the specific evaporation temperature:

Eq. 92

$$\alpha_r = 55 p^{*(0.12-0.2 log_{10} R_p)} (-log_{10} p^*)^{-0.55} q^{0.67} MOL^{-0.5}$$

where $p^*=p/p_{cr}$ is the reduced pressure, R_p the roughness as defined in German standard DIN 4762/1, q is the heat flux and MOL the molecular weight of the refrigerant.

The Cooper (1984) correlation reproduces the full load data points (refrigerant mass flow ratio>0.8) with a relative deviation of 15% for R134a, 3% for R1234yf, 4% for R1234ze(E), 35% for R600a, and 33% for R600 but the trend is consistent with the experimental data taken into account. Therefore, when the vapor super-heating at the outlet of the roll-bond evaporator approaches zero and two-phase heat transfer affects the whole heat transfer area, the dominant heat transfer regime on the refrigerant-side probably is the nucleate boiling.

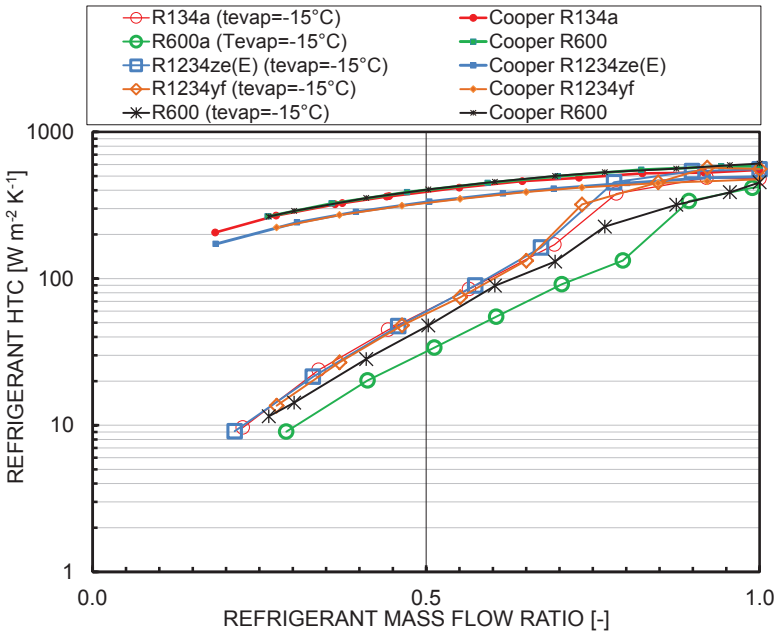

Figure 174 Refrigerant side heat transfer coefficient vs. the refrigerant heat flux at -15 °C of saturation temperature.

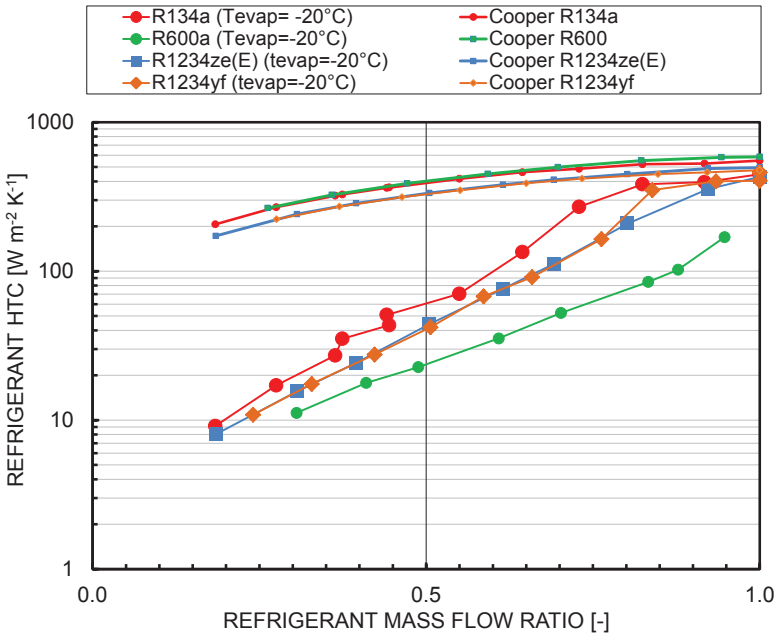

Figure 175 Refrigerant side heat transfer coefficient vs. the refrigerant heat flux at -20 °C of saturation temperature.

3.4 Heat pipe finned heat exchanger

3.4.1 Experimental results

Three different refrigerants were tested as two-phase fluid within the pipes of the same HPFHE: R134a which is nowadays a common refrigerant used in this kind of applications, R1234ze(E) a new low GWP fluid propose to directly replace the R134a, and R152a which shows very promising thermophysical properties for heat pipe applications.

For each refrigerant, four different sets of experimental tests were realized. The first two sets were conducted to simulate Mediterranean summer conditions where the exhaust air temperature is around 25 °C as it would come from an air conditioned environment, while the supply air temperature could reach 40 °C. For this reason, the first set consists of 13 runs in which the exhaust inlet air temperature was set at 25 °C ±0.1 °C with a relative humidity around 55%, and the supply inlet air temperature was kept at 35 °C ±0.1 °C with a relative humidity around 30%. The second set consists of 13 runs in which the exhaust inlet air temperature was maintained 25 °C ±0.1 °C with the same relative humidity around 55%, whereas the supply inlet air temperature was fixed at 40 °C ±0.1 °C with a relative humidity around 26%. The third and the fourth sets of data aimed at investigating the conditions of a Mediterranean winter season (i.e. an exhaust air temperature around 20 °C and a supply air temperature above 0 °C). The third set is composed by 13 data points where the exhaust temperature was fixed at 20 °C ±0.1 °C with a relative humidity approximately around 60%, and the supply air inlet temperature equal to 10 °C ± 0.1 °C with a humidity around 80%. Finally, the fourth set consists of 13 data points where the exhaust air temperature was maintained at 20 °C ±0.1 °C and the inlet temperature was set at 7 °C ± 0.1 °C with a relative humidity around 90%.

The volumetric air flow rate was varied in the range 430÷1000 m^3 h^{-1}. For both the winter and the summer conditions, part of the data was collected with the same flow rate on the exhaust and the supply air lines (C_{min}/C_{max}=1), while the other part was performed to analyze those conditions where the exhaust air flow rate is higher than the supply one. The latter refers to the case when part of the exhaust air flow is recirculated in the air conditioned ambient. For these runs, the C_{min}/C_{max} ratios equal to 0.9, 0.8, 0.7, 0.6, and 0.5 were analyzed.

Table 30, Table 31, and Table 32 report a brief summary on the entire experimental campaign conducted with R134a, R1234ze(E), and R152a respectively. The maximum and the minimum heat fluxes exchanged during each set of tests are highlighted.

Table 30 Summary of the experimental tests run with R134a in a finned heat pipe heat exchanger recuperator.

Set	**Mode**	**Runs**	**$T_{exh,in}$** [°C]	**$T_{supply,in}$** [°C]	**Q** [W]
1	Summer	13	25	35	998-565
2	Summer	13	25	40	1616-902
3	Winter	13	20	10	976-592
4	Winter	13	20	7	1140-772

Table 31 Summary of the experimental tests run with R1234ze(E) in a finned heat pipe heat exchanger recuperator.

Set	**Mode**	**Runs**	**$T_{exh,in}$** [°C]	**$T_{supply,in}$** [°C]	**Q** [W]
1	Summer	13	25	35	1011-613
2	Summer	13	25	40	1677-953
3	Winter	13	20	10	943-616
4	Winter	13	20	7	1135-784

Table 32 Summary of the experimental tests run with R152a in a finned heat pipe heat exchanger recuperator.

Set	**Mode**	**Runs**	**$T_{exh,in}$** [°C]	**$T_{supply,in}$** [°C]	**Q** [W]
1	Summer	13	25	35	1110-656
2	Summer	13	25	40	1666-982
3	Winter	13	20	10	1071-630
4	Winter	13	20	7	1403-855

3.4.1.1 Heat flow rate

The following graphs (from Figure 176 to Figure 181) represent the heat flow rate as a function of the air flow rate for the summer and the winter seasons respectively, obtained with the three different refrigerants tested. (Figure 176 and Figure 177 for R134a, Figure 178 and Figure 179 for R1234ze(E), and Figure 180 and Figure 181 for R152a).

As expected, the heat flow rate linearly increases with the air flow rate, calculate as the average value between the supply and the exhaust lines, and the temperature difference between the two air lines.

The maximum air flow rate was fixed at 1000 m^3 h^{-1} and the maximum heat flow rate achievable was 1616 W with R134a, 1667 W with R1234ze(E), and 1666 W with R152a (more data points are reported in Table 30, Table 31, and Table 32).

3.4.1.1.1.1 R134a

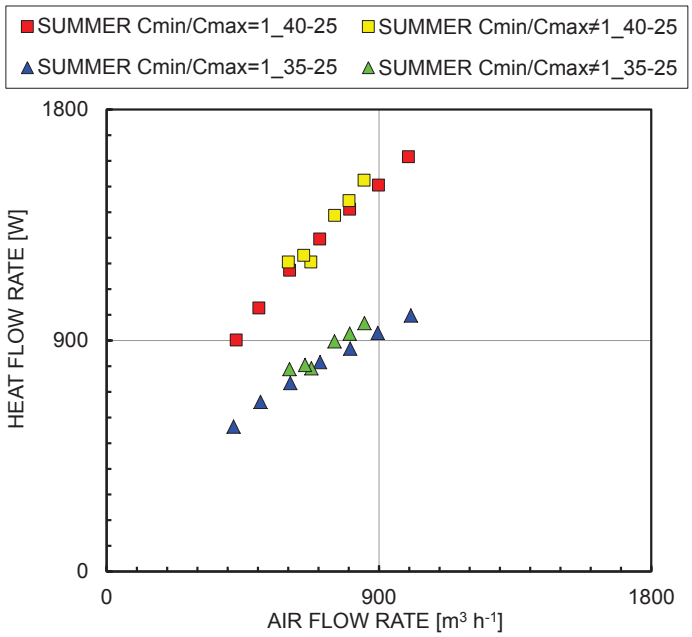

Figure 176 Heat flow rate vs. air flow rate during summer season tests with R134a.

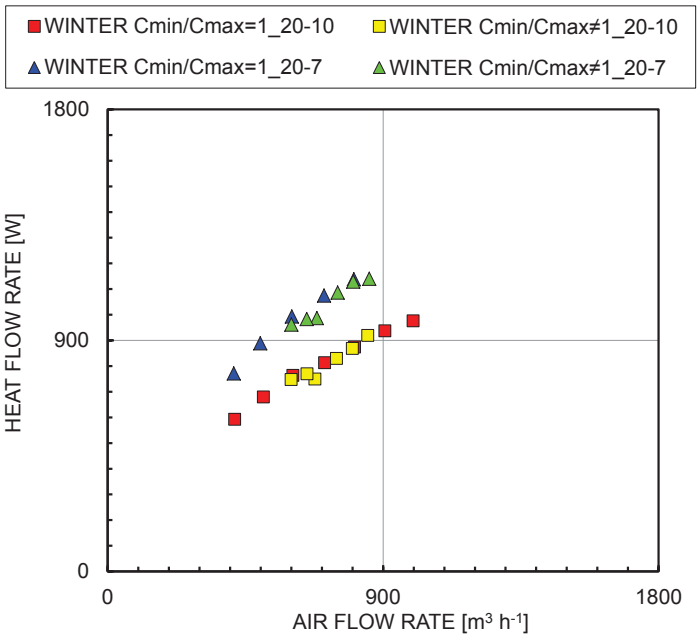

Figure 177 Heat flow rate vs. air flow rate during winter season tests with R134a.

3.4.1.1.1.2 R1234ze(E)

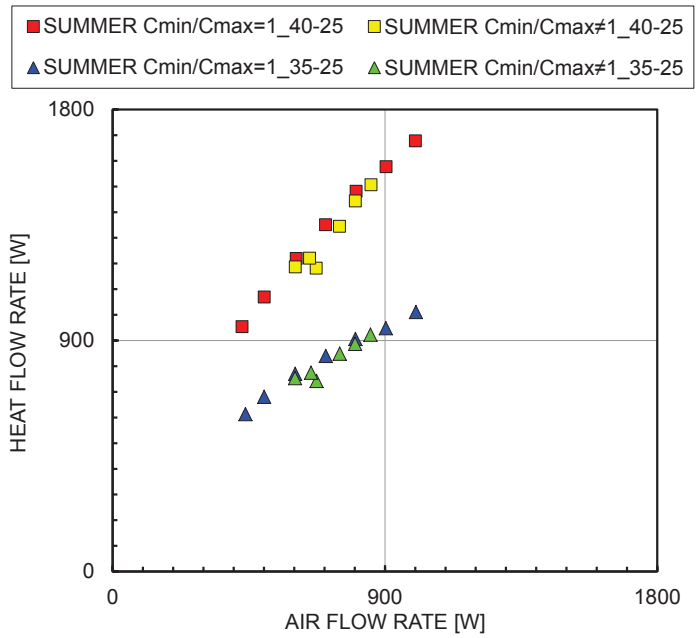

Figure 178 Heat flow rate vs. air flow rate during summer season tests with R1234ze(E).

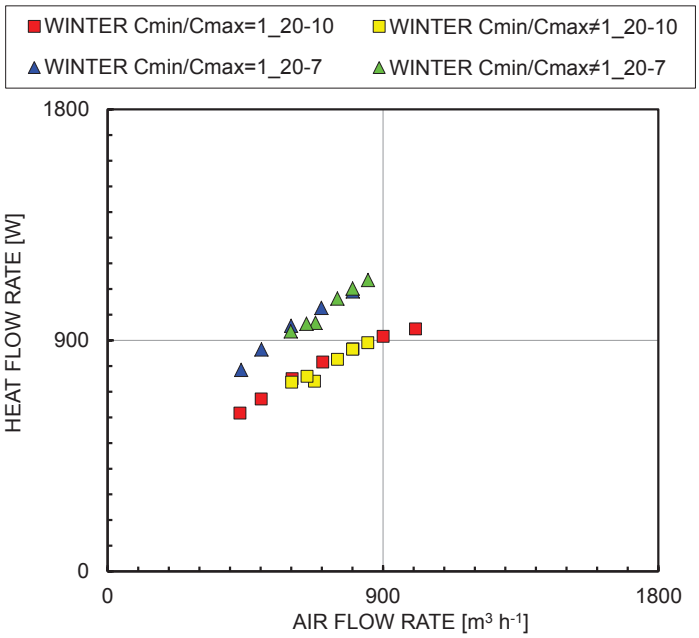

Figure 179 Heat flow rate vs. air flow rate during winter season tests with R1234ze(E).

3.4.1.1.1.3 R152a

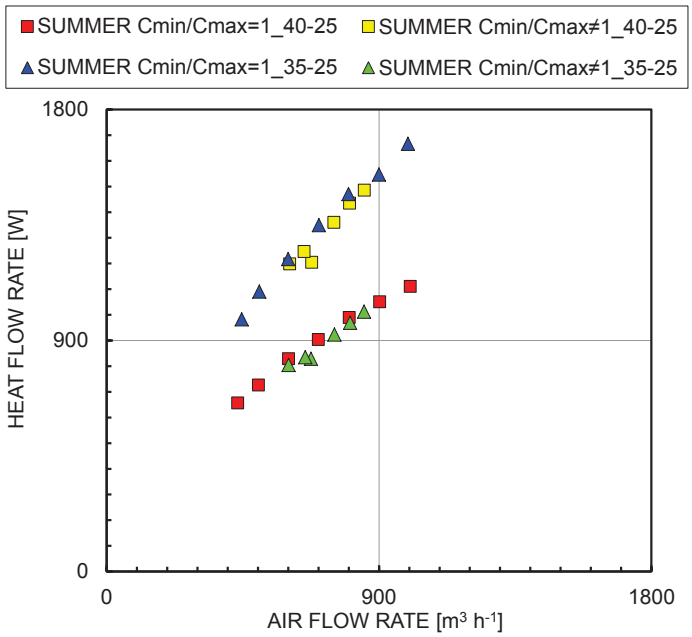

Figure 180 Heat flow rate vs. air flow rate during summer season tests with R152a.

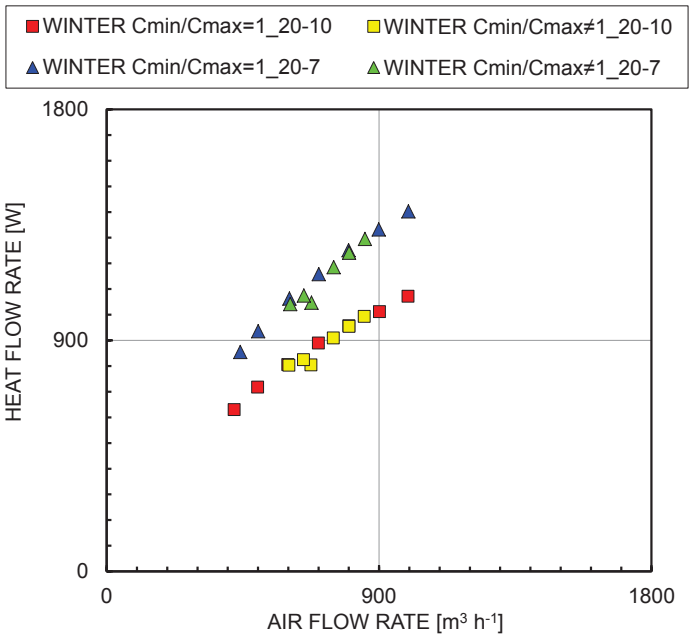

Figure 181 Heat flow rate vs. air flow rate during winter season tests with R152a.

3.4.1.2 Thermal effectiveness vs. number of transfer units

Figure 183 to Figure 187 plot the experimental thermal effectiveness against the Number of Transfer Units (NTU).

For each fluid tested the data have been sorted as a function of the heat capacity rates ratio that varies from 1 to 0.5.

Figure 183, Figure 185, and Figure 187 are relative to R134a, R1234ze(E), and R152a, respectively. Each of them presents 6 graphs in which the experimental thermal effectiveness vs. Number of Transfer Units (NTU) data for a single capacity rate ratio (C_{min}/C_{max}=1, C_{min}/C_{max}=0.9, C_{min}/C_{max}=0.8, C_{min}/C_{max}=0.7, C_{min}/C_{max}=0.6, and C_{min}/C_{max}=0.5, respectively) are shown. In addition, the theoretical values for a counter-flow heat exchanger having the same heat capacity rate ratio (C_{min}/C_{max}) are also reported.

Figure 182, Figure 184, and Figure 186 group together all the experimental data collected with R134a, R1234ze(E), and R152a, respectively plotted as thermal effectiveness against Number of Transfer Units (NTU). The theoretical trends for the maximum (C_{min}/C_{max}=1) and the minimum (C_{min}/C_{max}=0.5) capacity rate ratio are also reported.

In all the figures presented (from Figure 183 to Figure 187) the experimental data are consistent with the theoretical trends, confirming that a fin and coil with more than 4 rows of tubes is equivalent to a counter-flow heat exchanger (Kays and London; 1984).

The thermal effectiveness for this kind of devices is rather high, the average value during all the working condition tested is 0.40, 0.41 and 0.42 for R134a, R1234ze(E), and R152a, respectively. The maximum effectiveness, reached at C_{min}/C_{max}=1 and at the maximum air flow rate is equal to 0.52, 0.53 and 0.54 for R134a, R1234ze(E), and R152a, respectively.

3.4.1.2.1 R134a

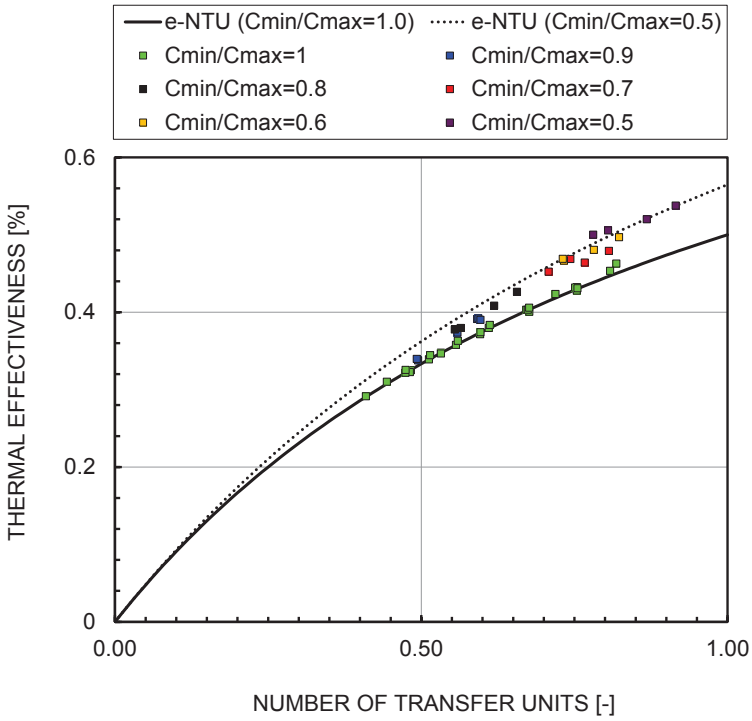

Figure 182 Thermal effectivness vs. Number of Transfer Units (NTU) of all the R134a data points. The lines represent the theoretical trends for C_{min}/C_{max}=1 and C_{min}/C_{max}=0.5.

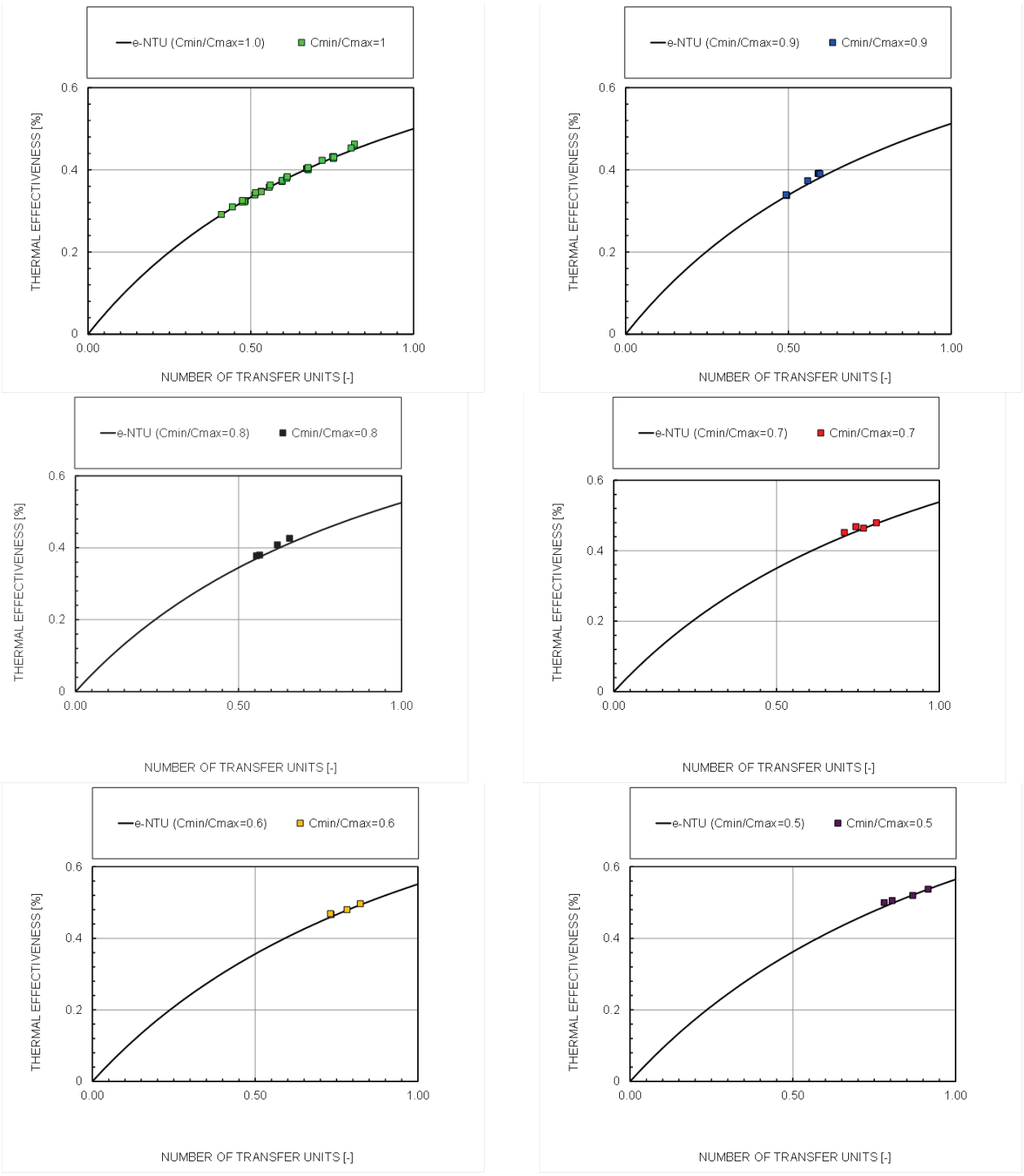

Figure 183 Thermal effectivness vs. Number of Transfer Units (NTU) of R134a data points having C_{min}/C_{max}=1, C_{min}/C_{max}=0.9, C_{min}/C_{max}=0.8, C_{min}/C_{max}=0.7, C_{min}/C_{max}=0.6, and C_{min}/C_{max}=0.5.

3.4.1.2.2 R1234ze(E)

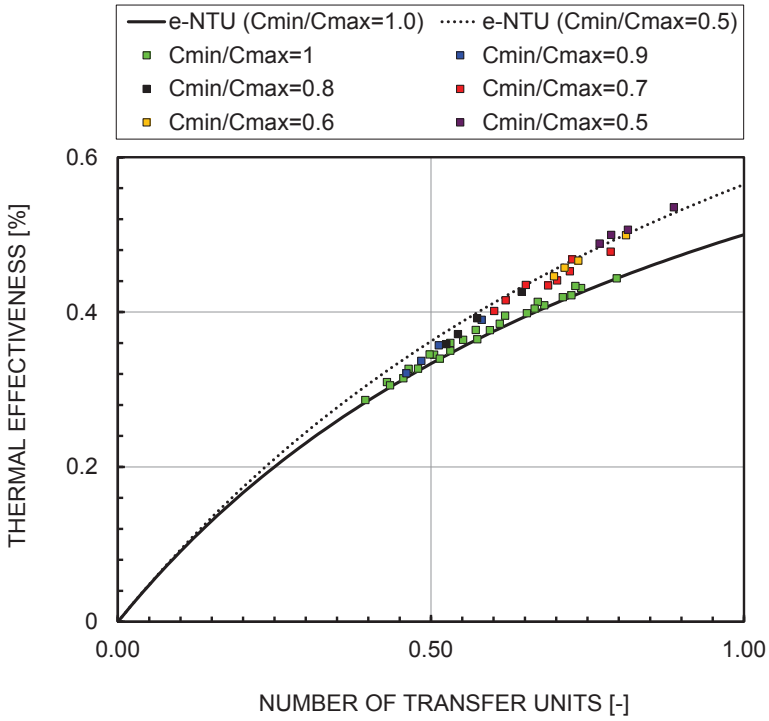

Figure 184 Thermal effectivness vs. Number of Transfer Units (NTU) of all the R1234ze(E) data points. The lines represent the theoretical trends for C_{min}/C_{max}=1 and C_{min}/C_{max}=0.5.

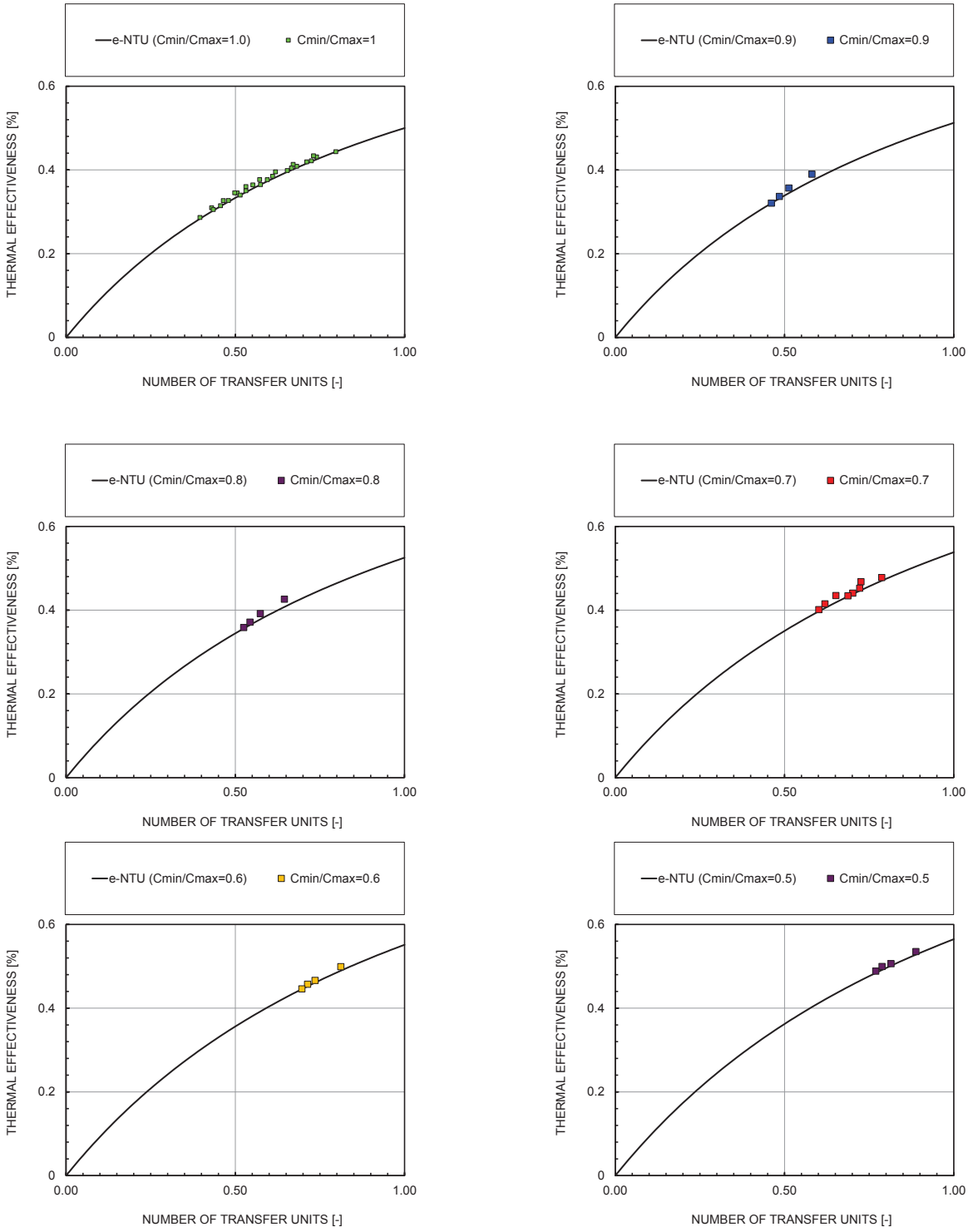

Figure 185 Thermal effectivness vs. Number of Transfer Units (NTU) of R1234ze(E) data points having C_{min}/C_{max}=1, C_{min}/C_{max}=0.9, C_{min}/C_{max}=0.8, C_{min}/C_{max}=0.7, C_{min}/C_{max}=0.6, and C_{min}/C_{max}=0.5.

3.4.1.2.3 R152a

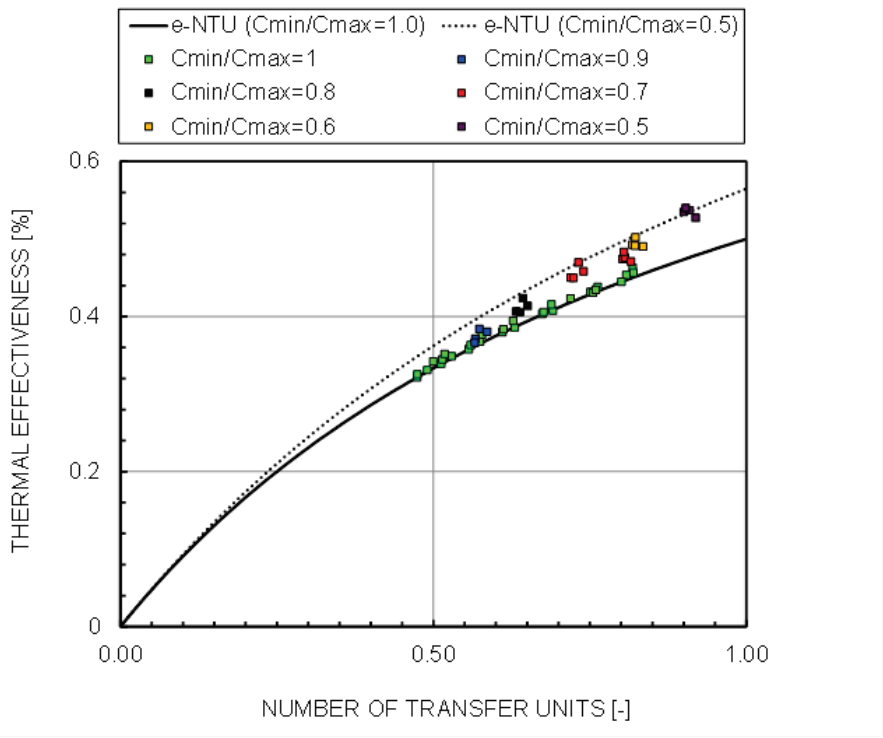

Figure 186 Thermal effectivness vs. Number of Transfer Units (NTU) of all the R152a data points. The lines represent the theoretical trends for C_{min}/C_{max}=1 and C_{min}/C_{max}=0.5.

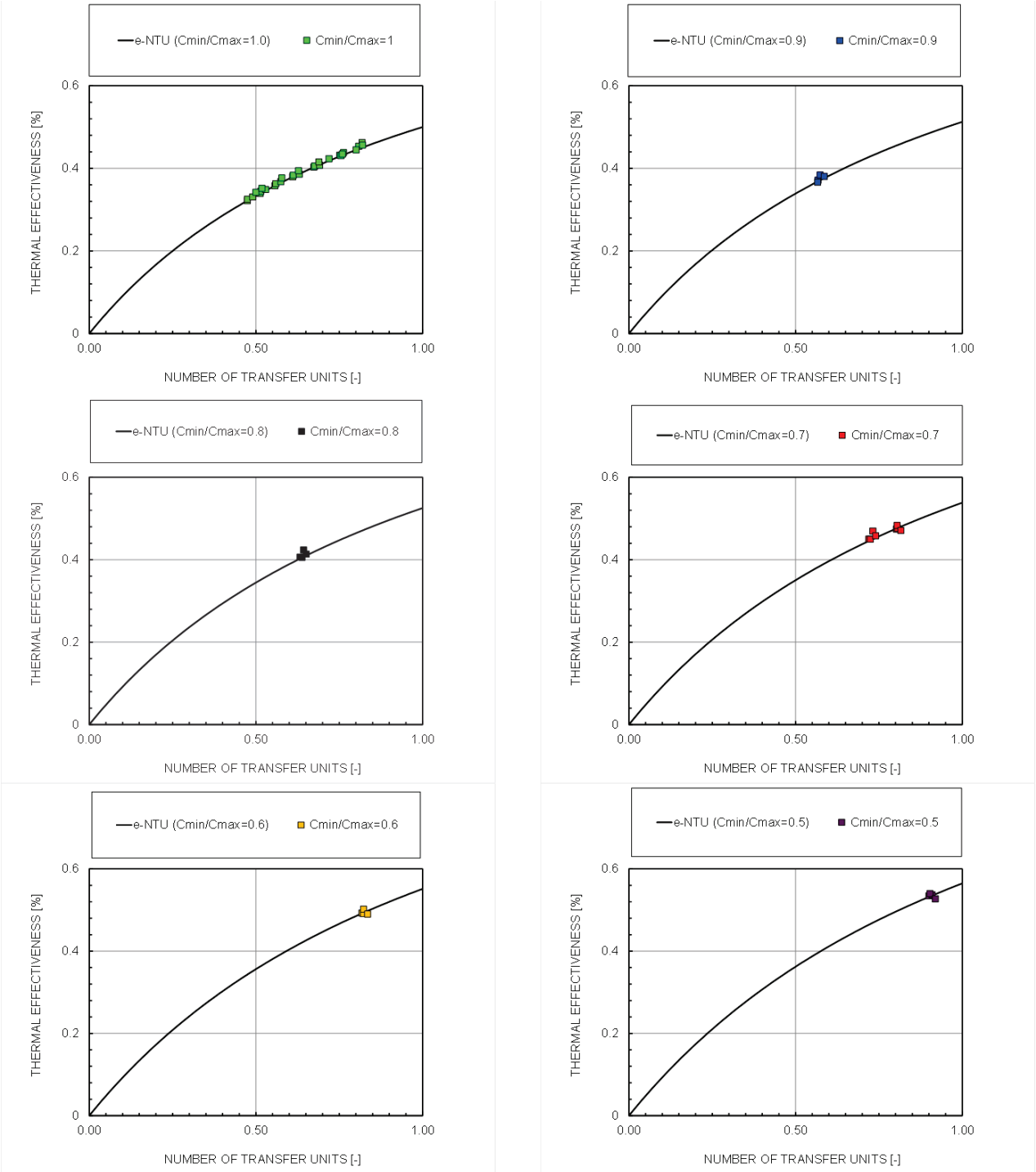

Figure 187 Thermal effectivness vs. Number of Transfer Units (NTU) of R152a data points having C_{min}/C_{max}=1, C_{min}/C_{max}=0.9, C_{min}/C_{max}=0.8, C_{min}/C_{max}=0.7, C_{min}/C_{max}=0.6, and C_{min}/C_{max}=0.5.

3.4.1.3 Air pressure drop

Figure 188 shows the experimental Fanning friction factor vs. the Reynolds number together with the trends predicted by the Wang *et al.* (2000) model when R134a is the heat pipe working fluid. The data points with a Reynolds number from 700 to 1700 are well predicted by the Wang *et al.* (2000) model and probably refer to turbulent flow, whereas the data points with a Reynolds number lower than 700. Similar results were also found for the other refrigerants sice the air pressure drops do not depend on the selected working fluid.

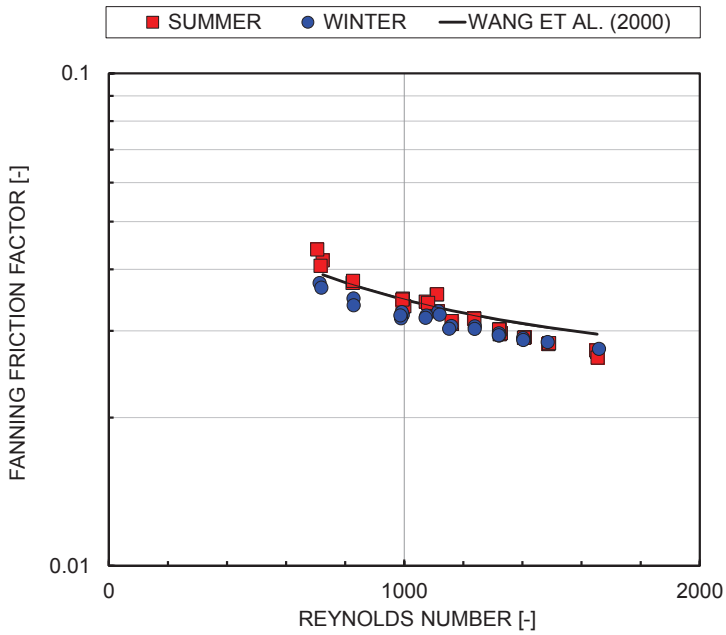

Figure 188 Fanning friction factor vs. Reynolds number during summer and winter tests with R134a. The black line rapresents the Wang *et al.* (2000) correlation.

3.4.2 Comparison against a new computational procedure

The heat transfer data experimentally collected and previously presented were compared against a new computational procedure.

This new procedure was developed to predict the data collected with R134a and R1234ze(E) as working fluid. Secondly, it was used to compare the experimental data with R152a as two-phase fluid in the pipes.

In this computational procedure the heat exchangers is divided into a series of ranks.

Some existing correlations, presented in Table 33, were evaluated inside the new computational procedure to estimate the condensation and the vaporization heat transfer coefficient of the refrigerant inside the tube and the heat transfer coefficient of the air. The mean deviation obtained with each group of models between the calculated results and the heat flux experimentally measured are listed in Table 33.

The correlation proposed by Gray and Webb (1986) and by Wang *et al.* (2000) have been tested for the air side, the correlations by Chen *et al.* (1984), Cohen and Bayley (from Japkise, 1973), Imura *et al.* (1979) and Shiraishi *et al.* (1981) for the evaporating region, and Nusselt (1916), Gross (1992), Wang and Ma (1987) and Bezrodnyi and Moklyak (1987) for the condensation region.

The group of correlations that better fits the experimental data is the one composed by the correlations of Gray and Webb (1986), Imura *et al.* (1979), and Nusselt (1916).

Table 33 Mean deviation between calculated and experimental heat flow rate values with R134a and R1234ze(E) as two phase fluid in the pipes.

Air side	**Refrigerant side (evaporation + condensation)**	**mean deviation**
Gray and Webb (1986)	Chen *et al.* (1984)+ Nusselt (1916)	-1.38
	Chen *et al.* (1984) + Gross (1992)	-5.17
	Chen *et al.* (1984) + Wang and Ma (1987)	4.51
	Chen *et al.* (1984) + Bezrodnyi and Moklyak (1987)	6.18
	Cohen and Bayley (1973) + Nusselt (1916)	-1.99
	Cohen and Bayley (1973) + Gross (1992)	-4.74
	Cohen and Bayley (1973) + Wang and Ma (1987)	4.9
	Cohen and Bayley (1973) + Bezrodnyi and Moklyak (1987)	6.5
	Imura *et al.* (1979) + Nusselt (1916)	**-0.97**
	Imura *et al.* (1979) + Gross (1992)	-4.67
	Imura *et al.* (1979) + Wang and Ma (1987)	4.82
	Imura *et al.* (1979) + Bezrodnyi and Moklyak (1987)	6.52
	Shiraishi *et al.* (1981) + Nusselt (1916)	1.43
	Shiraishi *et al.* (1981) + Gross (1992)	-1.83
	Shiraishi *et al.* (1981) + Wang and Ma (1987)	7.02
	Shiraishi *et al.* (1981) + Bezrodnyi and Moklyak (1987)	8.76
Wang *et al.* (2000)	Chen *et al.* (1984) + Nusselt (1916)	5.67
	Chen *et al.* (1984) + Gross (1992)	2.45
	Chen *et al.* (1984) + Wang and Ma (1987)	10.66
	Chen *et al.* (1984) + Bezrodnyi and Moklyak (1987)	12.64
	Cohen and Bayley (1973) + Nusselt (1916)	5.94
	Cohen and Bayley (1973) + Gross (1992)	3.62
	Cohen and Bayley (1973) + Wang and Ma (1987)	10.92

Wang *et al.* (2000)	Cohen and Bayley (1973) + Bezrodnyi and Moklyak (1987)	12.88
	Imura *et al.* (1979)+ Nusselt (1916)	5.95
	Imura *et al.* (1979)+ Gross (1992)	2.85
	Imura *et al.* (1979)+ Wang and Ma (1987)	10.91
	Imura *et al.* (1979)+ Bezrodnyi and Moklyak (1987)	12.85
	Shiraishi *et al.* (1981) + Nusselt (1916)	8.15
	Shiraishi *et al.* (1981) + Gross (1992)	5.2
	Shiraishi *et al.* (1981) + Wang and Ma (1987)	12.71
	Shiraishi *et al.* (1981) + Bezrodnyi and Moklyak (1987)	14.73

Within the tested operating conditions, the refrigerant condensate film Reynolds number was found to be always lower than 100. Accordingly, the condensation heat transfer coefficient was calculated with reference to the classical Nusselt theory (1916) for laminar condensation in vertical tubes.

$$\alpha_C = 0.943 \left[\frac{\rho_L(\rho_L - \rho_G) g \Delta h_{LG}{}' \lambda^3}{\mu_l L_c (T_{sat} - T_w)}\right]^{1/4} \quad \text{Eq. 93}$$

$$\Delta h_{LG}{}' = \Delta h_{LG} + \frac{3}{8} c_p (T_{sat} - T_w) \quad \text{Eq. 94}$$

The constant was further incremented by 30% to keep into account the wavy contribution created by the tube fins (similar approach, with 20% increment was proposed by McAdams (1954), for smooth tubes). The actual heat transfer area was considered as reference (i.e. keeping into account the whole fins area and the base tube).

The heat transfer coefficient on the evaporation part was evaluated according to Imura *et al.* (1979) equation (Eq. 95).

$$\alpha_e = 0.32 \left[\frac{\lambda_L^{0.3} \rho_L^{0.65} c_p^{0.7} g^{0.2} q_e^{0.4}}{\rho_G^{0.25} \Delta h_{LG}^{0.4} \mu_G^{0.1}}\right] \left[\frac{p_{sat}}{p_{atm}}\right]^{0.3} \quad \text{Eq. 95}$$

This approach was used also by Noie (2005) to fit his data inside a thermosyphon. The actual heat transfer area (including fins) was considered for heat flow rate calculations.
The air-side heat transfer coefficients are assumed to be uniform and they are evaluated through the Gray and Webb (1986) correlation. The air side pressure drops are evaluated according to Wang *et al.* (2000) correlation. The models of Gray and Webb (1986) and of Wang *et al.* (2000) were chosen because they accurately predict the experimental data of finned coil heat exchangers having the same geometrical characteristics of the tested coil.

Air temperature, relative humidity, and flow rate at the inlet of the condenser and the evaporator sections are the input data. The actual geometry of the heat exchanger (including, among others, the tube diameter and length, fin spacing, thickness, length and height) is an input as well.
The simulation proceeds by iterating on the saturation pressure of the fluid inside the heat pipes; given the subdivision of the HPFHE in ranks, the heat flow rate is assumed to be the same in each heat pipe on the same rank. A further iteration is on the overall heat exchanger: it starts by giving a guess value for the cold air at the heat exchanger exit. Each single rank is then simulated starting form the first one on the hot air direction. The output values for the first rank is then the input for the second one, etc. The iteration ends when the saturation temperature inside each rank allows the calculated exit temperature of the coil air to suitably approximate the initial guess value.

Figure 189, Figure 190, and Figure 191 show the comparison between the experimental heat flow rate exchanged and the values calculated by the computational procedure described above for R134a, R1234ze(E), and R152a, respectively.

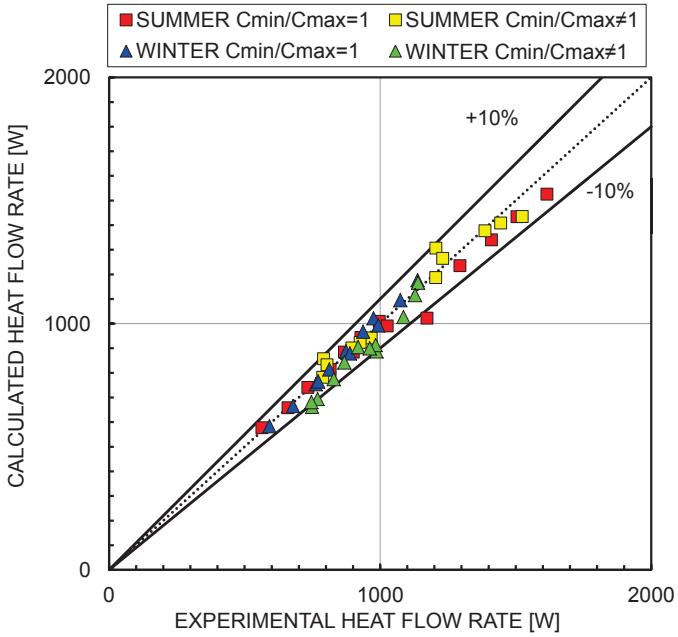

Figure 189 R134a calculated vs. experimental heat flow rate during both summer and winter season.

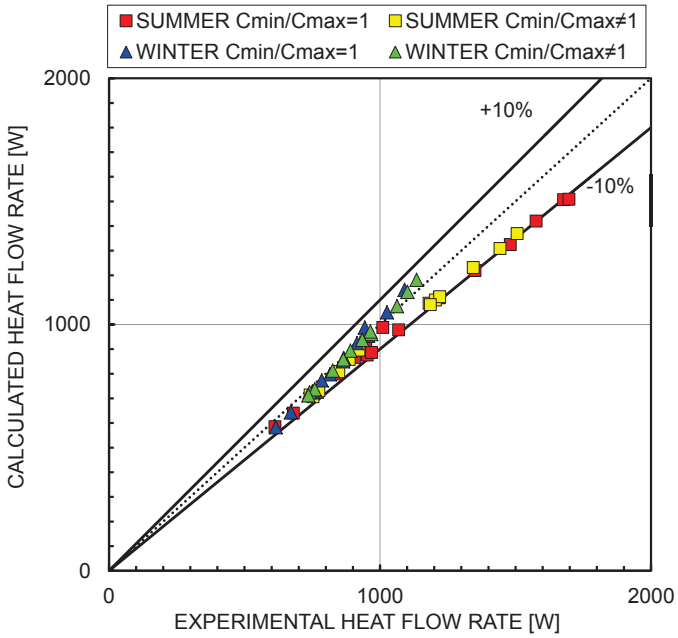

Figure 190 R1234ze(E) calculated vs. experimental heat flow rate during both summer and winter season.

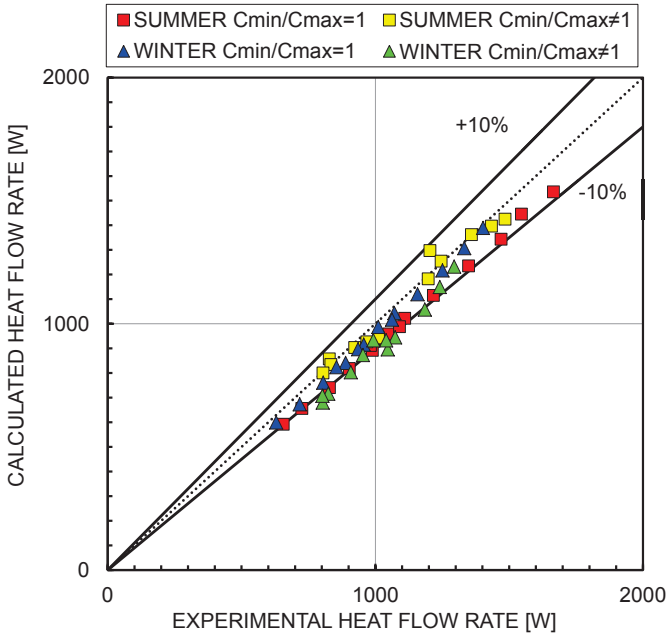

Figure 191 R152a calculated vs. experimental heat flow rate during both summer and winter season.

The mean absolute percentage deviation between calculated and experimental heat flow rate is around 0.6% for R134a, 4.5% for R1234ze(E), and 3.6% R152a which was not used during the present model developing.

Figure 192, Figure 193, and Figure 194 show the comparison between the experimental average saturation temperature of the refrigerant inside the pipes derived from the refrigerant pressure measurement on the third row and the calculated values by this new computational procedure for R134a, R1234ze(E), and R152a, respectively.

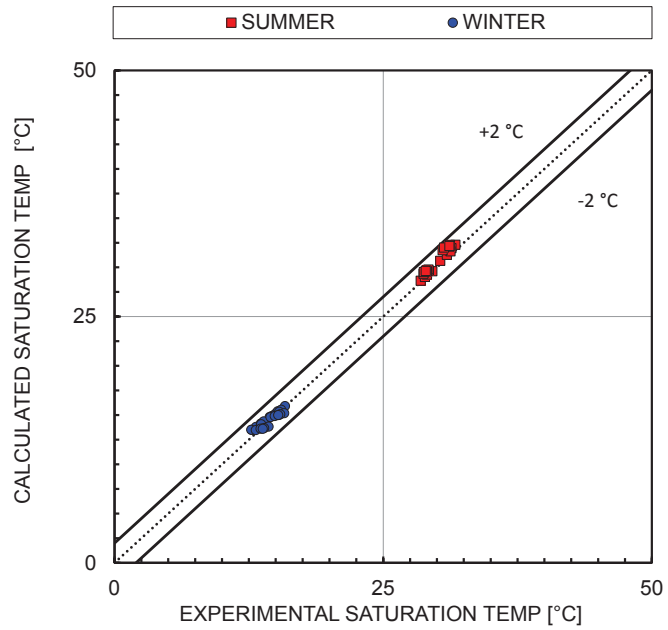

Figure 192 R134a calculated vs. experimental saturation temperature during both summer and winter season.

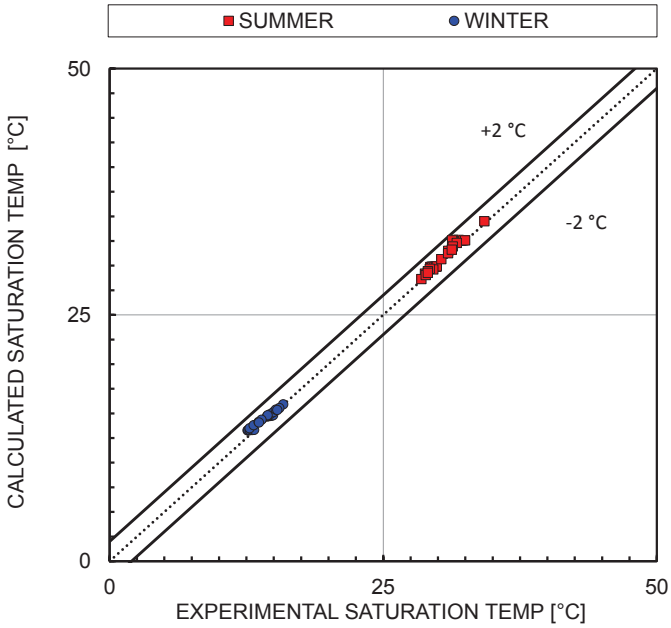

Figure 193 R1234ze(E) calculated vs. experimental saturation temperature during both summer and winter season.

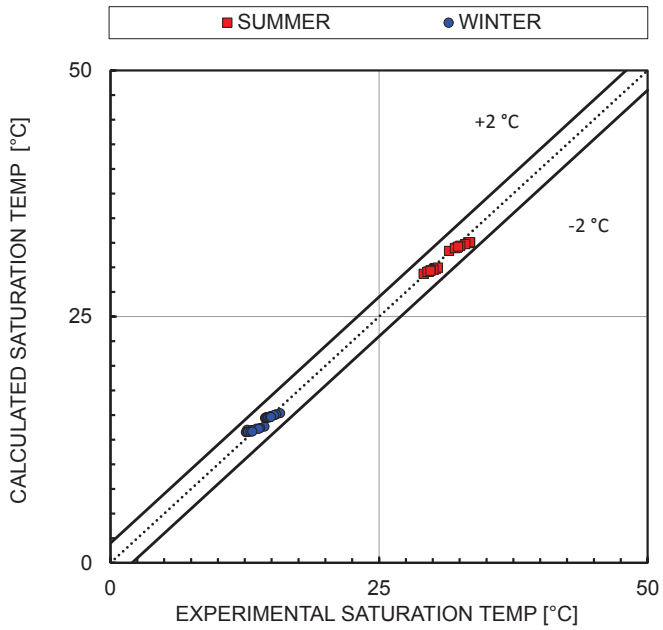

Figure 194 R152a calculated vs. experimental saturation temperature during both summer and winter season.

The mean absolute percentage deviation between calculated and experimental saturation temperature is around 1.2% for R134a, 1.6% for R1234ze(E), and 1.4% R152a which has not been included for the developing of the model.

Figure 195, Figure 196 , and Figure 197 show the comparison between the experimental pressure drop and the calculated values by the new computational procedure with R134a, R1234ze(E) and R152a, respectively.

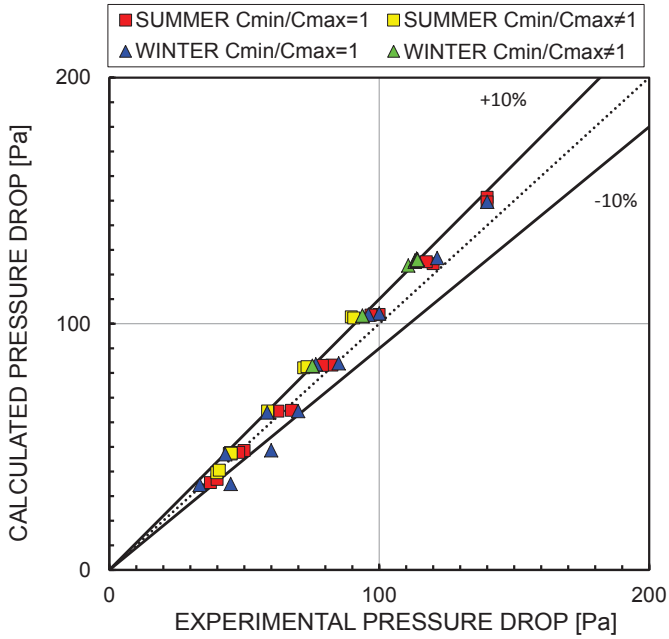

Figure 195 R134a calculated vs. experimental pressure drop during both summer and winter season.

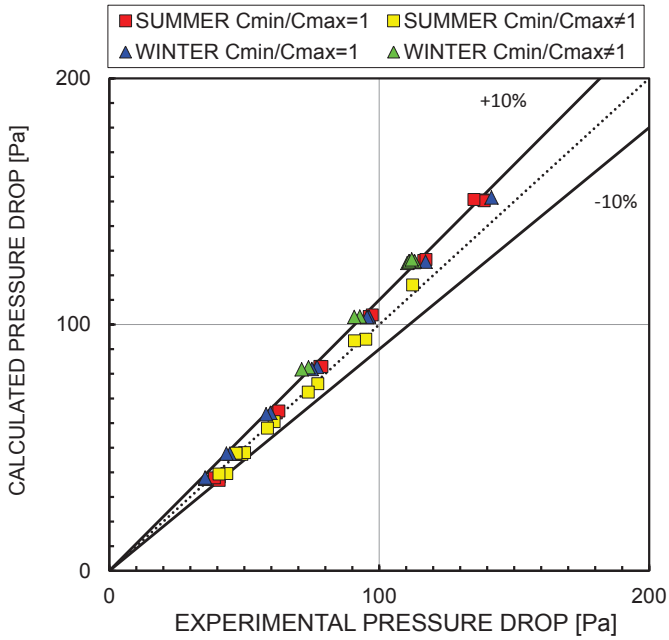

Figure 196 R1234ze(E) calculated vs. experimental pressure drop during both summer and winter season.

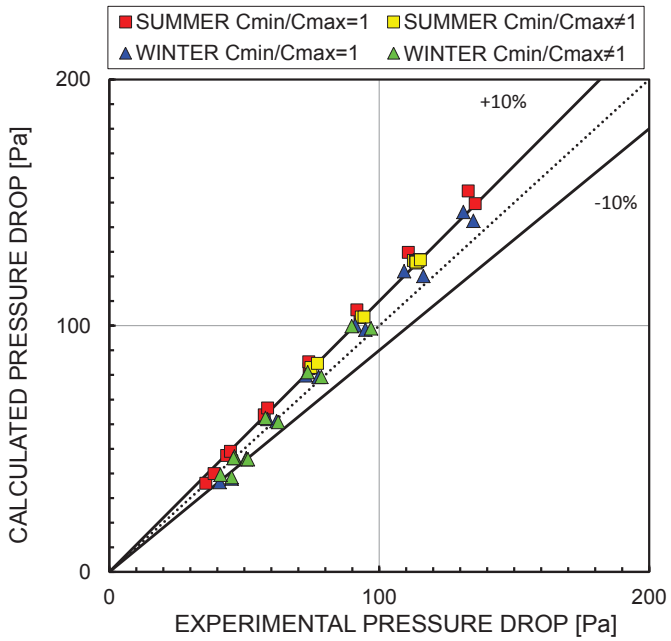

Figure 197 R152a calculated vs. experimental pressure drop during both summer and winter season.

The mean absolute percentage deviation between calculated and experimental saturation temperature is around 4.3% for R134a, 4.5% for R1234ze(E), and 6% for R152a.

The good agreement between experimental and calculated values confirms the ability of the model in simulating the HPFHE.

4 Fluid comparison and ranking

4.1 Horizontal smooth tube

Two couples of refrigerants were experimentally tested during the vaporization process inside a plain circular tube having an inner diameter of 4 mm.

Tests during two phase flow inside tubes are meaningful for technical purposes, due to tubes are the primary devices applied in air-cooled and water-cooled chillers and heat pumps, in tube-in-tube and shell-and-tube heat exchangers used in larger equipment operating with higher pressure drops. (Cavallini *et al.*, 2010).

The first couple of refrigerants taken into account is made up by R410A – a GWP=1725 and near-azeotropic mixture – ordinarily employed in many refrigeration fields (i.e. residential and commercial air conditioning) thanks to its high pressure and favorable thermophysical properties and by R32 (GWP= 677) already globally recognized as a valid substitute for R410A, able to lower its direct global warming impact by 1/3 or even more as its volumetric efficiency is higher than R410A one.

The second couple of refrigerants is composed by R134a, a GWP=1300 fluid, massively used for domestic and commercial refrigeration and automobile air conditioners, and by R1234ze(E) a relatively new molecule of the HFO group, proposed since 2010 (Cavallini *et al.*, 2012) to replace R134a and other refrigerants with similar application fields.

Following a comparison among the two couples of refrigerants during flow boiling inside a 4 mm horizontal smooth tube is presented and the effects of heat flux, refrigerant mass flux, mean vapor quality, and saturation temperature, investigated separately in section 3.1, are discussed.

4.1.1 R410A vs. R32

This couple of refrigerants was taken into account to propose a low GWP alternative to R410A.

In fact, R32 has a GWP around 675, mild flammability (ASHRAE classification A2L), operating pressure similar to R22 and R410A, and excellent heat transfer and pressure drop performance during phase change due to its relatively high liquid thermal conductivity and reduced pressure.

It was launched as low GWP alternative in air conditioners in Japan on November 1, 2012 and nowadays it is currently used in residential and commercial air conditioners in Japan, China, and India

as substitute for R410A. In order to reduce the residual risk associated with its mild flammability, R32 should be applied in heat transfer equipment with low refrigerant charge such as brazed plate heat exchangers, or small diameter tubes.

In Table 34 the main thermophysical properties, evaluated with Refprop 9.1 (2013) for both the refrigerants are reported at 5, 10, and 20 °C.

R32 has a similar saturation pressure to R410A (around 2% higher) but, due to its higher critical pressure, it has a lower reduced pressure (-15%) that disadvantages the pressure drops.

On the other hand the heat transfer properties are favorable, in fact R32 has higher liquid thermal conductivity (+40%) and higher specific heat (+15%). It also has a 40% higher vaporization latent heat that allows reducing the refrigerant flow rate at the same cooling capacity.

Table 34 Thermophysical properties of R32 and R410A at 5, 10, and 20 °C.

Refrigerant	**R32**	**R410A**	**R32**	**R410A**	**R32**	**R410A**
t sat [°C]	5	5	10	10	20	20
p in [bar]	9.51	9.33	11.07	10.85	14.75	14.43
p* [-]	0.165	0.19	0.191	0.221	0.255	0.294
λ_L [W m^{-1} K^{-1}]	0.1413	0.1003	0.1374	0.0974	0.1297	0.0918
λ_G [W m^{-1} K^{-1}]	0.0122	0.0126	0.0128	0.0132	0.0142	0.0146
c_{pL} [J kg^{-1} K^{-1}]	1773	1546	1806	1578	1886	1657
ρ_L [kg m^{-3}]	1037.7	1150	1019.7	1128.9	981.4	1083.6
ρ_G [kg m^{-3}]	25.9	35.9	30.2	41.9	40.9	56.8
μ_L [Pa s]	1.42E-04	1.52E-04	1.35E-04	1.43E-04	1.20E-04	1.26E-04
μ_G [Pa s]	1.18E-05	1.25E-05	1.20E-05	1.28E-05	1.25E-05	1.34E-05
σ [N m^{-1}]	1.01E-02	8.30E-03	9.26E-03	7.53E-03	7.59E-03	6.04E-03
Δh_{LG} [kJ kg^{-1}]	307.31	215.07	298.92	208.5	280.78	194.19
VCC [kJ m^{-1}]	7959	7721	9027	8736	11484	11030

This could be important to limit the refrigerant charge, and thus, limit the risks linked to a mildly flammable refrigerant and the emission of a low – but not zero – GWP fluid. Finally the Volumetric Cooling Capacity (VCC) is similar for the two fluids (R32 +3% than R410A) so they are compatible to a direct drop in operation.

4.1.1.1 Heat transfer

First of all, Figure 198, Figure 199, and Figure 200 present the refrigerant Heat Transfer Coefficient (HTC) as a function of the mean vapor quality at four different mass fluxes (G=200, 400, 600, and 800 kg m^{-2} s^{-1}), at a fixed heat flux (q=25 kW m^{-2}) and at 3 saturation temperatures: 20 °C, 10 °C, and 5 °C respectively.

At a first glance, HTC as a function of the vapor quality has a similar behavior for the two refrigerants and the onset of dry out occurs at similar vapor qualities.

The nucleate boiling is the dominant heat transfer mechanism, in fact generally the HTCs are poorly influenced by the mean vapor quality. Convective boiling effects are pointed out mainly at lower saturation temperatures and at higher mass fluxes, and R32 seems to be more affected by this heat transfer mechanism, maybe due to its lower vapor density (around -40%).

The heat transfer coefficients of R32 are up to 17% higher (on average +13%) than those of R410A at the same saturation temperature, mass flux, heat flux and vapor quality. This can be explained considering the differences in thermophysical properties (R32 presents liquid an higher thermal conductivity, a lower dynamic viscosity, and a higher surface tension than R410A) and thermodynamic properties (R32 has lower reduced pressure and higher latent heat of vaporization with respect to R410A), and also assuming a greater effect of the convective boiling heat transfer mechanism that occurs during R32 vaporization.

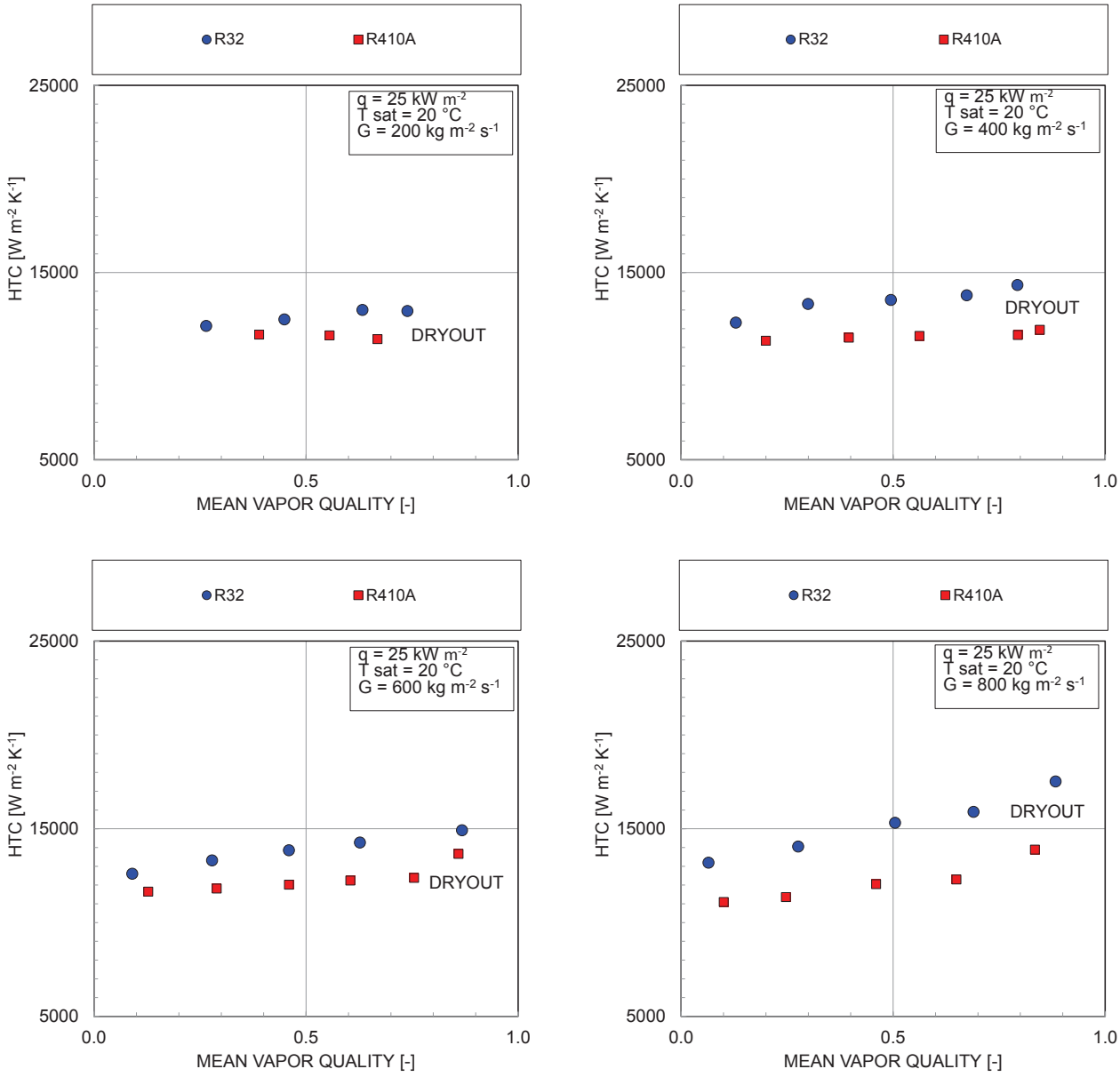

Figure 198 R32 vs. R410A Heat Transfer Coefficient (HTC) as a function of the mean vapor quality at four different mass fluxes (G=200, 400, 600, and 800 kg m^{-2} s^{-1}) at q=25 kW m^{-2} and t_{sat}=20 °C.

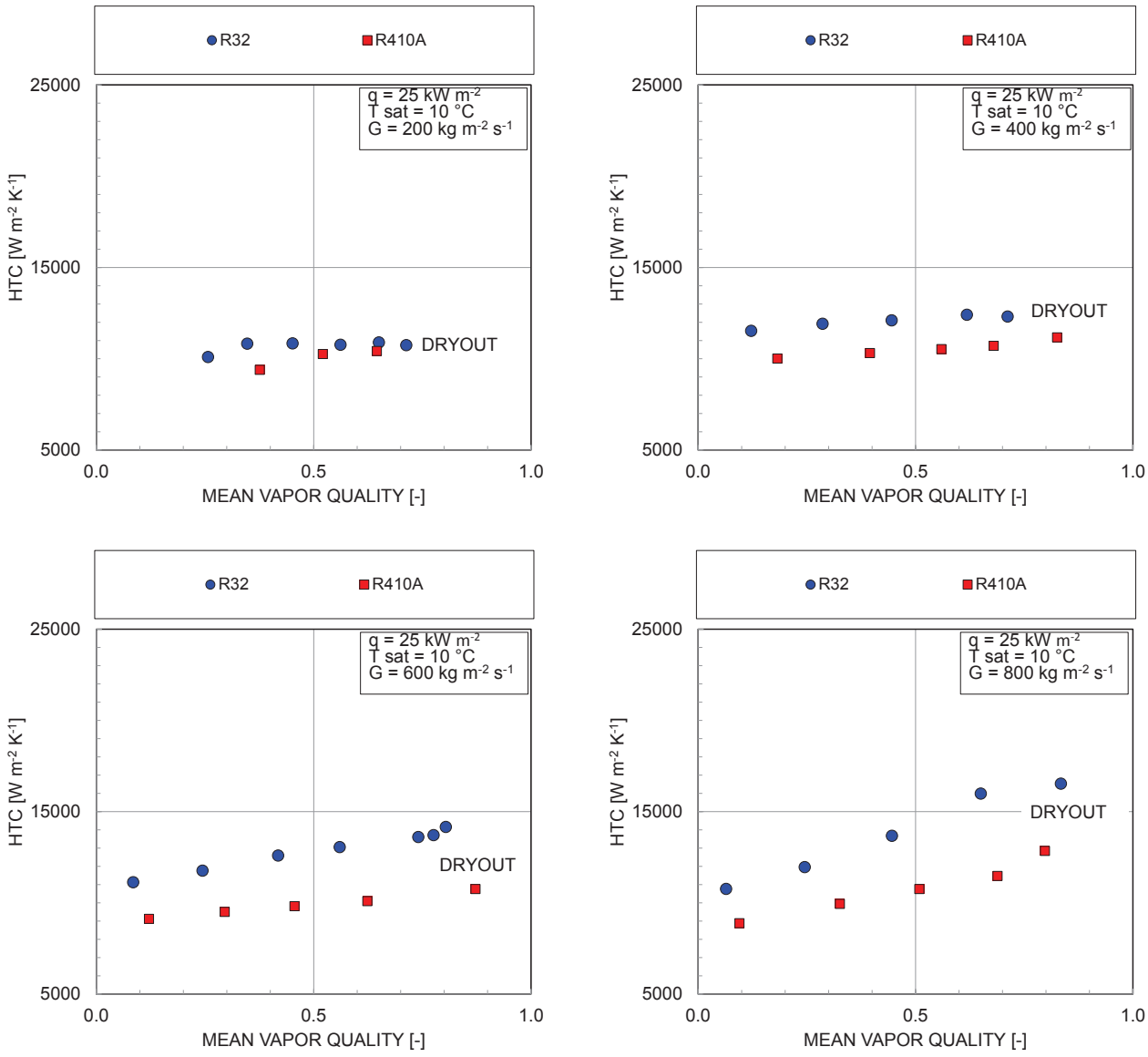

Figure 199 R32 vs. R410A Heat Transfer Coefficient (HTC) as a function of the mean vapor quality at four different mass fluxes (G=200, 400, 600, and 800 kg m^{-2} s^{-1}) at q=25 kW m^{-2} and t_{sat}=10 °C.

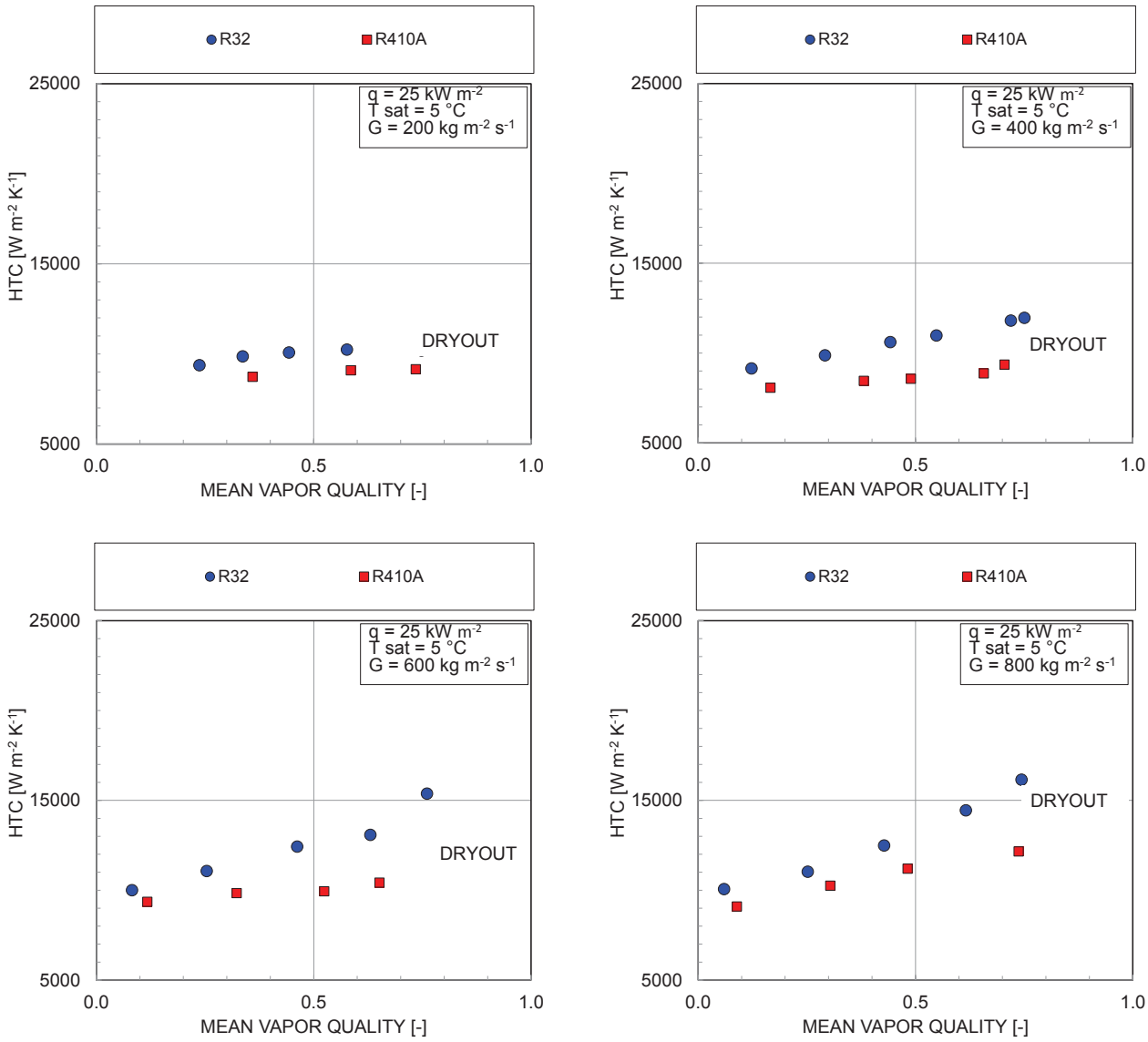

Figure 200 R32 vs. R410A Heat Transfer Coefficient (HTC) as a function of the mean vapor quality at four different mass fluxes (G=200, 400, 600, and 800 kg m^{-2} s^{-1}) and at q=25 kW m^{-2} and t_{sat}=5 °C.

Figure 201, Figure 202, and Figure 203, present the refrigerant Heat Transfer Coefficient (HTC) as a function of the mean vapor quality at four different heat fluxes (q=12, 25, 38, and 51 kW m^{-2}) at a fixed mass flux (G=400 kg m^{-2} s^{-1}) and at three saturation temperatures: 20 °C, 10 °C, and 5 °C respectively.

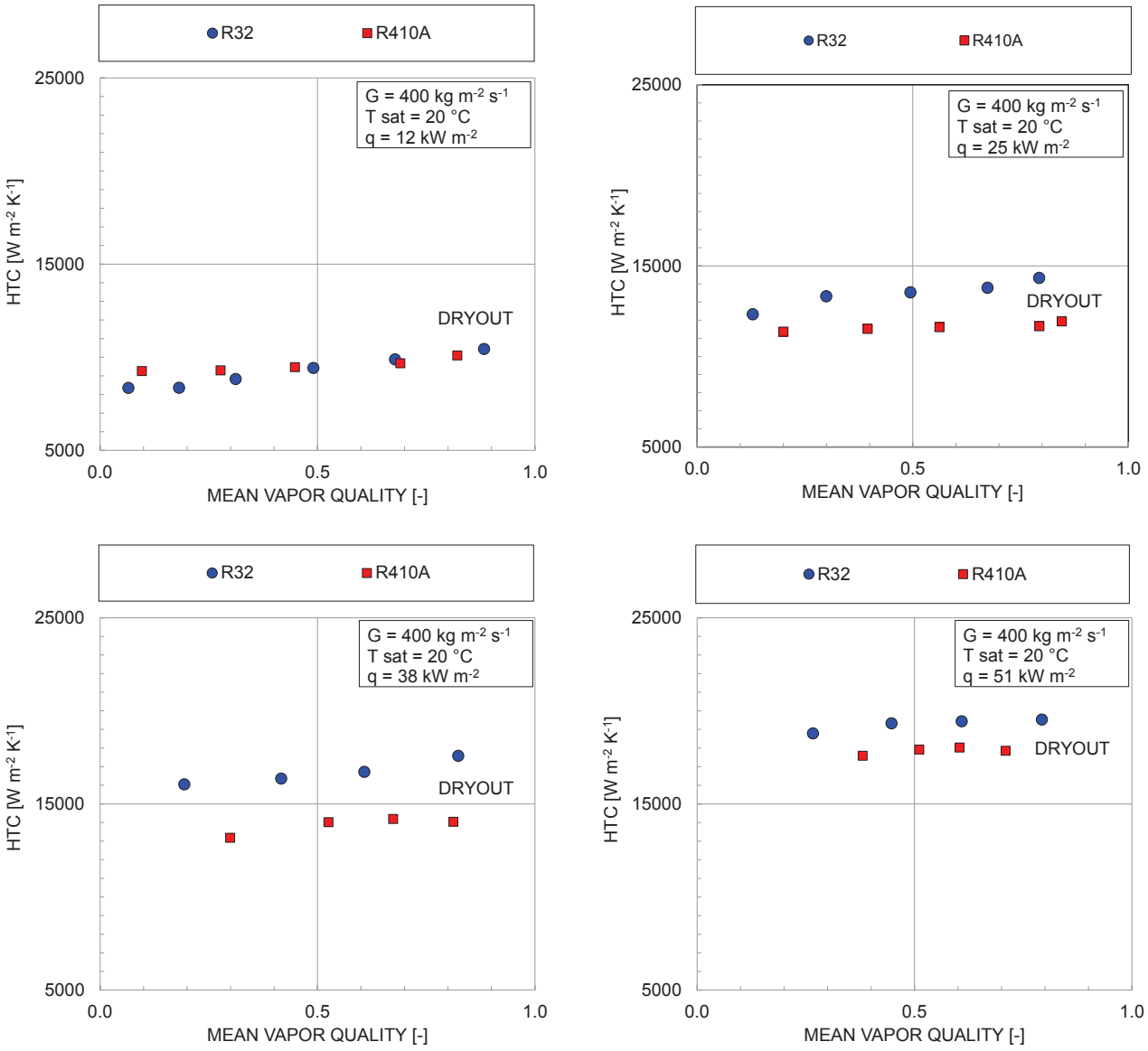

Figure 201 R32 vs. R410A Heat Transfer Coefficient (HTC) as a function of the mean vapor quality at four heat fluxes (q=12, 25, 38, and 50 kW m^{-2}) at G=400 kg m^{-2} $s^{-1}$and t_{sat}=20 °C.

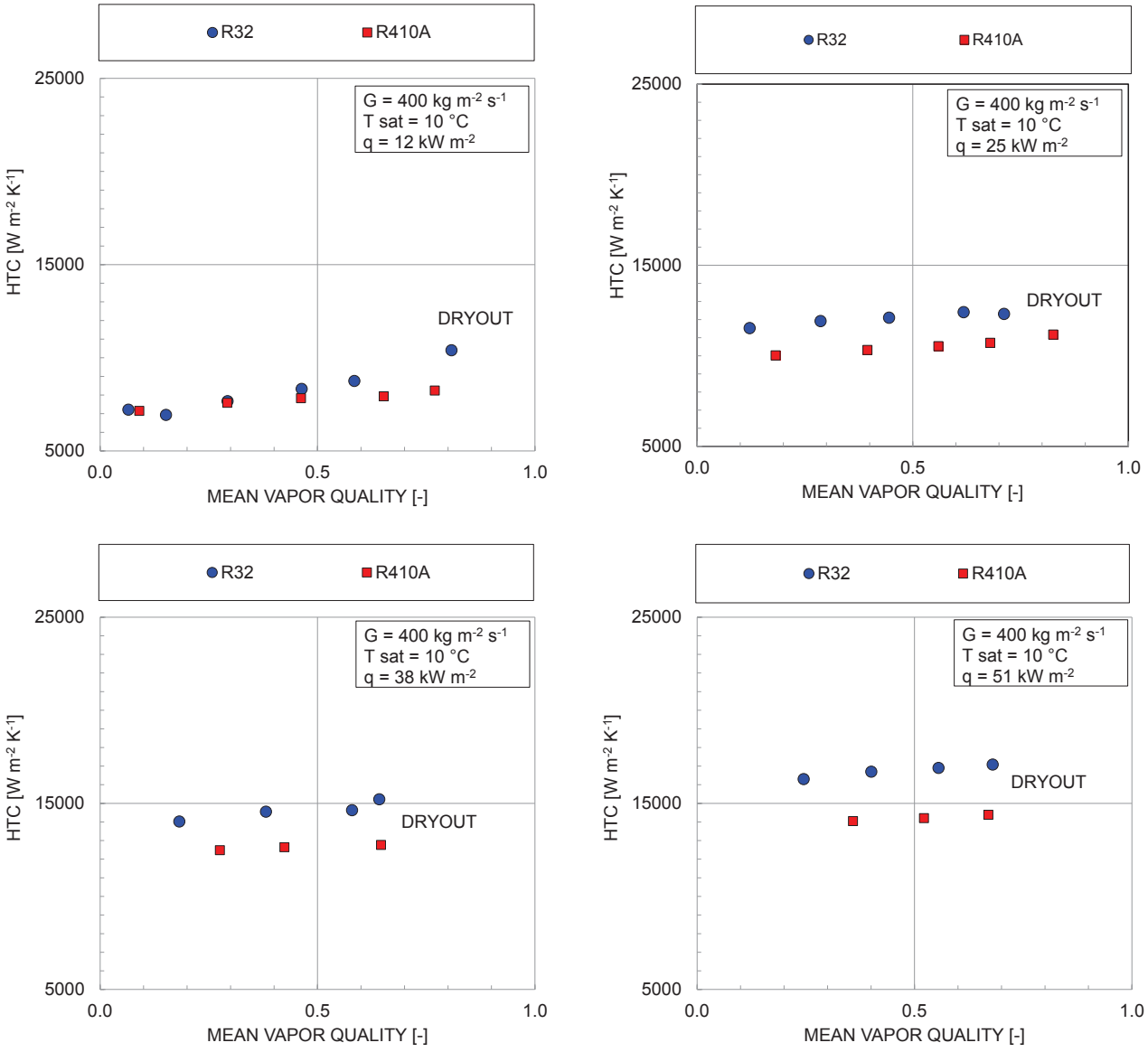

Figure 202 R32 vs. R410A Heat Transfer Coefficient (HTC) as a function of the mean vapor quality at four heat fluxes (q=12, 25, 38, and 50 kW m^{-2}) at G=400 kg m^{-2} $s^{-1}$and t_{sat}=10 °C.

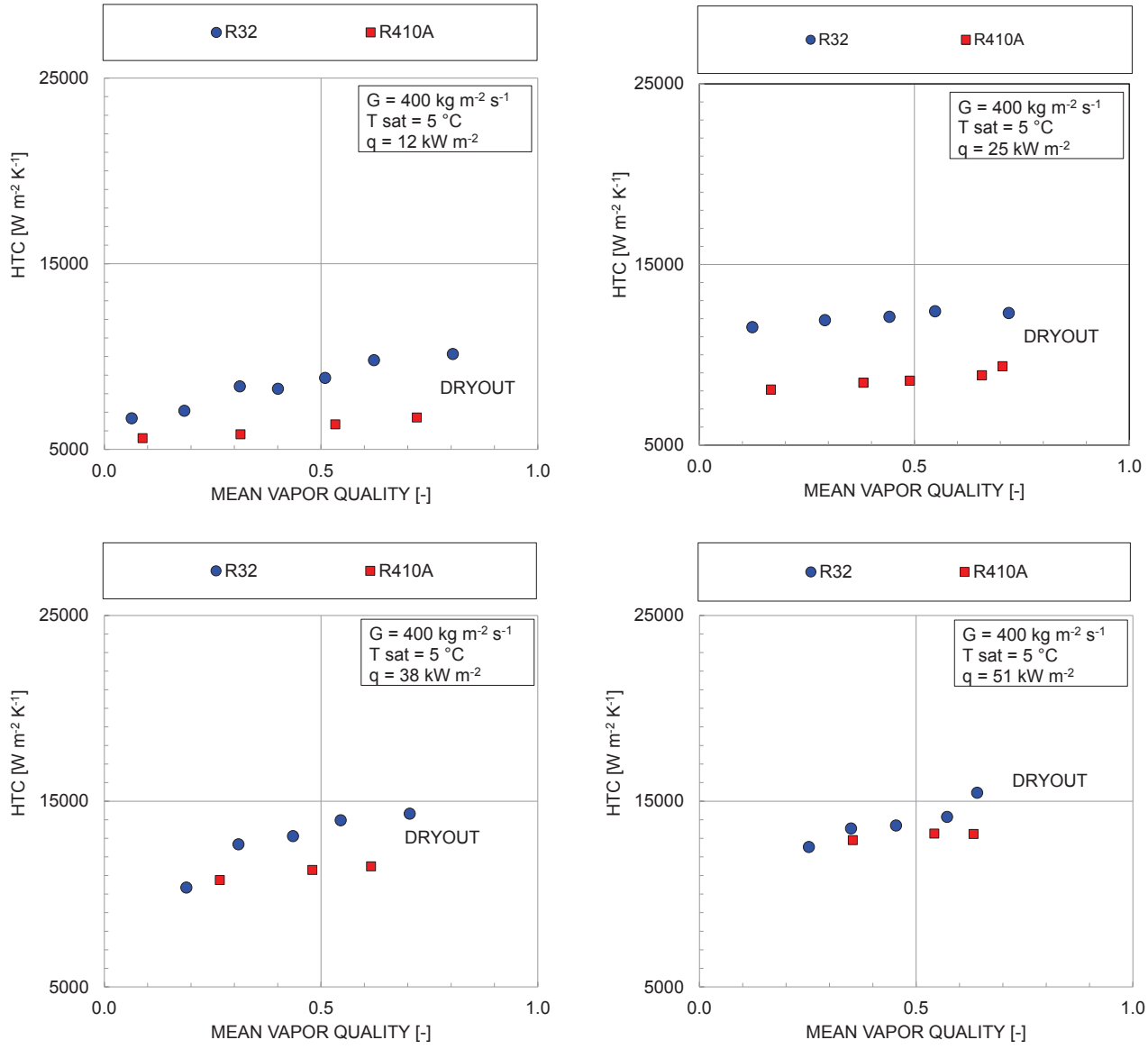

Figure 203 R32 vs. R410A Heat Transfer Coefficient (HTC) as a function of the mean vapor quality at four heat fluxes (q=12, 25, 38, and 50 kW m^{-2}) at G=400 kg m^{-2} $s^{-1}$and t_{sat}=5 °C.

When comparing the fluids at the same t_{sat}, G, q, and x, R32 heat transfer coefficients are higher than R410A ones (on average +15%).

As shown in section 3.1.1.1, the HTCs of both the refrigerants under these working conditions are strongly affected by the nucleate boiling mechanism. In fact they are remarkably influenced by heat flux while they show a negligible sensitivity to refrigerant mass flux and mean vapor quality.

This tendency is more relevant for R410A refrigerant. For example R410A at 20°C exhibits a 86-90% increase of the heat transfer coefficient when the heat flux varies from 12 kW m^{-2} to 51 kW m^{-2}, whereas R32 exhibits a 90% – 120% under the same conditions.
So, during R32 vaporization some convective boiling effects occur and this additional heat transfer contribution can enhance the R32 HTCs with respect to R410A. An example can be found in Figure 203 where at q=51 kW m^{-2} the two fluids HTCs are close to each other, while at q=15 kW m^{-2} (i.e. when the convective boiling is promoted) R32 has higher HTCs than R410A.

4.1.1.2 Pressure drop

Figure 204, Figure 205, and Figure 206 show the frictional pressure drop as a function of the mean vapor quality and of the mass flux (G=200, 400, 600, and 800 kg m^{-2} s^{-1}) at three different saturation temperatures: 20 °C, 10 °C, and 5 °C respectively and a fixed heat flux q=25 kW m^{-2}.
R32 frictional pressure drops are on average 18% higher than those of R410A under the same operating conditions (i.e. constant G, q, t_{sat}, and x). This can be explained mainly due to the R32 lower reduced pressure (-15%).

Despite the fact that the percentage differences of a single property between the two fluids are marginally affected by the saturation temperature (for instance, the reduced pressure increment between R32 and R410A is +15.7% at 5 °C and +15.4% at 20 °C) the R32 pressure drop is up to 60% higher than R410A at 20 °C while they are just up to 16% higher than R410A at 5 °C. So, probably, the flow regimes that occur at 20 °C are not the same than those occur at 5 °C. Further investigations should be done for determining the local flow regime as a function of the operating conditions.

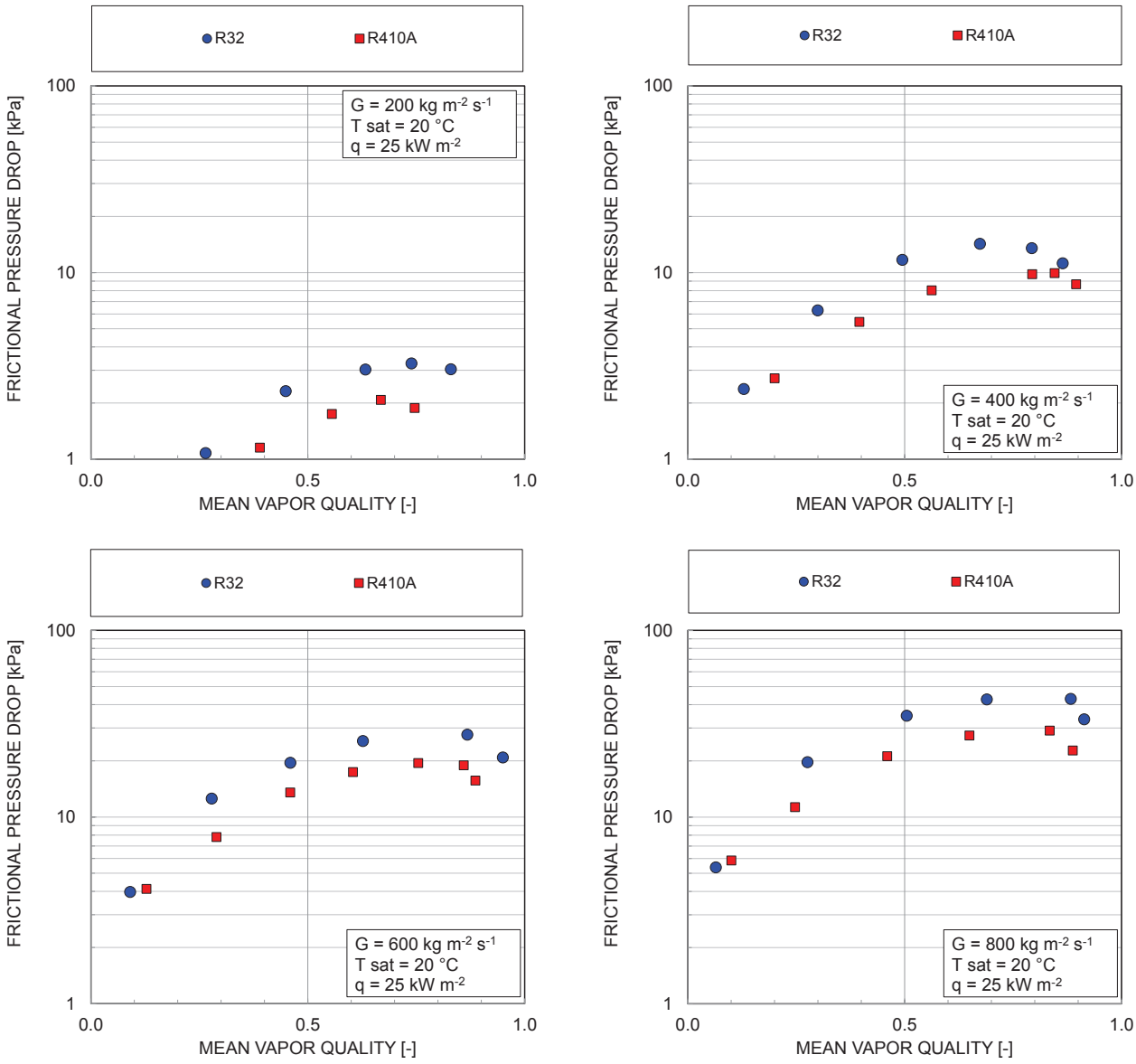

Figure 204 R32 vs. R410A frictional pressure drop as a function of the mean vapor quality and of the mass flux (G=200, 400, 600, and 800 kg m^{-2} s^{-1}) at t_{sat}=20 °C, and q=25 kW m^{-2}.

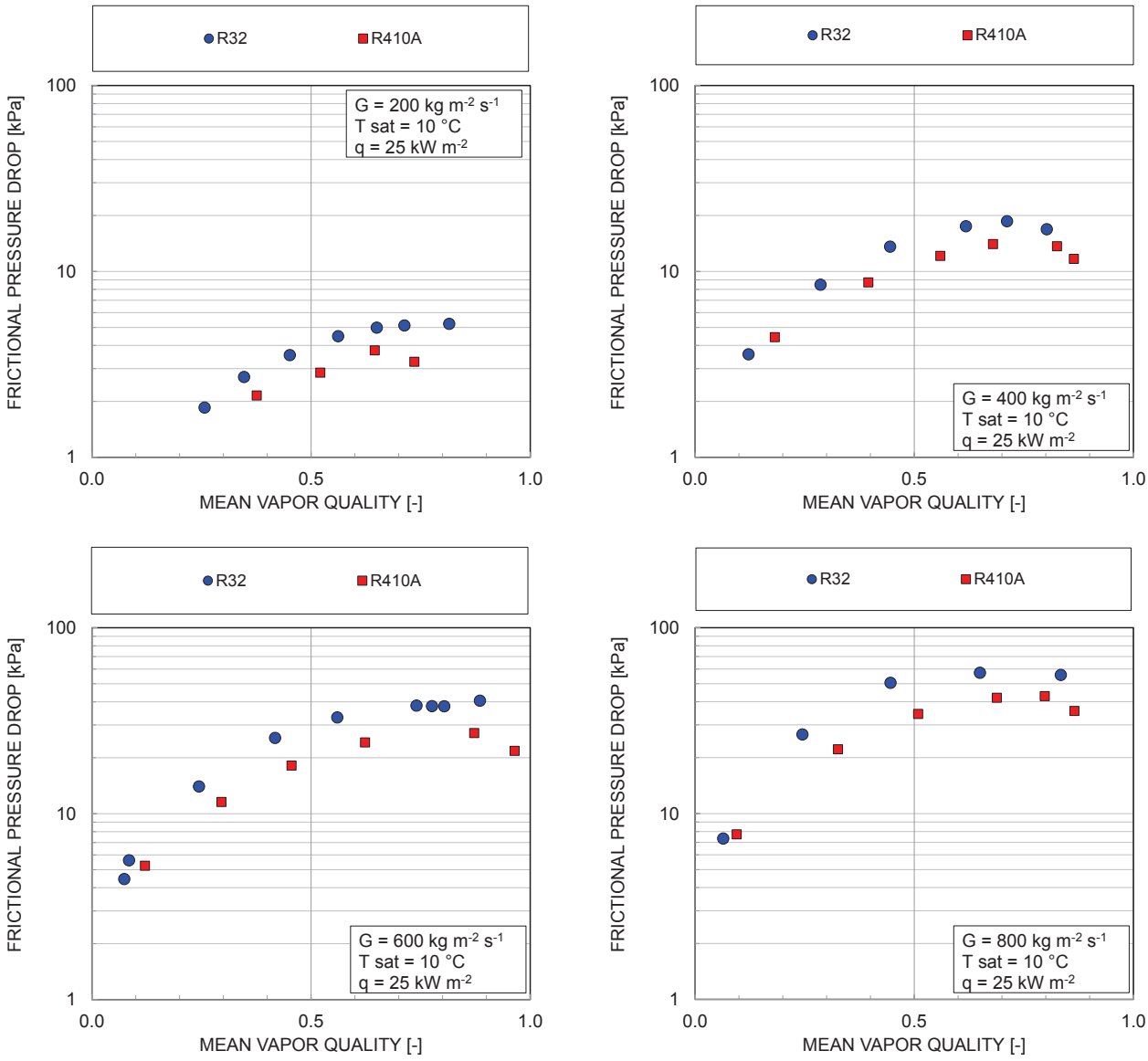

Figure 205 R32 vs. R410A frictional pressure drop as a function of the mean vapor quality and of the mass flux (G=200, 400, 600, and 800 kg m^{-2} s^{-1}) at t_{sat}=10 °C, and q=25 kW m^{-2}.

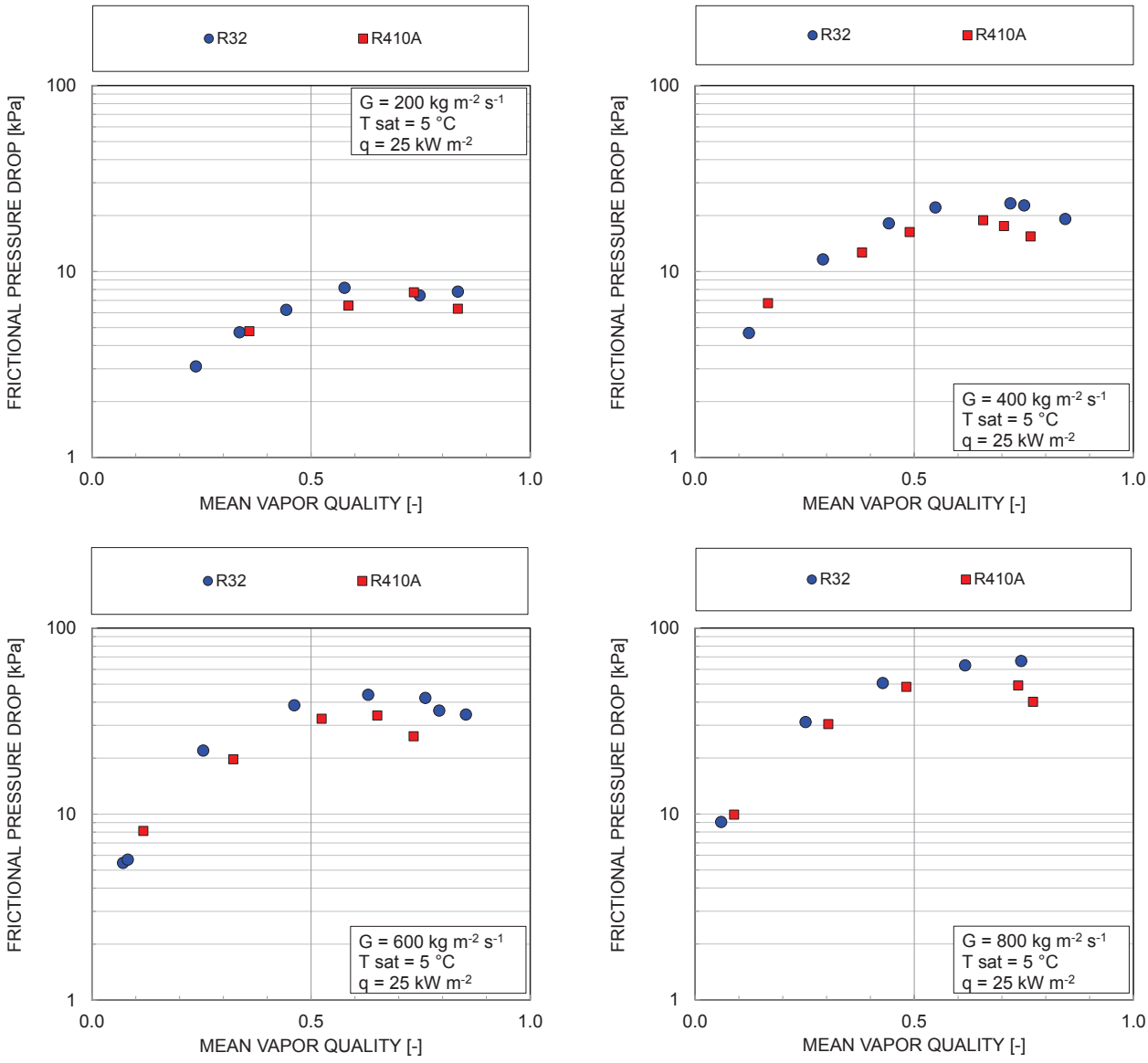

Figure 206 R32 vs. R410A frictional pressure drop as a function of the mean vapor quality and of the mass flux (G=200, 400, 600, and 800 kg m^{-2} s^{-1}) at t_{sat}=5 °C, and q=25 kW m^{-2}.

4.1.2 R134a vs. R1234ze(E)

R1234ze(E), together with R1234yf, is the most investigated HFO in the open literature. Its thermophysical properties have already been measured and it is commercially produced (Brown *et al.,* 2014). It has thermophysical properties not so far from the ones of R134a and a theoretical thermodynamic analysis collocates its performance close to R134a (Domanski *et al.*, 2014).

In the open literature R1234ze(E) has been proposed as R134a substitute since approximately 2010, when it was started to be investigated (Cavallini *et al.* 2012). As presented in the introduction (1.3.1) during years several assessments between R1234ze(E) and R134a have been made.

Table 35 summarizes the main thermophysical and thermodynamical properties of R1234ze(E) and R134a evaluated with Refprop 9.1 (2013) at 10, 15, and 20 °C.

Table 35 Thermophysical properties of R1234ze(E) and R134a at 10, 15, and 20 °C.

Refrigerant	**R1234ze(E)**	**R134a**	**R1234ze(E)**	**R134a**	**R1234ze(E)**	**R134a**
t sat [°C]	15	10	15	15	20	20
p in [bar]	3.08	4.15	3.64	4.88	4.27	5.72
p red [-]	0.085	0.102	0.1	0.12	0.118	0.141
$\mathbf{k_L}$ [W m^{-1} K^{-1}]	0.0828	0.0876	0.0777	0.0854	0.0759	0.0833
$\mathbf{k_v}$ [W m^{-1} K^{-1}]	0.0124	0.0124	0.0128	0.0129	0.0132	0.0133
$\mathbf{c_{pL}}$ [J kg^{-1} K^{-1}]	1342	1370	1355	1387	1370	1405
$\boldsymbol{\rho_L}$ [kg m^{-3}]	1210.4	1261	1195	1243.4	1179.3	1225.3
$\boldsymbol{\rho_V}$ [kg m^{-3}]	16.5	20.2	19.3	23.8	22.6	27.8
$\boldsymbol{\mu_L}$ [Pa s]	2.38E-04	2.35E-04	2.24E-04	2.21E-04	2.11E-04	2.07E-04
$\boldsymbol{\mu_V}$ [Pa s]	1.16E-05	1.11E-05	1.18E-05	1.13E-05	1.20E-05	1.15E-05
$\boldsymbol{\sigma}$ [N m^{-1}]	1.08E-02	1.00E-02	1.02E-02	9.36E-03	9.50E-03	8.69E-03
r [kJ kg^{-1} K^{-1}]	177.63	190.74	174.19	186.59	170.63	182.28
VCC [kJ m^{-1}]	2931	3853	3362	4441	3856	5067

The saturation pressure is quite different between the two refrigerants: the R134a one is around 35% higher than the R1234ze(E) one and also the R134a reduced pressure is about 20% higher. Furthermore the R134a vapor density is higher than the R1234ze(E) one (+23%), so theoretically R134a will perform lower pressure drops, and the R134a Volumetric Cooling Capacity (VCC) is higher, mainly due to an higher latent heat, so R1234ze(E) can not be consider as a directly drop-in fluid On the contrary, the liquid thermal conductivity is similar (around 5% higher for R134a), and also the surface tension (R134a: +9% than R1234ze(E)) and the latent heat (R134a: +7% R1234ze(E)) do not vary significantly.

Concluding, on the property basis, the two fluids should be good alternatives under the heat transfer point of view.

4.1.2.1 Heat transfer

Figure 207, Figure 208, and Figure 209 present the refrigerant Heat Transfer Coefficient (HTC) as a function of the mean vapor quality at four different mass fluxes (G=200, 300, 400, and 600 kg m^{-2} s^{-1}) and at a fixed heat flux (q=20 kW m^{-2}) at 3 saturation temperatures: 20 °C, 15 °C, and 10 °C respectively.

As outlined in the introduction of this section (see paragraph 4.1.2) there are not great differences in heat transfer coefficients among these two refrigerants: R134a HTCs are on average 5% higher than R1234ze(E) when G, q, t_{sat} and x are the same.

In can be supposed that the main discrepancy is given by the contribution that convective boiling gives to the heat transfer. In fact, as one can observe especially at low saturation temperatures and high mass fluxes (Figure 209), the R1234ze(E) heat transfer coefficients are more influenced by the mean vapor quality and thus by convective boiling, maybe due to the lower pressure and the lower vapor density. This mechanism makes the HTC increase and, in some conditions, the R1234ze(E) heat transfer coefficients are higher than the R134a ones (up to 25% at G=600 kg m^{-2} s^{-1} and t_{sat}=10 °C)

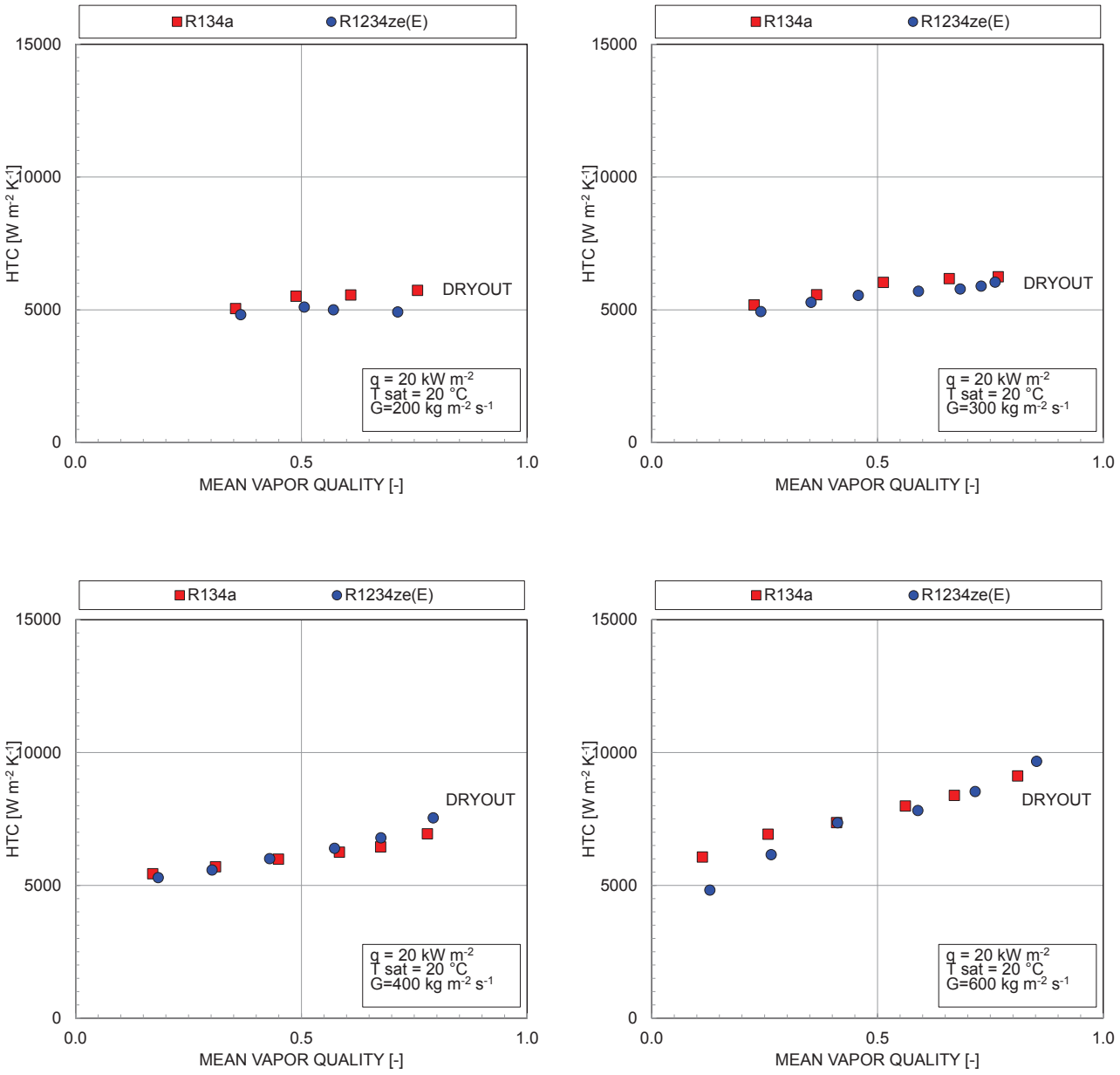

Figure 207 R134a vs. R1234ze(E) Heat Transfer Coefficients (HTCs) as a function of the mean vapor quality at four different mass fluxes (G=200, 300, 400, and 600 kg m^{-2} s^{-1}) and at q=20 kW m^{-2} and t_{sat}=20 °C.

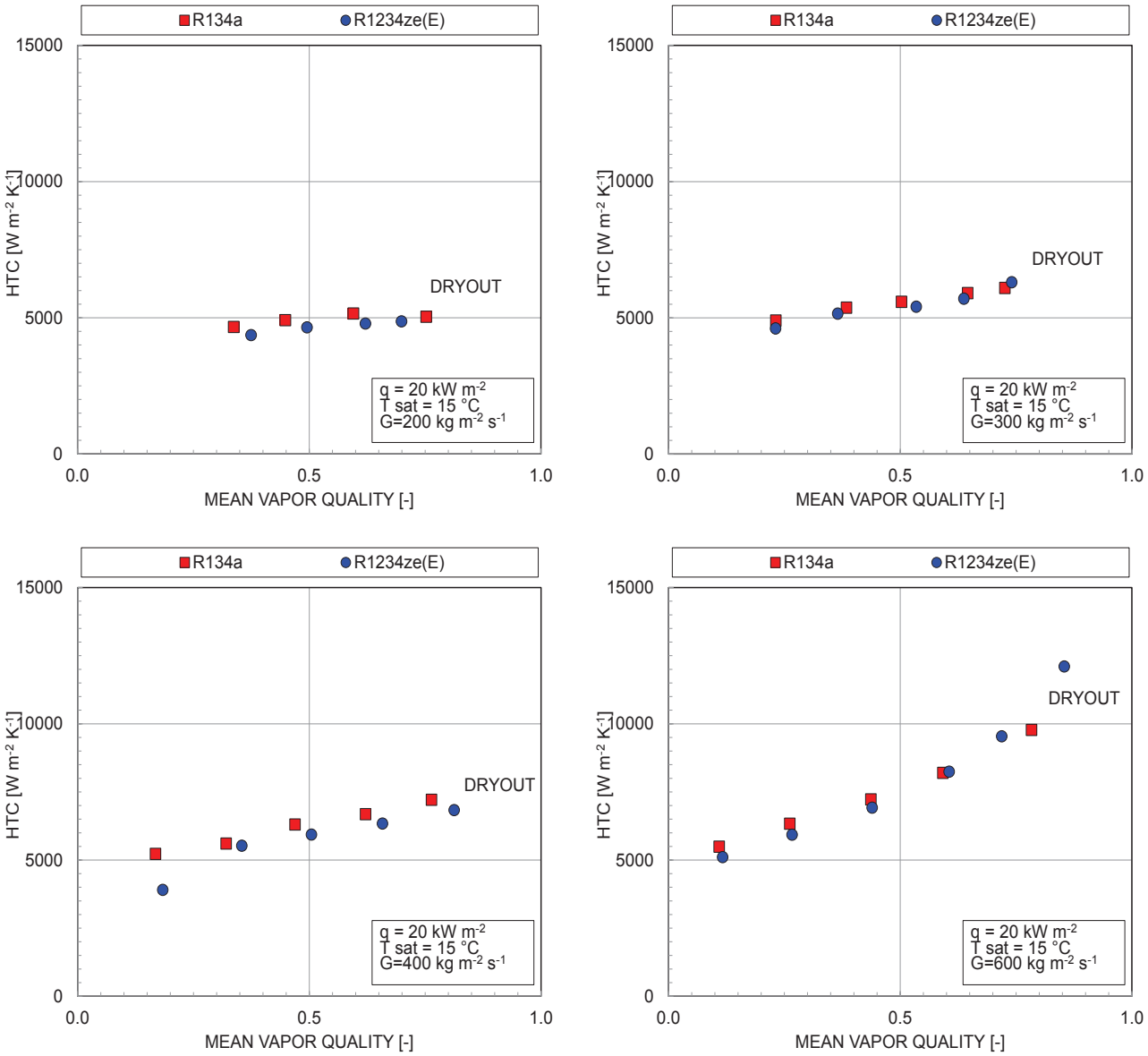

Figure 208 R134a vs. R1234ze(E) Heat Transfer Coefficients (HTCs) as a function of the mean vapor quality at four different mass fluxes (G=200, 300, 400, and 600 kg m^{-2} s^{-1}) and at q=20 kW m^{-2} and t_{sat}=15 °C.

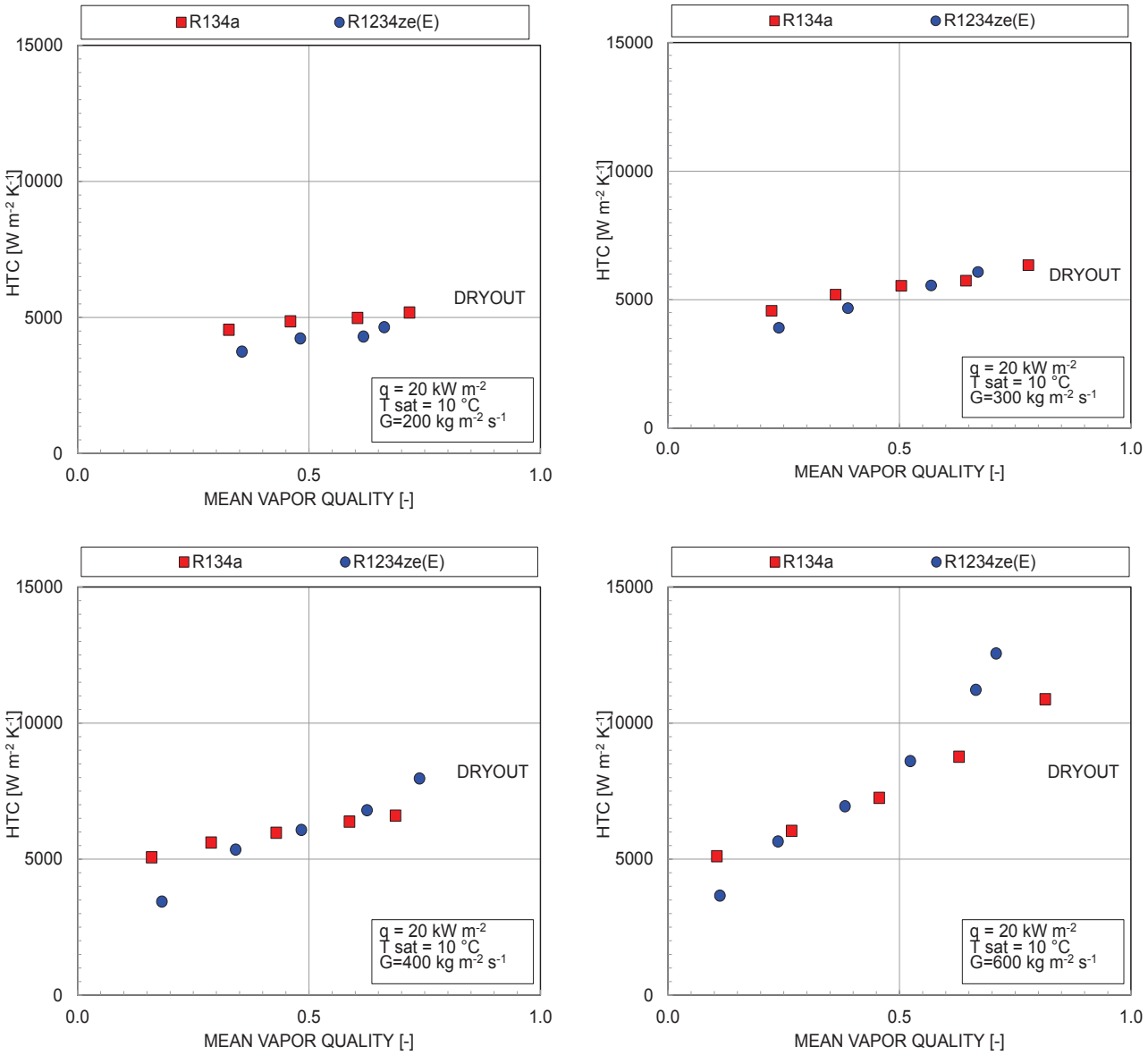

Figure 209 R134a vs. R1234ze(E) Heat Transfer Coefficients (HTCs) as a function of the mean vapor quality at four different mass fluxes (G=200, 300, 400, and 600 kg m^{-2} s^{-1}) and at q=20 kW m^{-2} and t_{sat}=10 °C.

Figure 210, Figure 211, and Figure 212 present the refrigerant Heat Transfer Coefficient (HTC) as a function of the mean vapor quality at four different heat fluxes (q=15, 20, 25, and 30 kW m^{-2}) and at a fixed mass flux (G=400 kg m^{-2} s^{-1}) at three saturation temperatures: 20 °C, 15 °C, and 10 °C respectively.

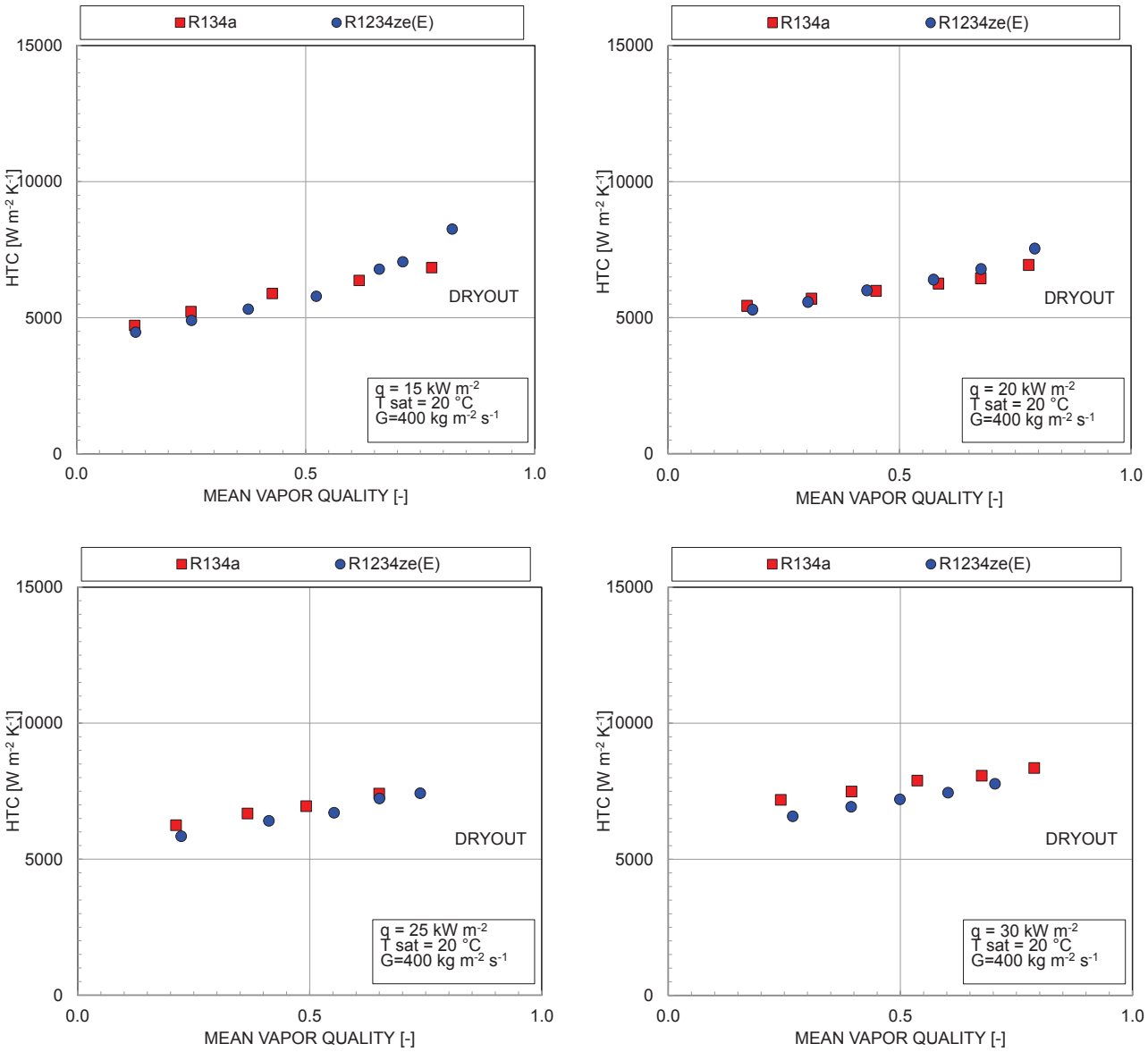

Figure 210 R134a vs. R1234ze(E) Heat Transfer Coefficients (HTCs) as a function of the mean vapor quality at four different heat fluxes (q=15, 20, 25, and 30 kW m^{-2}) at G=400 kg m^{-2} s^{-1} and t_{sat}=20 °C.

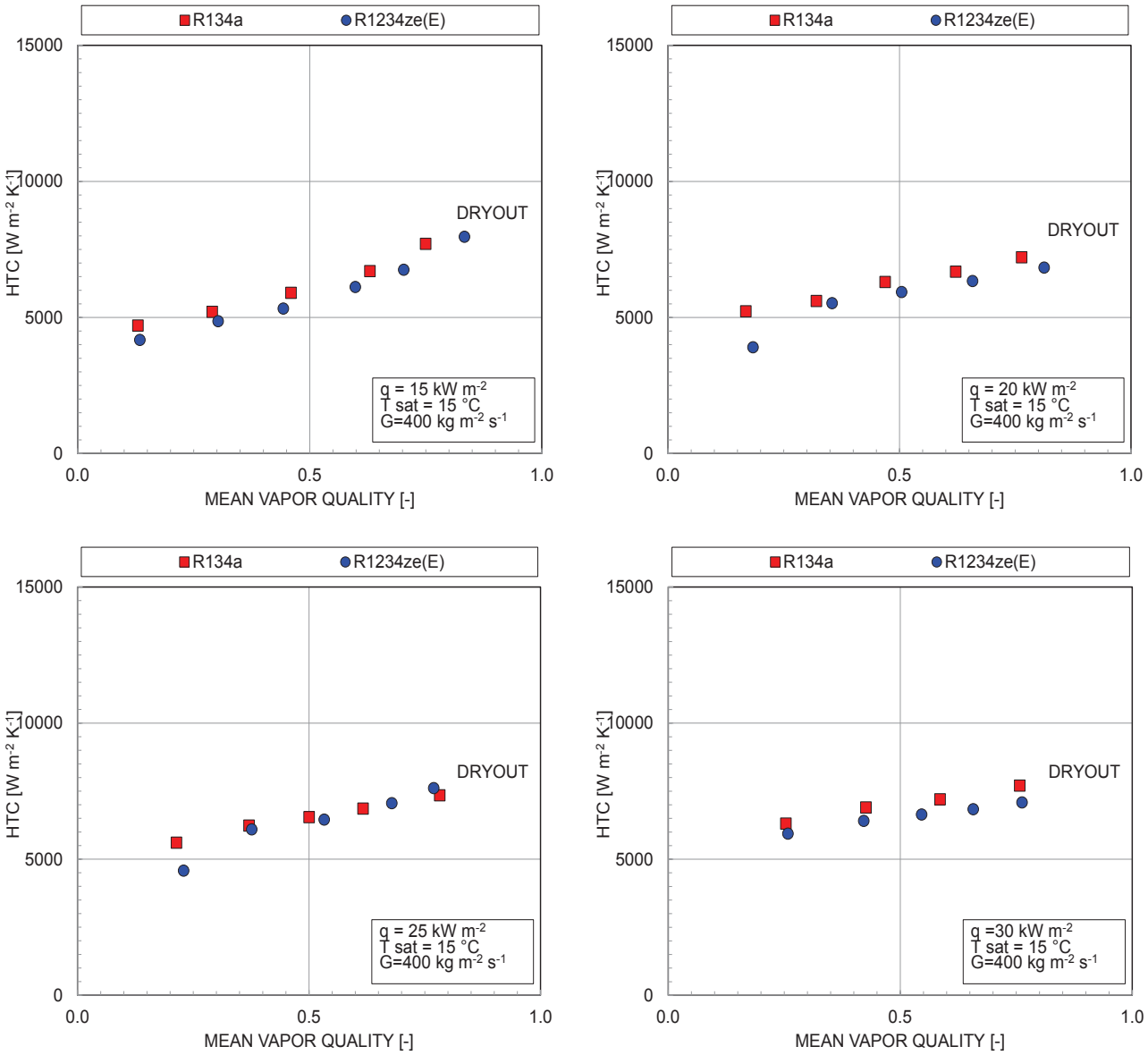

Figure 211 R134a vs. R1234ze(E) Heat Transfer Coefficients (HTCs) as a function of the mean vapor quality at four different heat fluxes (q=15, 20, 25, and 30 kW m^{-2}) at G=400 kg m^{-2} s^{-1} and t_{sat}=15 °C.

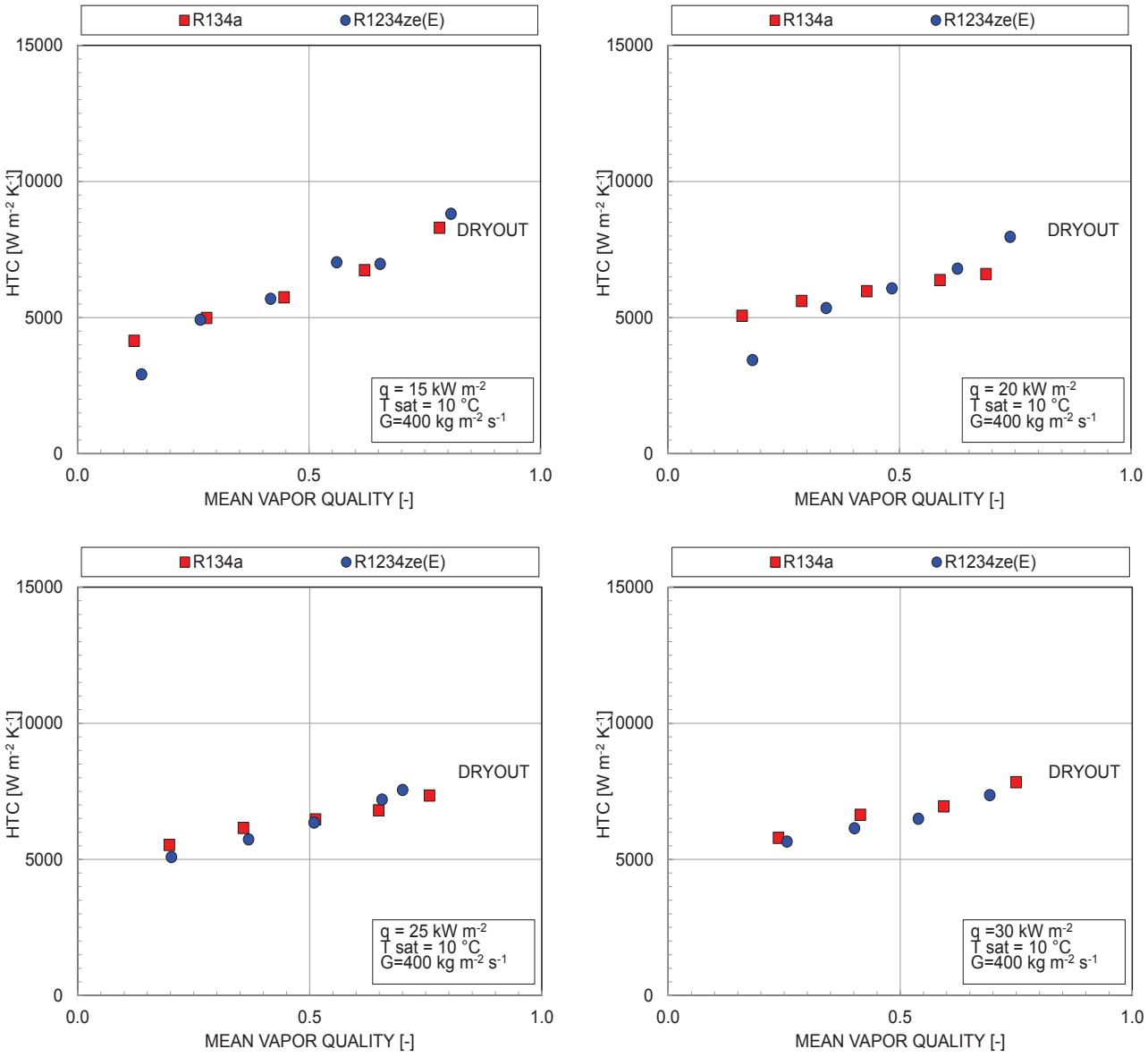

Figure 212 R134a vs. R1234ze(E) Heat Transfer Coefficients (HTCs) as a function of the mean vapor quality at four different heat fluxes (q=15, 20, 25, and 30 kW m^{-2}) and at G=400 kg m^{-2} s^{-1} and t_{sat}=10 °C.

The nucleate boiling heat transfer dominates the vaporization process at G=400 kg m^{-2} s^{-1} for both the refrigerants. In fact changes in vapor quality weakly affect the heat transfer coefficients. For this reason it is more difficult to identify in R1234ze(E) HTCs a higher convective boiling contribution as in Figure 209. Despite this, at low heat fluxes and saturation temperatures (see

Figure 212) the mean vapor quality lightly affects the HTCs that on average increase about 90% passing from a vapor quality around 0.15 to a vapor quality around 0.8. Under this working conditions and at high vapor qualities R1234ze(E) HTCs are around 10% higher than R134a, but al low vapor qualities they are significantly lower (up to -40%) than R134a.

4.1.2.2 Pressure drop

Figure 213, Figure 214, and Figure 215 show the frictional pressure drop as a function of the mean vapor quality and of the mass flux (G=200, 300, 400, and 600 kg m^{-2} s^{-1}) at three different saturation temperatures: 20 °C, 15 °C, and 10 °C respectively and a fixed heat flux q=20 kW m^{-2}.
The pressure drop trend as a function of the mean vapor quality is similar for the two refrigerants but, as presented in paragraph 4.1.2, especially due to the higher reduced pressure, R134a performs lower pressure drop (around 30% lower at 20 °C, yet only 5% lower at 10 °C).

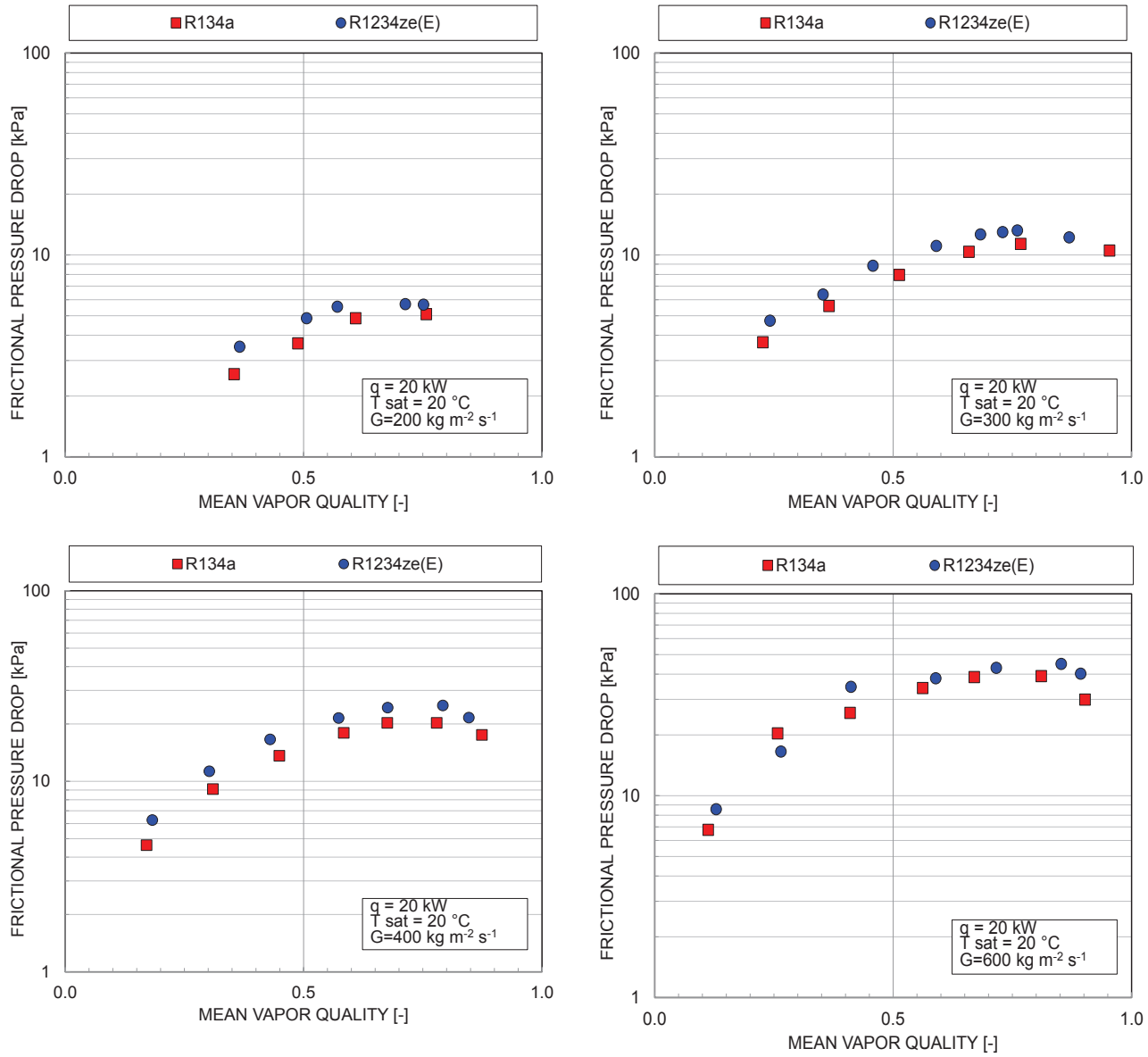

Figure 213 R134a vs. R1234ze(E) frictional pressure drop as a function of the mean vapor quality and of the mass flux (G=200, 400, 600, and 800 kg m^{-2} s^{-1}) at t_{sat}=20 °C, and q=20 kW m^{-2}.

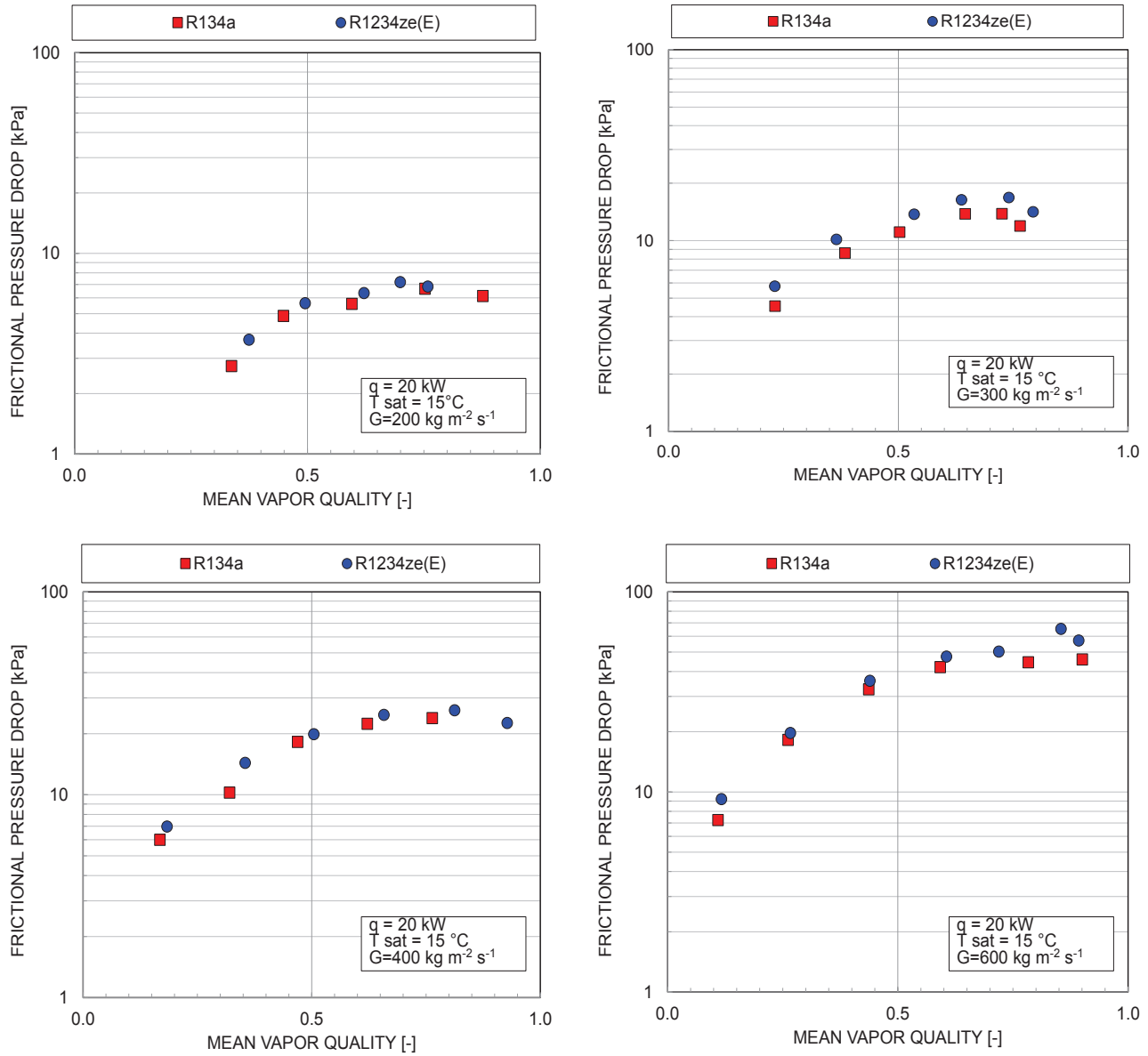

Figure 214 R134a vs. R1234ze(E) frictional pressure drop as a function of the mean vapor quality and of the mass flux (G=200, 400, 600, and 800 kg m^{-2} s^{-1}) at t_{sat}=15 °C, and q=20 kW m^{-2}.

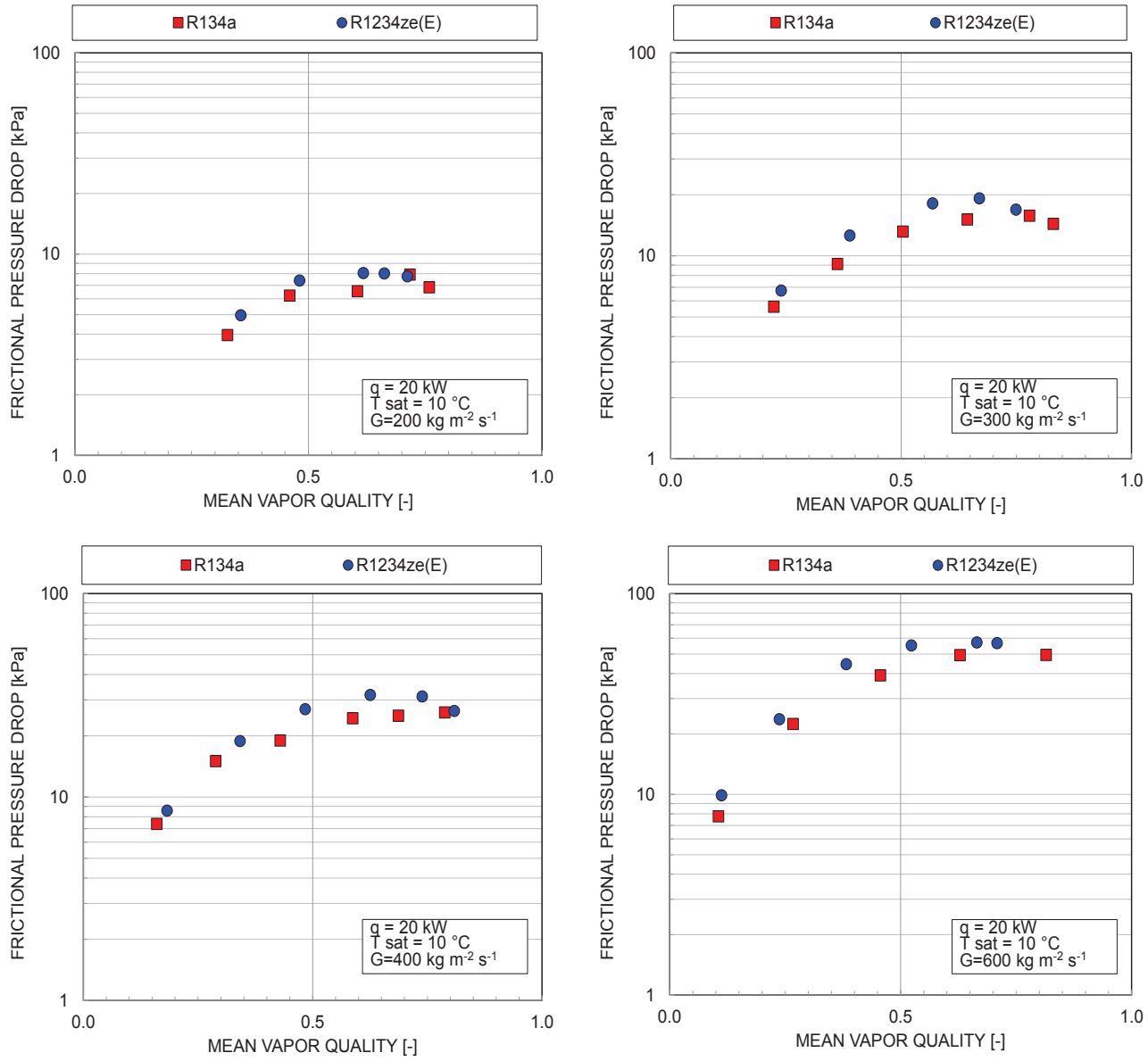

Figure 215 R134a vs. R1234ze(E) frictional pressure drop as a function of the mean vapor quality and of the mass flux (G=200, 400, 600, and 800 kg m^{-2} s^{-1}) at t_{sat}=10 °C, and q=20 kW m^{-2}.

4.1.3 Performance evaluation criteria and penalization terms

In the earlier paragraphs it has been proposed a comparison between couples of refrigerants on the basis of experimental data collected.

It has been noticed that the fluid properties affect both HTCs and pressure drops.

High heat transfer coefficients generally leads to high pressure drop but it is not straightforward that the percentage increment on HTC is equal to the one on pressure drop. Accordingly to rank the refrigerant performance only on the base of HTC or pressure drop separately is not complete.

So, to make a more complete analysis, it has been used the Performance Evaluation Criteria (PEC) proposed by Brown *et al.* (2013) that evaluates the flow boiling heat transfer performance potential of different refrigerants expressed as a combination of two temperature differences: the saturation temperature drop which occurs due to the refrigerant pressure drop ΔT_{sr}, and the driving temperature difference ΔT_{dr}.

Both ΔT_{sr} and ΔT_{dr} reduce the overall refrigeration system energetic and exergetic efficiencies by increasing the required compressor power to achieve the same refrigeration effect.

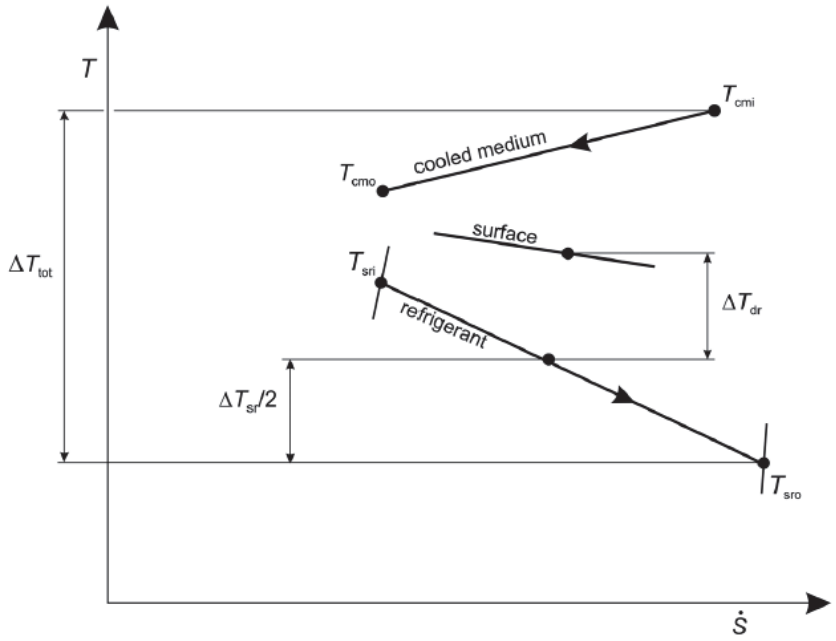

Figure 216 Idealized temperature profiles in a counter-flow evaporator Brown *et al.* (2013).

In Figure 216 are reported the idealized temperature profiles of refrigerant, surface, and cooling medium during the vaporization process inside a counter-flow heat exchanger and these two temperature differences (ΔT_{sr} and ΔT_{dr}) are highlighted.

ΔT_{sr} is the term linked to the pressure drops. It is defined as the difference between the refrigerant temperature at the inlet and at the outlet of the heat exchanger, as in Eq. 96

$$\Delta T_{sr} = t_{sat}(p_{in}) - t_{sat}(p_{out}) \quad \text{Eq. 96}$$

$$p_{out} = p_{in} - \Delta p_{tot} \quad \text{Eq. 97}$$

$$\Delta p_t = \Delta p_f + \Delta p_c - \Delta p_a - \Delta p_g \quad \text{Eq. 98}$$

The frictional pressure drop can be easily evaluated through a boiling frictional pressure drop correlation. In this particular case it has been chosen the Friedel (1979) model because is the one that better fits the experimental data collected during vaporization inside a circular tube (see paragraph 3.1.2.2).

Figure 217 and Figure 218 represent the ΔT_{sr} as a function of the heat transfer coefficient α for the two couples of refrigerants tested, respectively.

The heat transfer coefficient α was evaluated with the Kim and Mudawar (2014a) model for the couple R134a - R1234ze(E) and with the Sun and Mishima (2009) model for the couple R32 - R410A due to they are the ones that predict the experimental data with the lowest mean absolute percentage deviation (see paragraph 3.1.2.1).

The geometrical parameters used are the ones of the plain circular tube experimentally tested inside this thesis (see Table 8), the heat flux is set equal to 25 kW m^{-2} and the thermophysical properties are evaluated with Refprop 9.1 (2013) at the average temperature between inlet and outlet (inlet temperature of 20 °C).

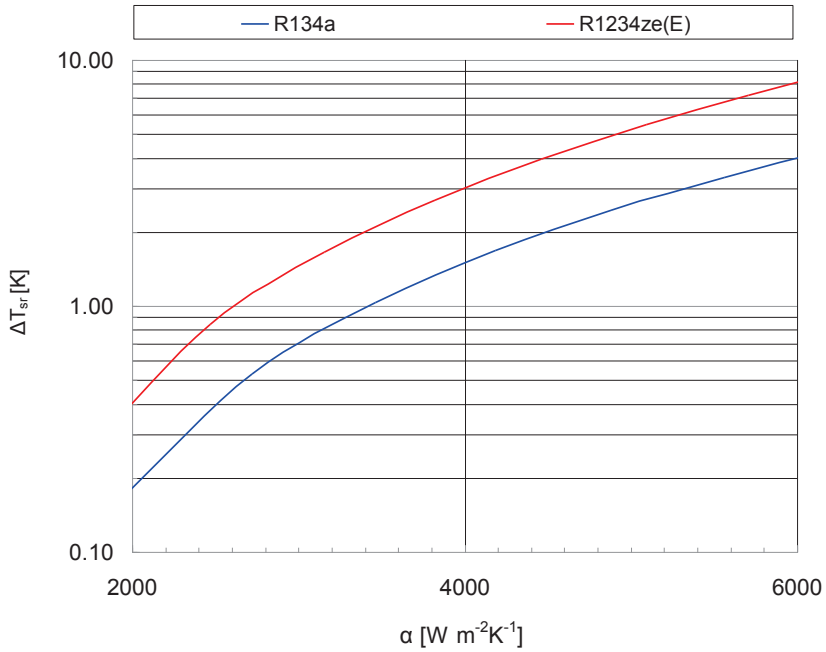

Figure 217 Refrigerant saturation temperature drops during vaporization of R134a and R1234ze(E) in a plain tube calculated using the heat transfer coefficient correlation of Kim and Mudawar (2014a) and the pressure drop correlation of Friedel (1979) at 20 °C of evaporator inlet temperature.

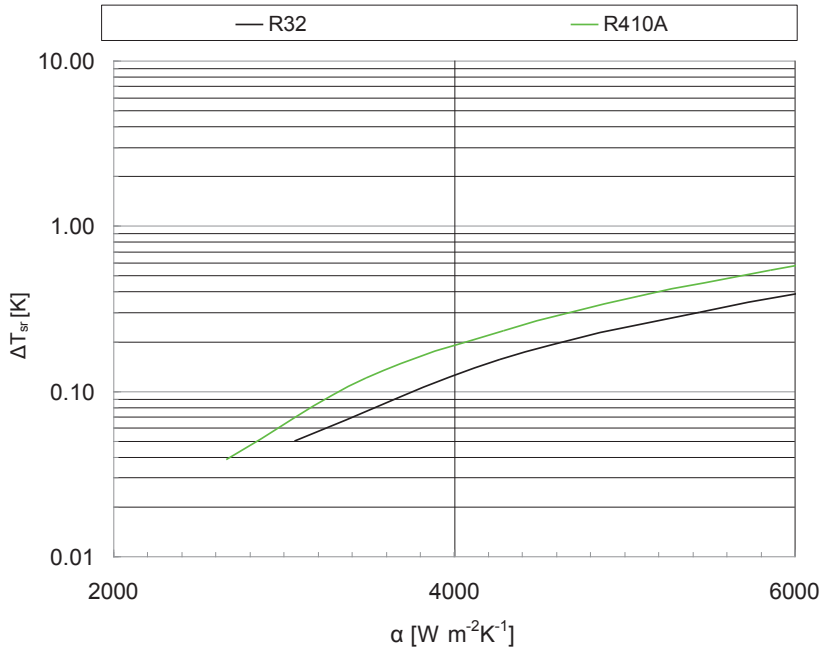

Figure 218 Refrigerant saturation temperature drops during vaporization of R32 and R410A in a plain tube calculated using the heat transfer coefficient correlation of Sun and Mishima (2009) and the pressure drop correlation of Friedel (1979) at 20 °C of evaporator inlet temperature.

In terms of refrigerant pressure drops, R134a performs better than R1234ze(E) at the same heat transfer coefficient value and R32 performs better than R410A.
In fact, if the heat transfer is held constant, a lower pressure drop penalization indicates lower exergy losses or entropy generations and thus higher energetic and exergetic efficiencies.
These results are consistent with the Brown *et al.* (2013) findings, where it is underlined that lower pressure refrigerants have higher pressure drop penalization terms than medium and higher pressure refrigerants (e.g., R32 and R410A). Moreover they found that the pressure drop penalization term for R1234ze(E) is approximately 88% greater than R134a.

Furthermore, it is possible to consider ΔT_{dr} (a term related to heat transfer) coupled with ΔT_{sr} (a term related to pressure drop) combined together into one single PEC called Total Temperature Penalization (TTP) which is defined as Eq. 99 (see Brown *et al.* 2013).

$$TTP = \Delta T_{dr} + 0.5\,\Delta T_{sr} \qquad \text{Eq. 99}$$

where:

$$\Delta T_{dr} = \dot{m}\,\Delta h_{LG}/\alpha \qquad \text{Eq. 100}$$

Figure 219 and Figure 220 represent the TTP as a function of the heat transfer coefficient α for the two couples of refrigerants tested. The heat transfer coefficient α was evaluated with the Kim and Mudawar (2014a) model for the couple R134a - R1234ze(E) and with the Sun and Mishima (2009) model for the couple R32 - R410A.

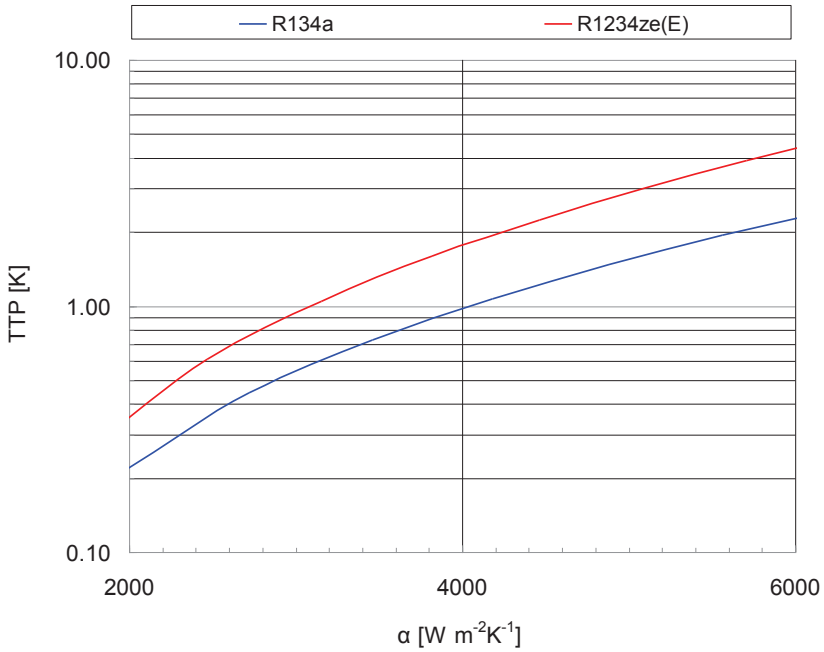

Figure 219 Total Temperature Penalization (TTP) during vaporization of R134a and R1234ze(E) in a plain tube calculated using the heat transfer coefficient correlation of Sun and Mishima (2009) and the pressure drop correlation of Friedel (1979).

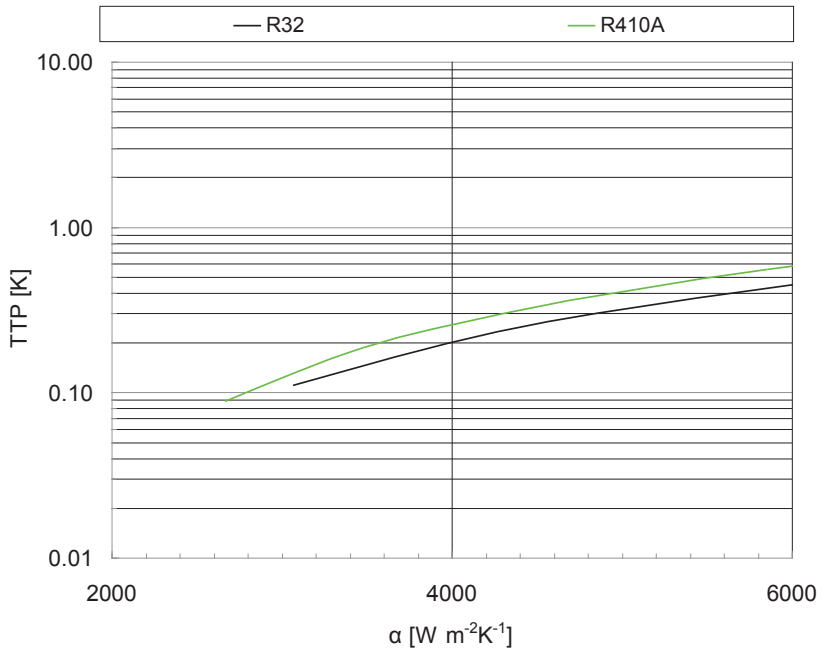

Figure 220 Total Temperature Penalization (TTP) during vaporization of R32 and R410A in a plain tube calculated using the heat transfer coefficient correlation of Sun and Mishima (2009) and the pressure drop correlation of Friedel (1979).

Consistently with the ΔT_{sr} results, also the analysis based on the TTP suggests that R134a performs better than R1234ze(E), having a TTP value lower at the same heat transfer coefficient, and similarly R32 gives better performance than R410A at the same HTC.

It can be concluded that the heat transfer performance potentials of refrigerants during vaporization can be expressed as temperature differences and this temperature differences are strongly affected by the refrigerant saturation pressure. In fact, higher pressure refrigerants have smaller pressure drop penalization values than medium and lower pressure refrigerants. So, on the basis of this analysis R1234ze(E) will have lower energetic and exergetic efficiencies than more traditional refrigerants such as R134a indicating the need to optimize the refrigerant circuitry (Brown *et al.*, 2013).

4.2 Brazed plate heat exchanger

Brazed Plate Heat Exchangers (BPHEs) are widely used in many application fields due to their compactness, their high efficiency in exchanging heat and their reliability in terms of low maintenance duties, long lifetime, safety in maintaining the two fluids separated, and high temperature and pressure resistance.
Furthermore BPHEs, which involve a reduction of the refrigerant charge of one order of magnitude as compared to the traditional tubular heat exchangers, are particularly interesting for limiting the risk of flammable or mildly flammable refrigerants such as HFOs Palm (2007). In fact the first attempt to reduce the risk of flammable refrigerants is to decrease the refrigerant charge.

4.2.1 Vaporization

In this thesis R1234ze(E) and R32 data during vaporization inside a BPHE have been presented in section 3.2.1.1.
Following this data will be compared against other data collected in the same test rig under the same working conditions using R134a, R1234yf and R410A as refrigerants. These latter data are presented in Longo and Gasparella (2007c), Longo (2012b), and Longo and Gasparella (2007b), respectively.

4.2.1.1 R134a vs. R1234ze(E) and R1234yf

The thermal and hydraulic performance of R1234ze(E) and R1234yf are going compared against those of R134a in the following.
In Table 36 are reported the main thermophysical properties of the three fluids evaluated at 20 °C (Refprop 9.1, 2013), but it should be interesting underlining some comparisons:

- R134a pressure is around 33% higher than R1234ze(E) and 4% lower than R1234yf, and also reduced pressure follows this ranking. So, theoretically, R134a pressure drops will be placed among the ones of the two HFOs with the R1234yf ones lower than the others;

- R134a liquid thermal conductivity, a property that affects the heat transfer coefficient, is 5% higher than R1234ze(E) and 21% higher than R1234yf;
- other relevant differences are to be found in the vapor density – R1234yf has the highest one, 18% higher than R134a and 31% higher than R1234ze(E) – and in the surface tension where R1234ze(E) has the highest one, 9% higher than R134a and 28% higher than R1234yf);
- finally the R1234yf latent heat of vaporization is the lowest one (-18% than that of R134a) and the Volumetric Cooling Capacity (VCC) is similar for R134a and R1234yf but it is lower for R1234ze(E) (-25%) that implies it cannot be used as direct drop in replacement.

Figure 222 show the comparison between R1234ze(E) and R1234yf and R134a saturated boiling heat transfer coefficients and frictional pressure drops, respectively, at 20 °C. The fluids were compared as a function of heat flux (Figure 221) and mass flux (Figure 222).

Table 36 Thermophysical properties of R134a, R1234yf, and R1234ze(E) at 20 °C.

Refrigerant	**R134a**	**R1234yf**	**R1234ze(E)**
p in [bar]	5.72	5.92	4.27
p * [-]	0.1408	0.1750	0.1175
λ_L [W m^{-1} K^{-1}]	0.0833	0.0652	0.0796
λ_G [W m^{-1} K^{-1}]	0.0133	0.0135	0.0132
c_{pL} [J kg^{-1} K^{-1}]	1404.86	1369.30	1369.77
ρ_L [kg m^{-3}]	1225.33	1109.86	1179.26
ρ_G [kg m^{-3}]	27.78	32.80	22.61
μ_L [Pa s]	2.07E-04	1.65E-04	2.11E-04
μ_G [Pa s]	1.15E-05	1.20E-05	1.20E-05
σ [N m^{-1}]	8.69E-03	6.77E-03	9.50E-03
Δh_{LG} [kJ kg^{-1}]	182.28	149.29	170.63
VCC [kJ m^{-1}]	5064	4896	3857

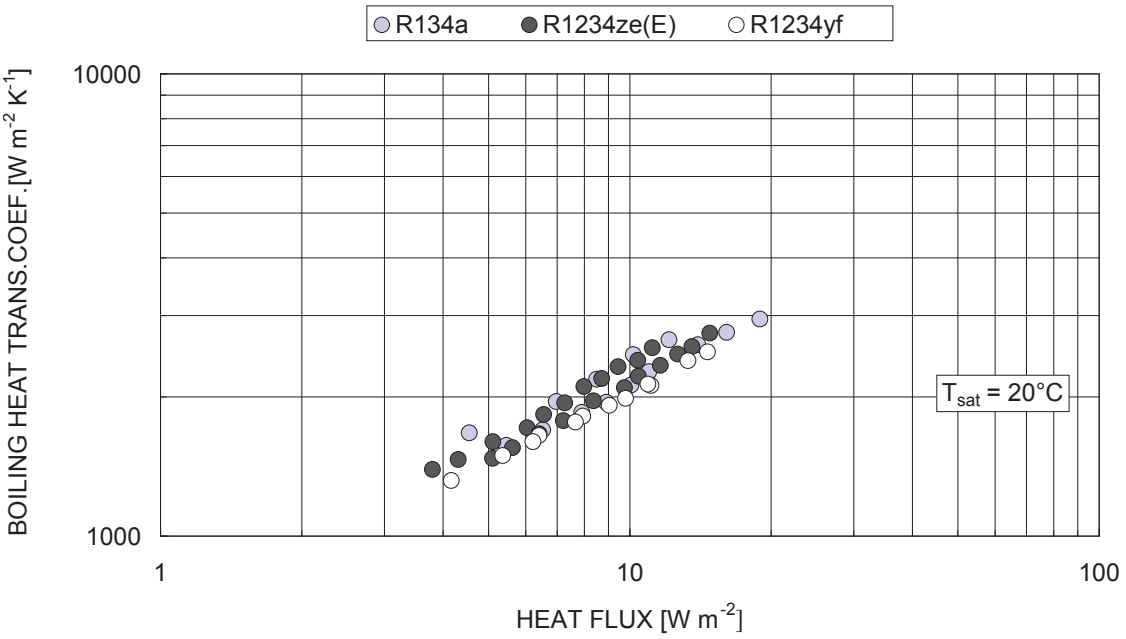

Figure 221 Comparison between R1234ze(E), R1234yf and R134a saturated boiling heat transfer coefficients inside a BPHE at 20°C.

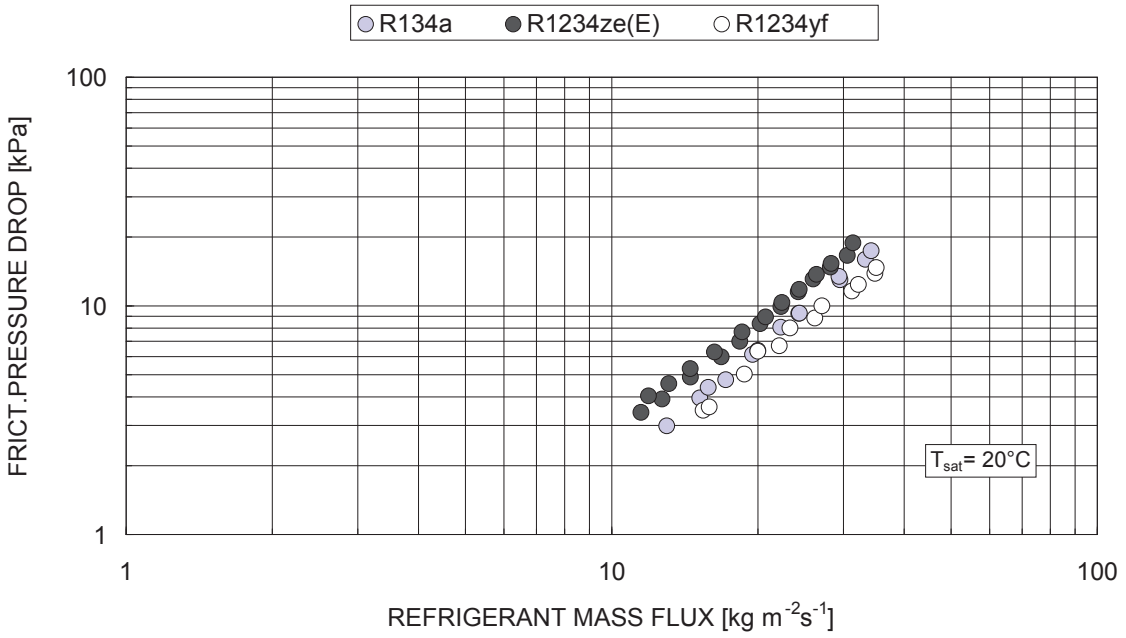

Figure 222 Comparison between R1234ze(E), R1234yf and R134a frictional pressure drop inside a BPHE at 20°C.

R1234ze(E) exhibits heat transfer coefficients very similar to R134a, while the R1234yf heat transfer coefficients are around 6-8% lower than those of R134a.
Despite having a similar slope, R1234ze(E) frictional pressure drops are around 23% higher than R134a, while R1234yf ones are slightly lower (around 10-18%) than R134a ones. This confirm the previous hypothesis based on the thermophysical properties that suggested that the higher pressure drop with R1234yf are due to the lower reduced pressure and higher vapor specific volume.

4.2.1.2 R410A vs. R32

R32 has already been used as low GWP R410A replacement, especially in residential and commercial air conditioning, but it could also be used in medium size chillers and residential heat pumps. In these applications BPHE are commonly used to make the systems more compact and to reduce the refrigerant charge. R32, which is classified as mildly flammable by ASHRAE (2013b), could benefit of a charge reduction and so its use is to be taken into account.
In this section R32 is going to be compared against R410A during vaporization inside a BPHE.
In Table 34 are reported the main thermophysical properties of this two fluids evaluated with Refprop 9.1 (2013) at 5, 10, and 20 °C. It could be interesting to remind that the two fluids have similar pressures but R32 has a lower reduced pressure (-15%), higher liquid thermal conductivity (+40%), higher specific heat (+15%), and higher vaporization latent heat (+40%) with respect to R410A.
Figure 223 presents the R32 and R410A heat transfer coefficient as a function of the heat flux at 20 °C of saturation temperature.
The R32 HTCs are on average 20-30% lower than the R410A ones, probably mainly due to the lower reduced pressure, a property that significantly influences the boiling heat transfer coefficient.
Figure 224 presents the R32 and R410A pressure drop as a function of the heat flux at 20 °C of saturation temperature.
R32 pressure drops are 30- 40% higher than those of R410A. Also this behavior can be explained with the R32 reduced pressure (-14% than R410 at 20 °C).

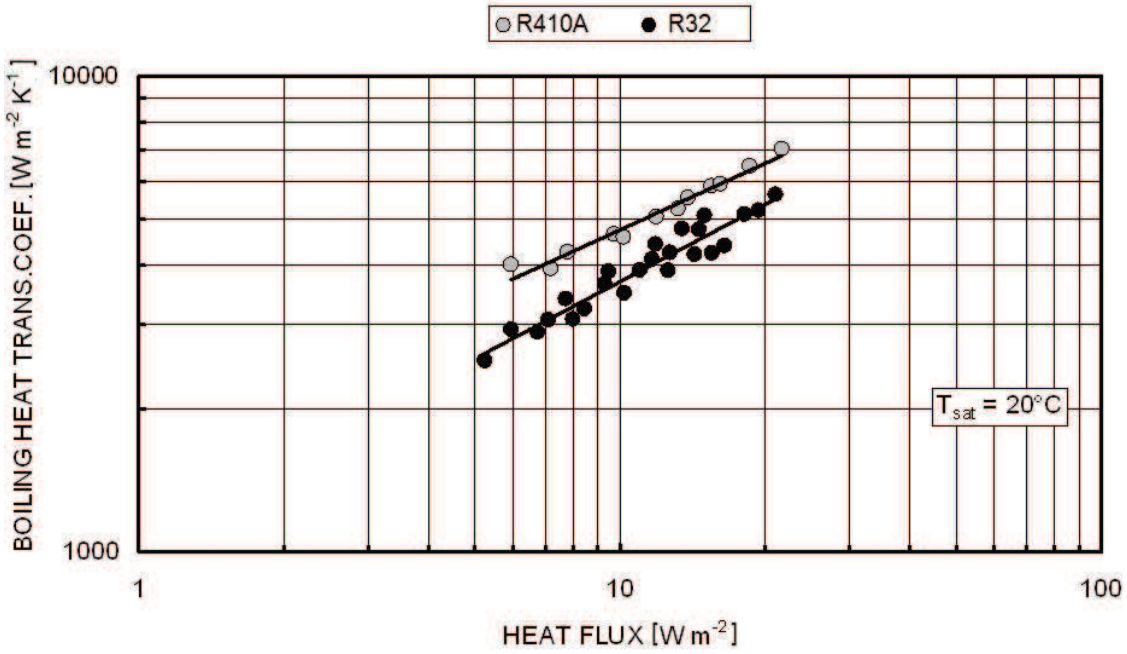

Figure 223 R32 and R410A heat transfer coefficient as a function of the heat flux at t_{sat}=20 °C.

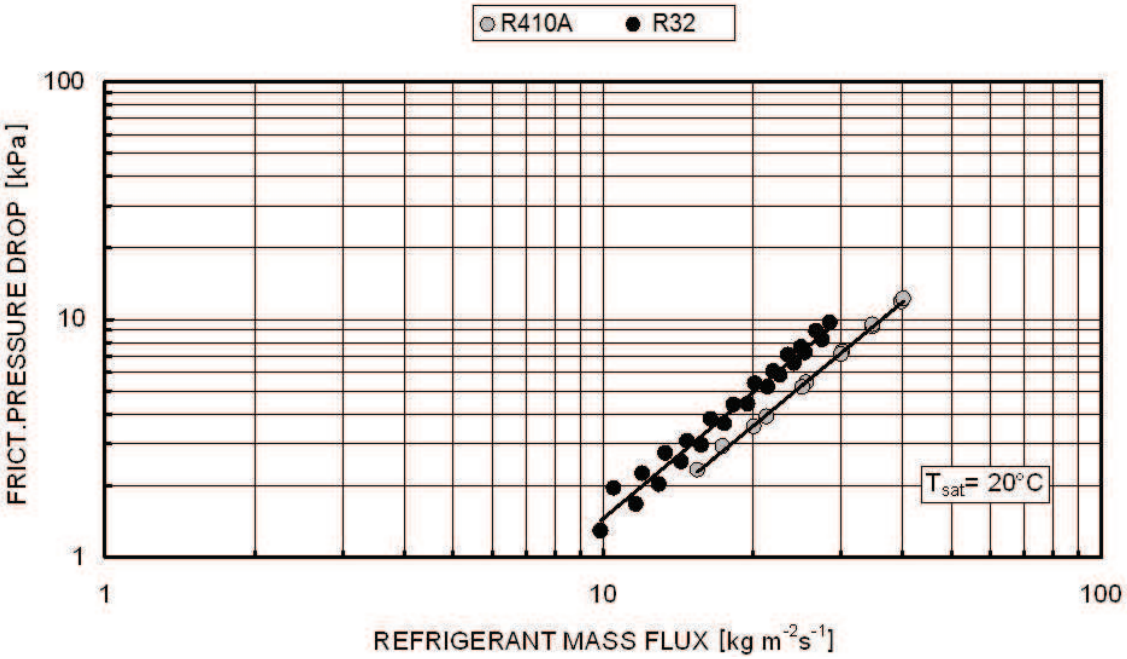

Figure 224 R32 and R410A pressure drop as a function of the heat flux at t_{sat}=20 °C.

4.2.2 Condensation

Four different refrigerants, namely R1234ze(E), R1234ze(Z), R152a, and R32, were tested during the condensation process inside a BPHE and the data obtained were reported in section 3.2.1.2.
The heat transfer performance and the pressure drop of these fluids were compared against the ones of other refrigerants (i.e. R134a, R1234yf, R290, R236fa, R600a, and R410A) under the same working conditions.

4.2.2.1 Air conditioning systems: R134a vs. R1234ze(E) and R1234yf

As introduced in section 4.2.1.1, R1234ze(E) and R1234yf are candidate to substitute R134a in air conditioning systems due to their interesting thermophysical properties, not so far from the R134a ones, and their low GWP value as presented in the previous paragraph.
In this section the heat transfer and hydraulic performances of the new HFOs refrigerants R1234ze(E) and R1234yf will be compared against those of R134a during condensation inside a BPHE.
The data of R1234ze(E) were presented in paragraph 3.2.1.2, while the ones of R134a and R1234yf, collected under the same working conditions, were published in Longo (2008) and Longo and Zilio (2013), respectively.
Figure 225 presents a comparison between R1234ze(E) heat transfer coefficients and R134a and R1234yf ones at different condensation temperatures, namely 25 °C, 30 °C, 35 °C, and 40 °C.
At a first glance, the global trend of HTC as a function of mass flux is similar for all the three tested refrigerants. R1234ze(E) heat transfer coefficients are slightly lower (4 to 6%) than those of R134a and slightly higher (4 to 6%) than those of R1234yf under the same operating conditions. This can be attributed mainly to the liquid thermal conductivity of R1234ze(E): lower with respect to R134a, but higher with respect to R1234yf.
Figure 226 presents a comparison between R1234ze(E) pressure drop and R134a and R1234yf ones at different condensation temperatures, namely 25 °C, 30 °C, 35 °C, and 40 °C.

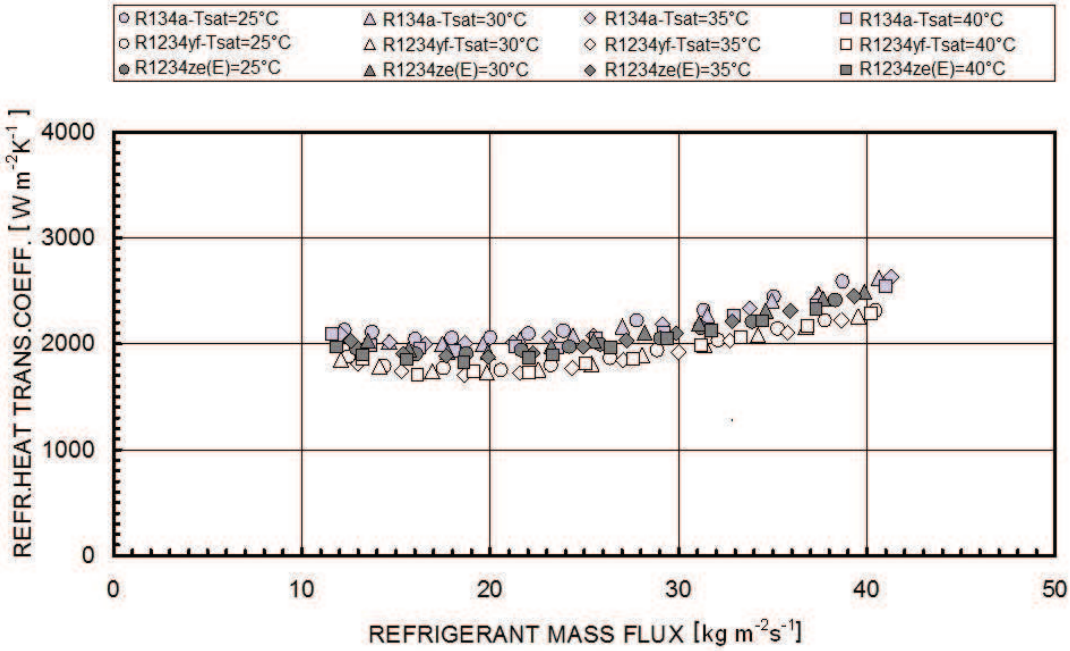

Figure 225 Comparison between R1234ze(E), R1234yf, and R134a condensation heat transfer coefficients vs. mass flux inside the tested BPHE.

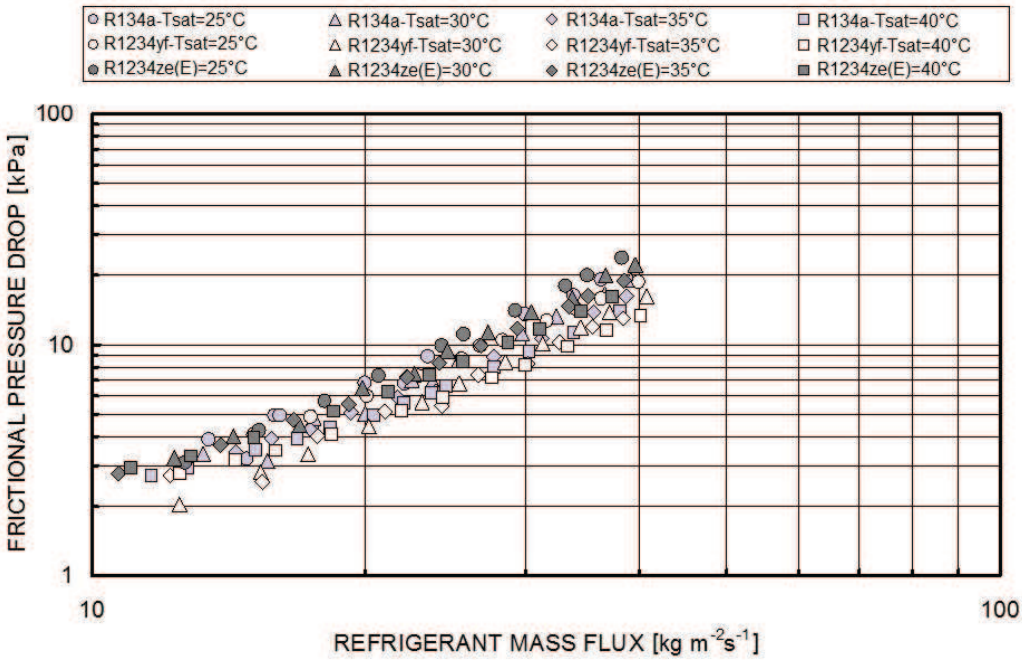

Figure 226 Comparison between R1234ze(E), R1234yf, and R134a frictional pressure drop during condensation vs. mass flux inside the tested BPHE.

The R1234ze(E) frictional pressure drops are higher both than those of R134a (10%) and those of R1234yf (20%) under the same operating conditions.
This can be explained due to the lower reduced pressure of R1234ze(E) with respect to the other refrigerants (around -25% at 40 °C).

4.2.2.2 Large chillers applications: R134a vs. R290, R1234ze(E) and R152a

In this section will be carried out a comparison between R134a and some candidates to replace it: a low GWP HFC, the R152a, one HC, the R290, and one HFO, the R1234ze(E).
One of the most promising R134a substitute in large chiller application with particular reference to turbo and screw compressor chillers seems to be the R152a due to its favorable thermodynamic properties.
In fact, a first simple thermodynamic assessment of refrigerants for large chiller application can be based on the properties reported in Table 37 where the critical temperature T_{crit}, the critical pressure p_{crit}, the saturation pressure p_{sat} at 5 °C, latent heat of vaporization Δh_{LG} at 5 °C (Refprop 9.1, 2013), the Volumetric Cooling Capacity (VCC), some efficiency data, such as the Coefficient of Performance (COP) for a simple vapor compression cycle (COP1) and for a vapor compression cycle with regenerative heat exchanger between liquid and suction lines (COP2) are shown.
The following assumptions were made for the reference vapor compression cycles:
– 5 °C evaporation temperature and 40 °C condensation temperature,
– no condenser sub-cooling and evaporator super-heat except for R1234ze(E),
– 3 °C evaporator superheat, that is the minimum to avoid wet isentropic compression, only with R1234ze(E),
– 100% compressor isentropic efficiency,
– 50% regenerative heat exchanger effectiveness,
– no evaporator, condenser and refrigerant lines pressure drop.
All the refrigerant properties were evaluated by Refprop 9.1 (2013).

Table 37 Comparison between different refrigerants for large chiller application.

Fluid	T crit	P sat	VCC	COP1	COP2
	[°C]	[bar]	[kJ m^{-3}]	[-]	[-]
R134a	101.0	3.497	3336	6.547	7.285
R1234ze(E)	109.3	2.593	2521	6.547	7.289
R290	134.6	5.513	4404	6.421	7.206
R152a	145.6	3.148	2988	6.796	7.268

R152a exhibits COP1 higher (+4%) and COP2 similar to R134a, R1234ze(E) presents both COP1 and COP2 almost similar to R134a, and R290 shows both the COP lower (-2%) than R134a. R290 presents VCC notably higher (+32%) than R134a, R152a shows VCC lower (-10%) than R134a, and R1234ze(E) exhibits VCC significantly lower (-25%) than R134a.

In spite of its slight flammability, R152a could be a low GWP substitute for R134a under a thermodynamic point of view, not only in domestic refrigerators and automotive air conditioning systems, but also in large chiller application.

Figure 227 presents a comparison between R134a heat transfer coefficients and R1234ze(E), R290 and R152a ones at different condensation temperatures, namely 25 °C, 30 °C, 35 °C, and 40 °C.

The data of R1234ze(E) and of R152a are presented as a function of the mass flux in section 3.2.1.2, while the ones of R134a and R290 were collected under the same working conditions and presented in Longo (2008) and Longo (2010b), respectively.

On average R152a exhibits heat transfer coefficients higher than those of all the other refrigerants considered in this paragraph, +19% than R134a, +13% than R290, and +23% than R1234ze(E).

The R152a high liquid thermal conductivity and latent heat of vaporization can be the main drivers of this behavior. In fact, for example at 40 °C, R152a exhibits a liquid thermal conductivity 23% higher than R134a, 25% higher than R1234ze(E) and 6% higher than R290. In addition it has a latent heat of condensation 59% higher than R134a, 68% higher than R1234ze(E), and 18% lower than R290.

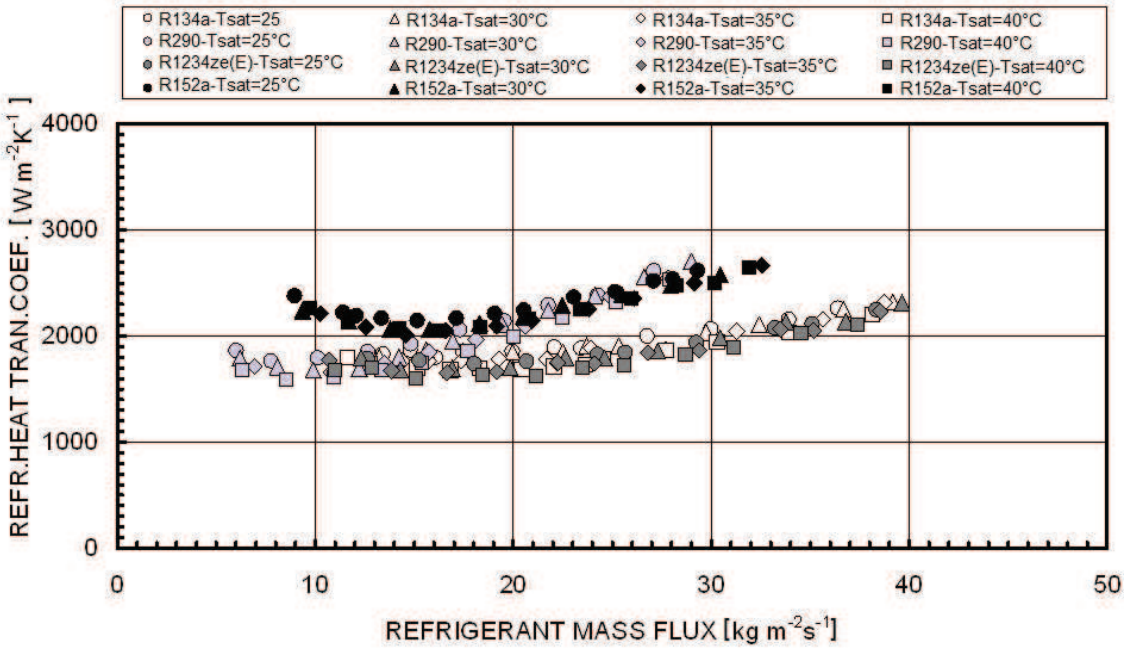

Figure 227 Comparison between R134a and R1234ze(E), R290, and R152a heat transfer coefficients vs. mass flux inside the tested BPHE.

Figure 228 presents a comparison between R134a pressure drop and R1234ze(E), R290 and R152a ones as a function of mass flux at different condensation temperatures, namely 25 °C, 30 °C, 35 °C, and 40 °C.

On average the slope of pressure drop at increasing mass flux is similar for all the refrigerants but R152a frictional pressure drop values are close to the R290 ones and lightly higher than R134a and R1234ze(E). This can be attributed mainly to the lower reduced pressure.

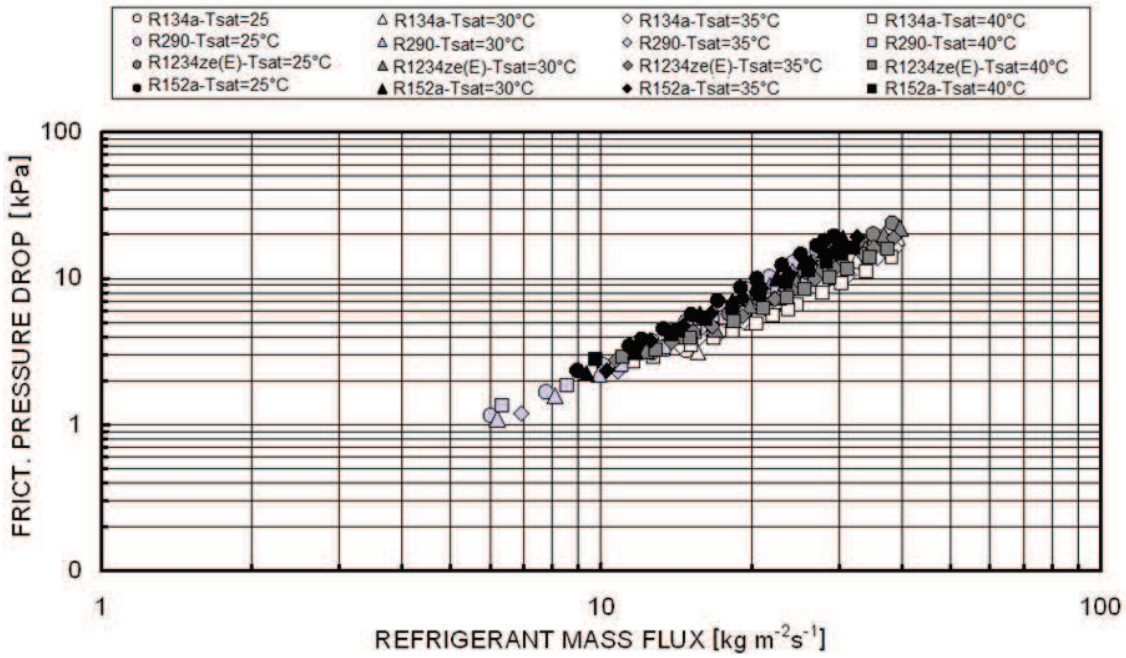

Figure 228 Comparison between R134a and R1234ze(E), R290, and R152a pressure drop vs. mass flux inside the tested BPHE.

4.2.2.3 High temperatures heat pumps: R134a, R236fa vs. R600a, R1234ze(E) and R1234ze(Z)

High-temperature heat pumps that work as hot dryers and steam generators for industrial purposes, such as concentration of beverages, sterilization of foods, drying lumber, solvent recovery, and distillation of petrochemical products are capable of increasing the temperature of the waste-heat source to a higher, more useful temperature. Therefore, replacing conventional combustion systems and electric heaters with heat pump systems can facilitate fuel savings and reduce CO_2 emissions (Fukuda *et al.*, 2014).

R1234ze(Z) is a potential refrigerant for high-temperature heat pumps, mainly due to its high critical temperature.

In this section it will be conducted a comparison between R1234ze(Z) and other refrigerants, namely R134a, R1234ze(E), R236fa, and R600a, during condensation inside a BPHE.

R236fa and R600a have been recently applied in high temperature heat pumps while R134a and R1234ze(E) are commonly used in medium temperature applications.

A summary table (Table 38) is proposed to analyze the thermophysical properties of these refrigerants evaluated with Refprop 9.1 (2013). The traditional CFC R114 was also added to set a target during the comparison.

R1234ze(E) has a relatively low critical temperature in comparison to R1234ze(Z), close to the R134a one. This is a limit in the use of these refrigerants that cannot condense at a temperature higher than 90 °C.

R236fa and R1234ze(Z) are the only fluids with a Volumetric Heating Capacity (VHC) similar to R114, whereas the other fluids display higher VHC values. A higher VHC value requires a change in the compressor design and so these fluids cannot be considered as candidates for drop-in replacement of R114. In addition, R1234ze(Z) exhibits the highest critical temperature. So, it seems to be very promising for high temperature heat pumps under a thermodynamic point of view.

Table 38 Comparison between different refrigerants for heat pump application.

Refrigerant	**R134a**	**R1234ze(E)**	**R1234ze(Z)**	**R600a**	**R236fa**	**R114**
Tcrit [K]	101.6	109.36	150.12	134.66	124.92	145.68
p in [bar]	10.17	7.66	2.9	5.31	4.37	3.38
p* [-]	0.25	0.211	0.082	0.146	0.136	0.104
λ_L [W m^{-1} K^{-1}]	7.47E-02	6.92E-02	8.46E-02	8.41E-02	6.84E-02	5.79E-02
ρ_L [kg m^{-3}]	1146.7	1111.5	1180.7	531.2	1306.5	1407.2
ρ_V [kg m^{-3}]	50.09	40.64	14.14	13.67	29.28	24.58
μ_L [Pa s]	1.61E-04	1.67E-04	2.33E-04	1.29E-04	2.36E-04	2.32E-04
μ_G [Pa s]	1.24E-05	1.29E-05	1.18E-05	7.91E-06	1.16E-05	1.12E-05
Δh_{LG} [kJ kg^{-1}]	163.02	154.8	196.36	311.52	136.36	121.96
VHC [kJ m^{-1}]	8165	6290	2776	4257	3993	2998

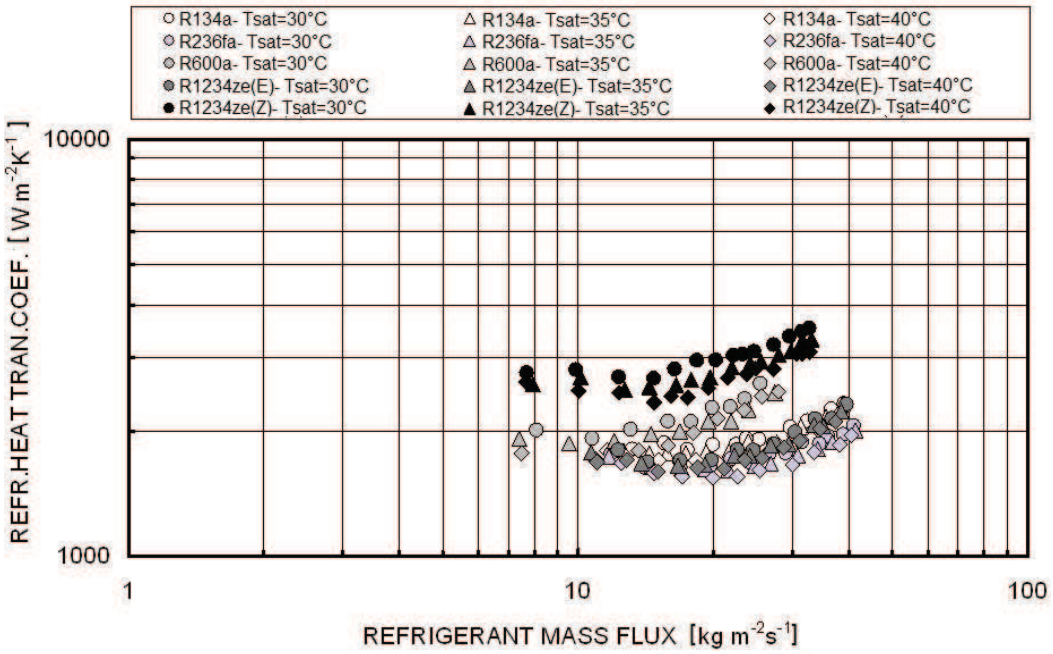

Figure 229 Comparison between R1234ze(Z) and other refrigerants heat transfer coefficients inside a BPHE.

Figure 229 presents the R1234ze(Z) heat transfer coefficient as a function of the refrigerant mass flux compared against HTCs of other refrigerants.

The heat transfer coefficients obtained with R1234ze(Z) are much higher than those obtained with all the other refrigerants analyzed in this paragraph. For example, at a condensation temperature of 40 °C, R1234ze(Z) shows heat transfer coefficients 35% higher than R600a, 65% higher than R134a, 72% higher than R1234ze(E), and 82% higher than R236fa. This is mainly due to the R1234ze(Z) higher liquid thermal conductivity, estimated by Brown *et al.* (2009) according to Sastri and Rao (2000) method (around +20% than R236fa and R1234ze(E), +12% than R134a) and latent heat of condensation, higher than all the other refrigerants, with the HC exception. The HTC trend is similar for all the HFC and HFO fluids, while the HC performs differently. In fact, as presented in section 3.2.2.2.2, the transition point between gravity controlled and forced convection condensation was found for an equivalent Reynolds number around 1600 which corresponds for the tested BPHE to a refrigerant mass flux around 20 kg $m^{-2}s^{-1}$ for HFC and HFO refrigerants and around 15 kg $m^{-2}s^{-1}$ for HC refrigerants. Figure 230 presents the refrigerant pressure drop as a function of the refrigerant mass flux for all the fluid considered in this section: R134a, R236fa, R600a, R1234ze(E), and R1234ze(Z).

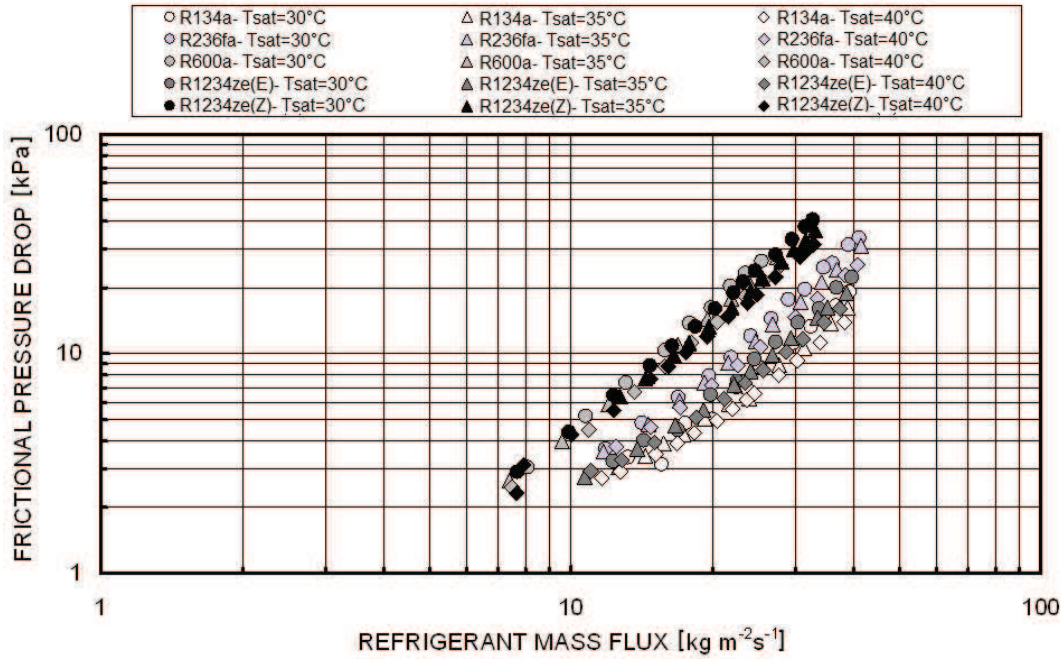

Figure 230 Comparison between R1234ze(Z) and other refrigerants pressure drop inside a BPHE.

The R1234ze(Z) frictional pressure drop is similar to R600a but higher than other refrigerants. For example at 40 °C R1234ze(Z) presents frictional pressure drop 5% lower than R600a but 166% higher than R134a, 125% higher than R1234ze(E), and 73% higher than R236fa. This can be attributed to the R1234ze(Z) lower reduced pressure with respect to the other refrigerants considered in the present comparative analysis (-78% R600a, -66% R236fa, -157% R1234ze(E), -205% R134a).

4.2.2.4 R410A vs. R32

In this section R32 heat transfer and hydraulic performances are going to be compared vs. R410A ones during condensation inside a BPHE. The vaporization process of these two fluids was already analyzed in paragraph 4.2.1.2.
Nowadays R32 has just been proposes and used as R410A replacement in residential and commercial air conditioners and medium size chillers and medium temperature applications.

Figure 231 shows the comparison between R32 heat transfer coefficients and those of R410A previously measured inside the same BPHE under the same operating conditions and presented in

Longo (2009) at different condensation temperatures (25 °C, 30 °C, 35 °C, and 40 °C) as a function of the refrigerant mass flux.

At the same mass flux and saturation temperature, R32 heat transfer coefficients are around 20% higher than those of R410A. This can be attributed mainly to the difference latent heat of vaporization and liquid thermal conductivity. For example, at 40°C R32 latent heat of condensation is 49% higher and the liquid thermal conductivity is 33% higher than those of R410A.

Figure 232 shows the comparison between R32 pressure drop and R410A ones as a function of the mass flux at different saturation temperatures (25 °C, 30 °C, 35 °C, and 40 °C).

The R32 frictional pressure drops, despite having a similar slope, are slightly higher than those of R410A. In fact R32 has a lower reduced pressure than R410A (-13% at 40 °C).

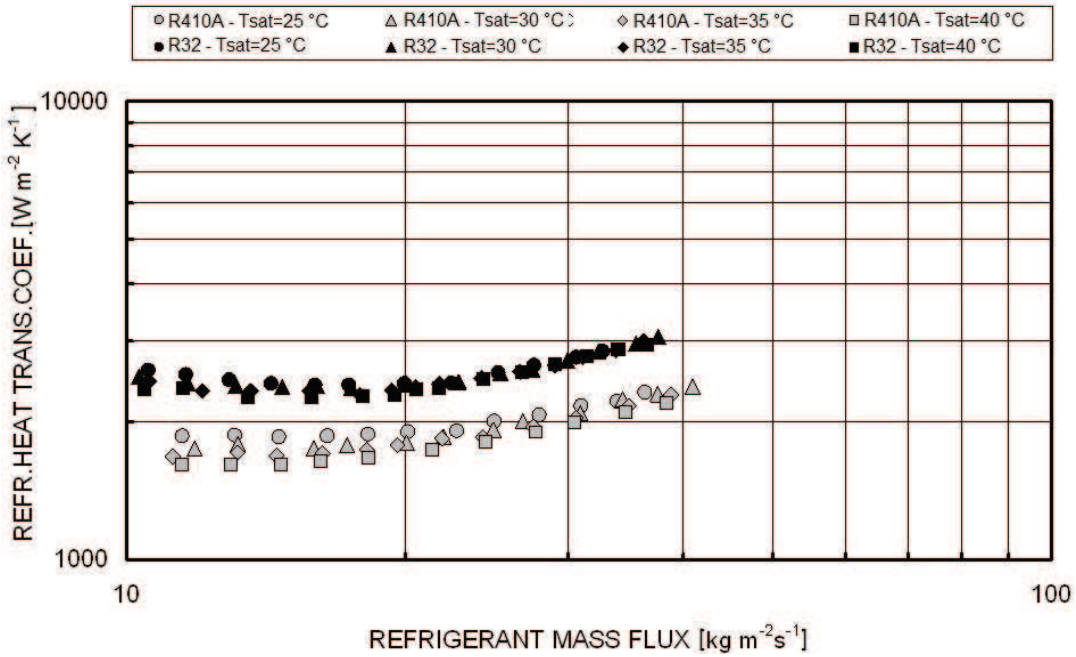

Figure 231 Comparison between R32 and R410A heat transfer coefficients vs. mass flux inside a BPHE.

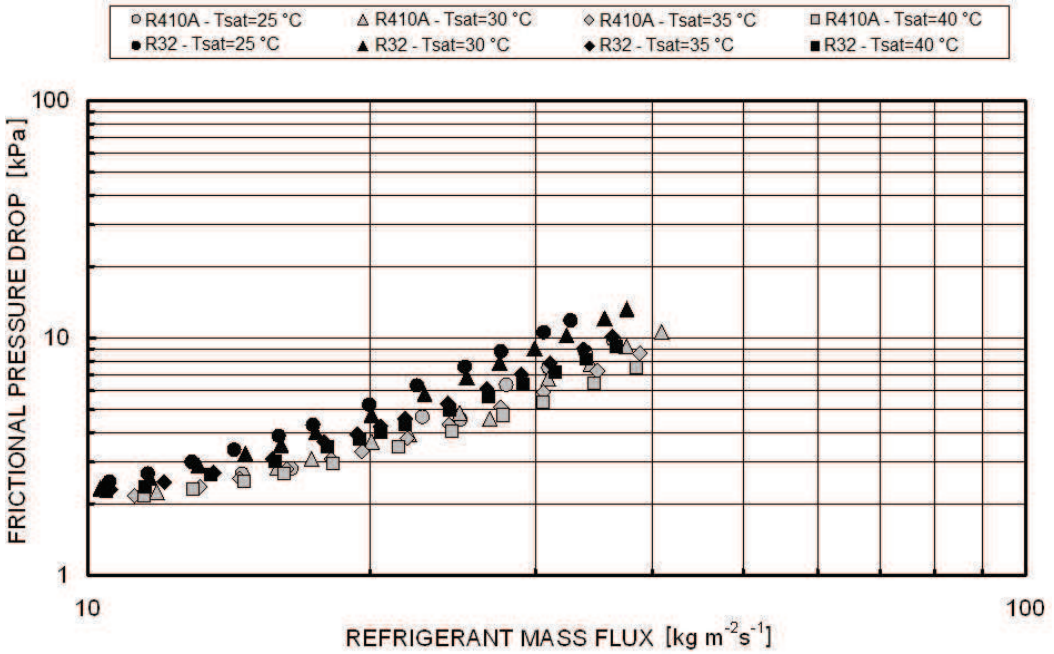

Figure 232 Comparison between R32 and R410A frictional pressure drop vs. mass flux inside a BPHE.

4.2.3 Performance evaluation criteria and penalization terms

Several performance evaluation criteria can be found in literature, but generally they are not applicable for two phase heat transfer. In fact, pressure drop in two-phase flow affects the working fluid saturation temperature, altering the heat transfer driving mean effective temperature difference, which cannot be ignored (Cavallini *et al.*, 2010).

An exhaustive analysis on the PEC applicable during a two phase flow inside tubes was made by Cavallini *et al.* (2000, 2001a, 2005, and 2010), Cavallini (2002), and Brown *et al.* (2013), but their study can be extended also to condensation and vaporization inside a brazed plate heat exchanger.

For taking into account the refrigerant saturation temperature drop, that affects the mean effective temperature difference (see paragraph 4.1.3), the local quantity to be optimized in the PEC is suggested to be Eq. 101, Cavallini *et al.* (2010).

$$\frac{dT_{sat}}{dx} = \frac{dT_{sat}}{dp_f}\frac{dp_f}{dz}\frac{dz}{dx}$$ Eq. 101

This quantity can be rewritten as Eq. 102, thanks to the Clausius-Clapeyron equation.

$$\frac{dT_{sat}}{dx} = \frac{G\ d\ T_{sat}}{4\ \alpha\ \Delta T_{dr}}\left(\frac{1}{\rho_L} - \frac{1}{\rho_G}\right)\frac{dp_f}{dz}$$ Eq. 102

In Eq. 102 two local energy penalization terms are contained: dT_{sat}/dx, which is associated with the frictional pressure drop of the refrigerant, and ΔT_{dr}, connected with the driving temperature difference for the heat transfer process.
During the shear dominated condensation process, for a specified refrigerant, saturation temperature, vapor quality, and geometry, Cavallini *et al.* (2000, 2001a, 2002, and 2005) showed that the product of the two penalization components can be expressed only as a function of α. In fact, under this working conditions both α and dp_f/dz can be considered independent of the local heat flux q.
This product was called Penalty Factor (PF) of the condensation process (Eq. 103).

$$PF = \frac{dT_{sat}}{dx}\ \Delta T_{dr} = \ \Delta T_{sr}\ \Delta T_{dr}$$ Eq. 103

Given a heat exchanger geometry, for the same value of α and q the heat transfer penalization term ΔT_{dr} is the same for all the refrigerants; thus, the PF becomes a useful tool for comparing among various fluids the relative frictional pressure drop penalizations and so for comparing the exergy losses associated with frictional pressure drop among various fluids.

4.2.3.1 Vaporization

To analyse the vaporization process inside a Brazed Plate Heat Exchanger (BPHE) it is here proposed an approach based on the Brown *et al.* (2013) Performance Evaluation Criteria (PEC).

This approach has been presented and used in section 4.1.3 to rank the refrigerant performance inside a plain circular tube and here it is going to be extended to the vaporization process in a BPHE. In fact a BPHE can be considered as a counter flow evaporator in which the idealized temperature profiles follow the general trend presented in Figure 216. Consequently, the definitions of refrigerant pressure drop, ΔT_{sr}, and of driving temperature difference, ΔT_{dr}, remain the same (see paragraph 4.1.3).
In this particular case the equation used to evaluate heat transfer coefficient is Eq. 76, proposed in section 3.2.2.1.1, which fits the experimental data within 4.7% (R32) and 7.1% (R1234ze(E).
So far as pressure drop is concerned, Eq. 104 is used to take into account the frictional pressure drops, while Eq. 41, Eq. 13, and Eq. 14 are utilized to calculate the gravity, the momentum, the inlet and outlet local pressure drops, respectively.

$$\Delta p_f = 1.85\ KE/V \qquad \text{Eq. 104}$$

where Δp_f are expressed in kPa and

$$KE/V = G^2/(2\ \rho_m) \qquad \text{Eq. 105}$$

Figure 233 represents the saturation temperature drop ΔT_{sr} linked to pressure drop as a function of the heat transfer coefficient α for a series of refrigerants.
The geometric parameter used in these relations are the ones of the real BPHE tested, reported in Table 10, the heat flux is equal to 10 kW m^{-2} and the thermophysical properties are evaluated with Refprop 9.1 (2013) at the mean temperature between inlet and outlet, where the inlet temperature is fixed equal to 20 °C and the outlet one depends on the pressure drops.
As debated in paragraph 4.1.3, a higher saturation temperature drop at the same heat transfer coefficient value is linked to a lower energetic and exergetic efficiency of the fluid itself.
For this reason refrigerants having lower saturation temperature drops are to be preferable.

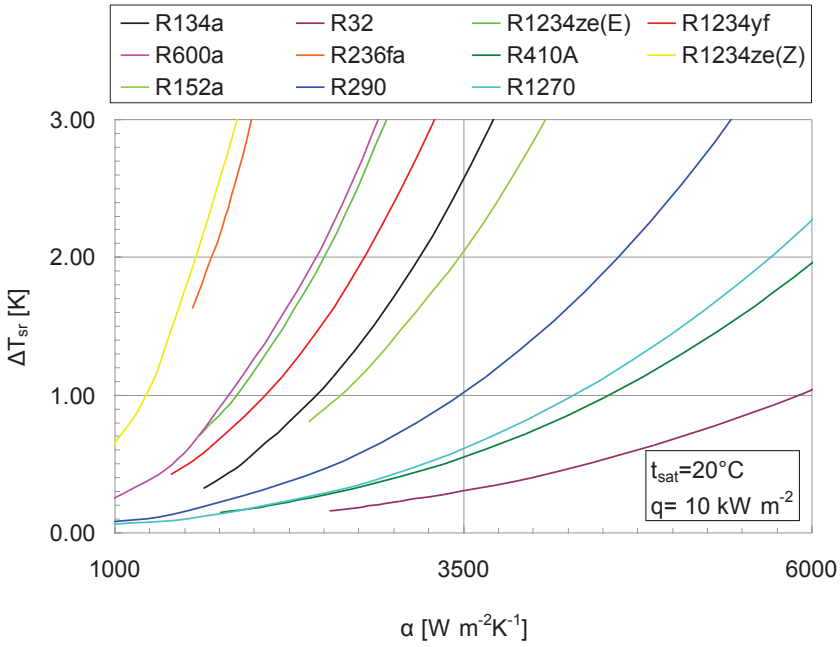

Figure 233 Saturation temperature drop as a function of the heat transfer coefficient for several refrigerants during evaporation inside a BPHE.

For the sake of clarity, in Figure 233 fluids are listed in this order (from the best one to the worst one): R32, R410A, R1270, R290, R152a, R134a, R1234yf, R1234ze(E), R600a, R236fa, and R1234ze(Z).

This ranking is not strictly linked to saturation pressure but, surely, saturation pressure is a useful parameter to discriminate the fluids. In fact, higher pressure refrigerants have smaller saturation temperature drop values than medium and lower pressure refrigerants. (See for example R32 and R410A vs. R1234ze(Z) and R236fa).

Focusing on the refrigerants experimentally tested during vaporization in this thesis (i.e. R1234ze(E) and R32, data presented in section 3.2.1.1) it is possible to notice that R32 is a good alternative to R410A on the basis of the saturation temperature drop. So, theoretically, it is going to have a lower penalization in terms of saturation temperature under the same heat transfer conditions.

The other refrigerant tested, R1234ze(E), has a higher saturation temperature drop than R134a mainly also due to its lower reduced pressure, so its global performance on the basis of this criterion is worse than the R134a one. On the contrary, in terms of environmental impact, R1234ze(E) has a really low GWP index, heat transfer coefficients comparable and pressure drop slightly higher than R134a, so it surely should be taken into account in the candidates to replace R134a.

4.2.3.2 Condensation

Similarly to what has been made for the vaporization process, a saturation temperature drop was defined also for the condensation process inside a Brazed Plate Heat Exchanger (BPHE).
It can be assumed that a BPHE during condensation works as an ideal counter-flow heat exchanger and so Figure 234 represents the idealized temperature profiles of refrigerant, surface and cooling medium that occur in it. The temperature differences ΔT_{sr} and ΔT_{dr} are another time highlighted due to they represent the penalization terms connected to the pressure drop and the driving temperature difference to the heat transfer.
On the base of the experimental results conducted and presented in this thesis, the correlation proposed in section 3.2.2.2.2 (Eq. 91) was used to evaluate the heat transfer coefficient during condensation, while Eq. 106 was used to calculate the frictional pressure drop (expressed in kPa).

$$\Delta p_f = 2\, KE/V \qquad \text{Eq. 106}$$

The total pressure drop used in the definition of saturation temperature drop is defined as Eq. 98.
Figure 235 represents the saturation temperature drop as a function of the heat transfer coefficient for several refrigerants.

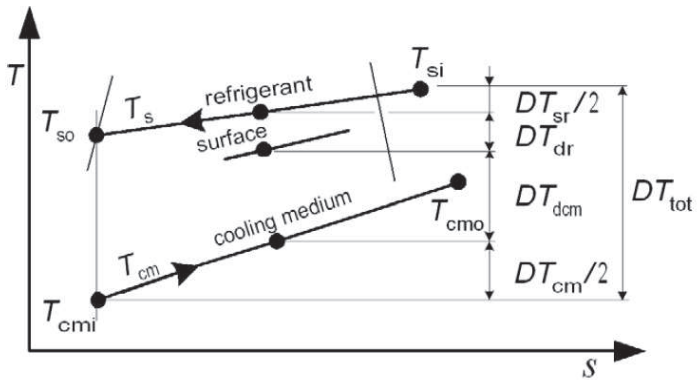

Figure 234 Idealized temperature profiles in a counter-flow condenser (Cavallini *et al.*, 2010).

The thermophysical properties are evaluated with Refprop9.1 (2013) at the mean temperature between the inlet at the condenser, 40 °C, and the outlet temperature that depends on the pressure drops. The heat flux is fixed equal to 10 kW m^{-2} and the geometric parameters are the same of the real BPHE tested ones (see Table 10). Due to the particular equation chosen to evaluate the heat transfer coefficient, only shear dominated condensation data are taken into account.

As for the vaporization case, the higher saturation temperature drop is, the lower the energetic and exergetic efficiency the fluid has. So, the refrigerants having low saturation temperature drops are to be preferable on the basis of this criterion.

Following the fluids investigated are listed from the one having the lower Δt_{sr} value in Figure 235 to the one having the higher one: R32, R410A, R290, R152a, R134a, R600a, R1234ze(E), R1234yf, R1234ze(Z), and R236fa.

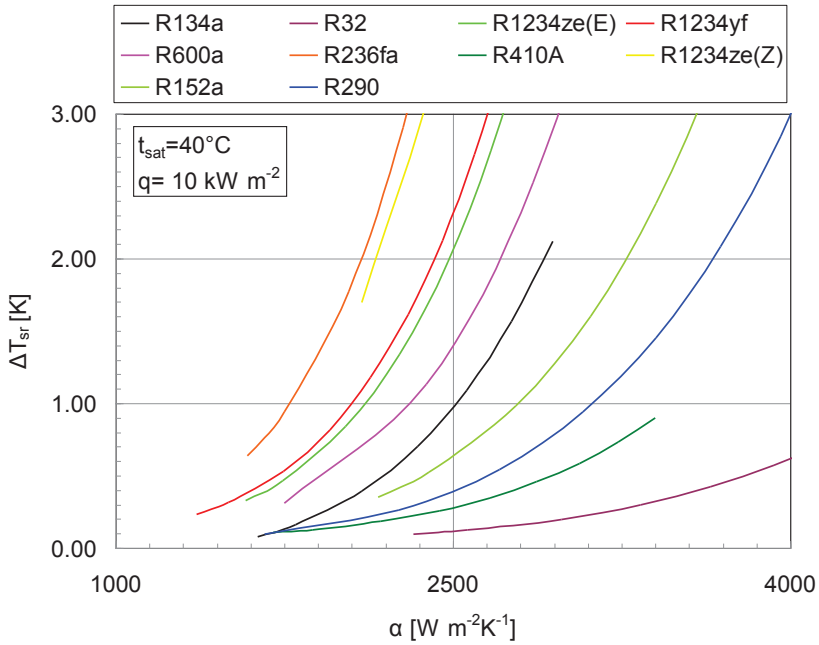

Figure 235 Saturation temperature drop as a function of the heat transfer coefficient for several refrigerants.

At a first glance, a fluid having a low saturation temperature drop during evaporation has also low ΔT_{sr} during condensation, but the ranking is not completely the same. In any case the higher pressure refrigerants group has smaller saturation temperature drop values than medium and lower pressure refrigerants.

Focusing on the refrigerants experimentally tested during condensation in this thesis (i.e. R152a, R1234ze(E), R1234ze(Z) and R32, data presented in section 3.2.1.2) it is possible to notice that:

- R152a and R1234ze(E) can be proposed as R134a substitutes. In terms of saturation temperature drop R152a is lightly better than R134a despite having a lower saturation pressure, while R1234ze(E) has higher ΔT_{sr} than R134a;
- R1234ze(Z) is a low pressure refrigerant and so its saturation temperature drop is strongly penalized. In a comparison among low pressure fluids, it shows a ΔT_{sr} lower than R236fa, so it can be consider as a fair alternative to R236fa;
- as presented for the vaporization process, the R32 ΔT_{sr} is lower than the R410A one also during condensation. Thus, the R32 energetic and exergetic efficiency should be higher than R410A.

In addition to the saturation temperature analysis, during the condensation process governed by shear stress it is possible to define a Penalty Factor (PF) as introduced in section 4.2.3 because the product between ΔT_{sr} and ΔT_{dr} is independent on the local heat flux q.

The PF combines the effects of pressure drop and heat transfer coefficient, so under these terms it is possible to conduct a more comprehensive analysis. At the same heat transfer coefficient value, a low PF implies lower penalizations to the heat transfer, so the smaller is the PF, the better is the performance potential of the refrigerant. (Cavallini *et al*., 2010).

Figure 236 presents the Penalty Factor as a function of the heat transfer coefficient during condensation governed by shear stress for several refrigerants.

The correlation used to evaluate the heat transfer coefficient is Eq. 91, while Eq. 98 is used for the pressure drop. The thermophysical properties are calculated with Refprop 9.1 (2013) at 40 °C. The heat flux is equal to 10 kW m^{-2} and the geometric parameters are the ones of the BPHE investigated in this thesis (see Table 10).

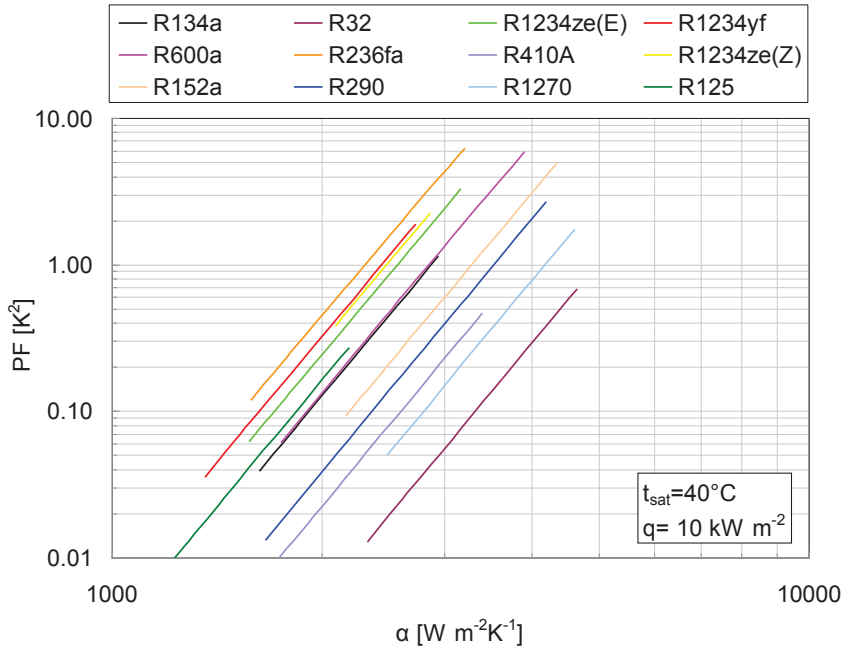

Figure 236 Penalty Factor (PF) as a function on the heat transfer coefficient during shear stress condensation for several refrigerants at t_{sat}=40 °C and q=10 kW m^{-2}.

R32 has PF lower than R410A in fact R410A is affected by the other component R125 having a higher PF value, while the HFOs group present PF values higher than R134a. That means that on the first hand proposing R32 as alternative to R410A is convenient under a refrigerant energetic and exergetic efficiency point of view, on the other hand substituting R134a with some HFOs can be less convenient and so to maintain a high efficiency it could be required an optimization of the heat transfer devices.

Generally, as for the ΔTt_{sr} analysis, fluids having high pressure have low PF and so they are preferable on the basis of this performance criterion.

Figure 237 plots the PF as a function of the critical temperature of several refrigerants at a fixed value of heat transfer coefficient α= 2500 $Wm^{-2}K^{-1}$, heat flux q=10 kWm^{-2} and saturation temperature t_{sat}=40 °C.

One can notice that the relation between PF and critical temperature is strong and that high critical temperature fluids (low reduced pressure) have high PF value. Of course, some kinds of applications require high critical temperature refrigerants, so this selection criterion could be overstepped.

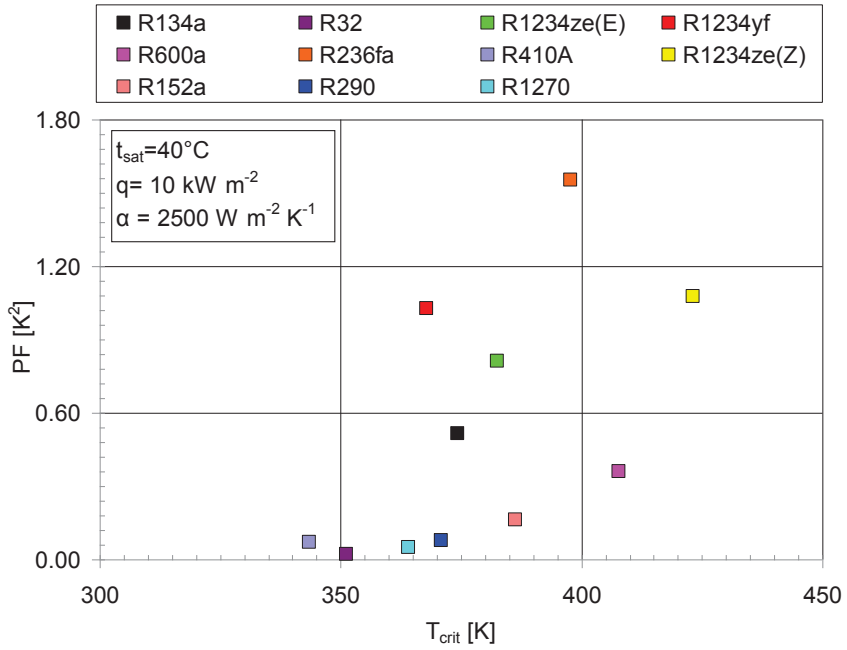

Figure 237 Penalty Factor (PF) as a function of the critical temperature at α= 2500 $Wm^{-2}K^{-1}$, q=10 kWm^{-2} and t_{sat}=40 °C.

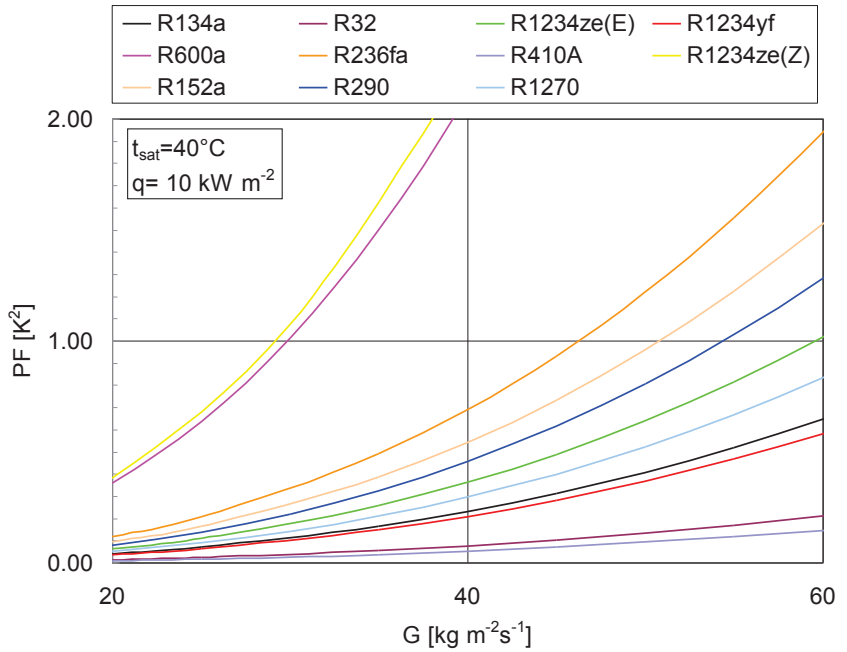

Figure 238 PF as a function of the refrigerant mass flux (kg $m^{-2}s^{-1}$) at q=10 kWm^{-2} and t_{sat}=40 °C.

Taking the same value of heat transfer coefficient means that the mass velocity is different moving from one refrigerant to another. For an engineering approach, it could be interesting comparing the fluids also at a constant value of mass flow rate. By increasing the mass velocity, higher heat transfer coefficients are obtained but, consequently, also higher frictional pressure gradients. So it is important to consider not only the pressure drop itself but the global energy penalization (e.g. PF)

Figure 238 presents the PF as a function of the refrigerant mass velocity. The PF is evaluated as previously explained at a saturation temperature of 40 °C and a heat flux of 10 kW m^{-2}.

The refrigerant ranking is slightly different from Figure 236. Here the refrigerants having high latent heat of condensation are less promoted. In fact R600a is relegated together with R1234ze(Z) at the top of the PF value list. Furthermore R1234yf seems to be a very promising fluid, even better than R134a and R32 becomes a little bit worse than R410A if compared at the same mass flux value. But the most of the times a refrigerant substitution has to be made guaranteeing the same heating (or cooling) capacity, so the analysis presented in Figure 238 as a function of refrigerant mass flux is as not as relevant as the one presented in Figure 236.

4.3 Roll-bond evaporator

As presented in section 1.5.3, roll-bond evaporators are commonly used inside domestic refrigerators. In the last decades, among the fluids proposed as refrigerants, R134a (GWP around 1430) has dominated this type of application. But, since the approval of some laws that limit the high GWP refrigerant use (e.g. in Europe the F-Gas regulation limits the use of refrigerants with GWP>150 in new domestic refrigerators from January 2015), other fluids should have been adopted.

The HydroCarbons (HCs) are already spread in Europe and Asia as working fluid in small domestic refrigerators and drink-coolers, but they are flammable (see 1.3).

On the other hand some HydroFluoroOlefins (HFOs), for example R1234yf and R1234ze(E), that are mildly flammable (A2L), are suitable candidates to be a direct replacement of R134a.

In this section it is going to be done a comparison between experimental data obtained with different refrigerants under the same working conditions. R134a, two HFOs: R1234ze(E) and R1234yf, and two HCs: R600a and R600 are investigated. All the data are presented in section 3.3.

The first comparison is executed as a function of the refrigerating capacity. In fact it is fundamental to compare different refrigerants at the same refrigerating capacity to highlight how they perform.

Figure 239 presents the overall heat transfer coefficient (K) as a function of the refrigerating capacity at two evaporation temperatures (-15 °C and -20 °C) for all the refrigerant tested.

At a first glance there are no big differences between the fluids under the same working conditions mainly due to the fact that the air side is the dominant heat transfer resistance. It is quite obvious remarking the effect of the saturation temperature, which is similar for all the refrigerants tested. An evaporation temperature of -20 °C shows an overall heat transfer coefficient up to 25% lower than an evaporation temperature of -15 °C.

After that, one can notice that the overall HTC is almost a linear function of the refrigerating capacity, except for the HCs (especially R600 and R600a at t_{evap}=-15 °C) which show an increment more than linear at high refrigerating capacities.

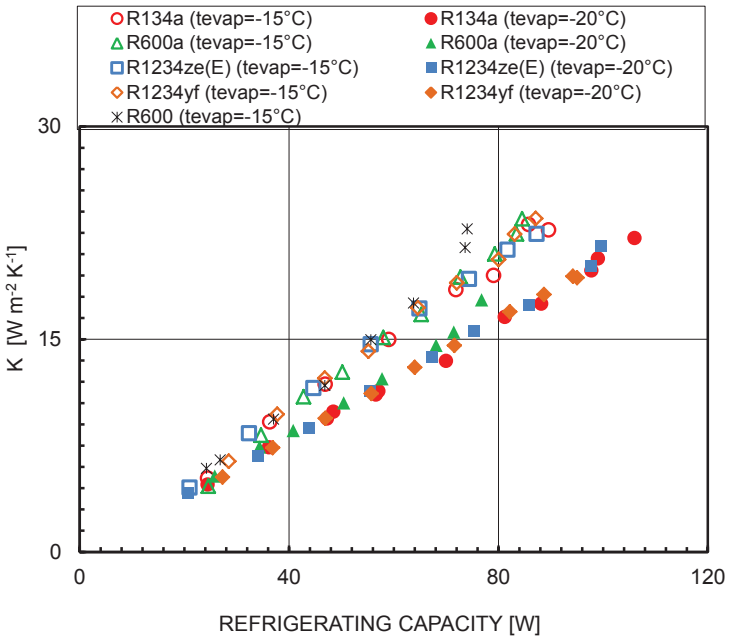

Figure 239 Overall heat transfer coefficient (K) as a function of the refrigerating capacity at two evaporation temperatures (-15 °C and -20 °C).

Figure 240 presents the refrigerant heat transfer coefficient α_r as a function of the refrigerating capacity at two evaporation temperatures (-15 °C and -20 °C) for all the refrigerant tested. Figure 241 presents the same data on a linear y axis.

Another time the differences between the refrigerants are limited. As for K, a lower saturation temperature brings to lower refrigerant side heat transfer coefficients (up to around 3 times lower passing from -20°C to -15 °C of saturation temperature).

The refrigerant HTC is not linear to the refrigerating capacity, but it increases asymptotically at low refrigerating capacities and more than linear at high refrigerating capacities. The trend of this function is opposite at the one of the percentage of superheating area of the plate when the refrigerant mass flow ratio increases. (from Figure 169 to Figure 173) because the refrigerant HTC depends on the super heating area (Eq. 46).

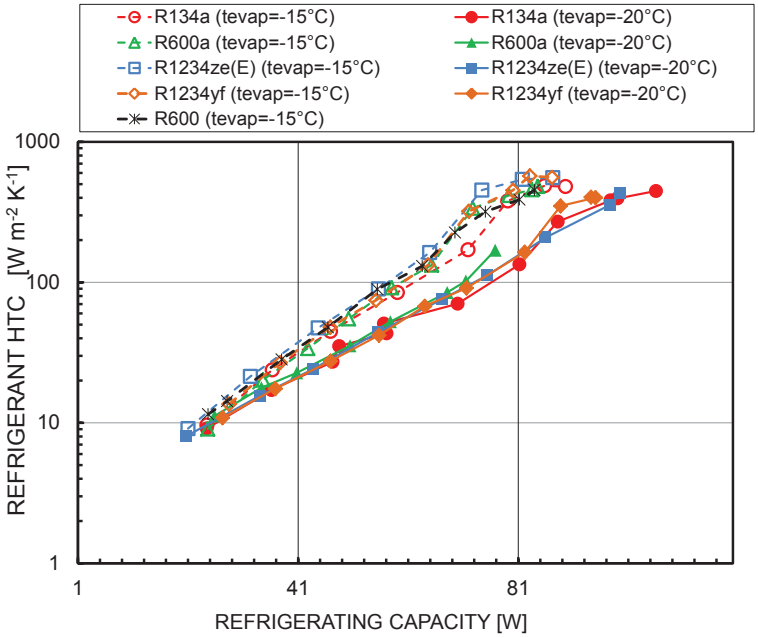

Figure 240 Refrigerant Heat Transfer Coefficient (HTC) as a function of the refrigerating capacity at two evaporation temperatures (-15 °C and -20 °C).

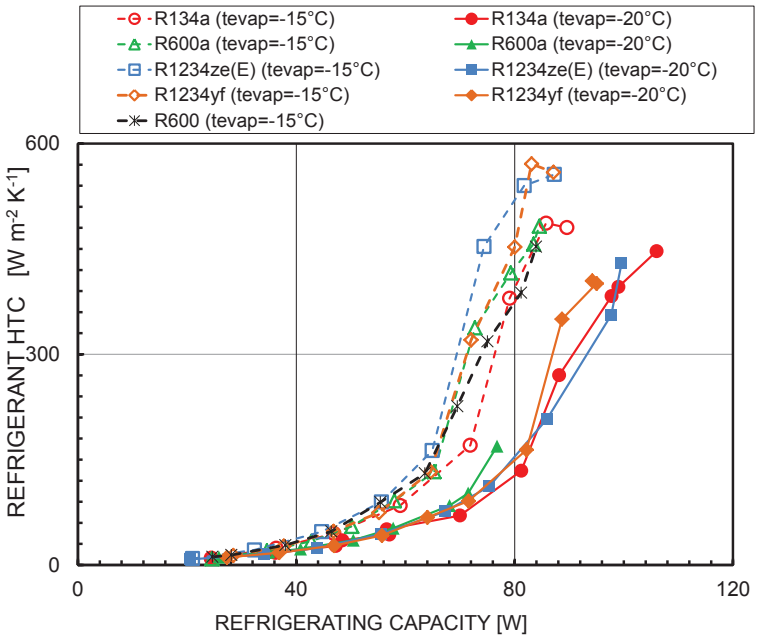

Figure 241 Refrigerant Heat Transfer Coefficient (HTC) as a function of the refrigerating capacity at two evaporation temperatures (-15 °C and -20 °C).

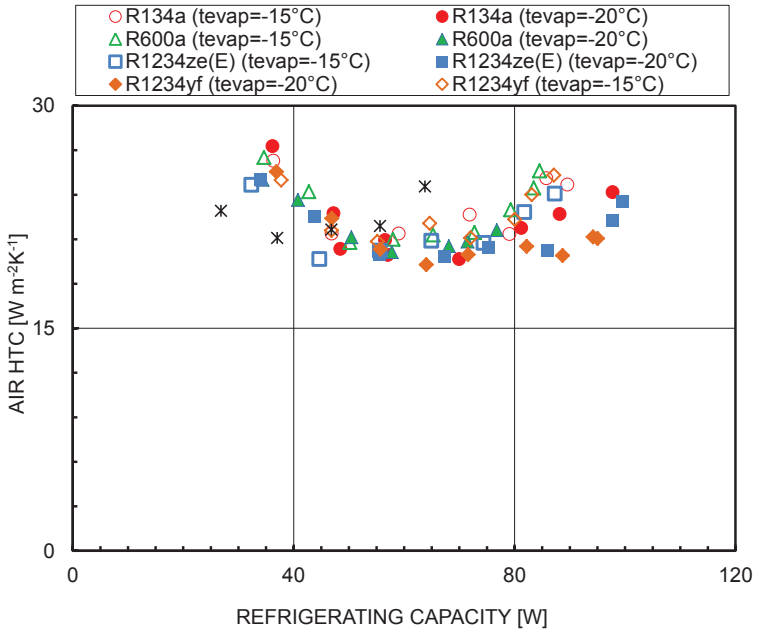

Figure 242 Air Heat Transfer Coefficient (HTC) as a function of the refrigerating capacity at two evaporation temperatures (-15 °C and -20 °C).

Figure 242 presents the air Heat Transfer Coefficient (HTC) as a function of the refrigerating capacity at two evaporation temperatures (-15 °C and -20 °C) for all the refrigerant tested.

The air side HTC does not depend strongly on the refrigerating capacity, on the saturation temperature and on the refrigerant type. It grows at low and high refrigerating capacities while it slightly decreases at refrigerating capacities included from 40 to 80 W. One can assume it as a quite constant value around 22 W m^{-2} K^{-1}, which is given by the average of all the experimental data collected.

Figure 243 presents the pressure drop through the evaporator as a function of the refrigerant mass flow rate at two evaporation temperatures (-15 °C and -20 °C) for all the refrigerant tested.

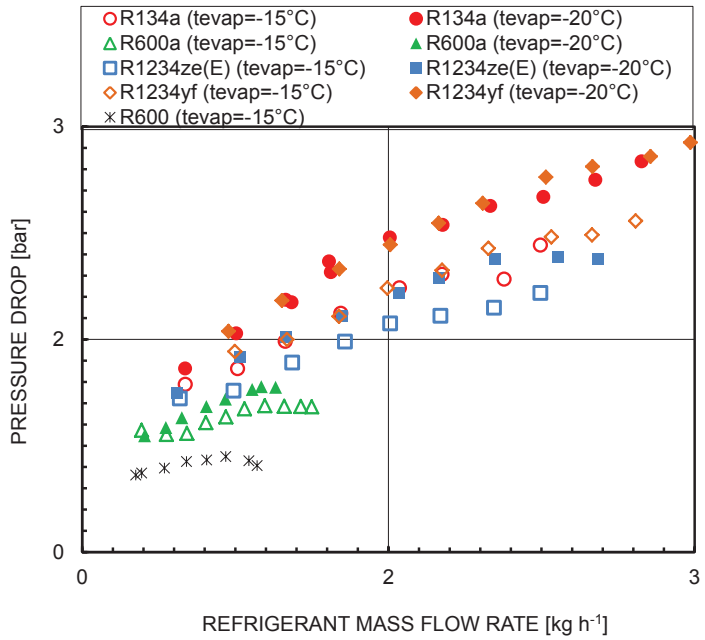

Figure 243 Pressure drop vs. refrigerant mass flow rate at two evaporation temperatures (-15 °C and -20 °C).

Lower evaporation temperatures cause higher pressure drop due to a lower pressure that implies lower density, so higher vapor velocity and thus higher pressure drop.

At the same refrigerant mass flow rate the HC refrigerants, especially the R600, induced to lower pressure drop than the other refrigerants. In addition they permit to work with lower refrigerant mass flow rate, (mainly due to their high latent heat, as shown in Table 4).

This fact can be highlighted by analyzing the refrigerant mass flow rate required to reach a determined heat flow rate.

Figure 244 presents the refrigerating capacity as a function of the refrigerant mass flow rate at two evaporation temperatures (-15 °C and -20 °C) for all the refrigerant tested.

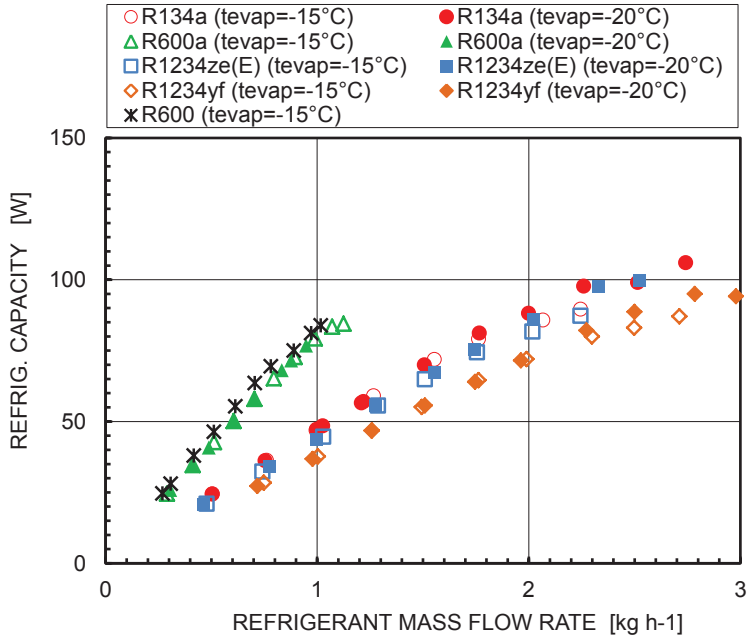

Figure 244 Refrigerating capacity vs. refrigerant mass flow rate at two evaporation temperatures (-15 °C and -20 °C).

The HC fluids need a refrigerant mass flow rate significantly lower than the other fluids tested. For example at 1 kg h^{-1} it can be obtained a cooling capacity around 80 W with an HC, while with the other tested refrigerants the cooling capacity achievable is lower than 50 W.

It is well known that it is possible to reduce the refrigerant charge using HCs instead of R134a or HFOs (Palm, 2008; Poggi *et al.*, 2008; and Mohanraj *et al.*, 2009b) and also in this application, the refrigerant charge can be reduced up to three times using a HC fluid.

After that it could be interesting also to analyze the maximum refrigerant flow rate, which is the flow rate required exchanging the maximum refrigerant capacity corresponding to saturated vapor conditions at the evaporator exit and so the flow rate that makes the super heating area approaching to zero. This value is reported in Table 39 for all the refrigerants tested. As can be seen by Figure 244 and Table 39, the maximum refrigerant flow rate is similar for R134a and for the two HFOs, while it is approximately 2.5 times lower for the HCs. This aspect can be highlighted by Figure 245, which presents the refrigerating capacity as a function of the refrigerant mass flow ratio defined as the ration between the refrigerant mass flow rate and the maximum refrigerant mass flow rate reached in the particular set of tests.at two evaporation temperatures (-15 °C and -20 °C) for all the fluids tested.

Table 39 Maximum refrigerant flow rate during vaporization tests inside a roll-bond type evaporator.

Refrigerant	**Evaporation temperature**	**Max refrigerant flow rate**
	[°C]	[kg h^{-1}]
R134a	-15	2.24
R134a	-20	2.74
R1234ze(E)	-15	2.24
R1234ze(E)	-20	2.53
R1234yf	-15	2.71
R1234yf	-20	2.98
R600a	-15	1.12
R600a	-20	0.947
R600	-15	1.01

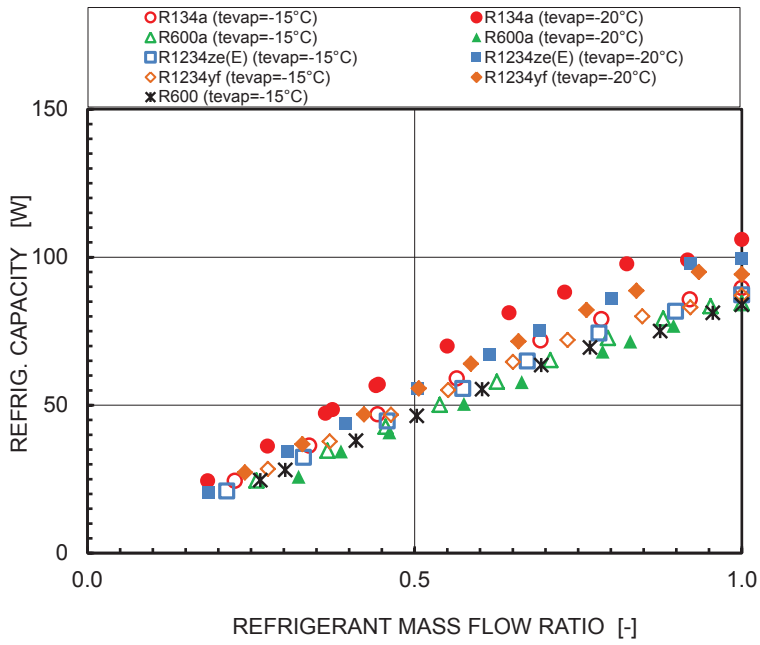

Figure 245 Refrigerating capacity vs. refrigerant mass flow ratio at two evaporation temperatures (-15 °C and -20 °C).

R134a permits to obtain an higher refrigerating capacity, up +36.8% the R600a one. At full load and at -20 °C of evaporation temperature, the R134a refrigerating capacity is +7%, +11.5%, +27.7%, +30.8% higher than the R1234ze(E), R1234yf, R600a, and R600 ones, respectively.

4.3.1 Refrigerant performance

In the case of a roll-bond evaporator finding a performance evaluation criteria becomes harder than the cases already described of a tube heat exchanger and of a BPHE (see paragraphs 4.1.3 and 4.2.3, respectively). The main reason is the lack of a valid equation able to estimate the heat transfer coefficient during all the working conditions (in section 3.3.8 some correlations have been tested only during the full load functioning). But from the experimental results conducted and presented in this thesis, one can notice that the heat transfer coefficients obtained using different refrigerants are comparable. So, it can be supposed that this feature is inconsequential under a refrigerant performance point of view also due to the fact that the air side resistance is much higher than the refrigerant side one.

The main difference between the tested refrigerants is in terms of pressure drops and, thus, of mass flow rate. In fact, the mass flow rate can be strongly reduced by using an HC instead of R134a and, consequently, also the pressure drop could be drastically limited.

On the other hand, the maximum refrigerating capacity of HFOs is close to the R134a one, while the maximum refrigerating capacity of the HCs is around 20% lower than the R134a one.

Finally, it has to be reminded that in the present tests the compressor speed has been adjusted to deliver the proper refrigerant mass flow rate. Only R1234yf exhibits a volumetric cooling capacity similar to R134a, therefore it only can be considered a direct drop-in alternative for R134a in domestic refrigerator.

4.4 Heat pipe finned heat exchanger

R134a is one of the most common two phase fluids inside heat pipe finned heat exchangers when used for air conditioning purposes. It has a relatively high GWP (i.e. GWP=1300) so it should be substituted with an environmentally friendly alternative.

Inside this thesis R134a, R1234ze(E), and R152a were experimentally tested and analyzed inside a commercial HPFHE and the results are presented in section 3.4.1.

R1234ze(E) is a quite new molecule having a GWP lower than 1, proposed to replace R134a in many application fields due to its thermophysical properties not so far from R134a and its drastically lower environmental impact. R152a is a HFC but, having a GWP equal to 140, can again be admitted by the new regulations.

Table 40 Thermophysical properties of R134a, R1234ze(E), and R152a at 20 °C.

Refrigerant	**R134a**	**R1234ze(E)**	**R152a**
p in [bar]	5.72	4.27	5.13
p* [-]	0.141	0.118	0.114
λ_L [W m^{-1} K^{-1}]	0.0833	0.0759	0.1
λ_G [W m^{-1} K^{-1}]	0.0133	0.0132	0.014183
c_{pL}[J kg^{-1} K^{-1}]	1405	1370	1776
ρ_L [kg m^{-3}]	1225.3	1179.3	912
ρ_G [kg m^{-3}]	27.78	22.61	15.91
μ_L [Pa s]	0.000207	0.000211	0.000173
μ_G [Pa s]	1.15E-05	0.000012	9.88E-06
σ [N m^{-1}]	0.00869	0.0095	0.0104
Δh_{LG} [kJ kg^{-1}]	182.28	170.63	285.32
VHC [kJ m^{-1}]	5064	3858	4539

It has a saturation pressure slightly lower (-25% at 20 °C) than the R134a one but it has higher liquid thermal conductivity (-32% at 20 °C) and latent heat of vaporization (-67% at 20 °C), so, theoretically, it should perform similar or better than R134a if used as working fluid inside an heat pipe (see Table 40 where the main thermophysical properties of these three refrigerants, evaluated with Refprop9.1(2013), are reported).

Following, the R1234ze(E) and R152a performance will be compared against the one of the reference refrigerant, R134a.

Figure 246 shows the heat flow rates vs. the air flow rates during the summer tests ($T_{supply.in}$=35 °C and $T_{supply.in}$=40 °C; $T_{exhaust.in}$=25 °C) at C_{min}/C_{max}=1 of the two low-GWP refrigerants, R152a and R1234ze(E), and of the reference refrigerant R134a.

The heat flow rates of the alternative refrigerants are comparable and even higher than that of the more traditional R134a. In particular, at the extreme summer conditions, $T_{supply.in}$=40 °C, they exchange similar heat flow rates, which are around 5% higher than those of R134a; but at lower inlet supply temperatures ($T_{supply.in}$=35 °C) R152a outperforms, showing heat flow rates up to 11% higher than those of the other fluids, which are similar.

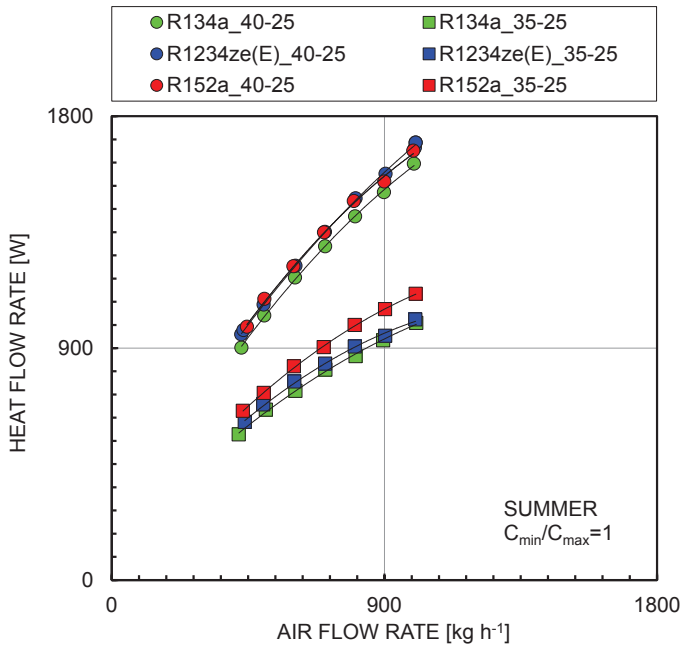

Figure 246 Heat flow rate vs. the air flow rate during the summer tests ($T_{supply.in}$=35 °C and $T_{supply.in}$=40 °C; $T_{exhaust.in}$=25 °C) at C_{min}/C_{max}=1 of R152a, R1234ze(E), and R134a.

Figure 247 shows the heat flow rates vs. the air flow rates during the winter conditions tests ($T_{supply.in}$=10 °C and $T_{supply.in}$=7 °C; $T_{exhaust.in}$=20 °C) at C_{min}/C_{max}=1 of the two low-GWP refrigerants, R152a and R1234ze(E) and of the reference refrigerant R134a.

In this conditions, R152a outperforms the other refrigerants which exhibit almost the same heat transfer performance. R152a shows heat flow rates 15% higher than those of R134a and R1234ze(E) under the same working conditions.

Figure 248 presents the heat flow rates vs. the air flow rates during the summer tests ($T_{supply.in}$=35 °C and $T_{supply.in}$=40 °C; $T_{exhaust.in}$=25 °C) at $C_{min}/C_{max}\neq1$ (i.e. C_{min}/C_{max}=0.9, C_{min}/C_{max}=0.8, C_{min}/C_{max}=0.7, C_{min}/C_{max}=0.6, and C_{min}/C_{max}=0.5) of the two low-GWP refrigerants, R152a and R1234ze(E) and of the reference refrigerant R134a.

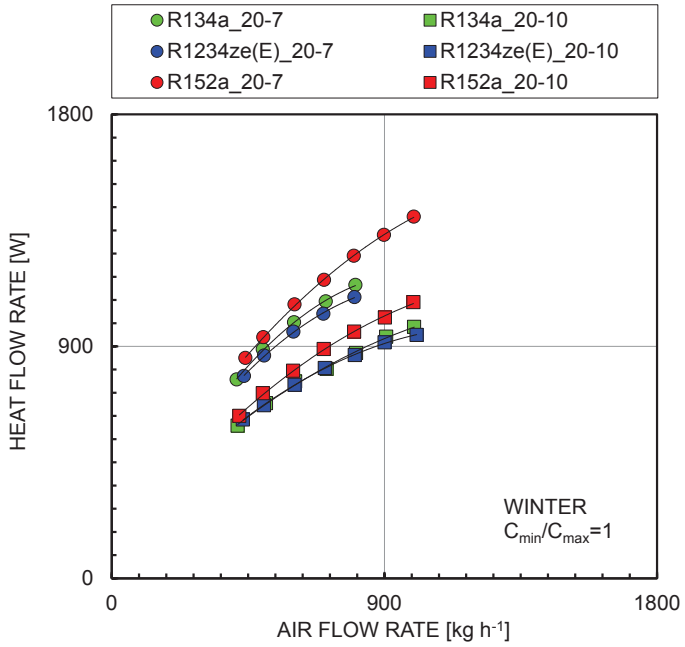

Figure 247 Heat flow rate vs. the air flow rate during the winter tests ($T_{supply.in}$=10 °C and $T_{supply.in}$=7 °C; $T_{exhaust.in}$=20 °C) at C_{min}/C_{max}=1 of R152a, R1234ze(E), and R134a.

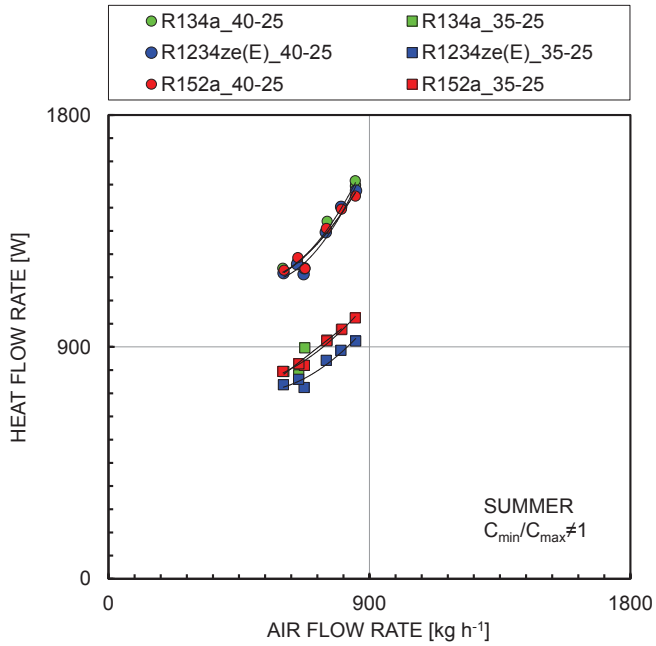

Figure 248 Heat flow rate vs. the air flow rate during the summer tests ($T_{supply.in}$=35 °C and $T_{supply.in}$=40 °C; $T_{exhaust.in}$=25 °C) at C_{min}/C_{max}≠1 of R152a, R1234ze(E), and R134a.

In this testing conditions the tree refrigerants performance is similar, especially at $T_{supply.in}$=40 °C where few differences can be founded in heat flow rate. At $T_{supply.in}$=35°C R1234ze(E) seems to have lower heat flow rates than the other two refrigerants (-4%).

Finally, Figure 249 represents the heat flow rates vs. the air flow rates during the winter conditions tests ($T_{supply.in}$=10 °C and $T_{supply.in}$=7 °C; $T_{exhaust.in}$=20 °C) at C_{min}/C_{max}≠1 (i.e. C_{min}/C_{max}=0.9, C_{min}/C_{max}=0.8, C_{min}/C_{max}=0.7, C_{min}/C_{max}=0.6, and C_{min}/C_{max}=0.5) of the two low-GWP refrigerants, R152a and R1234ze(E), and of the reference refrigerant R134a.

In these series of experimental tests, R152a presents the heat flow rates on average 10% higher than the other two refrigerants.

From these graphs (From Figure 246 to Figure 249) one can notice that R152a on average outperforms the other refrigerants of around 7%, but also that the higher increments can be found at the lower temperatures (for instance, +10% during the winter tests with C_{min}/C_{max}≠1 and +15% during the winter tests with C_{min}/C_{max}=1).

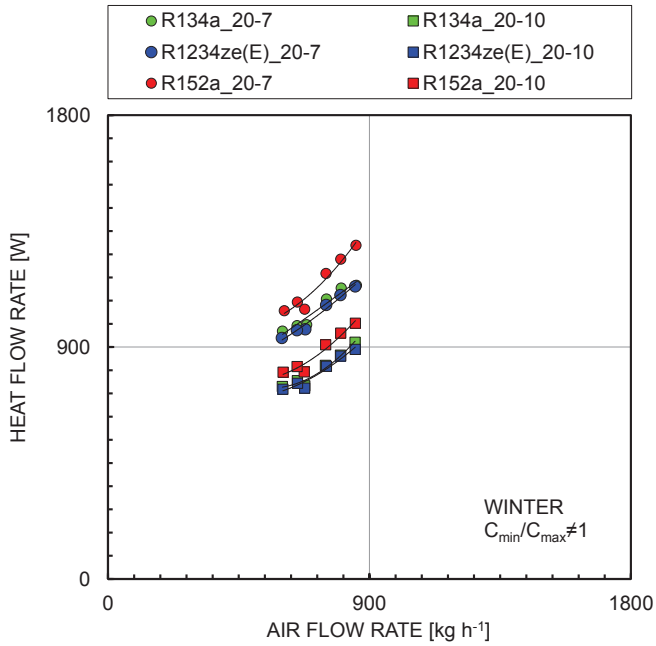

Figure 249 Heat flow rate vs. the air flow rate during the winter tests ($T_{supply.in}$=10 °C and $T_{supply.in}$=7 °C; $T_{exhaust.in}$=20 °C) at C_{min}/C_{max}≠1 of R152a, R1234ze(E), and R134a.

4.4.1 Refrigerant performance evaluation criteria

The air side dominates the heat transfer inside a HPFHE. Despite this, some light differences in terms of heat flow rate can be appreciated by changing the refrigerant inside the pipes.

So that, it could be useful defining a criterion to select a good fluid for this kind of applications. Basing on a performance criteria proposed by Reay and Kew (2006) for the single heat pipe, fluids suitable for heat pipe operation should display latent heat of vaporization as large as possible, high surface tension, and low liquid viscosity.

These properties have been mixed together in the so called Merit number (M), defined as Eq. 107.

$$\mathrm{M} = \frac{\rho_l \sigma_l \, r}{\mu_l} \qquad \text{Eq. 107}$$

The Reay and Kew (2006) criteria suggests that the higher the Merit number value is, the higher the efficiency of the heat pipe is.

In Table 41 and Table 42 the most relevant properties of different refrigerants evaluated with Refprop 9.1 (2013) at saturation temperature of 10 °C and 40 °C are listed for many fluids. These refrigerants were chosen because they are ones of the most used as two phase fluid inside heat pipes or because they belong to HFO group and so they may be considered low GWP candidate working fluids.
From the results reported in Table 41 and Table 42, with the exception of water that works with pressure very far from the R134a and ammonia that is not compatible to a directly drop-in in the tested copper HPFHE, R152a presents the highest merit number among the other fluids, approximately 63% higher than that of R134a at 10 °C and 78% at 50 °C. On the other hand R1234ze(E), the other fluid tested inside this thesis, has a Merit number close to the R134a one (-5% at 10 °C and +1% at 40 °C)

It seems that the Merit number criterion is a good way to ranking the refrigerant performance. In fact R1234ze(E), with a Merit number close to the R134a one, gives heat flow rates similar to the R134a ones. Furthermore R152a, with a Merit number higher to R134a, gives heat flow rates higher than R134a. But, on the other hand, the Merit number criteria does not explain the behavior during summer conditions, especially at $T_{supply.in}$=40 °C, where the three refrigerants performance are close to each other. In this case the refrigerant contribution to heat transfer seems to be negligible with respect to the air side.
Despite that, these results confirm the suitability of R152a, having a GWP of 138, as well as that of R1234ze(E) as viable options for replace R134a in heat pipe finned heat exchangers.

Table 41 Relevant thermodynamic and thermophysical properties of some working fluids at 10 °C.

	p_{sat} [bar]	Δh_{LG} [kJ kg^{-1}]	ρ_l [N m^{-1}]	σ [Pa s]	μ [Pa s]	M [N m^{-2}]
Water	0.01	2477.18	1000	7.42E-02	1.31E-03	1.41E+11
Ammonia	6.15	1225.54	625	2.40E-02	1.53E-04	1.20E+11
R152a	3.73	296.59	936	1.17E-02	1.94E-04	1.68E+10
R600	1.48	376.13	590	1.36E-02	1.83E-04	1.65E+10
R600a	2.21	344.63	569	1.17E-02	1.78E-04	1.29E+10
R1234ze(Z)	1.03	222.98	1300	1.53E-02	3.76E-04	1.18E+10
R134a	4.15	190.74	1261	1.00E-02	2.35E-04	1.03E+10
R1234ze(E)	3.08	177.63	1210	1.08E-02	2.38E-04	9.77E+09
R1234yf	4.38	156.60	1144	8.04E-03	1.86E-04	7.76E+09
R236fa	1.60	153.48	1410	1.14E-02	3.45E-04	7.15E+09

Table 42 Relevant thermodynamic and thermophysical properties of some working fluids at 40 °C.

	p_{sat} [bar]	Δh_{LG} [kJ kg^{-1}]	ρ_l [N m^{-1}]	σ [Pa s]	μ [Pa s]	M [N m^{-2}]
Water	0.07	2405.98	992	6.96E-02	6.53E-04	2.55E+11
Ammonia	15.55	1099.27	579	1.71E-02	1.14E-04	9.55E+10
R152a	9.09	259.93	860	7.75E-03	1.37E-04	1.26E+10
R600	3.78	345.44	555	1.02E-02	1.38E-04	1.43E+10
R600a	5.31	311.52	531	8.35E-03	1.29E-04	1.07E+10
R1234ze(Z)	2.97	205.83	1218	1.15E-02	2.64E-04	1.09E+10
R134a	10.17	163.02	1147	6.11E-03	1.61E-04	7.08E+09
R1234ze(E)	7.66	154.80	1112	6.96E-03	1.67E-04	7.17E+09
R1234yf	10.18	132.27	1034	4.42E-03	1.30E-04	4.65E+09
R236fa	4.37	136.36	1307	7.83E-03	2.36E-04	5.90E+09

5 Conclusions

The global warming is universally identified as a concrete and urgent concern. For this reason also the refrigeration fluids have to be evolved accordingly. The open literature remarks the fact that finding an ideal fluid able to replace the commonly used ones is extremely unlikely (see, for instance, McLinden *et al.*, 2014 and Calm, 2008). So, one of the actual refrigeration technology goals is to redesign the devices involved in this fluid substitution process in order to optimize their efficiencies when operating with the new working fluids, and to emphasize the strengths and the peculiar features of the new low GWP refrigerants.

For example, in this thesis it has been noticed how some HFO refrigerants, such as R1234ze(E), can potentially be valid alternatives to R134a in terms of heat transfer coefficient – that is comparable or even higher under some working conditions – but their pressure drops were experimentally assessed to be slightly higher than R134a. For this reason a heat exchanger that uses an HFO should be redesign to maintain the same (or a better) global heat transfer and fluid flow performance.

Sometimes the thermophysical properties (such as the latent heat or the density) of the new fluids could become an advantage. For example, as enucleated in Chapter 4, R152a presents a theoretical Coefficient of Performance, evaluated on the basis of the thermophysical properties, higher than R134a under the same conditions thus it could be a valid low GWP alternative in chiller applications. Another example is given by R32 having a volumetric efficiency higher than R410A, property that makes R32 attractive for being used in compression cycles, or by R1234ze(Z) that was proposed for high temperature heat pumps due to its high critical temperature and its Volumetric Cooling Capacity similar to the traditional R114 and R236fa, property that could permit a direct drop-in in the previous systems.

In this thesis the use of innovative refrigerants in refrigeration and thermal control applications was analyzed. To cover a great portion of the existing appliances, four different heat transfer devices were taken into account: tube heat exchangers, plate heat exchangers, roll-bond type heat exchangers and heat pipe finned heat exchangers. For each of the these groups, experimental tests during two phase flow were conducted using several refrigerants aiming to compare their performance.

The wide data set collected and here presented can help on the first hand to expand the literature database shared with the scientific community and, on the second hand, to increase the knowledge required in the optimization of the design of new components and thus of the whole refrigeration systems.

Furthermore, the experimental data collected in this thesis permitted to assess the reliability of several models from the literature and to propose and validate three new correlations for evaluating the heat transfer coefficient. These models can be adopted as guidelines in the development of new equipment, when some engineering approach calculations are required.

Besides, the experimental data set obtained with different refrigerants in several heat exchanger types can permit to highlight the peculiarities accountable to the single refrigerant and so to compare the behavior of the various fluid when applied under different working conditions, as described in Chapter 4.

Finally this thesis collected some Performance Evaluation Criteria (PEC), that help a potential designer in selecting the proper refrigerant for a given application, a very actual subject forced by international regulations. In some cases (for instance when a roll bond type evaporator is used) the two phase fluid does not affect in a meaningful way the heat exchanger performance, but in other cases (for example when a brazed plate heat exchanger is involved) the fluid plays a crucial role. The PEC here proposed and implemented gather together both the heat transfer coefficient and the pressure drop points of view, giving a more comprehensive ranking classification of the several fluids available on the market. It is also worth noticing that these criteria do not take into account other fundamental parameters involved in the refrigerant decision, such as price, availability, environmental compatibility, material affinity, etc. so the last choice is based on the designer experience.

6 Nomenclature

Symbol	Unit	Definition
A	m^2	heat transfer area
A’	m^2	heat transfer area of a single plate
a	m^2	nominal projected area
b	m	corrugation deep
Bo	–	Boiling number
C	$W\ K^{-1}$	heat capacity rate
c_p	$J\ kg^{-1}\ K^{-1}$	specific heat capacity
d	m	diameter
f	–	function
f	–	friction factor
F	–	factor
G	$kg\ m^{-2}\ s^{-1}$	mass flux
g	$m\ s^{-2}$	gravity acceleration
h	$J\ kg^{-1}$	specific enthalpy
h_g	m	groove depth
HTC	$W\ m^{-2}\ K^{-1}$	heat transfer coefficient
J_H	–	co-ordinate
k	–	coverage factor
K	$W\ m^{-2}\ K^{-1}$	overall heat transfer coefficient
KE/V	$J\ m^{-3}$	kinetic energy per unit volume
L	m	length
l_f	m	fin pitch
ln	–	logarithm
log	–	base 10 logarithm
l_r	m	row pitch
l_t	m	tube pitch

M	Nm^{-2}	merit number
$\dot{m}$	$kg\ s^{-1}$	mass flow rate
MFR	–	mass flow ratio
MOL	$kg\ kmol^{-1}$	molecular weight
N	–	number of plates
n	–	exponent
n_g	–	number of grooves
n_r	–	number of rows
n_t	–	number of tubes per row
NTU	–	number of transfer units
Nu	–	Nusselt number
p	Pa	pressure
P	m	corrugation pitch
p*	–	reduced pressure
PF	K^2	penalty factor
Pr	–	Prandtl number
Q	W	heat flow rate
q	$W\ m^{-2}$	heat flux
R_a	μm	roughness
Re	–	Reynolds number
R_p	μm	roughness
s	m	thickness
s_f	m	fin thichness
T	K	temperature
t	°C	temperature
TTP	K	total temperature penalization
v	m^3 kg-1	specific volume
VCC	$J\ kg^{-1}$	volumetric cooling capacity
VHC	$J\ kg^{-1}$	volumetric heating capacity

W	m	width
w	m s^{-1}	velocity
x	–	vapor quality
X	–	co-ordinate
Xtt	–	Martinelli parameter
Y	–	co-ordinate

Greek symbols

Symbol	**Unit**	**Definition**
α	W m^{-2} K^{-1}	heat transfer coefficient
β	°	corrugation angle
β_g	°	helix angle
Δ	-	difference
Δh_{LG}	J kg^{-1}	latent heat
Δp_a	Pa	manifold pressure drop
λ	W m^{-1} K^{-1}	thermal conductivity
μ	Pa s	dynamic viscosity
ρ	kg m-3	density
σ	N m^{-1}	surface tension
Φ	–	enlargement factor

Subscription

Symbol	**Definition**
a	air
atm	atmospheric
ave	average
b	boiling

c	manifold
calc	calculated
cb	convective boiling
cond	condensation
crit	critical
dr	driving
E	external channel
e	evaporator
eq	equivalent
exh	exhaust
ext	external
f	frictional
fc	single phase
g	gravity
G	gas
h	hydraulic
I	internal channel
in	inlet
L	liquid
lat	latent
ln	logarithmic
m	mean
max	maximum
min	minimum
nb	nucleate boiling
out	outlet
pb	pre-boiler
ps	pre-section
r	refrigerant

sat	saturation
sr	refrigerant pressure drop
sub	subcooling
sup	superheating
supply	supply
t	total
tot	total
V	vapor
w	water
wall	wall

7 References

Abadi G.B., Yun E., Kim K.C., 2016. Flow boiling characteristics of R134a and R245fa mixtures in a vertical circular tube, Experimental Thermal and Fluid Science, 72, pp. 112–124.

Abd El-Baky M.A., Mohamed M.M., 2007. Heat pipe heat exchanger for heat recovery in air conditioning, Applied Thermal Engineering, 27, pp. 795–801.

Agarwal R., Hrnjak P., 2015. Condensation in two phase and desuperheating zone for R1234ze(E), R134a and R32 in horizontal smooth tubes, International Journal of Refrigeration, 50, pp. 172–183.

AHRI Standard 410–2001, 2001. Forced-circulation air-cooling and air-heating coils, AHRI, Arlington, VA, USA.

Akash B.A., Said S.A., 2003. Assessment of LPG as a possible alternative to R-12 in domestic refrigerator, Energy Conversion Management, 44, pp. 381–388.

Akers W.W., Deans H.A., Crosser O.K., 1959, Condensing heat transfer within horizontal tubes, Chemical Engineering Program Symposium series vol. 55, pp. 171–176.

Almeida I.M.G., Barbosa C.R.F, Fontes F.A.O., 2010. Thermodynamic and hermophysical assessment of hydrocarbons application in household refrigerator. Thermal Engineering, 9 (01–02), pp. 19–27.

Alsaad M.A., Hammad M.A., 1998.The application of Propane/Butane mixture for domestic refrigerators. Applied Thermal Engineering, 18 (9–10), pp. 911–918.

Amalfi R.L., Vakili-Farahani F., Thome J.R., 2016. Flow boiling and frictional pressure gradients in plate heat exchangers. Part 1: Review and experimental database, International Journal of Refrigeration, 61, pp. 166–184.

ANSI/ASHRAE Standard 33–2000, 2000. Method of testing forced circulation air cooling and air heating coils, ASHRAE, Atlanta, GA, USA.

Anwar Z., Palm B., Khodabandeh R., 2015. Flow boiling heat transfer, pressure drop and dryout characteristics of R1234yf: Experimental results and predictions, Experimental Thermal and Fluid Science, 66, pp. 137–149.

ASHRAE 15-2013 – Safety Standard for Refrigeration Systems and Designation and Classification of Refrigerants.

ASHRAE 34-2013 – Designation and Safety Classification of Refrigerants.

ASHRAE Handbook Fundamentals, 1989. Fitting loss coefficients, 32.27–32.52.

Ayub Z.H., 2003. Plate heat exchanger literature survey and new heat transfer and pressure drop correlations for refrigerant evaporators, Heat Transfer Engineering, 24, pp. 3–16.

Baba D., Nakagawa T., Koyama S., 2012. Flow boiling heat transfer and pressure drop of R1234ze(E) and R32 in horizontal micro-fin tube. Proceedings of the 14th International Refrigeration and Air-Conditioning Conference at Purdue, West Lafayette, IN, July 16–19, 2012.

Bella B., Kaemmer N., Brignoli R., Zilio C., 2014. Energy Efficiency of a Chiller Using R410A or R32, 15th International Refrigeration and Air Conditioning Conference at Purdue, West Lafayette, IN, USA.

Belman-Flores J.M., Barroso-Maldonado J.M., Rodríguez-Muñoz A.P., Camacho-Vázquez G., 2015. Enhancements in domestic refrigeration, approaching a sustainable refrigerator – A review. Renewable and Sustainable Energy Reviews, 51, pp. 955–968.

Berger E., Heimel M., Almbauer R., Lang W., 2012. 1D heat exchanger simulation to capture the cycling transients of domestic refrigeration appliances working with R600a. International Refrigeration and Air Conditioning Conference at Purdue, July 16–19, 2012, West Lafayette, IN, USA.

Bezrodnyi M.K., Moklyak V.F., 1986. Heat transfer during condensation in vertical closed thermosyphons, Journal of Energy Physics, 51 (1), pp. 53–758.

Björk E., Palm B., Nordenberg J., 2010. A thermographic study ofthe on-off behavior of an all-refrigerator, Applied Thermal Engineering, 30, pp. 194–1984.

Bolaji B.O., 2010. Experimental study of R152a and R32 to replace R134a in a domestic refrigerator Energy, 35, pp. 3793–3798.

Bolaji B.O., Huan Z., 2013. ozone depletion and global warming: Case for the use of natural refrigerant – a review, Renewable and Sustinable Energy Reviews, 18, pp. 49–54.

Brown J.S., Zilio C., Brignoli R., Cavallini A., 2012. Heat transfer and pressure drop penalization terms (exergy losses) during flow boiling of refrigerants, International Journal of Energy research, 37, pp. 1669–1679.

Brown J.S., Zilio C., Brignoli R., Cavallini A., 2014. Thermophysical properties and heat transfer and pressure drop performance potentials of hydrofluoro-olefins, hydrochlorofluoro-olefins, and their blends, HVAC&R Research, 20(2), pp. 203–220.

Brown J.S., Zilio C., Cavallini A., 2009. The fluorinated olefin R-1234ze(Z) as a high-temperature heat pumping refrigerant, International Journal of Refrigeration, 32, pp. 1412–1422.

Calm J.M., 2008. The next generation of refrigerants- Historical review, considerations, and outlook, International Journal of Refrigeration, 31, pp. 1123–1133.

Calm J.M., Didion D.A., 1998. Trade-offs in refrigerant selections–past, present, and future. Refrigerants for the 21st Century, International Journal of Refrigeration, 21 (4), pp. 308–321.

Cavallini A., Brown J.S., Del Col D., Zilio C., 2010. In tube condensation performance of refrigerants considering penalization terms (exergy losses) for heat transfer and pressure drop, International Journal of Heat and Mass Transfer, 53, pp. 2885–2896.

Cavallini A., Brown J.S., Zilio C., 2012. Thermophysical Properties, Heat Transfer, and Pressure Drop of HFOs, ASHRAE/NIST Refrigerants Conference.

Cavallini A., Censi G., Del Col D., Doretti L., Longo G.A., Rossetto L., 2001a. Reduction of Global Warming Impact in the HP/AC Industry by Employing New HFC Refrigerants, Clima 2000, Napoli 2011.

Cavallini A., Censi G., Del Col D., Doretti L., Longo G.A., Rossetto L., 2001b. Experimental investigation on condensation heat transfer and pressure drop of new HFC refrigerants (R134a, R125, R32, R410A, R236ea) in a horizontal smooth tube, International Journal of Refrigeration, 24, pp. 73–87.

Cavallini A., Del Col D., Doretti L., Matkovic M., Rossetto L., Zilio C., Censi G., 2006. Condensation in Horizontal Smooth Tubes: A new Heat Transfer Model for Heat Exchanger Design, Heat Transfer Engineering, 27 (8), pp. 31–38.

Cavallini A., Del Col D., Doretti L., Rossetto L., Longo G.A., 2000. Condensation Heat Transfer of New Refrigerants: Advantages of High Pressure Fluids, International Refrigeration and Air Conditioning Conference at Purdue, West Lafayette, IN, USA, Paper 480.

Cavallini A., Del Col D., Mancin S., Rossetto L., 2009. Condensation of pure and near-azeotropic refrigerants in microfin tubes: A new computational procedure, International Journal of Refrigeration, 32, pp. 162–174.

Chang F.L., Hung Y.M., 2014. The coupled effects of working fluid and solid wall on thermal performance of micro heat pipes, International Journal of Heat and Mass Transfer, 73, pp. 76–87.

Chen J.C., 1963. A correlation for boiling heat transfer to saturated fluid in convective flow, ASME Paper 63-HT-34.

Chen J.C., 1966. Correlation for boiling heat transfer to saturated fluids in convective flow , Process Design and Development, 5, pp. 322–329.

Chen S.J., Reed J.G., Tien C.L., 1984. Reflux condensation in a two phase closed thermosyphon. International Journal of Heat and Mass Transfer, 27 (9), pp. 1587–1594.

Chien N.B., Oh J.T., Saito J.K., 2012. Heat transfer coefficient and pressure drop during evaporation of R1234yf, R134a and R22 in horizontal circular small tubes. Proceedings of the 3rd Workshop on Refrigerant Charge Reduction in Refrigerating Systems, Valencia, Spain, October 25–26, 2012.

Chien N.B., Vu P.Q., Choi K.I., Oh J.T., 2015. Heat Transfer Characteristics of R32, R410A and R1234yf During Evaporation Inside Horizontal Minichannel, ICR 2015, August 16 - 22 - Yokohama, Japan, Paper 282.

Choi K.I., Chien N.B., Oh J.T., 2013. Heat Transfer Coefficient during Evaporation of R-1234yf, R-134a, and R-22 in Horizontal Circular Small Tubes, Advances in Mechanical Engineering, Article ID 132397.

Cieslinski J.T., Fiuk A., 2013. Heat transfer characteristics of a two-phase thermosyphon heat exchanger, Applied Thermal Engineering, 51, pp. 112–118.

Claesson J., 2005. Correction of logarithmic mean temperature difference in a compact brazed plate evaporator assuming heat flux governed flow boiling heat transfer coefficient, International Journal of Refrigeration, 28, pp. 573–578.

Colbourne D., Suen K.O., 2015. Comparative evaluation of risk of a split air conditioner and refrigerator using hydrocarbon refrigerants, International Journal of Refrigeration, 59, pp. 295–303.

Cooper M.G., 1984. Heat flows rates in saturated pool boiling - a wide ranging examination using reduced properties, Advanced in Heat Transfer. Academic Press, Orlando, Florida, pp. 157–239.

Costa-Patry E., Olivier J., Thome J.R., 2012. Heat transfer characteristics in a copper micro-evaporator and flow pattern-based prediction method for flow boiling in microchannels, Frontiers in Heat and Mass Transfer, 3, article 013002.

da Silva L.W., Melo C., Pereira R.H., 1999. Heat transfer characteristics of roll-bond evaporators.20th IIR International Congress of Refrigeration. Sydney, Australia.

Del Col D., Azzolin M., Bortolin S., 2014. Two-Phase Flow and Heat Transfer of a Non-Azeotropic Mixture inside a Single Microchannel, International Refrigeration and Air Conditioning Conference at Purdue, West Lafayette, IN, USA, Paper 2556.

Del Col D., Bortolato M., Azzolin M., Bortolin S., 2015a. Condensation heat transfer and two-phase frictional pressure drop in a single minichannel with R1234ze(E) and other refrigerants, International Journal of Refrigeration, 50, pp. 87–103.

Del Col D., Bortolin S., Torresin D., Cavallini A., 2013b. Flow boiling of R1234yf in a 1 mm diameter channel. International Journal of Refrigeration, 36(2), pp. 353–362.

Del Col D., Bortolin, S., Rossetto, L., 2013a. Convective boiling inside a single circular microchannel, International Journal of Heat and Mass Transfer, 67, pp. 1231–1245.

Del Col D., Rossato M., Chinellato F., Muzzolon A., Rossetto L., 2015b. Flow Boiling Of R32 Inside A Brazed Plate Heat Exchanger, International Congress of Refrigeration, ICR 2015, August 16 - 22 - Yokohama, Japan.

Del Col D., Torresin D., Cavallini A., 2010. Heat transfer and pressure drop during condensation of the lowGWPrefrigerantR1234yf, International Journal of Refrigeration, 33(7), pp. 1307–18.

Devotta S., Kulkarni M.M., 1996. Use of hydrocarbon blends in Indian Household Refrigerators. Proceedings of the International Conference on Ozone Protection Technologies, Washington DC, USA, pp. 367–376.

Diani A., Mancin S., Cavallini A., Rossetto L., 2015c. R1234ze(E) Flow Boiling Heat Transfer And Pressure Drop Inside a 2.4 mm Microfin Tube, ICR 2015, August 16 - 22 - Yokohama, Japan, Paper 549.

Diani A., Mancin S., Doretti L., Rossetto L., 2015b. Low-GWP refrigerants flow boiling heat transfer in a 5 PPI copper foam, International Journal of Multiphase Flow, 76, pp. 111–121.

Diani A., Mancin S., Rossetto L., 2014. R1234ze(E) flow boiling inside a 3.4 mm ID microfin tube, International Journal of Refrigeration, 47, pp. 105–119.

Diani A., Mancin S., Rossetto L., 2015a. Flow boiling heat transfer of R1234yf inside a 3.4 mm ID microfin tube, Experimental Thermal and Fluid Science, 66, pp. 127–136.

Diani A., Rossetto L., 2015. Vaporization inside a mini microfin tune: experimental results and modeling, 3rd UIT (Italian Union of Thermo-fluid-dynamics) Heat Transfer Conference, Journal of Physics: Conference Series 655, pp. 012032.

Ding G., Hu H., Huang X., Deng B., Gao Y., 2009. Experimental investigation and correlation of two-phase frictional pressure drop of R410A–oil mixture flow boiling in a 5 mm microfin tube, International Journal of Refrigeration, 32, pp. 150–161.

Dittus F.W. , Boelter L. M.K., 1930. Heat transfer in automobile radiator of the tubular type, University of California Publications in Engineering, vol. 2, no. 13, pp. 443–461.

Djordjedvić E.M. , Kabelac S., Šerbanović S.P., 2007. Mean heat transfer coefficient and pressure drop during the evaporation of 1,1,1,2 tetrafluoroethane (R-134a) in a plate heat exchanger, Journal of Chemical Serbian Society, 72, pp. 833–846.

Djordjedvić E.M., Kabelac S., Šerbanović S.P., 2008. Heat transfer coefficient and pressure drop during refrigerant R134a condensation in a plate heat exchanger, Chemical Papers of the Serbian Society of Science, 62, pp. 78–85.

Djordjević E.M., Kabelac S., 2008. Flow Boiling of R134a and Ammonia in a Plate Heat Exchanger. International Journal of Heat and Mass Transfer, 51, pp. 6235–6242.

Domanski P.A., Brown J S., Jaehyeok H., Wojtusiak J., McLinden M.O., 2014. A thermodynamic analysis of refrigerants: Performance limits of the vapor compression cycle, International Journal of Refrigeration, 38, pp. 71–79.

Donowski, V.D., Kandlikar, S.G., 2000. Correlating evaporation heat transfer coefficient of refrigerant R134a in a plate heat exchanger, Engineering Foundation Conference on Pool and Flow Boiling, Alaska.

Dutto T., Blaise J.C., Benedic T., 1991. Performances of brazed plate heat exchanger set in heat pump, Proceedings of the 18th International Congress of Refrigeration, Montreal, Canada, pp. 1284–1288.

Ejarn, 2015. Retrieved from https://www.ejarn.com/news.asp?ID=30295.

El-Morsi M., 2015. Energy and exergy analysis of LPG (liquefied petroleum gas) as a drop in replacement for R134a in domestic refrigerators. Energy 86, pp. 344–353.

Engelhorn H.R., Reinhart A.M., 1990. Investigations on heat transfer in a plate evaporator. Chemical Engineering Process, 28, 143–146.

EPA ,U.S. Environmental Protection Agency, 2012. Acceptable Substitutes for CFC-114 and CFC-11 in Chillers and Other Refrigerants. Retrieved from www.epa.gov/ozone/snap/ refrigerants/lists/114cent.html.

Esen M., 2004. Thermal performance of a solar cooker integrated vacuum-tube collector with heat pipes containing different refrigerants, Solar Energy, 76, pp. 751–757.

Esen M., Esen H., 2005. Experimental investigation of a two-phase closed thermosyphon solar water heater, Solar Energy 79, pp. 459–468.

Fang X., 2013. A new correlation of flow boiling heat transfer coefficients based on R134a data, International Journal of Heat and Mass Transfer, 66, pp. 279–283.

Fang X., Li G., Li D., Xu Y., 2015. An experimental study of R134a flow boiling heat transfer in a 4.07 mm tube under Earth's gravity and hypergravity, International Journal of Heat and Mass Transfer, 87, pp. 399–408.

Fatouh M., El Kafafy M., 2006a. Assessment of propane/commercial butane mixtures as possible alternatives to R134a in domestic refrigerators, Energy Conversion and Management 47, pp. 2644–2658.

Fatouh M., El Kafafy M., 2006b. Experimental evaluation of a domestic refrigerator working with LPG, Applied Thermal Engineering, 26, pp. 1593–1603.

Feldman A., Marvillet C., Lebouché M., 2000. Nucleate and convective boiling in plate fin heat exchangers, International Journal of Heat and Mass Transfer, 43, pp. 3433–3442.

Fernando P., Palm B., Lundqvist P., Granryd E., 2004. Propane heat pump with low refrigerant charge: Design and laboratory tests, International Journal of Refrigeration 27 pp. 761–773.

Forster H.K., Zuber N., 1955. Dynamics of Vapor Bubbles and Boiling Heat Transfer, American Institute of Chemical Engineers Journal, 1, pp. 531-535.

Friedel L., 1979. Improved friction pressure drop correlations for horizontal and vertical two-phase pipe flow, European Two-Phase Group Meeting, Ispra, Italy, Paper E2.

Fujii T., 1991. Theory of Laminar Film Condensation. Springer Berlin, pp. 75–81, 83–87.

Fukuda S., Kondou C., Takata N., Koyama S., 2014. Low GWP refrigerants R1234ze(E) and R1234ze(Z) for high temperature heat pumps, International Journal of Refrigeration, 40, pp. 161–173.

Fukuda S., Zhang H., Takata N., Matsumoto T., Koyama S., 2015. Condensation of R1234ze(Z) inside a vertical plate-fin heat exchanger, ICR 2015, August 16 - 22 - Yokohama, Japan, Paper 361.

Gigiel A., 2004, Safety testing of domestic refrigerators using flammable refrigerants, International Journal of Refrigeration, 27, pp. 621–628.

Goetzler W., Sutherland T., Rassi M., Burgos J., 2014. Research & Development Roadmap for Next Generation Low Global Warming Potential Refrigerants, US Department of Energy Efficiency and Renewable Energy.

Gorenflo D., 1993. Pool boiling, VDI Heat Atlas, Dusseldorf, Germany.

Grauso S., Mastrullo R., Mauro A.W., Thome J.R., Vanoli G.P., 2013a. Flow pattern map, heat transfer and pressure drops during evaporation of R-1234ze(E) and R134a in a horizontal, circular smooth tube: Experiments and assessment of predictive methods, International Journal of Refrigeration, 36(2), pp. 478–491.

Grauso S., Mastrullo R., Mauro A.W., Vanoli G.P., 2013b. Flow boiling of R410A and CO_2 from low to medium reduced pressures in macro channels: Experiments and assessment of prediction methods, International Journal of Heat and Mass Transfer, 56, pp. 107–118.

Gray D.L., Webb R.L., 1986. Heat transfer and friction correlations for plate finned-tube heat exchangers having plain fins, Proceeding 8th International Journal of Heat Transfer Conference IHTC-8, 6, pp. 2745–2750.

Greco A., Vanoli G.P., 2005. Flow-boiling of R22, R134a, R507, R404A and R410A inside a smooth horizontal tube, International Journal of Refrigeration, 28, pp. 872–880.

Grooten M.H.M., van der Geld C.W.M., 2009. Predicting Heat Transfer In Long, R-134a Filled Thermosyphons, Journal of Heat Transfer, 131 (5), pp. 51–61.

Gross U., 1992. Reflux condensation heat transfer inside a closed thermosyphon, International Journal of Heat and Mass Transfer, 35 (2), pp. 279–294.

Gungor K.E. , Winterton R.H.S., 1986. A general correlation for flow boiling in tubes and annuli, International Journal of Heat and Mass Transfer, 29 (3), pp. 351–358.

Guo P., Ciepliski D.L., Besant R.W., 2011. A testing and HVAC design methodology for air-to-air heat pipe heat exchangers, HVAC&R Research, 4, pp. 3–26.

Guo W., Nutter D.W., 2009. An experimental study of axial conduction through a thermosyphon pipe wall, Applied Thermal Engineering, 29 (17–18), pp. 3536–3541.

Hammed M.A., Alsaad M.A., 1999. The use of hydrocarbon mixtures as refrigerants in domestic refrigerators, Applied Thermal Engineering, 19, pp. 1181–1189.

Han D., Lee K., Kim Y., 2003. Experiments on the characteristics of evaporation of R410A in brazed plate heat exchangers with different geometric configurations, Applied Thermal Engineering, 23, pp. 1209–1225.

Han H., Cui X., Zhu Y., Sun S., 2014. A comparative study of the behavior of working fluids and their properties on the performance of pulsating heat pipes (PHP), International Journal of Thermal Sciences, 82, pp. 138–147.

Han X., Li P., Yuan X., Wang Q., Chen G., 2013. The boiling heat transfer characteristics of the mixture HFO-1234yf/oil inside a micro-fin tube, International Journal of Heat and Mass Transfer, 67, pp. 1122–1130.

Hassan M.A.M., 2013. Investigation of performance of heat pipe as heat exchanger using alternative refrigerants, Journal of Energy Engineering, 139, pp. 18–24.

Hayes N., Jokar A., 2009. Study of carbon dioxide condensation in chevron plate exchangers, ASHRAE–D–RP–1394.

He M.G., Li T.C., Liu Z.G., Zhang Y., 2005. Testing of the mixing refrigerant HFC152a/HFC125 in domestic refrigerator, Applied Thermal Engineering, 25, pp. 1169–1181.

Hermes C.J.L., Melo C., Negrão C.O.R., 2008. A numerical simulation model for plate-type, roll-bond evaporators. International Journal of Refrigeration, 31, pp. 335–347.

Hodnebrog Ø., Etminan M., Fuglestvedt J.S., Marston G., Myhre G., Nielsen C.J., Shine K.P., Wallington T J., 2013. Global Warming Potentials and Radiative Efficiencies of Halocarbons and Related Compounds: A Comprehensive Review, Reviews of Geophysics, 51 (2), pp. 300-378.

Hossain M.A., Onaka Y., Hasan M.M., Miyara A., 2013. Heat transfer during evaporation of R1234ze(E), R32, R410A and a mixture of R1234ze(E) and R32 inside a horizontal smooth tube. International Journal of Refrigeration, 36(2), pp. 465–77.

Hossain M.A., Onaka Y., Miyara A., 2012. Experimental study on condensation heat transfer and pressure drop in horizontal smooth tube for R1234ze(E), R32 and R410A, International Journal of Refrigeration, 35(4), pp. 927–38.

HSE 2014. http://www.hse.gov.uk/statistics/sources.htm.

Hsieh Y.Y, Lin T.F., 2002. Saturated flow boiling heat transfer and pressure drop of refrigerant R-410A in a vertical plate heat exchanger, International Journal of Heat and Mass Transfer 45, pp.1033–1044.

Hsieh Y.Y., Chiang L.J., Lin T.F., 2002. Subcooled Flow Boiling Heat Transfer of R134a and the Associated Bubble Characteristics in a Vertical Plate Heat Exchanger, International Journal of Heat and Mass Transfer, 45, pp. 1791–1806.

Hsieh Y.Y., Lin T.F., 2003. Evaporation Heat Transfer and Pressure Drop of Refrigerant R410A Flow in a Vertical Plate Heat Exchanger, Journal of Heat Transfer, 125, pp. 852–857.

Hu H., Ding G., Wang K., 2008a. Heat transfer characteristics of R410A–oil mixture flow boiling inside a 7mm straight microfin tube, International Journal of Refrigeration, 31, pp. 1081–1093.

Hu H., Ding G., Wang K., 2008b. Measurement and correlation of frictional two-phase pressure drop of R410A/POE oil mixture flow boiling in a 7 mm straight micro-fin tube, Applied Thermal Engineering, 28, pp. 1272–1283.

Huang J., Sheer T.J., Bailey-McEwan M., 2012. Heat transfer and pressure drop in plate heat exchanger refrigerant evaporators, International Journal of Refrigeration, 35, pp. 325–335.

Huo X., Chen L., Tian Y.S., Karayiannis T.G., 2004. Flow boiling and flow regimes in small diameter tubes, Applied Thermal Engineering, 24, pp. 1225–1239.

Imura H., Kusuda H., Ogata J., Miyazaki T., Sakmoto N., 1979. Heat transfer in two-phase closed-type thermosyphons, HTJR 8, pp. 41–53.

Jafari D., Franco A., Filippeschi S., Di Marco P., 2016.Two-phase closed thermosyphons: A review of studies and solar applications, Renewable and Sustainable Energy Reviews, 53, pp. 575–593.

Japkise D., 1973. Advances in thermosyphon technology, Advances in heat transfer, 3, pp. 3–91.

Jassim E.W., Newell, T.A., Chato, J.C., 2006. Refrigerant Pressure Drop in Chevron and Bumpy Style Flat Plate Heat Exchangers. Experimental Thermal and Fluid Science, 30, pp. 213–222.

Jokar A., Hosni M.H., Eckels S.J., 2006. Dimensional Analysis on the Evaporation and Condensation of Refrigerant R-134a in Minichannel Plate Heat Exchangers, Applied Thermal Engineering, 26, pp. 2287–2300.

Jouhara H., Ezzuddin H., 2013. Thermal performance characteristics of a wraparound loop heat pipe (WLHP) charged with R134A, Energy, 61, pp. 128–138.

Joybari M.M., Hatamipour M.S., Rahimi A., Modarres F.G., 2013. Exergy analysis and optimization of R600a as a replacement of R134a in a domestic refrigerator system, International Journal of Refrigeration, 36, pp. 1233–1243.

Jun, D., Kim Y., Ko Y., Song K., 2003. Nucleate boiling heat transfer coefficients of pure halogenated refrigerants, International Journal of Refrigeration, 26, pp. 240–248.

Jung D.S., Kim C.B., Song K., Park B., 2000. Testing of propane/isobutane mixture in domestic refrigerators, International Journal of Refrigeration, 23, pp. 517–527.

Jung Y.K., Kim H.J., Lee H.S., Yong-Sung Lee Y.S., 2014. Heat Transfer and Pressure Drop Characteristics of Plate Heat Exchanger of R22 and R32, Twenty-fourth International Ocean and Polar Engineering Conference, Busan, Korea.

Jung, D., Kim, ANh, K., Park, J., 2004. Nucleate boiling heat transfer coefficients of HCFC22, HFC134a, HFC125, and HFC32 on various enhanced tubes, International Journal of Refrigeration, 27, pp. 202–206.

Jung, D., Kim, Y., Ko, Y., Song, K., 2003. Nucleate boiling heat transfer coefficients of pure halogenated refrigerants, International Journal of Refrigeration, 26, pp. 240–248.

Karber K.M., Abdelaziz O., Vineyard E.A., 2012. Experimental performance of R-1234yf and R-1234ze as drop-in replacements for R-134a in domestic refrigerators, International Refrigeration and Air Conditioning Conference at Purdue, July 16–19, 2012, West Lafayette, IN, USA.

Kays W.M., London A.L., 1984. Compact Heat Exchangers, third ed., Krieger Publishing Company, Malabar, FL, USA.

Kedzierski M.A., Park K.J., 2013. Horizontal Convective Boiling of R134a, R1234yf/R134a, and R1234ze(E) within a Micro-Fin Tube with Extensive Measurement and Analysis Details, NIST Technical Note 1807.

Kew P.A., 1982. Heat pumps for industrial waste heat recovery e a summary of required technical and economic criteria. Heat Recovery Systems, 2 (3), pp. 283–296.

Kim S.M., Mudawar I., 2013. Universal approach to predicting two-phase frictional pressure drop for mini/micro-channel saturated flow boiling, International Journal of Heat and Mass Transfer, 58, pp. 718–734.

Kim S.M., Mudawar I., 2014a. Review of databases and predictive methods for heat transfer in condensing and boiling mini/micro-channel flows, International Journal of Heat and Mass Transfer, 77, pp. 627–652.

Kim S.M., Mudawar I., 2014b. Review of databases and predictive methods for pressure drop in adiabatic, condensing and boiling mini/micro-channel flows, International Journal of Heat and Mass Transfer, 77, pp.74–97.

Kline S.J., McClintock F.A., 1953. Describing uncertainties in single-sample experiments. Mechanical Engineering, 75, pp. 3–8.

Kondou C., BaBa D., Mishima F., Koyama S., 2013c. Flow boiling of non-azeotropic mixture R32/R1234ze(E) in horizontal microfin tubes, International Journal of Refrigeration, 36, pp. 2236–2378.

Kondou C., Mishima F., Liu J.F., Koyama S., 2014a. Condensation and Evaporation of R744/R32/R1234ze(E) Flow in Horizontal Microfin Tubes, International Refrigeration and Air Conditioning Conference at Purdue, West Lafayette, IN, USA, Paper 1448.

Kondou C., Mishima F., Liu J.F., Koyama S., 2014b. Condensation and Evaporation of R134a, R1234ze(E) and R1234ze(Z) Flow in Horizontal Microfin Tubes at Higher Temperature, International Refrigeration and Air Conditioning Conference at Purdue, West Lafayette, IN, USA, Paper 1446.

Kumar, H., 1984. The plate heat exchanger: construction and design. Institute of Chemical Engineering Symposium Series.

Kundu A., Kumar R., Gupta A., 2014a. Heat transfer characteristics and flow pattern during two-phase flow boiling of R134a and R407C in a horizontal smooth tube, Experimental Thermal and Fluid Science, 57, pp. 344–352.

Kundu A., Kumar R., Gupta A., 2014b. Heat transfer characteristics and flow pattern during two-phase flow boiling of R134a and R407C in a horizontal smooth tube, Experimental Thermal and Fluid Science, 57, pp. 344–352.

Kundu A., Kumar R., Gupta A., 2014c. Comparative experimental study on flow boiling heat transfer characteristics of pure and mixed refrigerants, International Journal of Refrigeration, 45, pp. 136–147.

Kuo W.S., Lie Y.M., Hsieh Y.Y., Lin T.F., 2005. Condensation heat transfer and pressure drop of refrigerant R410A flow in a vertical plate heat exchanger, International Journal of Heat and Mass Transfer, 48, pp. 5205–5220.

Lazarek G.M., Black S.H., 1982. Evaporative heat transfer pressure drop and critical heat flux in a small vertical tube with R-113, International Journal of Heat and Mass Transfer, 25, pp. 945–960.

Lee H.S., Kim H.J., Cha S.W., Moon D.S., 2014. Performance Characteristics of Seawater Heat Pump Using R32/R152a Mixed Refrigerant, Twenty-fourth International Ocean and Polar Engineering Conference, Busan, Korea.

Leighton D., Hwang Y., Radermacher R., 2012. Modeling of household refrigerator performance with LGARs, ASHRAE Winter Conference, Chicago, IL, USA.

Lemmon E.W., Huber M.L., McLinden M.O., 2013. NIST Standard Reference Database23: Reference fluid Thermodynamic and Transport Properties – Refprop Version 9.1, NIST, Gaithersburgh, MD.

Li M., Dang C., Hihara E., 2012. Flow boiling heat transfer of HFO1234yf and R32 refrigerant mixtures in a smooth horizontal tube: Part I. Experimental investigation, International Journal of Heat Mass Transfer, 55(13–14), pp. 3437–3446.

Liu Z., Winterton R.H.S., 1991. A general correlation for saturated and subcooled flow boiling in tubes and annuli, based on a nucleate pool boiling equation, International Journal of Heat and Mass Transfer, 34, pp. 2759–2766.

Longo G.A., 2008. Refrigerant R134a condensation heat transfer and pressure drop inside a small brazed plate heat exchanger, International Journal of Refrigeration, 31, pp.780–789.

Longo G.A., 2009. R410A condensation inside a commercial brazed plate heat exchanger, Experimental Thermal and Fluid Science, 33, pp. 284–291.

Longo G.A., 2010a. Heat transfer and pressure drop during HFC refrigerant saturated vapor condensation inside a brazed plate heat exchanger, International Journal of Heat and Mass Transfer, 53, pp. 1079–1087.

Longo G.A., 2010b. Heat transfer and pressure drop during hydrocarbon refrigerant condensation inside a brazed plate heat exchanger, International Journal of Refrigeration, 33, pp. 944–953.

Longo G.A., 2011. The effect of vapor super-heating on hydrocarbon refrigerant condensation inside a brazed plate heat exchanger, Experimental Thermal and Fluid Science, 35, pp. 978–985.

Longo G.A., 2012a. Hydrocarbon refrigerant vaporization inside a brazed plate heat exchanger, ASME Journal of Heat Transfer, 134, pp. 101801-101810.

Longo G.A., 2012b. Vaporization of the low GWP refrigerant HFO1234yf inside a brazed plate heat exchanger, International Journal of Refrigeration, 35, pp. 952–961.

Longo G.A., Gasparella A., 2007a. Heat transfer and pressure drop during HFC refrigerant vaporization inside a brazed plate heat exchanger, International Journal of Heat and Mass Transfer 50, pp. 5194–5203.

Longo G.A., Gasparella A., 2007b. HFC-410A Vaporization inside a Commercial Brazed Plate Heat Exchanger, Experimental Thermal and Fluid Science, 32, pp. 107–116.

Longo G.A., Gasparella A., 2007c. Refrigerant R134a Vaporization Heat Transfer and Pressure Drop inside a Small Brazed Plate Heat Exchanger, International Journal of Refrigeration, 30, pp. 821–830.

Longo G.A., Gasparella A., Sartori R., 2004. Experimental Heat Transfer Coefficients During Refrigerant Vaporization and Condensation inside Herringbone-Type Plate Heat Exchangers with Enhanced Surfaces. International Journal of Heat and Mass Transfer, 47, pp. 4125–4136.

Longo G.A., Zilio C., 2013. Condensation of the low GWP refrigerant HFC1234yf inside a brazed plate heat exchanger, International Journal of Refrigeration, 36, pp. 612–621.

Lukitobudi A.R., Akbarzadeh A., Johnson A.W., Hendy P., 1995. Design, construction and testing of a thermosyphon heat exchanger for medium temperature heat recovery in bakeries. Heat Recovery Systems,15, pp. 481–91.

MacGregor R.W., Kew P.A., Reay D.A., 2013. Investigation of low Global Warming Potential working fluids for a closed two-phase thermosyphon, Applied Thermal Engineering, 51, pp. 917–925.

Makhnatch P., Khodabandeh R., 2014. The role of environmental metrics (GWP, TEWI, LCCP) in the selection of low GWP refrigerant, The 6th International Conference on Applied Energy -ICAE2014.

Manavela Chiapero E., Fernandino M., Dorao C.A., Experimental results on boiling heat transfer coefficient, frictional pressure drop and flow patterns for R134a at a saturation temperature of 34 °C, International Journal of Refrigeration, 40, pp. 317–327.

Mancin S., Del Col D., Rossetto L., 2010. Partial condensation of R407C and R410A refrigerants inside a plate heat exchanger, Experimental Thermal and Fluid Science, 36 (2011), 149–157.

Mancin S., Del Col D., Rossetto L., 2011. Partial condensation of R407C and R410A refrigerants inside a plate heat exchanger, Experimental Thermal Fluid Science, 36, pp. 149–157.

Mancin S., Del Col D., Rossetto L., 2012. Condensation of superheated vapor of R410A and R407C inside plate heat exchangers: experimental results and simulation procedure, International Journal of Refrigeration, 35, pp. 2003–2013.

Mancin S., Del Col D., Rossetto L., 2013. R32 partial condensation inside a brazed plate heat exchanger, International Journal of Refrigeration, 36, pp. 601–611.

Mancin S., Diani A., Rossetto L., 2014. R134a flow boiling heat transfer and pressure drop inside a 3.4 mm ID microfin tube, 68th Conference of the Italian Thermal Machines Engineering Association, ATI2013.

Mancin S., Diani A., Vezzù S., Rossetto L., 2015. Flow Boiling Heat Transfer Of R1234yf on a Microparticle Coated Copper Surface, ICR 2015, August 16 - 22 - Yokohama, Japan, Paper 564.

Margat, L., Thonon, B., Tadrist, L., 1997. Heat transfer and two phase flow characteristics during convective boiling in a corrugated channel. Compact Heat Exchangers For The Process Industry. Begell House.

Martinez F.J.R., Plasencia M.A.A., Gomez E.V., Diez F.V., Martin R.H., 2003. Design and experimental study of mixed energy recovery system, heat pipe and indirect evaporative equipment for air conditioning, Energy and Buildings, 35, pp. 1021–1030.

Mathur G.D., 1996. Enhancing performance of an air conditioning system with a two-phase heat recovery loop retrofit, Proceeding of the Intersociety Energy Conversion Engineering Conference, USA, pp. 2027–2032.

Mathur, G.D., 1997. Performance enhancement of existing air conditioning systems, Proceeding of the Intersociety Energy Conversion Engineering Conference, USA, pp. 1618–1623.

McAdams W.H., 1954. Heat Transmission, third ed., McGraw-Hill, New York.

McLinden M.O., 1990. Optimum refrigerants for non-ideal cycles: an analysis employing corresponding states. USNC/IIR Purdue Refrigeration Conference and ASHRAE Purdue CFC Conference, West Lafayette, IN.

McLinden M.O., Didion D.A., 1987. CFCs: quest for alternatives. ASHRAE Journal, 29 (12), pp.32–42.

McLinden M.O., Kazakov A.F., Brown J.S., Domanski P.A, 2014. A thermodynamic analysis of refrigerants: Possibilities and tradeoffs for Low-GWP refrigerants, International Journal of Refrigeration, 38, pp. 80–92.

Meena P., Rittidech S., Poomsa-ad N., 2007. Closed-loop oscillating heat-pipe with check valves (CLOHP/CVs) air-preheater for reducing relative humidity in drying systems, Applied Energy, 84, pp. 363–373.

Midgley Jr. T., 1937. From the periodic table to production. Industrial and Engineering Chemistry 29 (2), pp. 239–244.

Mishima K., Hibiki T., 1996. Some Characteristics of Air-Water Two-Phase Flow in Small Diameter Vertical Tubes, International Journal of Multi-phase Flow, 22 (4), pp.703–712.

Mishkinis D., Ochterbeck J. M., 2003. V Minsk International Seminar "Heat Pipes, Heat Pumps, Refrigerators" Minsk, Belarus , September 8-11, 2003.

Mitrovic, J., 2000. Effects of vapour superheating and condensate subcooling on laminar film condensation. Journal of Heat Transfer, 122, pp. 192–196.

Mohanraj M., 2013. Energy performance assessment of R430A as a possible alternative refrigerant to R134a in domestic refrigerators, Energy for Sustainable Development Journal, 17, pp. 471–476.

Mohanraj M., Jayaraj S., Muraleedharan C., 2007. Improved energy efficiency of a domestic refrigerator retrofitted with hydrocarbon refrigerant mixture (HC290/HC600a) as drop in substitute, Energy for Sustainable Development, 11, pp. 29–33.

Mohanraj M., Jayaraj S., Muraleedharan C., 2009a. Environment friendly alternatives to halogenated refrigerants- A review, International Journal of Greenhouse Gas Control, 3, pp. 108–119.

Mohanraj M., Jayaraj, S., Muraleedharan, C., Chandrasekar, P., 2009b. Experimental investigation of R290/R600a mixture as an alternative to R134a in a domestic refrigerator, International Journal of Thermal Science, 48, pp.1036–1042.

Moreno G., Narumanchi S., King C., 2011. Pool boiling heat transfer characteristics of HFO-1234yf with and without microporous enhanced surfaces. Proceedings of the ASME 2011 International Mechanical Engineering Congress and Exposition (IMECE2011), Denver, CO, November 11–17, 2011.

Mortada S., Zoughaib A., Arzano-Daurelle C., Clodic D., 2012. Boiling heat transfer and pressure drop ofR-134a and R-1234yf in minichannels for low mass fluxes, International Journal of Refrigeration, 35(4), pp. 962–973.

Mota-Babiloni A., Navarro-Esbrì J., Barragàn-Cervera A., Molés F., Peris B., 2015. Analysis based on EU Regulation No 517/2014 of new HFC/HFO mixtures as alternatives of high GWP refrigerants in refrigeration and HVAC systems, International Journal of Refrigeration, 52, pp. 21 –31.

Mota-Babiloni A., Navarro-Esbrí J., Molés F., Barragán Cervera Á., Peris B., Verdú G., 2015. A review of refrigerant R1234ze(E) recent investigations, Applied Thermal Engineering, http://dx.doi.org/doi: 10.1016/j.applthermaleng.2015.09.055.

Muley A., Manglik R.M., 1999. Experimental study of turbulent flow heat transfer and pressure drop in a plate heat exchanger with chevron plates, ASME Journal of Heat Transfer, 121, pp. 110–121.

Müller-Steinhagen H., Heck, K., 1986. A simple friction pressure drop correlation for two-phase flow in pipes, Chemical Engineering and Processing: Process Intensification, 20, pp. 297–308.

Nagata R., Nii N., Kondou C., Koyama S., 2015. Pool Boiling Heat Transfer Of Low GWP Refrigerants R1234ze(E), R1234ze(Z) and R1233zd(E) on a Horizontal Plane Tube, ICR 2015, August 16 - 22 - Yokohama, Japan, Paper 112.

Noie S.H., 2005. Heat transfer characteristics of a two-phase closed thermosyphon, Applied Thermal Engineering, 25, pp. 495–506.

Noie-Baghban S., Majideian G., 2000. Waste heat recovery using heat pipe heat exchanger (HPHE) for surgery rooms in hospitals, Applied Thermal Engineering, 20, pp. 1271–82.

Nusselt W., 1916. Die oberflachenkondensation des wasserdampfes, Z. Ver. Dt Ing. 60, pp. 541–575.

Oh H.K., Son C.H., 2011. Flow boiling heat transfer and pressure drop characteristics of CO_2 in horizontal tube of 4.57-mm inner diameter, Applied Thermal Engineering, 31, pp. 163–172.

Oh J.T., Choi K.I., Saito K., Jeong J.S., Oh H.K., 2012. Comparison of heat transfer coefficient during evaporation of natural refrigerants and R1234yf in horizontal small tubes. Proceedings of the 10th IIR Gustav Lorentzen Conference on Natural Working Fluids (GL2012), Delft, The Netherlands, June 25–27, 2012.

Ong K.S., 2014. Review of heat pipe heat exchangers for enhanced dehumidification and cooling in air conditioning systems, International Journal of Low-Carbon Technologies Advance Access,0, pp. 1–8.

Ouazia B., 2001. Evaporation Heat Transfer and Pressure Drop of HFC-R134a inside a Plate Heat Exchanger. ASME International Mechanical Engineering Congress and Exposition, IMECE2001/PID-25613, New York, NY, pp.115–123.

Padilla M., Revellin R., Bonjour J., 2012. Two-phase flow visualization and pressure drop measurements of HFO-1234yf and R-134a refrigerants in horizontal return bends, Experimental Thermal and Fluid Science, 39(5), pp. 98–11.

Padilla M., Revellin R., Haberschill P., Bensafi A., Bonjour J., 2011. Flow regimes and two-phase pressure gradient in horizontal straight tubes: Experimental results for HFO-1234yf, R-134a and R-410A. Experimental Thermal and Fluid Science, 35(6), pp. 1113–1126.

Padilla M., Revellin R., Wallet J., Bonjour J., 2013. Flow regime visualization and pressure drops of HFO-1234yf, R-134a and R-410A during downward two-phase flow in vertical return bends, International Journal of Heat and Fluid Flow, 40, pp. 116–134.

Padovan A., Del Col D., Rossetto L., 2011. Experimental study on flow boiling of R134a and R410A in a horizontal microfin tube at high saturation temperatures, Applied Thermal Engineering, 31, pp. 3814–3826.

Palm B., 2007. Refrigeration systems with minimum charge of refrigerant. Applied Thermal Engineering, 27, pp. 1693–1701.

Palm B., 2008. Hydrocarbons as refrigerants in small heat pump and refrigeration systems – A review, International Journal of Refrigeration, 31, pp. 552–563.

Palm B., Claesson J., 2006. Plate heat exchangers: calculation methods for single and two-phase flow, Heat Transfer Engineering, 27, pp. 88–98.

Palmer S.C., Payne W.V., Domanski P.A., 2000. Evaporation and Condensation Heat Transfer Performance of Flammable Refrigerants in a Brazed Plate Heat Exchanger, NIST IR 6541.

Park C.Y., Hrnjak P.S., 2007. CO_2 and R410A flow boiling heat transfer, pressure drop, and flow pattern at low temperatures in a horizontal smooth tube, International Journal of Refrigeration ,30 (2007), pp. 166–178.

Park J.E., Vakili-Farahani R., Consolini L., Thome J.R., 2011. Experimental study on condensation heat transfer in vertical minichannels for new refrigerant R1234ze(E) versus R134a and R236fa, Experimental Thermal and Fluid Science, 35(3), pp. 442–54.

Park J.H., Kim Y.S., 2004. Evaporation Heat Transfer and Pressure Drop Characteristics of R134a in the Oblong Shell and Plate Heat Exchanger. KSME International Journal, 18, pp. 2284–2293.

Park K.J., Jung D., 2010. Nucleate boiling heat transfer coefficients of R1234yf on plain and low fin surfaces. International Journal of Refrigeration, 33(3), pp.553–557.

Park K.J., Kang D.G., Jung D., 2011. Condensation heat transfer coefficients of R1234yf on plain, low fin, and Turbo-C tubes, International Journal of Refrigeration, 34(1), pp. 317–21.

Pelletier, O., Palm, B., 1997. Boiling of Hydrocarbons in Small Plate Heat Exchangers. International Institute of Refrigeration, Commission B1, College Park, USA.

Poggi F., Macchi-Tejeda H., Leducq D., Bontemps A., 2008. Refrigerant charge in refrigerating systems and strategies of charge reduction, International Journal of Refrigeration, 31, pp. 353–370.

Porkhial S., Khastoo B., Saffar-Avval M., 2004. Transient response of dry expansion evaporator in household refrigerators. Applied Thermal Engineering, 24, pp. 1465–1480.

Qiu J., Zhang H., Yu X., Qi Y., Lou J., Wang X., 2015. Experimental investigation of flow boiling heat transfer and pressure drops characteristic of R1234ze(E), R600a, and a mixture of R1234ze(E)/R32 in a horizontal smooth tube, Advances in Mechanical Engineering, 7(9), pp. 1–12.

Quiben J.M., Thome J.R., 2007. Flow pattern based two-phase frictional pressure drop model for horizontal tubes. Part I: Diabatic and adiabatic experimental study, International Journal of Heat and Fluid Flow, 28, pp. 1049–1059.

Ramírez-Rivera F., López-Belchí A., Vera-García F., García-Cascales J.R., Illán-Gómez F., 2015. Two phase flow pressure drop in multiport mini-channel tubes using R134a and R32 as working fluids, International Journal of Thermal Sciences, 92, pp. 17–33.

Rasti M., Aghamiri S.F., Hatamipour, M.S., 2013. Energy efficiency enhancement of a domestic refrigerator using R436A and R600a as alternative refrigerants to R134a, International Journal of Refrigeration, 74, pp. 86–94.

Rasti M., Hatamipour M.S., Aghamiri S.F., Tavakoli M., 2012. Enhancement of domestic refrigerator's energy efficiency index using a hydrocarbon mixture refrigerant, Measurement, 45, pp. 1807–1813.

Reay D.A., Harvey A., 2012. The role of heat pipes in intensified unit operations, Applied Thermal Engineering, 57, pp. 147–153.

Reay D.A., Kew P.A., 2006, Heat Pipes, fifth ed., Butterworth-Heinemann, Oxford.

Riffat S., Ma X., 2007. Recent developments in heat pipe technology and applications: a review, Int. J. Low Carbon Technology, 2, pp. 162–177.

Riffat S.B., Gan G., 1998. Determination of effectiveness of heat pipe heat recovery for naturally ventilated buildings, Applied Thermal Engineering, 18 pp. 121–30.

Rittidech S., Dangeton W., Soponronnarit S., 2005. Closed-ended oscillating heat pipe (CEOHP) air-preheater for energy thrift in a dryer, Applied Energy, 81, pp. 198–208.

Sabharwall P., Utgikar V., Gunnerson F., 2009. Dimensionless Numbers in Phase-Change Thermosyphon and Heat-Pipe Heat Exchangers, Nuclear Technology, 167 (2), pp. 325–332.

Saitoh S., Dang C., Nakamura Y., Hihara E., 2011. Boiling heat transfer of HFO-1234yf flowing in smooth small-diameter horizontal tube. International Journal of Refrigeration, 34(8), pp. 1846–1853.

Sastri, S.R.S., Rao, K.K., 2000. New method for predicting saturated liquid viscosity at temperatures above the normal boiling point, Fluid Phase Equilibria, 175, pp. 311–323.

Sattar M., Saidur R., Masjuki H., 2007. Performance investigation of domestic refrigerator using pure hydrocarbons and blends of hydrocarbons as refrigerants. Proceedings of World Academy of Science, Engineering and Technology, pp. 223–228.

Sekhar S.J., Mohanlal D., Renganarayanan S., 2004. Improved energy efficiency for CFC domestic refrigerators retrofitted with ozone friendly HFC134a/HC refrigerant mixture, International Journal of Thermal Sciences, 43, pp. 307–314.

Shah M.M., 1979. A general correlation for heat transfer during film condensation inside pipes, International Journal of Heat and Mass Transfer, 22, pp. 547–556.

Shah M.M., 1982. Chart correlation for saturated boiling heat transfer: equations and further study, ASHRAE Transactions, 88, pp. 185–196.

Shah R.K., Focke W.W., 1988. Plate heat exchangers and their design theory, Heat Transfer Equipment Design, Hemisphere, Washington, pp. 227–254.

Shi S.Y., Chen J.P., Grabenstein V., Kabelac S., 2010. Experimental investigation on condensation heat transfer and pressure drop of R134a in a plate heat exchanger, Heat and Mass Transfer, 46, pp. 1177–1185.

Shin J.Y., Kim M.S., Ro S.T., 1996. Experimental study on forced convective boiling heat transfer of pure refrigerants and refrigerant mixtures in a horizontal tube, International Journal of Refrigeration, 20(4), pp. 267–275.

Shiraishi M., Kikuchi K., Yamanishi T., 1981. Investigation of heat transfer characterisics of a two phase closed thermosyphon. Heat recovery systems, 4(1), pp. 287–297.

Slipcevic, B., 1988. Wärmeü bergang verdampfern in näturlicher stromüng und bemessung von ü berfluteten verdampfern. Handbuch der kältetechnik. Springer, Berlin.

Srimuang W., Amatachaya P., A review of the applications of heat pipe heat exchangers for heat recovery, Renewable and Sustainable Energy Review, 16, pp. 4303–4315.

Steiner D., Taborek, J., 1992. Flow Boiling Heat Transfer in Vertical Tubes Correlated by an Asymptotic Model, Heat Transfer Engineering, 13, pp. 43–68.

Stephan, K., Abdelsalam, M., 1980. Heat-transfer correlations for natural-convection boiling. International Journal of Heat and Mass Transfer, 23 (1), pp. 73–87.

Sukchana T., Jaiboonma C., 2012. Effect of Filling Ratios and Adiabatic Length on Thermal Efficiency of Long Heat Pipe Filled with R-134a, 10th Eco-Energy and Materials Science and Engineering (EMSES2012).

Sun L., Mishima K., 2009a. An evaluation of prediction methods for saturated flow boiling heat transfer in mini-channels International Journal of Heat and Mass Transfer, 52, pp. 5323–5329.

Sun L., Mishima K., 2009b. Evaluation analysis of prediction methods for two-phase flow pressure drop in mini-channels, International Journal of Multiphase Flow, 35, pp. 47–54.

Szczukiewicz S., Borhani N., Thome J.R., 2013. Two-phase heat transfer and high-speed visualization of refrigerant flows in 100 ×100 m^2 siliconmulti-microchannels, International Journal of Refrigeration, 36(2), pp. 402–413.

Táboas F., Vallés M., Bourouis M., Coronas A., 2012. Assessment of boiling heat transfer and pressure drop correlations of ammonia/water mixture in a plate heat exchanger, International Journal of Refrigeration, 35, pp. 633 – 644.

Tashtoush B., Tahat M., Shudeifat M.A., 2002. Experimental study of new refrigerant mixtures to replace R12 in domestic refrigerators, Applied Thermal Engineering, 22, pp. 495–506.

Thonon B., 1995. Design method for plate evaporators and condensers, in: Proceedings of 1st Int. Conf. Process Intensification for Chemical Industry, BHR Group Conference Series Publication, pp. 149-155.

Thonon B., Feldman A., Margat L., Marvillet C., 1997. Transition from nucleate boiling to convective boiling in compact heat exchangers, International Journal of Refrigeration, 20, pp. 592–597.

Tibiriçà C.B., Ribatski G., Thome J.R., 2012. Flow boiling characteristics for R1234ze(E) in 1.0 and 2.2mmcircular channels, Journal of Heat Transfer, 134(2), article 020906.

Tran T.N., Wambsganss M.W., France D.M., 1996. Small circular and rectangular channel boiling with two refrigerants, International Journal of Multiphase Flow, 22 (3), pp. 485–498.

Tribbe C., Müller-Steinhagen H., 2010. Gas/Liquid Flow in Plate-and-Frame Heat Exchangers- Part II: Two-Phase Multiplier and Flow Pattern Analysis, Heat Transfer Engineering, 22(1), pp. 12–21.

Vakili-Farahani F., Agostini B., Thome J.R., 2013. Experimental study on flow boiling heat transfer of multiport tubes with R245fa and R1234ze(E), International Journal of Refrigeration, 36(2), pp.335–52.

Van Rooyen E., Thome J.R., 2013. Pool boiling data and prediction method for enhanced boiling tubes with R-134a, R-236fa and R-1234ze(E). International Journal of Refrigeration 36(2), pp. 447–55.

Velders G.J.M., Fahey D.W., Daniel J.S., McFarland M., Andersen S.O., 2009. The large contribution of projected HFC emissions to future climate forcing, Proceedings of the National Academy of Sciences, 106, pp.10949–10954.

Wan J.W., Zhang J.L., Zhang W.M., 2007. The effect of heat pipe air handling coil on energy consumption in central air conditioning system, Energy and Buildings, 39, pp. 1035–1040.

Wang C.C., Chi K.Y., Chang C.J., 2000. Heat transfer and friction characteristics of plain fin-and-tube heat exchangers, part II: Correlation, Int. J. Heat Mass Transfer, 43, pp. 2693–2700.

Wang J.C.Y., Ma Y., 1987. Condensation heat transfer inside vertical and inclined thermosyphons, Journal of Heat Transfer, Transactions ASME, 113 (3), pp. 777–780.

Wang L., Dang C., Hihara E., 2012. Experimental study on condensation heat transfer and pressure drop of low GWP refrigerant HFO1234yf in a horizontal tube, International Journal of Refrigeration, 35, pp. 1418–1429.

Wang, C.C., Chiang, C.S., Lu, D.C., 1997. Visual observation of two-phase flow pattern of R-22, R-134a, and R-407C in a 6.5-mm smooth tube, Experimental Thermal and Fluid Science, 15, pp. 395–405.

Wattelet J.P., Chato J.C., Christoffersen B.R., et al., 1994. Heat transfer flow regimes of refrigerants in a horizontal-tube evaporator, ACRC TR-55.

Webb R.L., 1998. Convective condensation of superheated vapor, Journal of Heat Transfer – Trans. ASME, 120, pp. 418–421.

Wojtan L., Ursenbacher T., Thome J.R, 2005. Investigation of flow boiling in horizontal tubes: Part II — Development of a new heat transfer model for stratified-wavy, dryout and mist flow regimes, International Journal of Heat and Mass Transfer, 48, pp. 2970–2985.

Wongwises S., Chimres N., 2005. Experimental study of hydrocarbon mixtures to replace HFC134a in domestic refrigerators, Energy Conservation and Management, 46, pp.85–100.

Wu X., Zhu Y., Huang X., 2015. Influence of 0° helix angle micro fins on flow and heat transfer of R32 evaporating in a horizontal mini multichannel flat tube, Experimental Thermal and Fluid Science, 68, pp. 669–680.

Wu X.P., Johnson P., Akbarzadeh A., 1997. Application of heat-pipe exchangers for humidity control in an air conditioning system, Applied Thermal Engineering, 6, pp. 561–568.

Würfel R., Ostrowski N., 2004. Experimental investigations of heat transfer and pressure drop during the condensation process within plate heat exchangers of the herringbone-type, International Journal of Thermal Sciences 43, pp. 59–68.

www.epa.gov, U.S. Environmental Protection Agency, 28/10/2015.

www.ozone.unep.org, UNEP Ozone Secretariat, 09/12/2015.

Xu Y., Fang X., Li G., Li D., Yuan Y., 1996. An experimental study of flow boiling heat transfer of R134a and evaluation of existing correlations International Journal of Heat and Mass Transfer, 92, pp. 1143–1157.

Yan Y.Y., Lin T.F., 1999. Evaporation heat transfer and pressure drop of refrigerant R-134a in a plate heat exchanger, ASME Journal of Heat Transfer 121, pp. 118–127.

Yan Y.Y., Lio H.C., Lin T.F., 1999. Condensation heat transfer and pressure drop of refrigerant R134a in a plate heat exchanger, International Journal of Heat and Mass Transfer, 42, pp. 993–1006.

Yana Motta S.F., Vera Becerra E.D., Spatz M.W., 2010. Analysis of LGWP alternatives for small refrigeration (plugin) applications, International Refrigeration and Air Conditioning Conference at Purdue, July 12–15, 2010, West Lafayette, IN, USA.

Yang F., Yuan X., Lin G., 2003. Waste heat recovery using heat pipe heat exchanger for heating automobile using exhaust gas, Applied Thermal Engineering, 23, pp. 367–72.

Yau Y.H., 2006. Analysis of enthalpy change with/without a heat pipe heat exchanger in a tropical air conditioning system, International Journal of Energy Research, 30 (15), pp. 1251–1263.

Yau Y.H., 2008a. The heat pipe heat exchanger: a review of its status and its potential for coolness recovery in tropical buildings, Building Services Engineering Research and Technology, 29, pp. 291–310.

Yau Y.H., 2008b. The use of a double heat pipe heat exchanger system for reducing energy consumption of treating ventilation air in an operating theatre – a full year energy consumption model simulation, Energy and Buildings, 40, pp. 917–925.

Yau Y.H., Ahmadzadehtalatapeh M., 2010. A review on the application of horizontal heat pipe heat exchangers in air conditioning systems in the tropics, Applied Thermal Engineering, 3, pp. 77–84.

Yau Y.H., Tucker A.S., 2003. The performance of a wet six-row heat pipe heat exchanger operating in tropical buildings, International Journal of Energy Resources, 27, pp. 187–202.

Yu C.C., Teng T.P., 2014. Retrofit assessment of refrigerator using hydrocarbon refrigerants, Applied Thermal Engineering, 66, pp. 507-518.

Yu J., Momoki S., Koyama S., 1999. Experimental study of surface effect on flow boiling heat transfer in horizontal smooth tubes, International Journal of Heat and Mass Transfer, 42, pp. 1909–1918.

Yuan Y., Lu Y., Bao H., Wang Y., Wang W., Roskilly A.P., 2014. Investigation of a heat pipe heat exchanger integrated with a water spray for the heat recovery from boil exhaust gas, The 6th International Conference on Applied Energy – ICAE2014.

Zhang H., Shao S., Xu H., Zou H., Tian C., 2015. Integrated system of mechanical refrigeration and thermosyphon for free cooling of data centers, Applied Thermal Engineering, 75, 185–192.

Zhang W., Hibiki T., Mishima K., 2004. Correlation for flow boiling heat transfer in mini-channels, International Journal of Heat and Mass Transfer, 47, pp. 5749–5763.

Zhang Y., Faghri A., 2008. Advances and Unsolved Issues in Pulsating Heat Pipes, Heat Transfer Engineering, 29(1), pp. 20–44.

8 List of Publications

Papers on International Journals with Impact Factor

1 G. A. Longo, **G. Righetti**, C. Zilio, Development of an Innovative Raw Milk Dispenser Based on Nanofluid Technology, International Journal of Food Engineering, ISSN 1556-3758, ISSN 2194-5764, DOI 10.1515/ijfe-2015-0127.
IN PRESS

2 G. A. Longo, S. Mancin, **G. Righetti**, C. Zilio, HFC32 and HFC410A flow boiling inside a 4mm horizontal smooth tube, International Journal of Refrigeration, PII:S0140-7007(15)00278-9,
DOI:http://dx.doi.org/doi:10.1016/j.ijrefrig.2015.09.002.
IN PRESS

3 G. A. Longo, S. Mancin, **G. Righetti**, C. Zilio. Saturated flow boiling of HFC134a and its low GWP substitute HFO1234ze(E) inside a 4 mm horizontal smooth tube, International Journal of Refrigeration, DOI:10.1016/j.ijrefrig.2016.01.015.
IN PRESS

4 G. A. Longo, S. Mancin, **G. Righetti**, C. Zilio, A new model for refrigerant boiling inside Brazed Plate Heat Exchangers (BPHEs), International Journal of Heat and Mass Transfer, 91 (2015) 144-149.

5 G. A. Longo, S. Mancin, **G. Righetti**, C. Zilio, HFC32 vaporisation inside a Brazed Plate Heat Exchanger (BPHE): Experimental measurements and IR thermography analysis, International Journal of Refrigeration, 57(2015) 77-86.

6 **G. Righetti**, C. Zilio, G. A. Longo, Comparative performance analysis of the low GWP refrigerants HFO1234yf, HFO1234ze(E) and HC600a inside a roll-bond evaporator, International Journal of Refrigeration, 54 (2015) 1-9.

7 G. A. Longo, **G. Righetti**, C. Zilio, A new computational procedure for refrigerant condensation inside herringbone-type Brazed Plate Heat Exchangers, International Journal of Heat and Mass Transfer, 82 (2015) 530-536.

8 G. A. Longo, S. Mancin, **G. Righetti**, C. Zilio, HFC32, a low GWP substitute for

HFC410A in medium size chillers and heat pumps, International Journal of Refrigeration, 53 (2015) 62-68.

9 G. A. Longo, C. Zilio, **G. Righetti**, Condensation of the low GWP refrigerant HFC152a inside a Brazed Plate Heat Exchanger, Experimental Thermal and Fluid Science, 68 (2015) 509-515.

10 G. A. Longo, **G. Righetti**, C. Zilio, F. Bertolo, Experimental and theoretical analysis of a heat pipe heat exchanger operating with a low global warming potential refrigerant, Applied Thermal Engineering, 65 (2014) 361–368.

11 G. A. Longo, C. Zilio, **G. Righetti**, J. S. Brown, Experimental assessment of the low GWP refrigerant HFO-1234ze(Z) for high temperature heat pumps, Experimental Thermal and Fluid Science 57 (2014) 293–300

12 G. A. Longo, C. Zilio, **G. Righetti**, J. S. Brown, Condensation of the low GWP refrigerant HFO1234ze(E) inside a Brazed Plate Heat Exchanger, International Journal of Refrigeration, 38 (2014) 250–259.

13 S. Mancin, C. Zilio, **G. Righetti**, L. Rossetto, Mini Vapor Cycle System for high density electronic cooling applications, International Journal of Refrigeration, 36 (2013) 1119–1202.

Proceedings of international conferences

14 G. A. Longo, S. Mancin, **G. Righetti**, C. Zilio, HFC32 Vaporisation Inside A Brazed Plate Heat Exchanger, The 24th IIR International Congress Of Refrigeration, ICR 2015. August 16-22, 2015, Yokohama, JP.

15 **G. Righetti**, G. Pernigotto, C. Zilio, G. A. Longo, Numerical And Experimental Analysis On Poultry Freezing Time, The 24th IIR International Congress Of Refrigeration, ICR 2015. August 16-22, 2015, Yokohama, JP.

16 G. A. Longo, S. Mancin, **G. Righetti**, C. Zilio, A new model for refrigerant nucleate boiling inside a Brazed Plate Heat Exchanger (BPHE), The 24th IIR International Congress Of Refrigeration, ICR 2015. August 16-22, 2015, Yokohama, JP.

17 G. A. Longo, **G. Righetti**, C. Zilio, Development Of An Innovative Raw Milk Dispenser Based On Nanofluid Technology, The 24th IIR International Congress Of Refrigeration, ICR 2015. August 16-22, 2015, Yokohama, JP.

18 **G. Righetti**, S. Mancin, C. Zilio, G. A. Longo, Experimental And Theoretical Analysis Of A Heat Pipe Heat Exchanger Using HFC-152a As Working Fluid, The 24th IIR International Congress Of Refrigeration, ICR 2015. August 16-22, 2015, Yokohama, JP.

19 G. A. Longo, **G. Righetti**, C. Zilio, A New Model For Refrigerant Condensation Inside A Brazed Plate Heat Exchanger (BPHE), Proceedings of the 15th International Heat Transfer Conference, IHTC-15 August 10-15, 2014, Kyoto, JP.

20 G. A. Longo , C. Zilio, **G. Righetti**, J. S. Brown, HFO1234ze(Z) Saturated Vapour Condensation inside a Brazed Plate Heat Exchanger, 15th International Refrigeration and Air Conditioning Conference at Purdue, July 14-17, 2014, Purdue, Indiana, US.

21 **G. Righetti**, C. Zilio, G. A. Longo, Experimental Analysis of R134a and R1234ze(E) Flow Boiling Inside a Roll Bond Evaporator, 15th International Refrigeration and Air Conditioning Conference at Purdue, July 14-17, 2014, Purdue, Indiana, US.

22 G. A. Longo, C. Zilio, **G. Righetti**, J. S. Brown, HFO1234ze(E) Condensation Inside A Brazed Plate Heat Exchanger, 4th IIR Conference on Thermophysical Properties and Transfer Processes of Refrigerants, Delft, The Netherlands, 2013.

9 Acknowledgments

First of all, I would like to express my gratitude to my supervisor, Claudio Zilio, for believing in me and for encouraging me throughout the entire course of studies. A big thank you to him and to Giovanni Antonio Longo, for their expertise, their precious time dedicated me, their suggestions, and support.

I am very grateful to Simone Mancin, Giovanni Pernigotto, and Luca Doretti, for the good company and for assisting me in several ways. It's been my privilege to work with them.

In addition, I would also like to thank the DTG Department, most of all Professor Lazzarin, he staffs of the administrative offices, of the library, and Sergio.

I am extremely thankful to my Family, mum, dad, grandparents, and Damiano: my husband and team mate. I am where I am because of you all.

Last, but not least, thanks to all my relatives and to my special friends Andrea, Beatrice, Marta, Nadia, Silvia, Valentina, and Vittorio.

9 Ringraziamenti

Grazie innanzitutto al mio supervisore, Claudio Zilio, che ha voluto credere in me ancora da prima della laurea magistrale e, giorno dopo giorno, non ha mai smesso di darmi stima e fiducia. Grazie perché, con Giovanni Antonio Longo, mi sono stati di costante guida, esempio e supporto.

Grazie anche a Simone Mancin, Giovanni Pernigotto e Luca Doretti, per i consigli, la compagnia e i tanti lavori insieme: è sempre bello trascorrere il tempo con voi.

Ringrazio inoltre tutti gli afferenti al DTG che non mi hanno mai fatto mancare una parola gentile e un aiuto. Un grazie particolare al Professor Lazzarin, al personale delle segreterie e della biblioteca e a Sergio.

Un grandissimo grazie va ora alla mia famiglia, per l'affetto, la pazienza, il coraggio e la stima che non mancano mai di dimostrarmi. Grazie mamma, papà e nonni, e grazie a Damiano, mio marito e inseparabile compagno di avventure.

Grazie infine a tutte le persone che mi sono state vicine, agli zii, ai cugini e ai tantissimi amici, tra cui ricordo in particolare Andrea, Beatrice, Marta, Nadia, Silvia, Valentina e Vittorio che nei vari momenti della vita mi hanno regalato il loro sorriso.